molecules

Opioids and Their Receptors
Present and Emerging Concepts in Opioid Drug Discovery II

Edited by
Mariana Spetea and Richard M. van Rijn
Printed Edition of the Special Issue Published in *Molecules*

www.mdpi.com/journal/molecules

MDPI

Opioids and Their Receptors: Present and Emerging Concepts in Opioid Drug Discovery II

Opioids and Their Receptors: Present and Emerging Concepts in Opioid Drug Discovery II

Editors

Mariana Spetea
Richard M. van Rijn

Editors

Mariana Spetea
Department of
Pharmaceutical Chemistry
University of Innsbruck
Innsbruck
Austria

Richard M. van Rijn
Department of Medicinal
Chemistry and Molecular
Pharmacology
Purdue University
West Lafayette
United States

For citation purposes, cite each article independently as indicated on the article page online and as indicated below:

LastName, A.A.; LastName, B.B.; LastName, C.C. Article Title. *Journal Name* **Year**, *Volume Number*, Page Range.

Contents

About the Editors

Mariana Spetea

Mariana Spetea earned a M.Sc. degree in Biochemistry (1993) from the University of Bucharest (Romania) and her Ph.D. degree in Biology (1998) from the József Attila University (Szeged, Hungary). She spent two years (1998-–1999) as a post-doctoral fellow at the Karolinska Institute (Stockholm, Sweden), with research fellowships awarded by the Swedish Institute and the Wenner-Gren Center Foundation. In 2000, she joined the "Opioid Research Group" leaded by Prof. Helmut Schmidhammer at the University of Innsbruck (Austria), as a research associate and assistant professor, where she has habilitated in Pharmacology (2010). Since 2011, she is the head of the "Opioid Research Group". An important focus of her research is dedicated to opioid drug discovery and development. Central topics of her research include structure-activity relationships of new opioid ligands, modulation of the ligand/opioid receptor system in pathological pain and molecular mechanism of opioid actions. She has been a research leader and associate researcher of several research projects, as well as the scientific coordinator of a European Union research project. Besides science, Prof. Spetea is devoted to education in Pharmaceutical Sciences of undergraduate and graduate students at the Faculty of Chemistry and Pharmacy, University of Innsbruck. Her scientific achievements have been published in numerous peer-reviewed articles, reviews, conference proceedings and patents, and have been disseminated in popular science reports. Beside several numerous awards, she was also the receiver of "Science4Life Venture Cup 2003". Prof. Spetea is Editorial Board Member of Frontiers (Frontiers in Neuroscience, Pharmacology, Neurology, Psychiatry and Drug Discovery) and Molecules, and was a Guest Editor of Special Issues of Current Pharmaceutical Design (2013) and Molecules (2020 and 2021).

Richard M. van Rijn

Richard M. van Rijn received a B.S./M.S. degree in Bio-Pharmaceutical Sciences from Leiden University (The Netherlands). For his Ph.D. training, he joined the pharmacochemistry research group of Prof. Dr. Rob Leurs at VU University Amsterdam in 2002. After a brief stint in a research associate position at Biofocus DPI, a Galapagos subsidiary serving as contract research organization creating custom adenoviruses, he joined the laboratory of Dr. Jennifer Whistler at the Ernest Gallo Clinic and Research Center within the Department of Neuroscience at the University of California San Francisco in 2007. Here, he received post-doctoral training in the behavioral neuropharmacology of opioid receptors in the area of substance use-, pain-, and mood disorders. He was awarded a K99/R00 pathway to independence award from the National Institute on Alcohol Abuse and Alcoholism to study the delta opioid receptor as a target to treat alcohol use disorders. In 2013, he started his own laboratory in the Department of Medicinal Chemistry and Molecular Pharmacology at Purdue University. His research program combined high-throughput chemical library screening with natural product drug discovery to identify novel opioids with distinct and unique pharmacology to treat a variety of neurological disorders, focusing on biased signaling. He received multiple grants from the NIH and patents covering both opioids and adenylyl cyclase inhibitors. He received young investigator awards from the Brain and Behavior Foundation and the International Narcotics Research Conference. In 2020, he carried out a sabbatical in the laboratory of Dr. Brian Shoichet in the Department of Pharmaceutical Chemistry at UCSF. In 2021, he joined Septerna Inc., a pharmaceutical start-up company cofounded by Drs. Robert Lefkowitz, Arthur Christopoulos and Patrick Sexton specialized in small molecule drug discovery at G protein-coupled receptors.

Preface to "Opioids and Their Receptors: Present and Emerging Concepts in Opioid Drug Discovery II"

Few neurotransmitter systems have fascinated as much as the opioid system (i.e., opioid ligands and their receptors). Over the years, scientific studies of the endogenous opioid system have uncovered a complex and subtle system that exhibits impressive diversity, based on its critical role in modulating a large number of sensory, motivational, emotional and cognitive functions. Additionally, its important therapeutic value for the treatment of many human disorders, including pain, affective and addictive disorders, and gastrointestinal motility disorders, has been of persistent interest. This book specifically covers a broad area of the opioid research, offering up-to-date and new perspectives about opioid drug discovery. The diversity among the discussed topics ranging from medicinal chemistry to opioid pharmacology, from basic science to translational research, is a testimony to the complexity of the opioid system that results from the expression, regulation and functional role of opioid ligands and their receptors. This book will serve as a useful reference to scientists while also stimulating continuous research in the chemistry and pharmacology of the opioid system, with the prospect of finding improved therapies of human diseases where the opioid system plays a central role. We also thank all reviewers for their effort in evaluating the manuscripts. Last but not least, we would like to appreciate the editorial office of the *Molecules* journal for their support in preparing this book.

Mariana Spetea and Richard M. van Rijn
Editors

Editorial

Opioids and Their Receptors: Present and Emerging Concepts in Opioid Drug Discovery II

Richard M. van Rijn [1,2,*] and **Mariana Spetea** [3,*]

1   Department of Medicinal Chemistry and Molecular Pharmacology, Purdue Institute for Drug Discovery, and Purdue Institute for Integrative Neuroscience, Purdue University, West Lafayette, IN 47907, USA
2   Septerna Inc., San Francisco, CA 94080, USA
3   Department of Pharmaceutical Chemistry, Institute of Pharmacy and Center for Molecular Biosciences Innsbruck (CMBI), University of Innsbruck, 6020 Innsbruck, Austria
*   Correspondence: rvanrijn@purdue.edu (R.M.v.R.); mariana.spetea@uibk.ac.at (M.S.)

A few neurotransmitter systems have fascinated the research community, as much as the opioid system (i.e., opioid ligands and their receptors). Over the years, scientific studies of the endogenous opioid system have uncovered a complex and subtle system that exhibits impressive diversity, based on its critical role in modulating a large number of sensory, motivational, emotional, and cognitive functions. Additionally, its important therapeutic value for the treatment of many human disorders, including pain, affective and addictive disorders, and gastrointestinal motility disorders, has been of persistent interest.

The Special Issue, "Opioids and Their Receptors: Present and Emerging Concepts in Opioid Drug Discovery II", which follows a similar topical Special Issue published in 2020 [1], includes eleven research articles and three reviews. This Special Issue offers up-to-date and new perspectives about opioid drug discovery.

Three research articles cover the discovery of novel δ-opioid receptor (δOR) ligands with distinct pharmacological profiles [2–5]. Meqbil et al. identified a novel δOR agonist with a unique scaffold lacking basic nitrogen from a high-throughput screen [4]. Molecular dynamics simulations of the molecule in the presence or absence of a docked Leu[5]-enkephalin peptide suggests that this molecule interacts with δOR in a bitopic manner. Specifically, the molecule partly occupies the orthosteric pocket in which the enkephalin peptide resides, but it also fits in a generally idle subpocket of the binding pocket. Cellular assays indicate that the molecule has a 10-fold preference for binding to the δOR over μ- and κ-opioid receptors (μOR and κOR, respectively), and it competes with orthosteric ligands. However, modeling and competitive functional assays suggest that the molecule may possess some negative modulatory capabilities. The study by Karasawa et al. confirmed previous work by Cassell et al. showing rubiscolin-5 (Tyr-Pro-Leu-Asp-Leu) and rubiscolin-6 (Tyr-Pro-Leu-Asp-Leu-Phe) to selectively bind and activate δORs without recruiting β-arrestin 2 [2,6]. The authors noted significant changes in the efficacy of rubiscolin peptides to inhibit intracellular cAMP in cells co-expressing δOR and μOR, potentially indicating an affinity for putative δOR-μOR heteromers; however, this type of assay comes with multiple limitations in terms of controlling receptor expression and dissecting the cAMP signal that originates from the monomers, this could be better resolved in a model system that eliminates monomer signaling [7]. Tanguturi et al. reported on a couple of novel δOR inverse agonists [3,5]. This work was inspired by a prior study by Higashi et al. [8] and identified SRI-9342 as an irreversible antagonist and SRI-45128 as an inverse agonist. The high affinity and selectivity for δOR over μOR and κOR make these valuable tools, which could, for example, be used to investigate the utility of this class of δOR modulators in treating Alzheimers' disease. Similarly to the study by Karasawa et al., one exciting strength of the study by Tanguturi et al. is that it confirms findings by a different research team, providing much greater validity to the unique pharmacology, be it a G protein-biased peptide or an inverse agonist.

Wtorek et al. presented a continuation of their work on pentapeptide Tyr-c[D-Lys-Phe-Phe-Asp]NH$_2$ (RP-170), a stabilized bifunctional μOR and κOR agonist with central and peripheral antinociceptive properties [9]. In the current study [10], D-Lys was replaced with either an (*R*)-β^3-Lys (RP-171) or a (*S*)-β^3-Lys (RP-172). Both RP-171 and RP-172 lost affinity and potency relative to the parent compound, with RP-172 precipitously so. However, RP-171 gained μOR selectivity in both affinity (14-fold from 3-fold) and potency (7-fold from 2-fold) relative to RP-170. Molecular dynamics simulations suggested that RP-172 was less able to form or maintain hydrogen bonds and a salt bridge with Asp147.

Yucel et al. designed and synthesized novel molecules with thiazole and piperazine moieties [11], based on the rationale that many analgesic drugs, such as for example amoxapine and meloxicam, carry these structural motifs. Multiple synthesized molecules produced antinociception in mouse models of acute nociceptive (tail-clip and hot-plate tests) and visceral pain (acetic acid-induced writhing test) following oral administration. The authors found the effects to be naloxone reversible, which is suggestive of an opioid receptor mechanism. Molecular docking studies predict that the molecules can product meaningful interactions within the μOR and δOR binding pocket, whereas docking scores for the molecules within the κOR structure did not correlate with behavioral efficacy, i.e., inactive derivatives docked equally as active derivatives.

A study by Fritzwanker et al. examines μOR phosphorylation and dephosphorylation by SR-17018 compared to the canonical agonist DAMGO and the partial agonist buprenorphine [12]. The authors observed that SR-17018 has a delayed onset of μOR phosphorylation, but it otherwise matches the full agonist profile of phosphorylating μOR at multiple sites. Unlike the full agonist DAMGO, SR-17018-induced μOR phosphorylation persists and is resistant to washout suggestive of a slow off-rate that is, nevertheless, naloxone reversible. SR-17018 has been demonstrated to have a large therapeutic window between antinociception and respiratory depression [13], although there is a debate whether this profile is caused by the G protein bias [14,15]. The findings in this study suggest that SR-17018 clearly has a distinct binding mode that may begin to explain the opioid's pharmacology.

Other studies in this issue also explored the behavioral pharmacology of opioids in rodent models but outside of their antinociceptive properties. A study by Paul et al. investigated the development of tolerance to the locomotor effects of morphine after twice daily injection (b.i.d.) for a 10-day period [16]. The authors found significant hyperactivity on day 10 relative to day 1. The authors also reveal that tolerance induced by b.i.d. 10 mg/kg morphine treatment was reversed by switching to a 20 mg/kg q.d. dosing regimen. As the authors also tracked the establishment of antinociceptive tolerance, they were able to link antinociceptive tolerance switch to morphine-induced hyper-excitatory activity.

Targeting the κOR receptor is currently regarded as a viable strategy for developing pharmacotherapies for human disorders where the endogenous kappa opioid system (κOR/DYN) plays a central role, including pain, itch, neurological, and addictive disorders [17–19]. κOR agonists are under consideration for their antipruritic activity and one such agonist, nalfurafine, is approved in Japan for the treatment of resistant pruritus in hemodialysis patients [20], whereas in the United States, the peptide difelikefalin was approved to treat moderate-to-severe pruritis in the same patient population [21]. Nalbuphine is a third κOR agonist that is being clinically investigated as potential anti-pruritic agent [22]. In a report by Inan et al., in this Special Issue, a more detailed investigation on the antipruritic effects of nalbuphine is presented [23]. The authors tested nalbuphine at multiple doses (0.3–10 mg/kg) in three different acute itch mouse models of TAT-HIV-1 protein, deoxycholic acid, and chloroquine-induced scratching. Nalbuphine dose-dependently inhibited scratching in all three models. The authors also showed that nalbuphine is inactive in the chloroquine model when performed in κOR-knockout mice.

In this issue, Nosova et al. provided a review of epigenetic and transcriptional control of the prodynorphin (*PDYN*) gene in the human brain [24]. The review provides a detailed

analysis of different mRNAs produced from the *PDYN* gene as well splice variants and single nucleotide polymorphisms and the potential role of non-coding RNAs. Some of the protein products may serve as nuclear proteins that can impact gene transcription and epigenetic processes. The authors discuss possible transcription factors that can modulate the expression of the *PDYN* gene and the link of SNPs to differential regulation of prodynorphin expression in different neurological disorders. The authors review methylation patterns and discuss differential expressions of *PDYN* between neurons and glia. This review is a highly valuable resource and reference for researchers studying the pDYN/κOR system.

The availability of high-resolution crystal structures of all opioid receptors in active and inactive conformations offer a unique prospect for drug discovery, and has been a significant development for opioid research [25]. Multiple articles in this issue [4,10,11,26] utilized the power of computational techniques (molecular modeling and molecular dynamics simulations) to explore binding mechanisms of peptides and synthetic molecules under investigation using the crystal structures of the opioid receptors. The study by Yucel et al. provides an example of a phenotypic screen where molecular docking aided the investigation into the mechanism of action of the molecules bearing thiazole and piperazine moieties in producing opioid receptor-mediated antinociception [11].

Spetea et al. reported earlier on HS-731 as a full agonist at μOR and δOR, and a partial agonist at κOR [27]. Performing a structure-based molecular modeling study including molecular dynamics simulations and generation of dynamic 3D pharmacophore models (dynophores), Puls et al. provided important insights into dynamic interaction patterns of HS-731 with all opioid receptors [26]. The in silico study nicely rationalizes the experimental results on different binding and activity of HS-731 to each opioid receptor subtype. Two residues are highlighted for HS-731 recognition at μOR, δOR, and κOR, particularly the conserved residue 5.39 (K) and the non-conserved residue 6.58 (μOR: K, δOR: W and κOR: E). At μOR, HS-731 takes part in more frequent and stronger charge interactions than in δOR and κOR, in correlation with the highest affinity of HS-731 at μOR. A salt bridge between transmembrane helices 5 and 6 via K227$^{5.39}$ and E297$^{6.58}$ was postulated to be responsible for the κOR partial agonism of HS-731. Additionally, the lack of binding at the NOP receptor experimentally determined is rationalized by the morphinan phenol Y130$^{3.33}$.

Since the discovery of the NOP receptor as the fourth member of the opioid receptor family, its role in different physiological and pathophysiological processes, especially pain, and the development of potential pain therapeutics was increasingly explored [28] This issue contains a review by El Daibani and Che, highlighting the analgesic utility of the nociception/orphanin FQ receptor (NOP) system [29]. The authors provide a detailed overview of almost two dozen NOP ligands and underscored the need for more high-resolution structures to be resolved beyond the current three crystal structures of the NOP receptor. The authors also touch upon some of the complex behavioral pharmacology observed for NOP agonists depending on whether the animal is administered to rodents or non-human primates at spinal or supraspinal sites. The authors conclude that more studies into the NOP system are necessary, but that the therapeutic promise of NOP agonists as analgesics with reduced risk for respiratory depression persists.

Three articles in this Special Issue explore dimerization and intracellular interactions and positive or negative cooperativity between the μOR and angiotensin (AT2) receptors [30], serotonin (5HT$_{1A}$) receptor [31], and free fatty acid (FFA) receptors [32]. Kiraly et al. reviewed positive cooperativity between μOR analgesics and angiotensin receptor inhibition [30]. The premise of the review is based on studies, for example, that found angiotensin-converting enzyme inhibition enhancing morphine antinociception and reducing opioid antinociceptive tolerance [33] and that the activation of angiotensin AT2 receptor decreases morphine antinociception [34]. Only a handful studies have investigated the interplay between μOR and the angiotensin system, and some of the results have been

contradictory. Thus, further studies will be welcome to provide better insight into possible interactions and whether they can be exploited therapeutically.

Binienda et al. investigated but did not identify the presence of a synergistic interaction between the opioid receptor agonists and modulators of FFA receptors [32]. Specifically, the authors tested the μOR agonist DAMGO with FFAR2 antagonist GLPG-09734, FFAR4 agonist GSK 137647, and FFAR4 antagonist AH-7614 in a mouse model of colitis. The FFAR4 antagonist was also tested in the presence of the δOR agonist DPDPE but also without a strong effect. Finally, Radoi et al. utilized fluorescence cross-correlation spectroscopy to examine whether the opioids morphine, codeine, oxycodone, and fentanyl promoted heterodimerization between the serotonin $5HT_{1A}$ receptor and μOR [31]. The authors further assessed the ability of the four opioids to stimulate ERK1/2 and p38 phosphorylation in cells co-expressing μOR and $5HT_{1A}$ receptors. While the authors noted differences in phosphorylation strength MAPK subtype, the experimental design limited the conclusions that could be drawn from those findings. Since $5HT_{1A}$ receptors may have roles in nociception, the further examination of the $5HT_{1A}$R-μOR interaction may provide novel strategies to promote the effectiveness of opioid analgesics.

The final collection of articles in this Special issue covers a broad area of opioid research that encompass all four opioid receptors; in silico, in vitro, and in vivo approaches; and small molecules and peptide ligand design. Therefore, we are optimistic that there will be relevant and useful articles amongst the collection to suit any scientist or member of the public regardless of their specific research focus or interests.

We would like to thank all authors for their contributions to this second edition of the Special Issue covering current and emerging concepts in opioid drug discovery. We also thank all reviewers for their effort in evaluating the manuscripts. Last but not least, we would like to appreciate the editorial office of the *Molecules* journal for their support in preparing this Special Issue.

Institutional Review Board Statement: Not applicable.

Informed Consent Statement: Not applicable.

Data Availability Statement: Not applicable.

Conflicts of Interest: van Rijn is currently employed as a Principal Scientist at Septerna Inc. and holds stock options in the company. van Rijn holds a US patent (10,954,224) describing novel delta opioid receptor agonists. The funders had no role in writing the manuscript.

References

1. Spetea, M.; Schmidhammer, H. Opioids and Their Receptors: Present and Emerging Concepts in Opioid Drug Discovery. *Molecules* **2020**, *25*, 5658. [CrossRef] [PubMed]
2. Karasawa, Y.; Miyano, K.; Fujii, H.; Mizuguchi, T.; Kuroda, Y.; Nonaka, M.; Komatsu, A.; Ohshima, K.; Yamaguchi, M.; Yamaguchi, K.; et al. In Vitro Analyses of Spinach-Derived Opioid Peptides, Rubiscolins: Receptor Selectivity and Intracellular Activities through G Protein- and beta-Arrestin-Mediated Pathways. *Molecules* **2021**, *26*, 6079. [CrossRef] [PubMed]
3. Tanguturi, P.; Pathak, V.; Zhang, S.; Moukha-Chafiq, O.; Augelli-Szafran, C.E.; Streicher, J.M. Discovery of Novel Delta Opioid Receptor (DOR) Inverse Agonist and Irreversible (Non-Competitive) Antagonists. *Molecules* **2021**, *26*, 6693. [CrossRef] [PubMed]
4. Meqbil, Y.J.; Su, H.; Cassell, R.J.; Mores, K.L.; Gutridge, A.M.; Cummins, B.R.; Chen, L.; van Rijn, R.M. Identification of a Novel Delta Opioid Receptor Agonist Chemotype with Potential Negative Allosteric Modulator Capabilities. *Molecules* **2021**, *26*, 7236. [CrossRef]
5. Tanguturi, P.; Pathak, V.; Zhang, S.; Moukha-Chafiq, O.; Augelli-Szafran, C.E.; Streicher, J.M. Correction: Tanguturi et al. Discovery of Novel Delta Opioid Receptor (DOR) Inverse Agonist and Irreversible (Non-Competitive) Antagonists. *Molecules* **2021**, *26*, 6693, Correction in Molecules 2022, 27, 1969. [CrossRef]
6. Cassell, R.J.; Mores, K.L.; Zerfas, B.L.; Mahmoud, A.H.; Lill, M.A.; Trader, D.J.; van Rijn, R.M. Rubiscolins are Naturally Occurring G protein-biased Delta Opioid Receptor Peptides. *Eur. Neuropsychopharmacol.* **2019**, *29*, 450–456. [CrossRef]

7. Van Rijn, R.M.; Harvey, J.H.; Brissett, D.I.; DeFriel, J.N.; Whistler, J.L. Novel Screening Assay for the Selective Detection of G-protein-coupled Receptor Heteromer Signaling. *J. Pharmacol. Exp. Ther.* **2013**, *344*, 179–188. [CrossRef] [PubMed]

8. Higashi, E.; Hirayama, S.; Nikaido, J.; Shibasaki, M.; Kono, T.; Honjo, A.; Ikeda, H.; Kamei, J.; Fujii, H. Development of Novel delta Opioid Receptor Inverse Agonists without a Basic Nitrogen Atom and Their Antitussive Effects in Mice. *ACS Chem. Neurosci.* **2019**, *10*, 3939–3945. [CrossRef] [PubMed]

9. Perlikowska, R.; do-Rego, J.C.; Cravezic, A.; Fichna, J.; Wyrebska, A.; Toth, G.; Janecka, A. Synthesis and biological evaluation of cyclic endomorphin-2 analogs. *Peptides* **2010**, *31*, 339–345. [CrossRef]

10. Wtorek, K.; Lipinski, P.F.J.; Adamska-Bartlomiejczyk, A.; Piekielna-Ciesielska, J.; Sukiennik, J.; Kluczyk, A.; Janecka, A. Synthesis, Pharmacological Evaluation, and Computational Studies of Cyclic Opioid Peptidomimetics Containing β(3)-Lysine. *Molecules* **2021**, *27*, 151. [CrossRef]

11. Yucel, N.T.; Osmaniye, D.; Kandemir, U.; Evren, A.E.; Can, O.D.; Demir Ozkay, U. Synthesis and Antinociceptive Effect of Some Thiazole-Piperazine Derivatives: Involvement of Opioidergic System in the Activity. *Molecules* **2021**, *26*, 3350. [CrossRef] [PubMed]

12. Fritzwanker, S.; Schulz, S.; Kliewer, A. SR-17018 Stimulates Atypical μ-Opioid Receptor Phosphorylation and Dephosphorylation. *Molecules* **2021**, *26*, 4509. [CrossRef] [PubMed]

13. Schmid, C.L.; Kennedy, N.M.; Ross, N.C.; Lovell, K.M.; Yue, Z.; Morgenweck, J.; Cameron, M.D.; Bannister, T.D.; Bohn, L.M. Bias Factor and Therapeutic Window Correlate to Predict Safer Opioid Analgesics. *Cell* **2017**, *171*, 1165–1175.e13. [CrossRef] [PubMed]

14. Gillis, A.; Gondin, A.B.; Kliewer, A.; Sanchez, J.; Lim, H.D.; Alamein, C.; Manandhar, P.; Santiago, M.; Fritzwanker, S.; Schmiedel, F.; et al. Low Intrinsic Efficacy for G Protein Activation can Explain the Improved Side Effect Profiles of New Opioid Agonists. *Sci. Signal.* **2020**, *13*, eaaz3140. [CrossRef]

15. Stahl, E.L.; Bohn, L.M. Low Intrinsic Efficacy Alone Cannot Explain the Improved Side Effect Profiles of New Opioid Agonists. *Biochemistry* **2021**. [CrossRef]

16. Paul, A.K.; Gueven, N.; Dietis, N. Profiling the Effects of Repetitive Morphine Administration on Motor Behavior in Rats. *Molecules* **2021**, *26*, 4355. [CrossRef]

17. Tseng, P.Y.; Hoon, M.A. Molecular Genetics of Kappa Opioids in Pain and Itch Sensations. *Handb. Exp. Pharmacol.* **2022**, *271*, 255–274.

18. Aldrich, J.V.; McLaughlin, J.P. Peptide Kappa Opioid Receptor Ligands and Their Potential for Drug Development. *Handb. Exp. Pharmacol.* **2022**, *271*, 197–220.

19. French, A.R.; van Rijn, R.M. An updated Assessment of the Translational Promise of G-protein-biased Kappa Opioid Receptor Agonists to Treat Pain and Other Indications without Debilitating Adverse effects. *Pharmacol. Res.* **2022**, *177*, 106091. [CrossRef]

20. Inui, S. Nalfurafine hydrochloride to treat pruritus: A review. *Clin. Cosmet. Investig. Dermatol.* **2015**, *8*, 249–255. [CrossRef]

21. Deeks, E.D. Difelikefalin: First Approval. *Drugs* **2021**, *81*, 1937–1944. [CrossRef]

22. Pereira, M.P.; Stander, S. Novel drugs for the treatment of chronic pruritus. *Expert Opin. Investig. Drugs* **2018**, *27*, 981–988. [CrossRef]

23. Inan, S.; Dun, N.J.; Cowan, A. Antipruritic Effect of Nalbuphine, a Kappa Opioid Receptor Agonist, in Mice: A Pan Antipruritic. *Molecules* **2021**, *26*, 5517. [CrossRef]

24. Nosova, O.; Bazov, I.; Karpyak, V.; Hallberg, M.; Bakalkin, G. Epigenetic and Transcriptional Control of the Opioid Prodynorphine Gene: In-Depth Analysis in the Human Brain. *Molecules* **2021**, *26*, 3458. [CrossRef]

25. Zhao, B.; Li, W.; Sun, L.; Fu, W. The Use of Computational Approaches in the Discovery and Mechanism Study of Opioid Analgesics. *Front. Chem.* **2020**, *8*, 335. [CrossRef]

26. Puls, K.; Schmidhammer, H.; Wolber, G.; Spetea, M. Mechanistic Characterization of the Pharmacological Profile of HS-731, a Peripherally Acting Opioid Analgesic, at the Mu-, delta-, kappa-Opioid and Nociceptin Receptors. *Molecules* **2022**, *27*, 919. [CrossRef]

27. Spetea, M.; Rief, S.B.; Haddou, T.B.; Fink, M.; Kristeva, E.; Mittendorfer, H.; Haas, S.; Hummer, N.; Follia, V.; Guerrieri, E.; et al. Synthesis, Biological, and Structural Explorations of New Zwitterionic Derivatives of 14-*O*-Methyloxymorphone, as Potent mu/delta Opioid Agonists and Peripherally Selective Antinociceptives. *J. Med. Chem.* **2019**, *62*, 641–653. [CrossRef]

28. Toll, L.; Bruchas, M.R.; Calo, G.; Cox, B.M.; Zaveri, N.T. Nociceptin/Orphanin FQ Receptor Structure, Signaling, Ligands, Functions, and Interactions with Opioid Systems. *Pharmacol. Rev.* **2016**, *68*, 419–457. [CrossRef]

29. El Daibani, A.; Che, T. Spotlight on Nociceptin/Orphanin FQ Receptor in the Treatment of Pain. *Molecules* **2022**, *27*, 595. [CrossRef]

30. Kiraly, K.; Karadi, D.A.; Zador, F.; Mohammadzadeh, A.; Galambos, A.R.; Balogh, M.; Riba, P.; Tabi, T.; Zadori, Z.S.; Szoko, E.; et al. Shedding Light on the Pharmacological Interactions between mu-Opioid Analgesics and Angiotensin Receptor Modulators: A New Option for Treating Chronic Pain. *Molecules* **2021**, *26*, 6168. [CrossRef]

31. Radoi, V.; Jakobsson, G.; Palada, V.; Nikosjkov, A.; Druid, H.; Terenius, L.; Kosek, E.; Vukojevic, V. Non-Peptide Opioids Differ in Effects on Mu-Opioid (MOP) and Serotonin 1A (5-HT1A) Receptors Heterodimerization and Cellular Effectors (Ca(2+), ERK1/2 and p38) Activation. *Molecules* **2022**, *27*, 2350. [CrossRef]

32. Binienda, A.; Makaro, A.; Talar, M.; Krajewska, J.B.; Tarasiuk, A.; Bartoszek, A.; Fabisiak, A.; Mosinska, P.; Niewinna, K.; Dziedziczak, K.; et al. Characterization of the Synergistic Effect between Ligands of Opioid and Free Fatty Acid Receptors in the Mouse Model of Colitis. *Molecules* **2021**, *26*, 6827. [CrossRef]

33. Taskiran, A.S.; Avci, O. Effect of captopril, an Angiotensin-converting Enzyme Inhibitor, on Morphine Analgesia and Tolerance in Rats, and Elucidating the Inflammation and Endoplasmic Reticulum Stress Pathway in this Effect. *Neurosci. Lett.* **2021**, *741*, 135504. [CrossRef]

34. Yamada, Y.; Ohinata, K.; Lipkowski, A.W.; Yoshikawa, M. Angiotensin AT(2) Receptor Agonists act as Anti-opioids via EP(3) Receptor in Mice. *Peptides* **2009**, *30*, 735–739. [CrossRef]

MDPI

Article

In Vitro Analyses of Spinach-Derived Opioid Peptides, Rubiscolins: Receptor Selectivity and Intracellular Activities through G Protein- and β-Arrestin-Mediated Pathways

Yusuke Karasawa [1,2,3], Kanako Miyano [4], Hideaki Fujii [5], Takaaki Mizuguchi [5], Yui Kuroda [1,2,6], Miki Nonaka [2], Akane Komatsu [1,2,6], Kaori Ohshima [2], Masahiro Yamaguchi [1,2,7], Keisuke Yamaguchi [1,6], Masako Iseki [1,6], Yasuhito Uezono [1,2,*] and Masakazu Hayashida [1,6]

1 Department of Pain Medicine, Juntendo University Graduate School of Medicine, 2-1-1, Hongo, Bunkyo-ku, Tokyo 113-8421, Japan; yusuke.karasawa@viatris.com (Y.K.); y-kuroda@juntendo.ac.jp (Y.K.); a-komats@juntendo.ac.jp (A.K.); masahiro.yamaguchi@pfizer.com (M.Y.); keisuke@juntendo.ac.jp (K.Y.); miseki@juntendo.ac.jp (M.I.); hayashidatoday@yahoo.co.jp (M.H.)
2 Department of Pain Control Research, The Jikei University School of Medicine, 3-25-8, Nishi-Shimbashi, Minato-ku, Tokyo 105-8461, Japan; minonaka@jikei.ac.jp (M.N.); 3b14025@alumni.tus.ac.jp (K.O.)
3 Medical Affairs, Viatris Pharmaceuticals Japan Inc., 5-11-2, Toranomon, Minato-ku, Tokyo 105-0001, Japan
4 Division of Cancer Pathophysiology, National Cancer Center Research Institute, 5-1-1, Tsukiji, Chuo-ku, Tokyo 104-0045, Japan; kmiyano@ncc.go.jp
5 Laboratory of Medicinal Chemistry and Medicinal Research Laboratories, School of Pharmacy, Kitasato University, 5-9-1, Shirokane, Minato-ku, Tokyo 108-8641, Japan; fujiih@pharm.kitasato-u.ac.jp (H.F.); mizuguchit@pharm.kitasato-u.ac.jp (T.M.)
6 Department of Anesthesiology and Pain Medicine, Faculty of Medicine, Juntendo University, 2-1-1, Hongo, Bunkyo-ku, Tokyo 113-8421, Japan
7 Medical Affairs, Pfizer Japan Inc., 3-22-7, Yoyogi, Shibuya-ku, Tokyo 151-0053, Japan
* Correspondence: yuezono@jikei.ac.jp

Abstract: Activated opioid receptors transmit internal signals through two major pathways: the G-protein-mediated pathway, which exerts analgesia, and the β-arrestin-mediated pathway, which leads to unfavorable side effects. Hence, G-protein-biased opioid agonists are preferable as opioid analgesics. Rubiscolins, the spinach-derived naturally occurring opioid peptides, are selective δ opioid receptor agonists, and their p.o. administration exhibits antinociceptive effects. Although the potency and effect of rubiscolins as G-protein-biased molecules are partially confirmed, their in vitro profiles remain unclear. We, therefore, evaluated the properties of rubiscolins, in detail, through several analyses, including the CellKey™ assay, cADDis® cAMP assay, and PathHunter® β-arrestin recruitment assay, using cells stably expressing μ, δ, κ, or μ/δ heteromer opioid receptors. In the CellKey™ assay, rubiscolins showed selective agonistic effects for δ opioid receptor and little agonistic or antagonistic effects for μ and κ opioid receptors. Furthermore, rubiscolins were found to be G-protein-biased δ opioid receptor agonists based on the results obtained in cADDis® cAMP and PathHunter® β-arrestin recruitment assays. Finally, we found, for the first time, that they are also partially agonistic for the μ/δ dimers. In conclusion, rubiscolins could serve as attractive seeds, as δ opioid receptor-specific agonists, for the development of novel opioid analgesics with reduced side effects.

Keywords: analgesic; δ opioid receptor; G-protein-biased agonist; opioid peptide; rubiscolins

1. Introduction

Opioid analgesics are widely used as key medications for relief from pain, including perioperative pain, cancer pain, and nonmalignant chronic pain. However, their use is sometimes hampered in clinical practice owing to unfavorable side effects, such as tolerance, constipation, and respiratory depression [1,2]. Thus, the discovery of safer opioid analgesics is an urgent requirement. Opioid receptors (ORs), which belong to

the G-protein-coupled receptor (GPCR) family [3], are classified into three subtypes—μ (MOR), δ (DOR), and κ (KOR)—and opioid analgesics mainly bind to MOR to exert their effects [4]. Internal signals from ORs are transmitted through two major pathways after the ligand conjugates with Gi/o proteins, followed by internalization of membrane receptors; the two pathways are the G-protein-mediated pathway that is required for analgesia, which is induced by decreasing the intracellular cAMP levels, and the β-arrestin-mediated pathway, which is associated with side effects [5,6]. Therefore, a biased analgesic with a pharmacological profile of favoring the activation of the G protein-mediated pathway over that of the β-arrestin-mediated pathway is desirable because it is considered to be effective and has fewer adverse events [7,8]. From this perspective, some molecules have been studied and indicated as G-protein-biased agonists in the past decades [9,10]. Among them, TRV130 (oliceridine) has been evaluated by intravenous administration in clinical studies and was approved as the first G-protein-biased agonist that can be used in clinical practice [11].

Besides MOR-selective agonists, there are several compounds selective for DOR or KOR that have been investigated in the preclinical studies [12,13]. They are expected to become alternatives for MOR agonists, which can cause severe side effects [14]. Compared with MOR agonists, DOR agonists show weaker effects in modulating acute nociception [12] but obvious effects in treating chronic pain under experimental conditions [15–17]. DOR can also be a therapeutic target for treating emotional disorders, such as depression [13,18]. However, none of the DOR agonists have been developed as an analgesic. Among the DOR agonistic compounds, rubiscolins are naturally occurring opioid peptides isolated from spinach leaves, produced by a pepsin digestion of d-ribulose-1,5-bisphosphate carboxylase/oxygenase (RuBisCO), the most abundant protein on earth [19,20]. Two types of rubiscolin—rubiscolin-5 and rubiscolin-6—exist, which are composed of penta- or hexa-amino acid residues (Tyr-Pro-Leu-Asp-Leu: YPLDL and Tyr-Pro-Leu-Asp-Leu-Phe: YPLDLF), respectively (Figure 1). Interestingly, these peptides showed antinociceptive effects upon p.o. administration in mice [21], which never occurs for endogenous opioid peptides. Moreover, rubiscolins are promising in terms of their unique effects other than analgesia, such as memory consolidation [22], anxiolytic effect [23], stimulation of food intake [24], enhancement of glucose uptake in skeletal muscle [25], and antidepressant-like effect [26]. Although the potency and actions of rubiscolins as G-protein-biased molecules were partially confirmed in a previous study using DOR [27], their in vitro profiles have not been sufficiently revealed.

Rubiscolin-5   Rubiscolin-6
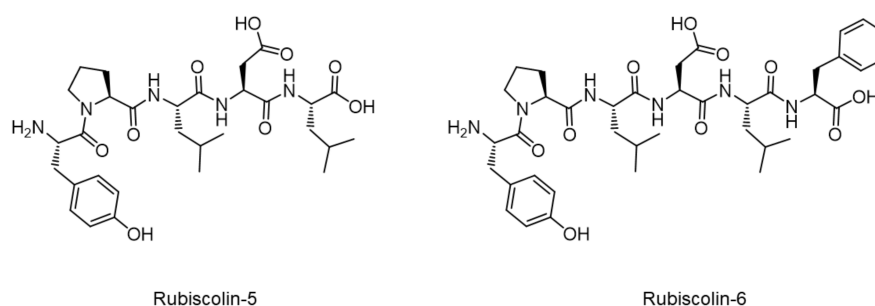
Figure 1. Molecular structures of rubiscolins.

The heterodimerization of ORs is also a noteworthy aspect [28,29]. It was recently revealed that ORs form heterodimers, which play an important role in pain modulation, and the selective ligand for the μ/δ opioid receptor (MOR/DOR) heteromer induced antinociception similar to that induced by morphine, but with less tolerance [30]. MOR/DOR heteromers have been reported to increase in cultured DRG neurons under pathophysiological conditions, such as chronic pain or subsequent exposure to morphine [31], and heterodimerization appears to be related to morphine-mediated antinociception and development of tolerance [32]. Therefore, MOR/DOR heteromers can also be targets for

developing safer and more effective opioid analgesics [33,34]. We believe that it is preferable for opioid compounds to activate MOR/DOR heteromers, in addition to having a G-protein-biased property.

In the present study, we investigated the in vitro properties of rubiscolins in detail, including the agonistic or antagonistic effects for ORs and intracellular activities through the G-protein- and β-arrestin-mediated pathways, using MOR, DOR, KOR, and MOR/DOR heteromer.

2. Results

2.1. Effects of Rubiscolins on the Functions of ORs Evaluated Using the CellKey^{TM} System

The effects of rubiscolins on the three types of ORs (MOR, DOR, and KOR) were evaluated using the CellKey^{TM} system (MDS Sciex, Foster City, CA, USA) in HEK293 cells stably expressing Halo-tag$^{®}$-MOR, T7-tag$^{®}$-DOR, or Halotag$^{®}$-KOR. Changes in cellular impedance were detected as activities of OR using this system. The changes in impedance induced by rubiscolins in positive controls of MOR (DAMGO), DOR (SNC-80), and KOR (U-50488H) were compared to confirm their agonistic effects on each OR. Rubiscolins showed dose-dependent effects only on DOR, whereas little effect was observed on MOR and KOR (Figure 2).
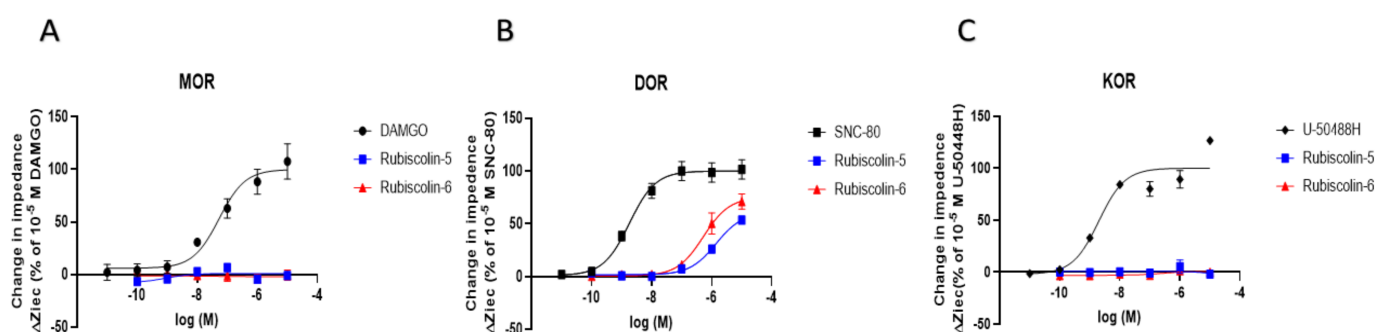
Figure 2. Effect of rubiscolins on MOR, DOR, and KOR, observed using the CellKey^{TM} system. The cells expressing MOR (**A**), DOR (**B**), and KOR (**C**) were treated with each compound (10^{-11}–10^{-5} M), and changes in impedance (ΔZiec) were measured using the CellKey^{TM} system. Concentration–response curves were prepared by calculating ΔZiec relative to the data obtained for each positive control: 10^{-5} M DAMGO for MOR (**A**), 10^{-5} M SNC-80 for DOR (**B**), and 10^{-5} M U-50488H for KOR (**C**). All data points are presented as means ± S.E.M. for three independent experiments (*n* = 3–5).

Moreover, we examined the antagonistic effects induced by a combination of rubiscolins with the positive control of MOR (DAMGO) or KOR (U-50488H), by comparing with the effect of a combination of each positive control with 10^{-5} concentration of a negative control for MOR (naloxone) or KOR (norbinaltorphimine: norBNI), respectively. Unlike for the combination with 10^{-5} concentration of negative control that completely suppressed the agonistic effects of the positive control for both MOR and KOR, rubiscolins had little antagonistic effects on MOR and KOR (Figure 3). These results suggest that rubiscolins act as selective DOR agonists without affecting the other subtypes (MOR and KOR) of ORs.
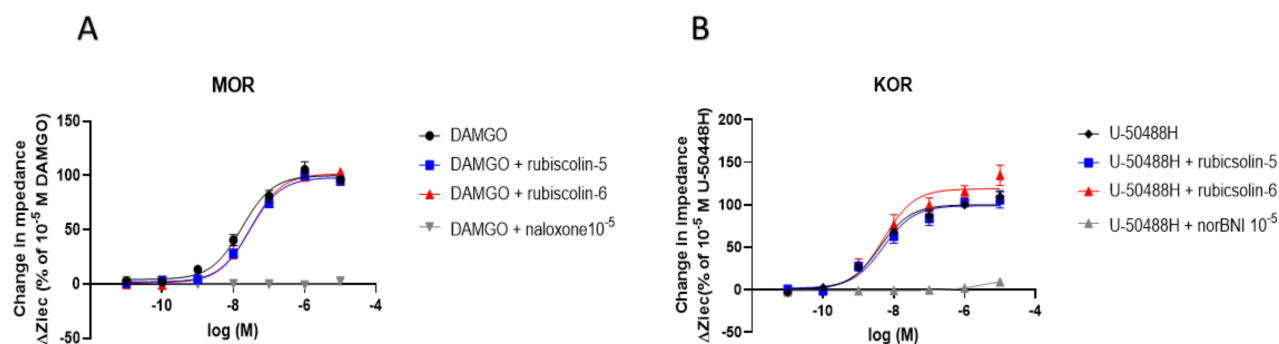
Figure 3. Evaluation of antagonistic effects induced by rubiscolins combined with positive control for MOR or KOR, observed using the CellKey^{TM} system. The cells expressing MOR (**A**) and KOR (**B**) were treated with each positive control alone or in combination with rubiscolin-5, rubiscolin-6, or 10^{-5} concentration of each negative control (10^{-11}–10^{-5} M), and changes in impedance (ΔZiec) were measured using the CellKey^{TM} system. Concentration–response curves were prepared by calculating ΔZiec relative to the data obtained for each positive control: 10^{-5} M DAMGO for MOR (**A**) and 10^{-5} M U-50488H for KOR (**B**). All data points are presented as means $\pm$ S.E.M. for three independent experiments (*n* = 3–4).

2.2. Effects of Rubiscolins on the Intracellular cAMP Levels Evaluated Using the cADDis® cAMP Assay

The activities of compounds through the G-protein-mediated pathway were evaluated by measuring the intracellular cAMP levels for each OR using HEK293 cells stably expressing Halotag®-MOR, T7-tag®-DOR, or Halotag®-KOR (Figure 4). After obtaining results for rubiscolins, SNC-80 (a positive control for DOR), and KNT-127 (an existing selective DOR agonist used as a competitor) [35], we compared the effects of rubiscolins with those of other compounds, including each of the positive controls for the three types of ORs. The E_{max} and EC_{50} values (pEC_{50} defined as the negative logarithm of the EC_{50}) for each OR were calculated (Table 1). As was observed for SNC-80 or KNT-127, rubiscolin-6 demonstrated a robust effect on DOR at 10^{-5} concentration. On the contrary, they had little effect on MOR and KOR; in contrast, KNT-127 showed full agonistic effects on both MOR and KOR. These results indicate that rubiscolins selectively activate the G-protein-mediated pathway of DOR to exert their pharmacological effects.
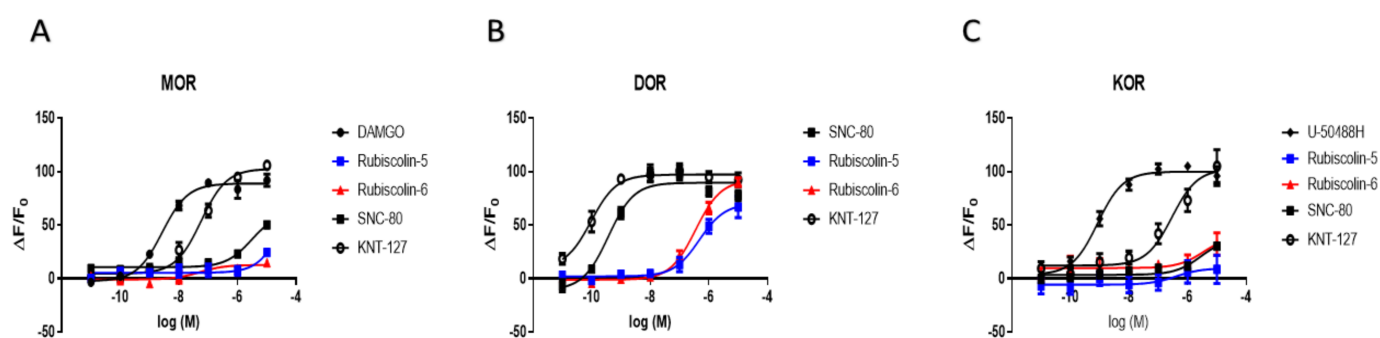
Figure 4. Changes in intracellular cAMP levels induced by rubiscolin-5, rubiscolin-6, and opioid compounds. Cells expressing MOR (**A**), DOR (**B**), or KOR (**C**) were treated with the listed compounds (10^{-11}–10^{-5} M), and intracellular cAMP levels were measured with the cADDis® cAMP assay. Concentration–response curves were prepared by calculating cAMP levels relative to the data obtained with 10^{-5} M DAMGO for MOR (**A**), 10^{-5} M SNC-80 for DOR (**B**), and 10^{-5} M U-50488H for KOR (**C**). Data are presented as means $\pm$ S.E.M. for three independent experiments (*n* = 3–5).

Table 1. E_{max} and pEC_{50} values for rubiscolins and opioid compounds obtained in the cAMP assay for MOR, DOR, and KOR.

		MOR	**DOR**	**KOR**
E_{max} (%)	DAMGO	100.0 ± 3.0	90.9 ± 8.9	-
	SNC-80	69.8 ± 6.2 *	100.0 ± 3.6	37.7 ± 6.9 [+]
	U-50488H	-	-	100.0 ± 3.0
	KNT-127	115.6 ± 4.3	108.4 ± 3.3	102.5 ± 9.5
	Rubiscolin-5	27.5 ± 5.5 *	78.4 ± 6.7 [#]	9.6 ± 9.0 [+]
	Rubiscolin-6	14.3 ± 3.2 *	103.0 ± 4.1	39.8 ± 20.5 [+]
pEC_{50} (M)	DAMGO	8.5 ± 0.1	6.2 ± 0.2 [#]	-
	SNC-80	5.5 ± 0.1 *	9.4 ± 0.1	5.6 ± 0.3 [+]
	U-50488H	-	-	9.1 ± 0.1
	KNT-127	7.2 ± 0.1 *	10.0 ± 0.2	6.5 ± 0.2
	Rubiscolin-5	n.d.	6.3 ± 0.2 [#]	n.d.
	Rubiscolin-6	n.d.	6.5 ± 0.1 [#]	n.d.

E_{max} (means $\pm$ S.E.M.) and pEC_{50} (-LogEC_{50}, means $\pm$ S.E.M.) were calculated according to the results shown in Figure 4. * $p < 0.05$ versus DAMGO, [#] $p < 0.05$ versus SNC-80, [+] $p < 0.05$ versus U-50488H. n.d.; not detected.

2.3. Effects of Rubiscolins on β-Arrestin Recruitment Measured Using the PathHunter® Assay

To determine the activities of rubiscolins through the β-arrestin-mediated pathway, we performed the PathHunter® β-arrestin recruitment assay using CHO-K1 cells stably expressing MOR and DOR (DiscoverX, Fremont, CA, USA), and U2OS cells stably expressing KOR (DiscoverX). We also evaluated the effects of SNC-80 and KNT-127. Compared with SNC-80, rubiscolins displayed little effect on DOR, as shown in Figure 5, whereas KNT-127 moderately recruited β-arrestin in DOR. Given these results, among the DOR-selective compounds used in the experiment, rubiscolin-5 and rubiscolin-6 were considered the most irrelevant with regard to the activity through the β-arrestin-mediated pathway. In contrast, all the DOR-selective compounds showed little effect on MOR and KOR, compared with each positive control.
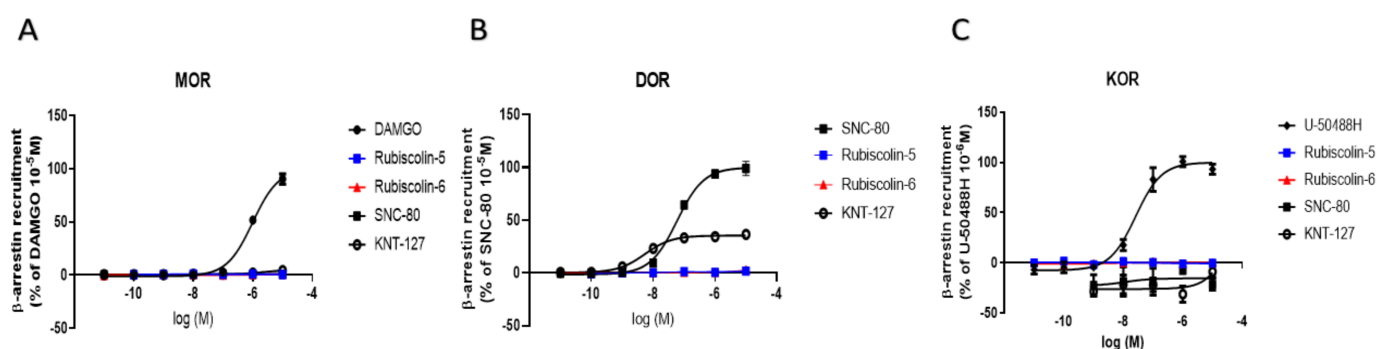
Figure 5. Levels of β-arrestin recruitment through OR induced by rubiscolin-5, rubiscolin-6, and opioid compounds. PathHunter® β-arrestin assay was performed in cells expressing MOR (**A**), DOR (**B**), and KOR (**C**) by treating with each compound (10^{-11}–10^{-5} M). Concentration–response curves were prepared by calculating intracellular β-arrestin levels relative to the data obtained for each positive control: 10^{-5} M DAMGO for MOR (**A**), 10^{-5} M SNC-80 for DOR (**B**), and 10^{-6} M of U-50488H for KOR (**C**). All data points are presented as means $\pm$ S.E.M. for three independent experiments ($n = 3$–6).

2.4. Effects of Rubiscolins on the MOR/DOR Heteromer

Finally, we examined the effects of rubiscolins on the MOR/DOR heteromer through the G-protein-mediated pathway using the cADDis® cAMP assay. As shown in Figure 6 and Table 2, rubiscolins acted as partial agonists, similarly to SNC-80, compared with ML335 [30], a specific agonist for MOR/DOR.
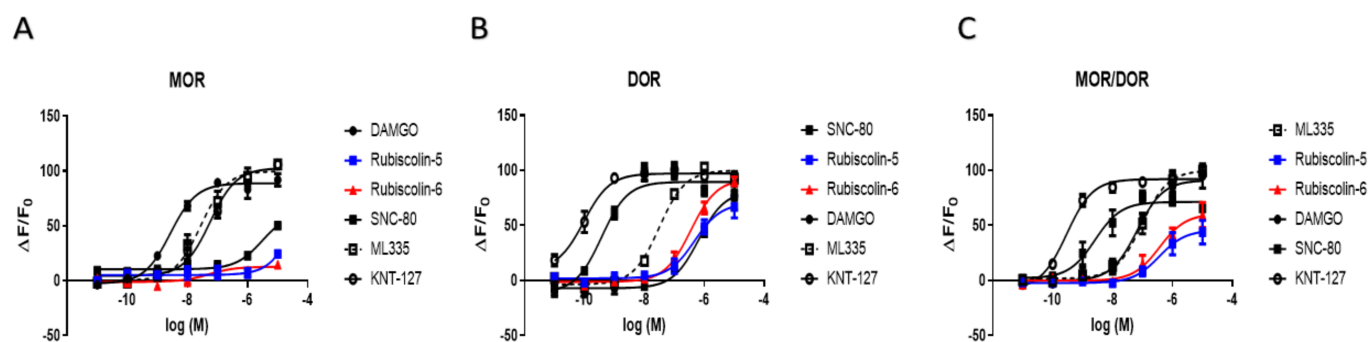
Figure 6. Changes in intracellular cAMP levels induced by rubiscolin-5, rubiscolin-6, and opioid compounds. Cells expressing MOR (**A**), DOR (**B**), or MOR/DOR (**C**) were treated with the listed compounds (10^{-11}–10^{-5} M), and the intracellular cAMP levels were measured with the cADDis® cAMP assay. Concentration–response curves were prepared by calculating cAMP levels relative to the data obtained with 10^{-5} M DAMGO for MOR (**A**), 10^{-5} M SNC-80 for DOR (**B**), and 10^{-5} M ML335 for MOR/DOR (**C**). Data are presented as means ± S.E.M. for three independent experiments (*n* = 6–8).

**Table 2.** E_{max} and pEC_{50} values for rubiscolins and opioid compounds obtained in the cAMP assay for MOR, DOR, and MOR/DOR.

		MOR	**DOR**	**MOR/DOR**
E_{max} (%)	DAMGO	100.0 ± 3.0	90.9 ± 8.9	91.1 ± 5.4
	SNC-80	69.8 ± 6.2 *	100.0 ± 3.6	71.4 ± 3.7 [+]
	ML335	112.5 ± 5.3	111.6 ± 3.6	100.0 ± 4.2
	KNT-127	115.6 ± 4.3	108.4 ± 3.3	92.1 ± 2.4
	Rubiscolin-5	27.5 ± 5.5 *	78.4 ± 6.7 [#]	45.8 ± 6.3 [+]
	Rubiscolin-6	14.3 ± 3.2 *	103.0 ± 4.1	60.6 ± 6.3 [+]
pEC_{50} (M)	DAMGO	8.5 ± 0.1	6.2 ± 0.2 [#]	7.2 ± 0.2
	SNC-80	5.5 ± 0.1 *	9.4 ± 0.1	8.6 ± 0.2 [+]
	ML335	7.6 ± 0.1 *	7.5 ± 0.1 [#]	7.0 ± 0.1
	KNT-127	7.2 ± 0.1 *	10.0 ± 0.2	9.5 ± 0.1 [+]
	Rubiscolin-5	n.d.	6.3 ± 0.2 [#]	6.4 ± 0.3
	Rubiscolin-6	n.d.	6.5 ± 0.1 [#]	6.4 ± 0.2

E_{max} (means ± S.E.M.) and pEC_{50} (-$LogEC_{50}$, means ± S.E.M.) were calculated according to the results shown in Figure 6. * $p < 0.05$ versus DAMGO, [#] $p < 0.05$ versus SNC-80, [+] $p < 0.05$ versus ML335. n.d.; not detected.

3. Discussion

In the present study, both rubiscolin-5 and -6 were indicated as G-protein-biased DOR full agonists without affecting MOR and KOR. The limited antagonistic effects of rubiscolins on MOR and KOR (Figure 3) confirmed using the three types of ORs, for the first time in this study, indicate that they rarely interfere with the cellular signaling mediated by endogenous or exogenous opioid ligands. The endogenous opioid system plays a critical role in modulating stress [36,37], anxiety [38,39], and the immune system [40]; hence, other than its role in analgesia, it is preferable that opioid agonists do not exert antagonistic effects on untargeted ORs, as these can lead to unexpected side effects that occur by attenuating the activities of endogenous ligands, such as enkephalins, β-endorphin, or dynorphin A. In addition, rubiscolins can potentially be administered in combination with exogenous ligands, such as MOR and KOR agonists and antagonists, without modulating their expected effects, which means that they are unique and attractive seeds that exhibit DOR selectivity, considering that the existing opioids can affect untargeted ORs to varying degrees [4]. As for the combination therapy of analgesics including opioids, opioid-sparing effects of non-opioid analgesics combined with opioids can reduce opioid consumption and its related side effects, especially in the perioperative pain management in terms of avoiding the toxicity and chronic use of opioids [41–43]. Rubiscolins can be novel candidates for use in combination with opioids. Therefore, further research is needed to

investigate the efficacy and safety of DOR agonists, including rubiscolins, in combination with MOR agonists.

In view of the results of our cAMP assay, rubiscolins can be considered DOR-biased agonists, consistent with previous reports. However, compared with the findings in a previous study on the bias factor of rubiscolins, which found that rubiscolin-5 was more G-protein-biased than rubiscolin-6 [27], our results indicate that rubiscolin-6 is relatively stronger than rubiscolin-5 in activating the G-protein-mediated intracellular pathway, and the β-arrestin recruitment levels induced by rubiscolin-5 or rubiscolin-6 are equivalently negligible (Table 1 and Figure 5). Indeed, there is a structural difference between the two peptides, as rubiscolin-6 has Phe, an additional aromatic residue, at the sixth position. Although its function is not clear, rubiscloin-6 has been shown to have a higher receptor affinity and is about twice as potent in analgesia as rubiscolin-5 [21], as was observed in our study. Rubiscolin-6 has also been reported to have broad beneficial effects related to the central nervous system, other than analgesia [22–26]. As an example, for the development of DOR selective agonists, considering such effects, NC-2800 is under Phase 1 clinical study to determine the indication of major depressive disorder (https://jrct.niph.go.jp/en-latest-detail/jRCT2071210033 accessed on 30 September 2021). The development of DOR-selective agonists as alternative antidepressants is expected to offer a solution for the unmet need related to the patient's adherence to the current treatment of depression, since their efficacy is independent of representative side effects of selective serotonin reuptake inhibitors, such as digestive symptoms [13]. Their antidepressant-like or anxiolytic-like activities are also desirable in the context of treating pain, considering psychological factors, such as depression and anxiety, are intimately associated with pain behavior, especially in chronic pain conditions [44–46]. Therefore, based on our results, we believe that rubiscolin-6 has more potential to be developed as a G-protein-biased DOR agonist than rubiscolin-5, not only as an analgesic but also as a medicine for treating other indications that are significantly different for DOR and MOR agonists, despite their mild analgesic properties compared with that of MOR agonists.

In OR signaling pathways, β-arrestin-mediated pathway is involved in unfavorable side effects, such as tolerance through the intracellular pathway in MOR or dysphoria through that of KOR. Interestingly, β-arrestin recruitment by rubiscolins on any type of OR was low, although moderate changes were observed even with KNT-127 for DOR (E_{max} (%): 35.4 ± 1.3), an existing selective DOR agonist [35], when compared with SNC-80 (E_{max} (%): 100.0 ± 2.6) (Figure 5B). Given these results, rubiscolins can be considered the safest among selective DOR agonists, possibly with fewer side effects, such as convulsion that sometimes occurs upon administration of DOR agonists [18], or increase in alcohol intake correlated with β-arrestin recruitment induced by DOR agonists [47].

Here, we report the effects of rubiscolins on MOR/DOR heteromers for the first time. Rubiscolins showed partial agonistic effects on the MOR/DOR heteromer (Figure 6C and Table 2). Moreover, the finding that rubiscolins have unique profiles in exerting their effects, mainly through the activation of the G-protein-mediated pathway in DOR, and in part through the MOR/DOR heteromer, is novel. In contrast, ML335 was reproduced as a full agonist of MOR/DOR, consistent with the findings in a previous study [30]. However, ML335 also acted as a full agonist for both MOR and DOR, and also partially recruited β-arrestin through both MOR and DOR. This suggests that there is still an unmet need to develop biased agonists that have more specific selectivity for MOR/DOR heteromers. A limitation of the present study is that we do not have data for the induction of β-arrestin recruitment on the MOR/DOR heteromer by rubiscolins, because it is not commercially available to investigate using the PathHunter® β-arrestin assay. In addition, although little evidence has been obtained on how DOR-selective agonists affect the MOR/DOR heteromer, interestingly, recent research has suggested that simultaneous treatment with MOR agonists and DOR antagonists can modulate tolerance induced by MOR agonists [48,49]. Therefore, further research is required to decipher how rubiscolins act as G-protein-biased

molecules for MOR/DOR heteromers, how they can contribute to analgesia and other effects, and to elucidate the utility of G-protein-biased MOR/DOR agonists.

Rubiscolins have the advantage of oral availability, although their absorption is not well known. In general, oligopeptides are thought to be metabolized by digestive enzymes (peptidases) and are then taken up in the form of dipeptides or tripeptides by the digestive organs, such as the stomach and small intestine. Whereas other opioid peptides are easily degraded, rubiscolins may not be disassembled and captured, and then pass through the blood–brain barrier to exhibit their antinociception [20]. They have been hypothesized to be resistant to proteolytic enzymes because of the Pro residue in the second position of their molecular structure, although it is not a characteristic feature of rubiscolins because the Tyr-Pro sequence at the N-terminus is generally present in the YP-type opioid peptides and is thought to be essential for opioid activity [21]. Thus, for the development of novel G-protein-biased DOR analgesics, further research is needed to decipher the mechanism of their uptake and to know whether some kind of active transporter is involved.

From a clinical perspective, the opioid crisis is currently a global challenge [50]. In general, opioid analgesics targeting MOR are shuffled to provide a "switching therapy", so as to balance the benefits and risks of individual opioids [51]; sometimes, a rescue dose with immediate effect is added for breakthrough pain in cancer patients. However, the kinds of opioid analgesics are limited, and their dosages often tend to increase owing to the loss in efficacy, opioid-induced hyperalgesia, or tolerance. Therefore, analgesics with safer and more effective profiles with new mechanisms of action, such as rubiscolins, appear to be promising alternatives. Hopefully, they could be used for reducing the dosage of current opioids and for resolving the opioid crisis, as part of the opioid rotation strategy, if their efficacy is proven to be on par with that of the existing opioids.

4. Materials and Methods

4.1. Chemicals

The following reagents were used: D-Ala(2)-*N*-Me-Phe(4)-Gly-ol(5)-enkephalin (DAMGO), (+)-4-[(a*R*)-a-((2*S*,5*R*)-4-allyl-2,5-dimethyl-1-piperazinyl)-3-methoxybenzyl]-*N*,*N*-diethylbenzamide (SNC-80), trans-3,4-dichloro-*N*-methyl-*N*-(2-(1-pyrrolidinyl)-cyclohexyl)-benzeneacetamide (U-50488H), naloxone, norbinaltorphimine, forskolin, KNT-127, ML335 (Sigma-Aldrich, St. Louis, MO, USA); rubiscolin-5 (H-Tyr-Pro-Leu-Asp-Leu-OH) and rubiscolin-6 (H-Tyr-Pro-Leu-Asp-Leu-Phe-OH) were chemically synthesized by standard solid-phase peptide synthesis as described in Supplementary Materials. Forskolin was diluted with dimethyl sulfoxide (DMSO) and other chemicals were diluted with water.

4.2. Cell Line

Human embryonic kidney 293 (HEK293) cells were obtained from American Type Culture Collection (ATCC®, Manassas, VA, USA), and HEK293 cells stably expressing Halotag®-MOR, T7-tag®-DOR, Halotag®-KOR, or Halotag®-MOR/T7-tag®-DOR were generated by transfection of the constructed plasmids using Lipofectamine reagent (Life Technologies, Carlsbad, CA, USA).

4.3. Cell Culture

HEK293 cells (stably expressing Halotag®-MOR, T7-tag®-DOR, Halotag®-KOR, or Halotag®-MOR/T7-tag®-DOR) were cultured in Dulbecco's modified Eagle's medium (DMEM) supplemented with 10% fetal bovine serum, 1% penicillin/streptomycin, and 5 µg/mL puromycin (InvivoGen, San Diego, CA, USA) for Halotag®-MOR, 250 µg/mL hygromycin B solution (FUJIFILM Wako Pure Chemical Corporation, Osaka, Japan) for T7-tag®-DOR, or 700 µg/mL genistein (Glico, Palo Alto, CA, USA) and 100 µg/mL hygromycin for Halotag®-KOR and Halotag®-MOR/T7-tag®-DOR. The incubation was done in a humidified atmosphere with 5% CO_2 at 37 °C.

4.4. Functional Analysis of ORs Using the CellKey^{TM} System

The analysis was performed as described previously [52]. In brief, cells were seeded at a density of 5.0×10^4 in CellKey^{TM} poly-D-Lysine (Sigma Aldrich, Saint Louis, MO, USA)-coated 96-well microplates with an embedded electrode at the bottom of each well and incubated for 24 h. After washing with CellKey^{TM} buffer composed of Hanks' balanced salt solution (1.3 mM $CaCl_2 \cdot 2H_2O$, 0.81 mM $MgSO_4$, 5.4 mM KCl, 0.44 mM KH_2PO_4, 4.2 mM $NaHCO_3$, 136.9 mM NaCl, 0.34 mM Na_2HPO_4, and 5.6 mM d-glucose) containing 20 mM 4-(2-hydroxyethyl)-1-piperazineethanesulfonic acid (HEPES) and 0.1% bovine serum albumin (BSA), cells were incubated for 30 min at 28 °C, and then treated with vehicle or one of the reagents. The change in impedance of an induced extracellular current (dZiec) in each well was measured for 25 min, following a 5 min baseline measurement. The magnitude of change in the dZiec value was defined as ΔZiec, and the value for rubiscolins was calculated as a percentage using the highest value for each positive control.

4.5. Intracellular cAMP Assay with cADDis$^{®}$

The assay was performed as described previously [53]. In brief, cells were seeded at 7.0×10^4 cells/well on black-walled, clear flat-bottom 96-well plates with recombinant BacMam virus expressing the cADDis sensor and 0.6 μM sodium butyrate, and incubated for 24 h at 5% CO_2 at 37 °C. The medium was replaced with 100 μL Krebs solution or pretreatment reagents. The 96-well plates were incubated at 28 °C for 30 min in the dark. Cell fluorescence was measured from the bottom of the plate using excitation/emission wavelengths of 485 and 525 nm, respectively, on FlexStation 3 (Molecular Devices, LLC., San Jose, CA, USA). Cells were stimulated with 50 μM forskolin to increase the cAMP levels. After 20 min, when the signal plateaued, cells were stimulated with the indicated drugs, and changes in fluorescence from each well were measured every 26 s for 40 min. Increase in fluorescence intensity reflects the decrease in cAMP, through the activation of Gi-coupled receptor. The data were transformed to changes in fluorescence over the initial fluorescence ($\Delta F/F_0$).

4.6. β-Arrestin Recruitment Assay with Pathhunter$^{®}$

This was performed as described previously [54]. In brief, U2OS OPRM1, CHO-K1 OPRD1, or U2OS OPRK1 cells were seeded at a density of 1.0×10^4 cells/well in 96-well clear-bottom white plates and incubated for 48 h. The cells were stimulated for 90 min (in the case of MOR and DOR) or 180 min (in the case of KOR) in a dilution series for each receptor at 37 °C under 5% CO_2 and the PathHunter$^{®}$ working detection solution was added. The luminescence intensity was measured using FlexStation 3 (BioTek Instruments Inc., Winooski, VT, USA) for 1 h at room temperature. Data are expressed as the maximum signal intensity of each test compound as a percentage of the maximum signal intensity of the positive control.

4.7. Statistical Analysis and Approval for the Study

Data are presented as means ± SEM for at least three independent experiments. Data from cADDis cAMP assays were analyzed using one-way ANOVA followed by Tukey's multiple comparison tests. A value of $p < 0.05$ was considered statistically significant. All analyses and concentration–response curve fitting were performed using Prism 8 (GraphPad Software, San Diego, CA, USA). All experiments were approved and performed in accordance with the Guide for Genetic Modification Safety Committee, National Cancer Center, Japan.

5. Conclusions

In the present study, we showed that rubiscolins are G-protein-biased full agonists for DOR, as well as partial agonists for the MOR/DOR heteromers, with limited effects on endogenous ligands or opioid analgesics that activate MOR or KOR. Considering the evidence obtained, we believe that rubiscolins could serve as promising seeds for the

development of novel, safer opioids and selective DOR agonists that can be orally used for treating pain.

References

1. Benyamin, R.; Trescot, A.M.; Datta, S.; Buenaventura, R.; Adlaka, R.; Sehgal, N.; Glaser, S.E.; Vallejo, R. Opioid complications and side effects. *Pain Physician* **2008**, *11* (Suppl. 2), S105–S120. [CrossRef]
2. Khademi, H.; Kamangar, F.; Brennan, P.; Malekzadeh, R. Opioid Therapy and its Side Effects: A Review. *Arch. Iran. Med.* **2016**, *19*, 870–876.
3. Machelska, H.; Celik, M. Advances in Achieving Opioid Analgesia Without Side Effects. *Front. Pharmacol.* **2018**, *9*, 1388. [CrossRef] [PubMed]
4. Trescot, A.M.; Datta, S.; Lee, M.; Hansen, H. Opioid pharmacology. *Pain Physician* **2008**, *11* (Suppl. 2), S133–S153. [CrossRef] [PubMed]
5. Raehal, K.M.; Schmid, C.L.; Groer, C.E.; Bohn, L.M. Functional selectivity at the μ-opioid receptor: Implications for understanding opioid analgesia and tolerance. *Pharmacol. Rev.* **2011**, *63*, 1001–1019. [CrossRef] [PubMed]
6. Schmid, C.L.; Kennedy, N.M.; Ross, N.C.; Lovell, K.M.; Yue, Z.; Morgenweck, J.; Cameron, M.D.; Bannister, T.D.; Bohn, L.M. Bias Factor and Therapeutic Window Correlate to Predict Safer Opioid Analgesics. *Cell* **2017**, *171*, 1165–1175. [CrossRef]
7. Chen, X.T.; Pitis, P.; Liu, G.; Yuan, C.; Gotchev, D.; Cowan, C.L.; Rominger, D.H.; Koblish, M.; Dewire, S.M.; Crombie, A.L.; et al. Structure-activity relationships and discovery of a G protein biased μ opioid receptor ligand, [(3-methoxythiophen-2-yl)methyl]({2-[(9R)-9-(pyridin-2-yl)-6-oxaspiro-[4.5]decan-9-yl]ethyl})amine (TRV130), for the treatment of acute severe pain. *J. Med. Chem.* **2013**, *56*, 8019–8031. [CrossRef]
8. Faouzi, A.; Varga, B.R.; Majumdar, S. Biased Opioid Ligands. *Molecules* **2020**, *25*, 4257. [CrossRef]
9. Bermudez, M.; Nguyen, T.N.; Omieczynski, C.; Wolber, G. Strategies for the discovery of biased GPCR ligands. *Drug Discov. Today* **2019**, *24*, 1031–1037. [CrossRef]
10. Kudla, L.; Przewlocki, R. Influence of G protein-biased agonists of μ-opioid receptor on addiction-related behaviors. *Pharmacol. Rep.* **2021**, *73*, 1033–1051. [CrossRef]
11. Miyano, K.; Manabe, S.; Komatsu, A.; Fujii, Y.; Mizobuchi, Y.; Uezono, E.; Ohshima, K.; Nonaka, M.; Kuroda, Y.; Narita, M.; et al. The G Protein Signal-Biased Compound TRV130; Structures, Its Site of Action and Clinical Studies. *Curr. Top. Med. Chem.* **2020**, *20*, 2822–2829. [CrossRef] [PubMed]
12. Vanderah, T.W. Delta and kappa opioid receptors as suitable drug targets for pain. *Clin. J. Pain* **2010**, *26* (Suppl. 10), S10–S15. [CrossRef] [PubMed]
13. Nagase, H.; Saitoh, A. Research and development of κ opioid receptor agonists and δ opioid receptor agonists. *Pharmacol. Ther.* **2020**, *205*, 107427. [CrossRef]
14. Turnaturi, R.; Chiechio, S.; Salerno, L.; Rescifina, A.; Pittalà, V.; Cantarella, G.; Tomarchio, E.; Parenti, C.; Pasquinucci, L. Progress in the development of more effective and safer analgesics for pain management. *Eur. J. Med. Chem.* **2019**, *183*, 111701. [CrossRef]

15. Kabli, N.; Cahill, C.M. Anti-allodynic effects of peripheral delta opioid receptors in neuropathic pain. *Pain* **2007**, *127*, 84–93. [CrossRef]

16. Rowan, M.P.; Ruparel, N.B.; Patwardhan, A.M.; Berg, K.A.; Clarke, W.P.; Hargreaves, K.M. Peripheral delta opioid receptors require priming for functional competence in vivo. *Eur. J. Pharmacol.* **2009**, *602*, 283–287. [CrossRef] [PubMed]

17. Commons, K.G. Translocation of presynaptic delta opioid receptors in the ventrolateral periaqueductal gray after swim stress. *J. Comp. Neurol.* **2003**, *464*, 197–207. [CrossRef]

18. Pradhan, A.A.; Befort, K.; Nozaki, C.; Gavériaux-Ruff, C.; Kieffer, B.L. The delta opioid receptor: An evolving target for the treatment of brain disorders. *Trends Pharmacol. Sci.* **2011**, *32*, 581–590. [CrossRef]

19. Yoshikawa, M.; Takahashi, M.; Yang, S. Delta opioid peptides derived from plant proteins. *Curr. Pharm. Des.* **2003**, *9*, 1325–1330. [CrossRef]

20. Perlikowska, R.; Janecka, A. Rubiscolins-Highly Potent Peptides Derived from Plant Proteins. *Mini Rev. Med. Chem.* **2018**, *18*, 104–112. [CrossRef]

21. Yang, S.; Yunden, J.; Sonoda, S.; Doyama, N.; Lipkowski, A.W.; Kawamura, Y.; Yoshikawa, M. Rubiscolin, a delta selective opioid peptide derived from plant Rubisco. *FEBS Lett.* **2001**, *509*, 213–217. [CrossRef]

22. Yang, S.; Kawamura, Y.; Yoshikawa, M. Effect of rubiscolin, a delta opioid peptide derived from Rubisco, on memory consolidation. *Peptides* **2003**, *24*, 325–328. [CrossRef]

23. Hirata, H.; Sonoda, S.; Agui, S.; Yoshida, M.; Ohinata, K.; Yoshikawa, M. Rubiscolin-6, a delta opioid peptide derived from spinach Rubisco, has anxiolytic effect via activating sigma1 and dopamine D1 receptors. *Peptides* **2007**, *28*, 1998–2003. [CrossRef]

24. Kaneko, K.; Lazarus, M.; Miyamoto, C.; Oishi, Y.; Nagata, N.; Yang, S.; Yoshikawa, M.; Aritake, K.; Furuyashiki, T.; Narumiya, S.; et al. Orally administered rubiscolin-6, a delta opioid peptide derived from Rubisco, stimulates food intake via leptomeningeal lipocallin-type prostaglandin D synthase in mice. *Mol. Nutr. Food Res.* **2012**, *56*, 1315–1323. [CrossRef] [PubMed]

25. Kairupan, T.S.; Cheng, K.C.; Asakawa, A.; Amitani, H.; Yagi, T.; Ataka, K.; Rokot, N.T.; Kapantow, N.H.; Kato, I.; Inui, A. Rubiscolin-6 activates opioid receptors to enhance glucose uptake in skeletal muscle. *J. Food Drug Anal.* **2019**, *27*, 266–274. [CrossRef] [PubMed]

26. Mitsumoto, Y.; Sato, R.; Tagawa, N.; Kato, I. Rubiscolin-6, a delta-Opioid Peptide from Spinach RuBisCO, Exerts Antidepressant-Like Effect in Restraint-Stressed Mice. *J. Nutr. Sci. Vitaminol.* **2019**, *65*, 202–204. [CrossRef] [PubMed]

27. Cassell, R.J.; Mores, K.L.; Zerfas, B.L.; Mahmoud, A.H.; Lill, M.A.; Trader, D.J.; van Rijn, R.M. Rubiscolins are naturally occurring G protein-biased delta opioid receptor peptides. *Eur. Neuropsychopharmacol.* **2019**, *29*, 450–456. [CrossRef]

28. Pinello, C.; Guerrero, M.; Eberhart, C.; Volmar, C.H.; Saldanha, S.A.; Cayanan, C.; Urbano, M.; Brown, S.J.; Ferguson, J.; Gomes, I.; et al. Characterization of an agonist probe for opioid receptor mu 1 (OPRM1)-opioid receptor delta 1 (OPRD1) heterodimerization. In *Probe Reports from the NIH Molecular Libraries Program*; National Center for Biotechnology Information (US): Bethesda, MD, USA, 2010.

29. Costantino, C.M.; Gomes, I.; Stockton, S.D.; Lim, M.P.; Devi, L.A. Opioid receptor heteromers in analgesia. *Expert Rev. Mol. Med.* **2012**, *14*, e9. [CrossRef]

30. Gomes, I.; Fujita, W.; Gupta, A.; Saldanha, S.A.; Negri, A.; Pinello, C.E.; Eberhart, C.; Roberts, E.; Filizola, M.; Hodder, P.; et al. Identification of a μ-δ opioid receptor heteromer-biased agonist with antinociceptive activity. *Proc. Natl. Acad. Sci. USA* **2013**, *110*, 12072–12077. [CrossRef]

31. Gupta, A.; Mulder, J.; Gomes, I.; Rozenfeld, R.; Bushlin, I.; Ong, E.; Lim, M.; Maillet, E.; Junek, M.; Cahill, C.M.; et al. Increased abundance of opioid receptor heteromers after chronic morphine administration. *Sci. Signal.* **2010**, *3*, ra54. [CrossRef]

32. He, S.Q.; Zhang, Z.N.; Guan, J.S.; Liu, H.R.; Zhao, B.; Wang, H.B.; Li, Q.; Yang, H.; Luo, J.; Li, Z.Y.; et al. Facilitation of μ-opioid receptor activity by preventing δ-opioid receptor-mediated codegradation. *Neuron* **2011**, *69*, 120–131. [CrossRef] [PubMed]

33. Milan-Lobo, L.; Enquist, J.; van Rijn, R.M.; Whistler, J.L. Anti-analgesic effect of the mu/delta opioid receptor heteromer revealed by ligand-biased antagonism. *PLoS ONE* **2013**, *8*, e58362. [CrossRef] [PubMed]

34. Spetea, M.; Rief, S.B.; Haddou, T.B.; Fink, M.; Kristeva, E.; Mittendorfer, H.; Haas, S.; Hummer, N.; Follia, V.; Guerrieri, E.; et al. Synthesis, Biological, and Structural Explorations of New Zwitterionic Derivatives of 14-O-Methyloxymorphone, as Potent μ/δ Opioid Agonists and Peripherally Selective Antinociceptives. *J. Med. Chem.* **2019**, *62*, 641–653. [CrossRef] [PubMed]

35. Nagase, H.; Nemoto, T.; Matsubara, A.; Saito, M.; Yamamoto, N.; Osa, Y.; Hirayama, S.; Nakajima, M.; Nakao, K.; Mochizuki, H.; et al. Design and synthesis of KNT-127, a δ-opioid receptor agonist effective by systemic administration. *Bioorg. Med. Chem. Lett.* **2010**, *20*, 6302–6305. [CrossRef] [PubMed]

36. Drolet, G.; Dumont, E.C.; Gosselin, I.; Kinkead, R.; Laforest, S.; Trottier, J.F. Role of endogenous opioid system in the regulation of the stress response. *Prog. Neuropsychopharmacol. Biol. Psychiatry* **2001**, *25*, 729–741. [CrossRef]

37. Bali, A.; Randhawa, P.K.; Jaggi, A.S. Stress and opioids: Role of opioids in modulating stress-related behavior and effect of stress on morphine conditioned place preference. *Neurosci. Biobehav. Rev.* **2015**, *51*, 138–150. [CrossRef] [PubMed]

38. Hang, A.; Wang, Y.J.; He, L.; Liu, J.G. The role of the dynorphin/κ opioid receptor system in anxiety. *Acta Pharmacol. Sin.* **2015**, *36*, 783–790. [CrossRef]

39. Van't Veer, A.; Carlezon, W.A., Jr. Role of kappa-opioid receptors in stress and anxiety-related behavior. *Psychopharmacology* **2013**, *229*, 435–452. [CrossRef]

40. Pomorska, D.K.; Gach, K.; Janecka, A. Immunomodulatory effects of endogenous and synthetic peptides activating opioid receptors. *Mini Rev. Med. Chem.* **2014**, *14*, 1148–1155. [CrossRef]

41. Kumar, K.; Kirksey, M.A.; Duong, S.; Wu, C.L. A Review of Opioid-Sparing Modalities in Perioperative Pain Management: Methods to Decrease Opioid Use Postoperatively. *Anesth. Analg.* **2017**, *125*, 1749–1760. [CrossRef]

42. Martinez, L.; Ekman, E.; Nakhla, N. Perioperative Opioid-sparing Strategies: Utility of Conventional NSAIDs in Adults. *Clin. Ther.* **2019**, *41*, 2612–2628. [CrossRef]

43. Barnett, T.; Denke, L. Managing postoperative pain with opioid-sparing therapies. *Nursing* **2020**, *50*, 60–63. [CrossRef]

44. Sheng, J.; Liu, S.; Wang, Y.; Cui, R.; Zhang, X. The Link between Depression and Chronic Pain: Neural Mechanisms in the Brain. *Neural Plast.* **2017**, *2017*, 9724371. [CrossRef]

45. Zhuo, M. Neural Mechanisms Underlying Anxiety-Chronic Pain Interactions. *Trends Neurosci.* **2016**, *39*, 136–145. [CrossRef] [PubMed]

46. Velly, A.M.; Mohit, S. Epidemiology of pain and relation to psychiatric disorders. *Prog. Neuropsychopharmacol. Biol. Psychiatry* **2018**, *87 Pt B*, 159–167. [CrossRef]

47. Chiang, T.; Sansuk, K.; van Rijn, R.M. β-Arrestin 2 dependence of δ opioid receptor agonists is correlated with alcohol intake. *Br. J. Pharmacol.* **2016**, *173*, 332–343. [CrossRef]

48. Ananthan, S.; Saini, S.K.; Dersch, C.M.; Xu, H.; McGlinchey, N.; Giuvelis, D.; Bilsky, E.J.; Rothman, R.B. 14-Alkoxy- and 14-acyloxypyridomorphinans: μ agonist/δ antagonist opioid analgesics with diminished tolerance and dependence side effects. *J. Med. Chem.* **2012**, *55*, 8350–8363. [CrossRef] [PubMed]

49. Bender, A.M.; Clark, M.J.; Agius, M.P.; Traynor, J.R.; Mosberg, H.I. Synthesis and evaluation of 4-substituted piperidines and piperazines as balanced affinity μ opioid receptor (MOR) agonist/δ opioid receptor (DOR) antagonist ligands. *Bioorg. Med. Chem. Lett.* **2014**, *24*, 548–551. [CrossRef]

50. Skolnick, P. The Opioid Epidemic: Crisis and Solutions. *Annu. Rev. Pharmacol. Toxicol.* **2018**, *58*, 143–159. [CrossRef] [PubMed]

51. Mercadante, S.; Bruera, E. Opioid switching in cancer pain: From the beginning to nowadays. *Crit. Rev. Oncol. Hematol.* **2016**, *99*, 241–248. [CrossRef] [PubMed]

52. Miyano, K.; Sudo, Y.; Yokoyama, A.; Hisaoka-Nakashima, K.; Morioka, N.; Takebayashi, M.; Nakata, Y.; Higami, Y.; Uezono, Y. History of the G protein-coupled receptor (GPCR) assays from traditional to a state-of-the-art biosensor assay. *J. Pharmacol. Sci.* **2014**, *126*, 302–309. [CrossRef] [PubMed]

53. Kuroda, Y.; Nonaka, M.; Kamikubo, Y.; Ogawa, H.; Murayama, T.; Kurebayashi, N.; Sakairi, H.; Miyano, K.; Komatsu, A.; Dodo, T.; et al. Inhibition of endothelin A receptor by a novel, selective receptor antagonist enhances morphine-induced analgesia: Possible functional interaction of dimerized endothelin A and μ-opioid receptors. *Biomed. Pharmacother.* **2021**, *141*, 111800. [CrossRef] [PubMed]

54. Yin, H.; Chu, A.; Li, W.; Wang, B.; Shelton, F.; Otero, F.; Nguyen, D.G.; Caldwell, J.S.; Chen, Y.A. Lipid G protein-coupled receptor ligand identification using beta-arrestin PathHunter assay. *J. Biol. Chem.* **2009**, *284*, 12328–12338. [CrossRef] [PubMed]

Discovery of Novel Delta Opioid Receptor (DOR) Inverse Agonist and Irreversible (Non-Competitive) Antagonists

Parthasaradhireddy Tanguturi [1] iD**, Vibha Pathak** [2]**, Sixue Zhang** [2]**, Omar Moukha-Chafiq** [2]**, Corinne E. Augelli-Szafran** [2] **and John M. Streicher** [1,*] iD

[1]   Department of Pharmacology, College of Medicine, University of Arizona, Tucson, AZ 85724, USA; parthasaradhit@arizona.edu

[2]   Department of Chemistry, Division of Drug Discovery, Southern Research Institute, Birmingham, AL 35205, USA; vibhabpathak@gmail.com (V.P.); szhang@southernresearch.org (S.Z.); omoukha-chafiq@southernresearch.org (O.M.-C.); caugelli-szafran@southernresearch.org (C.E.A.-S.)

*   Correspondence: jstreicher@arizona.edu; Tel.: +1-520-626-7495

Abstract: The delta opioid receptor (DOR) is a crucial receptor system that regulates pain, mood, anxiety, and similar mental states. DOR agonists, such as SNC80, and DOR-neutral antagonists, such as naltrindole, were developed to investigate the DOR in vivo and as potential therapeutics for pain and depression. However, few inverse agonists and non-competitive/irreversible antagonists have been developed, and none are widely available. This leaves a gap in our pharmacological toolbox and limits our ability to investigate the biology of this receptor. Thus, we designed and synthesized the novel compounds SRI-9342 as an irreversible antagonist and SRI-45128 as an inverse agonist. These compounds were then evaluated in vitro for their binding affinity by radioligand binding, their functional activity by ^{35}S-GTPγS coupling, and their cAMP accumulation in cells expressing the human DOR. Both compounds demonstrated high binding affinity and selectivity at the DOR, and both displayed their hypothesized molecular pharmacology of irreversible antagonism (SRI-9342) or inverse agonism (SRI-45128). Together, these results demonstrate that we have successfully designed new inverse agonists and irreversible antagonists of the DOR based on a novel chemical scaffold. These new compounds will provide new tools to investigate the biology of the DOR or even new potential therapeutics.

Keywords: delta opioid receptor; inverse agonist; irreversible antagonist; non-competitive antagonist; molecular pharmacology

1. Introduction

G-protein coupled receptors (GPCRs) are a superfamily of integral plasma membrane proteins and are involved in a broad array of signaling pathways and subsequent physiological processes. GPCRs are important drug targets, and over 25% of all approved drugs currently on the market are known to evoke their pharmaceutical effects through GPCRs [1]. The delta opioid receptor (DOR) is one such GPCR that has been linked to the regulation of pain, mood, depression, and similarly important brain states [2]. Numerous classical full/partial agonists, such as SNC80 and DPDPE, and neutral antagonists, such as naltrindole, have been developed or described for the DOR. However, there are far fewer inverse agonists and irreversible/non-competitive antagonists for this target.

A non-competitive antagonist is an insurmountable antagonist that can act either in one of two ways: via binding to an allosteric site of the receptor [3] or by irreversibly binding to the active site of the receptor. Although the mechanism of antagonism is different for both, they are called "non-competitive" since the end result of each are functionally the same. Unlike competitive antagonists, which commonly affect the amount of agonist necessary to achieve a maximal response but will not affect the magnitude of that maximal response, non-competitive antagonists decrease the level of the maximum response which

can be accomplished by any amount of agonist. This unique property receives the name as "non-competitive" because the effects cannot be overcome no matter how much agonist is present. One example is the commonly used beta-funaltrexamine, which is selective for the mu opioid receptor [4]. Only a few such ligands have been reported for the DOR, and none are widely available. These include a naphthalene-dialdehyde modification of 6′-aminonaltrindole [5] and 5′-naltrindole-isothiocyanate [6].

By contrast, an inverse agonist does have intrinsic activity at the orthosteric site. However, unlike an agonist, an inverse agonist shifts the energy landscape to further disfavor the receptor active state and favor the inactive state. This suppresses baseline receptor activity to the extent that it is below that of the unliganded state [3]. The first such described ligand for the DOR was ICI-174864, a peptidic inverse agonist reported by Costa and Herz [7]. Later, additional DOR inverse agonists were reported, such as (+)−KF4 [8], naltrindole (NTI) derivatives [9], amide/sulfonamide substituted NTI [10], as well as other peptidic [11–13] and nonpeptidic [14–17] molecules.

Here, we report the discovery and characterization of a new DOR non-competitive antagonist (SRI-9342) and a new inverse agonist (SRI-45128). These ligands have strong selectivity for the DOR and potent functional activity in vitro. The discovery of these ligands further expands the limited pharmacological tools available to probe the DOR and could even provide potential future therapeutics.

2. Results

2.1. Rational Design of DOR Ligands

The DOR ligands SRI-9342 (irreversible antagonist) and SRI-45128 (inverse agonist) were designed based on our previously published computational docking studies of the SRI-9409 scaffold core [18], as well as DOR ligands reported in the study, including SYK-623 [19]. When this core binds to the orthosteric site of DOR, the right-hand side indole moiety would face the extracellular opening of the binding pocket and be adjacent to the functionally important K214 of DOR [20], which is also a potentially reactive residue. Thus, the idea of adding a warhead to the scaffold to further increase its binding affinity to DOR was explored, which resulted in SRI-9342. The α,β-unsaturated pyridin group of SRI-9342 is supposed to be in a proper position to form a covalent bond with the nitrogen on the side chain of K214 via Michael's addition, turning it into an irreversible DOR antagonist. On the other hand, the cyclopropyl group of the scaffold would face the bottom of the binding pocket and form hydrophobic contact with the W274 of DOR, which is an important residue responsible for the switch between agonism and antagonism [20,21]. Therefore, chemical modifications were also explored at this position, which resulted in SRI-45128 with DOR inverse agonism. Notably, SRI-45128 was distinct from parent scaffold SRI-9409 in the sense that the introduction of carbonyl next to the cyclopropyl group (inspired by SYK-623) would reduce the basicity of the neighboring nitrogen of SRI-45128, which was no longer able to form a salt-bridge with key residue D128. In addition, SRI-45128 is distinguishable from SYK-623 in the sense that the former possessed a pyridine-4-phenylchloride moiety while the latter possessed an indole moiety on the right-hand side.

2.2. Synthesis of Novel DOR Irreversible Antagonist and Inverse Agonists

SRI-9342 (irreversible antagonist, Scheme 1) was synthesized with a 44% yield via the reaction of naltrexone hydrochloride and *trans*-4-hydrazino-2-stilbazole dihydrochloride following the same procedures previously reported [22,23]. SRI-45128 (inverse agonist, Scheme 2) was synthesized in nine steps by using the procedures reported in [24], subject to a few modifications. In our alternative route, the protecting group on the phenolic hydroxyl group of naltrexone (**1**) was changed from methyl to benzyl to achieve an overall improvement in yields. The 6-ketone group of compounds (**2**) was protected as 1,3-dioxolane, which was followed by acetylation of the 14-OH under refluxing in Ac_2O. The cyclopropyl methyl group of the resulting acetate compound (**3**) was exchanged for a trichloroethoxycarbonyl group at 140 °C with an excess amount of trichloroethoxycarbonyl

chloride to afford carbamate (**4**). The carbamate and the acetate group in compound (**4**) were further hydrolyzed with aqueous KOH at 110 °C to afford compound (**5**). The reaction of compound (**5**) with cyclopropyl carbonyl chloride in the presence of Et$_3$N afforded compound (**6**) with an 89% yield. Removal of the 1,3-dioxolane group in amide (**6**) was done by using HCl and MeOH at reflux conditions to afford ketone (**7**). Finally, further deprotection of the benzyl group in (**7**), followed by annulation with 2-(4-chlorophenyl)-3-hydroxy-prop-2-enal in the presence of ammonium acetate, afforded SRI-45128 in two steps. We also synthesized SYK-623 for use as a control group (inverse agonist, Scheme 3). This was achieved in two steps, from intermediate (**7**), by using the procedure reported in [19] with the following modifications: Compound (**7**) was reacted with phenyl hydrazine in acetic acid under reflux conditions followed by deprotection of the benzyl group to afford SYK-623. All compounds were confirmed for identity and high purity, which is sufficient for pharmacological characterization (see Methods).

Scheme 1. Reagents and conditions: (a) *trans*-4-hydrazino-2-stilbazole dihydrochloride, AcOH, 5 h, 120 °C.
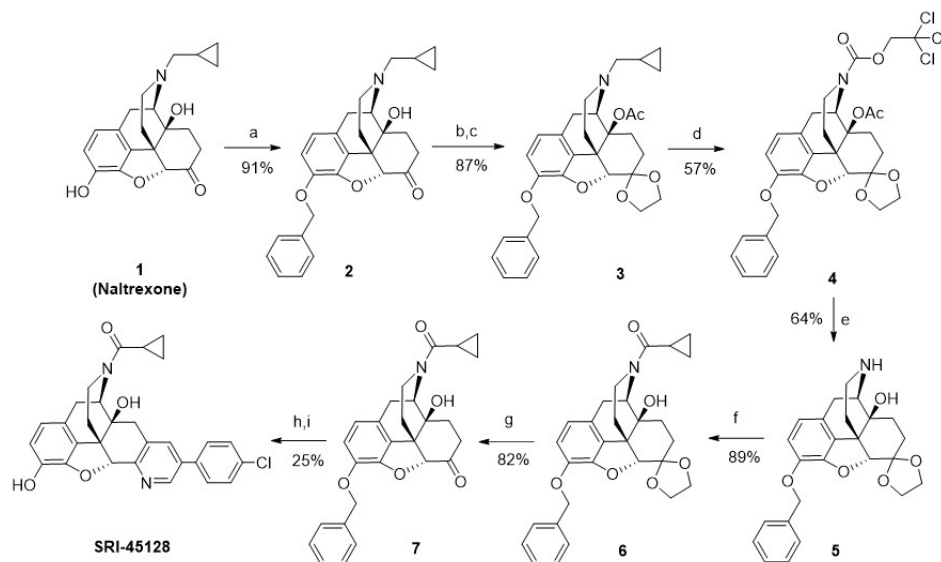
Scheme 2. Reagents and conditions: (a) BnBr, K$_2$CO$_3$, acetone, reflux; (b) ethylene glycol, p-TsOH.H$_2$O, toluene, reflux; (c) Ac$_2$O, reflux; (d) TrocCl, K$_2$CO$_3$, 1,1,2,2-tetrachloroethane, 140 °C; (e) KOH aq., DMSO, 110 °C; (f) cyclopropylcarbonyl chloride, Et$_3$N, CH$_2$Cl$_2$, rt; (g) HCl, MeOH, 80 °C; (h) 10% Pd/C, H$_2$, MeOH, no further purification of the obtained crude; (i) 2-(4-chlorophenyl)-3-hydroxy-prop-2-enal, ammonium acetate, AcOH, reflux.
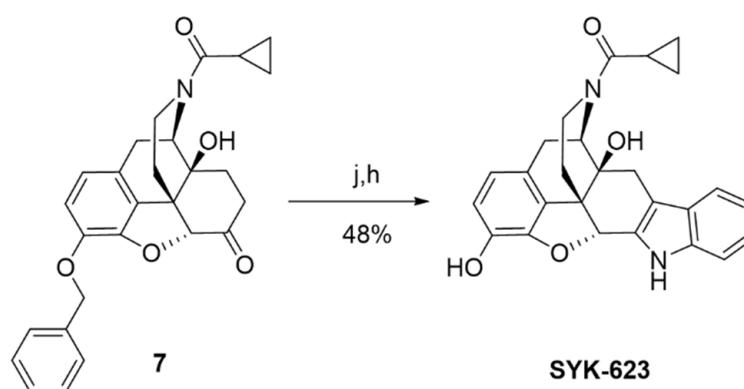
Scheme 3. Reagents and conditions: (j) phenyl hydrazine, AcOH, reflux; (h) 10% Pd/C, H_2, MeOH.

2.3. All Compounds Display High DOR Binding Affinity

All synthesized compounds were evaluated for binding to the human DOR using competition radioligand binding. All compounds showed one site full competition, suggesting full occupancy of the orthosteric binding site (Figure 1). Notably, the compounds are also bound to the DOR with high affinity with K_I values of 4.9–24 nM (Figure 1). We also tested SRI-45128 and SYK-623 for binding to the MOR and KOR, which would provide insight into compound selectivity. The compounds bound very weakly to the MOR, showing incomplete curves even at 10 μM. This suggests that both compounds are at least 120-fold selective for DOR over MOR. The compounds bound slightly better to the KOR, providing near-complete curves and K_I values, ranging from 2000 to 2500 nM, suggesting that both compounds are at least 104-fold selective for DOR over KOR (Figure 1). These results demonstrate that these compounds are high-affinity DOR ligands, and both inverse agonists display strong DOR selectivity. The expected performance of SYK-623 further confirms our findings.

Compound	Binding Affinity (K_I, nM)		
	DOR	MOR	KOR
Reference	200 ± 21	44 ± 0.6	7.2 ± 0.4
SRI-9342	4.9 ± 0.6	NT	NT
SYK-623	11 ± 1	>3,333	2000 ± 290
SRI-45128	24 ± 2	>3,333	2500 ± 510

Figure 1. Novel compounds bound to the DOR with high affinity. Compounds were tested as concentration curves competing with a fixed concentration of ^{3}H-diprenorphine (see Methods). N = 3 independent replicates performed, with summary curves shown for each set; affinity (K_I) was calculated separately for each experiment and then reported as the mean ± SEM. Experimental or reference compounds (naloxone for MOR and DOR, U50-488 for KOR) were tested at each receptor, DOR, MOR, or KOR, as noted. Reference compounds displayed expected affinities, validating the experiment, while all compounds demonstrated high affinities at the DOR. SRI-45128 and SYK-623 showed poor affinity at MOR and KOR, suggesting strong DOR selectivity.

2.4. SRI-9342 Displays Irreversible Antagonism at the DOR at Low Concentrations

Now that we showed that these compounds bound with high affinity to the DOR, we next sought to evaluate their functional activity. We tested the putative irreversible antagonist SRI-9342 for this activity using ^{35}S-GTPγS coupling. We ran SNC80 concentration curves with fixed and increasing concentrations of SRI-9342 present in each successive SNC80 curve. At 0.1 nM and 1 nM SRI-9342, we found that the SNC80 potency was actually better than the potency of SNC80 alone, while the efficacy was successively reduced to 92% and 84% (Figure 2). This behavior fits with the expected behavior of an irreversible antagonist, where potency is maintained at least initially, while efficacy is reduced. At higher concentrations (10–1000 nM), we observed large and successive shifts in both potency and measured efficacy, which is consistent with increasing receptor loss from the system. At 10,000 nM, we observed a puzzling partial recovery of both potency and efficacy. This may represent a non-specific effect at high concentrations (Figure 2). Overall, these findings are consistent with SRI-9342 displaying irreversible antagonism at low concentrations.

Condition	DOR Functional Activity	
	EC_{50} (nM)	E_{MAX} (%)
SNC80	33 ± 14	100
+ 0.1 nM	2.7 ± 0.9	92 ± 3
+ 1 nM	3.0 ± 0.6	84 ± 1
+ 10 nM	2200 ± 190	87 ± 1
+ 100 nM	>3,333	(29)
+ 1,000 nM	>3,333	(4.8)
+ 10,000 nM	950 ± 290	54 ± 1

Figure 2. SRI-9342 displayed DOR irreversible antagonism at low concentrations. SNC80 is a full DOR agonist, which was used to perform multiple full concentration curves using the ^{35}S-GTPγS assay (see Methods). Increasingly large fixed concentrations of SRI-9342 were included in subsequent SNC80 curves. N = 3 independent experiments performed, with summary curves shown. Potency (EC_{50}) and efficacy (E_{MAX}) were calculated separately for each experiment and reported as the mean ± SEM. SRI-9342 caused increasing loss of efficacy at 0.1 and 1 nM without decreasing potency (which was actually higher than SNC80 alone), suggesting irreversible antagonism. Beginning at 10 nM, potency loss was observed, which could indicate mixed activity or a very strong loss of receptors from the receptor pool due to irreversible antagonist activity.

2.5. SRI-45128 Displays DOR Inverse Agonism

Similar to SRI-9342, we sought to evaluate the inverse agonist functional activity of SRI-45128 with SYK-623 as a comparison control. The GTPγS assay used above has a generally low baseline receptor activity level, at least for the opioid receptors, so we switched assays to a live cell cAMP accumulation assay. This assay uses forskolin to stimulate cAMP levels, which are then inhibited/suppressed by the $Gα_I$-coupled activity of the DOR. As expected, SNC80 demonstrated potent and efficacious suppression of cAMP levels in DOR-CHO cells, which is in line with the expected activity of the receptor (Figure 3). By contrast, both SRI-45128 and SYK-623 showed efficacious inverse agonist activity and actually boosted cAMP levels, which is consistent with suppressing the baseline activity of the DOR (Figure 3). This activity was also efficacious, with an E_{MAX} of −67% and −56%, respectively. These results suggest that SRI-45128 is a robust inverse agonist, further confirmed by the performance of the SYK-623 comparison control.

Figure 3. SRI-45128 caused DOR inverse agonist activity. SRI-45128, positive control SYK-623, and SNC80 reference compounds were used to modulate the cAMP accumulation caused by forskolin treatment (see Methods). One independent experiment in triplicate was performed, and the potency (EC_{50}) and efficacy (E_{MAX}) were reported as the derived value with 95% confidence intervals (in parentheses). As expected, SNC80 caused high potency and efficacy cAMP inhibition, which is consistent with DOR agonist activity. SRI-45128 and SYK-623 caused efficacious cAMP increases, which is contrary to DOR agonism and consistent with DOR inverse agonism.

3. Discussion

As noted in the Introduction, a limited set of DOR irreversible antagonists and inverse agonists has been discovered and reported [5,11–17,19,25,26]. The ligands we report here were developed from a novel naltrexone scaffold and thus represent a significant contribution to the limited set of pharmacological tools available to probe the DOR. These ligands will help build the structure–activity relationship of irreversible antagonism and inverse agonism, and they could be used to investigate DOR function in vivo.

These novel compounds also have some possibility to inform future therapeutic candidates to target the DOR. For example, DOR activation has been associated with Alzheimer's disease, and DOR antagonism was shown to prevent and reverse Alzheimer's pathology in a mouse model [27]. Considering the long time-scales for Alzheimer's treatment, especially in a prevention paradigm, a long-lasting irreversible antagonist could be of considerable therapeutic benefit versus a short-acting competitive antagonist. Alternatively, an inverse agonist could be more effective than a standard neutral antagonist. DOR antagonists/inverse agonists have also not been associated with seizure activity as for some DOR agonists, suggesting their improved safety vs. agonists. This suggests that the active development of functionally selective DOR agonists to avoid seizures should not be necessary for these compounds [28,29]. However, one caution is that these compounds have only been tested for brief exposures in vitro and could thus possess other toxic effects. This will have to be examined in future studies.

Future works should also investigate these compounds in greater detail. Based on our binding studies, it is clear that all compounds bind selectively and with a high affinity to the DOR orthosteric site. However, the functional studies were not quite as clear. SRI-9342 displayed clear signs of irreversible antagonism at 0.1 and 1 nM. However, 10 nM caused a rapid loss of potency that continued at 100 nM and 1000 nM. The compound could be a full irreversible antagonist, and the activity at 10 nM could represent a rapid loss of receptors from the system that would eventually lead to the same reduction in potency as with other irreversible antagonists. Alternatively, the compound could have mixed activity, with irreversible antagonism at low concentrations and different functional activity, similar to competitive antagonism, at high concentrations. This mixed activity has been observed with other compounds, such as naloxonazine [30]. SRI-45128 also displayed clear inverse agonist activity. However, the potency of this activity was considerably less than

the binding affinity. This could represent the poor intrinsic efficacy of the compounds, or it could represent a relatively insensitive system for baseline receptor suppression. These details should be investigated for these compounds, working out the exact mechanisms of action and activity in different DOR-related signaling systems (e.g., ERK-MAPK activation instead of cAMP signaling). In addition, all compounds should be investigated for in vivo activity and whether the in vivo testing matches the predictions made via the in vitro testing reported here.

4. Materials and Methods

4.1. Chemical Synthesis and Characterization

All solvents and reagents were used as purchased without further purification. Unless otherwise stated, reactions were carried out under nitrogen atmosphere. Reaction conditions and yields were not optimized. The progress of all reactions was monitored by thin-layer chromatography (TLC) on pre-coated silica gel (60F254) aluminum plates (0.25 mm) from E. Merck and visualized using UV light (254 nm). Purification of compounds was performed on an Isco Teledyne Combiflash Rf200 with four channels to carry out sequential purification. Universal RediSep solid sample loading pre-packed cartridges (5.0 g silica) were used to absorb the crude product and purified on 12 g silica RediSep Rf Gold Silica (20–40 μm spherical silica) columns using appropriate solvent gradients. Melting points were determined in open capillary tubes with a Thomas–Hoover melting point apparatus or SRS OptiMelt automated melting point system and are uncorrected. High-resolution mass spectrometry (HRMS) or liquid chromatography with tandem mass spectrometry (LC-MS/MS) analysis was performed with an Agilent 1100 LC-MS TOF instrument using electrospray ionization (ESI) or with Agilent 1290 ultra-performance liquid chromatography (UPLC)/Sciex Triple Quad 6500+. ^{1}H NMR spectra were recorded at 400 MHz on an Agilent/Varian MR-400 spectrometer, and ^{13}C NMR spectra were recorded either at 100.574 MHz on an Agilent/Varian MR-400 spectrometer or at 125.76 MHz on a Bruker Avance III-HD 600 MHz Spectrometer. The chemical shifts (δ) are reported in parts per million (ppm) and referenced according to the deuterated solvent for ^{1}H spectra (CDCl$_3$, 7.26, DMSO-d_6, 2.50, or TMS 0.0) and ^{13}C spectra (CDCl$_3$, 77.2 or DMSO-d_6, 39.5). The purity of the final compounds was checked by analytical HPLC using an Agilent 1100 LC system equipped with a phenomenex Kinetex C18 column (5 μm, 4.6 × 150 mm) and a diode array detector (DAD) using the solvent system: solvent A: H$_2$O/0.1% trifluoroacetic acid, solvent B: CH$_3$CN/0.1% trifluoroacetic acid, 0–95% B over 22 min, flow rate 1 mL/min, λ 254 nm and λ 280 nm (System 1) or using a Waters HPLC system equipped with a Sunfire C18 column (5 μm, 4.6 × 150 mm) and a Waters 2998 photodiode array detector using the solvent system: solvent A: H$_2$O/0.1% formic acid, solvent B: CH$_3$CN/0.1% formic acid, 10–90% B over 20 min, flow rate 2 mL/min, λ 254 nm (System 2) or using an Agilent 1200 LC system equipped with phenomenex Kinetex Phenyl-Hexyl column (2.6 μm, 4.6 × 50 mm) and a diode array detector (DAD) using the solvent system: solvent A: H$_2$O/0.1% formic acid, solvent B: CH$_3$CN/0.1% formic acid, 0–95% B over 4.5 min, flow rate 2 mL/min, λ 254 nm (System 3). On the basis of NMR, HPLC-DAD, and HRMS (mass error less than 5 ppm), all final compounds were ≥95% pure.

4.1.1. (4b*S*,8*R*,8a*S*,14b*R*)-7-(Cyclopropylmethyl)-11-((E)-2-(pyridin-2-yl)vinyl)-5,6,7,8,14,14b-hexahydro-4,8-methanobenzofuro
[2,3-a]pyrido[4,3-b]carbazole-1,8a(9*H*)-diol (SRI-9342)

This compound was synthesized as previously described [22,23].

4.1.2. ((4b*S*,8*R*,8a*S*,13b*R*)-11-(4-Chlorophenyl)-1,8a-dihydroxy-5,6,8,8a,9,13b-hexahydro-7H-4,8-methanobenzofuro[3,2-h]pyrido[3,4-g]quinolin-7-yl)(cyclopropyl)methanone (SRI-45128)

This compound was synthesized by a modified procedure of the reported method [24] as described below.

4.1.3. 2,2,2-Trichloroethyl (4′*R*,7a′*R*,12b′*S*)-9′-(benzyloxy)-1′,2′,4′,6′-tetrahydro-3′*H*,7a′*H*-spiro[[1,3]dioxolane-2,7′-[4,12]methanobenzofuro[3,2-e]isoquinoline]-3′-carboxylate (**2**)

To a suspension of naltrexone (**1**) (5 g, 14.6 mmol) in acetone (200 mL), benzyl bromide (2.6 mL, 21.9 mmol) and potassium carbonate (4.0 mg, 29.3 mmol) were added. The reaction mixture was refluxed for 2 h; then, it was filtered, and the solid was washed with acetone (50 mL). The filtrate was concentrated under reduced pressure to afford a crude white solid, which was purified by the column chromatography over a column of silica gel, using EtOAc:Hexane, 1:3 as an eluant, to afford compound (**2**) (5.8 g, 58%) as a white solid. ^{1}H NMR (400 MHz, CDCl$_3$) δ 7.47–7.43 (m, 2H), 7.34 (ddt, *J* = 8.1, 6.5, 1.7 Hz, 2H), 7.31–7.26 (m, 1H), 6.71 (d, *J* = 8.2 Hz, 1H), 6.58–6.54 (m, 1H), 5.29 (d, *J* = 12.0 Hz, 1H), 5.21 (d, *J* = 8.9 Hz, 1H), 4.69 (s, 1H), 3.17 (d, *J* = 5.9 Hz, 1H), 3.09–2.98 (m, 2H), 2.69 (ddt, *J* = 12.1, 5.3, 1.3 Hz, 1H), 2.56 (ddd, *J* = 18.5, 6.1, 1.1 Hz, 1H), 2.47–2.38 (m, 3H), 2.31 (dt, *J* = 14.4, 3.2 Hz, 1H), 2.13 (td, *J* = 12.2, 3.8 Hz, 1H), 1.93–1.86 (m, 1H), 1.71–1.52 (m, 3H), 0.92–0.83 (m, 1H), 0.59–0.51 (m, 2H), 0.16–0.11 (m, 2H). ESI MS *m*/*z* 432 [M + H]$^{+}$.

4.1.4. (4′*R*,4a′*S*,7a′*R*,12b′*S*)-9′-(Benzyloxy)-3′-(cyclopropylmethyl)-1′,2′,3′,4′,5′,6′-hexahydro-4a′*H*,7a′*H*-spiro[[1,3]dioxolane-2,7′-[4,12]methanobenzofuro[3,2-e]isoquinolin]-4a′-yl acetate (**3**)

To a solution of compound (**2**) (5.0 g, 11.6 mmol) in toluene (50 mL) were added *p*-TsOH.H$_2$O (3.0 g, 17.4 mmol) and ethylene glycol (3.9 mL, 69.5 mmol), and the mixture was refluxed with a Dean–Stark apparatus for 17 h under an argon atmosphere. After cooling to room temperature, the reaction mixture was basified with potassium carbonate (3 g) and saturated aqueous NaHCO$_3$ solution (30 mL); then, it was extracted with CHCl$_3$ (3 × 100 mL). The organic layer was washed with brine, dried over Na$_2$SO$_4$, and concentrated under reduced pressure to afford a crude product as a colorless solid. The crude product was suspended in Ac$_2$O (35 mL), and the mixture was refluxed for 1 h under an argon atmosphere. After cooling to room temperature, the reaction mixture was concentrated and co-evaporated with toluene three times. The obtained residue was purified by column chromatography on silica gel using 0–5% MeOH in DCM to afford the desired compound (**3**) (3.8 g, 87% in two steps) as a white solid. ^{1}H NMR (400 MHz, CDCl$_3$) δ 7.42–7.27 (m, 5H), 6.86 (d, *J* = 8.2 Hz, 1H), 6.66 (d, *J* = 8.3 Hz, 1H), 5.36 (d, *J* = 5.2 Hz, 1H), 5.21–5.10 (m, 2H), 4.67 (s, 1H), 4.17 (ddd, *J* = 7.4, 6.6, 5.3 Hz, 1H), 4.01 (q, *J* = 6.6 Hz, 1H), 3.89 (dt, *J* = 7.4, 6.4 Hz, 1H), 3.78 (td, *J* = 6.6, 5.3 Hz, 1H), 3.46–3.32 (m, 2H), 3.23–3.06 (m, 2H), 3.02–2.89 (m, 2H), 2.66 (dt, *J* = 13.8, 3.2 Hz, 1H), 2.50 (s, 4H), 1.85 (td, *J* = 14.4, 2.8 Hz, 1H), 1.57 (dddd, *J* = 11.4, 8.5, 6.0, 3.2 Hz, 3H), 1.13–1.02 (m, 2H), 0.82–0.63 (m, 2H), 0.45 (ddt, *J* = 8.7, 5.7, 4.5 Hz, 1H). ESI MS *m*/*z* 518 [M + H]$^{+}$.

4.1.5. 2,2,2-Trichloroethyl (4′*R*,4a′*S*,7a′*R*,12b′*S*)-4a′-acetoxy-9′-(benzyloxy)-1′,2′,4′,4a′,5′,6′-hexahydro-3′*H*,7a′*H*-spiro[[1,3]dioxolane-2,7′-[4,12]methanobenzofuro[3,2-e]isoquinoline]-3′-carboxylate (**4**)

To a solution of compound (**3**) (3.0 g, 5.8 mmol) in 1,1,2,2-tetrachloroethane (25 mL) were added K$_2$CO$_3$ (5 g, 36.5 mmol) and 2,2,2-trichloroethyl chloroformate (5 mL, 36.5 mmol), and the mixture was stirred at 140 °C for 14 h under argon atmosphere. The reaction mixture was cooled to room temperature, and H$_2$O (20 mL) was added. The mixture was extracted with CHCl$_3$ (2 × 100 mL). The organic layer was washed with brine, dried over Na$_2$SO$_4$, and concentrated under reduced pressure to give a crude residue, which was purified by column chromatography on silica gel using 0–10% hexanes:EtOAc to afford compound (**4**) (2.1 g, 56%) as a light yellow amorphous solid. ^{1}H NMR (400 MHz, CDCl$_3$) δ 7.42 (tdd, *J* = 5.0, 4.0, 1.8 Hz, 2H), 7.39–7.28 (m, 3H), 6.83 (dd, *J* = 8.3, 1.3 Hz, 1H), 6.61 (dd, *J* = 8.3, 4.8 Hz, 1H), 5.62 (t, *J* = 4.5 Hz, 1H), 5.16 (q, *J* = 12.0 Hz, 2H), 4.93–4.85 (m, 1H), 4.70–4.63 (m, 1H), 4.60 (s, 1H), 4.21–4.15 (m, 1H), 4.07–3.98 (m, 2H), 3.91–3.86 (m, 1H), 3.80 (td, *J* = 6.6, 5.2 Hz,

1H), 3.09 (dt, *J* = 18.2, 6.0 Hz, 1H), 2.98–2.73 (m, 3H), 2.39 (tt, *J* = 12.6, 5.3 Hz, 1H), 2.07 (s, 1H), 2.05 (s, 1H), 1.86–1.77 (m, 1H), and 1.55–1.48 (m, 2H). ESI MS *m/z* 579.8 [M-AcOH]$^+$.

4.1.6. (4′*R*,4a′*S*,7a′*R*,12b′*S*)-9′-(Benzyloxy)-1′,2′,3′,4′,5′,6′-hexahydro-4a′*H*,7a′*H*-spiro[[1,3]dioxolane-2,7′-[4,12]methanobenzofuro[3,2-e]isoquinolin]-4a′-ol (**5**)

To a suspension of compound (**4**) (1.5 g, 2.6 mmol) in DMSO (20 mL) was added 12*M* aqueous KOH solution (7 mL), and the mixture was stirred for 6 h at 110 °C under an argon atmosphere. After cooling to room temperature, the reaction mixture was adjusted to pH 10 with saturated aqueous NH$_4$Cl solution (20 mL) and extracted with a mixed solution, *i*-PrOH/CHCl$_3$ = 1:3 (3 × 10 mL). The organic layer was washed with brine, dried over Na$_2$SO$_4$, and concentrated under reduced pressure to afford a crude residue, which was purified by chromatography on silica gel using 10% MeOH in DCM + 0.1% NH$_3$ to generate compound (**5**) (0.7 g, 64%) as a colorless solid. ^{1}H NMR (400 MHz, DMSO-*d*$_6$) δ 7.42–7.33 (m, 4H), 7.31–7.27 (m, 1H), 6.75 (d, *J* = 8.2 Hz, 1H), 6.52 (dd, *J* = 8.2, 0.8 Hz, 1H), 5.12–5.02 (m, 2H), 4.84 (s, 1H), 4.33 (s, 1H), 4.02–3.97 (m, 1H), 3.83 (q, *J* = 6.4 Hz, 1H), 3.78–3.66 (m, 2H), 2.89–2.78 (m, 3H), 2.55–2.49 (m, 1H), 2.34 (td, *J* = 12.6, 3.8 Hz, 1H), 2.15–1.98 (m, 2H), 1.40–1.28 (m, 3H), and 1.08–1.02 (m, 1H).

4.1.7. ((4′*R*,4a′*S*,7a′*R*,12b′*S*)-9′-(Benzyloxy)-4a′-hydroxy-1′,2′,4′,4a′,5′,6′-hexahydro-3′*H*,7a′*H*-spiro[[1,3]dioxolane-2,7′-[4,12]methanobenzofuro[3,2-e]isoquinolin]-3′-yl)(cyclopropyl)methanone (**6**)

To a stirred solution of compound (**5**) (500 mg, 1.14 mmol) in CH$_2$Cl$_2$ (12 mL) were added Et$_3$N (0.24 mL, 1.71 mmol) and cyclopropanecarbonyl chloride (143 mg, 1.37 mmol) at 0 °C under an argon atmosphere. After stirring for 2 h at room temperature, the reaction mixture was diluted with CH$_2$Cl$_2$ (10 mL) and washed with saturated aqueous NaHCO$_3$ solution (20 mL). The organic layer was washed with brine, dried over Na$_2$SO$_4$, and concentrated under reduced pressure to give a crude residue, which was purified by column chromatography on silica gel (80–100% EtOAc in n-hexane) to afford compound (**6**) (500 mg, 89%) as a colorless amorphous product. ^{1}H NMR (400 MHz, CDCl$_3$) δ 7.45–7.41 (m, 2H), 7.39–7.28 (m, 3H), 6.81 (d, *J* = 8.2 Hz, 1H), 6.59 (d, *J* = 8.0 Hz, 1H), 5.17 (q, *J* = 12.0 Hz, 2H), 4.94 (d, *J* = 5.9 Hz, 1H), 4.54 (d, *J* = 19.1 Hz, 1H), 4.40 (d, *J* = 21.2 Hz, 1H), 4.19–4.12 (m, 1H), 4.11–3.78 (m, 4H), 3.22–2.77 (m, 3H), 2.67–2.34 (m, 2H), 2.17 (t, *J* = 10.8 Hz, 1H), 1.71–1.45 (m, 5H), 1.10–0.92 (m, 2H), 0.80 (d, *J* = 9.8 Hz, 2H).

4.1.8. (4*R*,4a*S*,7a*R*,12b*S*)-9-(Benzyloxy)-3-(cyclopropanecarbonyl)-4a-hydroxy-2,3,4,4a,5,6-hexahydro-1H-4,12-methanobenzofuro[3,2-e]isoquinolin-7(7a*H*)-one (**7**)

A mixture of compound (**6**) (0.10 g, 0.20 mmol) in 1 *M* HCl (0.8 mL) was stirred for 15 h at 80 °C under an argon atmosphere. After cooling to room temperature, the reaction mixture was poured in 4*N* NaOH solution at 0 °C and extracted with CHCl$_3$, dried over Na$_2$SO$_4$, filtered, and concentrated to dryness to afford the crude material. The crude residue was purified by column chromatography on silica gel (5–15% (28% NH$_3$ aq/MeOH = 1:9) in CHCl3) to afford intermediate (**7**) (75 mg, 82%) as a colorless amorphous product with some impurities which was used as such in next step. ESI MS *m/z* 446 [M + H]$^+$.

4.1.9. ((4b*S*,8*R*,8a*S*,13b*R*)-11-(4-Chlorophenyl)-1,8a-dihydroxy-5,6,8,8a,9,13b-hexahydro-7H-4,8-methanobenzofuro[3,2-h]pyrido[3,4-g]quinolin-7-yl)(cyclopropyl)methanone (SRI-45128)

Compound (**7**) (150 mg, 0.3400 mmol) was dissolved in methanol (8 mL), and 10% palladium black (35.8 mg, 0.03 mmol) was added to the reaction. The reaction mixture was stirred under H$_2$ atmosphere (balloon) for 2 h at room temperature. The reaction mixture was filtered through a Celite pad, washed with MeOH (20 mL), and concentrated. To the solution of crude material in acetic acid (2 mL), ammonium acetate (43.4 mg, 0.56 mmol),

and (*E*)-2-(4-chlorophenyl)-3-hydroxy-prop-2-enal (77.07 mg, 0.42 mmol) were added, and the reaction mixture was refluxed overnight. The reaction mixture was cooled to room temperature, and acetic acid was removed. The obtained residue was diluted with water, neutralized with ammonium hydroxide to pH 7, extracted with DCM (3 × 10 mL), dried over Na_2SO_4, and purified by column chromatography using 0–10% MeOH in DCM to give a solid material, which was further purified by a preparative plate using 9:1 CHCl3-MeOH to afford SRI-45128 (35 mg, 25%) as a white solid. TLC (10% MeOH/DCM): R*f* = 0.35; ^{1}H NMR (400 MHz, CD_3OD) δ 8.60 (dd, *J* = 5.1, 2.2 Hz, 1H), 7.58 (dd, *J* = 3.6, 2.3 Hz, 1H), 7.50–7.44 (m, 2H), 7.42–7.37 (m, 2H), 6.66–6.58 (m, 2H), 5.42 (d, *J* = 2.7 Hz, 1H), 5.05 (d, *J* = 6.5 Hz, 0.5H), 4.74 (d, *J* = 6.5 Hz, 0.5H), 4.51–4.42 (m, 0.5H), 4.23 (dd, *J* = 14.0, 5.1 Hz, 0.5H), 3.38–3.30 (m, 1H), 3.28–3.15 (m, 1H), 2.88–2.75 (m, 2H), 2.55 (td, *J* = 12.8, 5.2 Hz, 0.5H), 2.40 (td, *J* = 12.8, 5.3 Hz, 0.5H), 2.33–2.22 (m, 1H), 2.16–1.96 (m, 1H), 1.73–1.53 (m, 2H), 1.20–1.06 (m, 1H), 1.02–0.93 (m, 1H), 0.89–0.80 (m, 3H). ^{13}C NMR (101 MHz, CD_3OD) δ 173.95, 145.50, 139.99, 136.28, 136.22, 135.33, 135.19, 134.23, 131.31, 128.88, 128.23, 128.19, 123.58, 119.41, 119.34, 117.64, 88.88, 71.56, 71.38, 47.38, 47.16, 47.01, 46.95, 46.94, 38.56, 36.28, 35.04, 32.45, 31.83, 29.71, 29.04, 11.06, 10.99, 6.91, 6.59, 6.53, 6.42. HRMS (ESI) *m/z* calcd for $C_{29}H_{25}ClN_2O_4$ [M + H]$^+$: 501.1576, found: 501.1570; HPLC (system 1) t_R = 10.7 min, purity = 99%.

4.1.10. Cyclopropyl((4bS,8R,8aS,14bR)-1,8a-dihydroxy-5,6,8a,9,14,14b-hexahydro-4,8-methanobenzofuro[2,3−a]pyrido [4,3−b]carbazol-7(8H)-yl)methanone (SYK-623)

This compound was prepared by a modification of the reported protocol [19]. A solution of compound (7) (200 mg, 0.45 mmol) in acetic acid (5 mL) was supplemented with phenylhydrazine (58.3 mg, 0.54 mmol), and the reaction mixture was refluxed for 2 h. After cooling to room temperature, the reaction mixture was concentrated and co-evaporated with toluene to afford a crude product. Saturated Na_2CO_3 was added, and the mixture was extracted with methylene chloride, dried over sodium sulfate, concentrated, chromatographed on an Isco Combiflash system using 0–5% MeOH in DCM to give a white solid which was dissolved in methanol (10 mL), and then 10% palladium black (24.6 mg, 0.02 mmol) was added to the reaction. The mixture was stirred under H_2 atmosphere (balloon) for 2 h at room temperature and filtered through celite. The celite pad was washed with MeOH (20 mL), and the filtrate was evaporated to give a white residue, which was purified by column chromatography using 0–10% MeOH in DCM to afford SYK-623 (50 mg, 48%) as a white solid. TLC (10% MeOH/DCM): R_f = 0.35; ^{1}H NMR (400 MHz, CD_3OD) δ 7.36 (ddt, *J* = 7.8, 6.7, 1.0 Hz, ^{1}H), 7.30 (ddt, *J* = 8.2, 4.1, 0.9 Hz, ^{1}H), 7.07 (dddd, *J* = 8.2, 7.0, 3.8, 1.2 Hz, ^{1}H), 6.94 (dddd, *J* = 8.0, 7.0, 4.7, 1.0 Hz, ^{1}H), 6.63–6.51 (m, ^{2}H), 5.61 (s, [0.5]H), 5.07 (d, *J* = 6.6 Hz, [0.5]H), 4.75 (d, *J* = 6.6 Hz, [0.5]H), 4.49–4.38 (m, [0.5]H), 4.18–4.08 (m, [0.5]H), 3.44 (dd, *J* = 18.5, 6.7 Hz, [0.5]H), 3.33–3.25 (m, ^{1}H), 3.15 (td, *J* = 13.4, 3.8 Hz, [0.5]H), 3.00–2.58 (m, [4]H), 2.51 (td, *J* = 12.8, 5.2 Hz, [0.5]H), 2.07 (tt, *J* = 7.9, 4.8 Hz, [0.5]H), 1.96–1.88 (m, [0.5]H), 1.71–1.62 (m, ^{1}H), 1.00–0.90 (m, ^{1}H), 0.89–0.74 (m, ^{3}H). HRMS (ESI) *m/z* calcd for $C_{26}H_{24}N_2O_4$ [M + H]$^+$: 429.1810, found: 429.1801; HPLC (system 1) t_R = 10.7 min, purity = 96%.

4.2. Cell Culture

A Chinese Hamster Ovary (CHO-K1) parental cell line expressing the human DOR was obtained from PerkinElmer (#RBHODM-K) and used for all experiments. Cells were maintained in 1:1 DMEM/F12 media with 1× penicillin/streptomycin supplement and 10% heat-inactivated fetal bovine serum (all from Invitrogen/ThermoFisher) in a 37 °C/5% CO_2 incubator. Maintenance cultures were further supplemented with 500 μg/mL of G418 to preserve receptor selection/expression (Invitrogen/ThermoFisher). Cells were generally passaged at 1:10 every 2 days. Similar cell lines for the human mu opioid receptor (PerkinElmer, #ES-542-C) and human kappa opioid receptor (PerkinElmer, #ES-541-C, Cambridge, MA, USA) were used for selectivity experiments and maintained as above.

4.3. Competition Radioligand Binding

Radioligand binding was generally carried out as reported in our previous work (e.g., [18,31–33]). Briefly, 30 μg of cell membrane protein was combined with 0.89 nM of ^{3}H-diprenorphine (PerkinElmer, #NET1121250UC) and concentration curves of experimental ligand or reference drug (see Figure Legends for details) in a 200 μL reaction volume. The reactions were incubated at room temperature for 1 h; then, they were collected onto GF/B filter plates (PerkinElmer) using a Brandel Cell Harvester. Then, the plates were read on a PerkinElmer Microbeta2 scintillation counter. The resulting data were normalized to vehicle-alone treatment (100%) and non-specific binding with 10 μM reference compound (0%) and fit to a one-site competition binding model using GraphPad Prism 9.0. The previously measured K_D of the diprenorphine in each cell line [34] was used to calculate the K_I of each ligand at each receptor.

4.4. ^{35}S-GTPγS Coupling

The ^{35}S-GTPγS coupling assay was also performed as in our previous work (e.g., [18,31,35]). Briefly, 15 μg of cell membrane protein was combined with 0.1 nM of ^{35}S-GTPγS (PerkinElmer, #NEG030H250UC) and concentration curves of ligand and SNC80 (see the figure legends for details) in a 200 μL reaction volume in the presence of 40 μM GDP. The reactions were incubated at 30 °C for 1 h; then, they were collected and read as above. The resulting data were normalized to stimulation caused by vehicle (0%) and 10 μM SNC80 (100%) and fit to a 3-variable (Hill Slope = 1) agonist model using GraphPad Prism 9.0.

4.5. cAMP Accumulation Assay

This assay was also carried out as reported in our previous work [31]. First, 20,000 cells/well were plated in a 96-well plate in growth medium as above for 24 h. Then, cells were serum-starved in DMEM/F12 for 4 h and then incubated with 500 μM IBMX for 20 min. Stimulation buffer contained 500 μM IBMX and 50 μM forskolin, which is a known cAMP inducer. Serial dilutions of SNC80, a known reference DOR agonist, or test compounds were added in stimulation buffer for 10 min. Then, incubation mixtures were halted by adding ice-cold assay buffer and heating the plate at 80 °C for 10 min. The plate was centrifuged at 4,000 rpm for 10 min at 4 °C; then, supernatants were transferred into a new 96-well plate. The supernatants were co-incubated with 1 pmol of ^{3}H-cAMP (PerkinElmer #NET1161250UC) and 7 μg of bovine protein kinase A (Sigma-Aldrich, St. Louis, MO, USA) in 0.05% bovine serum albumin for 1 h at room temperature. Then, the reactions were collected and measured as above. The data were normalized to cAMP suppression caused by vehicle (0%) or 10 μM SNC80 (100%) and fit to a 3-variable (Hill Slope = 1) agonist curve by GraphPad Prism 9.0.

4.6. Data Analysis

The data generated by the above pharmacological analyses include binding affinity (K_I) and functional potency/efficacy (EC_{50}/E_{MAX}). Each experiment was performed as 3 independent experiments using separate plates, drug dilutions, etc. (N = 3). The above values were calculated separately for each independent experiment and then reported as the mean $\pm$ SEM of the N = 3 set. Statistical comparisons are not typical for this sort of pharmacological characterization and were not employed here.

Institutional Review Board Statement: Not applicable.

Informed Consent Statement: Not applicable.

Data Availability Statement: All data sets are available from the Corresponding Author upon request.

Conflicts of Interest: J.M.S. has an equity stake in *Botanical Results, LLC* and is a co-founder of *Teleport Pharmaceuticals, LLC*; no company products or interests were tested in this study. The authors have no other relevant conflicts of interest to declare.

Sample Availability: Samples of the compounds are available from the authors.

References

1. Overington, J.P.; Al-Lazikani, B.; Hopkins, A.L. How many drug targets are there? *Nat. Rev. Drug Discov.* **2006**, *5*, 993–996. [CrossRef] [PubMed]
2. Bodnar, R.J. Endogenous opiates and behavior: 2013. *Peptides* **2014**, *62*, 67–136. [CrossRef] [PubMed]
3. Neubig, R.R.; Spedding, M.; Kenakin, T.; Christopoulos, A. International Union of Pharmacology Committee on Receptor Nomenclature and Drug Classification. XXXVIII. Update on terms and symbols in quantitative pharmacology. *Pharmacol. Rev.* **2003**, *55*, 597–606. [CrossRef] [PubMed]
4. Craft, R.M.; Tseng, A.H.; McNiel, D.M.; Furness, M.S.; Rice, K.C. Receptor-selective antagonism of opioid antinociception in female versus male rats. *Behav. Pharmacol.* **2001**, *12*, 591–602. [CrossRef] [PubMed]
5. Haris, S.P.; Zhang, Y.; Le Bourdonnec, B.; McCurdy, C.R.; Portoghese, P.S. o-Naphthalenedicarboxaldehyde derivative of 7'-aminonaltrindole as a selective delta-opioid receptor affinity label. *J. Med. Chem.* **2007**, *50*, 3392–3396. [CrossRef] [PubMed]
6. Portoghese, P.S.; Sultana, M.; Takemori, A.E. Naltrindole 5'-isothiocyanate: A nonequilibrium, highly selective delta opioid receptor antagonist. *J. Med. Chem.* **1990**, *33*, 1547–1548. [CrossRef]
7. Costa, T.; Herz, A. Antagonists with negative intrinsic activity at delta opioid receptors coupled to GTP-binding proteins. *Proc. Natl. Acad. Sci. USA* **1989**, *86*, 7321–7325. [CrossRef]
8. Carroll, F.I.; Zhang, L.; Mascarella, S.W.; Navarro, H.A.; Rothman, R.B.; Cantrell, B.E.; Zimmerman, D.M.; Thomas, J.B. Discovery of the first N-substituted 4beta-methyl-5-(3-hydroxyphenyl)morphan to possess highly potent and selective opioid delta receptor antagonist activity. *J. Med. Chem.* **2004**, *47*, 281–284. [CrossRef]
9. Nemoto, T.; Iihara, Y.; Hirayama, S.; Iwai, T.; Higashi, E.; Fujii, H.; Nagase, H. Naltrindole derivatives with fluorinated ethyl substituents on the 17-nitrogen as δ opioid receptor inverse agonists. *Bioorg. Med. Chem. Lett.* **2015**, *25*, 2927–2930. [CrossRef]
10. Iwamatsu, C.; Hayakawa, D.; Kono, T.; Honjo, A.; Ishizaki, S.; Hirayama, S.; Gouda, H.; Fujii, H. Effects of *N*-Substituents on the Functional Activities of Naltrindole Derivatives for the δ Opioid Receptor: Synthesis and Evaluation of Sulfonamide Derivatives. *Molecules* **2020**, *25*, 3792. [CrossRef]
11. Hosohata, K.; Burkey, T.H.; Alfaro-Lopez, J.; Hruby, V.J.; Roeske, W.R.; Yamamura, H.I. (2S,3R)TMT-L-Tic-OH is a potent inverse agonist at the human delta-opioid receptor. *Eur. J. Pharmacol.* **1999**, *380*, R9–R10. [CrossRef]
12. Martin, N.A.; Ruckle, M.B.; VanHoof, S.L.; Prather, P.L. Agonist, antagonist, and inverse agonist characteristics of TIPP (H-Tyr-Tic-Phe-Phe-OH), a selective delta-opioid receptor ligand. *J. Pharmacol. Exp. Ther.* **2002**, *301*, 661–671. [CrossRef] [PubMed]
13. Labarre, M.; Butterworth, J.; St-Onge, S.; Payza, K.; Schmidhammer, H.; Salvadori, S.; Balboni, G.; Guerrini, R.; Bryant, S.D.; Lazarus, L.H. Inverse agonism by Dmt-Tic analogues and HS 378, a naltrindole analogue. *Eur. J. Pharmacol.* **2000**, *406*, R1–R3. [CrossRef]
14. Zaki, P.A.; Keith, D.E., Jr.; Thomas, J.B.; Carroll, F.I.; Evans, C.J. Agonist-, antagonist-, and inverse agonist-regulated trafficking of the delta-opioid receptor correlates with, but does not require, G protein activation. *J. Pharmacol. Exp. Ther.* **2001**, *298*, 1015–1020. [PubMed]
15. Emmerson, P.J.; McKinzie, J.H.; Surface, P.L.; Suter, T.M.; Mitch, C.H.; Statnick, M.A. Na+ modulation, inverse agonism, and anorectic potency of 4-phenylpiperidine opioid antagonists. *Eur. J. Pharmacol.* **2004**, *494*, 121–130. [CrossRef]
16. Thomas, J.B.; Zhang, L.; Navarro, H.A.; Carroll, F.I. Highly potent and selective phenylmorphan-based inverse agonists of the opioid delta receptor. *J. Med. Chem.* **2006**, *49*, 5597–5609. [CrossRef]
17. Cheng, K.; Kim, I.J.; Lee, M.J.; Adah, S.A.; Raymond, T.J.; Bilsky, E.J.; Aceto, M.D.; May, E.L.; Harris, L.S.; Coop, A.; et al. Opioid ligands with mixed properties from substituted enantiomeric N-phenethyl-5-phenylmorphans. Synthesis of a micro-agonist delta-antagonist and delta-inverse agonists. *Org. Biomol. Chem.* **2007**, *5*, 1177–1190. [CrossRef]
18. Vekariya, R.H.; Lei, W.; Ray, A.; Sainai, S.K.; Zhang, S.; Molnar, G.; Barlow, D.; Karlage, K.L.; Bilsky, E.; Houseknecht, K.; et al. Synthesis and Structure-Activity Relationships of 5'-Aryl-14-alkoxypyridomorphinans: Identification of a Mu Opioid Receptor Agonist/Delta Opioid Receptor Antagonist Ligand with Systemic Antinociceptive Activity and Diminished Opioid Side Effects. *J. Med. Chem.* **2020**, *63*, 7663–7694. [CrossRef]

19. Higashi, E.; Hirayama, S.; Nikaido, J.; Shibasaki, M.; Kono, T.; Honjo, A.; Ikeda, H.; Kamei, J.; Fujii, H. Development of Novel delta Opioid Receptor Inverse Agonists without a Basic Nitrogen Atom and Their Antitussive Effects in Mice. *ACS Chem. Neurosci.* **2019**, *10*, 3939–3945. [CrossRef]

20. Fenalti, G.; Giguere, P.M.; Katritch, V.; Huang, X.P.; Thompson, A.A.; Cherezov, V.; Roth, B.L.; Stevens, R.C. Molecular control of delta-opioid receptor signalling. *Nature* **2014**, *506*, 191–196. [CrossRef]

21. Claff, T.; Yu, J.; Blais, V.; Patel, N.; Martin, C.; Wu, L.; Han, G.W.; Holleran, B.J.; Van der Poorten, O.; White, K.L.; et al. Elucidating the active delta-opioid receptor crystal structure with peptide and small-molecule agonists. *Sci. Adv.* **2019**, *5*, eaax9115. [CrossRef] [PubMed]

22. Peng, Y.; Keenan, S.M.; Zhang, Q.; Kholodovych, V.; Welsh, W.J. 3D-QSAR comparative molecular field analysis on opioid receptor antagonists: Pooling data from different studies. *J. Med. Chem.* **2005**, *48*, 1620–1629. [CrossRef] [PubMed]

23. Ananthan, S.; Johnson, C.A.; Carter, R.L.; Clayton, S.D.; Rice, K.C.; Xu, H.; Davis, P.; Porreca, F.; Rothman, R.B. Synthesis, opioid receptor binding, and bioassay of naltrindole analogues substituted in the indolic benzene moiety. *J. Med. Chem.* **1998**, *41*, 2872–2881. [CrossRef] [PubMed]

24. Nagase, H.; Yamamoto, N.; Yata, M.; Ohrui, S.; Okada, T.; Saitoh, T.; Kutsumura, N.; Nagumo, Y.; Irukayama-Tomobe, Y.; Ishikawa, Y.; et al. Design and Synthesis of Potent and Highly Selective Orexin 1 Receptor Antagonists with a Morphinan Skeleton and Their Pharmacologies. *J. Med. Chem.* **2017**, *60*, 1018–1040. [CrossRef]

25. Jiang, Q.; Takemori, A.E.; Sultana, M.; Portoghese, P.S.; Bowen, W.D.; Mosberg, H.I.; Porreca, F. Differential antagonism of opioid delta antinociception by [D-Ala2,Leu5,Cys6]enkephalin and naltrindole 5'-isothiocyanate: Evidence for delta receptor subtypes. *J. Pharmacol. Exp. Ther.* **1991**, *257*, 1069–1075.

26. Hirayama, S.; Iwai, T.; Higashi, E.; Nakamura, M.; Iwamatsu, C.; Itoh, K.; Nemoto, T.; Tanabe, M.; Fujii, H. Discovery of delta Opioid Receptor Full Inverse Agonists and Their Effects on Restraint Stress-Induced Cognitive Impairment in Mice. *ACS Chem. Neurosci.* **2019**, *10*, 2237–2242. [CrossRef]

27. Teng, L.; Zhao, J.; Wang, F.; Ma, L.; Pei, G. A GPCR/secretase complex regulates beta- and gamma-secretase specificity for Abeta production and contributes to AD pathogenesis. *Cell Res.* **2010**, *20*, 138–153. [CrossRef]

28. Burtscher, J.; Schwarzer, C. The Opioid System in Temporal Lobe Epilepsy: Functional Role and Therapeutic Potential. *Front. Mol. Neurosci.* **2017**, *10*, 245. [CrossRef]

29. Jutkiewicz, E.M.; Baladi, M.G.; Folk, J.E.; Rice, K.C.; Woods, J.H. The convulsive and electroencephalographic changes produced by nonpeptidic δ-opioid agonists in rats: Comparison with pentylenetetrazol. *J. Pharmacol. Exp. Ther.* **2006**, *317*, 1337–1348. [CrossRef]

30. Ling, G.S.; Simantov, R.; Clark, J.A.; Pasternak, G.W. Naloxonazine actions in vivo. *Eur. J. Pharmacol.* **1986**, *129*, 33–38. [CrossRef]

31. LaVigne, J.; Keresztes, A.; Chiem, D.; Streicher, J.M. The endomorphin-1/2 and dynorphin-B peptides display biased agonism at the mu opioid receptor. *Pharmacol. Rep.* **2020**, *72*, 465–471. [CrossRef] [PubMed]

32. Stefanucci, A.; Dimmito, M.P.; Macedonio, G.; Ciarlo, L.; Pieretti, S.; Novellino, E.; Lei, W.; Barlow, D.; Houseknecht, K.L.; Streicher, J.M.; et al. Potent, Efficacious, and Stable Cyclic Opioid Peptides with Long Lasting Antinociceptive Effect after Peripheral Administration. *J. Med. Chem.* **2020**, *63*, 2673–2687. [CrossRef] [PubMed]

33. LaVigne, J.E.; Hecksel, R.; Keresztes, A.; Streicher, J.M. Cannabis sativa terpenes are cannabimimetic and selectively enhance cannabinoid activity. *Sci. Rep.* **2021**, *11*, 8232. [CrossRef] [PubMed]

34. Olson, K.M.; Duron, D.I.; Womer, D.; Fell, R.; Streicher, J.M. Comprehensive molecular pharmacology screening reveals potential new receptor interactions for clinically relevant opioids. *PLoS ONE* **2019**, *14*, e0217371. [CrossRef]

35. Stefanucci, A.; Dimmito, M.P.; Molnar, G.; Streicher, J.M.; Novellino, E.; Zengin, G.; Mollica, A. Developing Cyclic Opioid Analogues: Fluorescently Labeled Bioconjugates of Biphalin. *ACS Med. Chem. Lett.* **2020**, *11*, 720–726. [CrossRef]

Correction

Correction: Tanguturi et al. Discovery of Novel Delta Opioid Receptor (DOR) Inverse Agonist and Irreversible (Non-Competitive) Antagonists. *Molecules* 2021, 26, 6693

Parthasaradhireddy Tanguturi [1] (ID)**, Vibha Pathak** [2]**, Sixue Zhang** [2]**, Omar Moukha-Chafiq** [2]**, Corinne E. Augelli-Szafran** [2] **and John M. Streicher** [1,*] (ID)

[1] Department of Pharmacology, College of Medicine, University of Arizona, Tucson, AZ 85724, USA; parthasaradhit@arizona.edu

[2] Department of Chemistry, Division of Drug Discovery, Southern Research Institute, Birmingham, AL 35205, USA; vibhabpathak@gmail.com (V.P.); szhang@southernresearch.org (S.Z.); omoukha-chafiq@southernresearch.org (O.M.-C.); caugelli-szafran@southernresearch.org (C.E.A.-S.)

* Correspondence: jstreicher@arizona.edu; Tel.: +1-520-626-7495

1. Text Correction

There was an error in the original publication [1]. The compound SYK-623 was unintentionally labeled as our own, SRI-45127, and treated as our original compound in the manuscript. SYK-623 was synthesized in another study as a control group. Our mistaken claim that this compound was our own was then exacerbated due to miscommunication amongst our scientific team. No malfeasance was intended by this mistake.

Corrections have been made throughout the text; correctly labeling SRI-45127 back to SYK-623 and adjusting the text accordingly. Further corrections have been made, with clear references and comparisons between SYK-623 and our own ligands, delineating what is unique about our compounds compared to theirs. These sections include: Abstract; Introduction Paragraphs 3 and 4; Results Sections 2.1, 2.2, 2.3, and 2.5; Discussion Paragraph 3; Materials and Methods Section 4.1.10.

Corrected Text

Abstract: The delta opioid receptor (DOR) is a crucial receptor system that regulates pain, mood, anxiety, and similar mental states. DOR agonists, such as SNC80, and DOR-neutral antagonists, such as naltrindole, were developed to investigate the DOR in vivo and as potential therapeutics for pain and depression. However, few inverse agonists and non-competitive/irreversible antagonists have been developed, and none are widely available. This leaves a gap in our pharmacological toolbox and limits our ability to investigate the biology of this receptor. Thus, we designed and synthesized the novel compounds SRI-9342 as an irreversible antagonist and SRI-45128 as an inverse agonist. These compounds were then evaluated in vitro for their binding affinity by radioligand binding, their functional activity by ^{35}S-GTPγS coupling, and their cAMP accumulation in cells expressing the human DOR. Both compounds demonstrated high binding affinity and selectivity at the DOR, and both displayed their hypothesized molecular pharmacology of irreversible antagonism (SRI-9342) or inverse agonism (SRI-45128). Together, these results demonstrate that we have successfully designed new inverse agonists and irreversible antagonists of the DOR based on a novel chemical scaffold. These new compounds will provide new tools to investigate the biology of the DOR or even new potential therapeutics.

Introduction Paragraphs 3 and 4

By contrast, an inverse agonist does have intrinsic activity at the orthosteric site. However, unlike an agonist, an inverse agonist shifts the energy landscape to further disfavor the receptor active state and favor the inactive state. This suppresses baseline

receptor activity to the extent that it is below that of the unliganded state [3]. The first such described ligand for the DOR was ICI-174864, a peptidic inverse agonist reported by Costa and Herz [7]. Later, additional DOR inverse agonists were reported, such as (+)−KF4 [8], naltrindole (NTI) derivatives [9], amide/sulfonamide substituted NTI [10], as well as other peptidic [11–13] and nonpeptidic [14–17] molecules.

Here, we report the discovery and characterization of a new DOR non-competitive antagonist (SRI-9342) and a new inverse agonist (SRI-45128). These ligands have strong selectivity for the DOR and potent functional activity in vitro. The discovery of these ligands further expands the limited pharmacological tools available to probe the DOR and could even provide potential future therapeutics.

Results Sections 2.1, 2.2, 2.3, 2.5

2.1. Rational Design of DOR Ligands

The DOR ligands SRI-9342 (irreversible antagonist) and SRI-45128 (inverse agonist) were designed based on our previously published computational docking studies of the SRI-9409 scaffold core [18], as well as DOR ligands reported in the study, including SYK-623 [19]. When this core binds to the orthosteric site of DOR, the right-hand side indole moiety would face the extracellular opening of the binding pocket and be adjacent to the functionally important K214 of DOR [20], which is also a potentially reactive residue. Thus, the idea of adding a warhead to the scaffold to further increase its binding affinity to DOR was explored, which resulted in SRI-9342. The α,β-unsaturated pyridin group of SRI-9342 is supposed to be in a proper position to form a covalent bond with the nitrogen on the side chain of K214 via Michael's addition, turning it into an irreversible DOR antagonist. On the other hand, the cyclopropyl group of the scaffold would face the bottom of the binding pocket and form hydrophobic contact with the W274 of DOR, which is an important residue responsible for the switch between agonism and antagonism [20,21]. Therefore, chemical modifications were also explored at this position, which resulted in SRI-45128 with DOR inverse agonism. Notably, SRI-45128 was distinct from parent scaffold SRI-9409 in the sense that the introduction of carbonyl next to the cyclopropyl group (inspired by SYK-623) would reduce the basicity of the neighboring nitrogen of SRI-45128, which was no longer able to form a salt-bridge with key residue D128. In addition, SRI-45128 is distinguishable from SYK-623 in the sense that the former possessed a pyridine-4-phenylchloride moiety while the latter possessed an indole moiety on the right-hand side.

2.2. Synthesis of Novel DOR Irreversible Antagonist and Inverse Agonists

SRI-9342 (irreversible antagonist, Scheme 1) was synthesized with a 44% yield via the reaction of naltrexone hydrochloride and *trans*-4-hydrazino-2-stilbazole dihydrochloride following the same procedures previously reported [22,23]. SRI-45128 (inverse agonist, Scheme 2) was synthesized in nine steps by using the procedures reported in [24], subject to a few modifications. In our alternative route, the protecting group on the phenolic hydroxyl group of naltrexone (**1**) was changed from methyl to benzyl to achieve an overall improvement in yields. The 6-ketone group of compounds (**2**) was protected as 1,3-dioxolane, which was followed by acetylation of the 14-OH under refluxing in Ac_2O. The cyclopropyl methyl group of the resulting acetate compound (**3**) was exchanged for a trichloroethoxycarbonyl group at 140 °C with an excess amount of trichloroethoxycarbonyl chloride to afford carbamate (**4**). The carbamate and the acetate group in compound (**4**) were further hydrolyzed with aqueous KOH at 110 °C to afford compound (**5**). The reaction of compound (**5**) with cyclopropyl carbonyl chloride in the presence of Et_3N afforded compound (**6**) with an 89% yield. Removal of the 1,3-dioxolane group in amide (**6**) was done by using HCl and MeOH at reflux conditions to afford ketone (**7**). Finally, further deprotection of the benzyl group in (**7**), followed by annulation with 2-(4-chlorophenyl)-3-hydroxy-prop-2-enal in the presence of ammonium acetate, afforded SRI-45128 in two steps. We also synthesized SYK-623 for use as a control group (inverse agonist, Scheme 3). This was achieved in two steps, from intermediate (**7**), by using the procedure reported in [19] with the following modifications: Compound (**7**) was reacted with phenyl hydrazine in acetic acid under reflux conditions

followed by deprotection of the benzyl group to afford SYK-623. All compounds were confirmed for identity and high purity, which is sufficient for pharmacological characterization (see Methods).

2.3. *All Compounds Display High DOR Binding Affinity*

All synthesized compounds were evaluated for binding to the human DOR using competition radioligand binding. All compounds showed one site full competition, suggesting full occupancy of the orthosteric binding site (Figure 1). Notably, the compounds are also bound to the DOR with high affinity with K_I values of 4.9–24 nM (Figure 1). We also tested SRI-45128 and SYK-623 for binding to the MOR and KOR, which would provide insight into compound selectivity. The compounds bound very weakly to the MOR, showing incomplete curves even at 10 μM. This suggests that both compounds are at least 120-fold selective for DOR over MOR. The compounds bound slightly better to the KOR, providing near-complete curves and K_I values, ranging from 2000 to 2500 nM, suggesting that both compounds are at least 104-fold selective for DOR over KOR (Figure 1). These results demonstrate that these compounds are high-affinity DOR ligands, and both inverse agonists display strong DOR selectivity. The expected performance of SYK-623 further confirms our findings.

2.5. *SRI-45128 Displays DOR Inverse Agonism*

Similar to SRI-9342, we sought to evaluate the inverse agonist functional activity of SRI-45128 with SYK-623 as a comparison control. The GTPγS assay used above has a generally low baseline receptor activity level, at least for the opioid receptors, so we switched assays to a live cell cAMP accumulation assay. This assay uses forskolin to stimulate cAMP levels, which are then inhibited/suppressed by the $G\alpha_I$-coupled activity of the DOR. As expected, SNC80 demonstrated potent and efficacious suppression of cAMP levels in DOR-CHO cells, which is in line with the expected activity of the receptor (Figure 3). By contrast, both SRI-45128 and SYK-623 showed efficacious inverse agonist activity and actually boosted cAMP levels, which is consistent with suppressing the baseline activity of the DOR (Figure 3). This activity was also efficacious, with an E_{MAX} of −67% and −56%, respectively. These results suggest that SRI-45128 is a robust inverse agonist, further confirmed by the performance of the SYK-623 comparison control.

Discussion Paragraph 3

Future works should also investigate these compounds in greater detail. Based on our binding studies, it is clear that all compounds bind selectively and with a high affinity to the DOR orthosteric site. However, the functional studies were not quite as clear. SRI-9342 displayed clear signs of irreversible antagonism at 0.1 and 1 nM. However, 10 nM caused a rapid loss of potency that continued at 100 nM and 1000 nM. The compound could be a full irreversible antagonist, and the activity at 10 nM could represent a rapid loss of receptors from the system that would eventually lead to the same reduction in potency as with other irreversible antagonists. Alternatively, the compound could have mixed activity, with irreversible antagonism at low concentrations and different functional activity, similar to competitive antagonism, at high concentrations. This mixed activity has been observed with other compounds, such as naloxonazine [30]. SRI-45128 also displayed clear inverse agonist activity. However, the potency of this activity was considerably less than the binding affinity. This could represent the poor intrinsic efficacy of the compounds, or it could represent a relatively insensitive system for baseline receptor suppression. These details should be investigated for these compounds, working out the exact mechanisms of action and activity in different DOR-related signaling systems (e.g., ERK-MAPK activation instead of cAMP signaling). In addition, all compounds should be investigated for in vivo activity and whether the in vivo testing matches the predictions made via the in vitro testing reported here.

Materials and Methods Section 4.1.10

4.1.10. Cyclopropyl((4bS,8R,8aS,14bR)-1,8a-dihydroxy-5,6,8a,9,14,14b-hexahydro-4,8-metha nobenzofuro[2,3−a]pyrido [4,3−b]carbazol-7(8H)-yl)methanone (SYK-623)

This compound was prepared by a modification of the reported protocol [19]. A solution of compound (7) (200 mg, 0.45 mmol) in acetic acid (5 mL) was supplemented with phenylhydrazine (58.3 mg, 0.54 mmol), and the reaction mixture was refluxed for 2 h. After cooling to room temperature, the reaction mixture was concentrated and co-evaporated with toluene to afford a crude product. Saturated Na_2CO_3 was added, and the mixture was extracted with methylene chloride, dried over sodium sulfate, concentrated, chromatographed on an Isco Combiflash system using 0–5% MeOH in DCM to give a white solid which was dissolved in methanol (10 mL), and then 10% palladium black (24.6 mg, 0.02 mmol) was added to the reaction. The mixture was stirred under H_2 atmosphere (balloon) for 2 h at room temperature and filtered through celite. The celite pad was washed with MeOH (20 mL), and the filtrate was evaporated to give a white residue, which was purified by column chromatography using 0–10% MeOH in DCM to afford SYK-623 (50 mg, 48%) as a white solid. TLC (10% MeOH/DCM): R_f = 0.35; ^{1}H NMR (400 MHz, CD_3OD) δ 7.36 (ddt, J = 7.8, 6.7, 1.0 Hz, ^{1}H), 7.30 (ddt, J = 8.2, 4.1, 0.9 Hz, ^{1}H), 7.07 (dddd, J = 8.2, 7.0, 3.8, 1.2 Hz, ^{1}H), 6.94 (dddd, J = 8.0, 7.0, 4.7, 1.0 Hz, ^{1}H), 6.63–6.51 (m, ^{2}H), 5.61 (s, [0.5]H), 5.07 (d, J = 6.6 Hz, [0.5]H), 4.75 (d, J = 6.6 Hz, [0.5]H), 4.49–4.38 (m, [0.5]H), 4.18–4.08 (m, [0.5]H), 3.44 (dd, J = 18.5, 6.7 Hz, [0.5]H), 3.33–3.25 (m, ^{1}H), 3.15 (td, J = 13.4, 3.8 Hz, [0.5]H), 3.00–2.58 (m, [4]H), 2.51 (td, J = 12.8, 5.2 Hz, [0.5]H), 2.07 (tt, J = 7.9, 4.8 Hz, [0.5]H), 1.96–1.88 (m, [0.5]H), 1.71–1.62 (m, ^{1}H), 1.00–0.90 (m, ^{1}H), 0.89–0.74 (m, ^{3}H). HRMS (ESI) *m/z* calcd for $C_{26}H_{24}N_2O_4$ [M + H]+: 429.1810, found: 429.1801; HPLC (system 1) t_R = 10.7 min, purity = 96%.

2. Figure/Table Legend

In the original publication, there was a labeling mistake as explained above in the legends for Figures 1–3. SYK-623 was labeled as SRI-45127. The correct legends appear below, in which the labeling has been changed from SRI-45127 to SYK-623.

Figure 1. Novel compounds bound to the DOR with high affinity. Compounds were tested as concentration curves competing with a fixed concentration of ^{3}H-diprenorphine (see Methods). N = 3 independent replicates performed, with summary curves shown for each set; affinity (K_I) was calculated separately for each experiment and then reported as the mean ± SEM. Experimental or reference compounds (naloxone for MOR and DOR, U50-488 for KOR) were tested at each receptor, DOR, MOR, or KOR, as noted. Reference compounds displayed expected affinities, validating the experiment, while all compounds demonstrated high affinities at the DOR. SRI-45128 and SYK-623 showed poor affinity at MOR and KOR, suggesting strong DOR selectivity.

Figure 2. SRI-9342 displayed DOR irreversible antagonism at low concentrations. SNC80 is a full DOR agonist, which was used to perform multiple full concentration curves using the ^{35}S-GTPγS assay (see Methods). Increasingly large fixed concentrations of SRI-9342 were included in subsequent SNC80 curves. N = 3 independent experiments performed, with summary curves shown. Potency (EC_{50}) and efficacy (E_{MAX}) were calculated separately for each experiment and reported as the mean ± SEM. SRI-9342 caused increasing loss of efficacy at 0.1 and 1 nM without decreasing potency (which was actually higher than SNC80 alone), suggesting irreversible antagonism. Beginning at 10 nM, potency loss was observed, which could indicate mixed activity or a very strong loss of receptors from the receptor pool due to irreversible antagonist activity.

Figure 3. SRI-45128 caused DOR inverse agonist activity. SRI-45128, positive control SYK-623, and SNC80 reference compounds were used to modulate the cAMP accumulation caused by forskolin treatment (see Methods). One independent experiment in triplicate was performed, and the potency (EC_{50}) and efficacy (E_{MAX}) were reported as the derived value

with 95% confidence intervals (in parentheses). As expected, SNC80 caused high potency and efficacy cAMP inhibition, which is consistent with DOR agonist activity. SRI-45128 and SYK-623 caused efficacious cAMP increases, which is contrary to DOR agonism and consistent with DOR inverse agonism.

3. Error in Figure/Table

In the original publication, there was a mistake in Scheme 3, Figures 1 and 3 as published. As above, SYK-623 was mislabeled as SRI-45127. The corrected Scheme/Figures appear below, in which the labeling has been corrected.

Scheme 3. Reagents and conditions: (j) phenyl hydrazine, AcOH, reflux; (h) 10% Pd/C, H_2, MeOH.

Compound	Binding Affinity (K_i, nM)		
	DOR	MOR	KOR
Reference	200 ± 21	44 ± 0.6	7.2 ± 0.4
SRI-9342	4.9 ± 0.6	NT	NT
SYK-623	11 ± 1	>3,333	2000 ± 290
SRI-45128	24 ± 2	>3,333	2500 ± 510

Figure 1. Novel compounds bound to the DOR with high affinity. Compounds were tested as concentration curves competing with a fixed concentration of ^{3}H-diprenorphine (see Methods). N = 3 independent replicates performed, with summary curves shown for each set; affinity (K_I) was calculated separately for each experiment and then reported as the mean ± SEM. Experimental or reference compounds (naloxone for MOR and DOR, U50-488 for KOR) were tested at each receptor, DOR, MOR, or KOR, as noted. Reference compounds displayed expected affinities, validating the experiment, while all compounds demonstrated high affinities at the DOR. SRI-45128 and SYK-623 showed poor affinity at MOR and KOR, suggesting strong DOR selectivity.

Figure 3. SRI-45128 caused DOR inverse agonist activity. SRI-45128, positive control SYK-623, and SNC80 reference compounds were used to modulate the cAMP accumulation caused by forskolin treatment (see Methods). One independent experiment in triplicate was performed, and the potency (EC_{50}) and efficacy (E_{MAX}) were reported as the derived value with 95% confidence intervals (in parentheses). As expected, SNC80 caused high potency and efficacy cAMP inhibition, which is consistent with DOR agonist activity. SRI-45128 and SYK-623 caused efficacious cAMP increases, which is contrary to DOR agonism and consistent with DOR inverse agonism.

4. Errors in References

In the original publication, the Reference [6] has been updated as [25]; the Reference [21] has been updated as [19]. Besides, due to adding new References, the numeration of References with respect to the original publication has been modified. References [2–5] will appear in the document as References [6,8–10] respectively.

The authors apologize for any inconvenience caused and state that the scientific conclusions are unaffected. The original publication has also been updated.

References

1. Tanguturi, P.; Pathak, V.; Zhang, S.; Moukha-Chafiq, O.; Augelli-Szafran, C.E.; Streicher, J.M. Discovery of Novel Delta Opioid Receptor (DOR) Inverse Agonist and Irreversible (Non-Competitive) Antagonists. *Molecules* **2021**, *26*, 6693. [CrossRef]
2. Portoghese, P.S.; Sultana, M.; Takemori, A.E. Naltrindole 5'-isothiocyanate: A nonequilibrium, highly selective delta opioid receptor antagonist. *J. Med. Chem.* **1990**, *33*, 1547–1548. [CrossRef]
3. Carroll, F.I.; Zhang, L.; Mascarella, S.W.; Navarro, H.A.; Rothman, R.B.; Cantrell, B.E.; Zimmerman, D.M.; Thomas, J.B. Discovery of the first N-substituted 4beta-methyl-5-(3-hydroxyphenyl)morphan to possess highly potent and selective opioid delta receptor antagonist activity. *J. Med. Chem.* **2004**, *47*, 281–284. [CrossRef]
4. Nemoto, T.; Iihara, Y.; Hirayama, S.; Iwai, T.; Higashi, E.; Fujii, H.; Nagase, H. Naltrindole derivatives with fluorinated ethyl substituents on the 17-nitrogen as δ opioid receptor inverse agonists. *Bioorg. Med. Chem. Lett.* **2015**, *25*, 2927–2930. [CrossRef]
5. Iwamatsu, C.; Hayakawa, D.; Kono, T.; Honjo, A.; Ishizaki, S.; Hirayama, S.; Gouda, H.; Fujii, H. Effects of *N*-Substituents on the Functional Activities of Naltrindole Derivatives for the δ Opioid Receptor: Synthesis and Evaluation of Sulfonamide Derivatives. *Molecules* **2020**, *25*, 3792. [CrossRef]

Identification of a Novel Delta Opioid Receptor Agonist Chemotype with Potential Negative Allosteric Modulator Capabilities

Yazan J. Meqbil [1,2], Hongyu Su [1], Robert J. Cassell [1], Kendall L. Mores [1], Anna M. Gutridge [1], Benjamin R. Cummins [3], Lan Chen [4] and Richard M. van Rijn [1,4,5,*]

1   Department of Medicinal Chemistry and Molecular Pharmacology, College of Pharmacy, Purdue University, West Lafayette, IN 47907, USA; ymeqbil@purdue.edu (Y.J.M.); serenata@umich.edu (H.S.); rcassell@purdue.edu (R.J.C.); kendall.mores@nm.org (K.L.M.); Agutridg@purdue.edu (A.M.G.)
2   Computational Interdisciplinary Life Sciences, Purdue University, West Lafayette, IN 47907, USA
3   Department of Chemistry, College of Science, Purdue University, West Lafayette, IN 47907, USA; bcummins96@gmail.com
4   Purdue Institute for Drug Discovery, Purdue University, West Lafayette, IN 47907, USA; chen2178@purdue.edu
5   Purdue Institute for Integrative Neuroscience, Purdue University, West Lafayette, IN 47907, USA
*   Correspondence: rvanrijn@purdue.edu; Tel.: +1-765-494-6461

Abstract: The δ-opioid receptor (δOR) holds great potential as a therapeutic target. Yet, clinical drug development, which has focused on δOR agonists that mimic the potent and selective tool compound SNC80 have largely failed. It has increasingly become apparent that the SNC80 scaffold carries with it potent and efficacious β-arrestin recruitment. Here, we screened a relatively small (5120 molecules) physical drug library to identify δOR agonists that underrecruit β-arrestin, as it has been suggested that compounds that efficaciously recruit β-arrestin are proconvulsant. The screen identified a hit compound and further characterization using cellular binding and signaling assays revealed that this molecule (R995045, compound **1**) exhibited ten-fold selectivity over μ- and κ-opioid receptors. Compound **1** represents a novel chemotype at the δOR. A subsequent characterization of fourteen analogs of compound **1**, however did not identify a more potent δOR agonist. Computational modeling and in vitro characterization of compound **1** in the presence of the endogenous agonist leu-enkephalin suggest compound **1** may also bind allosterically and negatively modulate the potency of Leu-enkephalin to inhibit cAMP, acting as a 'NAM-agonist' in this assay. The potential physiological utility of such a class of compounds will need to be assessed in future in vivo assays.

Keywords: chemotype; high-throughput screen; delta opioid receptor; allosteric modulation; beta-arrestin; molecular dynamics

1. Introduction

The δ-opioid receptor (δOR) has great potential as a therapeutic target to treat a myriad diseases and disorders. Preclinical use of δOR agonists suggest their utility to reduce anxiety, depression, alcohol use, migraine, neuropathic and inflammatory pain [1,2]. Yet, to this day roughly 30 years since the δOR was cloned [3,4] no δOR selective molecule has been FDA approved for clinical use. Between 2008–2010 a small set of δOR agonists entered phase II clinical trials (NCT00993863, NCT01058642, NCT00759395 and NCT00979953) for acute and chronic pain conditions as well as to treat depressive disorders [5]. However, none of these trials progressed to phase 3 clinical trials. A common shared feature of the phase 2 drug candidates, ADL5859, ADL5747 and AZD2327 was that their structure was based on that of previously developed potent and highly selective δOR agonists SNC80 and BW373U86 (SNC86), (Figure 1, [6–10]). A major concern with the original

SNC compounds was their propensity to induce severe seizures in rodents [11]. AZD2327 exhibited proconvulsant effects [8], whereas Adolor was able to modify the SNC structure enough to not observe tonic-clonic seizures [6,7]. However, recent studies have led to a better understanding of the mechanism by which SNC80 can cause seizures, implicating β-arrestin as a critical factor [12,13]. The SNC compounds are super-recruiters of β-arrestin, and it appears that ADL5859 and AZD2327, recruit β-arrestin on par with the endogenous agonist Leu-enkephalin, if not stronger [14–16]. In 2020, Conibear et al., developed a novel δOR agonist PN6047 (Figure 1), based on the SNC80 scaffold, which was not proconvulsant, and which recruited β-arrestin with efficacy slightly less than ARM390 (which in our hands has an Emax on par with Leu-enkephalin) [14,17]. Thus, PN6047 shared similarity with the failed Adolor and Astra Zeneca compounds, looking promising in terms of preclinical in vivo effects, but retaining high risk for a failure once moved into human clinical trials. Thus, in order for the δOR field to progess and produce a clinically viable candidate it is important to divert from the SNC80 scaffold. A handful of δOR selective small molecules have been produced that suggest this is possible: TAN-67 and KNT-127 (Figure 1) have distinct scaffolds and under-recruit β-arrestin, respectively with Emax for β-arrestin 2 recruitment of 30%, 70% and do not induce convulsions [14,18,19]. Similarly, kratom alkaloids, while displaying pan-opioid activity, are highly G-protein biased in that they do not show detectable β-arrestin 2 recruitment [20]. Our goal for this study was to identify novel δOR agonist scaffold(s) that under-recruit β-arrestin (relative to SNC80). In this study, we screened over 5000 chemical compounds from CNS-focused drug libraries. We were able to identify a molecule (compound **1**) with a novel chemical scaffold that was selective for δOR over the μ- and κ-opioid receptors (μOR and κOR) with micromolar affinity and potency. Computational modelling of compound **1** into the δOR crystal structure (PDB: 6PT3) suggests it is able to partially occupy the known orthosteric binding pocket as well as an allosteric binding pocket in the presence of Leu-enkephalin. Further in vitro analysis showed that compound **1** potentially negatively modulates the potency of Leu-enkephalin in an allosteric manner.
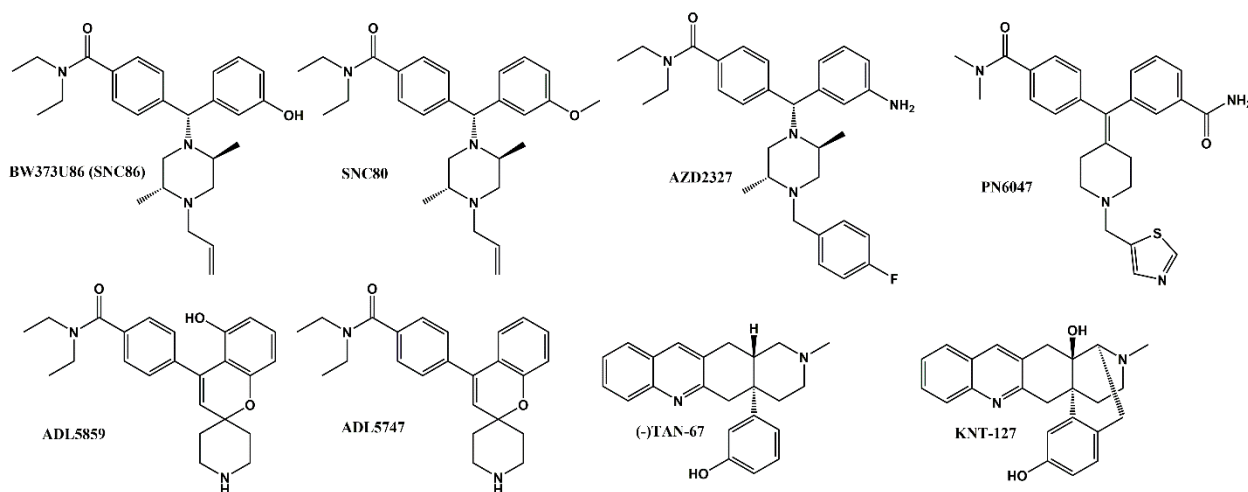
Figure 1. Chemical structure of δOR agonists. BW373U86 (SNC86), SNC80, AZD2327, PN6047, ADL5859, ADL5747, (-)TAN-67 and KNT-127.

2. Results

2.1. Identification of a Novel δOR Agonist with Sub-Maximal β-Arrestin Recruitment Efficacy

We have previously reported that SNC80 super-recruits β-arrestin 2 relative to Leu-enkephalin but has equal β-arrestin 1 recruitment efficacy [14,15]. Thus, for ease of setting a cut-off threshold we decided to perform a high-throughput screen with the β-arrestin 1 cells. We tested ~5100 compounds and identified a single positive hit, that, at a 10 μM concentration, displayed ~50% β-arrestin 1 recruitment relative to SNC80 (Figure 2).
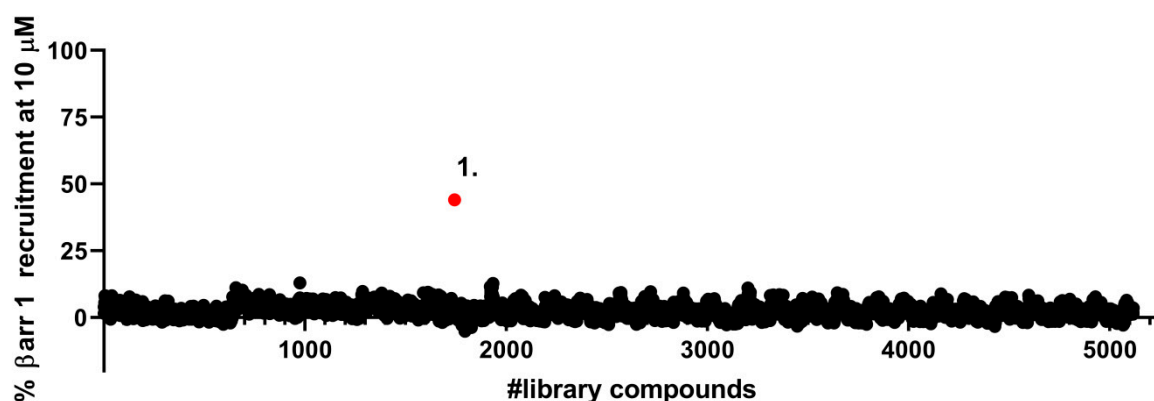
Figure 2. Screening of a CNS-targeted compound library for β-arrestin 1 recruitment at δOR. 5200 compounds from sixteen 384-well plates from diverse CNS-targeted drug libraries were tested at 10 μM for β-arrestin 1 recruitment at δORs in a PathHunter assay. The red dot represents the hit compound (**1**). 10 μM SNC80 was utilized for normalization.

2.2. Compound **1** Displays 10-Fold Selectivity over μOR and κOR

Pharmacological characterization of compound **1** revealed that it had a micromolar affinity (Figure 3A) and potency (Figure 3B) at the δOR, which was roughly 10-fold stronger than for the μOR and κOR (Table 1). Within the testable dose range (<100 μM) we were unable to detect any β-arrestin 2 recruitment for compound **1** at the μOR and κOR (Table 1, Figure 3C). At the highest concentration we were able to detect β-arrestin 1 and 2 recruitment at the δOR (Figure 3C), but we were unable to generate pEC_{50} or alpha values in these assays as we had not reached the maximum effect yet.
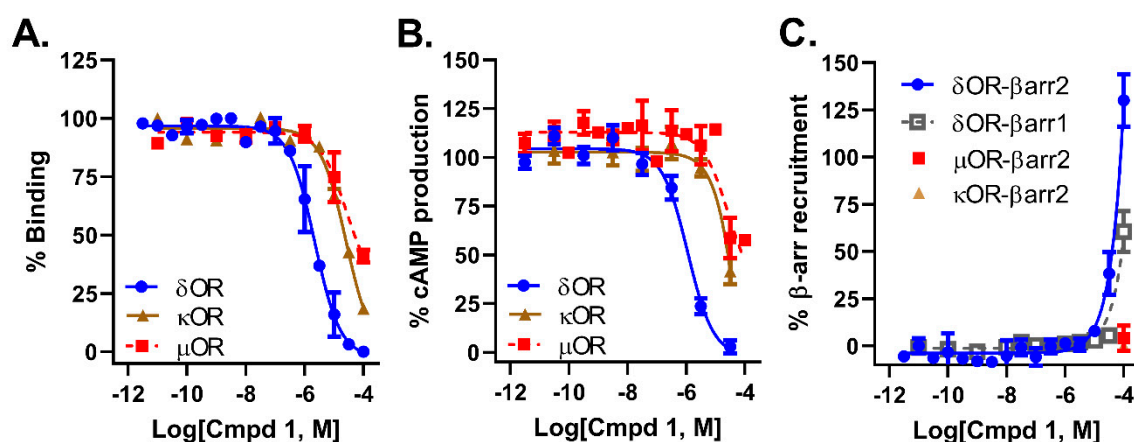
Figure 3. Pharmacological characterization of compound **1**. (**A**). Binding affinity for compound **1**. At δOR, μOR and κOR. (**B**). Inhibition of forskolin induced cAMP by compound **1** in cells expressing δOR, μOR and κOR. (**C**). β-arrestin recruitment for compound **1** following stimulation of δOR, μOR and κOR.

Table 1. Pharmacological characterization of compound **1**. All assays were run in three or more independent trials. ND = not detected.

Parameter	δOR	μOR	κOR
Affinity (pKi ± SEM)	5.94 ± 0.16	<5	<5
cAMP Potency (pIC_{50} ± SEM)	6.01 ± 0.09	<5	<5
β-ARR2 potency (pEC_{50})	<5	ND	ND
β-ARR1 potency (pEC_{50})	<5	-	-

2.3. Compound **1** Derivatives Exhibit Lower δOR Potency

The hit compound (**1**), *N'*-(2-hydroxy-3-methoxybenzylidene)-3-(2-thienyl)-1*H*-pyrazole-5-carbohydrazide, had a novel chemotype and in contrast to well-established δOR agonists Leu[5]-enkephalin, SNC80 and ADL5859 appears to lack a basic nitrogen. Next, we performed a structure activity relationship (SAR) by catalog using 14 analogs of compound **1** (Figure 4, Table 2) to investigate how compound **1** may bind to δOR and to possibly identify compounds with improved pharmacology. In our experience, potency for δOR agonism in the PathHunter β-arrestin assay is generally lower than for the cAMP assay [21]. Therefore, to assess if analogs of compound **1** displayed improved δOR potency we first characterized the compounds in the cAMP assay. We found that none of the purchased analogs had stronger potency for δOR activation than compound **1** (Table 2).
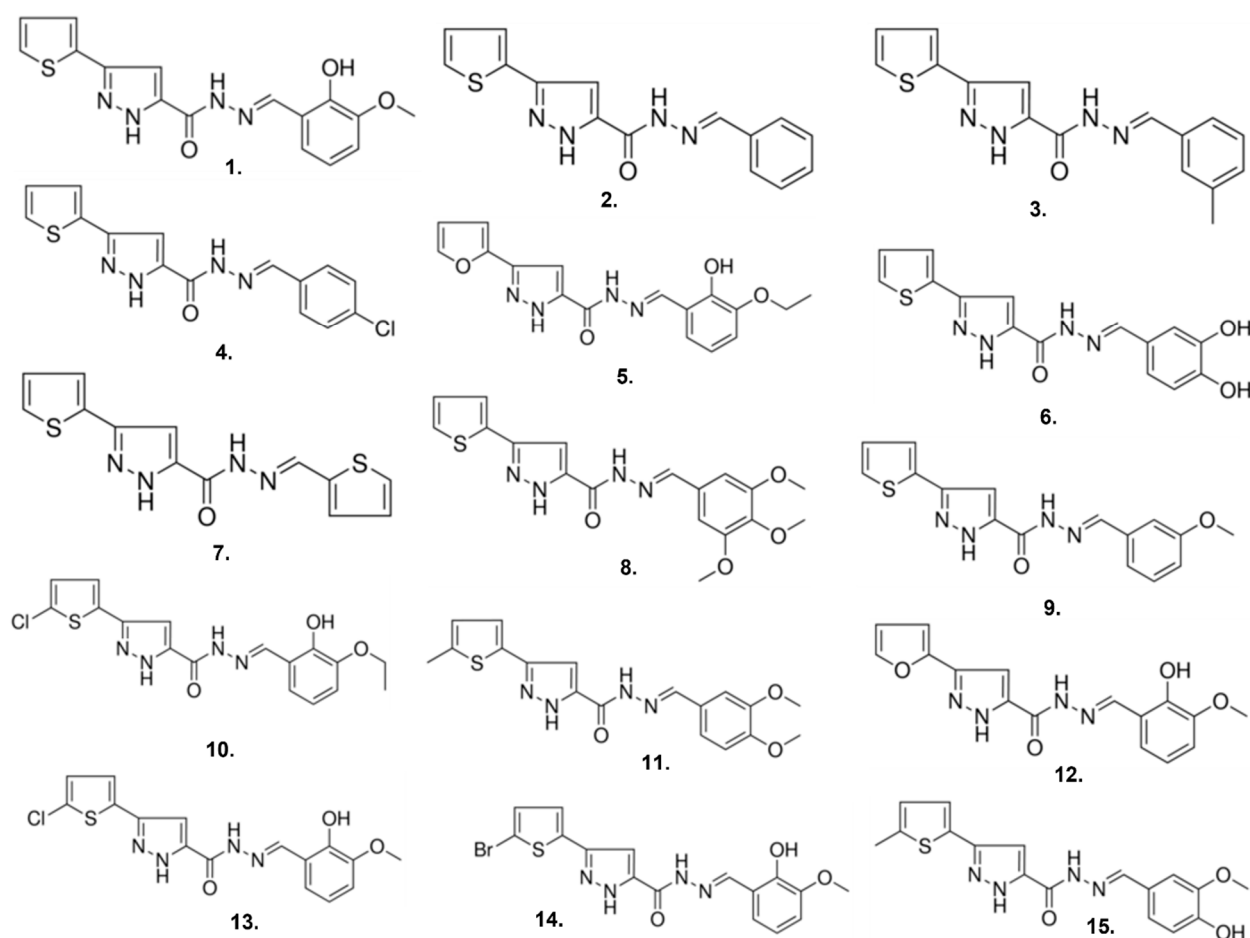
Figure 4. Chemical structures of compound **1** and **14** analogs of compound **1**.

Table 2. Potency (pIC$_{50}$) and standard error (SEM) of analogs of compound **1** to inhibit cAMP signaling at δOR. The sigma catalog number for each compound is provided. All compounds were tested in three or more independent trials.

Compound	Sigma Catalog Number	pIC50 $\pm$ SEM
1	R995045	6.0 $\pm$ 0.1
2	R563412	4.9 $\pm$ 0.1
3	R723622	5.1 $\pm$ 0.2
4	R443638	4.9 $\pm$ 0.2
5	R442488	5.0 $\pm$ 0.1
6	R910759	4.9 $\pm$ 0.2
7	R994944	ND
8	R817031	5.0 $\pm$ 0.1
9	R563420	4.8 $\pm$ 0.1
10	R729426	5.1 $\pm$ 0.2
11	R731501	5.4 $\pm$ 0.1
12	R455865	5.1 $\pm$ 0.2
13	R728691	5.1 $\pm$ 0.1
14	R729639	5.0 $\pm$ 0.1
15	L262382	5.0 $\pm$ 0.4
Leu^5-enkephalin	-	9.1 $\pm$ 0.1

*2.4. Compound **1** Engages Amino Acid Residues That Form the Orthosteric Binding Pocket*

Given the novelty of compound **1**'s scaffold, we wanted to model possible interactions of compound **1** at the δOR. We utilized the active-like crystal structure of δOR (PDB: 6PT3 [22]) to perform docking and molecular dynamics (MD) simulations in Schrödinger 2021-1. The crystal structure (6PT3) contains nine thermostabilizing mutations, three of which are near at the sodium binding pocket (N 90$^{2.45}$, D 95$^{2.50}$, N 131$^{3.35}$) and near ECL2 in transmembrane helix 2 (TM2) (Q105$^{2.60}$ and K108$^{2.62}$). Subsequently, we reverted all nine mutations to the wild-type (WT) residues (see methods and Supplementary Material). Our initial docking suggested that the thiophene ring of compound **1** occupies a hydrophobic pocket near the orthosteric site formed by W114^{ECL1}, V124$^{3.28}$, L125$^{3.29}$, C198^{ECL2} where it forms ionic bonds with K108$^{2.63}$ and hydrophobic interactions with W114^{ECL1} and C198^{ECL2} (Figure 5A). Additionally, compound **1** appeared to extend further into the orthosteric site where it was in proximity to and interacted with D128$^{3.32}$, Y129$^{3.33}$ and Y308$^{7.42}$ (Figure 5B). To confirm the initial docked poses, we docked compound **1** into multiple potential binding sites generated using SiteMap and confirmed similar interactions with residues within the hydrophobic pocket (Supplementary Figure S1). We then decided to further model the interactions of compound **1** at δOR using dynamic structures where we performed three independent all-atom MD simulations which showed a relatively stable pose for compound **1** where it interacts with residues in TM2, ECL1, TM3 and ECL2 (L200^{ECL2}) and occasionally with residues in TM5 (K214$^{5.40}$) and TM7 (Figure 5C,D, Supplementary Figures S2 and S3).
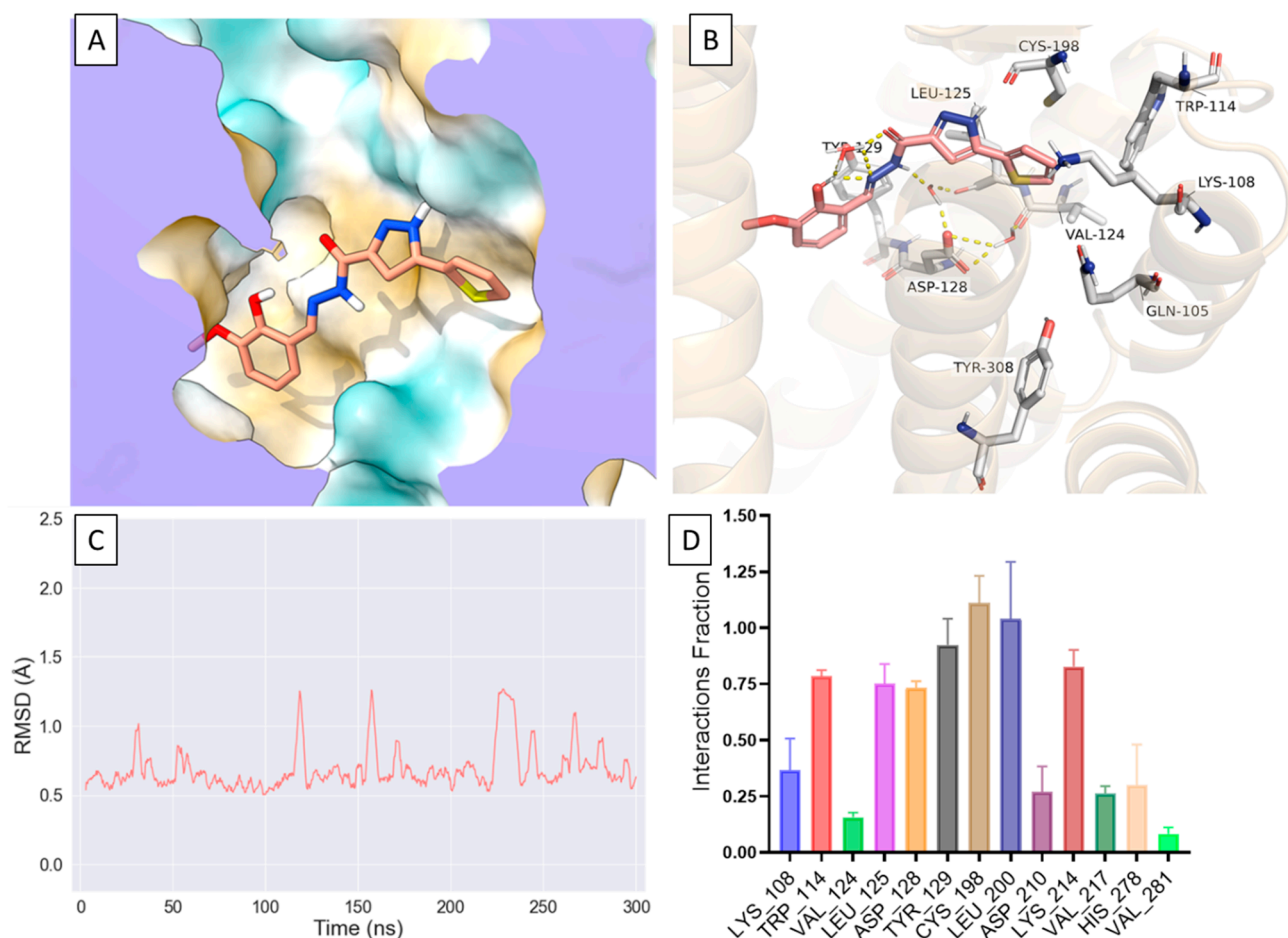
Figure 5. Molecular Dynamic simulation of Compound **1** binding to the δOR. (**A**). Compound **1** bound at δOR where its positioned within the hydrophobic pocket, a predicted allosteric site. (**B**). Compound **1** interacts with residues forming the hydrophobic pocket as well as with residues deeper into the orthosteric site K108$^{2.63}$, W114^{ECL1}, L125$^{3.29}$, D128$^{3.32}$, Y129$^{3.33}$, C198^{ECL2}, L200^{ECL2} and K214$^{5.40}$. (**C**). A rolling average of 3 ns of the RMSD of compound **1** in a 300 ns MD simulation showing a relatively stable binding pose for compound **1**. (**D**). Interaction fractions between compound **1** and the δOR in 3 different MD simulations.

2.5. Compound **1** Can Occupy an Allosteric Space alongside Leu-Enkephalin

Our modeling suggests that compound **1** interacts with residues in TM2 and TM7, which have been previously reported to interact, potentially, with the positive allosteric modulator BMS 986187 [23]. At the orthosteric site, compound **1** forms water-mediated interactions, hydrogen bonds and hydrophobic interactions with D128$^{3.32}$, Y129$^{3.33}$ and H278$^{6.62}$ residues which were reported to be involved in δOR activation [22]. Additionally, compound **1** interacts with W114^{ECL1} (π-π stacking), V124$^{3.28}$, L125$^{3.29}$, C198^{ECL2} where its thiophene moiety occupies a partially hydrophobic pocket that is adjacent to the orthosteric site (Figure 5A). These unique interactions which include amino acid residues in the orthosteric and the potential allosteric binding sites prompted us to model compound **1** in the presence of Leu-enkephalin using molecular dynamics (MD) simulations (Figure 6A, Supplementary Figure S4). Intriguingly, compound **1** appears to maintain a relatively stable orientation as shown by the relatively stable RMSD in three independent MD simulations whereas Leu-enkephalin undergoes more dramatic confirmational changes in the presence of compound **1** (Figure 6B–D). Specifically, the presence of compound **1** appears to disrupt the π-π interaction between Leu-enkephalin with W284$^{6.58}$ where the phenyl group of Phe^4 rotates away from W284$^{6.58}$ (Figure 6C). We also observed an inward shift in ICL2 as well as conformational changes at the intracellular side of δOR in ICL2, TM5 and TM6 when compared to the thermostabilized crystal structure (Supplementary Figure S5).
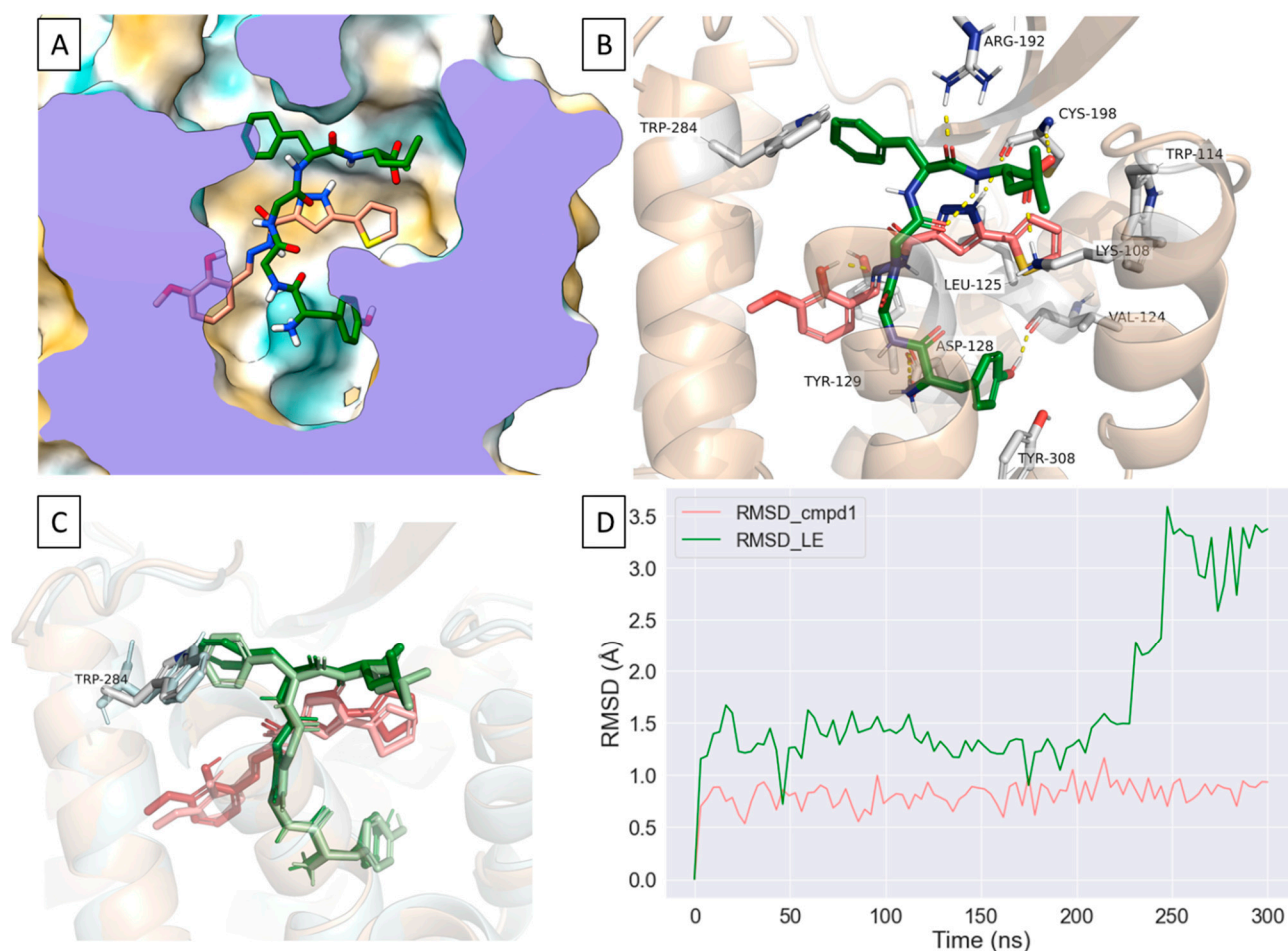
Figure 6. Molecular dynamic simulation of Compound **1** bound to the δOR in the presence of Leu-enkephalin. (**A**). a representative binding pose for compound **1** in the presence of Leu-enkephalin obtained from a 300 ns MD simulation where compound **1** stably occupies the partially hydrophobic pocket. (**B**). Leu-enkephalin forms H-bonds and water mediated interactions with K108$^{2.63}$, D128$^{3.32}$, R192^{ECL2}, C198^{ECL2}, H301$^{7.35}$, C303$^{7.37}$ and hydrophobic interactions with Y308$^{7.42}$ whereas compound **1** mostly interacts with W114^{ECL1}, L125$^{3.29}$, C198^{ECL2} and L200^{ECL2} and K214$^{5.40}$. (**C**). Poses of Leu-enkephalin and compound **1** showing the first frame of a 300 ns MD simulation (Leu-enkephalin: light green, compound **1**: light pink, W284: cyan) aligned on the clustered poses of Leu-enkephalin and compound **1** (Leu-enkephalin: dark green, compound **1**: red, W284$^{6.58}$: light grey). (**D**). A rolling average of 3 ns of the RMSD of compound **1** in the presence of Leu-enkephalin obtained from a 300 ns MD simulation showing a relatively stable pose for compound **1** whereas the disruption of Leu-enkephalin's interaction with W284$^{6.58}$ causes a relatively large change in its RMSD.

2.6. Compound **1** Potentially Negatively Modulates Potency of Leu-Enkephalin through an Allosteric Mechanism

Given that our modelling efforts suggested binding poses in a slightly allosteric binding pocket, we next decided to measure to what degree compound **1** modulated the activity profile of leu-enkephalin in the cAMP glosensor assay. We noted an increase in baseline (or τ_β) when Leu-enkephalin was co-incubated with increasing concentrations of compound **1** (Figure 7A,B), without observing a chance in E$_{max}$ (β = 1). We observed a left-shift in Leu-enkephalin potency suggestive of a negative allosteric modulation that is affinity (or α) driven (Figure 7A,B). As such, compound **1** appears to act as a negative allosteric modulator (NAM)-agonist [24] in the cAMP glosensor assay. It is well known that, for example, irreversible antagonists by lowering the receptor reserve will right-shift the potency of an agonist [25]. Thus, the potency shift could also be driven by the decrease in receptors available for Leu-enkephalin to bind to since radioligand binding indicates that compound **1** can bind and displace agonists (Figure 3) from the binding pocket.
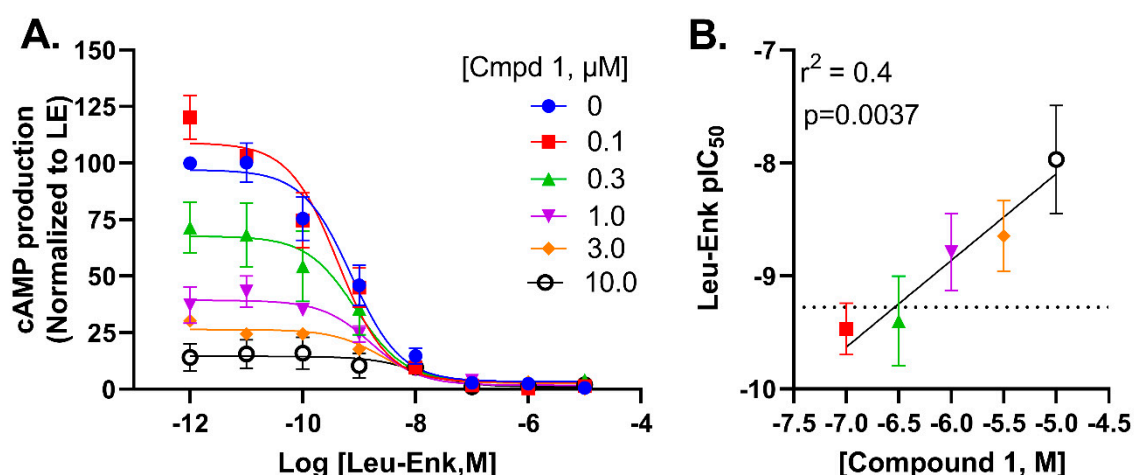
Figure 7. Compound **1** acts as a negative allosteric modulator for leu-enkephalin potency in the cAMP glosensor assay. (**A**). Dose-dependent inhibition of forskolin-mediated cAMP production by Leu-enkephalin (Leu-Enk) in the absence or presence of increasing concentrations of compound **1**. (**B**). The decrease in Leu-enkephalin pIC50 is correlated with increasing concentration of compound **1**.

3. Discussion

Here we report on a novel δOR-selective agonist chemotype that was identified from a 5120-compound high-throughput screen of CNS-targeted chemical libraries. The scaffold lacks a basic protonated amine, which is generally considered a hallmark feature of opioid ligands, needed to form a stable salt-bridge with aspartate $D^{3.32}$ [22]. Using MolgpKa [26], the predicted pKa of the basic nitrogen in the pyrazole ring of compound **1** is 1.4, in sharp contrast with the pKa for protonated basic amines that is closer to physiological pH. A second interesting feature of compound **1** is the apparent negative allosteric modulation of the endogenous agonist Leu-enkephalin. Positive allosteric modulators (PAMs) have been identified for the opioid receptors, including the G-protein-biased δOR 'PAM-agonist' BMS 986187 (Figure 8) [24,27–29]. Cannabidiol and tetrahydrocannabinol have been proposed to be allosteric modulators of the δOR, specifically accelerating naltrindole dissociation rate [30], however to our knowledge no NAM-agonist has previously been reported.
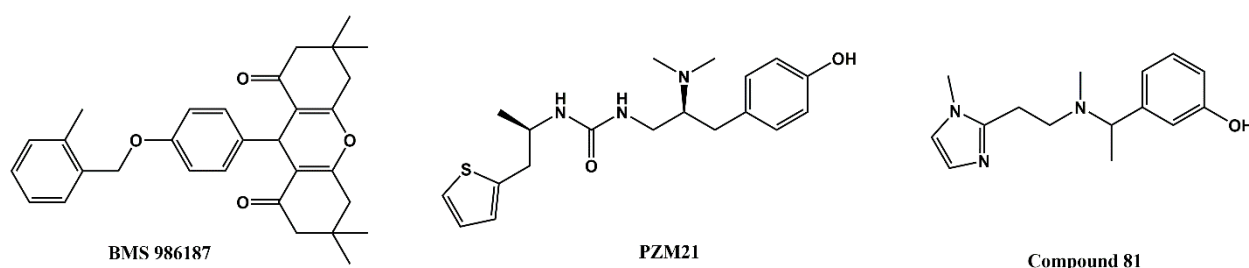
Figure 8. Chemical structures of the allosteric G-protein-biased δOR modulator BMS 986187, the G-protein-biased μOR agonist PZM21 and the G-protein-biased κOR agonist compound 81.

The PAM-agonist BMS 986187 does not possess an ionizable group and thus resembles our compound **1**, which also lacks the protonated amine commonly present in opioids. However, comparisons between the suggested mode of binding of BMS 986187 and compound **1** at δOR show distinct interactions that could account for the differences in their mode of action. Notably, in the presence of the endogeneous peptide Leu-enkephalin, compound **1** appears to occupy a partially hydrophobic pocket adjacent to the orthosteric site which allows compound **1** to interact with residues in ECL1 (W114[ECL1]), ECL2 (C198, L200) and TM7, whereas BMS 986187 is reported to interact with residues in TM2 and TM7 in its lowest relative free-energy state in the presence of SNC80 [23]. Moreover, most of the residues reported to interact with BMS 986187 were shown to interact

with residues in the active-like structures of δOR that constitute the orthosteric binding site [22,23]. These differences in the interactions could account for the distinct pharmacology of compound **1** and BMS 986187. Intriguingly, in the presence or absence of Leu-enkephalin, compound **1** maintains a relatively stable orientation that enables it to retain its hydrophobic and water-mediated interactions at the thiophene and pyrazole rings, respectively (Figure 6A,D). The presence of Leu-enkephalin, however, appears to disrupt the water-mediated interactions between compound **1** and orthosteric residues D128$^{3.32}$ and Y129$^{3.33}$ (Figure 6B) and changes the number of hydrogen donors or acceptors in compound **1** (Supplementary Figure S5). On the other hand, the presence of compound **1** disrupts the hydrophobic interaction between Phe^4 and δOR by causing the phenyl group of Leu-enkephalin to rotate away from the side chain of W284$^{6.58}$ (Figure 6C). Additionally, H-bond and water-mediated interactions between Leu-enkephalin and R192^{ECL2} appear to move ECL2 toward Leu-enkephalin which could open a cryptic binding site similar to a previously reported allosteric binding site in the angiotensin II (AngII) type 1 receptor [31] (Figure 6B, Supplementary Figure S6). As such, we predict that compound **1** may induce NAM activity by either destabilizing Leu-enkephalin or by playing an analogous role to BMS 986187 where it stabilizes the Na$^+$ binding at δOR which increases the likelihood of receptor deactivation. It should be noted that comparisons between the binding modes of compound **1** and BMS 986187 at the δOR are limited due to the differences in the crystal structures used for modeling (agonist-bound vs antagonist-bound, respectively), chemotype differences between compound **1** and BMS 986187, the modeling method utilized, and the co-simulated ligand. Hence, future studies should examine the binding of compound **1** at the δOR in the presence of small molecule agonists and the implementation of enhanced sampling methods to model its interactions in the presence or absence of δOR agonists.

After identifying compound **1** in our screen, we had hoped to find analogs with higher potency, through a SAR by catalog. However, none of the purchased analogs displayed improved potency for the δOR. Our choice of catalog analogs was driven primarily by price and availability and much less guided by intelligent design. As a result of this strategy, we were only able to explore minor derivatization at the thiopene moiety and the 2-hydroxy-3-methoxybenzene moiety. Therefore, it is possible that compound **1** may still be improved on, for example, by altering or substituting on the pyrazole group, or by adding hydrogen bond-forming and/or accepting groups on the thiophene moiety.

Another feature we set out to find in our screen was a δOR agonist that underrecruited β-arrestin. Much effort has been devoted to identify opioids that display a preference to recruit and activate G-proteins relative to β-arrestin recruitment [17,21,32–34]. Our screen was designed with the purpose of finding molecules that underrecruit β-arrestin, but that are not G-protein-selective i.e., that entirely avoid β-arrestin recruitment and as such, compound **1** does still recruit β-arrestin. Surprisingly, we noted an unusual steep increase in β-arrestin recruitment at the δOR when stimulated with 100 μM compound **1**, such that we were unable to accurately predict an Emax. The sharp rise in β-arrestin recruitment at 100 μM did not appear to be a pan- interference assay effect, as we did not observe a similar response in our μOR and κOR PathHunter cell lines (Figure 3C). The mechanism or implication of compound **1**′s β-arrestin recruitment at 100 μM will require further investigation.

With increased availability of apo-state, antagonist-bound and agonist bound opioid structures, drug screening has moved away from screening physical libraries to screening virtual libraries. A computational model created using the crystal structure of an antagonist bound κOR [35] supported a virtual chemical library screen of 5 million molecules at κOR resulting in the identification of compound 81 (Figure 8), which is a G-protein-biased agonist with an 0.16 μM affinity and 0.53 μM potency at the κOR [36]. A virtual screen of 3 million molecules docked at a computational model of the μOR based on the antagonist-bound μOR crystal structure [37] resulted in the identification of a hit with 2.5 μM affinity at the μOR, which through an analog screen was improved to a lead compound with a 42 nM affinity and G protein bias. Further structure guided optimization of the lead compound

resulted in the design of PZM21 (Figure 8), a G-protein-biased μOR-selective agonist with 1 nM affinity and unique chemotype [32]. Recent advances now allow for virtual screening of libraries containing more than a billion compounds [38,39]. While it is undeniable that large virtual screens can identify completely novel chemical matter, the ability to discover molecules with novel pharmacology may be more limited or biased by the type of structure (e.g., an orthosteric agonist-bound structure stabilized by a heterotrimeric G-protein or nanobody-mimic in a single active conformation) used for docking. Thus, in conclusion, our results highlight a current persisting value of chemical library screens in identifying molecules with unique binding modes and pharmacology.

4. Materials and Methods

4.1. Chemicals

Leu[5]-enkephalin, compounds **1–15** and forskolin were purchased from Sigma-Aldrich (St. Louis, MO USA). [D-Ala[2], N-MePhe[4], Gly-ol] enkephalin (DAMGO), SNC80 and U50,488 were purchased from Tocris Bioscience (Minneapolis, MN, USA). Radiolabels were from Perkin Elmer (Waltham, MA, USA).

4.2. Library Screen

In consultation with the Chemical Genomics Facility within the Purdue Institute for Drug Discovery, we screened sixteen 384-well plates that were part of CNS-targeted drug libraries. Specifically, we screened eleven plates part of a CNS-Chemdiv library, three plates part of a Chembridge ion channel library, and two plates part of a CNS-TimTec library. Each plate contained 320 compounds and four spare columns that were utilized to run positive (10 μM SNC80, 32 wells) and negative controls (0.02% DMSO, 32 wells), which were used to calculate Z-factors (average: Z′= 0.53, hit plate: Z′= 0.58) and normalize the data across plates. Using an Echo 525 acoustic liquid handler (Labcyte, San Jose, CA, USA), depending on the stock concentration (1, 10 or 20 mM) of the library plate 5, 10 or 100 nL of each compound was transferred from the library plate to the assay plate, the final concentration of each library compound was 10 μM.

4.3. Radioligand Binding Assay

Radioligand binding was performed as previously described [40,41]. For the binding assay 50 μL of a dilution series of peptide was added to 50 μL of 3.3 nM [^{3}H]DPDPE (K_d = 3.87 nM) or 2.35 nM of [^{3}H]DAMGO (K_d = 1.07 nM) or 0.8 nM of [^{3}H]U69,593 (K_d = 1.2 nM) in a clear 96 well plate. Next, 100 μL of membrane suspension containing 7 μg protein was added to the agonist wells and incubated for 90 min at room temperature. The reaction mixture was then filtered over a GF-B filter plate (Perkin Elmer) followed by four quick washes with ice-cold 50 mM Tris HCl. The plate was dried overnight, after which 50 μL scintillation fluid (Ultimagold uLLT) was added and radioactivity was counted on a Packard TopCount NXT scintillation counter. All working solutions were prepared in a radioligand assay buffer containing 50 mM Tris HCl, 10 mM MgCl$_2$, and 1 mM ethylenediaminetetraacetic acid at pH 7.4.

4.4. Cellular Signaling Assays

cAMP inhibition and β-arrestin 1 and 2 recruitment assays were performed as previously described [18]. In brief, for cAMP inhibition assays HEK 293 (Life Technologies, Grand Island, NY, USA) cells were transiently transfected in a 1:3 ratio with FLAG-mouse δOR, or HA-mouse μOR and pGloSensor22F-cAMP plasmids (Promega, Madison, WI, USA) using Xtremegene9 (Sigma). Two days post-transfection cells (20,000 cells/well, 7.5 μL) were seeded in low volume Greiner 384-well plates (#82051-458, VWR, Batavia, IL, USA) and were incubated with Glosensor reagent (Promega, 7.5 μL, 2% final concentration) for 90 min at room temperature. Cells were stimulated with 5 μL drug solution for 20 min at room temperature prior to stimulation with 5 μL forskolin (final concentration 30 μM), for an additional 15 min at room temperature. For β-arrestin recruitment assays, CHO-

human µOR PathHunter β-arrestin 2 cells, CHO-human δOR PathHunter β-arrestin 2 cells, U2OS κOR PathHunter β-arrestin 2 cells or U2OS PathHunter β-arrestin 1 cells (DiscoverX, Fremont, CA, USA) were plated (2500 cells/well, 10 µL) one day prior to stimulation with 2.5 µL or 5–100 nL (in the screen) drug solution for 90 min at 37 °C/5% CO_2, after which cells were incubated with 6 µL cell PathHunter assay buffer (DiscoverX) for 60 min at room temperature as per the manufacturer's protocol. Luminescence for each of these assays was measured using a FlexStation3 plate reader (Molecular Devices, Sunnyvale, CA, USA). As positive control we utilized Leu[5]-enkephalin or SNC80 (in the screen) for δOR, [D-Ala[2], N-MePhe[4], Gly-ol] enkephalin (DAMGO) for µOR and U50,488 for κOR.

4.5. Assessment of Allosteric Modulation

We ran log-step concentration response curves for Leu-enkephalin (10 µM–1 pM) in the presence of 0, 0.1, 0.3, 1, 3, or10 µM compound **1** in the δOR glosensor cAMP assay.

4.6. Data and Statistical Analysis

All data are presented as means ± standard error of the mean, and analysis was performed using GraphPad Prism 8 software (GraphPad Software, La Jolla, CA, USA). For in vitro assays, nonlinear regression was conducted to determine pIC_{50} (cAMP) or pEC_{50} (β-arrestin recruitment). Technical replicates were used to ensure the reliability of single values, specifically each data point for binding and β-arrestin recruitment was run in duplicate, and for the cAMP assay in triplicate. The averages of each independent run were counted as a single experiment and combined to provide a composite curve in favor of providing a 'representative' curve.

4.7. Receptor and Ligand Preparation for Molecular Modeling

The crystal structure of the active-like δOR (PDB: 6PT3) bound to small molecule agonist, DPI-287, was obtained from the Protein Data Bank (PDB) [22]. Molecular modeling was performed via Maestro (Schrödinger suite 2021-1, Schrödinger, Inc., New York, NY, USA). The *Protein Preparation Wizard* was used to prepare the structures before docking. The crystal structure was preprocessed to cap the N-terminus, remove the BRIL tag, membrane lipids and other crystal waters or ions not involved in mediating receptor-ligand interaction. Preliminary modeling and energy minimization of the thermostabilized receptor [22] and the WT-reverted receptor (data not shown) showed the feasibility of performing MD simulations using a truncated version of the WT receptor (residues 41–289) where all 9-thermostabilizing mutations were reverted to the WT (Supplementary Figure S5). Missing loops and side chains in the crystal structure were modeled using *Prime* within Schrödinger [42–44]. H-bond were assigned using the PROPKA algorithm [45,46]. All-atom MD simulations were performed on the modeled receptor using Desmond (Schrödinger, Inc.) implementing the OPLS4 force field. Compound **1** was prepared using LigPrep where the ionization states were assigned using Epik at pH 7.0 ± 2.0 [47,48]. Docking grids were generated for a representative structure from the MD simulations using *Receptor Grid Generation* in Schrödinger Release 2021-1 (Schrödinger, Inc.) using default parameters.

4.8. Ligand Docking Using Glide

Compound **1** and a set of known δOR ligands (Table 1) were docked into a model WT δOR using Glide (Table 2) [49–51]. Further structural optimization was needed to improve the docking accuracy of the model WT δOR (Supplemental Table S3). Additionally, given the novelty of the compound **1**'s chemotype, δOR ligands were docked into several models with predicted binding sites that were generated using SiteMap [52,53]. The best model was selected for further production MD simulations. Standard precision (SP) scoring function in Schrodinger 2021-1 was used for the initial docking of the molecules. The extra precision (XP) scoring function was then to further refine the docked poses. Post-docking energy minimization was performed for the top 50 poses of each small molecule, after which top 10 poses were visually inspected. The top 50 docked poses were also

scored using Prime MM-GBSA scoring [54]. The best pose (based on docking, visual inspection and MM-GBSA score) was selected for subsequent production MD simulations (Supplemental Tables S4–S6).

4.9. Molecular Dynamics Simulations of Compound **1** at δOR

Production molecular dynamics simulations (MD) were performed in Desmond as reported previously [55]. Ligand-receptor complexes were embedded in a POPC membrane contained in a SPC-solvated orthorhombic box while maintaining a 10 Å distance from box boundaries. Na^+ and Cl^- ions at a concentration of 0.15 M were added to mimic biological conditions using System Builder in Schrodinger 2021-1. The default membrane relaxation protocol in Desmond was used for membrane relaxation. Then a constant pressure and temperature (NPT) equilibration run was performed for 100 ns. The RESPA integrator with a 2 fs integration step for bonded interactions and a 6 fs step for non-bonded interactions. The Nosé-Hoover thermostat (and Martyna-Tobias-Klein barostat with semi-isotropic coupling to maintain temperature at 300 K and pressure at 1 bar. For the production MD simulations, three independent 200 ns NPT simulations were carried out for compound **1** in complex with modeled δOR or compound **1** and Leu-enkephalin in complex with modeled δOR. Each trajectory was assembled into 10 clusters using the trajectory clustering protocol implemented in Desmond. The top five clusters with the most interacting members were further assessed using Prime MM-GBSA (Supplemental Tables S7 and S8). The top poses were further inspected and used for analyses and figures presented here.

Supplementary Materials: The following are available, Figure S1: Binding sites within the δOR structure generated using SiteMap, Figure S2: $C\alpha$ RMSD of δOR and compound **1** obtained from 3 independent MD simulations with varying trajectory time lengths and starting points, Figure S3: Receptor and ligand RMSD across several MD simulations, Figure S4: Summary of key δOR amino acid interactions with compound **1** and Leu-Enkephalin in the presence of compound **1**, Figure S5: Pharmacophore mapping analysis using the receptor-ligand complex. Figure S6: Comparison of the thermostabilized and simulated wild-type agonist-bound δOR structures. Table S1: Smiles of δOR agonists and antagonists used to validate the initial docking models, Table S2: Docking and glide scores for known δOR agonists and antagonists used to validate the initial docking model before structural optimization of the model δOR, Table S3: Docking and glide scores for known δOR agonists and antagonists used to validate the initial docking model after structural optimization, Table S4: Compound **1** docking scores using the SP scoring function. Top 10 poses were rescored XP scoring function, Table S5: Top 15 Leu-enkephalin poses docked into model δOR in the presence of compound **1**, Table S6: Rescoring of top 50 poses of Leu-enkephalin docked into model δOR using Prime MM-GBSA, Table S7: MM-GBSA scoring of top 5 clusters from a 300 ns MD simulation for Leu-enkephalin and compound **1**, Table S8: MM-GBSA scoring of top 5 clusters from a 300 ns MD simulation for compound **1**.

Author Contributions: Conceptualization, R.M.v.R. and Y.J.M.; methodology, L.C., Y.J.M.; validation, Y.J.M. and H.S.; formal analysis, R.M.v.R., Y.J.M., H.S. and R.J.C.; investigation, R.M.v.R., Y.J.M., H.S., R.J.C., K.L.M., A.M.G. and B.R.C.; writing—original draft preparation, R.M.v.R. and Y.J.M.; writing—review and editing, R.M.v.R. and Y.J.M.; visualization, R.M.v.R. and Y.J.M.; supervision, R.M.v.R.; project administration, R.M.v.R.; funding acquisition, R.M.v.R. All authors have read and agreed to the published version of the manuscript.

Institutional Review Board Statement: Not applicable.

Informed Consent Statement: Not applicable.

Data Availability Statement: Not applicable.

Conflicts of Interest: The authors declare no conflict of interest.

Sample Availability: The compounds are available from commercial vendors e.g., Sigma.

References

1. Pradhan, A.A.; Befort, K.; Nozaki, C.; Gaveriaux-Ruff, C.; Kieffer, B.L. The delta opioid receptor: An evolving target for the treatment of brain disorders. *Trends Pharm. Sci.* **2011**, *32*, 581–590. [CrossRef]
2. Van Rijn, R.M.; Defriel, J.N.; Whistler, J.L. Pharmacological traits of delta opioid receptors: Pitfalls or opportunities? *Psychopharmacology* **2013**, *228*, 1–18. [CrossRef]
3. Evans, C.J.; Keith, D.E., Jr.; Morrison, H.; Magendzo, K.; Edwards, R.H. Cloning of a delta opioid receptor by functional expression. *Science* **1992**, *258*, 1952–1955. [CrossRef] [PubMed]
4. Kieffer, B.L.; Befort, K.; Gaveriaux-Ruff, C.; Hirth, C.G. The delta-opioid receptor: Isolation of a cDNA by expression cloning and pharmacological characterization. *Proc. Natl. Acad. Sci. USA* **1992**, *89*, 12048–12052. [CrossRef] [PubMed]
5. Nagase, H.; Saitoh, A. Research and development of kappa opioid receptor agonists and delta opioid receptor agonists. *Pharm. Ther.* **2020**, *205*, 107427. [CrossRef]
6. Le Bourdonnec, B.; Windh, R.T.; Ajello, C.W.; Leister, L.K.; Gu, M.; Chu, G.H.; Tuthill, P.A.; Barker, W.M.; Koblish, M.; Wiant, D.D.; et al. Potent, orally bioavailable delta opioid receptor agonists for the treatment of pain: Discovery of *N,N*-diethyl-4-(5-hydroxyspiro[chromene-2,4′-piperidine]-4-yl)benzamide (ADL5859). *J. Med. Chem.* **2008**, *51*, 5893–5896. [CrossRef]
7. Le Bourdonnec, B.; Windh, R.T.; Leister, L.K.; Zhou, Q.J.; Ajello, C.W.; Gu, M.; Chu, G.H.; Tuthill, P.A.; Barker, W.M.; Koblish, M.; et al. Spirocyclic delta opioid receptor agonists for the treatment of pain: Discovery of *N,N*-diethyl-3-hydroxy-4-(spiro[chromene-2,4′-piperidine]-4-yl) benzamide (ADL5747). *J. Med. Chem.* **2009**, *52*, 5685–5702. [CrossRef] [PubMed]
8. Hudzik, T.J.; Maciag, C.; Smith, M.A.; Caccese, R.; Pietras, M.R.; Bui, K.H.; Coupal, M.; Adam, L.; Payza, K.; Griffin, A.; et al. Preclinical pharmacology of AZD2327: A highly selective agonist of the delta-opioid receptor. *J. Pharmacol. Exp. Ther.* **2011**, *338*, 195–204. [CrossRef]
9. Calderon, S.N.; Rothman, R.B.; Porreca, F.; Flippen-Anderson, J.L.; McNutt, R.W.; Xu, H.; Smith, L.E.; Bilsky, E.J.; Davis, P.; Rice, K.C. Probes for narcotic receptor mediated phenomena. 19. Synthesis of (+)-4-[(alpha R)-alpha-((2S,5R)-4-allyl-2,5-dimethyl-1-piperazinyl)-3-methoxybenzyl]-*N,N*-diethylbenzamide (SNC 80): A highly selective, nonpeptide delta opioid receptor agonist. *J. Med. Chem.* **1994**, *37*, 2125–2128. [CrossRef]
10. Chang, K.J.; Rigdon, G.C.; Howard, J.L.; McNutt, R.W. A novel, potent and selective nonpeptidic delta opioid receptor agonist BW373U86. *J. Pharmacol. Exp. Ther.* **1993**, *267*, 852–857.
11. Broom, D.C.; Jutkiewicz, E.M.; Folk, J.E.; Traynor, J.R.; Rice, K.C.; Woods, J.H. Convulsant activity of a non-peptidic delta-opioid receptor agonist is not required for its antidepressant-like effects in Sprague-Dawley rats. *Psychopharmacology* **2002**, *164*, 42–48. [CrossRef]
12. Vicente-Sanchez, A.; Dripps, I.J.; Tipton, A.F.; Akbari, H.; Akbari, A.; Jutkiewicz, E.M.; Pradhan, A.A. Tolerance to high-internalizing delta opioid receptor agonist is critically mediated by arrestin 2. *Br. J. Pharmacol.* **2018**, *175*, 3050–3059. [CrossRef]
13. Blaine, A.T.; Palant, S.; Yuan, J.; Van Rijn, R.M. Role of β-arrestin Isoforms in Delta Opioid Receptor Agonist-Induced Seizures. *FASEB J.* **2021**, *35*. [CrossRef]
14. Chiang, T.; Sansuk, K.; van Rijn, R.M. Beta-arrestin 2 dependence of delta opioid receptor agonists is correlated with alcohol intake. *Br. J. Pharmacol.* **2016**, *173*, 323–343. [CrossRef] [PubMed]
15. Ko, M.J.; Chiang, T.; Mukadam, A.A.; Mulia, G.E.; Gutridge, A.M.; Lin, A.; Chester, J.A.; van Rijn, R.M. beta-Arrestin-dependent ERK signaling reduces anxiety-like and conditioned fear-related behaviors in mice. *Sci. Signal.* **2021**, *14*, eaba0245. [CrossRef] [PubMed]
16. Crombie, A.; Arezzo, J.; Cowan, C.; DeWire, S.; Gowen-McDonald, W.; Hawkins, M.; Jutkiewicz, E.; Kramer, M.; Koblish, M.; Lark, M.; et al. TRV250: A novel G protein-biased ligand at the delta receptor for the potential treatment of migraine. *Postgrad. Med.* **2015**, *127* (Suppl. 1), S61.
17. Conibear, A.E.; Asghar, J.; Hill, R.; Henderson, G.; Borbely, E.; Tekus, V.; Helyes, Z.; Palandri, J.; Bailey, C.; Starke, I.; et al. A Novel G Protein-Biased Agonist at the delta Opioid Receptor with Analgesic Efficacy in Models of Chronic Pain. *J. Pharmacol. Exp. Ther.* **2020**, *372*, 224–236. [CrossRef] [PubMed]
18. Nagase, H.; Nemoto, T.; Matsubara, A.; Saito, M.; Yamamoto, N.; Osa, Y.; Hirayama, S.; Nakajima, M.; Nakao, K.; Mochizuki, H.; et al. Design and synthesis of KNT-127, a delta-opioid receptor agonist effective by systemic administration. *Bioorg. Med. Chem. Lett.* **2010**, *20*, 6302–6305. [CrossRef]
19. Nagase, H.; Wakita, H.; Kawai, K.; Endoh, T.; Matsura, H.; Tanaka, C.; Takezawa, Y. Syntheses of non-peptidid delta opioid agonists and their structure activity relationships. *Jpn. J. Pharmacol.* **1994**, *64*. [CrossRef]
20. Gutridge, A.M.; Robins, M.T.; Cassell, R.J.; Uprety, R.; Mores, K.L.; Ko, M.J.; Pasternak, G.W.; Majumdar, S.; van Rijn, R.M. G protein-biased kratom-alkaloids and synthetic carfentanil-amide opioids as potential treatments for alcohol use disorder. *Br. J. Pharmacol.* **2020**, *177*, 1497–1513. [CrossRef]
21. Cassell, R.J.; Sharma, K.K.; Su, H.; Cummins, B.R.; Cui, H.; Mores, K.L.; Blaine, A.T.; Altman, R.A.; van Rijn, R.M. The Meta-Position of Phe(4) in Leu-Enkephalin Regulates Potency, Selectivity, Functional Activity, and Signaling Bias at the Delta and Mu Opioid Receptors. *Molecules* **2019**, *24*, 4542. [CrossRef]

22. Claff, T.; Yu, J.; Blais, V.; Patel, N.; Martin, C.; Wu, L.; Han, G.W.; Holleran, B.J.; Van der Poorten, O.; White, K.L.; et al. Elucidating the active delta-opioid receptor crystal structure with peptide and small-molecule agonists. *Sci. Adv.* **2019**, *5*, eaax9115. [CrossRef] [PubMed]

23. Shang, Y.; Yeatman, H.R.; Provasi, D.; Alt, A.; Christopoulos, A.; Canals, M.; Filizola, M. Proposed Mode of Binding and Action of Positive Allosteric Modulators at Opioid Receptors. *ACS Chem. Biol.* **2016**, *11*, 1220–1229. [CrossRef] [PubMed]

24. Christopoulos, A.; Changeux, J.P.; Catterall, W.A.; Fabbro, D.; Burris, T.P.; Cidlowski, J.A.; Olsen, R.W.; Peters, J.A.; Neubig, R.R.; Pin, J.P.; et al. International Union of Basic and Clinical Pharmacology. XC. multisite pharmacology: Recommendations for the nomenclature of receptor allosterism and allosteric ligands. *Pharmacol. Rev.* **2014**, *66*, 918–947. [CrossRef]

25. Kelly, E. Efficacy and ligand bias at the mu-opioid receptor. *Br. J. Pharmacol.* **2013**, *169*, 1430–1446. [CrossRef]

26. Pan, X.; Wang, H.; Li, C.; Zhang, J.Z.H.; Ji, C. MolGpka: A Web Server for Small Molecule pKa Prediction Using a Graph-Convolutional Neural Network. *J. Chem. Inf. Model.* **2021**, *61*, 3159–3165. [CrossRef]

27. Stanczyk, M.A.; Livingston, K.E.; Chang, L.; Weinberg, Z.Y.; Puthenveedu, M.A.; Traynor, J.R. The delta-opioid receptor positive allosteric modulator BMS 986187 is a G-protein-biased allosteric agonist. *Br. J. Pharmacol.* **2019**, *176*, 1649–1663. [CrossRef]

28. Burford, N.T.; Clark, M.J.; Wehrman, T.S.; Gerritz, S.W.; Banks, M.; O'Connell, J.; Traynor, J.R.; Alt, A. Discovery of positive allosteric modulators and silent allosteric modulators of the mu-opioid receptor. *Proc. Natl. Acad. Sci. USA* **2013**, *110*, 10830–10835. [CrossRef]

29. Burford, N.T.; Wehrman, T.; Bassoni, D.; O'Connell, J.; Banks, M.; Zhang, L.; Alt, A. Identification of selective agonists and positive allosteric modulators for micro- and delta-opioid receptors from a single high-throughput screen. *J. Biomol. Screen.* **2014**, *19*, 1255–1265. [CrossRef]

30. Kathmann, M.; Flau, K.; Redmer, A.; Trankle, C.; Schlicker, E. Cannabidiol is an allosteric modulator at mu- and delta-opioid receptors. *Naunyn. Schmiedebergs. Arch. Pharmacol.* **2006**, *372*, 354–361. [CrossRef] [PubMed]

31. Singh, K.D.; Jara, Z.P.; Harford, T.; Saha, P.P.; Pardhi, T.R.; Desnoyer, R.; Karnik, S.S. Novel allosteric ligands of the angiotensin receptor AT1R as autoantibody blockers. *Proc. Natl. Acad. Sci. USA* **2021**, *118*. [CrossRef] [PubMed]

32. Manglik, A.; Lin, H.; Aryal, D.K.; McCorvy, J.D.; Dengler, D.; Corder, G.; Levit, A.; Kling, R.C.; Bernat, V.; Hubner, H.; et al. Structure-based discovery of opioid analgesics with reduced side effects. *Nature* **2016**, *537*, 185–190. [CrossRef]

33. Schmid, C.L.; Kennedy, N.M.; Ross, N.C.; Lovell, K.M.; Yue, Z.; Morgenweck, J.; Cameron, M.D.; Bannister, T.D.; Bohn, L.M. Bias Factor and Therapeutic Window Correlate to Predict Safer Opioid Analgesics. *Cell* **2017**, *171*, 1165–1175.e13. [CrossRef] [PubMed]

34. Chen, X.T.; Pitis, P.; Liu, G.; Yuan, C.; Gotchev, D.; Cowan, C.L.; Rominger, D.H.; Koblish, M.; Dewire, S.M.; Crombie, A.L.; et al. Structure-activity relationships and discovery of a G protein biased mu opioid receptor ligand, [(3-methoxythiophen-2-yl)methyl]({2-[(9R)-9-(pyridin-2-yl)-6-oxaspiro-[4.5]decan- 9-yl]ethyl})amine (TRV130), for the treatment of acute severe pain. *J. Med. Chem.* **2013**, *56*, 8019–8031. [CrossRef] [PubMed]

35. Wu, H.; Wacker, D.; Mileni, M.; Katritch, V.; Han, G.W.; Vardy, E.; Liu, W.; Thompson, A.A.; Huang, X.P.; Carroll, F.I.; et al. Structure of the human kappa-opioid receptor in complex with JDTic. *Nature* **2012**, *485*, 327–332. [CrossRef]

36. Zheng, Z.; Huang, X.P.; Mangano, T.J.; Zou, R.; Chen, X.; Zaidi, S.A.; Roth, B.L.; Stevens, R.C.; Katritch, V. Structure-Based Discovery of New Antagonist and Biased Agonist Chemotypes for the Kappa Opioid Receptor. *J. Med. Chem.* **2017**, *60*, 3070–3081. [CrossRef]

37. Manglik, A.; Kruse, A.C.; Kobilka, T.S.; Thian, F.S.; Mathiesen, J.M.; Sunahara, R.K.; Pardo, L.; Weis, W.I.; Kobilka, B.K.; Granier, S. Crystal structure of the micro-opioid receptor bound to a morphinan antagonist. *Nature* **2012**, *485*, 321–326. [CrossRef]

38. Lyu, J.; Wang, S.; Balius, T.E.; Singh, I.; Levit, A.; Moroz, Y.S.; O'Meara, M.J.; Che, T.; Algaa, E.; Tolmachova, K.; et al. Ultra-large library docking for discovering new chemotypes. *Nature* **2019**, *566*, 224–229. [CrossRef]

39. Stein, R.M.; Kang, H.J.; McCorvy, J.D.; Glatfelter, G.C.; Jones, A.J.; Che, T.; Slocum, S.; Huang, X.P.; Savych, O.; Moroz, Y.S.; et al. Virtual discovery of melatonin receptor ligands to modulate circadian rhythms. *Nature* **2020**, *579*, 609–614. [CrossRef]

40. Cassell, R.J.; Mores, K.L.; Zerfas, B.L.; Mahmoud, A.H.; Lill, M.A.; Trader, D.J.; van Rijn, R.M. Rubiscolins are naturally occurring G protein-biased delta opioid receptor peptides. *Eur. Neuropsychopharmacol.* **2019**, *29*, 450–456. [CrossRef]

41. Creed, S.M.; Gutridge, A.M.; Argade, M.D.; Hennessy, M.R.; Friesen, J.B.; Pauli, G.F.; van Rijn, R.M.; Riley, A.P. Isolation and Pharmacological Characterization of Six Opioidergic Picralima nitida Alkaloids. *J. Nat. Prod.* **2021**, *84*, 71–80. [CrossRef] [PubMed]

42. Farid, R.; Day, T.; Friesner, R.A.; Pearlstein, R.A. New insights about HERG blockade obtained from protein modeling, potential energy mapping, and docking studies. *Bioorg. Med. Chem.* **2006**, *14*, 3160–3173. [CrossRef]

43. Sherman, W.; Beard, H.S.; Farid, R. Use of an induced fit receptor structure in virtual screening. *Chem. Biol. Drug. Des.* **2006**, *67*, 83–84. [CrossRef] [PubMed]

44. Sherman, W.; Day, T.; Jacobson, M.P.; Friesner, R.A.; Farid, R. Novel procedure for modeling ligand/receptor induced fit effects. *J. Med. Chem.* **2006**, *49*, 534–553. [CrossRef] [PubMed]

45. Olsson, M.H.; Sondergaard, C.R.; Rostkowski, M.; Jensen, J.H. PROPKA3: Consistent Treatment of Internal and Surface Residues in Empirical pKa Predictions. *J. Chem. Theory. Comput.* **2011**, *7*, 525–537. [CrossRef] [PubMed]

46. Sondergaard, C.R.; Olsson, M.H.; Rostkowski, M.; Jensen, J.H. Improved Treatment of Ligands and Coupling Effects in Empirical Calculation and Rationalization of pKa Values. *J. Chem. Theory. Comput.* **2011**, *7*, 2284–2295. [CrossRef]

47. Greenwood, J.R.; Calkins, D.; Sullivan, A.P.; Shelley, J.C. Towards the comprehensive, rapid, and accurate prediction of the favorable tautomeric states of drug-like molecules in aqueous solution. *J. Comput. Aided. Mol. Des.* **2010**, *24*, 591–604. [CrossRef]

48. Shelley, J.C.; Cholleti, A.; Frye, L.L.; Greenwood, J.R.; Timlin, M.R.; Uchimaya, M. Epik: A software program for pK(a) prediction and protonation state generation for drug-like molecules. *J. Comput. Aided. Mol. Des.* **2007**, *21*, 681–691. [CrossRef] [PubMed]

49. Friesner, R.A.; Banks, J.L.; Murphy, R.B.; Halgren, T.A.; Klicic, J.J.; Mainz, D.T.; Repasky, M.P.; Knoll, E.H.; Shelley, M.; Perry, J.K.; et al. Glide: A new approach for rapid, accurate docking and scoring. 1. Method and assessment of docking accuracy. *J. Med. Chem.* **2004**, *47*, 1739–1749. [CrossRef]

50. Friesner, R.A.; Murphy, R.B.; Repasky, M.P.; Frye, L.L.; Greenwood, J.R.; Halgren, T.A.; Sanschagrin, P.C.; Mainz, D.T. Extra precision glide: Docking and scoring incorporating a model of hydrophobic enclosure for protein-ligand complexes. *J. Med. Chem.* **2006**, *49*, 6177–6196. [CrossRef]

51. Halgren, T.A.; Murphy, R.B.; Friesner, R.A.; Beard, H.S.; Frye, L.L.; Pollard, W.T.; Banks, J.L. Glide: A new approach for rapid, accurate docking and scoring. 2. Enrichment factors in database screening. *J. Med. Chem.* **2004**, *47*, 1750–1759. [CrossRef]

52. Halgren, T. New method for fast and accurate binding-site identification and analysis. *Chem. Biol. Drug. Des.* **2007**, *69*, 146–148. [CrossRef] [PubMed]

53. Halgren, T.A. Identifying and characterizing binding sites and assessing druggability. *J. Chem. Inf. Model.* **2009**, *49*, 377–389. [CrossRef] [PubMed]

54. Sastry, G.M.; Adzhigirey, M.; Day, T.; Annabhimoju, R.; Sherman, W. Protein and ligand preparation: Parameters, protocols, and influence on virtual screening enrichments. *J. Comput. Aided. Mol. Des.* **2013**, *27*, 221–234. [CrossRef] [PubMed]

55. Zhou, Y.; Ramsey, S.; Provasi, D.; El Daibani, A.; Appourchaux, K.; Chakraborty, S.; Kapoor, A.; Che, T.; Majumdar, S.; Filizola, M. Predicted Mode of Binding to and Allosteric Modulation of the mu-Opioid Receptor by Kratom's Alkaloids with Reported Antinociception In Vivo. *Biochemistry* **2021**, *60*, 1420–1429. [CrossRef] [PubMed]

Synthesis, Pharmacological Evaluation, and Computational Studies of Cyclic Opioid Peptidomimetics Containing β³-Lysine

Karol Wtorek [1] , **Piotr F. J. Lipiński** [2] , **Anna Adamska-Bartłomiejczyk** [1], **Justyna Piekielna-Ciesielska** [1],
Jarosław Sukiennik [3], **Alicja Kluczyk** [4] and **Anna Janecka** [1,*]

1   Department of Biomolecular Chemistry, Medical University of Lodz, Mazowiecka 6/8, 92-215 Lodz, Poland;
    karol.wtorek@umed.lodz.pl (K.W.); anna.adamska@umed.lodz.pl (A.A.-B.);
    justyna.piekielna@umed.lodz.pl (J.P.-C.)
2   Department of Neuropeptides, Mossakowski Medical Research Institute, Polish Academy of Sciences,
    Pawińskiego 5, 02-106 Warsaw, Poland; plipinski@imdik.pan.pl
3   TriMen Chemicals Ltd., 92-318 Lodz, Poland; sukiennik@trimen.pl
4   Faculty of Chemistry, University of Wroclaw, 50-383 Wroclaw, Poland; alicja.kluczyk@chem.uni.wroc.pl
*   Correspondence: anna.janecka@umed.lodz.pl

Abstract: Our formerly described pentapeptide opioid analog Tyr-c[D-Lys-Phe-Phe-Asp]NH₂ (designated **RP-170**), showing high affinity for the mu (MOR) and kappa (KOR) opioid receptors, was much more stable than endomorphine-2 (EM-2) in the rat brain homogenate and displayed remarkable antinociceptive activity after central (intracerebroventricular) and peripheral (intravenous) administration. In this report, we describe the further modification of this analog, which includes the incorporation of a β³-amino acid, (R)- and (S)-β³-Lys, instead of D-Lys in position 2. The influence of such replacement on the biological properties of the obtained analogs, Tyr-c[(R)-β³-Lys-Phe-Phe-Asp]NH₂ (**RP-171**) and Tyr-c[(S)-β³-Lys-Phe-Phe-Asp]NH₂, (**RP-172**), was investigated in vitro. Receptor radiolabeled displacement and functional calcium mobilization assays were performed to measure binding affinity and receptor activation of the new analogs. The obtained data revealed that only one of the diastereoisomeric peptides, **RP-171**, was able to selectively bind and activate MOR. Molecular modeling (docking and molecular dynamics (MD) simulations) suggests that both compounds should be accommodated in the MOR binding site. However, in the case of the inactive isomer **RP-172**, fewer hydrogen bonds, as well as instability of the canonical ionic interaction to Asp¹⁴⁷, could explain its very low MOR affinity.

Keywords: opioid receptors; β-amino acids; peptide synthesis; receptor binding studies; functional assay

1. Introduction

Among the three opioid receptors, mu (MOR), delta (DOR), and kappa (KOR), MOR plays the most important role in the modulation of pain signals and, therefore, is an important target in medicinal chemistry and drug development [1]. The two endogenous compounds activating MOR are endomorphin-1 (EM-1, Tyr-Pro-Trp-Phe-NH₂) and endomorphin-2 (EM-2, Tyr-Pro-Phe-Phe-NH₂) [2]. Over the years, numerous chemical modifications of these ligands have been reported in order to provide specific information on their structure–activity relationship and to find drug candidates with improved therapeutic properties [3–5]. Among various modifications of opioid peptides, cyclization of their linear structures was used to restrict flexibility and to obtain better-defined conformations, allowing for the identification of receptor binding sites [6–9].

Endomorphins are very short peptides lacking reactive side chain groups, which makes their cyclization difficult. One of the structural elements considered essential for their binding to MOR is the free cationic amino group of Tyr¹ [10–12], and this feature does not encourage head-to-tail cyclization. In order to obtain cyclic analogs based on the structure of

EM-2 but still to preserve the free N-terminal amino group, we introduced into the sequence of EM-2 additional amino acids with functionalized side chains. A pentapeptide analog Tyr-c[D-Lys-Phe-Phe-Asp]NH$_2$ (designated **RP-170**), in which cyclization was achieved through the amide bond between D-Lys and Asp side chains, displayed high affinity for MOR, was much more stable than EM-2 in the rat brain homogenate and showed remarkable antinociceptive activity after central (i.c.v.) and peripheral (i.v.) administration [13]. The presence of a D-amino acid in position 2 (as in opioid peptides isolated from amphibian skin) was shown to enforce a different conformation of a peptide, greatly improving MOR binding as compared with Tyr-c[Lys-Phe-Phe-Asp]NH$_2$ [14]. Molecular docking studies of **RP-170** revealed that the amino group of Tyr[1] provided ionic interactions with Asp[147] residue in the transmembrane helice TM III of the receptor, while Asp amide effectively interacted with Asp[216] and Cys[217] belonging to the extracellular loop EL II. The presence of a Lys residue allowed for the formation of another strong interaction between Asp[147] and Lys-NH [15].

Further modifications of **RP-170** produced analogs with different opioid receptor preferences. Introduction of Dmt instead of Tyr[1] increased cyclopeptide affinity to MOR [16]. The reduction in the ring size increased MOR selectivity [17]. Substitution of the Phe residues by amino acids fluorinated in the aromatic ring (4-F-Phe, 2,4-diF-Phe, 4-CF$_3$Phe) produced either high-affinity MOR/KOR agonists, non-selective MOR/DOR/KOR agonists, or selective KOR agonists [18], indicating that even small modifications in the side chains can completely change their orientation in the receptor cavity.

In the present study, we investigated the influence of a β-amino acid on the biological properties of **RP-170**. D-Lys was replaced by (*R*)- or (*S*)-β^3-Lys, obtained by homologation of D- or L-ornitine (Orn). This modification produced compounds isomeric to **RP-170** with the same size of the macrocyclic ring (17-membered), as in the parent peptide. Opioid receptor binding and activation were studied, and the obtained results were rationalized by molecular docking and molecular dynamics (MD) simulations.

2. Results

2.1. Synthesis of Protected (R)- and (S)-β^3-Lys

(*R*)- and (*S*)-Fmoc-β^3-Lys (Mtt), which are not available commercially, were obtained by homologation of D- and L-Orn, respectively, according to the general procedure [19]. The synthetic protocol is outlined in Scheme 1.
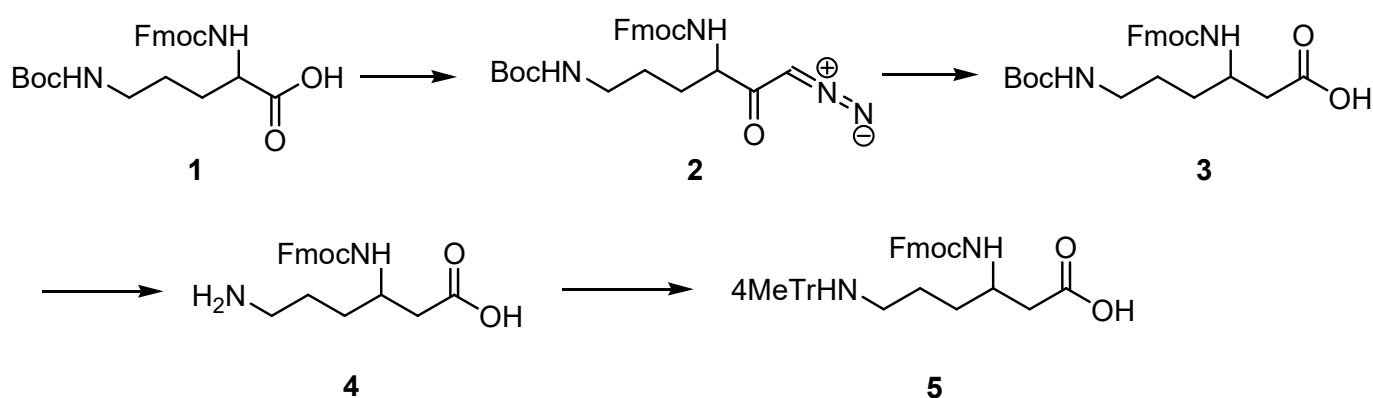
Scheme 1. Synthesis of Fmoc-(R)- and (S)-β^3-Lys(Mtt).

2.2. Synthesis of Cyclopeptides

Cyclopeptides containing a β-amino acid, Tyr-c[(*R*)-β^3-Lys-Phe-Phe-Asp]NH$_2$ (**RP-171**) and Tyr-c[(*S*)-β^3-Lys-Phe-Phe-Asp]NH$_2$ (**RP-172**) (Figure 1) were synthesized on the solid support, using Fmoc/t-Bu strategy, with the hyper-acid labile groups (Mtt and O-2-PhiPr) for the selective protection of amine/carboxyl side chains of (*R*)- and (*S*)-β^3-Lys and Asp, engaged in cyclization. After deprotection of the functionalized side chains, the linear

sequences were cyclized through amide bond formation. Final products were obtained with a purity greater than 95%, as assessed by semi-preparative RP-HPLC. The detailed analytical data of the synthesized peptides are provided in the Supplementary Materials (Table S1, Figures S2 and S3).
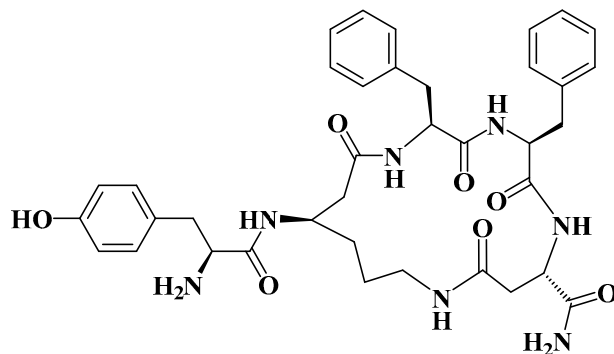
Tyr-c[(*R*)-β^3-Lys-Phe-Phe-Asp]NH$_2$ **RP-171**
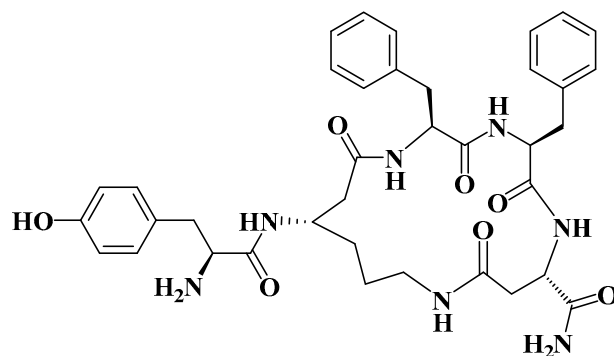
Tyr-c[(*S*)-β^3-Lys-Phe-Phe-Asp]NH$_2$ **RP-172**

Figure 1. Chemical structure of **RP-171** and **RP-172**.

2.3. LC-MS, LC-MS^n, and Quantum Chemical Calculation Studies

During the routine LC-MS analysis of analogs **RP-171** and **RP-172**, we noticed a distinct difference in retention times and MS^n patterns for these diastereoisomeric peptides. To confirm our observation, we subjected a mixture of these peptides to LC-MS and MS^n experiments. The HPLC analysis in reversed-phase mode revealed that the isomeric peptides separate easily, using both C$_{18}$ column (Aeris Peptide) and biphenyl column (Kinetex Biphenyl), known for additional π-π interactions [20], with a nearly 0.5 min retention time difference in both cases in a 10 min gradient run from 5 to 80% acetonitrile in water (Figure 2 and Figures S4–S6). Such a difference in retention time suggests altered interactions with the stationary phase, probably due to the shape of the molecules. It is interesting that the elution order from the biphenyl column was the same as from the C$_{18}$ column.

To assign the order of isomeric peptides in the LC-MS experiment on the **RP-171** and **RP-172** peptide mixture (Figure 2), we used retention times obtained during analysis of pure peptides, supported by MS^n spectra. As expected, the MS spectra of peptides **RP-171** and **RP-172** were identical (panels **RP-171** MS and **RP-172** MS), and the difference in their collision-induced dissociation (MS^2, panels **RP-171** MS/MS, and **RP-172** MS/MS) was related to an intensity of 586 *m/z* fragment ion. To find a more reliable distinction, the MS^3 spectra were obtained for the precursors 586 from MS^2 spectra (panels **RP-171** MS/MS/MS and **RP-172** MS/MS/MS, MS^3 discussion in the Supplementary Materials).
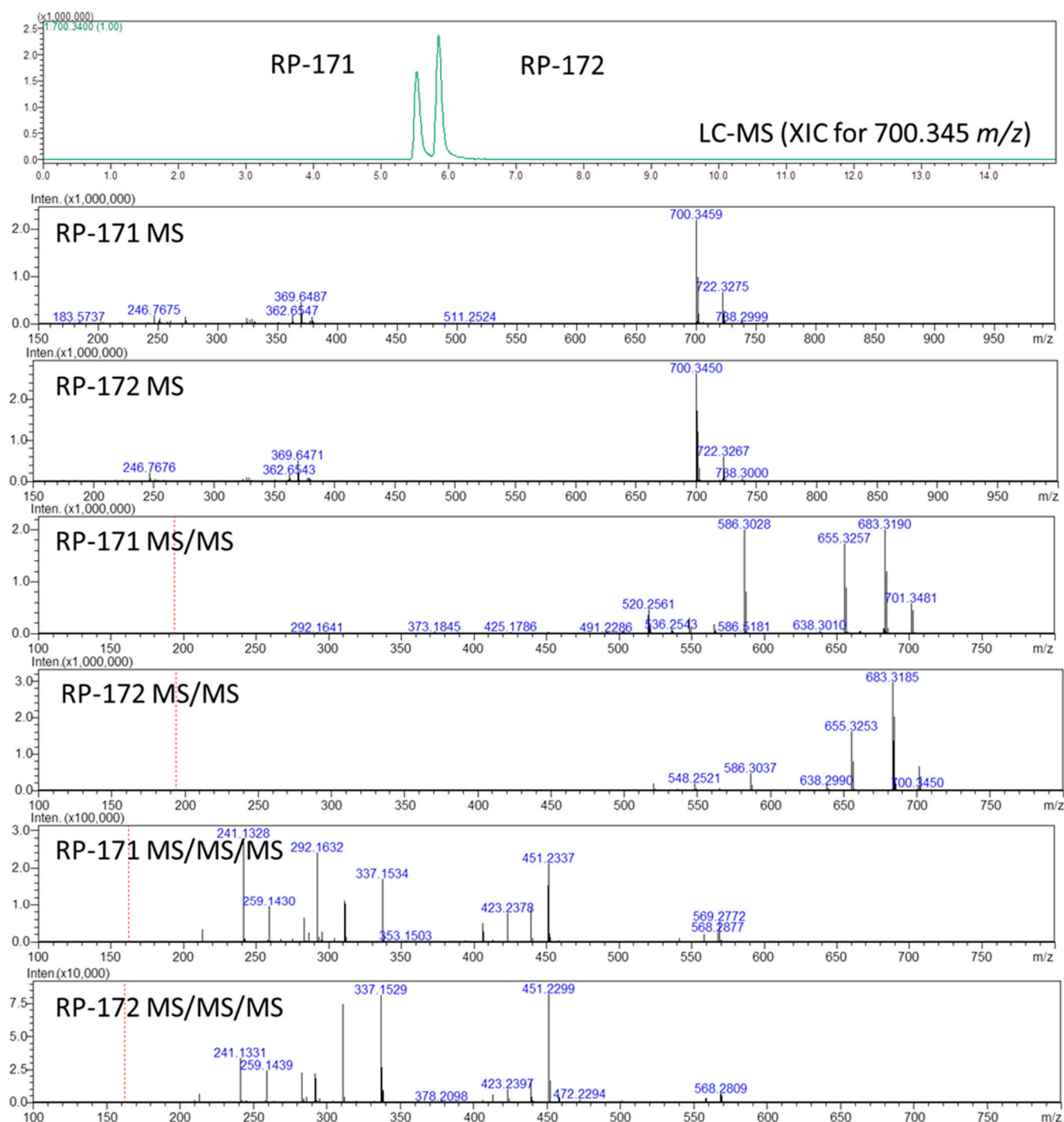
Figure 2. LC-MS[n] analysis of peptides **RP-171** and **RP-172**. Extracted ion chromatogram (XIC) showing two peaks for the mixture of peptides (top panel): MS panels, all spectra recorded for the retention time of indicated peaks; MS spectra, MS/MS spectra for the precursor ions *m/z* 700.34, and MS/MS/MS spectra for the precursor ions *m/z* 586.30.

The fragment ions observed in the MS/MS spectra were typical for peptide amides (consecutive loss of ammonia, 683 *m/z*, and carbon monoxide 655 *m/z*), whereas the 586 ion resulted from ring-opening and removal of the Asp residue. The difference in intensity of the 586 *m/z* ions in panels **RP-171** MS/MS and **RP-172** MS/MS suggests that the fragmentation of peptide **RP-171** occurs easier than in the case of **RP-172**, suggesting that peptide **RP-172** containing (S)-β^3-Lys is more stable.

This observation corresponds to the results of quantum chemical calculations (performed with Gaussian09 [21], Table S2) for both isomers. The lowest-lying (at the B3LYP/6-31G(d,p) level) gas-phase conformer of the [(S)-β^3-Lys^2]- analog is more stable by 3.5 kcal/mol (ΔG_{298}) than the lowest-lying conformer of the [(R)-β^3- Lys]- analog. The structures differ with respect to the intramolecular hydrogen bonds present (Figure 3). In the [(R)-β^3-Lys]- analog, the Tyr^1 amino group interacts with the backbone carbonyl oxygens of Phe^4 and Asp^5. This arrangement might facilitate internal cyclization upon the Asp residue loss. On the other hand, in **RP-172**, the Tyr^1 amino group interacts with the carbonyl oxygens of (S)-β^3-Lys^2 and of the exocyclic $CONH_2$.

RP-171   **RP-172**
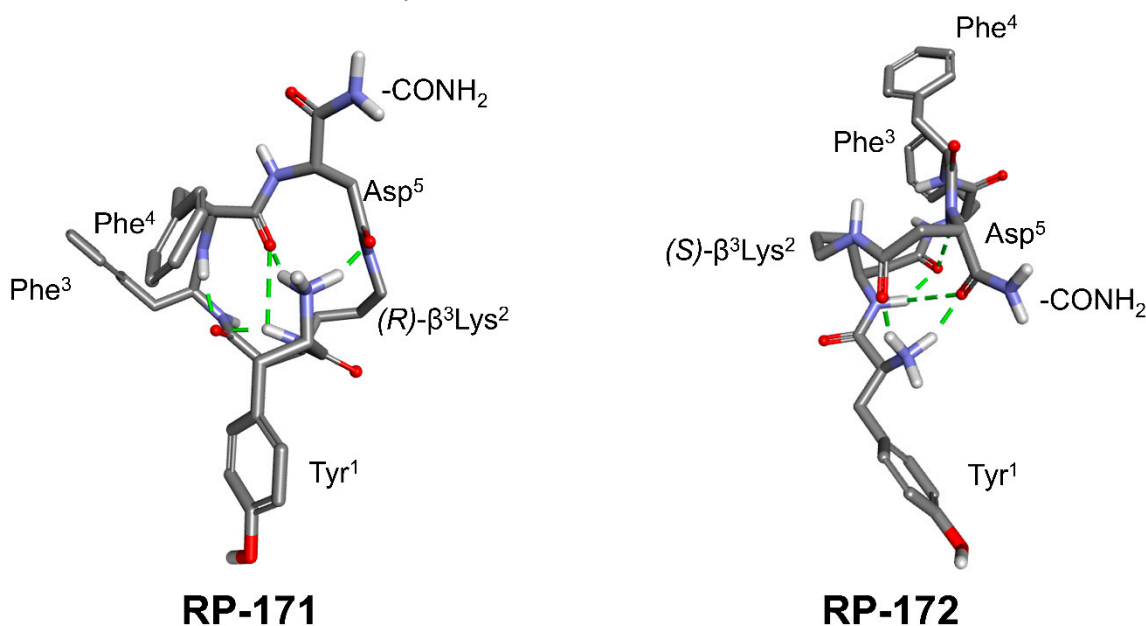
Figure 3. The lowest-lying conformers of **RP-171** and **RP-172** (at the B3LYP/6-31G(d,p) in the gas phase. Green dots show intramolecular hydrogen bonding.

2.4. Receptor Binding and Functional Activity

The binding affinities of cyclopeptides **RP-171** and **RP-172** toward MOR, DOR, and KOR were determined by competitive binding against [^{3}H]DAMGO, [^{3}H][D-Ala^2]deltorphin-2, and U-69593, respectively, using membranes of CHO cells transfected with opioid receptors and are summarized in Table 1.

Table 1. Receptor binding affinities (K_i) of novel cyclic analogs at MOR, DOR, KOR.

No.	Sequence	K_i [a] [nM]		
		MOR	**DOR**	**KOR**
RP-170	Tyr-c[D-Lys-Phe-Phe-Asp]NH$_2$	0.55 ± 0.02	198 ± 4.5	1.52 ± 0.20
RP-171	Tyr-c[(R)-β^3-Lys-Phe-Phe-Asp]NH$_2$	29 ± 4.32	>1000	420 ± 23
RP-172	Tyr-c[(S)-β^3-Lys-Phe-Phe-Asp]NH$_2$	950 ± 45	>1000	>1000

[a] Binding affinities were determined by competitive displacement of the selective radioligands, [^{3}H]DAMGO (MOR), [^{3}H]deltorphin-2 (DOR), and [^{3}H]U-69593 (KOR) using commercial membranes of CHO cells transfected with human opioid receptors. Values are expressed as mean $\pm$ SEM, n = 3.

The parent compound **RP-170** displayed subnanomolar affinity to MOR, nanomolar to KOR, and did not show substantial DOR affinity. Replacement of D-Lys with (R)-β^3-Lys generated **RP-171**, which showed about 50-fold lower affinity for MOR but did not bind to the other two opioid receptors, which made this analog much more selective. The diastereoisomeric **RP-172**, incorporating (S)-β^3-Lys, did not bind to any of the three opioid receptors, showing that affinity of these analogs depended on the configuration of the β-amino acid.

The functional activities of the cyclopeptides in vitro were assessed at all three opioid receptors in calcium mobilization assay in which CHO cells co-expressing human recombinant opioid receptors and chimeric G proteins were used to monitor changes of intracellular calcium levels, reflecting activation of the G protein-coupled receptors (GPCR) [22,23].

The obtained results are summarized in Table 2. Agonist potencies of peptides are given as the negative logarithm of the molar concentration of an agonist that produces 50% of the maximal possible effect (pEC_{50}). Ligand efficacy was expressed as intrinsic activity (α). Dermorphin, DPDPE, and dynorphin A were used as standard agonists for calculating efficacy at MOR, DOR, and KOR, respectively. In CHO-MOR cells, the parent analog **RP-170** induced a significant concentration-dependent release of Ca^{2+} ions ($pEC_{50} = 8.93$, $\alpha = 1.00$), with efficacy and potency even higher than those of dermorphin ($pEC_{50} = 8.57$, $\alpha = 1.00$). For peptides **RP-171** and **RP-172**, the calculated pEC_{50} values were 6.87 and 5.45, respectively (for concentration-response curves, see Figure S7). In CHO-DOR cells, DPDPE elicited a strong concentration-dependent Ca^{2+} release, showing high potency and maximal effect ($pEC_{50} = 7.23$, $\alpha = 1.00$), while all three cyclopeptides were inactive. In CHO-KOR cells, dynorphin A induced a significant concentration-dependent Ca^{2+} release ($pEC_{50} = 9.04$, $\alpha = 1.00$). The potency of **RP-170** was only slightly lower, showing high potency and maximal effect ($pEC_{50} = 8.60$, $\alpha = 1.00$), **RP-171** displayed significantly lower potency but high efficacy ($pEC_{50} = 5.99$, $\alpha = 0.82$), and **RP-172** was inactive. Summing up, in this assay, **RP-171** had similar receptor preferences as the parent **RP-170,** while **RP-172** was completely inactive, which points to the importance of the R-chirality at position 2 of these cyclopeptides.

Table 2. Effect of new analogs at human recombinant opioid receptors coupled with calcium signaling via chimeric G proteins.

Peptide	MOR		DOR		KOR	
	pEC_{50} (CL$_{95\%}$)	$\alpha \pm$ SEM	pEC_{50} (CL$_{95\%}$)	$\alpha \pm$ SEM	pEC_{50} (CL$_{95\%}$)	$\alpha \pm$ SEM
Dermorphin	8.57 ± 0.07	1.00	inactive		inactive	
DPDPE	inactive		7.23 ± 0.22	1.00	inactive	
Dynorphin A	6.67 ± 0.50	0.83 ± 0.10	7.73 ± 0.27		9.04 ± 0.05	1.00
RP-170	8.93 ± 0.05	1.00	inactive		8.60 ± 0.14	1.00 ± 0.03
RP-171	6.87 ± 0.14	0.82 ± 0.02	inactive		5.99 ± 0.05	0.82 ± 0.05
RP-172	5.45 ± 0.91	0.45 ± 0.02	inactive		inactive	

Dermorphin, DPDPE, and dynorphin A were used as reference agonists for calculating intrinsic activity at MOR, DOR, and KOR, respectively: pEC50, aAgonist potency values; α, befficacy values; n ≥ 3.

2.5. Molecular Modeling

In order to obtain insight into the structural basis for the observed affinities, the analogs **RP-171** and **RP-172** were docked into the structure of the activated MOR (PDB accession code: 6DDF [24]) using AutoDock 4.2.6 [25]. The best scored poses were then subjected to molecular dynamics (MD) simulations (100 ns production, see Figure S8 for RMSD plots).

A general view of the binding pose of **RP-171**, as found in the MD simulations at t = 100.0 ns, is shown in Figure 4A. The interaction scheme is presented in Figure 4B. The compound is anchored in the MOR binding site first and foremost by the canonical interaction of the protonated amino group of Tyr[1] with Asp[147]. Additionally, the amide hydrogen of the peptide bond joining Tyr[1] and β^3-Lys[2] interacts with Asp[147]. These two interactions are stable throughout the simulation (Figure 4C,D). Other polar contacts stabilizing the complex are hydrogen bonds between the exocyclic carbonyl oxygen and Gln[124] or Asn[127], but these interactions fluctuate in the simulation time (Figure 4E,F). The remaining contacts are of apolar character. The aromatic ring of Tyr[1] is involved with π-π stacking with Tyr[148] and π-alkyl interactions with Ala[240] and Val[236] side chains. Other residues in the close vicinity of this aromatic ring are Met[151] and His[297]. The aromatic ring of the Phe[3] residue approaches Trp[318], Lys[303], and Ala[304], while the Phe[4] aromatic ring is

exposed to the solvent close to the extracellular outlet of the binding site. For other residues participating in van der Waals contacts, refer to Figure 4B.
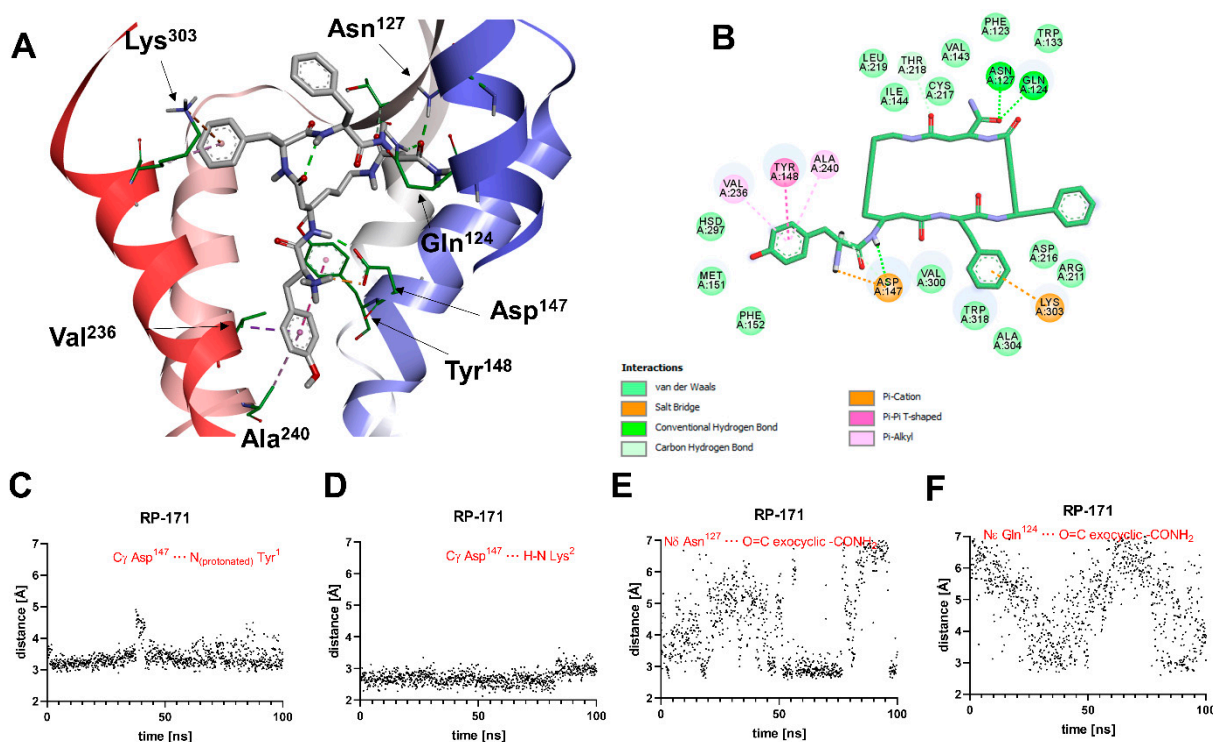
Figure 4. (**A**) Binding mode of **RP-171** (white sticks) in the MOR binding site, as found at t = 100.0 ns of the MD production run. The receptor is shown in a simplified manner, with only selected helices (ribbons) and side chains (thin sticks) shown. Display of nonpolar hydrogens is suppressed for clarity. (**B**) Diagram showing interactions between **RP-171** and the MOR binding site (interaction types colored according to the legend). (**C**–**F**) Time evolutions of selected distances associated with protein–ligand interactions during the MD simulations.

A general view of the binding pose of **RP-172**, as found in the MD simulations at t = 100.0 ns, is shown in Figure 5A. The interaction scheme is presented in Figure 5B. The only polar contact that is consistently present throughout the whole MD production is the H-bond interaction of amide hydrogen of the peptide bond joining Tyr^1 and β^3-Lys^2 interacts with Asp^{147} (Figure 5D). Contrary to what was found for **RP-171**, and contrary to what would be expected for strong MOR agonists, the interaction between the protonated amino group of Tyr^1 and Asp^{147} is unstable (Figure 5C). This H-bond, while present in the binding pose found by docking, is broken after the 65 ns of the MD simulations. Another polar contact that is broken during the MD run involves the interaction of exocyclic carbonyl oxygen with the Arg^{211} side chain guanidine group. By the end of the simulation, the carbonyl oxygen of Phe^3 starts with backbone amide hydrogen of Leu^{218} and hydroxyl hydrogen of Thr^{219} (Figure 5E,F). With respect to apolar contacts (found in the final snapshots of the simulation), the Tyr^1 aromatic ring interacts with the Met^{151} side chain (π-alkyl interaction). The Phe^3 aromatic ring approaches Trp^{318} and participates in π-alkyl interactions with the side chains of Leu^{219}, Lys^{233}, and Val^{236}. Other receptor residues interacting with the peptide are shown in Figure 5B.
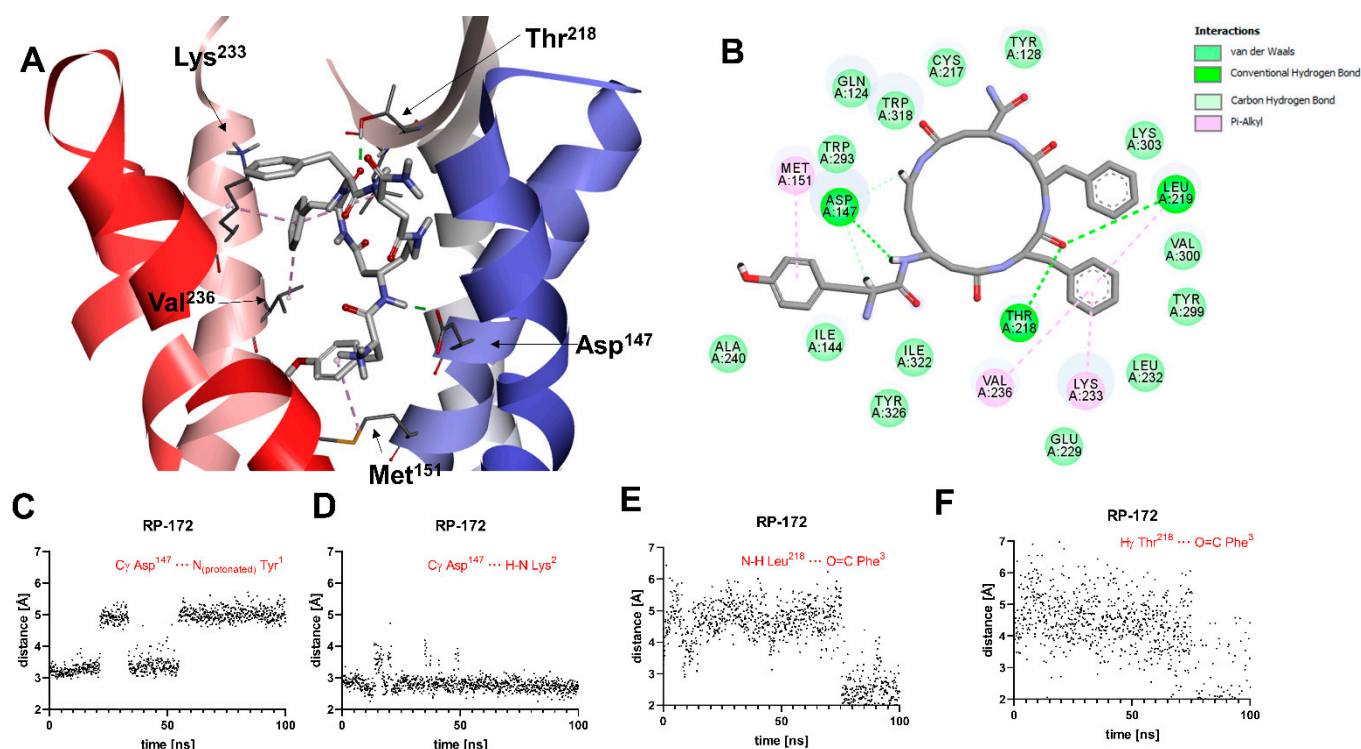
Figure 5. (**A**) Binding mode of **RP-172** (white sticks) in the MOR binding site, as found at t = 100.0 ns of the MD production run. The receptor is shown in a simplified manner, with only selected helices (ribbons) and side chains (thin sticks) shown. Display of nonpolar hydrogens is suppressed for clarity. (**B**) Diagram showing interactions between **RP-172** and the MOR binding site (interaction types colored according to the legend). (**C**–**F**) Time evolutions of selected distances associated with protein–ligand interactions during the MD simulations.

3. Discussion

β-Amino acids, although much less abundant than their α-analogs, are also present in nature and exhibit interesting pharmacological properties. The difference between α- and β-amino acids is in the number of carbon atoms (one or two, respectively) that separate an amino and a carboxy termini. β-Amino acids with side chains other than H can exist as *R* or *S* isomers at either the α (C2) carbon or the β (C3) carbon, producing β^2- or β^3-amino acids, respectively.

The most common naturally occurring β-amino acid is β-alanine, which is a component of pantothenic acid (vitamin B_5), which, in turn, is a component of coenzyme A. Another example of a natural β-amino acid is (1*R*,2*S*)-2-aminocyclopentanecarboxylic acid (cispentacin), an antifungal antibiotic isolated from *Bacillus cereus* [26].

β-Peptides (made of only β-amino acids) in general do not appear in nature, though among the opioid peptides, there are examples of such synthetic analogs [27]. More often mixed α/β-peptides, in which one or more β-residues are incorporated instead of some α-amino acids, were constructed [28–34].

An important advantage of peptide analogs incorporating β-amino acids over natural peptides is their stability against proteolytic degradation [35,36], which makes β-amino acids desirable building blocks in the preparation of peptide-based drugs [37].

In this report, we used (*R*)- and (*S*)-β^3-Lys to assess the influence of a β-amino acid on the conformation of the macrocycle of Tyr-c[D-Lys-Phe-Phe-Asp]NH$_2$ (**RP-170**), which has nanomolar MOR and KOR affinity. The obtained diastereoisomeric analogs **RP-171** and **RP-172** are also isomers of the parent compound **RP-170**, with which they share the same number of atoms in the whole structure and in the macrocycle. The difference between **RP-171**/**RP-172** and the parent **RP-170** is the point at which the exocyclic Tyr[1] is attached

to the ring (one carbon atom shift as compared with **RP-170**). The experimental evaluation of the binding affinity and functional activity of **RP-171** showed that such minor structural change had a significant effect on the biological properties causing 53- and 276-fold loss of affinity for MOR and KOR, respectively, as compared with the parent. The inversion of the configuration of β^3-Lys in **RP-172** induced an almost complete loss of affinity of this peptide for the opioid receptors.

The diastereomers **RP-171** and **RP-172** exhibit slightly different lipophilicity, as could be seen from their chromatographic behavior in the reversed-phase liquid chromatography on a C_{18} column. No additional effects were observed when the biphenyl stationary phase was used, which may suggest that the arrangement of aromatic rings in the isomers was not suitable for interactions with a biphenyl motif.

Further differences between isomers were revealed after a thorough analysis of fragmentation patterns in the MS^n experiments. Peptide **RP-172** containing (*S*)-β^3-Lys turned out to be more stable, and this observation corresponds with the results of conformational analysis and quantum chemical calculations. They show a significant difference in the structure and the energetics of the lowest-lying conformers of both diastereoisomers.

In our former work [33], we devised an interaction model for **RP-170** and its analogs, in which the peptides were anchored in the MOR binding pocket by interactions at the three key binding subsites. According to that model, in the S1 subsite, the protonable amino group of Tyr^1 interacts with Asp^{147} (a typical contact for high-affinity MOR agonists of both peptide [24] and non-peptide character [38]). In the S2 and S3 subsites reside the aromatic rings of the Phe residues. Our analyses suggested that the ability to place Tyr^1, Phe^3, and Phe^4 in these subsites is important for high MOR affinity.

The present results seem to corroborate this model. Replacement of D-Lys by (R)- or (S)-β3-Lys produced a topographical shift of Phe^3 and Phe^4 in regard to Tyr^1. As a conse-quence (according to the molecular docking and molecular dynamics), neither **RP-171** nor **RP-172** could accommodate their Phe^3 and Phe^4 aromatic rings in the way the parent compound did. This explains the lower MOR affinity of **RP-171**. This compound exhibits, however, the canonical interaction between the Tyr^1 amino group and Asp^{147}. On the contrary, for **RP-172**, such interaction (while present in the docked pose) is unstable in the MD simulations. This could be correlated to a much-diminished MOR affinity found experimentally for this analog. The obtained experimental and theoretical data form the basis for further work on **RP-170** analogs, an important element of which will be ADME/T evaluation.

4. Materials and Methods

4.1. Materials

All protected α-amino acids were purchased from Bachem A (Bubendorf, Switzerland). Opioid radioligands, [^{3}H]DAMGO, [^{3}H]deltorphin-2, and [^{3}H]U-69593, and human recombinant opioid receptors were purchased from PerkinElmer (Krakow, Poland). GF/B glass fiber strips were obtained from Whatman (Brentford, UK). Purity of peptides was determined by RP-HPLC and exact mass. Analytical and semi-preparative RP-HPLC was performed using Waters Breeze instrument (Milford, MA, USA) with dual absorbance detector (Waters 2487, Milford, MA, USA). All ESI-MS experiments were performed on a Shimadzu IT-TOF mass spectrometer (Shimadzu, Japan) equipped with ESI source connected to Nexera HPLC system (Shimadzu, Japan). The instrument was operated in the positive-ion mode. Peptide solutions (1 μL) were introduced in a 0.2 mL/min flow of mobile phase. For LC-MS experiments, Aeris Peptide C_{18} and Kinetex Biphenyl (Phenomenex, Torrance, CA, USA) were used, in a gradient reversed-phase mode, from 5 to 80% acetonitrile in water (both containing 0.1% HCOOH). ^{1}H NMR spectra were recorded on a 500 MHz Brucker instrument in DMSO-d_6, using residual DMSO as a resonance reference at 2.5 ppm.

4.2. Synthesis of Fmoc-Protected (R)- and (S)-β³-Lys(Mtt)

To the 500 mL three-necked, round bottom flask with Liebig's condenser equipped with thermometer, magnetic stirrer and protected from moisture with a tube with anhydrous calcium chloride, a solution of Fmoc-D-Orn-(Boc)-OH (**1**) (3 g, 6.6 mmol, 1 eq) in 50 mL of tetrahydrofuran (THF) was added, stirred and cooled to −30 °C. Then, N-methylmorpholine (1.52 mL, 13.9 mmol, 2.1 eq) was added, followed by methyl chloroformate (0.56 mL, 7.3 mmol, 1.1 eq) added dropwise, and stirring was continued for 30 min at −30 °C. Next, the diazomethane obtained, using standard procedure, from Diazald®(8.48 g, 13.9 mmol, 6 eq.) was distilled along with diethyl ether directly to the flask. The temperature in the flask was maintained below −10 °C, and after 1 h, the cooling bath was removed. The reaction was completed in 2 h (LC-MS analysis). Acetic acid (5 mL) was added to decompose the excess diazomethane, and stirring was continued for 30 min. Then, 100 mL of diethyl ether was added, and the solution was washed with water (2 × 100 mL), 5% NaHCO₃ (2 × 50 mL), and brine. The organic fraction was dried over MgSO₄ to obtain, after evaporation, 3 g (95%) of diazoketone (**2**), which was used in the next step without further purification.

Diazoketone (**2**) (3 g, 6.3 mmol, 1 eq) was dissolved in the mixture of THF and water (55 mL; 10:1) in a 250 mL round bottom flask. Triethylamine (1.78 mL, 17.5 mmol, 2.8 eq) and silver trifluoroacetate (0.15 g, 0.7 mmol, 0.11 eq) were added, and stirring was continued for 30 min. The solution was diluted with diethyl ether (200 mL), followed by 5% NaHCO₃ (200 mL). The white precipitate was filtrated off and combined with the aqueous phase. Its pH was adjusted to 2 with 2 M HCl, and the product was extracted with ethyl acetate (3 × 150 mL). The organic solution was washed with brine (100 mL) and dried over MgSO₄. Evaporation of the solvent gave a white product, which, after purification by flash chromatography (hexane:ethyl acetate = 1:1; Rf = 0.3), yielded 1.5 g (51%) of **3**.

A total of 0.9 g of **3** was dissolved in dioxane (5 mL); 4N HCl/dioxane (10 mL) was added, and the mixture was stirred until the reaction was completed (LC-MS). The solid residue obtained after evaporation was suspended in propylene oxide (10 mL) and refluxed for 2 h until all chloride ions reacted with the silver nitrate solution. Then, diethyl ether was added, and the white precipitate was filtered and dried. The obtained zwitterionic product **4** (0.71 g, yield ~100%) was used in the next step without further purification.

In total, 0.71 g (1.92 mmol, 1 eq) of **4** was suspended in DCM (20 mL). N,O-bis(trimethylsilyl) acetamide (0.535 g, 2.5 mmol, 1.3 eq) was added and stirred for 30 min. Next, 4-methyltrityl chloride (0.562 g, 1.92 mmol, 1 eq) was added along with DIPEA (2.5 mmol, 0.44 mL, 1.3 eq). The reaction was kept overnight at r.t. and controlled with LC-MS. When completed, the solvent was evaporated, and the residue was dissolved in ethyl acetate (200 mL) and washed with 5% NaHCO₃ (2 × 100 mL) and brine (100 mL). The organic layer was dried over MgSO₄ and evaporated. The product was purified by flash chromatography (Rf = 0.2 in DCM:MeOH = 10:1), giving 0.67 g of the final product **5** with a 50% yield. ¹H NMR spectrum (Figure S1) confirmed the structure.

4.3. Peptide Synthesis

Synthesis of linear precursors of cyclopeptides was performed by the standard manual solid-phase procedure on MBHA Rink-Amide resin (100–200 mesh, 0.8 mmol/g), using 9-fluorenylmethoxycarbonyl (Fmoc) protection for the α-amino groups of amino acids. Nᵋ-amino group of (R)- and (S)-β³-Lys was protected by the 4-methyltrityl (Mtt), β-carboxy group of Asp by 2-phenyl-isopropyl ester (O-2 PhiPr) and hydroxy group of Tyr by t-butyl (t-Bu). Piperidine in DMF (20%) was used for the deprotection of Fmoc groups, and 2-(1H-benzotriazol-1-yl)-1,1,3,3-tetramethyluronium tetrafluoroborate (TBTU) was employed as a coupling agent and diisopropylethylamine (DIEA) as a neutralizing base. Fully assembled Fmoc-protected peptides were treated with 1% trifluoroacetic acid (TFA) in dichloromethane (DCM) to remove the side chain Mtt and O-2PhiPr protecting groups, followed by on-resin cyclization (TBTU). Cleavage from the resin was accomplished by treatment with TFA/triisopropylsilane (TIS)/water (95:2.5:2.5) for 3 h at room temperature.

Crude peptides were purified by preparative reversed-phase HPLC on a Vydac C_{18} column (10 μm, 22 × 250 mm), flow rate 2 mL/min, 20 min linear gradient from water/0.1% (*v*/*v*) TFA to 80% acetonitrile/20% water/0.1% (*v*/*v*) TFA. The purity of the final peptides was verified by analytical HPLC employing a Vydac C_{18} column (5 μm, 4.6 × 250 mm), flow rate 1 mL/min, and the same solvent system over 50 min. The purity of the obtained peptides was >95%. Calculated values for protonated molecular ions were in agreement with those determined by high-resolution mass spectroscopy with electrospray ionization (ESI-MS) (Table S1).

4.4. Opioid Receptor Binding Assays

The opioid receptor binding assays were performed according to the described method [39], using commercial membranes of Chinese Hamster Ovary (CHO) cells transfected with human opioid receptors. The binding affinities for MOR, DOR, and KOR were determined by radioligand competition analysis using [^{3}H]DAMGO, [^{3}H]deltorphin-2, and [^{3}H]U-69593, respectively, as specific radioligands, respectively. Membrane preparations were incubated at 25 °C for 120 min with appropriate concentrations of a tested peptide in the presence of 0.5 nM radioligand in a total volume of 0.5 ml of 50 mM Tris/HCl (pH 7.4) containing bovine serum albumin (BSA) (1 mg/mL), bacitracin (50 μg/mL), bestatin (30 μM), and captopril (10 μM). Non-specific binding was determined in the presence of 1 μM naloxone. Incubations were terminated by the rapid filtration through the GF/B Whatman (Brentford, UK) glass fiber strips (pre-soaked for 2 h in 0.5% (*v*/*v*) polyethylamine) using Millipore Sampling Manifold (Billerica, MA, USA). The filters were washed three times with 4 ml of ice-cold Tris buffer solution. The bound radioactivity was measured in a Packard Tri-Carb 2100 TR liquid scintillation counter (Ramsey, MN, USA) after overnight extraction of the filters in 4 mL of a Perkin Elmer Ultima Gold scintillation fluid (Wellesley, MA, USA). Three independent experiments for each assay were carried out in duplicate. The data were analyzed by a nonlinear least square regression analysis computer program Graph Pad PRISM 6.0 (Graph Pad Software Inc., San Diego, CA, USA). The IC_{50} values were determined from the logarithmic concentration–displacement curves, and the values of the inhibitory constants (K_i) were calculated according to the equation of Cheng and Prusoff [40].

4.5. Calcium Mobilization Assay

Calcium mobilization assay was performed, as reported in detail elsewhere [41], using CHO cells stably co-expressing human recombinant MOR or KOR and the C-terminally modified $G\alpha_{qi5}$ and CHO cells co-expressing human recombinant DOR and the $G\alpha_{qG66Di5}$ chimeric protein (a generous gift from Prof. Girolamo Calo, University of Padova, Italy). Cells were cultured in a culture medium consisting of Dulbecco's MEM/HAMS F12 (1:1) supplemented with 10% fetal bovine serum, penicillin (100 IU/mL), streptomycin (100 μg/mL), L-glutammine (2 mM), fungizone (1 μg/mL), geneticin (G418; 200 μg/mL) and hygromycin B (100 μg/mL). Cell cultures were kept at 37 °C in 5% CO_2/humidified air. Cells were seeded at a density of 50,000 cells/well into 96-well black, clear-bottom plates. After 24 h incubation, the cells were loaded with a medium supplemented with probenecid (2.5 mM), calcium-sensitive fluorescent dye Fluo-4 AM (3 μM), pluronic acid (0.01%), and HEPES (20 mM) and kept for 30 min at 37 °C. Then, the loading solution was aspirated, and 100 μL/well of assay buffer (HBSS supplemented with 20 mM HEPES, 2.5 mM probenecid, and 500 μM Brilliant Black) was added. After placing both plates (cell culture and compound plate) into the FlexStation II (Molecular Device, Union City, CA, USA), the on-line additions were carried out in a volume of 50 μL/well and the fluorescence changes were measured. Ligand efficacies, expressed as the intrinsic activity (α), were calculated as the E_{max} ratio of the tested compound and the standard agonist. At least three independent experiments for each assay were carried out in duplicate.

Curve fittings were performed using Graph Pad PRISM 5.0 (GraphPad Software Inc., San Diego, CA, USA). Data have been statistically analyzed with one-way ANOVA followed by the Dunnett's test for multiple comparisons; *p* values < 0.05 were considered significant.

4.6. Quantum Chemical Calculations

One hundred conformers for compounds **RP-171** and **RP-172** were generated by an in-house Python script using the improved ETKDG method [42]. The compounds were protonated at the N-terminal nitrogen atom. The geometries were optimized in Gaussian09 [21] at the B3LYP/6-31G level in a gas phase or in water using the PCM solvent model. The resulting geometries were then reoptimized at the B3LYP/6-31G(d,p) level. Further attempts to increase the theory level were unsuccessful for the lack of convergence. Top conformers were subject to harmonic frequency calculations at the B3LYP/6-31G(d,p) level in order to ascertain that the geometries are minima (no imaginary frequencies) and to calculate thermochemical values.

4.7. Molecular Docking

One hundred conformers of **RP-171** and **RP-172** (obtained as described in Section 4.6) were docked into the activated structure of the MOR (PDB accession code: 6DDF [24], a complex of mu opioid receptor with Gi protein, with DAMGO peptide in the orthosteric binding site) using AutoDock 4.2.6 [25]. The ligands and the protein were processed in AutoDock Tools 4 [25]. The ligands' side chains were allowed to rotate, and the receptor structure was kept rigid. The docking box was set around the position of the DAMGO molecule in the 6DDF structure [24]. The grids ($82 \times 78 \times 104$ points, with 0.375 Å spacing) were calculated with AutoGrid, and the docking was performed using Lamarckian Genetic Algorithm local searches according to the pseudo-Solis and Wets algorithm. Each docking consisted of 100 runs. The results were clustered, and the top scored solutions were visually inspected to examine their conformity to the known literature data on ligand MOR interactions [43]. Molecular graphics were prepared in Biovia Discovery Studio Visualizer [44].

4.8. Molecular Dynamics

The complexes of MOR with **RP-171** and **RP-172** (obtained by molecular docking, described in Section 4.7) were subject to molecular dynamics simulations in GROMACS 5.1.2 [45]. The complexes were embedded in a lipid bilayer of POPC molecules (128 molecules) solvated with water molecules (TIP3P type, 13,000 molecules) and supplied with ions (Na^+ and Cl^-, 0.154 M). These steps were performed with the CHARMM-GUI service [46]. CHARMM 36 force field was used for modeling the proteins, lipids, water, and ions. The ligands were modeled using CHARMM CGenFF [47].

The complexes were minimized and equilibrated, whereafter 100 ns production was performed (NPT ensemble, temperature = 303.15 K, integration step = 2 fs, cut-off scheme Verlet, Nose-Hoover thermostat, Parrinello–Rahman barostat, LINCS H-bonds constraints).

References

1. Janecka, A.; Fichna, J.; Janecki, T. Opioid receptors and their ligands. *Curr. Top. Med. Chem.* **2004**, *4*, 1–17. [CrossRef] [PubMed]
2. Fichna, J.; Janecka, A.; Costentin, J.; Do Rego, J.C. The endomorphin system and its evolving neurophysiological role. *Pharmacol. Rev.* **2007**, *59*, 88–123. [CrossRef]
3. Liu, W.X.; Wang, R. Endomorphins: Potential roles and therapeutic indications in the development of opioid peptide analgesic drugs. *Med. Res. Rev.* **2012**, *32*, 536–580. [CrossRef] [PubMed]
4. Gu, Z.H.; Wang, B.; Kou, Z.Z.; Bai, Y.; Chen, T.; Dong, Y.L.; Li, H.; Li, Y.Q. Endomorphins: Promising Endogenous Opioid Peptides for the Development of Novel Analgesics. *Neurosignals* **2017**, *25*, 98–116. [CrossRef] [PubMed]
5. Zhang, Y.Z.; Yang, W.J.; Wang, X.F.; Wang, M.M.; Zhang, Y.; Gu, N.; Wang, C.L. The spinal anti-allodynic effects of endomorphin analogs with C-terminal hydrazide modification in neuropathic pain model. *Peptides* **2020**, *134*, 170407. [CrossRef] [PubMed]
6. Piekielna, J.; Perlikowska, R.; Gach, K.; Janecka, A. Cyclization in opioid peptides. *Curr. Drug Targets* **2013**, *14*, 798–816. [CrossRef] [PubMed]
7. Vu, Q.N.; Young, R.; Sudhakar, H.K.; Gao, T.; Huang, T.; Tan, Y.S.; Lau, Y.H. Cyclisation strategies for stabilising peptides with irregular conformations. *RSC Med. Chem.* **2021**, *12*, 887–901. [CrossRef]
8. White, C.J.; Yudin, A.K. Contemporary strategies for peptide macrocyclization. *Nat. Chem.* **2011**, *3*, 509–524. [CrossRef] [PubMed]
9. Stefanucci, A.; Dimmito, M.P.; Molnar, G.; Streicher, J.M.; Novellino, E.; Zengin, G.; Mollica, A. Developing Cyclic Opioid Analogues: Fluorescently Labeled Bioconjugates of Biphalin. *ACS Med. Chem. Lett.* **2020**, *11*, 720–726. [CrossRef]
10. Leitgeb, B. Structural investigation of endomorphins by experimental and theoretical methods: Hunting for the bioactive conformation. *Chem. Biodivers.* **2007**, *4*, 2703–2724. [CrossRef]
11. Janecka, A.; Gentilucci, L. Cyclic endomorphin analogs in targeting opioid receptors to achieve pain relief. *Future Med. Chem.* **2014**, *6*, 2093–2101. [CrossRef]
12. Borics, A.; Tóth, G. Structural comparison of mu-opioid receptor selective peptides confirmed four parameters of bioactivity. *J. Mol. Graph. Model.* **2010**, *28*, 495–505. [CrossRef]
13. Perlikowska, R.; do-Rego, J.C.; Cravezic, A.; Fichna, J.; Wyrebska, A.; Toth, G.; Janecka, A. Synthesis and biological evaluation of cyclic endomorphin-2 analogs. *Peptides* **2010**, *31*, 339–345. [CrossRef]
14. Janecka, A.; Fichna, J.; Kruszynski, R.; Sasaki, Y.; Ambo, A.; Costentin, J.; do-Rego, J.C. Synthesis and antinociceptive activity of cyclic endomorphin-2 and morphiceptin analogs. *Biochem. Pharmacol.* **2005**, *71*, 188–195. [CrossRef]
15. Perlikowska, R.; Piekielna, J.; Gentilucci, L.; De Marco, R.; Cerlesi, M.C.; Calo, G.; Artali, R.; Tömböly, C.; Kluczyk, A.; Janecka, A. Synthesis of mixed MOR/KOR efficacy cyclic opioid peptide analogs with antinociceptive activity after systemic administration. *Eur. J. Med. Chem.* **2016**, *109*, 276–286. [CrossRef]
16. Fichna, J.; Perlikowska, R.; Wyrębska, A.; Gach, K.; Piekielna, J.; do-Rego, J.C.; Toth, G.; Kluczyk, A.; Janecki, T.; Janecka, A. Effect of 2′,6′-dimethyl-L-tyrosine (Dmt) on pharmacological activity of cyclic endomorphin-2 and morphiceptin analogs. *Bioorg. Med. Chem.* **2011**, *19*, 6977–6981. [CrossRef]
17. Piekielna, J.; Kluczyk, A.; Gentilucci, L.; Cerlesi, M.C.; Calo', G.; Tomböly, C.; Łapiński, K.; Janecki, T.; Janecka, A. Ring size in cyclic endomorphin-2 analogs modulates receptor binding affinity and selectivity. *Org. Biomol. Chem.* **2015**, *13*, 6039–6046. [CrossRef]
18. Piekielna, J.; Perlikowska, R.; do-Rego, J.C.; do-Rego, J.L.; Cerlesi, M.C.; Calo, G.; Kluczyk, A.; Łapiński, K.; Tömböly, C.; Janecka, A. Synthesis of mixed opioid affinity cyclic endomorphin-2 analogues with fluorinated phenylalanines. *ACS Med. Chem. Lett.* **2015**, *6*, 579–583. [CrossRef]
19. Matthews, J.L.; Braun, C.; Guibourdenche, C.; Overhand, M.; Seebach, D. *Enantioselective Synthesis of β-Amino Acids*; Juaristi, E., Ed.; Wiley-VCH: Weinheim, Germany, 1996; pp. 105–126.
20. Fang, Z.; Baghdady, Y.Z.; Schug, K.A.; Chowdhury, S.M. Evaluation of different stationary phases in the separation of inter-cross-linked peptides. *J. Proteome Res.* **2019**, *18*, 1916–1925. [CrossRef]
21. Frisch, M.J.; Trucks, G.W.; Schlegel, H.B.; Scuseria, G.E.; Robb, M.A.; Cheeseman, J.R.; Scalmani, G.; Barone, V.; Mennucci, B.; Petersson, G.A.; et al. *Gaussian 09, Revision D.01*; Gaussian Inc.: Wallingford, CT, USA, 2013.
22. Caers, J.; Peymen, K.; Suetens, N.; Temmerman, L.; Janssen, T.; Schoofs, L.; Beets, I. Characterization of G protein-coupled receptors by a fluorescence-based calcium mobilization assay. *J. Vis. Exp.* **2014**, *89*, e51516. [CrossRef]

23. Camarda, V.; Calo', G. Chimeric G proteins in fluorimetric calcium assays: Experience with opioid receptors. *Methods Mol. Biol.* **2013**, *937*, 293–306.

24. Koehl, A.; Hu, H.; Maeda, S.; Zhang, Y.; Qu, Q.; Paggi, J.M.; Latorraca, N.R.; Hilger, D.; Dawson, R.; Matile, H.; et al. Structure of the μ-opioid receptor–Gi protein complex. *Nature* **2018**, *558*, 547–552. [CrossRef]

25. Morris, G.M.; Huey, R.; Lindstrom, W.; Sanner, M.F.; Belew, R.K.; Goodsell, D.S.; Olson, A.J. AutoDock4 and AutoDockTools4: Automated docking with selective receptor flexibility. *J. Comput. Chem.* **2009**, *30*, 2785–2791. [CrossRef]

26. Konishi, M.; Nishio, M.; Saitoh, K.; Miyaki, T.; Oki, T.; Kawaguchi, H. Cispentacin, a new antifungal antibiotic. I. Production, isolation, physico-chemical properties and structure. *J. Antibiot. (Tokyo)* **1989**, *42*, 1749–1755. [CrossRef]

27. Wilczynska, D.; Kosson, P.; Kwasiborska, M.; Ejchart, A.; Olma, A. Synthesis and receptor binding of opioid peptide analogues containing $β^3$-homo-amino acids. *J. Pept. Sci.* **2009**, *15*, 777–782. [CrossRef]

28. Keresztes, A.; Szucs, M.; Borics, A.; Kövér, K.E.; Forró, E.; Fülöp, F.; Tömböly, C.; Péter, A.; Páhi, A.; Fábián, G.; et al. New endomorphin analogues containing alicyclic β-amino acids: Influence on bioactive conformation and pharmacological profile. *J. Med. Chem.* **2008**, *51*, 4270–4279. [CrossRef]

29. Lesma, G.; Salvadori, S.; Airaghi, F.; Murray, T.F.; Recca, T.; Sacchetti, A.; Balboni, G.; Silvani, A. Structural and biological exploration of Phe^3-Phe^4-modified endomorphin-2 peptidomimetics. *ACS Med. Chem. Lett.* **2013**, *4*, 795–799. [CrossRef]

30. Mollica, A.; Pinnen, F.; Costante, R.; Locatelli, M.; Stefanucci, A.; Pieretti, S.; Davis, P.; Lai, J.; Rankin, D.; Porreca, F.; et al. Biological active analogues of the opioid peptide biphalin: Mixed $α/β^3$-peptides. *J. Med. Chem.* **2013**, *56*, 3419–3423. [CrossRef]

31. Fraczak, O.; Lasota, A.; Kosson, P.; Lesniak, A.; Muchowska, A.; Lipkowski, A.W.; Olma, A. Biphalin analogs containing β3-Homo-amino acids at the 4,4positions: Synthesis and opioid activity profiles. *Peptides* **2015**, *66*, 13–18. [CrossRef]

32. Fraczak, O.; Lasota, A.; Tymecka, D.; Kosson, P.; Muchowska, A.; Misicka, A.; Olma, A. Synthesis, binding affinities and metabolic stability of dimeric dermorphin analogs modified with β 3-Homo-amino acids. *J. Pept. Sci.* **2016**, *22*, 222–227. [CrossRef]

33. Adamska-Bartłomiejczyk, A.; Lipiński, P.F.J.; Piekielna-Ciesielska, J.; Kluczyk, A.; Janecka, A. Pharmacological profile and molecular modeling of cyclic opioid analogues incorporating various phenylalanine derivatives. *Chem. Med. Chem.* **2020**, *15*, 1322–1329. [CrossRef]

34. Tymecka, D.; Lipiński, P.F.J.; Kosson, P.; Misicka, A. $β^2$-*Homo*-Amino Acid Scan of μ-Selective Opioid Tetrapeptide TAPP. *Molecules* **2020**, *25*, 2461. [CrossRef]

35. Seebach, D.; Beck, A.K.; Bierbaum, D.J. The world of beta- and gamma-peptides comprised of homologated proteinogenic amino acids and other components. *Chem. Biodivers.* **2004**, *1*, 1111–1239. [CrossRef]

36. Torino, D.; Mollica, A.; Pinnen, F.; Lucente, G.; Feliciani, F.; Davis, P.; Lai, J.; Ma, S.W.; Porreca, F.; Hruby, V.J. Synthesis and evaluation of new endomorphin analogues modified at the Pro(2) residue. *Bioorg. Med. Chem. Lett.* **2009**, *19*, 4115–4118. [CrossRef]

37. Beke, T.; Somlai, C.; Perczel, A. Toward a rational design of beta-peptide structures. *J. Comput. Chem.* **2006**, *27*, 20–38. [CrossRef]

38. Huang, W.; Manglik, A.; Venkatakrishnan, A.J.; Laeremans, T.; Feinberg, E.N.; Sanborn, A.L.; Kato, H.E.; Livingston, K.E.; Thorsen, T.S.; Kling, R.C.; et al. Structural insights into μ-opioid receptor activation. *Nature* **2015**, *524*, 315–321. [CrossRef]

39. Janecka, A.; Kruszynski, R.; Fichna, J.; Kosson, P.; Janecki, T. Enzymatic degradation studies of endomorphin-2 and its analogs containing N-methylated amino acids. *Peptides* **2006**, *27*, 131–135. [CrossRef]

40. Cheng, Y.; Prusoff, W.H. Relationship between the inhibition constant (K1) and the concentration of inhibitor which causes 50 per cent inhibition (I50) of an enzymatic reaction. *Biochem. Pharmacol.* **1973**, *22*, 3099–3108.

41. Perlikowska, R.; Malfacini, D.; Cerlesi, M.C.; Calo', G.; Piekielna, J.; Floriot, L.; Henry, T.; do-Rego, J.C.; Tömböly, C.; Kluczyk, A.; et al. Pharmacological characterization of endomorphin-2-based cyclic pentapeptides with methylated phenylalanine residues. *Peptides* **2014**, *55*, 145–150. [CrossRef]

42. Wang, S.; Witek, J.; Landrum, G.A.; Riniker, S. Improving conformer generation for small rings and macrocycles based on distance geometry and experimental torsional-angle preferences. *J. Chem. Inf. Model.* **2020**, *60*, 2044–2058. [CrossRef]

43. Williams, J.T.; Ingram, S.L.; Henderson, G.; Chavkin, C.; Von Zastrow, M.; Schulz, S.; Koch, T.; Evans, C.J.; Christie, M.J. Regulation of mu -Opioid Receptors: Desensitization, Phosphorylation, Internalization, and Tolerance. *Mol. Pharmacol.* **2013**, *65*, 223–254.

44. *Biovia Discovery Studio Visualizer v.19*; Dassault Systèmes: San Diego, CA, USA, 2018.

45. Abraham, M.J.; Murtola, T.; Schulz, R.; Páll, S.; Smith, J.C.; Hess, B.; Lindahl, E. GROMACS: High performance molecular simulations through multi-level parallelism from laptops to supercomputers. *SoftwareX* **2015**, *1*, 19–25. [CrossRef]

46. Lee, J.; Cheng, X.; Swails, J.M.; Yeom, M.S.; Eastman, P.K.; Lemkul, J.A.; Wei, S.; Buckner, J.; Jeong, J.C.; Qi, Y.; et al. CHARMM-GUI Input Generator for NAMD, GROMACS, AMBER, OpenMM, and CHARMM/OpenMM Simulations Using the CHARMM36 Additive Force Field. *J. Chem. Theory Comput.* **2016**, *12*, 405–413. [CrossRef] [PubMed]

47. Vanommeslaeghe, K.; Hatcher, E.; Acharya, C.; Kundu, S.; Zhong, S.; Shim, J.; Darian, E.; Guvench, O.; Lopes, P.; Vorobyov, I.; et al. CHARMM general force field: A force field for drug-like molecules compatible with the CHARMM all-atom additive biological force fields. *J. Comput. Chem.* **2009**, *31*, 671–690. [CrossRef]

Synthesis and Antinociceptive Effect of Some Thiazole-Piperazine Derivatives: Involvement of Opioidergic System in the Activity

Nazlı Turan Yücel [1],*, Derya Osmaniye [2], Ümmühan Kandemir [3], Asaf Evrim Evren [4], Özgür Devrim Can [1] and Ümide Demir Özkay [1]

[1] Faculty of Pharmacy, Department of Pharmacology, Anadolu University, Eskişehir 26470, Turkey; ozgurdt@anadolu.edu.tr (Ö.D.C.); udemir@anadolu.edu.tr (Ü.D.Ö.)
[2] Faculty of Pharmacy, Department of Pharmaceutical Chemistry, Anadolu University, Eskişehir 26470, Turkey; dosmaniye@anadolu.edu.tr
[3] Institute of Health Sciences, Department of Pharmacology, Anadolu University, Eskişehir 26470, Turkey; ummuhan_kandemir@hotmail.com
[4] Vocational School of Health Services, Pharmacy Services, Bilecik Şeyh Edebali University, Bilecik 11230, Turkey; asafevrim.evren@bilecik.edu.tr
* Correspondence: nazlituran@anadolu.edu.tr

Abstract: In this study, we aimed to design and synthesize novel molecules carrying both the thiazole and piperazine rings in their structures and to investigate their antinociceptive activity. Targeted compounds were obtained by reacting thiosemicarbazide derivative and appropriate 2-bromoacetophenone in ethanol. The structures of the obtained compounds were determined using data from various spectroscopic methods (IR, ^{1}H-NMR, ^{13}C-NMR, and LCMSMS). Experimental data from in vivo tests showed that test compounds **3a–3c**, **3f**, and **3g** (50 mg/kg) significantly prolonged reaction times of animals in tail-clip and hot-plate tests compared to the controls, indicating that these compounds possess centrally mediated antinociceptive activities. Furthermore, these compounds reduced the number of writhing behaviors in the acetic acid-induced writhing tests, showing that the compounds also possess peripheral antinociceptive activity. In the mechanistic studies, naloxone pre-treatments abolished the antinociceptive activities of compounds **3a–3c**, **3f**, and **3g**, indicating that opioidergic mechanisms were involved in their antinociceptive effects. Molecular docking studies demonstrating significant interactions between the active compounds and μ- and δ-opioid receptor proteins supported the pharmacological findings. This study is the first showing that molecules designed to bear thiazole and piperazine moieties together on their structure exert centrally and peripherally mediated antinociceptive effects by activating the opioid system.

Keywords: thiazole; piperazine; tail-clip; hot-plate; acetic acid-induced writhing test; opioid

1. Introduction

Pain is a health problem affecting the quality of life of patients due to its prevalence and accompanying disabilities. The pharmacological agents used in the treatment of pain include nonsteroidal anti-inflammatory drugs (NSAID), opioid analgesics, and analgesic adjuvants (such as antidepressants and local anesthetics) [1]. Although there are various analgesics used in clinics today, pain management is still a challenge due to concomitant undesirable side effects of these drugs. Long-term NSAID intake increases the risk of gastrointestinal complications, renal damage, and cardiovascular effects [2], while currently used opioid analgesics have negative effects such as sedation, respiratory depression, addiction, and tolerance [3]. Therefore, studies on the discovery and development of safer alternative drugs with comparable or better analgesic efficacy than conventional drugs are ongoing.

Nitrogen- and sulfur-containing heterocycles are frequently used in drug synthesis. Thiazole, a five-membered ring system carrying three carbons, one nitrogen, and one sulfur atom, is one such structure. It has been reported that thiazole-bearing compounds have some central nervous system (CNS)-related effects, such as anti-schizophrenic [4], anti-parkinsonian [5], neuroprotective [6], acetylcholinesterase inhibitory [7], anticonvulsant [8], antidepressant [9], and sedative-hypnotic [10] effects. Another heterocyclic structure, piperazine, is a 6-membered saturated ring system containing two nitrogen atoms in the first and fourth positions. Piperazine structure is present in several currently used CNS-related drugs, such as amoxapine, trazodone, hydroxyzine, buspirone, clozapine, aripiprazole [11], and vortioxetine [12].

A considerable amount of research data have been reported on the analgesic and anti-inflammatory effects of compounds carrying thiazole [13–21] or piperazine moieties [22–31]. Inhibition of COX isoenzymes [13,16], modulation of glutamatergic system through metabotropic and ionotropic (NMDA) receptors [20], inhibition of cytokine (TNF-α and IL-1β) signaling [20], involvement of α_2 adrenergic, adenosinergic, and $D_{2/3}$ dopaminergic receptors [22,23], blockage of T-type calcium channels [24], participation of 5-HT$_{1A}$ and 5-HT$_{2A}$ serotonergic receptors [25,26], and contribution of opioid system [21,30,31] have been suggested as some possible mechanisms underlying the aforementioned analgesic effects.

The chemical structures of some analgesic agents that contain thiazole, secondary amine, or methylsulfonyl groups, similar to our test compounds, are provided in Figure 1.
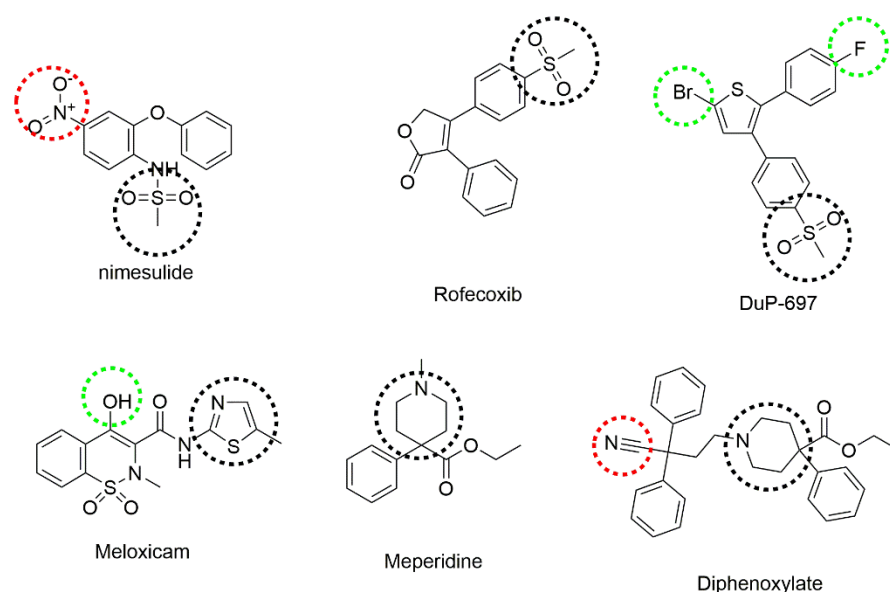
Figure 1. Some analgesic agents containing thiazole, secondary amine, or methylsulfonyl groups. Thiazole, secondary amine, or methylsulfonyl groups are marked in black, electron-donating substituents are marked with green, and electron-withdrawing substituents are marked with red.

Based on the antinociceptive activities of thiazole and piperazine ring systems, we designed and synthesized eight novel compounds containing both moieties and investigated their possible antinociceptive activities by well-validated in vivo methods. In addition, studies on the mechanism of action were performed with naloxone, a non-selective opioid receptor antagonist, to examine the possible involvement of the opioidergic mechanisms in the activity. Binding properties of test compounds to µ-, δ-, and k-opioid receptors were evaluated by in silico studies.

2. Results

2.1. Chemistry

The compounds **3a–3h** were synthesized as outlined in Figure 2.

Figure 2. Synthesis pathway of target compounds (**3a–3h**).
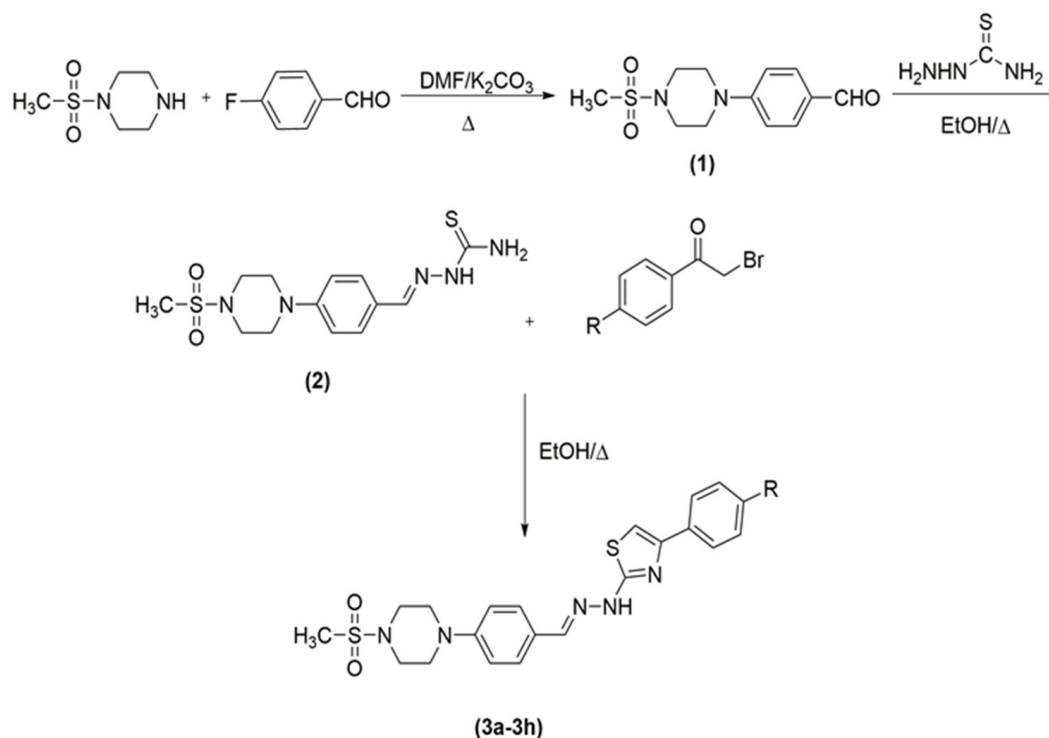
Compounds	R
3a	-H
3b	-CH₃
3c	-OCH₃
3d	-CN
3e	-NO₂
3f	-F
3g	-Cl
3h	-CF₃

Firstly, 4-(4-(methylsulphonyl)piperazin-1-yl) benzaldehyde (**1**) were prepared by reacting 1-(methylsulphonyl) piperazine with 4-fluorobenzaldehyde. Secondly, 4-(4-(methylsulphonyl) piperazin-1-yl) benzaldehyde (**1**) was changed to its corresponding thiosemicarbazone by reacting compound **1** with hydrazinecarbothioamide. Finally, target compounds (**3a–3h**) were generated via ring closure reaction. The final compounds (**3a–3h**) were purified, and their structures were determined using ^{1}H-NMR, ^{13}C-NMR, and LCMSMS (see Supplementary Materials Figures S1–S32).

2.2. Prediction of ADME Parameters

Strong pharmacological activity and low toxicity profile of molecules are not sufficient to make it a certain drug candidate—candidate drugs need to possess appropriate pharmacokinetics [32]. Therefore, we calculated various physicochemical parameters of the synthesized compounds (**3a–3h**) using the Molinspiration program to estimate their absorption, distribution, metabolism, and excretion (ADME) profiles.

The theoretical calculations of ADME parameters (topological polar surface area (TPSA), molecular volume (MV), number of hydrogen acceptors (AHB), number of hydrogen donors (DHB), partition coefficient (log P), and molecular weight (MW)) are presented in Table 1.

Table 1. Some physicochemical parameters of the compounds **3a–3h** used in the prediction of ADME profiles.

Compounds	R	MW	TPSA	logP	AHB	DHB	MV	Vio
3a	-H	444.58	77.90	3.33	7	1	379.00	0
3b	-CH$_3$	455.61	77.90	3.77	7	1	395.56	0
3c	-OCH$_3$	471.61	87.14	3.38	8	1	404.55	0
3d	-CN	466.59	101.69	3.08	8	1	395.86	0
3e	-NO$_2$	486.58	123.72	3.29	10	1	402.34	0
3f	-F	459.57	77.90	3.49	7	1	383.94	0
3g	-Cl	476.03	77.90	4.00	7	1	392.54	0
3h	-CF$_3$	509.58	77.90	4.22	7	1	410.30	1

The Molinspiration program is based on the principle of Lipinski's five rules that determine the properties a candidate drug molecule must have to be active in humans—an orally administrated drug should not violate more than one rule. The data obtained for compounds **3a–3h** did not violate any Lipinski rule, indicated good pharmacokinetic profiles, and increased their therapeutic potentials. On the other hand, it should also be noted that the Lipinski rule is not sufficient on its own and further pharmacokinetic studies are needed to draw solid conclusions.

2.3. Pharmacology

Figures 3 and 4 show the effects of compounds **3a–3h** (50 mg/kg, p.o.) and morphine (10 mg/kg, i.p.) as MPE % values in the tail-clip (F(9,60) = 20.01, $p < 0.001$) and hot-plate tests (F(9,60) = 20.86, $p < 0.001$) respectively, in mice.
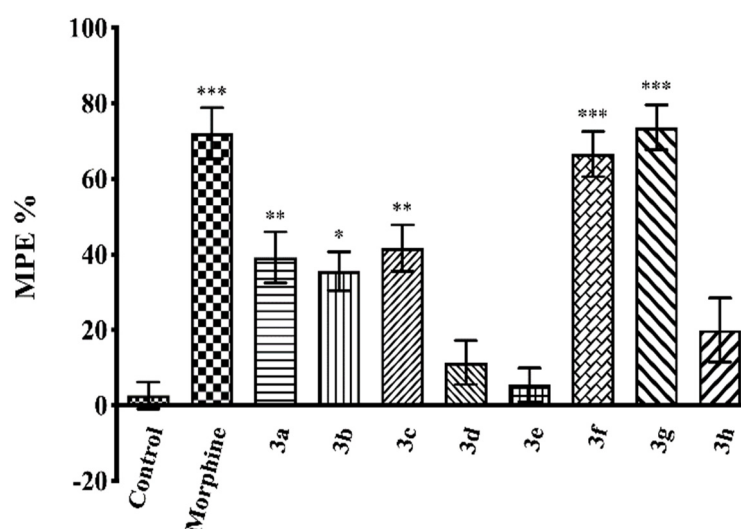
Figure 3. Effects of test compounds (**3a–3h**, 50 mg/kg, p.o., administered 60 min before testing) and morphine (10 mg/kg, i.p., administered 30 min before testing), on MPE % values in the mice tail-clip test. Significance against control group * $p < 0.05$, ** $p < 0.01$, *** $p < 0.001$. Values are mean ± SEM. One-way ANOVA and post-hoc Tukey's test, $n = 7$.
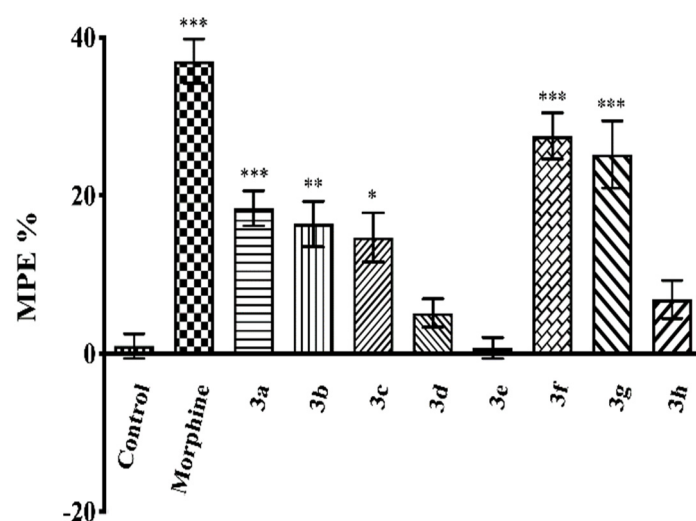
Figure 4. Effects of test compounds (**3a**–**3h**, 50 mg/kg, p.o., administered 60 min before testing) and morphine (10 mg/kg, i.p., administered 30 min before testing) on MPE % values in the mice hot-plate test. Significance against control group * $p < 0.05$, ** $p < 0.01$, *** $p < 0.001$. Values are mean ± SEM. One-way ANOVA and post-hoc Tukey's test, $n = 7$.

Results of the multiple comparison tests indicated that administration of compounds **3a**–**3c**, **3f**, and **3g** (50 mg/kg, p.o.) significantly increased the calculated MPE % values compared to the corresponding control group in both tests. Compounds **3d**, **3e**, and **3h** were ineffective.

Figure 5 illustrates the effects of test compounds **3a**–**3h** and morphine on the number of writhing behaviors scored in the acetic acid-induced writhing test ($F_{(9,60)} = 9.13$, $p < 0.001$). Results of the multiple comparison tests indicated that compounds **3a**–**3c**, **3f**, and **3g** significantly decreased the acetic acid-induced writhing responses compared to the control group. The percentage inhibitions of writhing behaviors in the acetic acid writhing test are presented in Table 2.
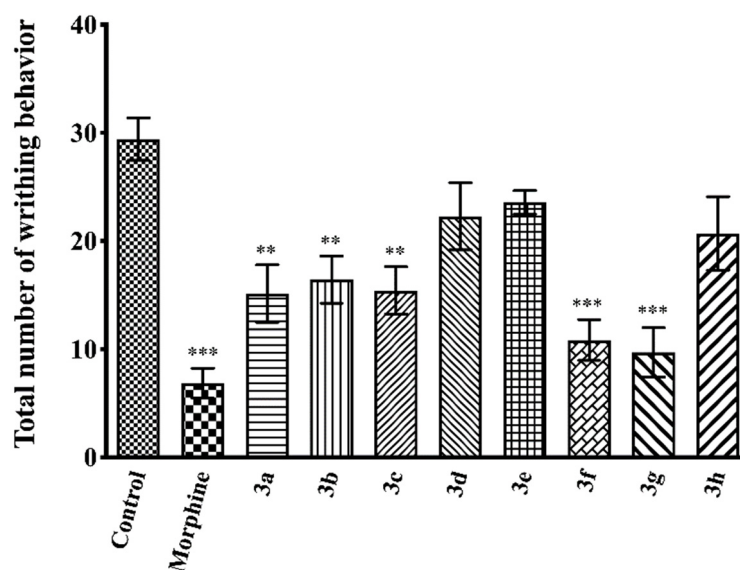
Figure 5. Effects of test compounds **3a**–**3h** (50 mg/kg, p.o., administered 60 min before testing) and morphine (10 mg/kg, i.p., administered 30 min before testing) on the number of writhing behaviors of mice in the acetic acid-induced writhing test. Significance against control group ** $p < 0.01$, *** $p < 0.001$. Values are mean ± SEM. One-way ANOVA and post-hoc Tukey's test, $n = 7$.

Table 2. Effects of test compounds (50 mg/kg, p.o.) and morphine (10 mg/kg, i.p.) on protection (%) values of mice in the acetic acid-induced writhing test.

Treatment	Protection %
Control	-
Morphine	76.69
3a	48.54
3b	44.17
3c	47.57
3d	24.27
3e	19.90
3f	63.10
3g	66.99
3h	29.61

Morphine (10 mg/kg, i.p.), used as a reference drug, presented its antinociceptive activity in all tests, as expected (Figures 3–5).

The effects of the test compounds on falling latencies recorded in the Rota-Rod tests are shown in Figure 6. The data show that test compounds did not cause any significant alteration in the mice's motor coordination ($F_{(8,54)} = 0.57$, $p > 0.05$).
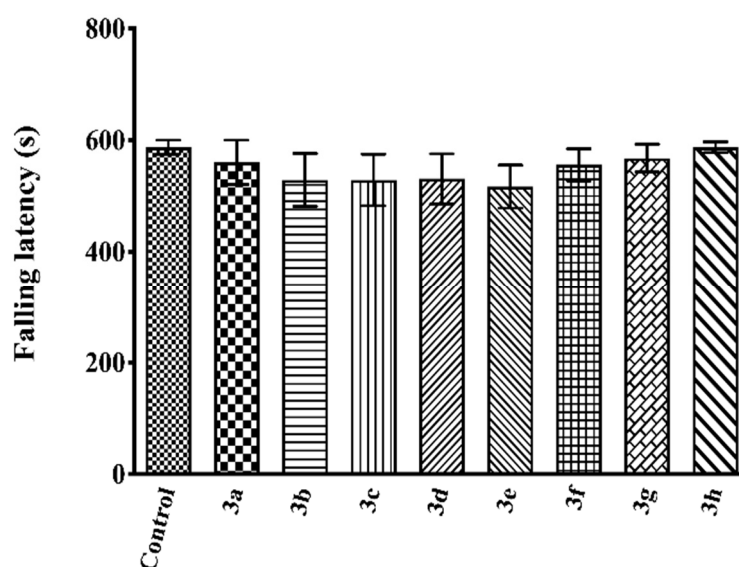
Figure 6. Effects of test compounds **3a–3h** (50 mg/kg) on falling latencies of mice in the Rota-Rod test. Values are mean $\pm$ SEM. One-way ANOVA and post-hoc Tukey's test, $n = 7$.

The effects of naloxone pre-treatment on the antinociceptive effects of test compounds in the tail-clip ($F_{(11,72)} = 28.53$, $p < 0.001$) and hot-plate ($F_{(11,72)} = 16.87$, $p < 0.001$) tests are shown in Figures 7 and 8, respectively. In both tests, naloxone pre-treatments significantly reversed the increase in MPE % values induced by compounds **3a–3c**, **3f**, and **3g**.
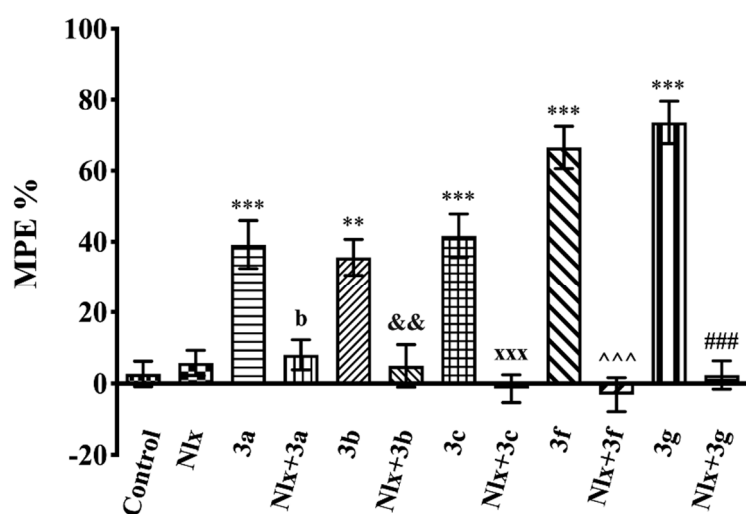
Figure 7. Effect of naloxone (5.48 mg/kg, i.p.) pre-treatment on antinociceptive activity induced by compounds **3a**–**3c**, **3f**, and **3g** in the tail-clip test. Significance against control group ** $p < 0.01$, *** $p < 0.001$; significance against compound groups: **3a** [b] $p < 0.01$; **3b** [&&] $p < 0.01$; **3c** [xxx] $p < 0.001$; **3f** [^^^] $p < 0.001$; **3g** [###] $p < 0.001$. Values are mean $\pm$ SEM. One-way ANOVA and post-hoc Tukey's test, $n = 7$.
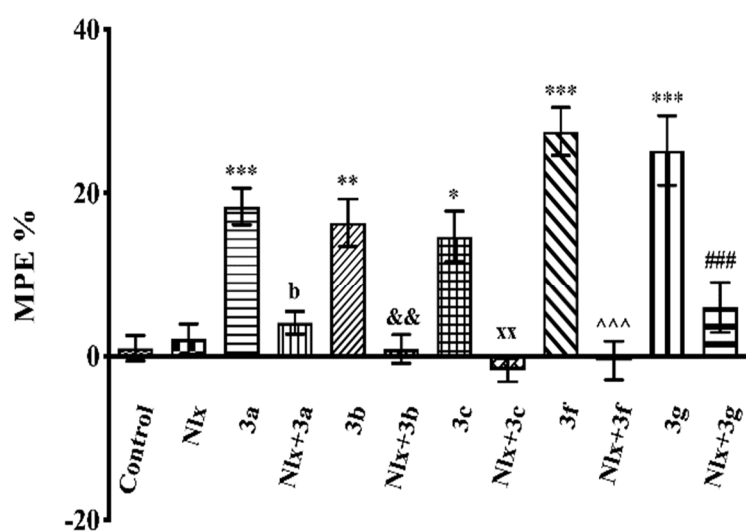
Figure 8. Effect of naloxone (5.48 mg/kg, i.p.) pre-treatment on antinociceptive activity induced by compounds **3a**–**3c**, **3f**, and **3g** in the hot-plate test. Significance against control group * $p < 0.05$, ** $p < 0.01$, *** $p < 0.001$; significance against compound groups: **3a** [b] $p < 0.01$; **3b** [&&] $p < 0.01$; **3c** [xx] $p < 0.01$; **3f** [^^^] $p < 0.001$; **3g** [###] $p < 0.001$. Values are mean $\pm$ SEM. One-way ANOVA and post-hoc Tukey's test, $n = 7$.

The effects of naloxone pre-treatment on the antinociceptive effects of the test compounds in the acetic acid-induced writhing test are shown in Figure 9. Naloxone pre-treatments significantly antagonized the decrease in the number of writhing movements and reversed the antinociceptive effect of compounds **3a**–**3c**, **3f**, and **3g** ($F_{(11,72)} = 12.03$, $p < 0.001$).
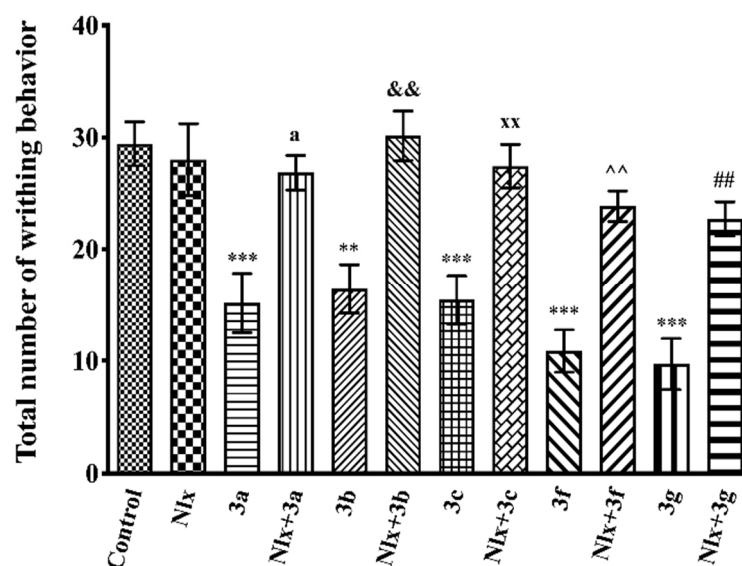
Figure 9. Effect of naloxone (5.48 mg/kg, i.p.) pre-treatment on antinociceptive activity induced by compounds **3a**–**3c**, **3f**, and **3g** in the acetic acid-induced writhing test. Significance against control group ** $p < 0.01$, *** $p < 0.001$; significance against compound groups: **3a** ^{a} $p < 0.05$; **3b** $^{\&\&}$ $p < 0.01$; **3c** ^{xx} $p < 0.01$; **3f** $^{\wedge\wedge}$ $p < 0.01$; **3g** $^{\#\#}$ $p < 0.01$. Values are mean ± SEM. One-way ANOVA and post-hoc Tukey's test, $n = 7$.

2.4. Molecular Docking Studies

Molecular docking studies were performed to clarify binding profiles of the tested derivatives to active sites of opioid receptors. For this purpose, the crystal structures of μ-opioid receptor (PDB ID: 5C1M) [33], δ-opioid receptor (PDB ID: 4N6H) [34], and k-opioid receptor (PDB ID: 6B73) [35] were retrieved from the Protein Data Bank server (www.pdb.org, accessed date 28 April 2021). The two-dimensional and three-dimensional docking poses of all compounds against all receptors are presented in Figures 10–24, and Supplementary Materials Figures S33–S68.
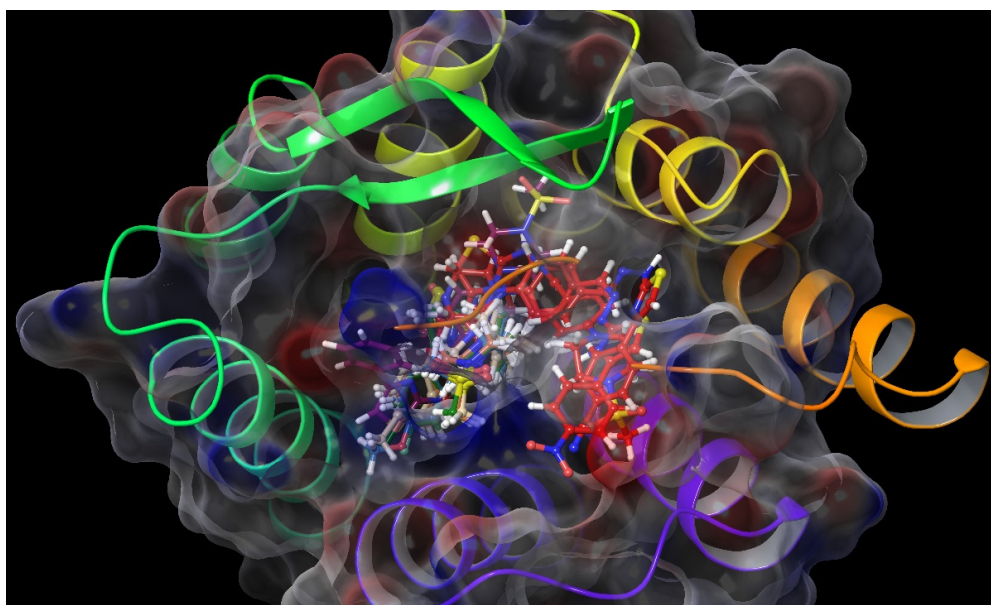
Figure 10. The three-dimensional pose of the interaction of all compounds with the μ-opioid receptor (PDB Code: 5C1M) active site. The inactive compounds (**3d**, **3e**, and **3h**) are presented by a tube model colored with red.
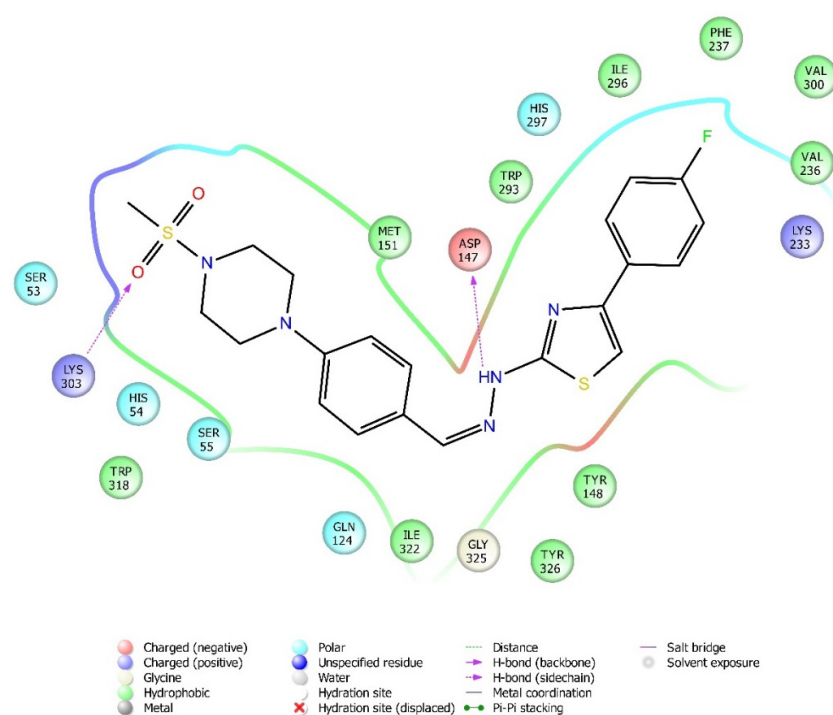
Figure 11. The two-dimensional interacting mode of compound **3f** in the active region of μ-opioid receptor (PDB Code: 5C1M).
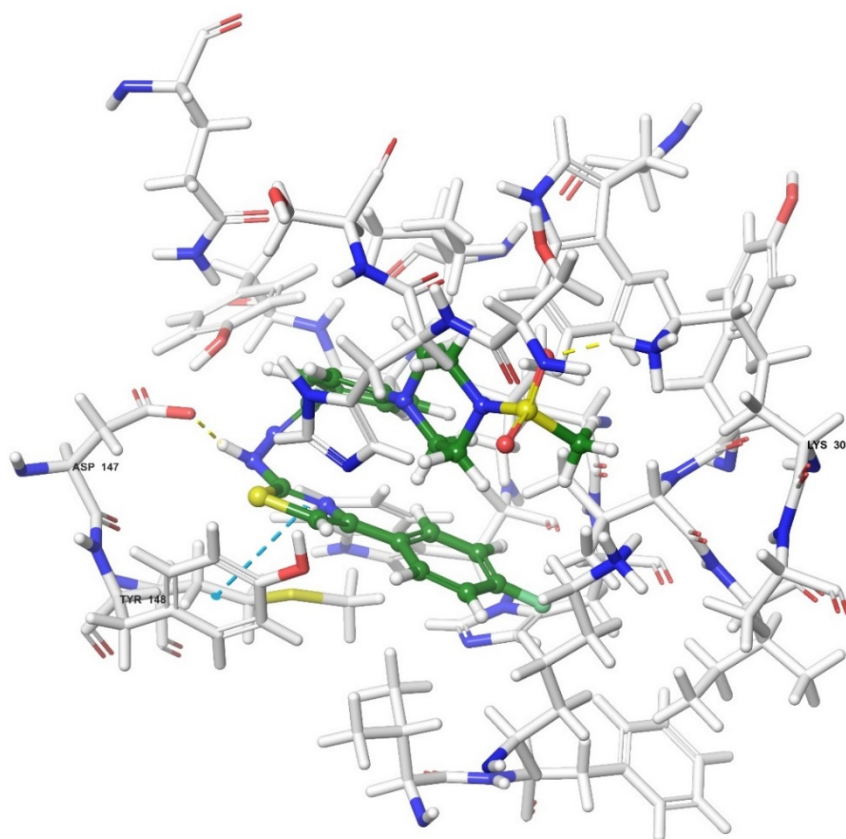
Figure 12. The three-dimensional interacting mode of compound **3f** in the active region of μ-opioid receptor. The ligand and significant residues of the active site of the receptor are presented by a tube model colored with green and white, respectively (PDB Code: 5C1M).
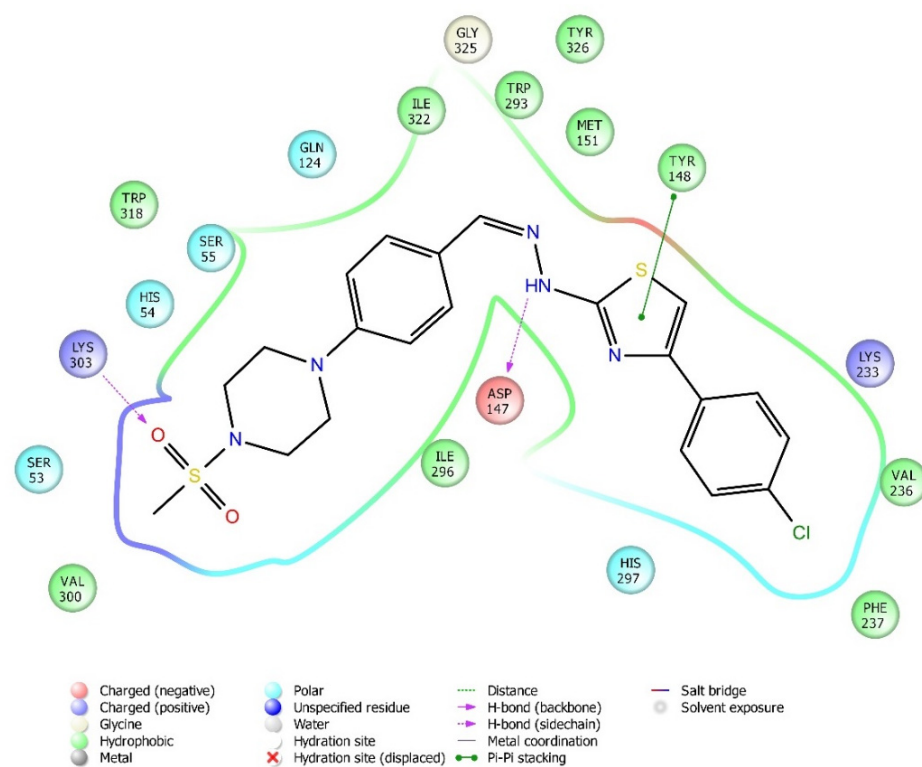
Figure 13. The two-dimensional interacting mode of compound **3g** in the active region of μ-opioid receptor (PDB Code: 5C1M).
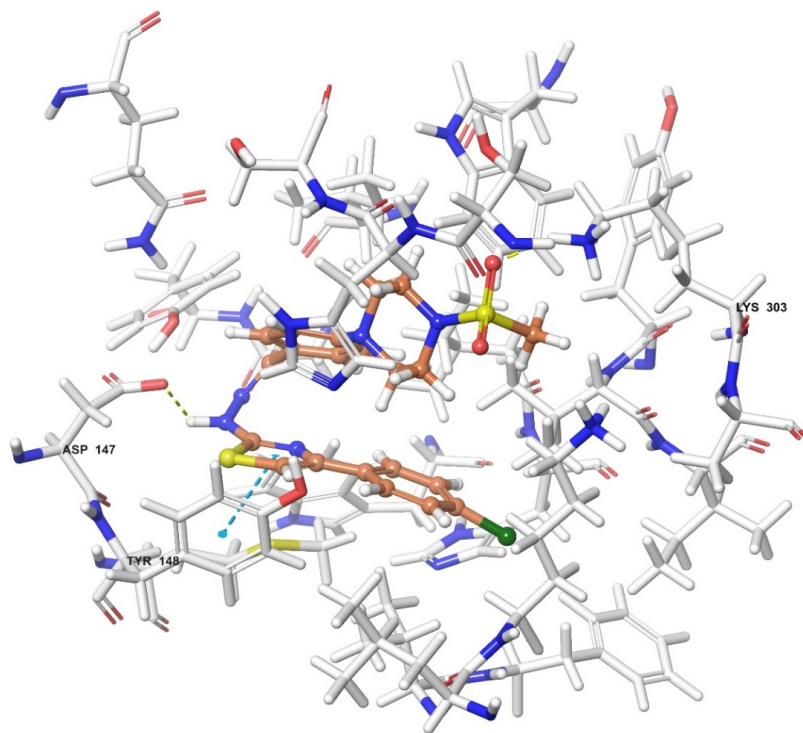
Figure 14. The three-dimensional interacting mode of compound **3g** in the active region of μ-opioid receptor. The ligand and significant residues of the active site of the receptor are presented by a tube model colored with orange and white, respectively (PDB Code: 5C1M).
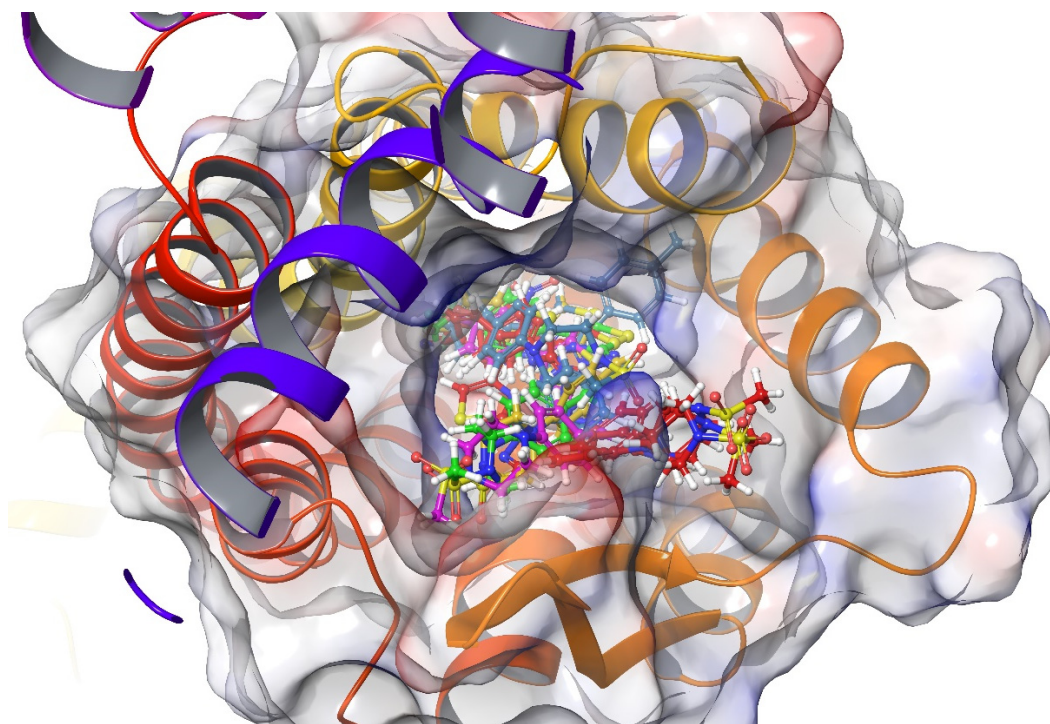
Figure 15. The three-dimensional pose of the interaction of all compounds with the δ-opioid receptor (PDB Code:4N6H) active site. The inactive compounds (**3d**, **3e**, and **3h**) are presented by a tube model colored with red.
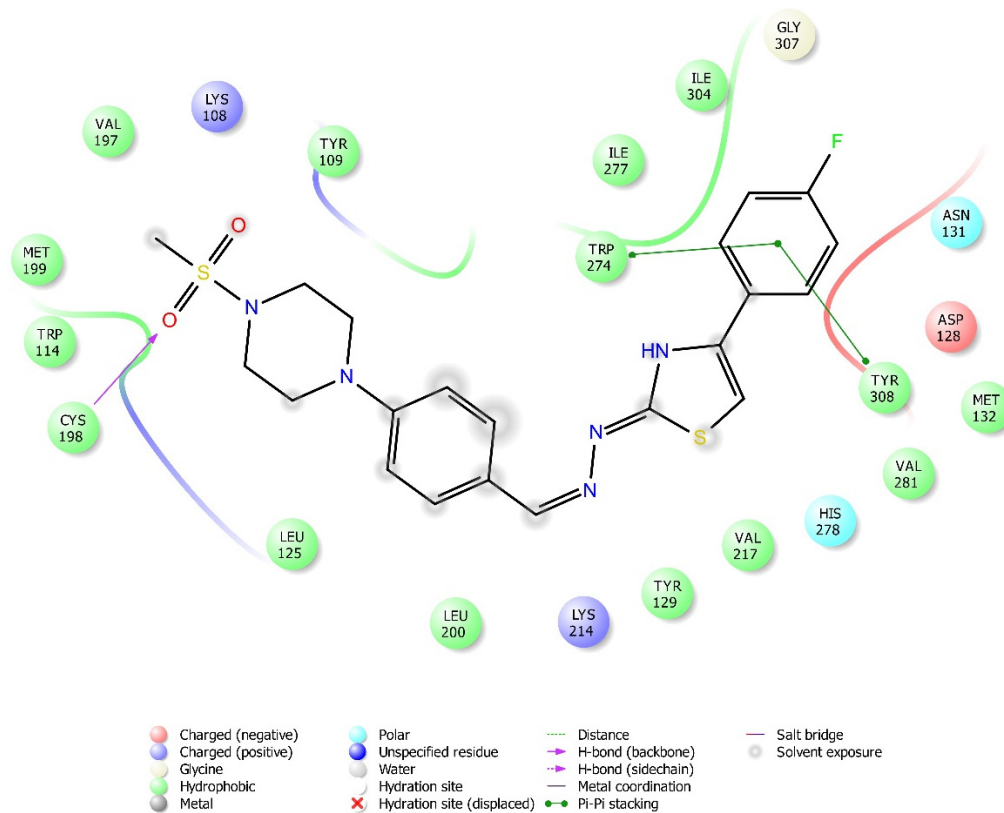
Figure 16. The two-dimensional interacting mode of compound **3f** in the active region of δ-opioid receptor (PDB Code: 4N6H).
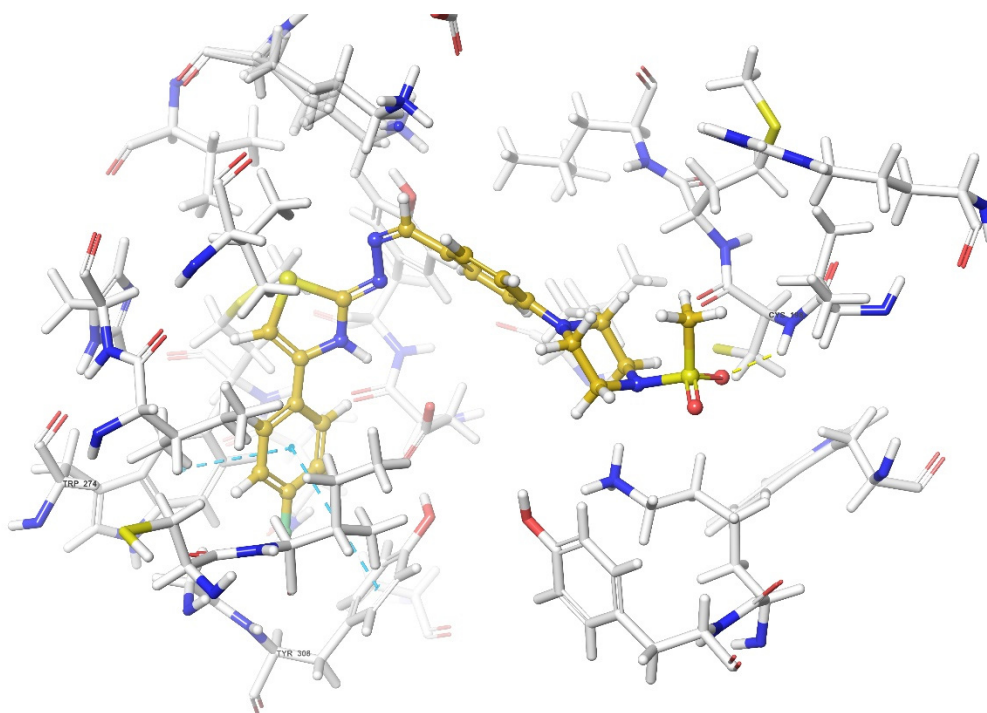
Figure 17. The three-dimensional interacting mode of compound **3f** in the active region of δ-opioid receptor. The ligand and significant residues of the active site of the receptor are presented by a tube model colored with yellow and white, respectively (PDB Code: 4N6H).
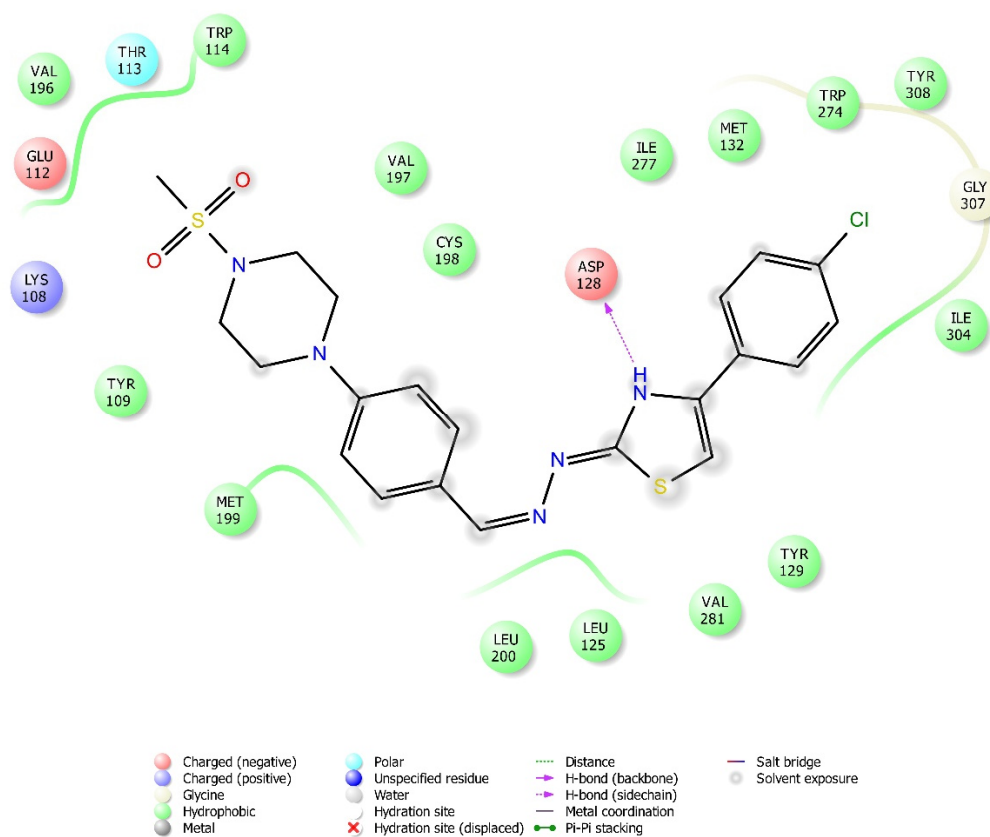
Figure 18. The two-dimensional interacting mode of compound **3g** in the active region of δ-opioid receptor (PDB Code: 4N6H).
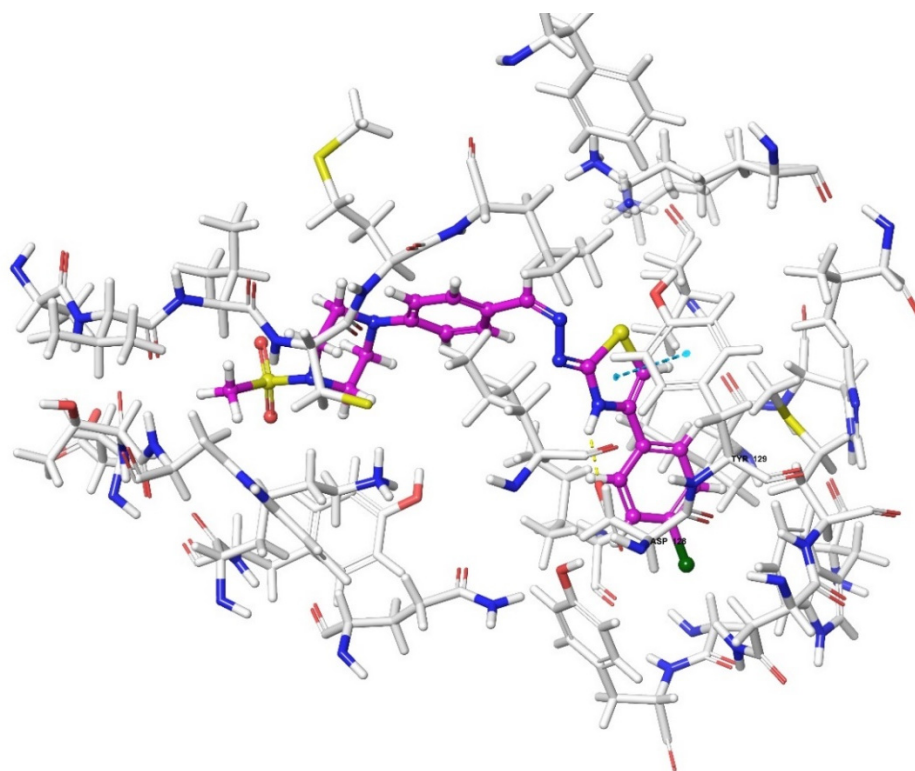
Figure 19. The three-dimensional interacting mode of compound **3g** in the active region of δ-opioid receptor. The ligand and significant residues of the active site of the receptor are presented by a tube model colored with purple and white, respectively (PDB Code: 4N6H).
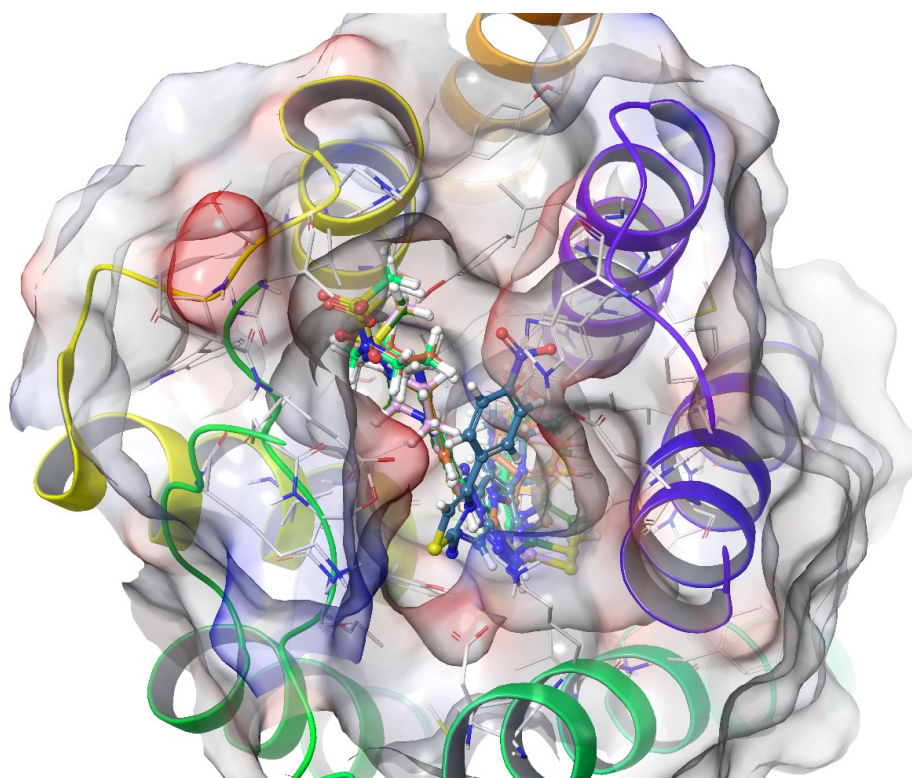
Figure 20. The three-dimensional pose of the interaction of all compounds with the k-opioid receptor (PDB Code:6B73) active site. The compound **3e** is presented by a tube model colored with blue.
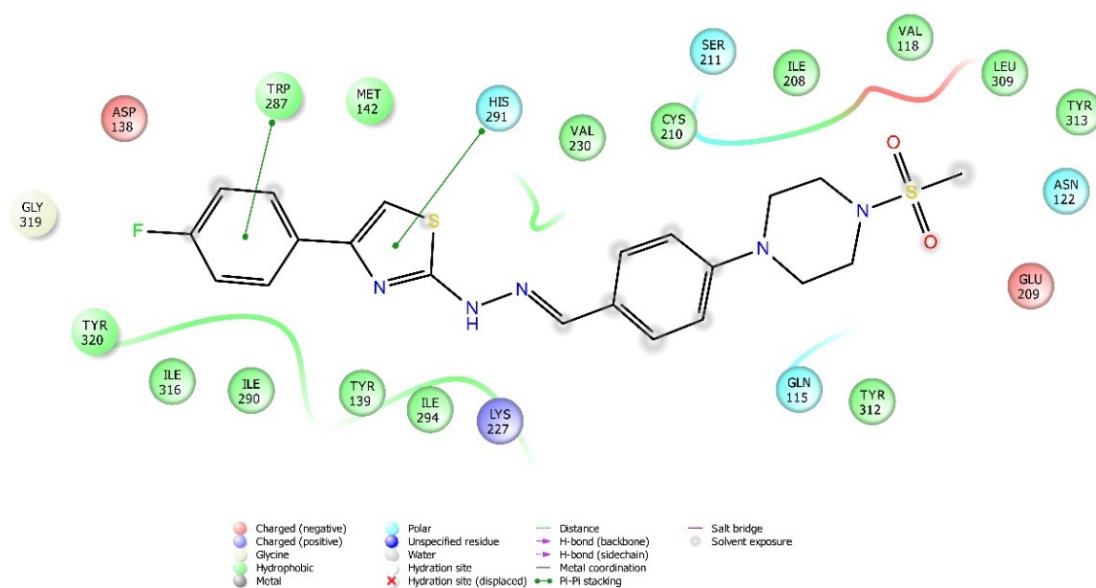
Figure 21. The two-dimensional interacting mode of compound **3f** in the active region of k-opioid receptor (PDB Code: 6B73).
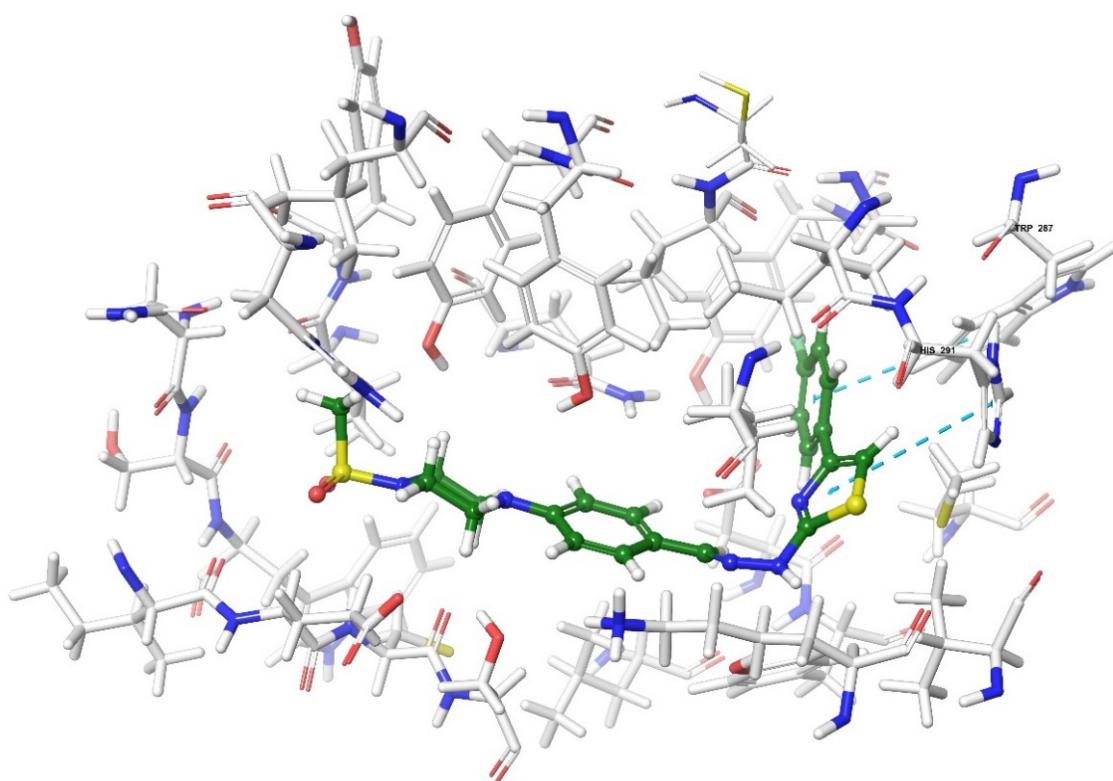
Figure 22. The three-dimensional interacting mode of compound **3f** in the active region of k-opioid receptor. The ligand and significant residues of the active site of the receptor are presented by a tube model colored with green and white, respectively (PDB Code: 6B73).
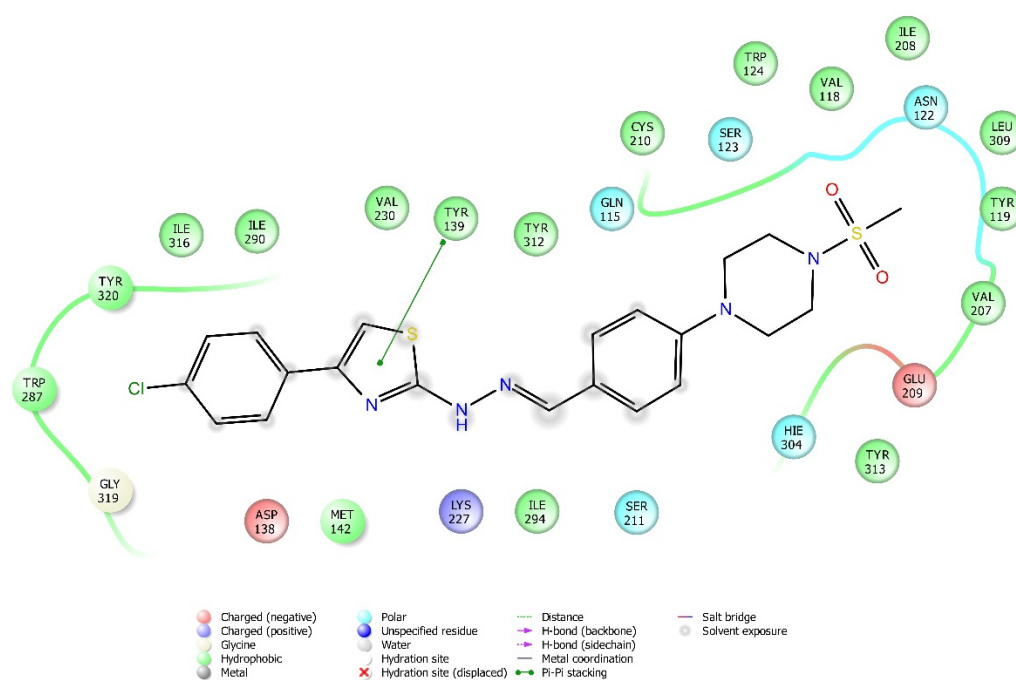
Figure 23. The two-dimensional interacting mode of compound **3g** in the active region of k-opioid receptor (PDB Code: 6B73).
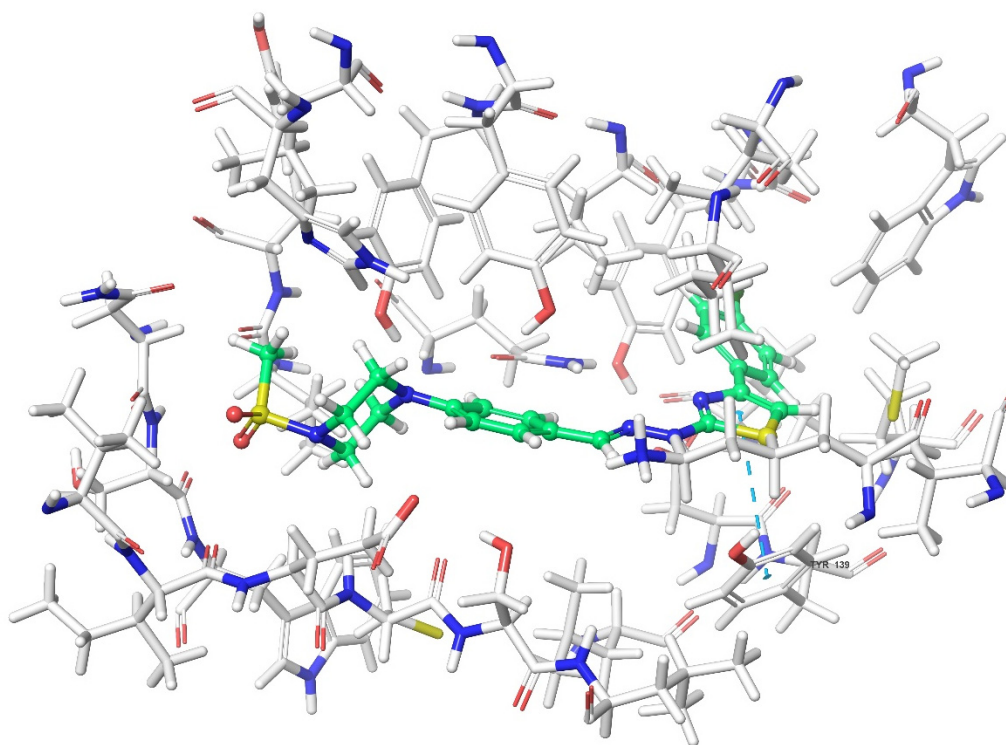
Figure 24. The three-dimensional interacting mode of compound **3g** in the active region of k-opioid receptor. The ligand and significant residues of the active site of the receptor are presented by a tube model colored with green and white, respectively (PDB Code: 6B73).

According to the crystallographic X-ray structure of the μ-opioid receptor (PDB ID:5C1M), the rendered docking poses of all compounds are shown in Figures 10–14 and in Supplementary Materials Figures S33–S44. When the compounds were analyzed all together, it is seen that compounds **3a**–**3c**, **3f**, and **3g** fit well to the active site of the receptor, whereas **3d**, **3e**, and **3h** do not place properly (compounds colored in red) (Figure 10). The presented 2D

and 3D docking poses of the test compounds exhibited that pharmacologically ineffective derivatives cannot achieve to build necessary interactions with the receptor protein (See Supplementary Materials Figures S33–S44).

When the interactions are analyzed in terms of binding to the μ-opioid receptor, π-π interactions are observed between the thiazole rings of compounds **3b**, **3c**, and **3g** and the phenyl group of Tyr148. Additionally, the phenyl ring of compounds **3a** and **3h** formed a π-π interaction with imidazole group of His54. Hydrogen bonds were the other bonds constructing between the ligands and μ-opioid receptors. The sulfonyl moieties of compounds **3b**, **3c**, **3f**, and **3g** formed single hydrogen bonds with the amine groups of Lys303. Another hydrogen bond is observed between the hydrazine groups of compounds **3c**, **3f**, and **3g** and hydroxy group of Asp147. These results are in accordance with the previous literature [36]. Moreover, compound **3d** did not interact with this opioid receptor subtype, while compound **3e** is observed to form only a salt bridge with Lys303 amino acid of μ-opioid receptor protein.

According to the crystallographic X-ray structure of the δ-opioid receptor (PDB ID: 4N6H), the rendered docking poses of all compounds are provided in Figures 15–19 and in Supplementary Materials Figures S45–S56. Obtained findings indicated that compounds **3a**–**3c**, **3f**, and **3g** fit well to the active site of the receptor, whereas **3d**, **3e**, and **3h** do not (compounds colored in red) (Figure 15). The presented 2D and 3D docking poses of the test compounds exhibited that pharmacologically ineffective derivatives are not able to form required interactions with the receptor protein (See Supplementary Materials Figures S45–S56).

Docking findings obtained from δ-opioid receptor studies revealed that there are two π-π interactions between the phenyl on thiazole ring of compound **3a** and the phenyl groups of Tyr308 and Trp274. Similar bonds are also observed for compound **3f**. Another π-π interaction is observed between the thiazole ring of compound **3b** and phenyl group of Tyr129. It is also seen that the active molecules form notable hydrogen bonds with the receptor. The sulfonyl moieties of compounds **3a** and **3f** formed hydrogen bonds with Cys198. Moreover, sulfonyl moiety and hydrazine nitrogen of compound **3b** displayed hydrogen bond interactions with Lys214 and Asp128, respectively. Thiazole ring of compound **3g** also formed a hydrogen bond with Asp128. Besides, compound **3e** is observed to form a π-cation interaction with His278. Although compound **3c** fitted to the active site of the δ-receptor, no interaction was observed.

According to the crystallographic X-ray structure of the k-opioid receptor (PDB ID: 6B73), the rendered docking poses of obtained compounds are provided in Figures 20–24 and in Supplementary Materials Figures S57–S68. As seen in the 3D pose, all compounds are located in the active site (Figure 20). It is observed that π-π interactions occur between the thiazole rings of compounds **3a** and **3g**, and phenyl group of Tyr139. Another π-π interaction is seen between the phenyl rings of compounds **3a**, **3b**, and **3f** and indole group of Trp287. Moreover, thiazole rings of compounds **3d**, **3f**, and **3h** are observed to form π-π interactions with imidazole group of His291. Settlement of compound **3e** on this receptor protein was quite different from those of other compounds. This compound formed a π-π interaction with Try139, a salt-bridge with Lys227, Glu297, and a π-cation interaction with Lys227 and Tyr312. On the other hand, compound **3c** did not interact with the k receptors.

Results of the docking studies are summarized in Table 3.

Table 3. Interaction sites of opioidergic receptor subtypes with the test compounds.

Compound	Receptor *	H-Bond	π-π Interaction	Salt Bridge	π-Cation Interaction
3a	MOR		His54		
	DOR	Cys198	Trp274, Tyr308		
	KOR		Try139, Trp287		
3b	MOR	Lys303	Tyr148		
	DOR	Lys214, Asp128	Tyr129		
	KOR		Trp287		
3c	MOR	Lys303, Asp147	Tyr148		
	DOR				
	KOR				
3d	MOR				
	DOR				
	KOR		His291		
3e	MOR			Lys303	
	DOR				His278
	KOR		Try139	Lys227, Glu297	Lys227, Tyr312
3f	MOR	Lys303, Asp147			
	DOR	Cys198	Trp274, Tyr308		
	KOR		His291, Trp287		
3g	MOR	Lys303, Asp147	Tyr148		
	DOR	Asp128			
	KOR		Tyr139		
3h	MOR		His54		
	DOR				
	KOR		His291		

* Receptor crystals retrieved from the protein data bank. The PDBIDs for MOR, DOR, and KOR were 5C1M, 4N6H, and 6B73, respectively.

3. Discussion

Eight novel compounds (**3a**–**3h**) carrying thiazole-piperazine ring systems were synthesized and investigated for their possible acute antinociceptive activities, in this study.

In antinociceptive activity screening studies, methods that evaluate the nociceptive behaviors of animals induced by nociceptive mechanical, thermal, or chemical stimuli are used. Stimuli applied to create pain perception in experimental animals should be measurable, reproducible, and non-invasive [37].

In this study, antinociceptive activities after oral administration of the compounds against mechanical nociceptive stimulus were investigated by the tail-clip tests. The administration of compounds **3a**–**3c**, **3f**, and **3g**, at doses of 50 mg/kg, significantly increased the MPE % values of mice compared to the control group (Figure 3), indicating that these compounds possess antinociceptive activity by affecting the neuronal pathways carrying mechanical stimuli. Moreover, based on the knowledge that this test is predominantly related to nociceptive transmission at the spinal level [38,39], it can be assumed that spinal mechanisms play a role in the antinociceptive effects of these compounds.

The antinociceptive activities after oral administration of the test compounds against thermal nociceptive stimulus were examined by the hot-plate test. Results showed that administrations of the compounds **3a–3c**, **3f**, and **3g** significantly enhanced the MPE % values compared to the control group (Figure 4), indicating that these compounds affect the nociceptive pathways carrying the thermal as well as the mechanical stimuli. Based on the well-documented association of this test with supraspinal nociceptive transmission [38–41], it can be assumed that supraspinal mechanisms play a role in the antinociceptive effects of these compounds, together with the spinal mechanisms. When MPE % values of the compounds are examined in both tests, it is seen that compounds **3f** and **3g** (50 mg/kg, p.o.) are as effective as the reference drug morphine (10 mg/kg, i.p.) in tail-clip tests, unlike the effects in hot-plate tests. These findings may be due to the fact that the antinociceptive effects of the compounds **3f** and **3g** on the spinal pathways are stronger than those in the supraspinal pathways, or because these two compounds affect the mechanical nociceptive pathways more strongly than the thermal ones.

Peripheral antinociceptive effects of test compounds were investigated by an acid-induced writhing test that models visceral pain [42]. In this test, acetic acid administrated by i.p. route acts in direct (by activating the nociceptors) or indirect (by triggering the release of autacoid mediators) ways [43] to stimulate the peripheral receptors on the surface of the peritoneal cavity [44]. This stimulation causes a writhing behavior in animals characterized by contraction of the abdominal muscles and backward stretching of the hind legs [41,45]. Oral administration of compounds **3a–3c**, **3f**, and **3g** significantly inhibited the writhing of animals (Figure 5 and Table 2), indicating that these compounds exhibit peripheral antinociceptive effects on the neuronal pathways that transfer chemical painful stimuli. The peripheral antinociceptive activities of these compounds may be related to the reduced release of inflammatory mediators and/or direct blockage of their receptors. Possible increase in the nociceptive thresholds or interruption in the transmission of pain stimuli in the nerve fiber may also be other mechanisms underlying the observed antinociception [40,41,46].

It is known that possible effects of the test compounds on the motor performances of animals may cause false-positive results in nociceptive tests [40,41]. Therefore, Rota-Rod tests were conducted to evaluate the motor coordination of mice. Data show that none of the test compounds caused significant alterations in the motor activities of mice (Figure 6), indicating that the antinociceptive effects exhibited in this study are specific.

After demonstrating the antinociceptive efficacies of compounds **3a–3c**, **3f**, and **3g**, the possible involvement of opioidergic mechanisms in the presented pharmacological activity was investigated by naloxone studies. Naloxone pre-treatment reversed the antinociceptive activities of these compounds in all of the nociceptive tests (Figures 7–9), indicating that opioidergic mechanisms participate in the antinociceptive activity of these compounds. Then, we performed docking studies in order to clarify the interactions of our molecules with opioid receptors.

Results of the docking studies on the μ-opioid receptor indicated that compounds **3a–3c**, **3f**, and **3g** formed π-π interactions and/or hydrogen bonds with His54, Asp147, Tyr148, and Lys303 amino acids of the receptor protein, probably conferring antinociceptive activity to these derivatives. Actually, these findings are in accordance with previous knowledge obtained from the fragment molecular orbital (FMO) method, which revealed that His54 (N-terminus), Asp147 (TM3), and Lys303 (TM6) are the most significant residues contributing to the μ-opioid receptor-mediated analgesic efficacy of opioids [36]. It was determined that π-π interactions between the pharmacologically active compounds **3b**, **3c**, and **3g** and μ-opioid receptors occurred through the Tyr148 amino acid of the receptor protein. Moreover, His54 was the only amino acid involved in the π-π interactions between the μ-receptor protein and compound **3a**. Therefore, it can be speculated that interactions with Tyr148 and His54 amino acids may be supportive of the antinociceptive activities of these molecules. Nevertheless, compound **3h** is the exception. The fact that compound **3h** does not show an antinociceptive effect although it shows π-π interactions with His54 may be related to the

inability of this molecule to enter the active pocket due to the CF3 group it carries. Although docking studies have revealed various π-π interactions between the active compounds and the μ-receptor protein, hydrogen bonds seem to be major contributors of the antinociceptive effect. It is observed that compounds **3f**, **3g**, and **3c**, whose phenyl ring is substituted with the electron-donating groups (F, Cl, and OCH_3, respectively), formed hydrogen bonds with Lys303 and Asp147 amino acids of the μ-opioid receptors. Besides, compound **3b**, carrying another electron-donating group (CH_3) on its phenyl ring, also formed hydrogen bonds with Lys303 amino acids. On the other hand, no hydrogen bonds have formed between these receptor subtypes and compounds **3d**, **3e**, and **3h**, which have phenyl rings, substituted with electron-withdrawal groups such as CN, NO_2, and CF3. Therefore, it may be speculated that substitution of phenyl ring with electron-donating groups supports the hydrogen bond formation with μ-opioid receptor subtype.

Compounds **3a**, **3b**, **3f**, and **3g** were observed to form π-π interactions and/or hydrogen bonds with Asp128, Tyr129, Cys198, Lys214, Trp274, and Tyr308 amino acids of the δ-opioid receptor protein. These interactions pointed out that δ-opioid receptors, together with μ-receptor subtypes, play roles in the antinociceptive activities of these compounds. Among the pharmacologically active compounds, only **3a** and **3f** were detected to form π-π interactions with both of the Trp274 and Tyr308 amino acids of the δ-opioid receptors. Another π-π interaction was seen between the compound **3b** and Tyr129. Active compounds **3a**, **3b**, **3f**, and **3g** were observed to form hydrogen bonds with Cys198, Asp128, and Lys214 amino acids of δ-opioid receptor protein. Since compounds **3f**, **3g**, and **3b** have phenyl rings substituted by F, Cl, and CH_3, it can be assumed that substitution of the phenyl ring with electron-donating groups can promote the formation of strong hydrogen bonds between the test compounds and δ-opioid receptors, as in the μ-receptor subtype. Indeed, absence of any hydrogen bonding or π-π interactions between inactive test compounds (**3d**, **3e**, and **3h**) carrying phenyl rings substituted by electron-withdrawal groups and δ-opioid receptors confirms this idea. On the other hand, another active compound **3c** did not interact with the δ-receptor protein, although it fits into the active site of the receptor. Thus, it is possible that compound **3c** induced its antinociceptive activity via μ-opioid receptors that we know to form hydrogen bonds and π-π interactions with this compound, rather than δ-receptors.

Docking findings obtained from the k-opioid receptor studies were different from the results of μ- and δ-subtypes. Not only active derivatives but also pharmacologically inactive compounds settled down to the k-receptor protein, successfully. It was observed that active compounds **3a**, **3b**, **3f**, and **3g** formed π-π interactions with the Tyr139, Trp287, and His291 amino acids of k receptor protein, while no hydrogen bonds were detected. On the other hand, compounds **3d** and **3h**, having π-π interactions with His291, and compound **3e**, having the same type of interaction with Try139, were inactive in the nociceptive tests. Since these π-π interactions are common for all of the active and inactive compounds, the only significant binding might be the π-π interaction formed with Trp287 amino acid. Nevertheless, it should also be noted that the contributions of the weak π-π interactions to the antinociceptive effects of these compounds are limited. Moreover, it was observed that compound **3c**, an active derivative in the serial, did not show any interaction with the k-receptor protein. All these findings pointed out that there is not a significant settlement/binding and activity relationship between the molecules and k-opioid receptor protein. Therefore, it can be suggested that k-opioid receptors did not mediate the antinociceptive effects of the active compounds presented in this study.

Data obtained from the docking studies indicated that thiazole rings in the compounds seem responsible to form π-π interactions with all of the μ-, δ-, and k-opioid receptor subtypes. Thiazole ring even constructs a hydrogen bond between compound **3g** and δ-opioid receptor protein. In addition, hydrazine groups of compound **3f** and compound **3b** were shown to build hydrogen bonds with μ- and δ-receptors, respectively. More importantly, methylsulfonyl residues of the active derivatives seem to build strong hydrogen bonds with the active sites of μ- and δ-receptor subtypes, which seem to be critical for the pre-

sented antinociceptive effect in this study. The same residues, on the other hand, did not show similar interactions with k-opioid receptors, which seem to be irrelevant to the activity. This difference in binding properties of methylsulfonyl residues may be related to conformational arrangement of the substituents, which alter the settlements on opioid receptors and affect interactions with them.

Differences in the electronic properties of the compounds can also change their pharmacological activity profiles. For example, electron-donating substituents (CH_3, OCH_3, F, and Cl) in the chemical structures of the derivatives seem to support μ- and δ-opioid receptor bindings and antinociceptive activity, more than electron-withdrawing groups such as cyano, nitro, and trifluoromethyl (**3d**, **3e**, and **3h**). Substitutions with CN (**3d**) and NO_2 (**3e**) groups increased TPSA values, reflecting the increased polarity of the molecules, possibly resulting in reduced transport of molecules across membranes. These compounds were indeed ineffective in activity tests. In addition, substitutions with Cl (**3g**) and CF_3 (**3h**) increased the lop P values, reflecting the enhanced lipofility of these compounds. Really, **3g** was active in the nociceptive tests. However, **3h** was not. The ineffectiveness of the CF_3-substituted compound **3h** may possibly be related to its high MW and MV values, hindering the molecule from placing on the μ- and δ-opioid receptors. Furthermore, it was observed that compound **3e**, which has a higher number of hydrogen acceptors than the other molecules (Table 1), did not form any hydrogen bonds to opioid receptors. The probable reason for this is that this molecule is improperly located on the receptor and therefore is not able to form any bond with it.

Future Directions

In the present study, the opioid system-mediated antinociceptive activities of some novel compounds, bearing both of the thiazole and piperazine ring systems together on their structures, have been evidenced. Although the binding potential of active molecules to opioid receptors has been shown by an in silico method in this study, it will be useful to verify this binding by further methods, such as radioligand binding. Moreover, based on the fact that pain transmission and antinociception are complex processes affected by various endogenous mechanisms [47,48], possible contributions of different mechanisms such as GABAergic, glutamatergic, cannabinoidergic, cholinergic, nitrergic systems, ion channels, or enzymes (such as COX isoenzymes) [49,50], which may be underlying the pharmacological effects of these compounds, need to be clarified with further studies.

Since this study was planned as a synthesis and antinociceptive activity screening study, we contended with the calculation of the ADME parameters, which provides an overview regarding the pharmacokinetic properties of the molecules. On the other hand, dose-response curves can be drawn by using pharmacological responses induced by different doses of each compound, various pharmacodynamic parameters, such as E_{max} and ED_{50}, can be calculated, and more detailed pharmacodynamic data for each active molecule can be obtained in the next step of this study.

An important point regarding the potential of new compounds to become analgesic drugs is the side effect profiles of these molecules. Although the tested compounds did not show undesirable side effects such as death, paralysis, ataxia, convulsions, or diarrhea, promising that they do not have a serious toxicity potential, the efficacy and safety of these compounds should be investigated by further detailed studies. In this context, it is of great importance to evaluate active molecules in terms of possible side effects such as respiratory depression, emesis, addiction, and tolerance development, which are typical side effects of opioid drugs [51].

4. Materials and Methods

4.1. Chemicals

All reagents were purchased from commercial suppliers and were used without further purification. Morphine sulphate and naloxone hydrochloride were acquired from Sigma-Aldrich (St. Louis, MO, USA).

4.2. Chemistry

Melting points (m.p.) were determined on the Mettler Toledo-MP90 Melting Point System and were uncorrected. IR spectra were recorded on an IR Affinity-1S Infrared spectrophotometer (Shimadzu, Tokyo, Japan). ^{1}H NMR and ^{13}C NMR spectra in DMSO-d_6 were recorded on a Bruker Fourier 300 (Bruker Bioscience, Billerica, MA, USA), respectively. MS studies were performed on an LCMS-8040 tandem mass system (Shimadzu, Tokyo, Japan). Chemical purities of the compounds were checked by classical TLC applications performed on silica gel 60 F254 (Merck KGaA, Darmstadt, Germany). The Rf values of the synthesized compounds were measured using the solution system of petroleum ether:ethyl acetate (1:1).

4.2.1. Synthesis of 4-(4-(methylsulphonyl)piperazin-1-yl)benzaldehyde (1)

1-(Methylsulphonyl)piperazine (2.8 g, 0.017 mol), 4-fluorobenzaldehyde (1.82 mL, 0.017 mol), and potassium carbonate (2.35 g, 0.017 mol) were refluxed in DMF (10 mL). The complete reaction content was poured into ice-water, and the precipitated product was washed with water, filtered, dried, and recrystallized from EtOH.

4.2.2. Synthesis of 2-(4-(4-(methylsulphonyl)piperazin-1-yl)benzylidene)hydrazine-1-carbothioamide (2)

A mixture of 4-(4-(methylsulphonyl)piperazin-1-yl)benzaldehyde (1) (4 g, 0.014 mol) and hydrazinecarbothioamide (1.36 g, 0.014 mol) was refluxed in ethanol (50 mL) for 10 h. The reaction mixture was cooled, and the precipitated product was filtered, washed with cooled ethanol, and dried.

4.2.3. General Procedure for the Synthesis of Target Compounds (**3a**–**3h**)

2-(4-(4-(methylsulphonyl)piperazin-1-yl)benzylidene) hydrazine-1-carbothioamide (2) (0.48 g, 0.0014 mol) and the appropriate 2-bromo-1-(4-substituted)ethan-1-one (0.0014 mol) derivatives were stirred for 5 h in EtOH at 150 °C. The reaction mixture was cooled, and the precipitated product was filtered, and washed with cooled EtOH.

1-Methylsulphonyl-4-(4-{[2-(4-phenyl-1,3-thiazol-2-yl)hydrazinylidene]methyl}phenyl) piperazine (**3a**)

Yield: 85%, Rf = 0.57, M.P. = 210–212 °C, FTIR (ATR, cm^{-1}): 3294 (N-H), 2843 (C-H), 771, 711. ^{1}H-NMR (300 MHz, DMSO-d_6): δ = 2.93 (3H, s, -CH$_3$), 3.23–3.26 (4H, m, piperazine), 3.33–3.37 (4H, m, piperazine), 6.98 (2H, d, J = 8.9 Hz, Monosubstituephenyl), 7.03 (2H, d, J = 8.9 Hz, 1,4-Disubstituephenyl), 7.27–7.32 (2H, m, Monosubstituephenyl + Thiazole), 7.41 (2H, t, J = 7.5 Hz, Monosubstituephenyl), 7.53 (2H, d, J = 8.9 Hz, 1,4-Disubstituephenyl), 7.85 (2H, d, J = 7.2 Hz, Monosubstituephenyl), 7.95 (1H, s, -CH=N-), 11.97 (1H, s, -NH). ^{13}C-NMR (75 MHz, DMSO-d_6): δ = 34.32, 45.59, 47.76, 103.67, 115.93, 125.65, 125.96, 127.90, 129.05, 131.91, 135.20, 142.06, 150.92, 151.46, 168.79. ESI-MS (*m/z*): [M + H]$^+$: 442.09.

1-Methylsulphonyl-4-[{2-[4-(4-methylphenyl)-1,3-thiazol-2-yl]hydrazinylidene}methyl] piperazine (**3b**)

Yield: 82%, Rf = 0.68, M.P. = 226–230 °C, FTIR (ATR, cm^{-1}): 3294 (-NH), 2856 (C-H), 817. ^{1}H-NMR (300 MHz, DMSO-d_6): δ = 2.32 (3H, s, -CH$_3$), 2.93 (3H, s, -CH$_3$), 3.23–3.26 (4H, m, piperazine), 3.33–3.36 (4H, m, piperazine), 7.03 (2H, d, J = 8.9 Hz, 1,4-Disubstituephenyl), 7.19–7.22 (3H, m, 4-Methylphenyl + Thiazole), 7.53 (2H, d, J = 8.9 Hz, 1,4-Disubstituephenyl), 7.74 (2H, d, J = 8.1 Hz, 4-Methylphenyl), 7.94 (1H, s, -CH=N-), 11.93 (1H, s, -NH). ^{13}C-NMR (75 MHz, DMSO-d_6): δ = 21.27, 34.32, 45.59, 47.77, 102.74, 115.93, 125.67, 125.91, 127.89, 128.75, 129.62, 132.56, 137.19, 141.98, 151.45, 168.69. ESI-MS (*m/z*): [M + H]$^+$: 456.11.

1-Methylsulphonyl-4-[{2-[4-(4-methoxyphenyl)-1,3-thiazol-2-yl]hydrazinylidene}methyl] piperazine (**3c**)

Yield: 87%, Rf = 0.77, M.P. = 175–178 °C, FTIR (ATR, cm^{-1}): 3294 (N-H), 2845 (C-H), 819. ^{1}H-NMR (300 MHz, DMSO-d_6): δ = 2.93 (3H, s, -CH$_3$), 3.23–3.25 (4H, m, piperazine), 3.33–3.36 (4H, m, piperazine), 3.78 (3H, s, -OCH$_3$), 6.96 (2H, d, *J* = 8.9 Hz, 4-Methoxyphenyl), 7.02 (2H, d, *J* = 8.9 Hz, 1,4-Disubstituephenyl), 7.10 (1H, s, Thiazole), 7.52 (2H, d, *J* = 8.9 Hz, 1,4-Disubstituephenyl), 7.78 (2H, d, *J* = 8.9 Hz, 4-Methoxyphenyl), 7.93 (1H, s, -CH=N-), 11.93 (1H, s, -NH). ^{13}C-NMR (75 MHz, DMSO-d_6): δ = 34.31, 45.59, 47.77, 55.55, 101.51, 114.03, 114.40, 115.93, 125.69, 127.28, 127.88, 128.07, 141.96, 151.44, 159.20, 168.68. ESI-MS (*m/z*): [M + H]$^+$: 472.10.

1-Methylsulphonyl-4-[{2-[4-(4-cyanophenyl)-1,3-thiazol-2-yl]hydrazinylidene}methyl] piperazine (**3d**)

Yield: 89%, Rf = 0.34, M.P. = 237–239 °C, FTIR (ATR, cm^{-1}): 3292 (N-H), 2845 (C-H), 2222 (C≡N), 817. ^{1}H-NMR (300 MHz, DMSO-d_6): δ = 2.92 (3H, s, -CH$_3$), 3.23–3.26 (4H, m, piperazine), 3.33–3.37 (4H, m, piperazine), 7.02 (2H, d, *J* = 8.9 Hz, 1,4-Disubstituephenyl), 7.53 (2H, d, *J* = 8.9 Hz, 1,4-Disubstituephenyl), 7.59 (1H, s, Thiazole), 7.86 (2H, d, *J* = 8.5 Hz, 4-Cyanophenyl), 7.96 (1H, s, -CH=N-), 8.03 (2H, d, *J* = 8.5 Hz, 4-Cyanophenyl), 12.01 (1H, s, -NH). ^{13}C-NMR (75 MHz, DMSO-d_6): δ = 34.42, 45.58, 47.76, 107.58, 109.98, 115.90, 119.47, 125.51, 126.56, 127.99, 133.13, 139.32, 142.57, 149.27, 151.55, 169.13. ESI-MS (*m/z*): [M + H]$^+$: 467.09.

1-Methylsulphonyl-4-[{2-[4-(4-nitrophenyl)-1,3-thiazol-2-yl]hydrazinylidene}methyl] piperazine (**3e**)

Yield: 88%, Rf = 0.79, M.P. = 220–223 °C, FTIR (ATR, cm^{-1}): 3305 (N-H), 2845 (C-H), 1504, 1334 (NO$_2$), 819. ^{1}H-NMR (300 MHz, DMSO-d_6): δ = 2.92 (3H, s, -CH$_3$), 3.23–3.26 (4H, m, piperazine), 3.34–3.37 (4H, m, piperazine), 7.02 (2H, d, *J* = 8.9 Hz, 1,4-Disubstituephenyl), 7.53 (2H, d, *J* = 8.9 Hz, 1,4-Disubstituephenyl), 7.67 (1H, s, Thiazole), 7.96 (1H, s, -CH=N-), 8.10 (2H, d, *J* = 9.0 Hz, 4-Nitrophenyl), 8.27 (2H, d, *J* = 9.0 Hz, 4-Nitrophenyl), 12.05 (1H, s, -NH). ^{13}C-NMR (75 MHz, DMSO-d_6): δ = 34.42, 45.58, 47.75, 108.60, 115.89, 124.55, 125.47, 126.77, 128.01, 141.22, 142.66, 146.63, 148.97, 151.57, 169.22. ESI-MS (*m/z*): [M + H]$^+$: 487.08.

1-Methylsulphonyl-4-[{2-[4-(4-fluorophenyl)-1,3-thiazol-2-yl]hydrazinylidene}methyl] piperazine (**3f**)

Yield: 79%, Rf = 0.31, M.P. = 190–193 °C, FTIR (ATR, cm^{-1}): 3344 (N-H), 2841 (C-H), 817. ^{1}H-NMR (300 MHz, DMSO-d_6): δ = 2.92 (3H, s, -CH$_3$), 3.23–3.25 (4H, m, piperazine), 3.33–3.35 (4H, m, piperazine), 6.98 (2H, d, *J* = 8.9 Hz, 1,4-Disubstituephenyl), 7.22–7.27 (2H, m, 4-Fluorophenyl + Thiazole), 7.49–7.52 (1H, m, 4-Fluorophenyl), 7.64 (2H, d, *J* = 8.9 Hz, 1,4-Disubstituephenyl), 7.83–7.86 (2H, m, 4-Fluorophenyl), 7.96 (1H, s, -CH=N-), 11.24 (1H, s, -NH). ^{13}C-NMR (75 MHz, DMSO-d_6): δ =34.42, 45.58, 47.64, 47.79, 103.41, 115.75 (*J* = 26.08 Hz), 125.20, 125.64, 127.92, 128.99, 142.19, 143.07, 151.49, 151.85, 162.04 (*J* = 244.24 Hz), 168.90, 177.84. ESI-MS (*m/z*): [M + H]$^+$: 460.08.

1-Methylsulphonyl-4-[{2-[4-(4-chlorophenyl)-1,3-thiazol-2-yl]hydrazinylidene}methyl] piperazine (**3g**)

Yield: 81%, Rf = 0.71, M.P. = 204–208 °C, FTIR (ATR, cm^{-1}): 3300 (N-H), 2835 (C-H), 817. ^{1}H-NMR (300 MHz, DMSO-d_6): δ = 2.93 (3H, s, -CH$_3$), 3.23–3.26 (4H, m, piperazine), 3.34–3.37 (4H, m, piperazine), 7.03 (2H, d, *J* = 8.9 Hz, 1,4-Disubstituephenyl), 7.36 (1H, s, Thiazole), 7.46 (2H, d, *J* = 8.6 Hz, 4-Chlorophenyl), 7.53 (2H, d, *J* = 8.9 Hz, 1,4-Disubstituephenyl), 7.87 (2H, d, *J* = 8.6 Hz, 4-Chlorophenyl), 7.95 (1H, s, -CH=N-), 11.98 (1H, s, -NH). ^{13}C-NMR (75 MHz, DMSO-d_6): δ = 34.34, 45.57, 47.78, 106.55, 115.95, 125.57, 126.04, 126.08, 126.50, 127.99, 138.82, 142.50, 149.30, 151.48, 169.07. ESI-MS (*m/z*): [M + H]$^+$: 476.05.

1-Methylsulphonyl-4-[{2-[4-(4-trifluoromethylphenyl)-1,3-thiazol-2-yl]hydrazinylidene} methyl]piperazine (**3h**)

Yield: 77%, Rf = 0.78, M.P. = 142–145 °C, FTIR (ATR, cm^{-1}): 3304 (N-H), 2827 (C-H), 844. ^{1}H-NMR (300 MHz, DMSO-d_6): δ = 2.93 (3H, s, -CH$_3$), 3.23–3.26 (4H, m, piperazine), 3.34–3.36 (4H, m, piperazine), 7.04 (2H, d, *J* = 8.9 Hz, 1,4-Disubstituephenyl), 7.52–7.55 (3H, m, 1,4-Disubstituephenyl + Thiazole), 7.76 (2H, d, *J* = 8.3 Hz, 4-Trifluoromethylphenyl), 7.96 (1H, s, -CH=N-), 8.06 (2H, d, *J* = 8.1 Hz, 4-Trifluoromethylphenyl), 12.06 (1H, s, -NH). ^{13}C-NMR (75 MHz, DMSO-d_6): δ = 34.42, 45.58, 47.64, 104.56, 115.58, 120.89, 125.20, 127.98, 128.99, 129.97, 131.96, 142.30, 143.07, 151.85, 177.84. ESI-MS (*m/z*): [M + H]$^+$: 510.08.

4.3. Pharmacology

4.3.1. Animals

Adult Balb/c male mice (aged 12–15 weeks, body weight 30–35 g), obtained from the Anadolu University Research Unit for Experimental Animals, Eskişehir, Turkey, were used in the study. The animals were housed in well-ventilated rooms with a 12/12 h dark/light cycle at a temperature of 24 ± 1 °C. The food in the cages was withdrawn 12 h before the experiments to avoid a possible food interference with the absorption of the test compounds.

The experimental protocol of this research has been approved by the Local Ethical Committee on Animal Experimentation of Anadolu University, Eskişehir, Turkey.

4.3.2. Administration of the Test Compounds

The mice were divided into 10 groups of seven animals each. The test compounds were dissolved in sunflower oil and administered (p.o.) to animals at doses of 50 mg/kg in a volume of 0.1 mL [52]. Sunflower oil was used as a no-drug control and morphine sulphate (10 mg/kg, i.p.) was selected as a reference drug [40].

Measurements were taken 60 min after the administration of the test compounds or sunflower oil, and 30 min after the administration of morphine [53].

4.3.3. Evaluation of the Antinociceptive Activity

Tail-Clip Test

A tail-clip test was used to assess the response of animals to mechanically induced noxious stimuli. A metal artery clamp that applies standardized pressure was placed 2–2.5 cm from the base of the tail and latency for turning and biting the clamp was recorded by a stopwatch [54]. A sensitivity test was performed before the test session, and mice that did not respond to the clip for 10 s were eliminated from the experiments. The cut-off time for this test was accepted as 10 s to avoid possible tail damage. Tail-clip tests were performed before and after the test compound administrations, with the prolongations in the reaction times being considered as a parameter for the antinociceptive effect [41].

Hot-Plate Test

A hot-plate test was used to assess the reaction of animals against thermal noxious stimuli. The hot-plate device consists of a heated surface kept at a constant temperature of 55 ± 1.0 °C (Ugo Basile, 7280, Varese, Italy). The animals were placed on the surface of the aluminum plate and pain thresholds were determined before and after the test compounds' administrations. Paw licking or jumping latencies of each animal were recorded in seconds. In sensitivity tests, animals that failed to show a nociceptive response within 15 s were discarded from the experiments. The cut-off time for this test was accepted as 30 s to avoid an injury to the paws [40,55].

In both the tail-clip and hot-plate tests, analgesic efficacies of the test compounds were expressed as a percentage of the maximum possible effect (MPE %) using the following equation:

$$\text{MPE \%} = ((\text{post-drug latency} - \text{pre-drug latency})/(\text{cut-off time} - \text{pre-drug latency})) \times 100 \quad (1)$$

Acetic Acid-Induced Writhing Test

The acetic acid-induced writhing test was used to evaluate the responses of animals to chemically induced noxious stimuli elicited by i.p. injection of 0.6% *v/v* acetic acid in a volume of 0.1 mL/10 g. The mice were then placed in transparent boxes and the number of writhing behaviors was recorded for 10 minutes, 5 minutes after acetic acid injections [53,56]. Reductions in the number of writhing behaviors were considered as evidence for the antinociceptive effect. The inhibition percentage of the nociceptive behavior was calculated according to the following equation:

$$\text{Inhibition\%} = ([(\text{mean number of writhes (control)} - \text{mean number of writhes (treatment)}]/\text{mean number of writhes (control)}) \times 100 \quad (2)$$

Mechanistic Studies

The possible involvement of opioid receptors in the antinociceptive effects of test compounds was examined by mechanistic studies using a non-selective opioid receptor antagonist, naloxone. For antagonism studies, mice were pre-treated with naloxone at a dose of 5.48 mg/kg 15 min before the administrations of test compounds [40,41]. Then, experiments were carried out as explained previously.

4.3.4. Evaluation of the Motor Activity
Rota-Rod Test

The Rota-Rod test device (Ugo Basile, 47600, Varese, Italy) was used to evaluate the possible effects of test compounds on the motor coordination of animals. Before experiments, mice were trained on the rotating rod of the apparatus set at 16 rpm for 3 consecutive days. Animals that could stay on the rotating mill for more than 180 s were used for the tests. The falling time of the mice was considered as a parameter for motor coordination. The cut-off time for this test was accepted as 10 min [40,41,57].

4.3.5. Statistical Analysis

Statistical evaluation of the experimental data was carried out using GraphPad Prism ver. 8.4.3 software (GraphPad Software, La Jolla, CA, USA). The data used in the statistical analyses were acquired from seven animals in each group. The differences between experimental groups were determined by one-way analysis of variance (ANOVA) followed by a post-hoc Tukey's test. The results were presented as mean ± standard error of the mean (SEM) and considered statistically significant when $p < 0.05$.

GraphPad Prism ver. 8.4.3 software were used for creating the figures.

4.4. Molecular Docking Studies

Molecular docking studies were performed using an in silico procedure to define the binding modes of obtained compounds in active regions of opioid receptors. X-ray crystal structures of μ-opioid receptor (PDB ID: 5C1M) [33], δ-opioid receptor (PDB ID: 4N6H) [34], and k-opioid receptor (PDB ID: 6B73) [35] were retrieved from the Protein Data Bank server (www.pdb.org, accessed date 28 April 2021). Active conformations of these receptors were used.

The structures of proteins were built using the Schrödinger Maestro [58] interface and were then submitted to the Protein Preparation Wizard protocol of the Schrödinger Suite 2016 Update 2 [59]. The ligands were prepared using LigPrep 3.8 [60] to correctly assign the protonation states at pH 7.4 ± 1.0, as well as the atom types. Bond orders were assigned, and hydrogen atoms were added to the structures. The grid generation was formed using the Glide 7.1 [61] program and docking runs were performed with standard precision docking mode (SP).

5. Conclusions

To the best of our knowledge, this is the first study showing that molecules designed to carry thiazole and piperazine moieties together on their structures have convenient

pharmacokinetic profiles and show notable antinociceptive efficacies mediated by the opioid receptors at the spinal, supraspinal, and peripheral sites.

Supplementary Materials: The following are available online. Figure S1. IR spectra of compound **3a**. Figure S2. ^{1}H-NMR spectra of compound **3a**. Figure S3. ^{13}C-NMR spectra of compound **3a**. Figure S4. LCMSMS spectra of compound **3a**. Figure S5. IR spectra of compound **3b**. Figure S6. ^{1}H-NMR spectra of compound **3b**. Figure S7. ^{13}C-NMR spectra of compound **3b**. Figure S8. LCMSMS spectra of compound **3b**. Figure S9. IR spectra of compound **3c**. Figure S10. ^{1}H-NMR spectra of compound **3c**. Figure S11. ^{13}C-NMR spectra of compound **3c**. Figure S12. LCMSMS spectra of compound **3c**. Figure S13. IR spectra of compound **3d**. Figure S14. 1H-NMR spectra of compound **3d**. Figure S15. 13C-NMR spectra of compound **3d**. Figure S16. LCMSMS spectra of compound **3d**. Figure S17. IR spectra of compound **3e**. Figure S18. ^{1}H-NMR spectra of compound **3e**. Figure S19. ^{13}C-NMR spectra of compound **3e**. Figure S20. LCMSMS spectra of compound **3e**. Figure S21. IR spectra of compound **3f**. Figure S22. ^{1}H-NMR spectra of compound **3f.** Figure S23. ^{13}C-NMR spectra of compound **3f.** Figure S24. LCMSMS spectra of compound **3f**. Figure S25. IR spectra of compound **3g**. Figure S26. ^{1}H-NMR spectra of compound **3g**. Figure S27. ^{13}C-NMR spectra of compound **3g**. Figure S28. LCMSMS spectra of compound **3g**. Figure S29. IR spectra of compound **3h**. Figure S30. ^{1}H-NMR spectra of compound **3h**. Figure S31. ^{13}C-NMR spectra of compound **3h**. Figure S32. LCMSMS spectra of compound **3h.** Figure S33. The two-dimensional interacting mode of compound **3a** in the active region of μ-opioid receptor (PDB Code: 5C1M). Figure S34. The three-dimensional interacting mode of compound **3a** in the active region of μ -opioid receptor. The ligand and significant residues of the active site of the receptor are presented by a tube model colored with purple and white, respectively (PDB Code: 5C1M). Figure S35. The two-dimensional interacting mode of compound **3b** in the active region of μ-opioid receptor. (PDB Code: 5C1M). Figure S36. The three-dimensional interacting mode of compound **3b** in the active region of μ-opioid receptor. The ligand and significant residues of the active site of the receptor are presented by a tube model colored with orange and white, respectively (PDB Code: 5C1M). Figure S37. The two-dimensional interacting mode of compound **3c** in the active region of μ-opioid receptor. (PDB Code: 5C1M). Figure S38. The three-dimensional interacting mode of compound **3c** in the active region of μ-opioid receptor. The ligand and significant residues of the active site of the receptor are presented by a tube model colored with blue and white, respectively (PDB Code: 5C1M). Figure S39. The two-dimensional interacting mode of compound **3d** in the active region of μ-opioid receptor. (PDB Code: 5C1M). Figure S40. The three-dimensional interacting mode of compound **3d** in the active region of μ-opioid receptor. The ligand and significant residues of the active site of the receptor are presented by a tube model colored with red and white, respectively (PDB Code: 5C1M). Figure S41. The two-dimensional interacting mode of compound **3e** in the active region of μ-opioid receptor. (PDB Code: 5C1M). Figure S42. The three-dimensional interacting mode of compound **3e** in the active region of μ-opioid receptor. The ligand and significant residues of the active site of the receptor are presented by a tube model colored with red and white, respectively (PDB Code: 5C1M). Figure S43. The two-dimensional interacting mode of compound **3h** in the active region of μ-opioid receptor. (PDB Code: 5C1M). Figure S44. The three-dimensional interacting mode of compound **3h** in the active region of μ-opioid receptor. The ligand and significant residues of the active site of the receptor are presented by a tube model colored with red and white, respectively (PDB Code: 5C1M). Figure S45. The two-dimensional interacting mode of compound **3a** in the active region of δ-opioid receptor. (PDB Code: 4N6H). Figure S46. The three-dimensional interacting mode of compound **3a** in the active region of δ-opioid receptor. The ligand and significant residues of the active site of the receptor are presented by a tube model colored with blue and white, respectively (PDB Code: 4N6H). Figure S47. The two-dimensional interacting mode of compound **3b** in the active region of δ-opioid receptor. (PDB Code: 4N6H). Figure S48. The three-dimensional interacting mode of compound **3b** in the active region of δ-opioid receptor. The ligand and significant residues of the active site of the receptor are presented by a tube model colored with blue and white, respectively (PDB Code: 4N6H). Figure S49. The two-dimensional interacting mode of compound **3c** in the active region of δ-opioid receptor. (PDB Code: 4N6H). Figure S50. The three-dimensional interacting mode of compound **3c** in the active region of δ-opioid receptor. The ligand and significant residues of the active site of the receptor are presented by a tube model colored with green and white, respectively (PDB Code: 4N6H). Figure S51. The two-dimensional interacting mode of compound **3d** in the active region of δ-opioid receptor. (PDB Code: 4N6H). Figure S52. The three-dimensional interacting mode of compound **3d** in the active region of δ-opioid receptor. The

ligand and significant residues of the active site of the receptor are presented by a tube model colored with red and white, respectively (PDB Code: 4N6H). Figure S53. The two-dimensional interacting mode of compound **3e** in the active region of δ-opioid receptor. (PDB Code: 4N6H). Figure S54. The three-dimensional interacting mode of compound **3e** in the active region of δ-opioid receptor. The ligand and significant residues of the active site of the receptor are presented by a tube model colored with red and white, respectively (PDB Code: 4N6H). Figure S55. The two-dimensional interacting mode of compound **3h** in the active region of δ-opioid receptor. (PDB Code: 4N6H). Figure S56. The three-dimensional interacting mode of compound **3h** in the active region of δ-opioid receptor. The ligand and significant residues of the active site of the receptor are presented by a tube model colored with red and white, respectively (PDB Code: 4N6H). Figure S57. The two-dimensional interacting mode of compound **3a** in the active region of k-opioid receptor. (PDB Code: 6B73). Figure S58. The three-dimensional interacting mode of compound **3a** in the active region of k-opioid receptor. The ligand and significant residues of the active site of the receptor are presented by a tube model colored with green and white, respectively (PDB Code: 6B73). Figure S59. The two-dimensional interacting mode of compound **3b** in the active region of k-opioid receptor. (PDB Code: 6B73). Figure S60. The three-dimensional interacting mode of compound **3b** in the active region of k-opioid receptor. The ligand and significant residues of the active site of the receptor are presented by a tube model colored with pink and white, respectively (PDB Code: 6B73). Figure S61. The two-dimensional interacting mode of compound **3c** in the active region of k-opioid receptor. (PDB Code: 6B73). Figure S62. The three-dimensional interacting mode of compound **3c** in the active region of k-opioid receptor. The ligand and significant residues of the active site of the receptor are presented by a tube model colored with orange and white, respectively (PDB Code: 6B73). Figure S63. The two-dimensional interacting mode of compound **3d** in the active region of k-opioid receptor. (PDB Code: 6B73). Figure S64. The three-dimensional interacting mode of compound **3d** in the active region of k-opioid receptor. The ligand and significant residues of the active site of the receptor are presented by a tube model colored with yellow and white, respectively (PDB Code: 6B73). Figure S65. The two-dimensional interacting mode of compound **3e** in the active region of k-opioid receptor. (PDB Code: 6B73). Figure S66. The three-dimensional interacting mode of compound **3e** in the active region of k-opioid receptor. The ligand and significant residues of the active site of the receptor are presented by a tube model colored with blue and white, respectively (PDB Code: 6B73). Figure S67. The two-dimensional interacting mode of compound **3h** in the active region of k-opioid receptor. (PDB Code: 6B73). Figure S68. The three-dimensional interacting mode of compound **3h** in the active region of k-opioid receptor. The ligand and significant residues of the active site of the receptor are presented by a tube model colored with pink and white, respectively (PDB Code: 6B73).

Author Contributions: Conceptualization, N.T.Y., D.O., and Ü.D.Ö.; methodology, D.O., N.T.Y., and A.E.E.; software, A.E.E., D.O., and N.T.Y.; validation, N.T.Y. and Ü.K.; formal analysis, Ö.D.C. and Ü.D.Ö.; investigation, D.O., N.T.Y., and Ü.K.; resources, D.O., N.T.Y., Ö.D.C., and Ü.D.Ö.; data curation, D.O., N.T.Y., and Ü.K.; writing—original draft preparation, N.T.Y., Ö.D.C., Ü.D.Ö., D.O., A.E.E.; writing—review and editing, Ö.D.C.; visualization, Ö.D.C. and Ü.D.Ö.; supervision, Ö.D.C. and Ü.D.Ö.; project administration, D.O. and N.T.Y.; funding acquisition, Ü.D.Ö. All authors have read and agreed to the published version of the manuscript.

Institutional Review Board Statement: The study was approved by the Local Ethical Committee on Animal Experimentation of Anadolu University, Eskişehir, Turkey (protocol code 2018-22 and 13 April 2018).

Informed Consent Statement: Not applicable.

Data Availability Statement: All relevant data are included within the article or Supplementary Materials. The raw data are available upon request from the corresponding author.

Conflicts of Interest: The authors declare no conflict of interest.

Sample Availability: Samples of the compounds are available from the authors.

References

1. Ruel, H.L.; Steagall, P.V. Adjuvant Analgesics in Acute Pain Management. *Vet. Clin. N. Am. Small Anim. Pract.* **2019**, *49*, 1127–1141. [CrossRef]
2. Harirforoosh, S.; Asghar, W.; Jamali, F. Adverse effects of nonsteroidal antiinflammatory drugs: An update of gastrointestinal, cardiovascular and renal complications. *J. Pharm. Pharm. Sci.* **2013**, *16*, 821–847. [CrossRef]
3. Imam, M.Z.; Kuo, A.; Ghassabian, S.; Smith, M.T. Progress in understanding mechanisms of opioid-induced gastrointestinal adverse effects and respiratory depression. *Neuropharmacology* **2018**, *131*, 238–255. [CrossRef]
4. Jaen, J.C.; Wise, L.D.; Caprathe, B.W.; Tecle, H.; Bergmeier, S.; Humblet, C.C.; Heffner, T.G.; Meltzer, L.T.; Pugsley, T.A. 4-(1,2,5,6-Tetrahydro-1-alkyl-3-pyridinyl)-2-thiazolamines: A novel class of compounds with central dopamine agonist properties. *J. Med. Chem.* **1990**, *33*, 311–317. [CrossRef] [PubMed]
5. Perez-Lloret, S.; Rey, M.V.; Ratti, L.; Rascol, O. Pramipexole for the treatment of early Parkinson's disease. *Expert Rev. Neurother.* **2011**, *11*, 925–935. [CrossRef] [PubMed]
6. Storch, A.; Burkhardt, K.; Ludolph, A.C.; Schwarz, J. Protective Effects of Riluzole on Dopamine Neurons. *J. Neurochem.* **2008**, *75*, 2259–2269. [CrossRef]
7. Das Neves, A.M.; Berwaldt, G.A.; Avila, C.T.; Goulart, T.B.; Moreira, B.C.; Ferreira, T.P.; Soares, M.S.P.; Pedra, N.S.; Spohr, L.; De Souza, A.A.A.; et al. Synthesis of thiazolidin-4-ones and thiazinan-4-ones from 1-(2-aminoethyl)pyrrolidine as acetylcholinesterase inhibitors. *J. Enzym. Inhib. Med. Chem.* **2019**, *35*, 31–41. [CrossRef] [PubMed]
8. Verma, P.K.; Khatkar, A. Anticonvulsant and Neurological Profile of Benzothiazoles: A Mini-Review. *Central Nerv. Syst. Agents Med. Chem.* **2015**, *15*, 11–16. [CrossRef]
9. Jin, Q.; Fu, Z.; Guan, L.; Jiang, H. Syntheses of Benzo[d]Thiazol-2(3H)-One Derivatives and Their Antidepressant and Anticonvulsant Effects. *Mar. Drugs* **2019**, *17*, 430. [CrossRef] [PubMed]
10. Tikhonova, T.A.; Rassokhina, I.V.; Kondrakhin, E.A.; Fedosov, M.A.; Bukanova, J.V.; Rossokhin, A.V.; Sharonova, I.N.; Kovalev, G.I.; Zavarzin, I.V.; Volkova, Y.A. Development of 1,3-thiazole analogues of imidazopyridines as potent positive allosteric modulators of GABAA receptors. *Bioorg. Chem.* **2020**, *94*, 103334. [CrossRef]
11. Shaquiquzzaman, M.; Verma, G.; Marella, A.; Akhter, M.; Akhtar, W.; Khan, M.F.; Tasneem, S.; Alam, M.M. Piperazine scaffold: A remarkable tool in generation of diverse pharmacological agents. *Eur. J. Med. Chem.* **2015**, *102*, 487–529. [CrossRef] [PubMed]
12. Sanchez, C.; Asin, K.E.; Artigas, F. Vortioxetine, a novel antidepressant with multimodal activity: Review of preclinical and clinical data. *Pharmacol. Ther.* **2015**, *145*, 43–57. [CrossRef] [PubMed]
13. Thore, S.N.; Gupta, S.V.; Baheti, K.G. Docking, synthesis, and pharmacological investigation of novel substituted thiazole derivatives as non-carboxylic, anti-inflammatory, and analgesic agents. *Med. Chem. Res.* **2013**, *22*, 3802–3811. [CrossRef]
14. Kalkhambkar, R.; Kulkarni, G.; Shivkumar, H.; Rao, R.N. Synthesis of novel triheterocyclic thiazoles as anti-inflammatory and analgesic agents. *Eur. J. Med. Chem.* **2007**, *42*, 1272–1276. [CrossRef] [PubMed]
15. Raj, K.V.; Narayana, B.; Ashalatha, B.; Kumari, N.S.; Sarojini, B. Synthesis of some bioactive 2-bromo-5-methoxy-N′-[4-(aryl)-1,3-thiazol-2-yl]benzohydrazide derivatives. *Eur. J. Med. Chem.* **2007**, *42*, 425–429. [CrossRef]
16. Ochi, T.; Motoyama, Y.; Goto, T. The analgesic effect profile of FR122047, a selective cyclooxygenase-1 inhibitor, in chemical nociceptive models. *Eur. J. Pharmacol.* **2000**, *391*, 49–54. [CrossRef]
17. Saravanan, G.; Alagarsamy, V.; Prakash, C.R.; Dinesh-Kumar, P.; Selvam, T.P. Synthesis of novel thiazole derivatives as analgesic agents. *Am. J. Pol. Sci.* **2011**, *1*, 134–138.
18. Salem, M.A.; Thabet, H.K.H.; Helal, M.H.; Abdelaal, A.S.; Ammar, Y.A. Synthesis and pharmacological evaluation of some pyrazoles, thiazolopyrimidine, triazolopyrimidine, pyridone and 2-iminochromene containing naproxenoyl moiety as NSAIDs. *Chem. Sci. J.* **2011**, *2*, 32.
19. Venkateshwarlu, E.; Rao, J.V.; Umasankar, K.; Dheeraj, G. Study of anti-inflammatory, analgesic and antipyretic activity of novel isatin derivatives. *Asian J. Pharm. Clin. Res.* **2012**, *5*, 187–190.
20. Martins, D.F.; Rosa, A.O.; Gadotti, V.M.; Mazzardo-Martins, L.; Nascimento, F.P.; Egea, J.; Lopez, M.G.; Santos, A.R. The Antinociceptive Effects of AR-A014418, a Selective Inhibitor of Glycogen Synthase Kinase-3 Beta, in Mice. *J. Pain* **2011**, *12*, 315–322. [CrossRef]
21. Yoon, S.-Y.; Woo, J.; Park, J.-O.; Choi, E.-J.; Shin, H.-S.; Roh, D.-H.; Kim, K.-S. Intrathecal RGS4 Inhibitor, CCG50014, Reduces Nociceptive Responses and Enhances Opioid-Mediated Analgesic Effects in the Mouse Formalin Test. *Anesthesia Analg.* **2015**, *120*, 671–677. [CrossRef] [PubMed]
22. Abdel-Salam, O.M.; El-Batran, S. Pharmacological Investigation of Trimetazidine in Models of Inflammation, Pain and Gastric Injury in Rodents. *Pharmacology* **2005**, *75*, 122–132. [CrossRef]
23. Biancalani, C.; Giovannoni, M.P.; Pieretti, S.; Cesari, N.; Graziano, A.; Vergelli, C.; Cilibrizzi, A.; Di Gianuario, A.; Colucci, M.; Mangano, G.; et al. Further Studies on Arylpiperazinyl Alkyl Pyridazinones: Discovery of an Exceptionally Potent, Orally Active, Antinociceptive Agent in Thermally Induced Pain. *J. Med. Chem.* **2009**, *52*, 7397–7409. [CrossRef]
24. Kam, Y.L.; Rhee, H.-K.; Rhim, H.; Back, S.K.; Na, H.S.; Choo, H.-Y.P. Synthesis and T-type calcium channel blocking activity of novel diphenylpiperazine compounds, and evaluation of in vivo analgesic activity. *Bioorg. Med. Chem.* **2010**, *18*, 5938–5944. [CrossRef]
25. Chen, Y.; Wang, G.; Xu, X.; Liu, B.-F.; Li, J.; Zhang, G. Design, Synthesis and Biological Activity Evaluation of Arylpiperazine Derivatives for the Treatment of Neuropathic Pain. *Molecules* **2011**, *16*, 5785–5806. [CrossRef]

26. Chae, E.; Yi, H.; Choi, Y.; Cho, H.; Lee, K.; Moon, H. Synthesis and pharmacological evaluation of carbamic acid 1-phenyl-3-(4-phenyl-piperazine-1-yl)-propyl ester derivatives as new analgesic agents. *Bioorg. Med. Chem. Lett.* **2012**, *22*, 2434–2439. [CrossRef]

27. Papadopoulou, C.; Geronikaki, A.; Hadjipavlou-Litina, D. Synthesis and biological evaluation of new thiazolyl/benzothiazolyl-amides, derivatives of 4-phenyl-piperazine. *Il Farm.* **2005**, *60*, 969–973. [CrossRef]

28. Ahmadi, A.; Khalili, M.; Nafarie, A.; Yazdani, A.; Nahri-Niknafs, B. Synthesis and anti-inflammatory effects of new piperazine and ethanolamine derivatives of H(1)-antihistaminic drugs. *Mini Rev. Med. Chem.* **2012**, *12*, 1282–1292. [CrossRef]

29. Salat, K.; Moniczewski, A.; Salat, R.; Janaszek-Mańkowska, M.; Filipek, B.; Malawska, B.; Więckowski, K. Analgesic, anticonvulsant and antioxidant activities of 3-[4-(3-trifluoromethyl-phenyl)-piperazin-1-yl]-dihydrofuran-2-one dihydrochloride in mice. *Pharmacol. Biochem. Behav.* **2012**, *101*, 138–147. [CrossRef] [PubMed]

30. Metcalf, M.D.; Yekkirala, A.S.; Powers, M.D.; Kitto, K.F.; Fairbanks, C.A.; Wilcox, G.L.; Portoghese, P.S. The δ Opioid Receptor Agonist SNC80 Selectively Activates Heteromeric μ-δ Opioid Receptors. *ACS Chem. Neurosci.* **2012**, *3*, 505–509. [CrossRef] [PubMed]

31. Yi, S.P.; Kong, Q.H.; Li, Y.L.; Pan, C.L.; Yu, J.; Cui, B.Q.; Wang, Y.F.; Wang, G.L.; Zhou, P.L.; Wang, L.L.; et al. The opioid receptor triple agonist DPI-125 produces analgesia with less respiratory depression and reduced abuse liability. *Acta Pharmacol. Sin.* **2017**, *38*, 977–989. [CrossRef]

32. Van De Waterbeemd, H.; Gifford, E. ADMET in silico modelling: Towards prediction paradise? *Nat. Rev. Drug Discov.* **2003**, *2*, 192–204. [CrossRef] [PubMed]

33. Huang, W.; Manglik, A.; Venkatakrishnan, A.J.; Laeremans, T.; Feinberg, E.N.; Sanborn, A.L.; Kato, H.E.; Livingston, K.E.; Thorsen, T.S.; Kling, R.C.; et al. Structural insights into μ-opioid receptor activation. *Nat. Cell Biol.* **2015**, *524*, 315–321. [CrossRef] [PubMed]

34. Fenalti, G.; Giguere, P.M.; Katritch, V.; Huang, X.-P.; Thompson, A.A.; Cherezov, V.; Roth, B.L.; Stevens, R.C. Molecular control of δ-opioid receptor signalling. *Nat. Cell Biol.* **2014**, *506*, 191–196. [CrossRef] [PubMed]

35. Che, T.; Majumdar, S.; Zaidi, S.A.; Ondachi, P.; McCorvy, J.D.; Wang, S.; Mosier, P.D.; Uprety, R.; Vardy, E.; Krumm, B.E.; et al. Structure of the Nanobody-Stabilized Active State of the Kappa Opioid Receptor. *Cell* **2018**, *172*, 55–67.e15. [CrossRef]

36. Jarończyk, M.; Lipiński, P.F.J.; Dobrowolski, J.C.; Sadlej, J. The FMO analysis of the molecular interaction of fentanyl derivatives with the μ-opioid receptor. *Chem. Pap.* **2017**, *71*, 1429–1443. [CrossRef]

37. Le Bars, D.; Gozariu, M.; Cadden, S.W. Animal models of nociception. *Pharmacol. Rev.* **2001**, *53*, 597–652. [PubMed]

38. Wong, C.H.; Dey, P.; Yarmush, J.; Wu, W.-H.; Zbuzek, V.K. Nifedipine-Induced Analgesia After Epidural Injection in Rats. *Anesthesia Analg.* **1994**, *79*, 303–305. [CrossRef] [PubMed]

39. Gabra, B.H.; Sirois, P. Beneficial effect of chronic treatment with the selective bradykinin B1 receptor antagonists, R-715 and R-954, in attenuating streptozotocin-diabetic thermal hyperalgesia in mice. *Peptides* **2003**, *24*, 1131–1139. [CrossRef]

40. Kasap, M.; Can, Ö.D. Opioid system mediated anti-nociceptive effect of agomelatine in mice. *Life Sci.* **2016**, *163*, 55–63. [CrossRef] [PubMed]

41. Özkay, Ü.D.; Can, Ö.D. Anti-nociceptive effect of vitexin mediated by the opioid system in mice. *Pharmacol. Biochem. Behav.* **2013**, *109*, 23–30. [CrossRef]

42. De Souza, M.; Pereira, M.; Ardenghi, J.; Mora, T.; Bresciani, L.; Yunes, R.; Monache, F.D.; Cechinel-Filho, V. Filicene obtained from Adiantum cuneatum interacts with the cholinergic, dopaminergic, glutamatergic, GABAergic, and tachykinergic systems to exert antinociceptive effect in mice. *Pharmacol. Biochem. Behav.* **2009**, *93*, 40–46. [CrossRef]

43. Ayumi, R.R.; Mossadeq, W.M.S.; Zakaria, Z.A.; Bakhtiar, M.T.; Kamarudin, N.; Hisamuddin, N.; Talib, M.; Sabar, A.M. Antinociceptive Activity of Asiaticoside in Mouse Models of Induced Nociception. *Planta Med.* **2020**, *86*, 548–555. [CrossRef]

44. Ishola, I.O.; Akindele, A.J.; Adeyemi, O.O. Analgesic and anti-inflammatory activities of Cnestis ferruginea Vahl ex DC (Connaraceae) methanolic root extract. *J. Ethnopharmacol.* **2011**, *135*, 55–62. [CrossRef]

45. Park, S.-H.; Sim, Y.-B.; Kang, Y.-J.; Kim, S.-S.; Kim, C.-H.; Kim, S.-J.; Seo, J.-Y.; Lim, S.-M.; Suh, H.-W. Hop Extract Produces Antinociception by Acting on Opioid System in Mice. *Korean J. Physiol. Pharmacol.* **2012**, *16*, 187–192. [CrossRef]

46. Coelho, L.P.; Reis, P.A.; De Castro, F.L.; Gayer, C.R.M.; Lopes, C.D.S.; Silva, M.C.D.C.E.; Sabino, K.C.D.C.; Todeschini, A.R.; Coelho, M.G.P. Antinociceptive properties of ethanolic extract and fractions of *Pterodon pubescens* Benth. seeds. *J. Ethnopharmacol.* **2005**, *98*, 109–116. [CrossRef]

47. Argoff, C. Mechanisms of pain transmission and pharmacologic management. *Curr. Med. Res. Opin.* **2011**, *27*, 2019–2031. [CrossRef] [PubMed]

48. Millan, M.J. Descending control of pain. *Prog. Neurobiol.* **2002**, *66*, 355–474. [CrossRef]

49. Liaras, K.; Fesatidou, M.; Geronikaki, A. Thiazoles and Thiazolidinones as COX/LOX Inhibitors. *Molecules* **2018**, *23*, 685. [CrossRef]

50. Yam, M.F.; Loh, Y.C.; Tan, C.S.; Adam, S.K.; Manan, N.A.; Basir, R. General Pathways of Pain Sensation and the Major Neurotransmitters Involved in Pain Regulation. *Int. J. Mol. Sci.* **2018**, *19*, 2164. [CrossRef] [PubMed]

51. Friderichs, E. *Analgesics: From Chemistry and Pharmacology to Clinical Application*; Wiley: Hoboken, NJ, USA, 2002.

52. Sarigol, D.; Uzgoren-Baran, A.; Tel, B.C.; Somuncuoglu, E.I.; Kazkayasi, I.; Ozadali-Sari, K.; Unsal-Tan, O.; Okay, G.; Ertan, M.; Tozkoparan, B. Novel thiazolo[3,2-*b*]-1,2,4-triazoles derived from naproxen with analgesic/anti-inflammatory properties: Synthesis, biological evaluation and molecular modeling studies. *Bioorg. Med. Chem.* **2015**, *23*, 2518–2528. [CrossRef]

53. Kaplancikli, Z.A.; Turan-Zitouni, G.; Özdemir, A.; Can, Ö.D.; Chevallet, P. Synthesis and antinociceptive activities of some pyrazoline derivatives. *Eur. J. Med. Chem.* **2009**, *44*, 2606–2610. [CrossRef]

54. D'Amour, F.E.; Smith, D.L. A method for determining loss of pain sensation. *J. Pharmacol. Exp. Ther.* **1941**, *72*, 74–79.

55. Pavin, N.F.; Donato, F.; Cibin, F.W.; Jesse, C.R.; Schneider, P.H.; De Salles, H.D.; Soares, L.D.A.; Alves, D.; Savegnago, L. Antinociceptive and anti-hypernociceptive effects of Se-phenyl thiazolidine-4-carboselenoate in mice. *Eur. J. Pharmacol.* **2011**, *668*, 169–176. [CrossRef] [PubMed]

56. Koster, R.; Anderson, M.; Beer, E. Acetic acid for analgesic screening. *Fed. Proc.* **1959**, *18*, 412.

57. Dunham, N.W.; Miya, T.S. A Note on a Simple Apparatus for Detecting Neurological Deficit in Rats and Mice. *J. Am. Pharm. Assoc.* **1957**, *46*, 208–209. [CrossRef]

58. Schrödinger LLC. *Maestro, Version 10.6*; Schrödinger, LLC: New York, NY, USA, 2016.

59. Schrödinger LLC. *Schrödinger Suite*; Schrödinger, LLC: New York, NY, USA, 2016.

60. Schrödinger LLC. *LigPrep, Version 3.8*; Schrödinger, LLC: New York, NY, USA, 2016.

61. Schrödinger LLC. *Glide, Version 7.1*; Schrödinger, LLC: New York, NY, USA, 2016.

SR-17018 Stimulates Atypical μ-Opioid Receptor Phosphorylation and Dephosphorylation

Sebastian Fritzwanker, Stefan Schulz * and **Andrea Kliewer ***

Department of Pharmacology and Toxicology, Jena University Hospital, Friedrich Schiller University Jena, Drackendorfer Straße 1, D-07747 Jena, Germany; Sebastian.Fritzwanker@med.uni-jena.de
* Correspondence: stefan.schulz@med.uni-jena.de (S.S.); andrea.kliewer@med.uni-jena.de (A.K.)

Abstract: Opioid-associated overdoses and deaths due to respiratory depression are a major public health problem in the US and other Western countries. In the past decade, much research effort has been directed towards the development of G-protein-biased μ-opioid receptor (MOP) agonists as a possible means to circumvent this problem. The bias hypothesis proposes that G-protein signaling mediates analgesia, whereas ß-arrestin signaling mediates respiratory depression. SR-17018 was initially reported as a highly biased μ-opioid with an extremely wide therapeutic window. It was later shown that SR-17018 can also reverse morphine tolerance and prevent withdrawal via a hitherto unknown mechanism of action. Here, we examined the temporal dynamics of SR-17018-induced MOP phosphorylation and dephosphorylation. Exposure of MOP to saturating concentrations of SR-17018 for extended periods of time stimulated a MOP phosphorylation pattern that was indistinguishable from that induced by the full agonist DAMGO. Unlike DAMGO-induced MOP phosphorylation, which is reversible within minutes after agonist washout, SR-17018-induced MOP phosphorylation persisted for hours under otherwise identical conditions. Such delayed MOP dephosphorylation kinetics were also found for the partial agonist buprenorphine. However, buprenorphine, SR-17018-induced MOP phosphorylation was fully reversible when naloxone was included in the washout solution. SR-17018 exhibits a qualitative and temporal MOP phosphorylation profile that is strikingly different from any other known biased, partial, or full MOP agonist. We conclude that detailed analysis of receptor phosphorylation may provide novel insights into previously unappreciated pharmacological properties of newly synthesized MOP ligands.

Keywords: μ-opioid receptor; DAMGO; SR-17018; buprenorphine

1. Introduction

Opioids are the most effective drugs for the treatment of severe pain. However, their clinical use in acute and chronic pain is limited by severe adverse side effects such as respiratory depression, constipation, dependence, and development of tolerance [1,2]. Currently, opioid-associated overdoses and deaths due to respiratory depression from prescription opioids are a major public health problem in the US and other Western countries. It is believed that one way to solve this problem may be the development of biased μ-opioid receptor (MOP) agonists. These compounds have been developed based on the hypothesis that selective activation of the G-protein signal pathway via MOP mediates the analgesic effect by avoiding stimulation of ß-arrestin signaling, which is believed to induce adverse opioid effects such as respiratory depression and constipation.

SR-17018 is one of the most recently described G-protein-biased agonists [3,4]. Schmid et al. (2017) demonstrated an extremely high bias factor in different G-protein assays over ß-arrestin 2 recruitment in vitro, and significant separation between antinociception and respiratory side effects in vivo. In addition to the extremely wide therapeutic window, it was reported later that SR-17018 does not produce tolerance in the hot-plate antinociception assay [5]. Furthermore, it was shown that SR-17018 can reverse morphine tolerance and prevent withdrawal via an unknown mechanism of action [5].

In contrast, a more recent study by Gillis et al. (2020) showed that SR-17018 consistently exhibited low intrinsic efficacy across a variety of assays and showed no statistically significant bias towards or away from any G-protein activation. Furthermore, similar kinetics were observed between antinociception and respiratory depressant effects. Similar in vitro results were obtained with the partial agonist buprenorphine, albeit with an increased therapeutic window regarding respiratory depression [4,6,7]. In clinical settings, buprenorphine is used as an alternative to methadone in the treatment of heroin addiction, due to its mixed agonist–antagonist properties [8]. Collectively, these findings suggest that SR-17018 may be similar to buprenorphine and exhibit partial agonistic properties.

In the past decade, we have shown that the phosphorylation barcode of the MOP carboxyl-terminal tail is dependent on agonist efficacy and indicative of ß-arrestin recruitment and receptor internalization [9,10]. High-efficacy MOP agonists like DAMGO and fentanyl induce a robust hierarchical and sequential multisite receptor phosphorylation, whereas low-efficacy agonists like morphine, oxycodone, and buprenorphine, trigger only phosphorylation at Ser^{375}. Recent phosphorylation studies with SR-17018 have reported an unusual phosphorylation pattern which is limited to Ser^{375} during the first 20 min of stimulation, corresponding to a low-efficacy agonist [4]. In contrast, incubation for >30 min leads to a multisite receptor phosphorylation, which corresponds to a high-efficacy agonist. Furthermore, SR-17018-induced MOP phosphorylation is driven by GRK2/3 and is naloxone sensitive.

Given its unusual pharmacological profile and unknown mechanism of action, we performed a series of MOP phosphorylation and dephosphorylation experiments in vitro and compared the effects of SR-17018 with the partial agonist buprenorphine.

2. Results

SR-17018 was developed as a G-protein-biased MOP agonist, but exhibits a number of pharmacological effects which cannot be explained by the biased signaling hypothesis. To better understand SR-17018 ligand properties, we performed a series of MOP phosphorylation and dephosphorylation experiments comparing SR-17018 to the low-efficacy agonist buprenorphine and the full agonist DAMGO as internal standard.

2.1. Agonist-Induced Dose-Dependent MOP Phosphorylation

First, we evaluated dose- and time-dependent MOP phosphorylation induced by DAMGO, SR-17018 or buprenorphine (Figure 1). As shown in Figure 2, 30 min exposure at 37 °C to saturating concentrations of SR-17018 induced a multisite phosphorylation that was indistinguishable from that induced by DAMGO. In contrast, buprenorphine induced only a robust Ser^{375} phosphorylation under otherwise identical conditions.
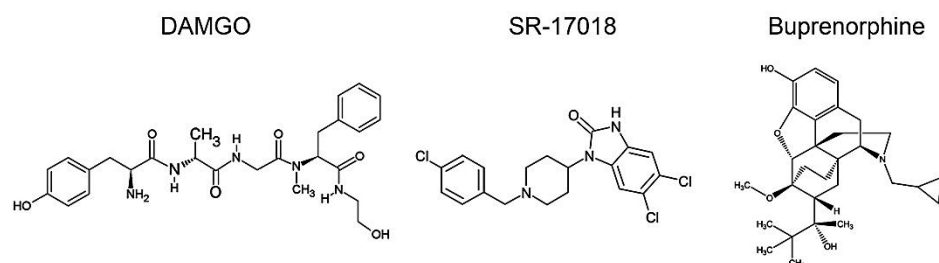
Figure 1. Chemical structures of DAMGO, SR-17018, and buprenorphine.
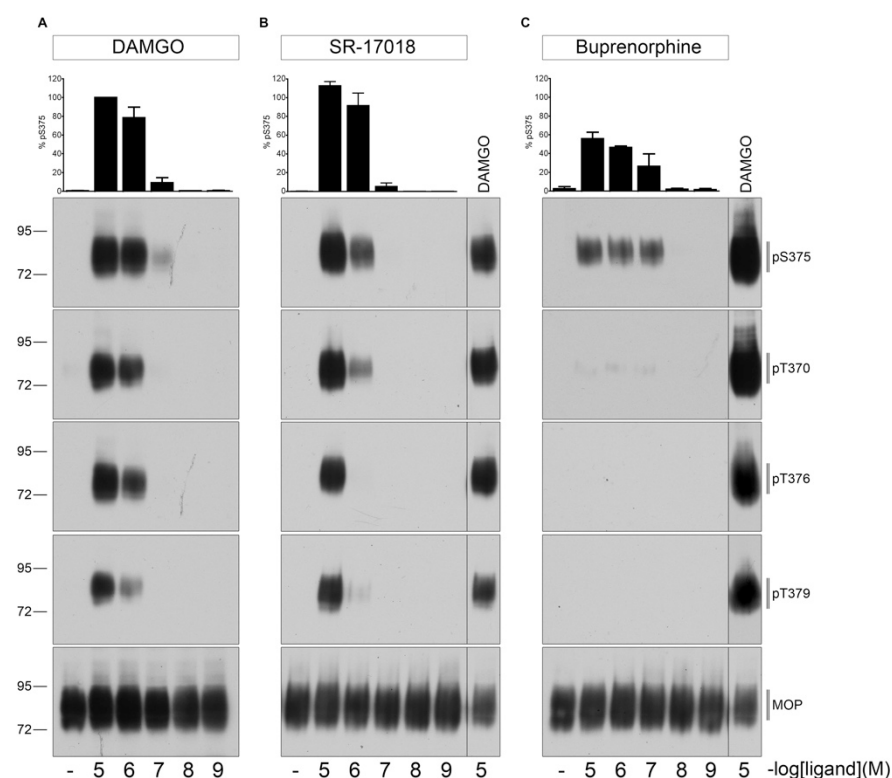
Figure 2. Dose-dependent multisite phosphorylation by DAMGO, SR-17018, and buprenorphine. HEK293 cells stably expressing HA-MOP were either treated with (**A**) DAMGO, (**B**) SR-17018, or (**C**) buprenorphine with concentrations ranging from 10 µM to 1 nM for 30 min at 37 °C. Cells were lysed and immunoblotted with the anti-pT370 (pT370), anti-pT376 (pT376), anti-pT379 (pT379), or anti-pSer375 (pS375) antibodies. Blots were stripped and reprobed with the phosphorylation-independent anti-HA-tag antibody to confirm equal loading of the gels. S375 phosphorylation was quantified (upper panel) and expressed as percentage of maximal phosphorylation in control cells, which was set at 100%. Data correspond to mean ± SEM from three independent experiments. Positions of molecular mass markers are indicated on the left (in kDa). ((**B**,**C**) right lane) 10 µM DAMGO samples were used as a control to visualize different development times on X-ray films. Blots are representative of three independent experiments.

2.2. Agonist-Induced Time-Dependent MOP Phosphorylation

As depicted in Figure 3A, DAMGO-stimulated MOP phosphorylation occurred rapidly within seconds to minutes at RT. S375 is the initial site of a hierarchical phosphorylation cascade. The following phosphorylation at T370, T379, and T376 requires priming S375 phosphorylation [9]. In contrast, both SR-17018- and buprenorphine-mediated MOP phosphorylation required extended exposure times (>20 min). Furthermore, SR-17018 and DAMGO promoted a robust internalization, which resulted in a receptor accumulation in the perinuclear recycling compartment (Figure 3B). In contrast, buprenorphine failed to stimulate any detectable MOP endocytosis (Figure 3B).

2.3. PBS Buffer Washout of Agonist-Induced Phosphorylation

Next, we evaluated the temporal dynamics of MOP dephosphorylation after extensive ligand washout with PBS (Figure 4). The DAMGO-induced phosphorylation was quickly reversed within 5 to 10 min after agonist removal. T370 and T379 were dephosphorylated immediately, whereas S375 and T376 dephosphorylation required between 10 and 20 min. In contrast, SR-17018-mediated MOP phosphorylation was retained for hours under otherwise identical conditions (Figure 4B). Similar, the buprenorphine-stimulated Ser[375] phosphorylation was also resistant to PBS washout (Figure 4A).
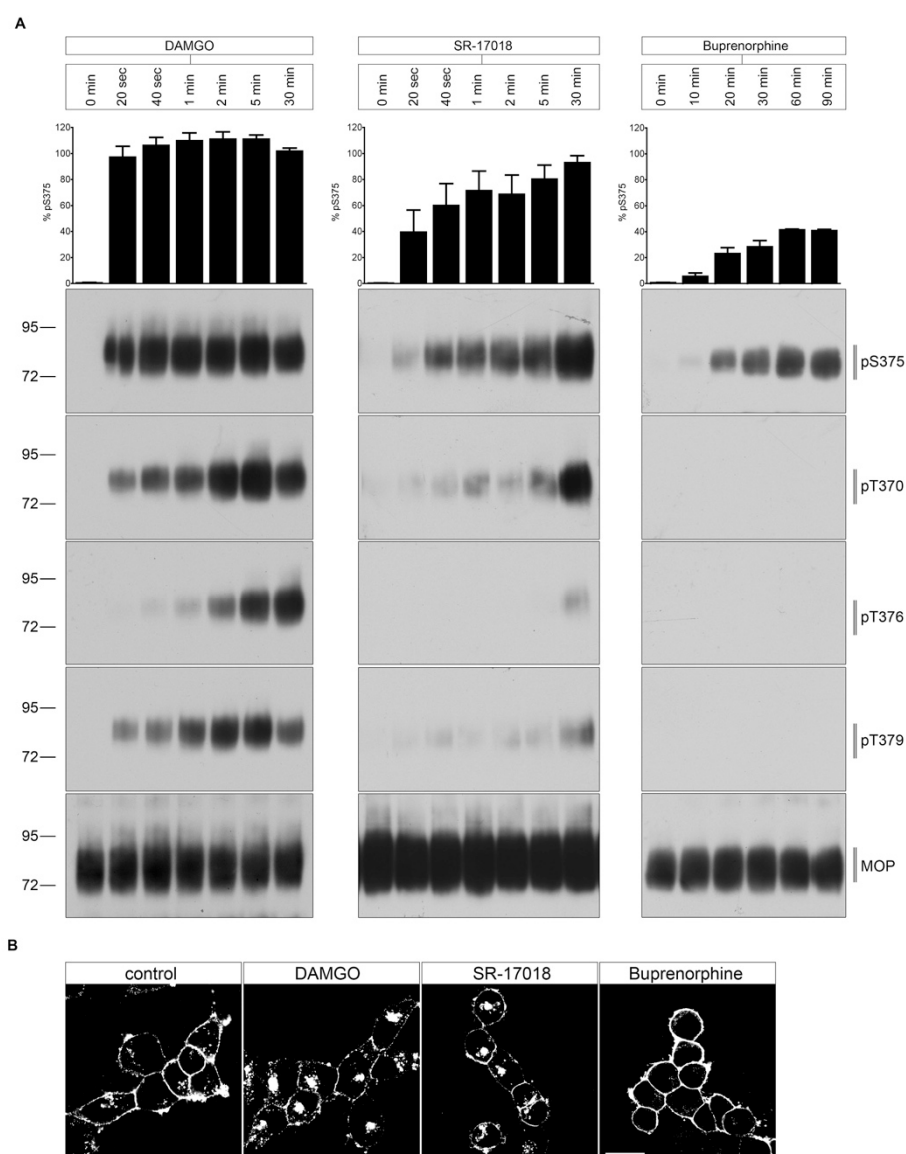
Figure 3. Time course of multisite phosphorylation by DAMGO, SR-17018, and buprenorphine. (**A**) HEK293 cells stably expressing HA-MOP were incubated with (left panel) 10 μM DAMGO, (middle panel) 10 μM SR-17018, or (right panel) buprenorphine for the indicated time periods at RT. Cells were lysed and immunoblotted with the anti-pT370 (pT370), anti-pT376 (pT376), anti-pT379 (pT379), or anti-pSer375 (pS375) antibodies. Blots were stripped and reprobed with the phosphorylation-independent anti-HA-tag antibody to confirm equal loading of the gels (MOP). S375 phosphorylation was quantified (upper panel) and expressed as percentage of maximal phosphorylation in control cells, which was set at 100% (data not shown). Data correspond to mean ± SEM from three independent experiments. Positions of molecular mass markers are indicated on the left (in kDa). Blots are representative of three independent experiments. (**B**) HEK293 HA-MOP cells were pre-incubated with anti-HA antibody for 2 h at 4 °C. Afterwards, cells were treated with either 10 μM DAMGO, 10 μM SR-17018, or 10 μM buprenorphine for 30 min at 37 °C. After fixation, the cells were incubated with Alexa488-conjugated secondary antibody and examined using confocal microscopy. Figure shows representative images of three independent experiments. Scale bar: 20 μm.
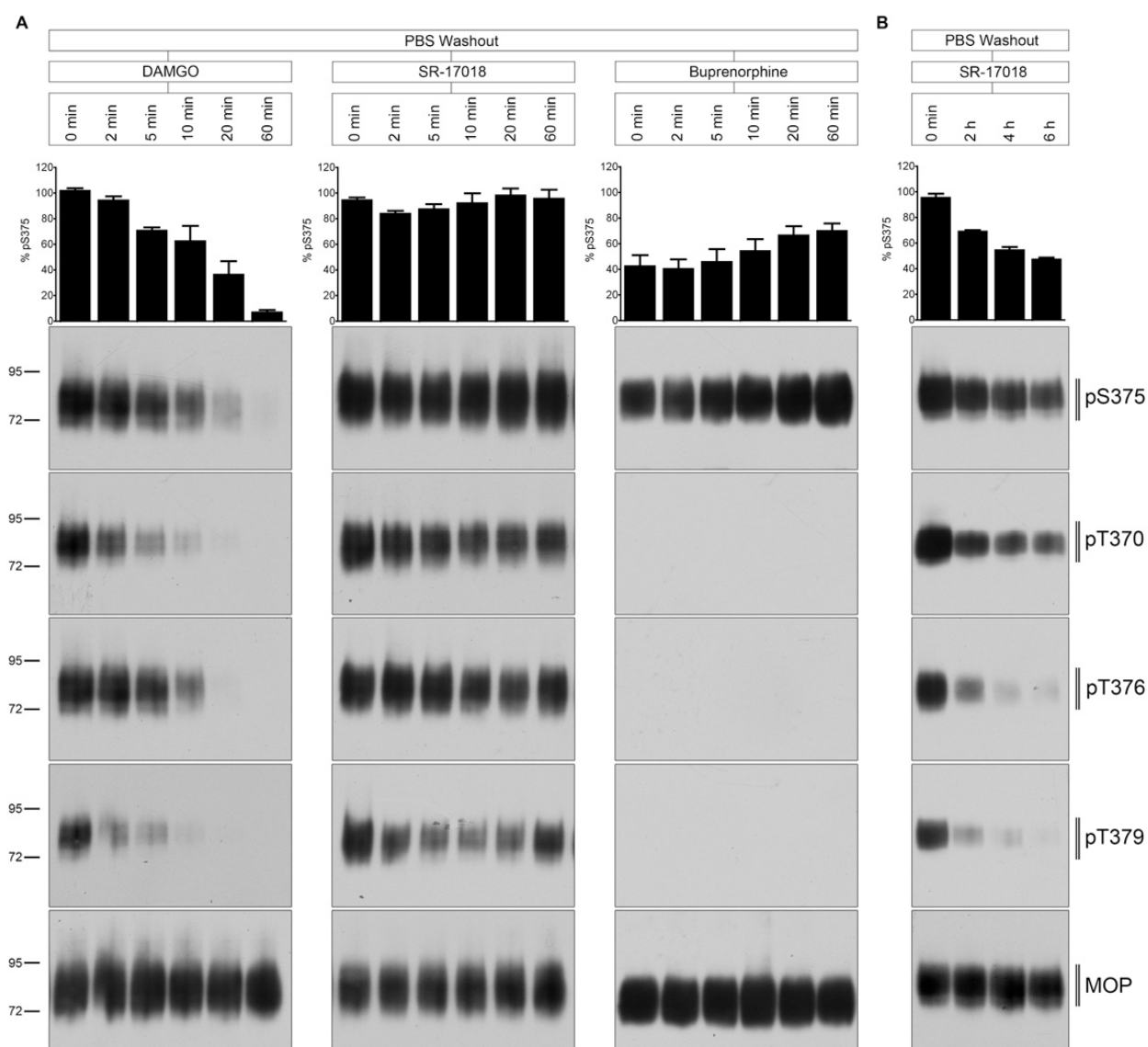
Figure 4. Time course of multisite dephosphorylation after PBS buffer washout. (**A**) HEK293 cells stably expressing HA-MOP were incubated with (left panel) 10 μM DAMGO, (middle panel) 10 μM SR-17018, or (right panel) buprenorphine for 30 min at 37 °C. Cells were washed three times with PBS buffer (PBS washout) and then incubated in the absence of agonist for 0, 2, 5, 10, 20, or 60 min at 37 °C. (**B**) HEK293 cells stably expressing HA-MOP were incubated with 10 μM SR-17018 for 30 min. Cells were washed three times with PBS buffer and then incubated in the absence of agonist for 0, 2, 4, or 6 h at 37 °C. (**A,B**) Cells were lysed and immunoblotted with the anti-pT370 (pT370), anti-pT376 (pT376), anti-pT379 (pT379), or anti-pSer375 (pS375) antibodies. Blots were stripped and reprobed with the phosphorylation-independent anti-HA-tag antibody to confirm equal loading of the gels (MOP). S375 phosphorylation was quantified (upper panel) and expressed as percentage of maximal phosphorylation in control cells, which was set at 100% (data not shown). Data correspond to mean ± SEM from three independent experiments. Positions of molecular mass markers are indicated on the left (in kDa). Blots are representative of three independent experiments.

2.4. Naloxone Washout of Agonist-Induced Phosphorylation

Interestingly, when 10 μM naloxone was included into the washout solution, MOP dephosphorylation was strongly facilitated in SR-17018-treated but not in buprenorphine-treated cultures (Figure 5).
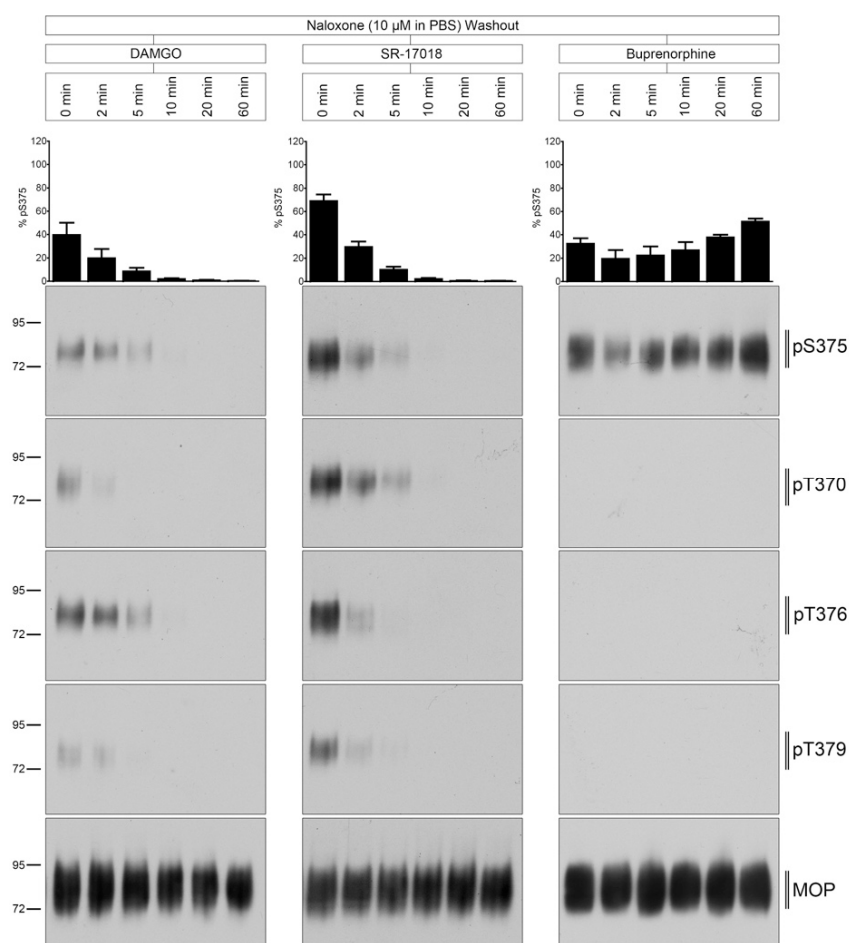
Figure 5. Time course of multisite dephosphorylation after naloxone washout. HEK293 cells stably expressing HA-MOP were incubated with (left panel) 10 μM DAMGO, (middle panel) 10 μM SR-17018, or (right panel) 10 μM buprenorphine for 30 min at 37 °C. Cells were washed three times with 10 μM naloxone and then incubated in the absence of agonist for 0, 2, 5, 10, 20, or 60 min at 37 °C. Cells were lysed and immunoblotted with the anti-pT370 (pT370), anti-pT376 (pT376), anti-pT379 (pT379), or anti-pSer375 (pS375) antibodies. Blots were stripped and reprobed with the phosphorylation-independent anti-HA-tag antibody to confirm equal loading of the gels (MOP). S375 phosphorylation was quantified (upper panel) and expressed as percentage of maximal phosphorylation in control cells, which was set at 100% (data not shown). Data correspond to mean ± SEM from at least three independent experiments. Positions of molecular mass markers are indicated on the left (in kDa). Blots are representative of three independent experiments.

3. Discussion

SR-17018 is unique in that it exhibits an atypical MOP phosphorylation and dephosphorylation profile [4]. Saturating concentrations of SR-17018 stimulate a full agonist-like multisite phosphorylation of MOP but with delayed onset (>20 min). Similar slow phosphorylation kinetics are observed with the partial agonist buprenorphine, whereas the full agonist DAMGO induces full MOP phosphorylation within seconds. At least three kinases contribute to agonist-induced MOP phosphorylation namely GRK2, GRK3, and GRK5 [9,11]. The most likely explanation is that SR-17018, buprenorphine, and DAMGO restrain the receptor in different conformations, which exhibit different affinities for individual GRKs [4]. In fact, the selective engagement of different GRKs to differently activated MOP receptors could be a major source of biased signaling as it is the driving force for recruitment of arrestin isoforms 1 and 2 to the receptor [9,10]. Thus, different GRK-mediated phosphorylation patterns should be taken into account in the development of new MOP agonists with beneficial side-effect profiles.

For many years, the biased signaling concept has been reduced to analysis of G-protein signaling versus ß-arrestin 2 recruitment, and the resulting bias factor has been proposed as a predictor of the therapeutic window. SR-17018 is one candidate compound that was developed based on the biased signaling hypothesis [3]. While the initial study reported an extremely high bias factor in different G-protein assays over ß-arrestin 2 recruitment, later work showed no statistically significant bias towards or away from any G-protein activation [4]. Nevertheless, the present study revealed a unique MOP phosphorylation and internalization profile for SR-17018 that does not support the initial report of an extremely high bias factor.

Conversely, dephosphorylation of DAMGO-activated MOPs occurred within minutes after agonist washout. In contrast, SR-17018-stimulated MOP phosphorylation occurred in a delayed manner similar to that observed with buprenorphine and persisted for hours after agonist washout. These data suggest that SR-17018 remains tightly bound to the MOP receptor after washout, while preventing receptor dephosphorylation. However, SR-17018-induced MOP phosphorylation was reversible when the antagonist naloxone was included in aqueous washout solutions. In contrast, buprenorphine-stimulated MOP phosphorylation was not reversible by naloxone. These results predict that SR-17018 has a very slow off-rate at MOP, similar to that known for buprenorphine [4,12]. However, SR-17018 has a much lower affinity than buprenorphine so it can easily be displaced by naloxone [3,12].

SR-17018 exhibits a peculiar pharmacological profile in preclinical animal models, where it has been shown to prevent opioid withdrawal signs [3,5]. Such activity has previously been observed for buprenorphine but not for any other biased MOP agonist [8,13]. This suggests that opioids with delayed dephosphorylation kinetics may be useful for opioid maintenance therapy. Nevertheless, SR-17018 differs from buprenorphine in that its effects are easily reversible with naloxone.

4. Materials and Methods

4.1. Reagents and Antibodies

[D-Ala^2, N-Me-Phe^4, Gly^5-ol]-Enkephalin acetate salt (DAMGO) was purchased from Sigma Aldrich (Munich, Germany). SR-17018 was obtained from MedChemExpress (Monmouth Junction, NJ, USA), buprenorphine from Indivior (Dublin, Ireland), and naloxone from Ratiopharm (Ulm, Germany). Pierce^{TM} HA epitope tag antibody was obtained from Thermo Scientific (Rockford, IL, USA). The rabbit polyclonal phosphosite-specific μ-opioid receptor antibodies anti-pT370 (7TM0319B), anti-pT376 (7TM0319D), anti-pT379 (7TM0319E), anti-pS375 (7TM0319C) and anti-HA antibody (7TM000HA) were obtained from 7TM Antibodies (Jena, Germany) [9,11,14,15]. The secondary horseradish peroxidase (HRP)-linked anti-rabbit antibody was purchased from Cell Signaling (Frankfurt, Germany).

4.2. Cell Culture and Transfection

HEK293 cells were originally obtained from the German Resource Centre for Biological Material (DSMZ, Braunschweig, Germany) and grown in Dulbecco's modified Eagle's medium supplemented with 10% fetal calf serum, 2 mM L-glutamine, and 100 U/mL penicillin/streptomycin and cultured in a humidified atmosphere containing 5% CO_2. Cells were stably transfected with mouse MOP-HA and the assays performed have been extensively characterized in previous publications [9,11].

4.3. Western Blot Assay

HEK293 cells stably expressing HA-MOP were seeded onto poly-L-lysine-coated 60 mm dishes and grown to 90% confluency. After agonist stimulation, cells were lysed in RIPA buffer (50 mM Tris-HCl, pH 7.4, 150 mM NaCl, 5 mM EDTA, 1% Nonidet P-40, 0.5% sodium deoxycholate, 0.1% SDS) containing protease and phosphatase inhibitors (Complete mini and PhosSTOP; Roche Diagnostics, Mannheim, Germany). When indicated, cells were washed three times with either PBS buffer (PBS washout) or PBS supplemented with

10 µM naloxone (naloxone washout). After removal of agonist, the cells were incubated in the absence of agonist at 37 °C as indicated and lysed in RIPA buffer containing protease and phosphatase inhibitors, as described previously. The assays were performed at both physiological temperature (37 °C) and at room temperature (22 °C) to slow down the cellular processes if indicated. Pierce^{TM} HA epitope tag antibody beads (Thermo Scientific, Rockford, IL, USA) were used to enrich HA-tagged MOP. The samples were washed several times afterwards. To elute proteins from the beads, the samples were incubated in SDS sample buffer for 25 min at 43 °C. Supernatants were separated from the beads, loaded onto 8% SDS polyacrylamide gels, and then immunoblotted onto nitrocellulose membranes afterwards. After blocking, membranes were incubated with anti-pT370 (7TM0319B), anti-pS375 (7TM0319C), anti-pT376 (7TM0319D), or anti-pT379 (7TM0319E) antibody overnight at 4 °C (7TM Antibodies, Jena, Germany). Membranes were incubated in HRP-linked secondary antibody for 2 h, followed by detection using a chemiluminescence system (90 mM *p*-coumaric-acid, 250 mM luminol, 30% hydrogen peroxide). Blots were subsequently stripped and incubated again with the phosphorylation-independent anti-HA antibody to confirm equal loading of the gels. Protein bands on Western blots were exposed to X-ray films.

4.4. Immunocytochemistry

HEK293 cells stably expressing HA-MOP were seeded onto poly-L-lysine coated 24-well plates overnight. On the next day, cells were pre-incubated with anti-HA antibody for 2 h at 4 °C. Cells were then transferred to 37 °C, exposed to 10 µM agonist for 30 min at 37 °C and fixed with 4% paraformaldehyde and 0.2% picric acid in phosphate buffer (pH 6.9) for 30 min at room temperature (RT). After washing the coverslips with PBS *w/o* Ca^{2+}/Mg^{2+} buffer several times, cells were blocked with phosphate buffer containing 3% NGS for 2 h and were then incubated with Alexa488-conjugated secondary antibody (1:2000) (LifeTechnologies, Thermo Fisher Scientific A11008) overnight at 4 °C. On the next day, cells were washed several times with PBS *w/o* Ca^{2+}/Mg^{2+} and specimens were mounted with Roti®-MountFluorCare DAPI (Carl Roth, HP20.1) and examined using a Zeiss LSM510 META laser scanning confocal microscope (Zeiss, Jena, Germany).

4.5. Data Availability

The authors declare that all data supporting the findings of this study are presented within the paper and its supporting information files. The data that support the findings of this study are available from the authors upon reasonable request.

5. Conclusions

Together, the present study reveals a mechanism of action for SR-17018 that is clearly different from any other known MOP agonist. Our findings also demonstrate that newly synthesized compounds should be fully characterized, including detailed analysis of their receptor phosphorylation kinetics, before classification as biased, partial, or full agonists.

Author Contributions: A.K. and S.S. initiated the project and designed all experiments with S.F. S.F. performed all in vitro studies. The manuscript was written by A.K., S.S. and S.F. All authors have read and agreed to the published version of the manuscript.

References

1. Koob, G.F. Neurobiological substrates for the dark side of compulsivity in addiction. *Neuropharmacology* **2009**, *56* (Suppl. 1), 18–31. [CrossRef] [PubMed]

2. Williams, J.T.; Ingram, S.L.; Henderson, G.; Chavkin, C.; von Zastrow, M.; Schulz, S.; Koch, T.; Evans, C.J.; Christie, M.J. Regulation of mu-opioid receptors: Desensitization, phosphorylation, internalization, and tolerance. *Pharm. Rev.* **2013**, *65*, 223–254. [CrossRef] [PubMed]

3. Schmid, C.L.; Kennedy, N.M.; Ross, N.C.; Lovell, K.M.; Yue, Z.; Morgenweck, J.; Cameron, M.D.; Bannister, T.D.; Bohn, L.M. Bias factor and therapeutic window correlate to predict safer opioid analgesics. *Cell* **2017**, *171*, 1165–1175. [CrossRef] [PubMed]

4. Gillis, A.; Gondin, A.B.; Kliewer, A.; Sanchez, J.; Lim, H.D.; Alamein, C.; Manandhar, P.; Santiago, M.; Fritzwanker, S.; Schmiedel, F.; et al. Low intrinsic efficacy for g protein activation can explain the improved side effect profiles of new opioid agonists. *Sci. Signal.* **2020**, *13*, e3140. [CrossRef] [PubMed]

5. Grim, T.W.; Schmid, C.L.; Stahl, E.L.; Pantouli, F.; Ho, J.H.; Acevedo-Canabal, A.; Kennedy, N.M.; Cameron, M.D.; Bannister, T.D.; Bohn, L.M. A G protein signaling-biased agonist at the mu-opioid receptor reverses morphine tolerance while preventing morphine withdrawal. *Neuropsychopharmacology* **2020**, *45*, 416–425. [CrossRef] [PubMed]

6. McPherson, J.; Rivero, G.; Baptist, M.; Llorente, J.; Al-Sabah, S.; Krasel, C.; Dewey, W.L.; Bailey, C.P.; Rosethorne, E.M.; Charlton, S.J.; et al. Mu-opioid receptors: Correlation of agonist efficacy for signalling with ability to activate internalization. *Mol. Pharm.* **2010**, *78*, 756–766. [CrossRef] [PubMed]

7. Pergolizzi, J.; Aloisi, A.M.; Dahan, A.; Filitz, J.; Langford, R.; Likar, R.; Mercadante, S.; Morlion, B.; Raffa, R.B.; Sabatowski, R.; et al. Current knowledge of buprenorphine and its unique pharmacological profile. *Pain Pract.* **2010**, *10*, 428–450. [CrossRef] [PubMed]

8. Lutfy, K.; Eitan, S.; Bryant, C.D.; Yang, Y.C.; Saliminejad, N.; Walwyn, W.; Kieffer, B.L.; Takeshima, H.; Carroll, F.I.; Maidment, N.T.; et al. Buprenorphine-induced antinociception is mediated by mu-opioid receptors and compromised by concomitant activation of opioid receptor-like receptors. *J. Neurosci.* **2003**, *23*, 10331–10337. [CrossRef] [PubMed]

9. Just, S.; Illing, S.; Trester-Zedlitz, M.; Lau, E.K.; Kotowski, S.J.; Miess, E.; Mann, A.; Doll, C.; Trinidad, J.C.; Burlingame, A.L.; et al. Differentiation of opioid drug effects by hierarchical multi-site phosphorylation. *Mol. Pharm.* **2013**, *83*, 633–639. [CrossRef] [PubMed]

10. Miess, E.; Gondin, A.B.; Yousuf, A.; Steinborn, R.; Mosslein, N.; Yang, Y.; Goldner, M.; Ruland, J.G.; Bunemann, M.; Krasel, C.; et al. Multisite phosphorylation is required for sustained interaction with grks and arrestins during rapid mu-opioid receptor desensitization. *Sci. Signal.* **2018**, *11*, eaas9609. [CrossRef] [PubMed]

11. Doll, C.; Poll, F.; Peuker, K.; Loktev, A.; Gluck, L.; Schulz, S. Deciphering micro-opioid receptor phosphorylation and dephosphorylation in hek293 cells. *Br. J. Pharm.* **2012**, *167*, 1259–1270. [CrossRef] [PubMed]

12. Pedersen, M.F.; Wrobel, T.M.; Marcher-Rorsted, E.; Pedersen, D.S.; Moller, T.C.; Gabriele, F.; Pedersen, H.; Matosiuk, D.; Foster, S.R.; Bouvier, M.; et al. Biased agonism of clinically approved mu-opioid receptor agonists and trv130 is not controlled by binding and signaling kinetics. *Neuropharmacology* **2020**, *166*, 107718. [CrossRef] [PubMed]

13. Fishman, M.A.; Kim, P.S. Buprenorphine for chronic pain: A systemic review. *Curr. Pain Headache Rep.* **2018**, *22*, 83. [CrossRef] [PubMed]

14. Yousuf, A.; Miess, E.; Sianati, S.; Du, Y.P.; Schulz, S.; Christie, M.J. Role of phosphorylation sites in desensitization of micro-opioid receptor. *Mol. Pharm.* **2015**, *88*, 825–835. [CrossRef] [PubMed]

15. Pfeiffer, M.; Koch, T.; Schroder, H.; Laugsch, M.; Hollt, V.; Schulz, S. Heterodimerization of somatostatin and opioid receptors cross-modulates phosphorylation, internalization, and desensitization. *J. Biol. Chem.* **2002**, *277*, 19762–19772. [CrossRef] [PubMed]

Profiling the Effects of Repetitive Morphine Administration on Motor Behavior in Rats

Alok K. Paul [1],[*] , Nuri Gueven [1] and Nikolas Dietis [2],[*]

[1] School of Pharmacy and Pharmacology, University of Tasmania, Hobart, TAS 7001, Australia; nuri.guven@utas.edu.au
[2] Medical School, University of Cyprus, Nicosia 1678, Cyprus
[*] Correspondence: alokkpaul@gmail.com (A.K.P.); dietis.nikolas@ucy.ac.cy (N.D.)

Abstract: Efficient repetitive clinical use of morphine is limited by its numerous side effects, whereas analgesic tolerance necessitates subsequent increases in morphine dose to achieve adequate levels of analgesia. While many studies focused on analgesic tolerance, the effect of morphine dosing on non-analgesic effects has been overlooked. This study aimed to characterize morphine-induced behavior and the development and progression of morphine-induced behavioral tolerance. Adult male Sprague–Dawley rats were repetitively treated with subcutaneous morphine for 14 days in two dose groups (A: 5 mg/kg/day (b.i.d.) → 10 mg/kg/day; B: 10 mg/kg/day (b.i.d.) → 20 mg/kg/day). Motor behavior was assessed daily (distance traveled, speed, moving time, rearing, rotation) in an open-field arena, before and 30 min post-injections. Antinociception was measured using tail-flick and hot-plate assays. All measured parameters were highly suppressed in both dosing groups on the first treatment day, followed by a gradual manifestation of behavioral tolerance as the treatment progressed. Animals in the high-dose group showed increased locomotor activity after 10 days of morphine treatment. This excitatory phase converted to an inhibition of behavior when a higher morphine dose was introduced. We suggest that the excitatory locomotor effects of repetitive high-dose morphine exposure represent a signature of its behavioral and antinociceptive tolerance.

Keywords: morphine dosing; behavior; locomotor activity; tolerance

1. Introduction

Long-term clinical use of opioids such as morphine is limited by its significant side effects such as drowsiness, itching, respiratory depression, constipation, addiction, and dependence [1–3]. Although predicting the appearance of morphine-induced side effects is important for effective pain relief, the relationship between opioid dosing and the appearance of drug-induced side effects is currently not well established. In the clinic, pain relief and side effects appear to correlate poorly [4]. Behavioral side effects of morphine in different clinical studies are described as dose-dependent, such as pruritus [5], and dose-independent, such as nausea and vomiting [6,7]. It therefore is important to understand how the dosing regimen can affect behavioral effects. Noticeably, antinociceptive tolerance largely depends on morphine dose and dosing protocol, and a high starting dose or a high follow-up dose of morphine produces less antinociceptive tolerance [8]. We previously measured antinociception and antinociceptive tolerance in rats using four different morphine dosing regimens. Antinociception and antinociceptive tolerance were measured using two independent assays (tail-flick and hot-plate assays) [8]. Behavioral measurements are more complex than nociceptive pain measurements, and therefore, only two morphine dosing regimens were selected for the present study. Our previous study confirmed the manifestation of antinociceptive tolerance in rats using these dosage regimens [8]. However, antinociceptive tolerance differed between these dosage groups, which suggested that these dosages regimens might also differentially affect behavioral tolerance [8]. Therefore, the current study correlated behavioral and antinociceptive tolerance

in rats using the same morphine dosage regimen (starting dose, follow-up dose, frequency of dosing, and duration of treatment) [8].

The current literature shows inconsistent effects of morphine on animal behavior. These inconsistencies are likely due to the use of different species/strains, routes of administration, types or formulations of morphine, age of animals, and various treatment protocols (dose, frequency, or duration of treatment) [9–12]. Locomotor activity has been widely assessed to characterize behavioral effects of morphine-treated animals. While lower morphine doses mostly left locomotor activities unaffected, higher doses produced stimulatory or biphasic effects when morphine was administered acutely [10,13–16]. Similarly, long-term morphine treatment with lower doses (1.25 to 5 mg/kg i.p.) showed no effects on locomotion, while higher doses (10 to 40 mg/kg i.p.) produced a biphasic effect with initial suppressive and subsequent increased locomotor activities [14]. Basic locomotor activity alone cannot reflect the complete behavioral side effects profile of morphine, while concomitant measurement of locomotor activities together with other behavioral parameters was shown to be better suited to model the behavioral side effects of morphine [13]. In this study, 20 mg/kg of intraperitoneal morphine increased, while 10 mg/kg of morphine decreased horizontal movements in female mice, while both doses decreased rearing and grooming activities [13]. In contrast, no dose-dependent differences were detected in male rats in response to intracerebroventricular morphine injections [10]. These discrepancies illustrate that morphine-induced behavioral changes are, among other parameters such as route of administration and species, influenced by gender. This is not surprising, since female animals are more sensitive to morphine treatment [17,18] and showed increased distance and rearing duration compared to male mice in response to morphine treatment [18]. Moreover, different environmental settings have been used for behavioral tests. Especially, changes to the illumination conditions such as brightly illuminated [18–20], moderately illuminated [9,13], or low illuminated environments [14] have been reported. Since rodents are more active under low illumination conditions, brightly lit open-field arenas may distract the animals, which likely alters the results compared to experiments performed under low illumination conditions. Besides, most studies only tested the animal's acute responses 30 min after morphine administration [9,10,13], which completely disregarded the known biphasic behavioral pattern in response to morphine exposure [14,21].

Although some studies combined several behavioral activities such as distance traveled, rearing, immobility, or grooming after acute morphine treatment [9,10,13], possible connections between locomotion and other behavioral effects have not been established for repetitive long-term morphine treatment. Therefore, a significant gap of knowledge is evident regarding the relationship between antinociceptive and behavioral effects of morphine and its long-term effect on behavioral and antinociceptive tolerance. This study measured multiple behavioral effects before, during, and after long-term morphine treatment in rats. Animals were treated with two different morphine dosing regimens to establish the influence of dosing regimens on behavior. Seven behavioral parameters were measured automatically in an open-field arena, which has been rarely performed before [10]. The present study is an exploratory study to understand the behavioral tolerance profile of the same group of animals over the course of a two week treatment instead of comparing them to a different group of control animals. We aimed to generate a detailed behavioral profile of long-term morphine treatment, behavioral tolerance, and the influence of two different morphine dosage regimens, to reflect existing relationships between behavioral and antinociceptive tolerance.

2. Results

2.1. Time-Dependent Effects of a Single Dose of Morphine to Locomotor Behaviors: Hypoactivity vs. Hyperactivity

To acquire a basic understanding of how repeated morphine administration affects rat behaviors, rats were treated daily with 10 mg/kg (b.i.d.) morphine over a period of 10 days, and their activities were recorded and assessed daily at regular intervals, for a total of 180 min after administration. Daily basal levels of activity ($t = 0$ min) were similar with no

significant differences over the treatment period. Therefore, no residual effects of morphine from previous administrations on the examined behavior were observed at the beginning of each daily experiment (Supplementary Figures S1 and S2). A separate control group of animals (*n* = 6) was used to assess the impact of vehicle (0.9% *w/v* sodium chloride solution, b.i.d.) over repeated treatments (Supplementary Figure S3). Control animals, treated similarly with the vehicle for three days, did not change locomotor behavior at the 30 min post-injection time-point. Since no differences in basal behavioral activities were observed over 14 days and no changes in the behavior of saline-treated animals over three days of consecutive treatment were detected, repeated treatment did not change the baseline behavioral activities of rats (Supplementary Figures S1–S3).

Behavioral scoring at every time-point was compared between days 1 and 10 using unpaired *t*-tests and is shown in Figures 1 and 2 (basic locomotion, Figure 1; rearing and rotation, Figure 2). Statistical analysis was also performed using two-way ANOVA that produced similar results. For basic locomotion, at day 1 of morphine administration, suppression of locomotor activities was observed after 30 min at all parameters analyzed (one-way ANOVA; $F_{(11, 46)} = 12.43$; $p < 0.01$(distance); $F_{(11, 54)} = 8.96$; $p < 0.0001$ (moving time); $F_{(11, 57)} = 22.12$; $p < 0.001$ (speed)), which persisted until 60 min after administration (Figure 1A–C). The repression of all examined parameters of locomotion returned to their basal levels within 180 min after administration. However, after 10 days of daily repetitive administration of morphine (day 10), general locomotion manifested as hyperactivity, as shown by significant increases in the traveled distance (one-way ANOVA; $F_{(11, 46)} = 12.43$; $p < 0.0001$) and moving speed (one-way ANOVA; $F_{(11, 57)} = 22.12$; $p < 0.0001$), along with non-significant differences in moving time compared to basal levels. This change in the activity profile towards hyperactivity was accompanied by a shift of its peak at 15 min after morphine administration and a faster recovery to basal levels within 180 min of treatment.
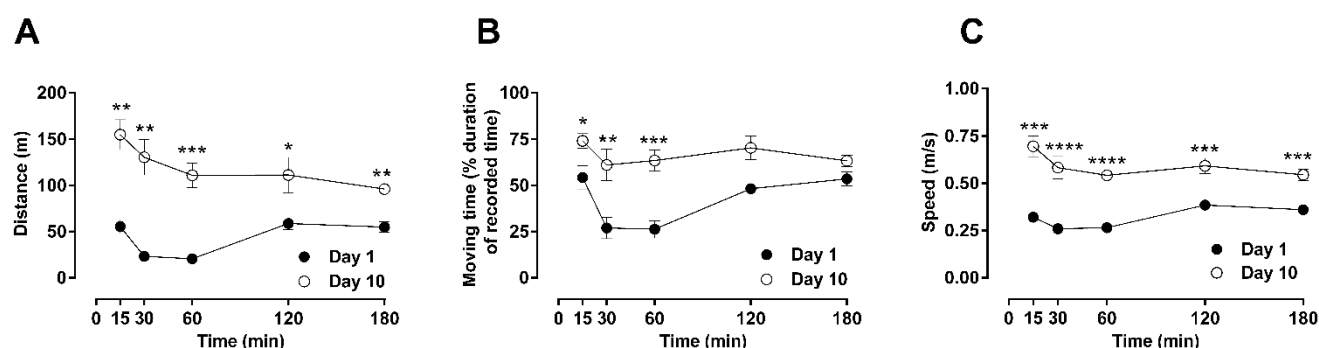
Figure 1. Time-resolved basic locomotor activity after repeated morphine administration (10 mg/kg, b.i.d. over 10 days). Locomotor parameters were recorded in an open-field arena after a single subcutaneous injection of morphine on day 1 or day 10 in male Sprague–Dawley rats. The motor behavior of treated animals was assessed by quantification of total distance traveled (**A**), total moving duration (**B**), or average speed (**C**), for a period of 180 min post-administration. Statistically significance ($p < 0.05$) at a specific time-point against the effects of day 1 is shown as * $p < 0.05$, ** $p < 0.01$, *** $p < 0.001$, and **** $p < 0.0001$ and was calculated using unpaired *t*-test. Values are presented as mean ± SEM (*n* = 6 animals per group). Error bars are sometimes too small to be visible. The behavioral differences between these two days are shown as the differences in their area under the curves (AUC) in Table 1, which indicates that differences were observed in the distance, moving time, and speed.

The specific locomotor behaviors of rotation and rearing were also analyzed in a similar time-resolved manner in terms of the total score (numbers; Figure 2A,C) and duration (time; Figure 2B,D). Rotational behavior was suppressed by morphine on day 1 in a similar fashion as general locomotion in terms of peak and recovery timing (one-way ANOVA; $F_{(11, 42)} = 31.56$; $p < 0.05$). Similar to general locomotion, rotational behavior was also significantly increased at day 10 compared to basal levels (one-way ANOVA; $F_{(11, 42)} = 31.56$; $p < 0.01$). Rearing was significantly suppressed by morphine on day 1, similarly to general locomotion (one-way ANOVA; $F_{(11, 39)} = 45.85$; $p < 0.0001$). This

behavior remained suppressed at day 10 without contributing to the hyperactivity usually seen in the previously recorded parameters on day 10 (Figure 2B,C).

Table 1. Comparison of motor behaviors from day 1 after repeated morphine administration. Total scoring of motor behavior was recorded over 180 min after subcutaneous administration of morphine 10 mg/kg (b.i.d.) over 10 days of repeated treatment. Parameters (presented as the area under curve; AUC) were calculated from the behavioral curves in Figures 1 and 2. Statistically significant differences between AUCs of each behavior were assessed using an unpaired *t*-test.

Behavioral Parameter	AUC Units	Day 1 (Dose Group B)	Day 10 (Dose Group B)	Significance (*p*-Value)
Distance	meter × days	8958 ± 995	19,492 ± 1562	<0.001
Moving time	% of recorded time × days	8349 ± 643	11,715 ± 643	<0.01
Speed	(meter/sec) × days	60.22 ± 1.25	99.51 ± 3.34	<0.0001
Rotation numbers	incidences × days	8374 ± 550	25,423 ± 1761	<0.0001
Rotation time	% of recorded time × days	2464 ± 240	3704 ± 199	<0.01
Rearing numbers	incidences × days	3018 ± 308	3717 ± 206	0.096
Rearing time	% of recorded time × days	2116 ± 171	2803 ± 458	0.2269
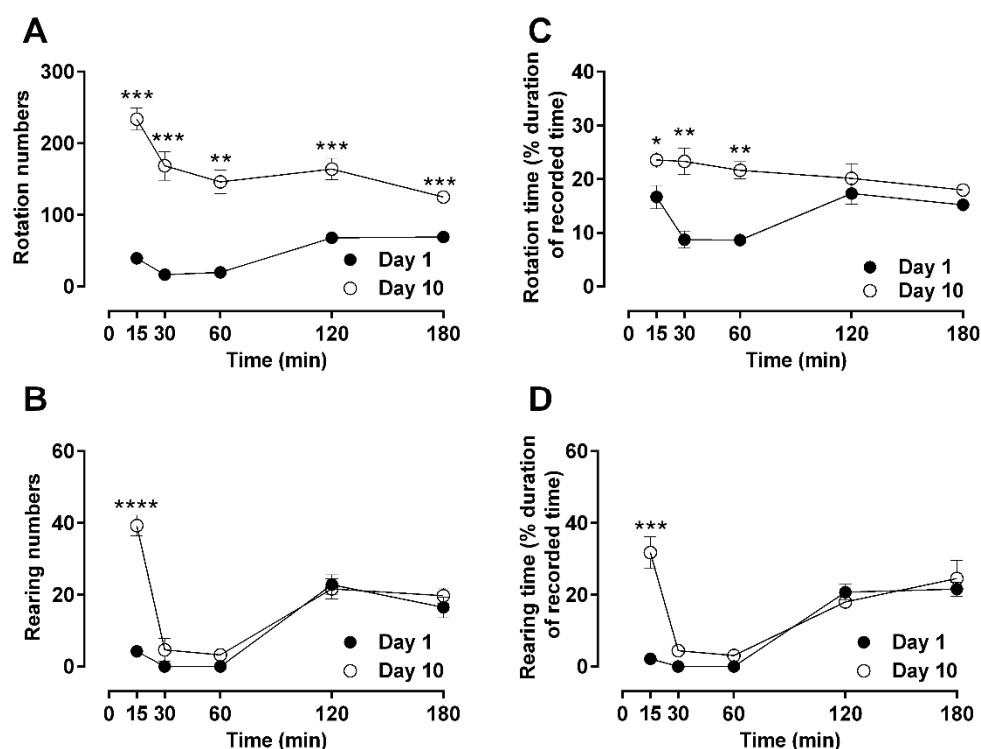
Figure 2. Time-resolved advanced locomotor activity (rotation and rearing) after repeated morphine administration (10 mg/kg, b.i.d. over 10 days). Open-field turning and rearing activities after a single subcutaneous injection of morphine on day 1 or day 10 were measured in male Sprague–Dawley rats. Activities of treated animals were measured as rotation numbers (**A**), rearing numbers (**B**), rotation time (**C**), and rearing time (**D**) over a period of 180 min. Statistical significance ($p < 0.05$) at a specific time-point against the effects of day 1 is shown as * $p < 0.05$, ** $p < 0.01$, *** $p < 0.001$, and **** $p < 0.0001$ and was calculated using unpaired *t*-test. Values are presented as mean ± SEM ($n = 6$ animals per group). Error bars are sometimes too small to be visible. The behavioral differences between day 1 and day 10 are shown as the differences in their area under the curves (AUC) in Table 1, which indicates that differences were observed in rotation, but not in rearing behaviors.

To evaluate the overall behavioral effects of repeated morphine administration over a period of 10 days, the overall scores of Figures 1 and 2 were quantified as area under the curves (AUC) and presented in Table 1. Morphine significantly stimulated locomotion after 10 days of repetitive administration compared to day 1, where it significantly suppressed

locomotion, with the notable exception of rearing behavior that was persistently suppressed at day 10 (Table 1). The corresponding behavioral activities of morphine 5 mg/kg (b.i.d.) for 5 days of repeated treatment are shown in Supplementary Figures S4 and S5.

2.2. Dose-Dependent Effects of Repetitive Morphine Administration and Incremental Changes of Dosing on Locomotor Behavior: Hypoactivity vs. Hyperactivity

To investigate the effect of morphine dosing regimens on locomotion and related behavior, animals were treated with two dosing regimens that differ in dose and duration (5 mg/kg/day b.i.d. or 10 mg/kg/day b.i.d.), followed by a subsequent change in the administration of morphine (double-dosing in single daily injections) until day 14 of treatment (Figure 3). Noticeably, no differences between basal locomotion, rotation, or rearing activities over the total treatment period of 14 days were observed, which were recorded daily (every morning) immediately before morphine injections (Supplementary Figures S1 and S2).

Table 2. Overall comparison of motor behaviors between different dosing groups. Total scoring of recorded motor behaviors (presented as area under curve; AUC) were calculated from the behavioral curves in Figures 3 and 4. Statistically significant differences between AUCs of each behavior were assessed using an unpaired *t*-test.

Behavioral Parameter	AUC Units	Dose Group A	Dose Group B	Significance (*p*-Value)
Distance	meter × days	369.6 ± 71.6	982.3 ± 134.3	<0.01
Moving time	% of recorded time × days	305.5 ± 32.6	700.2 ± 51.4	<0.001
Speed	(meter/sec) × days	3.80 ± 0.23	5.69 ± 0.42	<0.01
Rotation numbers	incidences × days	255.8 ± 48.4	1200 ± 124.2	<0.001
Rotation time	% of recorded time × days	103.1 ± 12.6	233.4 ± 22.2	<0.001
Rearing numbers	incidences × days	48.0 ± 15.5	97.4 ± 30.1	0.174
Rearing time	% of recorded time × days	19.4 ± 2.86	40.6 ± 9.9	0.130

In the 'low' starting dose treatment group (5 mg/kg b.i.d. → 10 mg/kg/day; Figure 3A), moving distance was significantly reduced days 1 and 2 (one-way ANOVA; $F_{(14, 48)} = 4.26$; $p < 0.05$), with a slow but steady recovery until day 5. The subsequent change in the method of administration of morphine (from twice daily 5 mg/kg to once daily 10 mg/kg) on day 6 onwards somewhat increased the suppressive effect of morphine on moving distance, returning the difference from basal back to significant levels (one-way ANOVA; $F_{(14, 48)} = 4.26$; $p < 0.001$). No behavioral recovery was observed from day 6 to the end of the treatment period (day 14). The parameter of moving time (Figure 3B) and moving speed (Figure 3C) showed very similar responses as for the distance parameter.

In the second group of 'high' morphine dosing (10 mg/kg/day b.i.d. till day 10 → 20 mg/kg/day till day 14), the same locomotive parameters were assessed, where a marked change in the overall profile was observed (Figure 3D–F). The 10 mg/kg/day b.i.d. morphine significantly reduced moving distance at day 1 compared to basal (one-way ANOVA; $F_{(14, 47)} = 19.20$; $p < 0.01$); however, the recovery to basal values was not only fast and steady despite repetitive morphine administration, but also significantly increased distance traveled compared to basal values, from day 6 (one-way ANOVA; $F_{(14, 47)} = 19.20$; $p < 0.05$) until it reached a hyperactivity plateau at day 10. When morphine administration changed to a single dose of 20 mg/kg/day from day 11 (Figure 3D), the suppressive effect of morphine returned to the observed levels of day 1 (one-way ANOVA; $F_{(14, 47)} = 19.20$; $p < 0.05$) and remained suppressed until the end of the treatment period (day 14). This pattern of morphine-induced changes observed for traveled distance was also replicated by the other experimental parameters of general locomotion (moving time; Figure 3E and speed of movement; Figure 3F) and rotational behavior (Figure 4A,C).
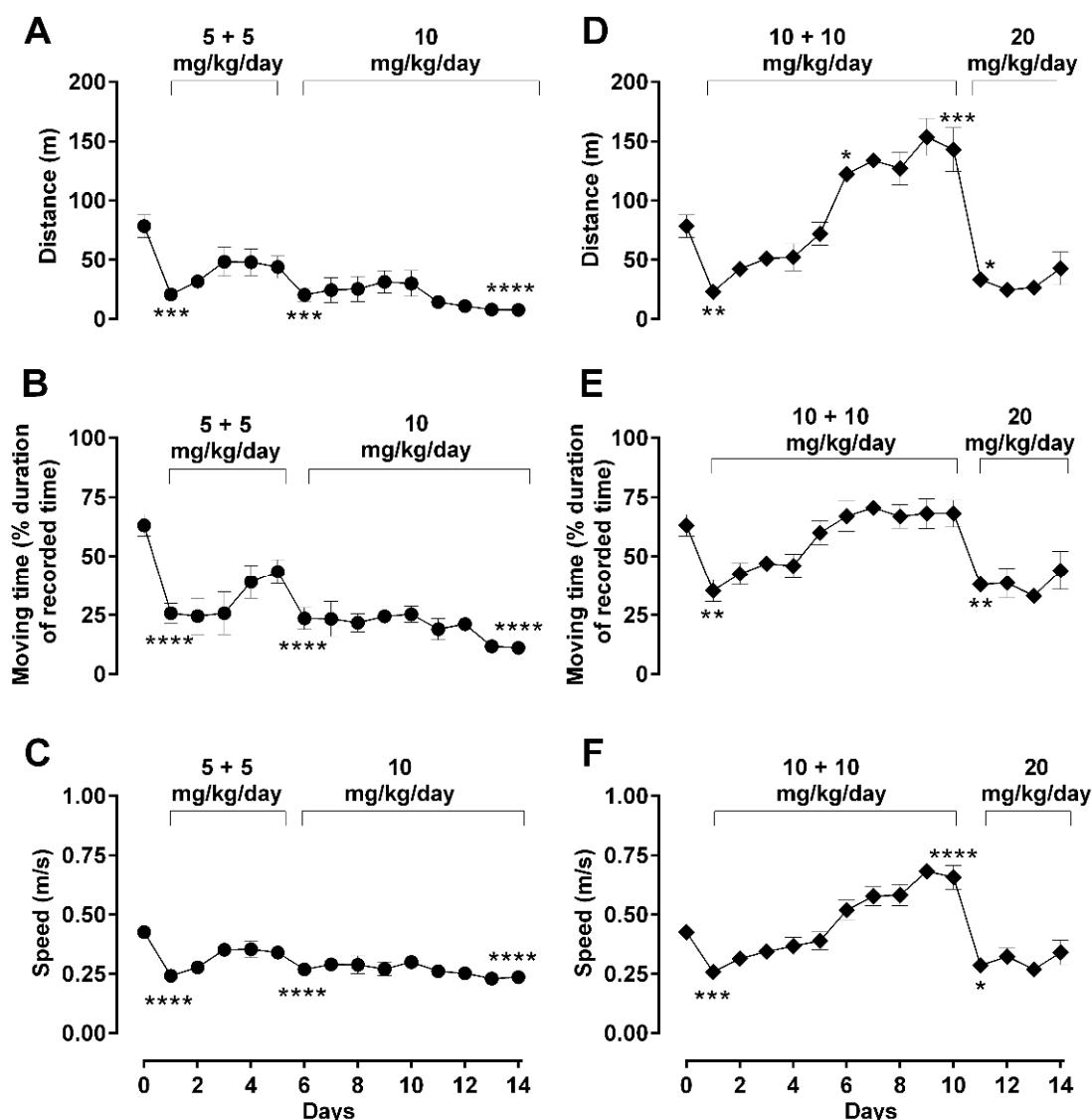
Figure 3. Effect of dosing regimen changes on basic locomotor activity during long-term morphine administration. Locomotor parameters were recorded daily in an open-field arena 30 min after daily subcutaneous injections of morphine in male Sprague–Dawley rats, during a 5 min recording period. Motor behavior of treated animals was assessed by quantification of distance travelled (**A**,**D**), moving duration (**B**,**E**), or average speed (**C**,**F**). Two morphine regimens were respectively used in two different groups of animals: 5 (b.i.d.) → 10 mg/kg (**A**–**C**) and 10 (b.i.d.) → 20 mg/kg (**D**–**F**) over a total period 14 days, as described in *Methods*. Values are presented as mean $\pm$ SEM (n = 6 animals per group). Error bars are sometimes too small to be visible. Statistically significant ($p < 0.05$) differences compared against day 0 are shown as * $p < 0.05$, ** $p < 0.01$, *** $p < 0.001$, and **** $p < 0.0001$ and were calculated using one-way ANOVA with Dunnett's multiple comparisons test. The behavioral differences between these two dosing groups are shown as the differences in their area under the curves (AUC) in Table 2, which indicates that differences were observed in all three behavioral parameters.

For rearing behavior, a similar morphine effect during repetitive administration for both 'low' and 'high' dose groups was observed (Figure 4B,D). Morphine significantly suppressed rearing from day 1 until day 14 (one-way ANOVA; F $(14, 53)$ = 35.57; $p < 0.0001$) without any recovery or observed increase in recorded activity, even when morphine administration was changed from twice daily to a daily single double-dose (5 mg/kg/day b.i.d. → 10 m/kg/day; Figure 4B, 10 mg/kg/day b.i.d. → 20 mg/kg/day; Figure 4D), essentially staying suppressed over the entire treatment period.
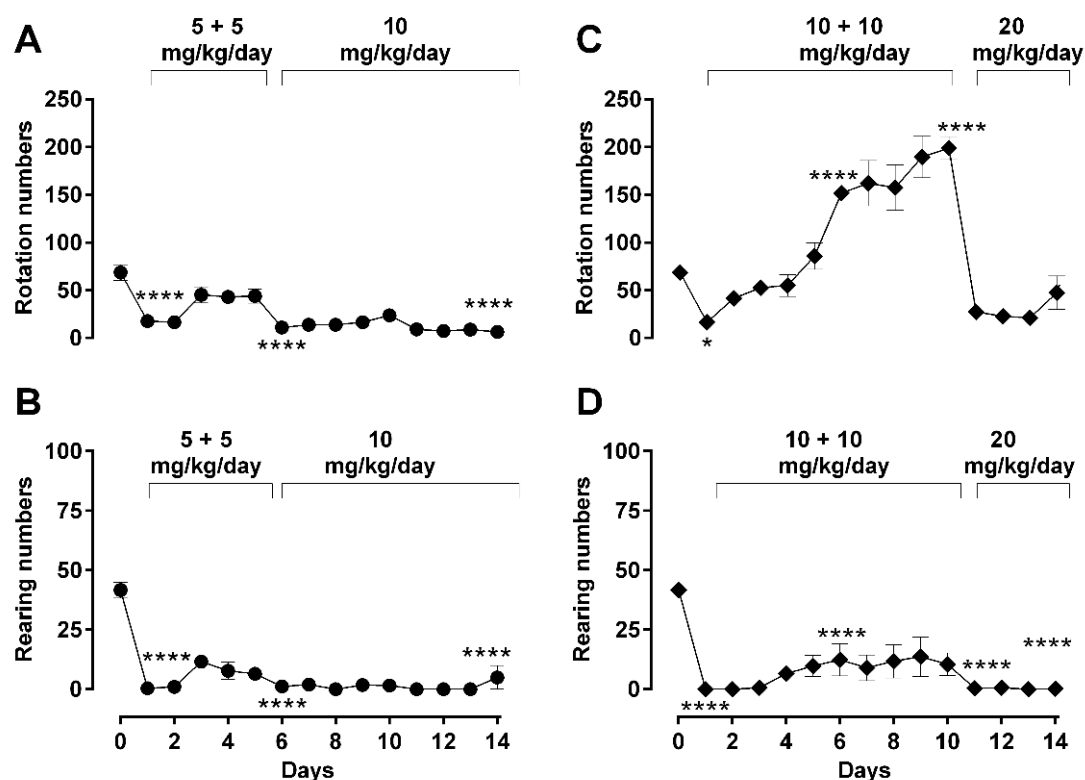
Figure 4. Effect of dosing regimen changes on advanced locomotor activity parameters (rearing and rotation) during long-term morphine administration. Rotation and rearing behaviors were recorded in an open-field arena after daily subcutaneous injections of morphine in male Sprague–Dawley rats, at a daily 30 min mark post-administration during a 5 min recording period. Activities of treated animals were measured as rotation numbers (**A,C**) and rearing numbers (**B,D**). Two morphine regimens were respectively used in two different groups of animals: 5 (b.i.d.) → 10 mg/kg (A, B) and 10 (b.i.d.) → 20 mg/kg (**C,D**) over a total period 14 days, as described in *Methods*. Values are presented as mean ± SEM (*n* = 6 animals per group). Error bars are sometimes too small to be visible. Statistically significant (*p* < 0.05) differences compared against day 0 are shown as * *p* < 0.05, and **** *p* < 0.0001 and were calculated using one-way ANOVA with Dunnett's multiple comparisons test. The behavioral differences between these two dosing groups are shown as the differences in their area under the curves (AUC) in Table 2, which indicates that differences were observed in rotation but not in rearing behavior.

Regimen-dependent behavioral changes were also expressed as the area under the curves (AUCs) over the whole treatment period of 14 days, and a comparison between the groups is shown in Table 2. The AUCs of behavioral parameters of the higher dosing paradigm (10 mg/kg/day b.i.d. → 20 mg/kg/day) were significantly higher than the AUCs of the lower treatment paradigm (5 mg/kg/day b.i.d. → 10 mg/kg/day), except for rearing numbers and rearing time. Thus, morphine 10 mg/kg (b.i.d.) → 20 mg/kg/day treated animals showed more locomotor and rotational behavioral changes (hyper-activity) than the morphine 5 mg/kg (b.i.d.) → 10 mg/kg/day group.

2.3. Relationship between Antinociceptive Tolerance and Locomotor Activities

To better understand the clinical significance of the biphasic behavioral effects of morphine on locomotor behavior between different dosing regimens, we aimed to compare these effects with morphine's major pharmacological drawback, antinociceptive tolerance. Antinociception was measured using two assays (tail-flick and hot-plate), and tolerance was defined as a significant reduction in antinociceptive efficacy, whereas distance traveled was measured using open-field test over a period of 180 min after injections at day 5 or day 10, as described in *Methods*. The area under the curves (AUC) of the first treatment day (day 1), day 5 for Group A (5 mg/kg/day b.i.d.), or day 10 for Group B (10 mg/kg/day

b.i.d.) were compared using unpaired *t*-tests (Figure 5). Animals in the first dose group (5 mg/kg b.i.d.) showed no difference in distance travelled between days 1 and 5, although they exhibited significant antinociceptive tolerance in both assays used (tail-flick; unpaired *t*-test; *t* (10) = 8.48; *p* < 0.0001 and hot-plate; unpaired *t*-test; *t* (10) = 9.80; *p* < 0.0001, as shown in (Figure 5A)). However, animals in the higher dose group (10 mg/kg b.i.d.) showed hyperactivity (e.g., significantly higher locomotion) at day 10 when antinociceptive tolerance first manifested, compared to day 1 (unpaired *t*-test; *t* (7) = 7.04; *p* < 0.001) (Figure 5B). These data collectively show that antinociceptive tolerance due to repetitive morphine administration is an independent effect to morphine's effects on locomotor behavior, where the profile is largely dependent on the dosage regimen used.
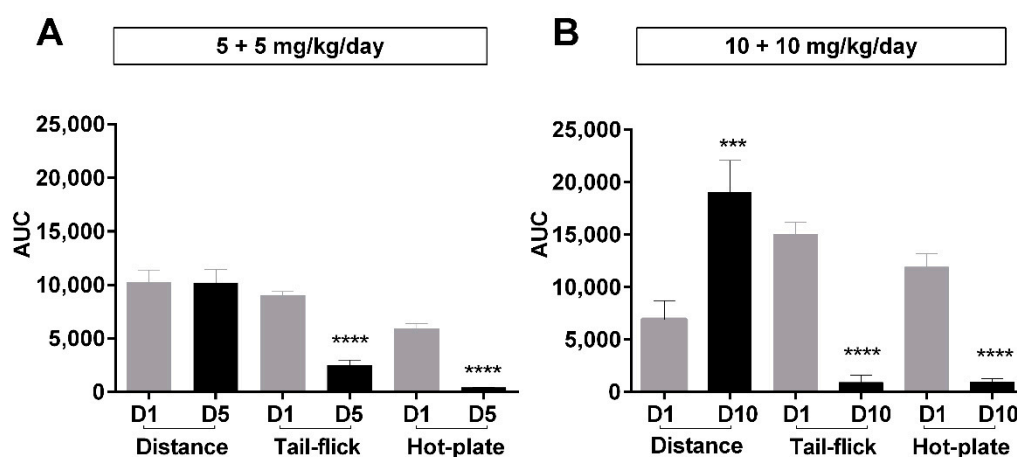
Figure 5. Overall behavioral and antinociceptive effects after long-term morphine administration. Area under the curves (AUC) for distance travelled and antinociception over a period of 180 min post-administration of subcutaneous morphine at different days through a treatment period. The curves used to calculate these AUC values are shown in Figure 1A and Supplementary Figures S4A and S6. Morphine was administered daily as 5 mg/kg (b.i.d.) (**A**), 10 mg/kg b.i.d. over 5 days, or (**B**) 10 mg/kg b.i.d. over 10 days. D1, D5, and D10 represent day 1, day 5, and day 10, respectively. Antinociception was assessed by tail-flick assay (TF) and hot-plate assay (HP). Values are presented as mean ± SEM (*n* = 6 animals per group). Statistically significant (*p* < 0.05) differences from day 1 for all treatment groups are shown as *** *p* < 0.001, **** *p* < 0.0001 and were calculated using unpaired *t*-tests. Error bars are present in all graphs but are sometimes too small to be visible.

3. Discussion

Morphine is the gold standard for the treatment of chronic or cancer pain. Nevertheless, long-term use of morphine is severely limited by its biphasic effects on motor behavior (inhibitory or excitatory) and the manifestation of analgesic tolerance (i.e., reduced analgesic efficacy). Despite increased knowledge of the different activities of morphine, little is known about how dosing regimens affect the manifestation of motor behavioral effects. Euphoria, lethargy, or drowsiness are very common clinical side effects of morphine [22,23] and are mirrored by morphine-induced hypoactivity reported in rodents [24]. The relationship between the behavioral effects of morphine, antinociceptive tolerance, and morphine dosing has been elusive, mainly due to reported inconsistencies in experimental results, which are likely the consequence of different experimental approaches with regards to the route of administration, formulation of morphine, type of animals used, as well as treatment protocols (dose, frequency, or duration of treatment) [9,10,12,25]. All these experimental variables are likely to influence the effect of morphine on motor behavior and therefore highlight the need to examine the relationship between morphine's behavioral effects and dosing in a unified model. Understanding how morphine dosing contributes to behavior is crucial for future clinical strategies to reduce morphine's side effects.

We assessed hypoactivity by monitoring the major parameters of locomotor activity (distance, speed, moving time, rotational behavior, and rearing), as surrogate markers for morphine-induced motor side effects. Locomotor activity was previously used to assess behavioral side effects after acute or chronic treatment with morphine [12–14]. However, basic locomotion alone cannot represent all facets of drug-induced behavioral changes—combining it with additional behavioral parameters is a much more promising approach [13].

This study confirmed that subcutaneous administration of morphine produces locomotor suppression in rats after acute administration, which is in agreement with previous studies [10,13,14,26]. We also showed that repetitive morphine administration (twice a day) resulted in locomotor tolerance after 5 days, the extent of which depended on the dose administered (partial tolerance at 5 mg/kg b.i.d. and full tolerance at 10 mg/kg b.i.d.). The tolerance profile for the behavioral effect of morphine seemed to manifest in parallel to antinociceptive tolerance, as we recently described [8]. Similar to the basal antinociceptive effects reported previously [8], basal locomotor activities (locomotor, rotation, and rearing activities) were also unaffected by repeated morphine dosing over two weeks, which supports a previous report [17]. Therefore, morphine showed no residual effects on behavior or antinociception after repeated dosing over two weeks. Noticeably, no behavioral changes in control rats were observed in comparison to the effects of day 1, which indicated that the 0.9% *w/v* sodium chloride solution or repeated measurements did not affect the development of behavioral tolerance. However, future follow-up studies should include longer periods of vehicle treatment, similar to morphine treatment regimens to provide more evidence for this observation.

The biphasic motor effect of morphine has been known for quite a while but has been mainly described in acute and short-term morphine administration protocols [9,12–14,26–28]. The present study described the manifestation profile of behavioral excitatory state (i.e., rate of increase and timing of expression) in detail, which is vital to understand the underlying mechanisms. This study also described the effect of the morphine dosing regimen for the expression of morphine-induced hyperactivity. When the morphine dosing regimen changes after the occurrence of hyperactivity, such as 10 mg/kg (b.i.d.) → 20 mg/kg/day (once daily), the strong suppressive effect of morphine returns to the pro-hyperactivity levels and results in morphine-induced hypoactivity manifestation (Figure 3). Our data also show that the morphine-induced excitatory effect results from morphine-induced tolerance on motor behavior, which can be reversed by an increased dose, similarly to how antinociceptive tolerance can be reversed by a dose increase [8].

Activation of the MOP receptor by an agonist (e.g., morphine) increases dopamine levels in the brain [29,30]. Morphine-induced hyperactivity can be reduced by blocking dopaminergic receptors, but these are not specific to the dopaminergic system [12,31]. The higher AUC of behavioral activities of animals treated with morphine over a few days clearly indicates that the locomotion-related behavioral effects changed over this time using a specific dose. In our study, the effects of morphine were dependent on the dose administered and the dosage regimen, as the AUCs of locomotor activities were statistically lower (over the entire 14 days) with lower doses compared to the higher dose group.

Opioid-induced turning, circling, or rotation is mainly mediated by the dopaminergic system [32,33], and circling animal models have been used to assess anti-Parkinson's disease drugs [34]. The rotating or turning behavior in this study was suppressed in line with a suppression of general locomotion after acute treatment of morphine with a similar time kinetic, which replicates previous studies [35,36]. We also showed that the rotational behavior is subjected to morphine-induced tolerance, similarly to locomotion (Figure 2), suggesting a strong link of this behavior to the opioidergic system.

Rearing activity is an exploratory behavior of rodents related to information gathering or cognitive behavior [37]. Little or no rearing in the open field may indicate motor impairment [38]. Therefore, unsurprisingly, changes in rearing behavior are also influenced by benzodiazepine treatment [39], which suggests that other neuronal systems might

be more important for this behavior. Rearing is related to gamma-aminobutyric (GABA) neurotransmission controlled by the GABA$_A$ receptor in the hippocampus [40]. Locomotion and rearing are positively correlated and are very reliable factors for exploratory behavior in untreated animals [9,41]. Here, we showed that morphine reduces rearing activities due to repetitive treatment with both low and high doses of morphine, in line with previous studies [42]. However, the morphine-induced suppression of rearing was not associated with tolerance, irrespective of the morphine dose used, the changes in dosing regimen, and the length of treatment (Figure 2). The different effects on rearing behavior compared to the rest of the motor behaviors tested (free moving and rotation) could indicate that additional non-opioidergic systems that affect brain areas involved in motor control of this behavior alleviate or delay the manifestation of tolerance in rearing.

In summary, our results illustrate that a lower morphine dose reduced motor behavior, which was subject to behavioral tolerance after repetitive administration but did not lead to subsequent behavioral hyperexcitation. In contrast, animals treated with a higher morphine dose developed acute motor-suppressive behavior that quickly desensitized to basal levels and progressed to an excitatory phase after 10 days, which was parallel to the development of antinociceptive tolerance [8]. Therefore, morphine dosing plays a crucial role in the manifestation of motor behavioral tolerance that follows a similar pattern to antinociceptive tolerance. The kinetics of morphine-induced suppression of motor behavior and subsequent behavioral tolerance were similar to those of antinociception and antinociceptive tolerance, as reported previously [8]. In contrast, rearing showed a distinctive resistance to tolerance and dosing changes. Our results suggest that morphine dosing determines the expression profile of behavioral effects by morphine and that antinociceptive tolerance is linked to the morphine-induced hyper-excitatory phase of behavior.

4. Materials and Methods

4.1. Animal Maintenance and Care

Eighteen male Sprague–Dawley (SD) rats (234.0 ± 6.1 g, 8 weeks) were housed as three littermates per cage at 22 °C with 50–60% humidity under an automated 12-h day/night cycle (lights on at 7:00 a.m.) with free access to food and water. All procedures were approved by the University of Tasmania Animal Ethics Committee (A0013864) and were conducted according to The Australian Code for the Care and Use of Animals for Scientific Purposes and in compliance with the ARRIVE guidelines [43,44]. Animals were handled for 5–6 days before starting the experiments and acclimatized to the test environment for 2 h in home cases prior to daily experiments.

4.2. Treatment Protocol

Body weight was recorded daily immediately before experiments. Animals were divided into three subgroups using a completely randomized design as previously described [45]. Two sub-groups of animals received different morphine dosing. Group A (*n* = 6): morphine sulfate 5 mg/kg (twice daily) for 5 days, followed by a single dose (once daily) of 10 mg/kg from day 6 to 14. Group B (*n* = 6): morphine sulfate 10 mg/kg (twice daily) for 10 days, followed by a single dose (once daily) of 20 mg/kg from day 11 to 14, as described in a previous study [8]. Commercially available 30 mg/mL morphine sulfate solution (Hameln Pharmaceuticals GmbH, Hamelin, Germany) was administered by daily subcutaneous injections between the left thigh and the spinal cord for group B. For group A, morphine sulfate was diluted to 15 mg/mL with sterile 0.9% *w/v* sodium chloride solution immediately before injections, as we described previously in another study [15]. The third sub-group, group C (*n* = 6), was a control group of animals were treated similarly with sterile 0.9% *w/v* sodium chloride solution in water (b.i.d.) for 3 days. Injection volumes, morphine doses, dilution, and timing of injections were selected based on our previous results [8]. The illumination intensity of the laboratory was reduced prior to and during experiments to minimize discomfort to the animals. At the end of each study,

animals were anesthetized with 5% (w/v) isoflurane in oxygen at a flow rate of 1 L/min before decapitation.

4.3. Locomotor Activity Measurements

Behavior was tested in an open-field arena in an automated Multi-Conditioning System (MCS) (TSE GmbH, Homburg, Germany) pre- and post- (15, 30, 60, 120 and 180 min) administration of morphine over 5 min on the first and the last treatment day of the same dose, since a 5 min observation period is widely used [9,13,15]. On all other treatment days, the rats were tested only for baseline behavior (pre-) and 30 min post-administration of morphine, representing the time-point of morphine-induced maximal behavioral suppression on day 1. Similarly, open-field behaviors of control-group animals were measured after 30 min post-injection time-point for three consecutive days. Behavioral testing included seven different parameters (moving time, total distance traveled, speed, rotation numbers, rearing numbers, rotation time, and rearing time). Speed (m/s) was calculated as distance traveled (m) divided by the corresponding moving time (s). Rotation numbers were calculated as the sum of clockwise and counterclockwise rotations. MCS included an internal noise/light/temperature insulation system and a 3D infrared beam frame that provided fast (100 Hz) and accurate animal movement (TSE ActiMot) combined with high-resolution video monitoring. The open-field arena was thoroughly cleaned and dried between each animal. A background noise (20 dB) was used to cancel out any unexpected laboratory sounds during experiments. The area under the curves (AUC) was calculated by the trapezoid method using GraphPad Prism V6 software (GraphPad Software Inc., La Jolla, CA, USA). Morphine treatment and behavioral measurements at different time-points are represented in a schematic diagram (Figure 6).
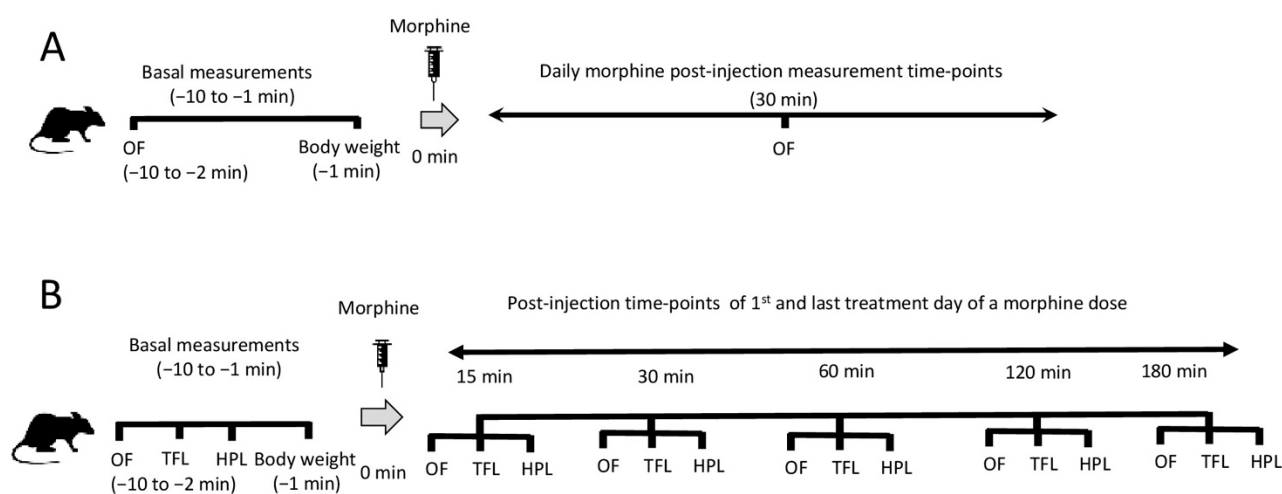
Figure 6. Schematic representation of the morphine treatment as well as behavioral and antinociception assessments used in the study. Animals were treated daily for baseline behavior (pre-) and 30 min post-administration of morphine (**A**), or pre- and post- (15, 30, 60, 120 and 180 min) administration of morphine on the first and the last treatment day of a morphine dose (**B**). The main assessment of motor behavior was calculated using data from open-field tests (OF). Antinociception was followed in order to validate the effect of morphine on the animals and be able to relate morphine's antinociceptive effect with the produced motor behaviors after repeated drug administrations. Antinociception assessment was performed using tail-flick (TFL) and hot-plate (HPL) tests.

4.4. Assessment of Antinociception

Nociceptive thresholds were measured by tail-flick and hot-plate assay using equipment purchased from Ugo Basile (Comerio, Italy. Animals were tested randomly to avoid any bias effects due to multiple repeated measurements. The maximum exposure to the nociceptive thermal stimulus was 15 s for the tail-flick (basal latency: 4.3 ± 0.2 s) and

30 s for the hot-plate assay (basal latency: 5.7 ± 0.3 s). The infrared intensity of the tail-flick photocell was set at 30, whereas the plate temperature of the hot-plate was set at $54 \pm 0.5\ ^\circ C$. The experimental settings for antinociceptive measurements used in this study were previously described [8,46–48]. Every rat was tested immediately prior to morphine administration as well as 15, 30, 60, and 120 min post-administration using both assays only on the first and the last treatment day (Figure 6). Measurements were conducted in a blinded manner, and the mean of three independent measurements for each time-point with a 1 min interval between measurements was recorded to minimize the operator's handling effects. The maximum possible effect (MPE) was defined as MPE % = $100 \times$ [(test latency–basal latency)/(cut-off time–basal latency)] as previously described [49]. The area under the curves (AUC) was calculated by the trapezoid method using GraphPad Prism V6 software (GraphPad Software Inc., La Jolla, CA, USA).

4.5. Statistical Analysis

The area under the curves (AUC) was calculated by the trapezoid method using GraphPad Prism V6 software (GraphPad Software Inc., La Jolla, CA, USA). Data are expressed as mean $\pm$ SEM and analyzed by one-way ANOVA with Dunnett's multiple comparisons test (for comparisons between three or more animal groups) or unpaired *t*-test (for comparisons between two groups of animals). Multiple comparisons (Dunnett's test) were employed when F achieved $p < 0.05$, and there was no significant variance in the homogeneity. A '*p*' value less than 0.05 was considered statistically significant.

References

1. CDC. Prescription Opioids: Side Effects. Centers for Disease Control and Prevention. Available online: https://www.cdc.gov/drugoverdose/opioids/prescribed.html (accessed on 29 December 2020).
2. TG. Principles of Nonsteroidal Anti-Inflammatory Drug Use for Musculoskeletal Conditions in Adults. In eTG Complete Melbourne: Therapeutic Guidelines Limited. Available online: https://tgldcdp.tg.org.au/index (accessed on 29 December 2020).
3. Azevedo Neto, J.; Costanzini, A.; De Giorgio, R.; Lambert, D.G.; Ruzza, C.; Calò, G. Biased versus Partial Agonism in the Search for Safer Opioid Analgesics. *Molecules* **2020**, *25*, 3870. [CrossRef]
4. Droney, J.M.; Gretton, S.K.; Sato, H.; Ross, J.R.; Branford, R.; Welsh, K.I.; Cookson, W.; Riley, J. Analgesia and central side-effects: Two separate dimensions of morphine response. *Br. J. Clin. Pharmacol.* **2013**, *75*, 1340–1350. [CrossRef]
5. Dominguez, J.E.; Habib, A.S. Prophylaxis and treatment of the side-effects of neuraxial morphine analgesia following cesarean delivery. *Curr. Opin. Anaesthesiol.* **2013**, *26*, 288–295. [CrossRef] [PubMed]

6. Girgin, N.K.; Gurbet, A.; Turker, G.; Aksu, H.; Gulhan, N. Intrathecal morphine in anesthesia for cesarean delivery: Dose-response relationship for combinations of low-dose intrathecal morphine and spinal bupivacaine. *J. Clin. Anesth.* **2008**, *20*, 180–185. [CrossRef] [PubMed]

7. Raffaeli, W.; Marconi, G.; Fanelli, G.; Taddei, S.; Borghi, G.B.; Casati, A. Opioid-related side-effects after intrathecal morphine: A prospective, randomized, double-blind dose-response study. *Eur. J. Anaesthesiol.* **2006**, *23*, 605–610. [CrossRef]

8. Paul, A.K.; Gueven, N.; Dietis, N. Morphine dosing strategy plays a key role in the generation and duration of the produced antinociceptive tolerance. *Neuropharmacology* **2017**, *121*, 158–166. [CrossRef] [PubMed]

9. Hollais, A.W.; Patti, C.L.; Zanin, K.A.; Fukushiro, D.F.; Berro, L.F.; Carvalho, R.C.; Kameda, S.R.; Frussa-Filho, R. Effects of acute and long-term typical or atypical neuroleptics on morphine-induced behavioural effects in mice. *Clin. Exp. Pharmacol. & physiology* **2014**, *41*, 255–263. [CrossRef]

10. Kahveci, N.; Gulec, G.; Ozluk, K. Effects of intracerebroventricularly-injected morphine on anxiety, memory retrieval and locomotor activity in rats: Involvement of vasopressinergic system and nitric oxide pathway. *Pharmacol. Biochem. Behav.* **2006**, *85*, 859–867. [CrossRef] [PubMed]

11. Belknap, J.K.; Riggan, J.; Cross, S.; Young, E.R.; Gallaher, E.J.; Crabbe, J.C. Genetic determinants of morphine activity and thermal responses in 15 inbred mouse strains. *Pharmacol. Biochem. Behav.* **1998**, *59*, 353–360. [CrossRef]

12. Rodriguez-Arias, M.; Broseta, I.; Aguilar, M.A.; Minarro, J. Lack of specific effects of selective D(1) and D(2) dopamine antagonists vs. risperidone on morphine-induced hyperactivity. *Pharmacol. Biochem. Behav.* **2000**, *66*, 189–197. [CrossRef]

13. Patti, C.L.; Frussa-Filho, R.; Silva, R.H.; Carvalho, R.C.; Kameda, S.R.; Takatsu-Coleman, A.L.; Cunha, J.L.; Abilio, V.C. Behavioral characterization of morphine effects on motor activity in mice. *Pharmacol. Biochem. Behav.* **2005**, *81*, 923–927. [CrossRef]

14. Babbini, M.; Davis, W.M. Time-dose relationships for locomotor activity effects of morphine after acute or repeated treatment. *Br. J. Pharmacol.* **1972**, *46*, 213–224. [CrossRef]

15. Paul, A.K.; Gueven, N.; Dietis, N. Age-dependent antinociception and behavioral inhibition by morphine. *Pharmacol. Biochem. Behav.* **2018**, *168*, 8–16. [CrossRef]

16. Paul, A.K.; Gueven, N.; Dietis, N. Data on prolonged morphine-induced antinociception and behavioral inhibition in older rats. *Data Brief.* **2018**, *19*, 183–188. [CrossRef]

17. Holtman, J.R., Jr.; Sloan, J.W.; Wala, E.P. Morphine tolerance in male and female rats. *Pharmacol. Biochem. Behav.* **2004**, *77*, 517–523. [CrossRef]

18. Zhan, B.; Ma, H.Y.; Wang, J.L.; Liu, C.B. Sex differences in morphine-induced behavioral sensitization and social behaviors in ICR mice. *Zool. Res.* **2015**, *36*, 103–108.

19. Barros, H.M.; Tannhauser, S.L.; Tannhauser, M.A.; Tannhauser, M. The effects of GABAergic drugs on grooming behaviour in the open field. *Pharmacol. Toxicol.* **1994**, *74*, 339–344. [CrossRef] [PubMed]

20. Rex, A.; Voigt, J.P.; Voits, M.; Fink, H. Pharmacological evaluation of a modified open-field test sensitive to anxiolytic drugs. *Pharmacol. Biochem. Behav.* **1998**, *59*, 677–683. [CrossRef]

21. Costall, B.; Fortune, D.H.; Naylor, R.J. Biphasic changes in motor behaviour following morphine injection into the nucleus accumbens [proceedings]. *Br. J. Pharmacol.* **1976**, *57*, 423.

22. Bounes, V.; Charriton-Dadone, B.; Levraut, J.; Delangue, C.; Carpentier, F.; Mary-Chalon, S.; Houze-Cerfon, V.; Sommet, A.; Houze-Cerfon, C.H.; Ganetsky, M. Predicting morphine related side effects in the ED: An international cohort study. *Am. J. Emerg. Med.* **2017**, *35*, 531–535. [CrossRef]

23. Riley, J.L., 3rd; Hastie, B.A.; Glover, T.L.; Fillingim, R.B.; Staud, R.; Campbell, C.M. Cognitive-affective and somatic side effects of morphine and pentazocine: Side-effect profiles in healthy adults. *Pain Med.* **2010**, *11*, 195–206. [CrossRef] [PubMed]

24. Wilkinson, V.E.; Jackson, M.L.; Westlake, J.; Stevens, B.; Barnes, M.; Swann, P.; Rajaratnam, S.M.; Howard, M.E. The accuracy of eyelid movement parameters for drowsiness detection. *J. Clin. Sleep Med.* **2013**, *9*, 1315–1324. [CrossRef] [PubMed]

25. Iwai, S.; Kiguchi, N.; Kobayashi, Y.; Fukazawa, Y.; Saika, F.; Ueno, K.; Yamamoto, C.; Kishioka, S. Inhibition of morphine tolerance is mediated by painful stimuli via central mechanisms. *Drug Discov. Ther.* **2012**, *6*, 31–37. [CrossRef] [PubMed]

26. Domino, E.F.; Vasko, M.R.; Wilson, A.E. Mixed depressant and stimulant actions of morphine and their relationship to brain acetylcholine. *Life Sci.* **1976**, *18*, 361–376. [CrossRef]

27. Brady, L.S.; Holtzman, S.G. Locomotor activity in morphine-dependent and post-dependent rats. *Pharmacol. Biochem. Behav.* **1981**, *14*, 361–370. [CrossRef]

28. Tulunay, F.C.; Ayhan, I.H.; Sparber, S.B. The effects of morphine and delta-9-tetrahydrocannabinol on motor activity in rats. *Psychopharmacology* **1982**, *78*, 358–360. [CrossRef] [PubMed]

29. Vander Weele, C.M.; Porter-Stransky, K.A.; Mabrouk, O.S.; Lovic, V.; Singer, B.F.; Kennedy, R.T.; Aragona, B.J. Rapid dopamine transmission within the nucleus accumbens: Dramatic difference between morphine and oxycodone delivery. *Eur. J. Neurosci.* **2014**, *40*, 3041–3054. [CrossRef]

30. Di Chiara, G.; Imperato, A. Opposite effects of mu and kappa opiate agonists on dopamine release in the nucleus accumbens and in the dorsal caudate of freely moving rats. *J. Pharmacol. Exp. Ther.* **1988**, *244*, 1067–1080.

31. Murphy, N.P.; Lam, H.A.; Maidment, N.T. A comparison of morphine-induced locomotor activity and mesolimbic dopamine release in C57BL6, 129Sv and DBA2 mice. *J. Neurochem.* **2001**, *79*, 626–635. [CrossRef]

32. Barber, D.L.; Blackburn, T.P.; Greenwood, D.T. An automatic apparatus for recording rotational behaviour in rats with brain lesions. *Physiol. Behav.* **1973**, *11*, 117–120. [CrossRef]

33. Christie, J.E.; Crow, T.J. Turning behaviour as an index of the action of amphetamines and ephedrines on central dopamine-containing neurones. *Br. J. Pharmacol.* **1971**, *43*, 658–667. [CrossRef]

34. Pycock, C.J. Turning behaviour in animals. *Neuroscience* **1980**, *5*, 461–514. [CrossRef]

35. Blundell, C.; Crossman, A.R.; Slater, P. The effect of morphine on turning behaviour in rats and mice with unilateral 6-hydroxydopamine lesions [proceedings]. *Br. J. Pharmacol.* **1976**, *57*, 456p.

36. Jacquet, Y.F.; Carol, M.; Russell, I.S. Morphine-induced rotation in naive, nonlesioned rats. *Science* **1976**, *192*, 261–263. [CrossRef]

37. Lever, C.; Burton, S.; O'Keefe, J. Rearing on hind legs, environmental novelty, and the hippocampal formation. *Rev. Neurosci.* **2006**, *17*, 111–133. [CrossRef] [PubMed]

38. Rodriguiz, R.M.; Wetsel, W.C. Frontiers in Neuroscience Assessments of Cognitive Deficits in Mutant Mice. In *Animal Models of Cognitive Impairment*; Levin, E.D., Buccafusco, J.J., Eds.; CRC Press/Taylor & Francis, Taylor & Francis Group, LLC.: Boca Raton, FL, USA, 2006.

39. Van Lier, H.; Drinkenburg, W.H.; van Eeten, Y.J.; Coenen, A.M. Effects of diazepam and zolpidem on EEG beta frequencies are behavior-specific in rats. *Neuropharmacology* **2004**, *47*, 163–174. [CrossRef]

40. Alves, R.; Carvalho, J.G.B.d.; Venditti, M.A.C. High-and Low-Rearing Rats Differ in the Brain Excitability Controlled by the Allosteric Benzodiazepine Site in the GABA A Receptor. *J. Behav. Brain Sci.* **2012**, *2*, 315–325. [CrossRef]

41. Walsh, R.N.; Cummins, R.A. The Open-Field Test: A critical review. *Psychol. Bull.* **1976**, *83*, 482–504. [CrossRef]

42. Kuzmin, A.; Sandin, J.; Terenius, L.; Ogren, S.O. Dose- and time-dependent bimodal effects of kappa-opioid agonists on locomotor activity in mice. *J. Pharmacol. Exp. Ther.* **2000**, *295*, 1031–1042. [PubMed]

43. Kilkenny, C.; Browne, W.J.; Cuthill, I.C.; Emerson, M.; Altman, D.G. Improving bioscience research reporting: The ARRIVE guidelines for reporting animal research. *PLoS Biol.* **2010**, *8*, e1000412. [CrossRef]

44. NHMRC. *Australian Code for the Care and Use of Animals for Scientific Purposes*, 8th ed.; National Health and Medical Research Council: Canberra, Australia, 2013.

45. Festing, M.F.; Altman, D.G. Guidelines for the design and statistical analysis of experiments using laboratory animals. *ILAR J.* **2002**, *43*, 244–258. [CrossRef]

46. Heilborn, U.; Rost, B.R.; Arborelius, L.; Brodin, E. Arthritis-induced increase in cholecystokinin release in the rat anterior cingulate cortex is reversed by diclofenac. *Brain Res.* **2007**, *1136*, 51–58. [CrossRef] [PubMed]

47. Duan, B.; Cheng, L.; Bourane, S.; Britz, O.; Padilla, C.; Garcia-Campmany, L.; Krashes, M.; Knowlton, W.; Velasquez, T.; Ren, X.; et al. Identification of spinal circuits transmitting and gating mechanical pain. *Cell* **2014**, *159*, 1417–1432. [CrossRef]

48. Khroyan, T.V.; Polgar, W.E.; Cami-Kobeci, G.; Husbands, S.M.; Zaveri, N.T.; Toll, L. The first universal opioid ligand, (2S)-2-[(5R,6R,7R,14S)-N-cyclopropylmethyl-4,5-epoxy-6,14-ethano-3-hydroxy-6-meth oxymorphinan-7-yl]-3,3-dimethylpentan-2-ol (BU08028): Characterization of the in vitro profile and in vivo behavioral effects in mouse models of acute pain and cocaine-induced reward. *J. Pharmacol. Exp. Ther.* **2011**, *336*, 952–961. [CrossRef] [PubMed]

49. Harris, L.S.; Pierson, A.K. Some narcotic antagonists in the benzomorphan series. *J. Pharmacol. Exp. Ther.* **1964**, *143*, 141–148. [PubMed]

Antipruritic Effect of Nalbuphine, a Kappa Opioid Receptor Agonist, in Mice: A Pan Antipruritic

Saadet Inan [1,*], Nae J. Dun [2] and Alan Cowan [1,2,†]

[1] Department of Neural Sciences, Center for Substance Abuse Research, Lewis Katz School of Medicine at Temple University, Philadelphia, PA 19104, USA

[2] Department of Pharmacology, Lewis Katz of Medicine at Temple University, Philadelphia, PA 19104, USA; ndun@temple.edu

* Correspondence: sinan@temple.edu

† This author has passed away.

Abstract: Antipruritic effects of kappa opioid receptor (KOR) agonists have been shown in rodent models of acute and chronic scratching (itchlike behavior). Three KOR agonists, nalfurafine, difelikefalin, and nalbuphine, are in clinical studies for antipruritic effects in chronic itch of systemic and skin diseases. Nalfurafine (in Japan) and difelikefalin (in the USA) were approved to be used in the treatment of chronic itch in hemodialysis patients. The FDA-approved nalbuphine has been used in clinic for over 40 years, and it is the only narcotic agonist that is not scheduled. We aimed to study (a) antiscratch activity of nalbuphine against TAT-HIV-1 protein (controls HIV transcription)-, deoxycholic acid (DCA, bile acid)-, and chloroquine (CQ)-induced scratching in a mouse model of acute itch; and (b) whether the effect of nalbuphine is produced via KORs. First, dose–responses were developed for pruritogens. Mice were pretreated with nalbuphine (0.3–10 mg/kg) and then a submaximal dose of pruritogens were administered and the number of scratching bouts was counted. To study if the antiscratch effect of nalbuphine is produced via KOR, we used KOR knock out mice and pharmacologic inhibition of KORs using nor-binaltorphimine, a KOR antagonist. For this aim, we used CQ as a pruritogen. We found that: (a) TAT-HIV-1 protein elicits scratching in a dose-dependent manner; (b) nalbuphine inhibits scratching induced by TAT-HIV-1, DCA, and CQ dose-dependently; and (c) nalbuphine inhibits scratching induced by CQ through KORs. In conclusion, nalbuphine inhibits scratching elicited by multiple pruritogens.

Keywords: nalbuphine; kappa opioid receptor agonist; pruritis; scratching; mice; TAT-HIV; cholestasis; chloroquine; deoxycholic acid

1. Introduction

As of today, three kappa opioid receptor (KOR) agonists, nalfurafine (TRK-820, Remich®), difelikefalin (CR845, Korsuva™), and nalbuphine (Haduvio™, KOR agonist and a weak mu opioid receptor partial agonist) (Figure 1) are in clinical studies for treating chronic itch of chronic kidney disease, cholestatic liver disease, and atopic dermatitis [1–4]. Further, nalfurafine was approved in Japan and recently, difelikefalin was approved by the FDA in the USA (https://korsuva.com) (accessed on 2 September 2021) for the treatment of chronic itch in hemodialysis patients. Evidence for the involvement of KORs and for the antipruritic activity of KOR agonists go back to early 1980s. Gmerek and Cowan [5] introduced a rat model that allowed quantitative measurements of scratching (itch like behavior) by intracerebroventricular administration of bombesin, a tetradecapeptide originally isolated from frog skin and a homolog of mammalian gastrin-releasing factor (GRP). Bombesin induced excessive grooming and scratching of the face, head, and neck with the hindpaws in a dose-dependent manner [5]. Later, GRP was identified as one of the mediators for itch transmission at the spinal cord level [6,7]. For the first time, Gmerek and Cowan reported that systemic administration of early benzomorphan KOR agonists

(e.g, bremazocine, cyclazocine, ketocyclazocine and pentazocine) significantly reduced bombesin-induced grooming and scratching in rats in a dose-dependent manner in 1984 [8]. Another early piece of evidence was the observation of excessive scratching in monkeys during withdrawal from chronic administration of the KOR agonist U50,488 [9]. Recently, it was shown that B5-I inhibitory neurons express Dynorphin, an endogenous KOR agonist, and inhibit itch sensation at the spinal level [10,11].
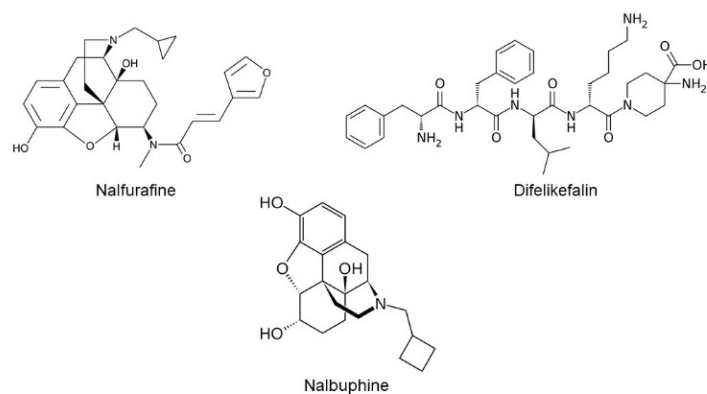
Figure 1. Chemical structures of nalfurafine, difelikefalin, and nalbuphine.

Our interest was predominantly in nalbuphine, an FDA-approved analgesic that has been known over 40 years. It is the only narcotic agonist currently unscheduled. Based on GTPgS binding assays, nalbuphine was described as a full agonist on kappa opioid receptors and a weak partial agonist on mu opioid receptors. Nalbuphine both stimulated [35S] GTPgS binding mediated by the mu opioid receptor and inhibited DAMGO-stimulated [35S] GTPgS binding in cultured cells [12–14]. The results of the earliest preclinical and clinical studies suggest that nalbuphine is a highly effective analgesic with minimal respiratory depression, inhibition of gastrointestinal transit, analgesic tolerance, physical dependence, and psychotomimetic potential (dysphoria only at doses beyond the therapeutic range) [15]. Hawi et al. [16] showed antiscratch activity of nalbuphine in mice against Substance-P-induced acute scratching. We reported that acute systemic administration of nalbuphine also significantly reduced scratching in mice with chronic contact dermatitis [17]. Chronic itch is a very unpleasant symptom of skin and systemic diseases such as chronic kidney disease, cholestatic liver disease, some cancers, hematologic diseases, psychiatric diseases, and neuropathies, or is idiopathic with no reason. One third of the dermatology patients have chronic itch [18] and, overall, nearly 15% of the general population have this symptom [19,20]. The quality of life of patients with chronic itch is affected seriously. Patients can suffer from sleep deprivation, agitation, depression, suicidal thoughts, and difficulty concentrating [21,22]. Chronic itch is also reported in HIV-infected patients with or without skin conditions [23,24]. Chronic itch could be related common forms of dermatosis, such as seborrheic dermatitis, psoriasis, prurigo nodularis, as well as HIV-associated pruritic popular eruptions, and eosinophilic folliculitis. TAT-HIV-1, a viral protein that controls HIV-transcription, plays an important role in the development of HIV-1 infection as well as in the pathogenesis of complications such as dementia, cardiovascular diseases, and retinal diseases. For example, it was shown that exposure of TAT-HIV-1 induces cytotoxic effects in human brain microvascular endothelial cells [25] and causes apoptotic cell death in retinal pigment epithelial cells [26]. We aimed to study whether nalbuphine would be effective against scratching in mouse models of HIV and cholestasis, as well as chloroquine (CQ)-induced scratching. We first studied whether behind the neck injection of TAT-HIV-1 protein would elicit scratching in mice. We used previously shown induction of scratching by behind the neck injection of a bile acid, deoxycholic acid to study cholestasis [27,28]. We had shown previously that nalfurafine inhibits scratching induced by CQ [29], so lastly, we studied whether nalbuphine, like nalfurafine, would inhibit scratching in mice. We also studied whether antiscratch activity of nalbuphine is produced through KORs in

mice injected with CQ. The results of these studies will be beneficial for treatment of HIV- and cholestasis-related chronic itch, as well as itch due to CQ for treatment for malaria in susceptible individuals [30].

2. Results

2.1. TAT-HIV-1 Induces Scratching and Nalbuphine Inhibits Scratching in a Dose-Dependent Manner

As seen in Figure 2a, behind the neck (s.c.) administration of TAT-HIV-1 elicited scratching dose-dependently in mice. TAT-HIV-1 at 0.3 and 1 mg/kg doses induced scratching behavior significantly compared to saline (one-way ANOVA followed by Dunnett's multiple comparison, *** $p < 0.001$, **** $p < 0.0001$). At 1 mg/kg, 124 ± 6 scratching bouts was observed in 30 min. Next, we pretreated (-30 min) mice with either saline or nalbuphine (0.3–10 mg/kg, s.c.) and then a submaximum dose (0.3 mg/kg) of TAT-HIV-1 was injected the nape of the mice. Nalbuphine alleviated TAT-HIV-1-induced scratching in a dose-dependent manner (Figure 2b). Nalbuphine at 3 and 10 mg/kg inhibited scratching significantly compared to control (* $p < 0.05$, ** $p < 0.01$). As seen in Figure 2c, nalbuphine at 10 mg/kg also significantly inhibited scratching elicited by the maximum dose of TAT-HIV-1 (1 mg/kg) (**** $p < 0.0001$).

(**a**)

(**b**)

Figure 2. *Cont.*

(**c**)
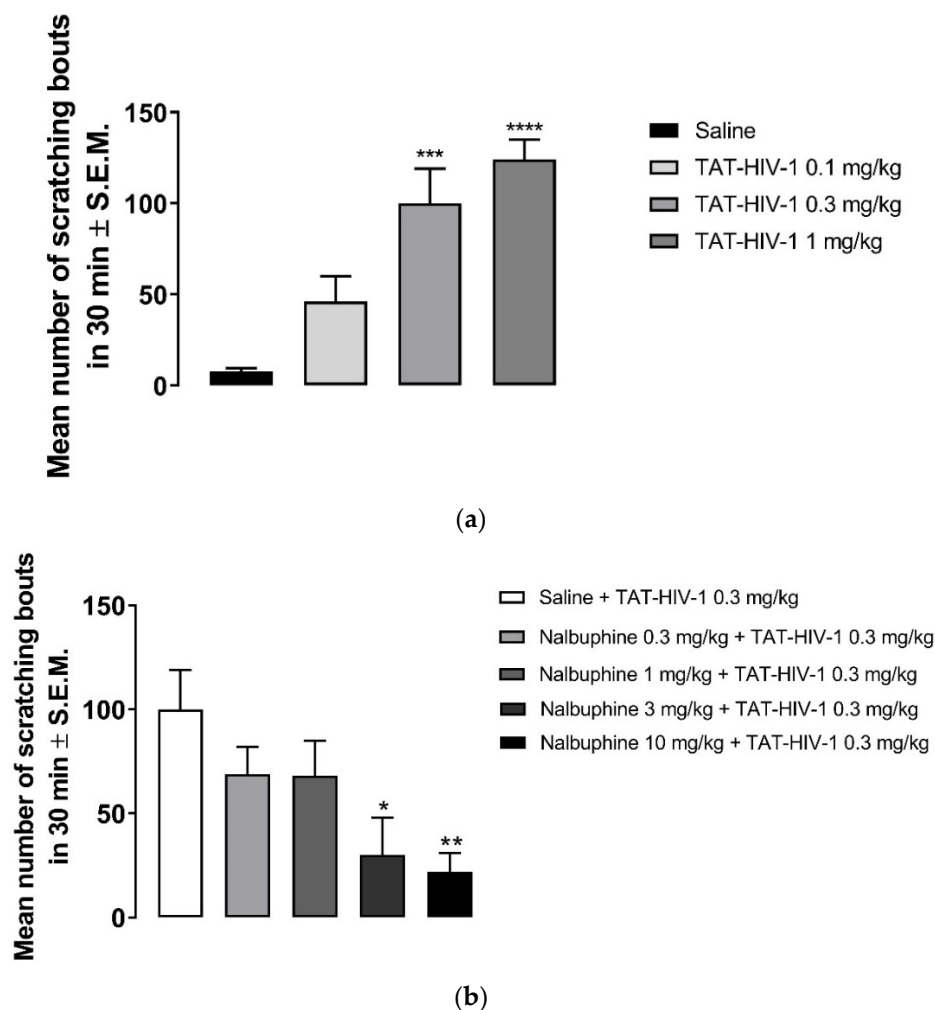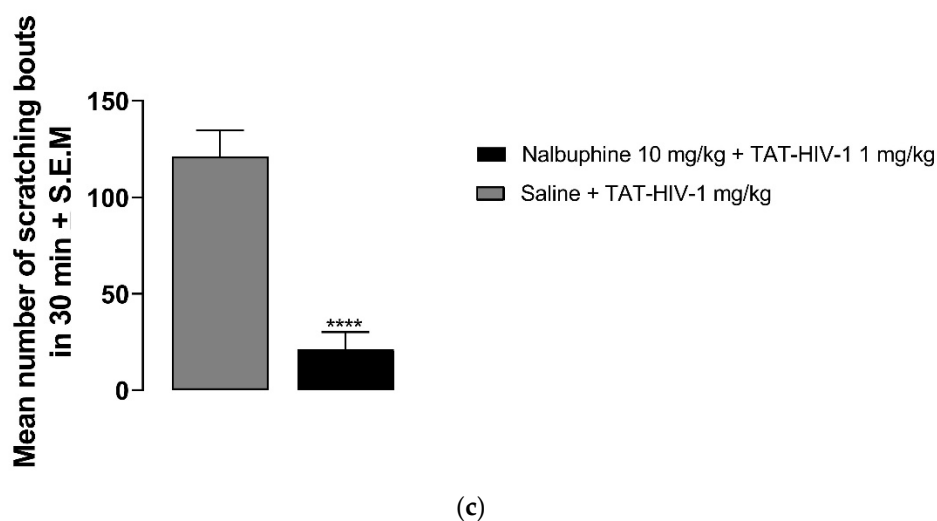
Figure 2. Subcutaneous behind the neck injection of TAT-HIV-1 induces scratching in a dose-dependent manner. (**a**) Mice were administered saline (s.c., flank area) and then 30 min later they were injected with either saline or TAT-HIV-1 (0.1–1 mg/kg, behind the neck). One min following injections, the number of scratching bouts was counted for 30 min. Both TAT-HIV-1 at 0.3 and 1 mg/kg elicited scratching significantly compared to saline (one-way ANOVA followed by Dunnett's multiple comparison; *** $p < 0.001$, **** $p < 0.0001$; n = 6). Nalbuphine inhibits TAT-HIV-1-induced scratching in a dose-dependent manner; (**b**) Nalbuphine at 3 and 10 mg/kg doses inhibited scratching elicited by submaximal dose of TAT-HIV-1 (0.3 mg/kg) significantly compared to control (one-way ANOVA followed by Dunnett's multiple comparison; * $p < 0.05$, ** $p < 0.01$; n = 6). Nalbuphine at 10 mg/kg also alleviated scratching induced by maximum dose of TAT-HIV-1 (1 mg/kg); (**c**) (unpaired Student's *t*-test; **** $p < 0.0001$; n = 6). Swiss–Webster mice were used for these studies.

2.2. Nalbuphine Inhibits Deoxycholic Acid-Induced Scratching

Deoxycholic acid in doses of 0.3–10 mg/kg induced scratching (Figure 3a). While the number of scratching bouts was 47.5 ± 11 at 0.3 mg/kg, 144 ± 40 scratching bouts was observed at 10 mg/kg dose of DCA. Nalbuphine at 10 mg/kg was administered 30 min before DCA 3 mg/kg to test whether nalbuphine also inhibits DCA-induced scratching. As seen in Figure 3b, nalbuphine significantly reduced scratching bouts induced by DCA (Unpaired Student's *t*-test; ** $p < 0.01$).

(**a**)

Figure 3. *Cont.*

(**b**)
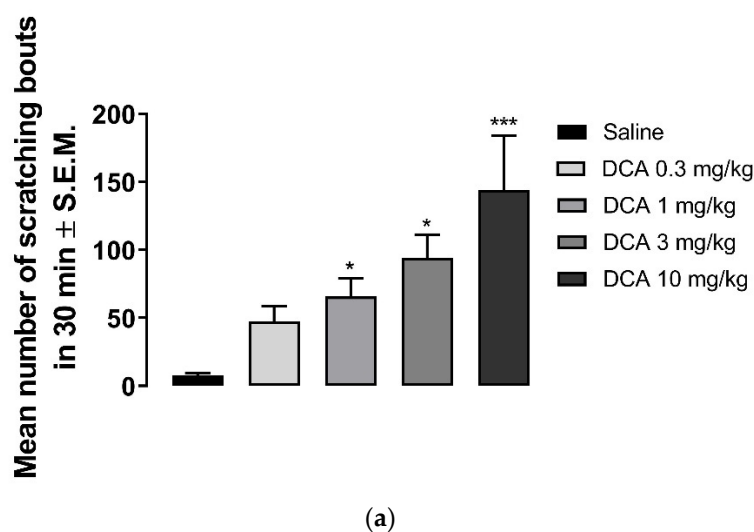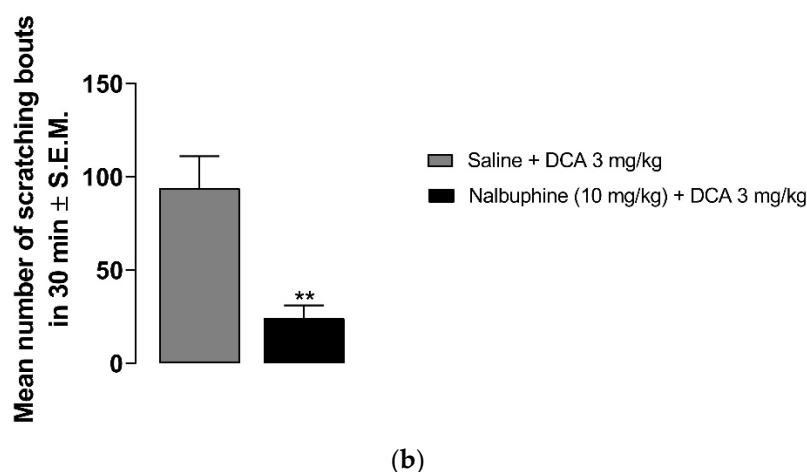
Figure 3. Nalbuphine inhibits DCA-induced scratching. DCA at 1, 3, and 10 mg/kg induces significant scratching compared to saline. (**a**) (one-way ANOVA followed by Dunnett's multiple comparison; * $p < 0.05$, *** $p < 0.001$; n = 7–8). Pretreatment with nalbuphine 10 mg/kg significantly reduces the number of scratching bouts in 30 min; (**b**) (unpaired Student's *t*-test; ** $p < 0.01$); n = 6). Swiss–Webster mice were used for these studies.

2.3. Nalbuphine Inhibits CQ-Induced Scratching through KOR

Nalbuphine (1–10 mg/kg) significantly inhibited scratching bouts induced by submaximal dose of CQ, as seen in Figure 4a (* $p < 0.05$, *** $p < 0.001$). Next, we studied whether the antipruritic effects of nalbuphine function via through KORs. WT C57BL/6J mice did not respond to nalbuphine 10 mg/kg in the same manner as did Swiss–Webster mice. As seen in Figure 4b, nalbuphine at 10 mg/kg did not significantly reduced the number of scratching bouts induced by CQ. Then, we tried nalbuphine at 20 mg/kg in C57BL/6J mice. The animals moved freely and did not show behavioral depression against a higher dose of nalbuphine. A significant decrease in scratching was observed with nalbuphine on WT mice. However, nalbuphine did not have any effect on KOR KO mice. The pharmacological inhibition of KORs using nor-BNI also showed similar results. In Swiss–Webster mice pretreated with nor-BNI, nalbuphine did not inhibit CQ-induced scratching (Figure 4c).

(**a**)

Figure 4. *Cont.*

(**b**)

(**c**)
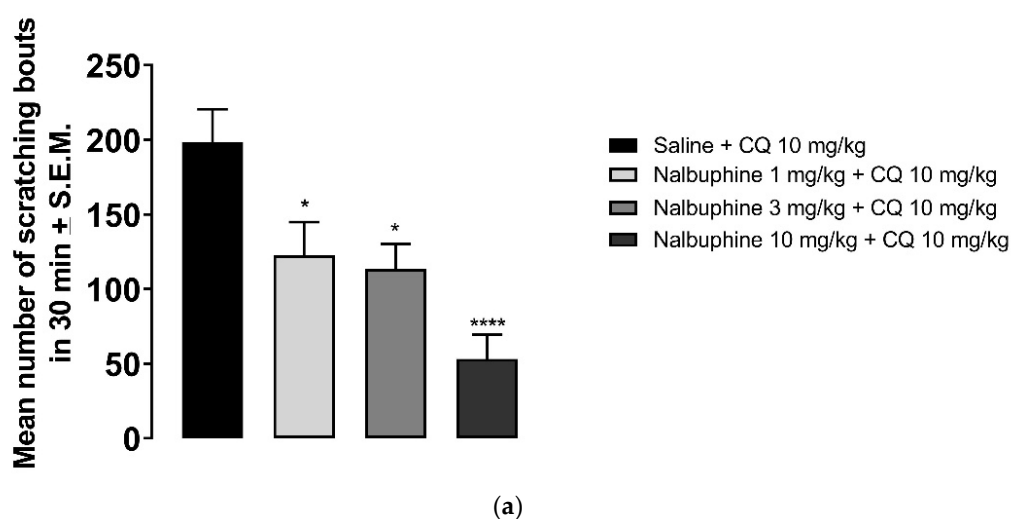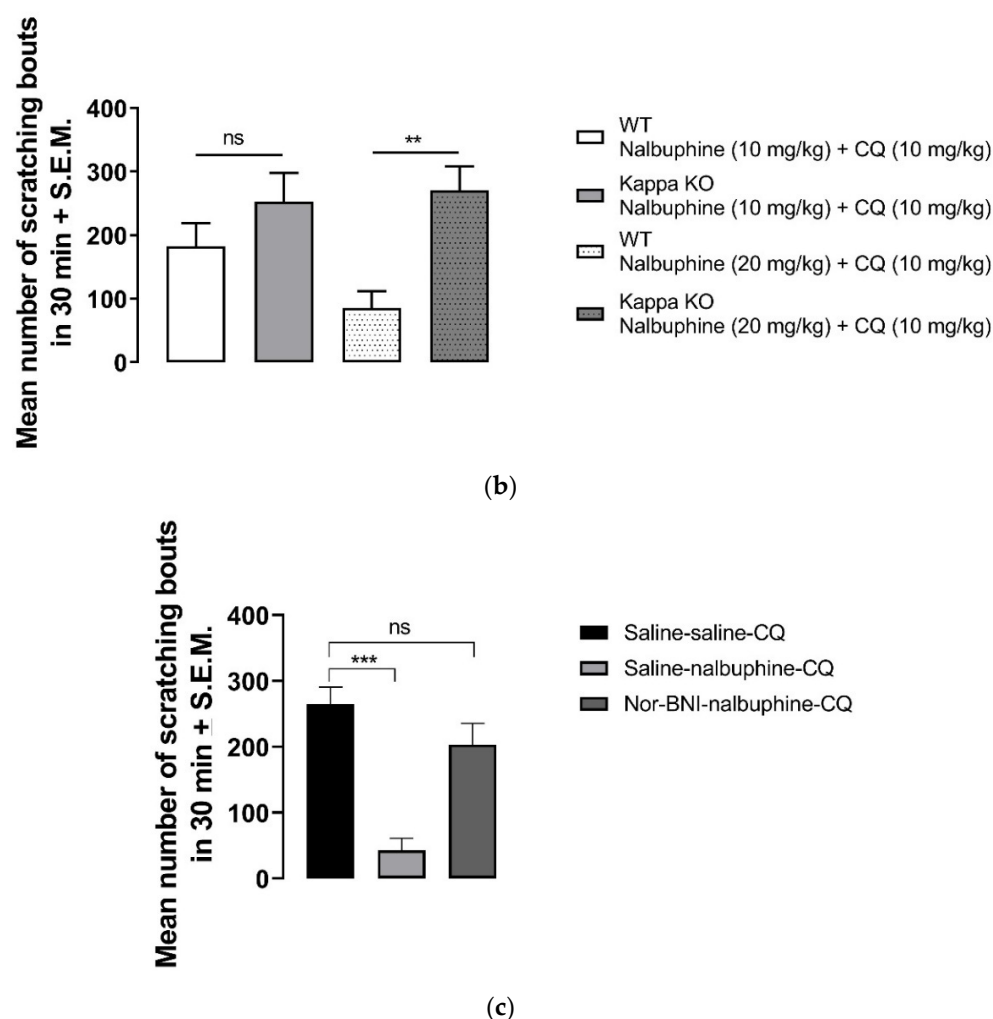
Figure 4. Nalbuphine significantly reduced CQ-induced scratching bouts in a dose-dependent manner. (**a**) Swiss–Webster mice were injected with either saline or nalbuphine (1, 3, or 10 mg/kg). Thirty min later, they were administered a submaximal dose (10 mg/kg, s.c., behind the neck) of CQ. Then, the number of scratching bouts was counted for 30 min. Nalbuphine did not decrease scratching in KOR KO mice; (**b**) Nalbuphine at 10 mg/kg did not have significant effect in C57BL/6J WT mice as in Swiss–Webster. Nalbuphine at 20 mg/kg significantly reduced scratching induced by CQ in WT mice, but not in KOR KO mice. Nalbuphine had no antiscratch effect in Swiss–Webster mice pretreated with nor-BNI; (**c**) Mice were administered with nor-BNI or saline 20 h before the nalbuphine injection. Then, mice received either saline or nalbuphine. Thirty min later, they were injected with CQ. Nalbuphine significantly reduced scratching in mice pretreated with saline the day before; however, no significant effect was observed in mice pretreated with nor-BNI. (one-way ANOVA followed by Dunnett's multiple comparison; * $p < 0.05$, ** $p < 0.01$, *** $p < 0.001$, **** $p < 0.0001$; n = 7–8).

3. Discussion

The results of these studies clearly indicate that nalbuphine, a kappa opioid receptor agonist, alleviate scratching bouts elicited by chemically different pruritogens, TAT-HIV-1 protein, DCA, and chloroquine. Additionally, we have shown that antiscratch effect of nalbuphine in CQ-induced scratching operates via KORs. Here, for the first time we report that TAT-HIV-1 protein induces scratching behavior in mice in a dose-dependent manner when it is given s.c. behind the neck. As expected, DCA also elicited scratching in our study in mice, as previously reported [27,28]. Nalbuphine inhibited scratching induced by CQ as well.

As seen in Figure 2a, the TAT-HIV-1 protein elicited scratching behavior dose-dependently. The highest dose (1 mg/kg) that we used caused average of 124 ± 6 scratching bouts in 30 min. Pretreating mice with nalbuphine (10 mg/kg) significantly reduced scratching to an average of 20 ± 7 (Figure 2b). Previously, it was reported that U50,488, a KOR agonist, inhibited HIV-1 expression in human microglia and macrophages [31,32]. Additionally, neurotoxicity-induced by HIV-1 was suppressed by U50, 488 in human microglia cell culture [32]. In the same study, the authors additionally reported that neuroprotective effect of U50,488 was through KORs. In another study, inhibition of TAT-HIV-1-induced production of chemokine, chemoattractant protein-1 in human astrocytes by U50,488 was reported via KORs since nor-BNI blocked the effect of U50,488 [33]. Skin diseases can develop in almost 90% of HIV-positive patients [24,34,35]. Prevalence of chronic pruritus in HIV-positive patients has been reported as 31% from a study conducted in Spain [36] and 45% from a study conducted in southeastern United States [37]. In the later study, itch was found to have a significant negative impact on quality of patient life. In a study including over 4000 HIV patients, it was shown that African Americans are at a higher risk of developing pruritic skin conditions compared to race-matched controls and white patients [38]. TAT-HIV-1 protein might be a contributing factor in the pathogenesis of chronic itch in HIV-positive patients. HIV-infected patients can be targeted with the antipruritic effect of nalbuphine in clinical studies.

As expected, the behind the neck injection of DCA induced scratching beginning at 1 mg/kg in a dose-dependent manner (Figure 3a). Nalbuphine 10 mg/kg was studied against one dose of DCA (3 mg/kg) and it was found that nalbuphine significantly reduced DCA-induced scratching bouts, as shown in Figure 3b. Pathogenesis of chronic pruritus of cholestasis is still elusive. It was reported that multiple mediators contribute in the same way as bile acids (by activating TGR5 receptors), endogenous opioid peptides, activation of autotoxin [39,40]. Still, there is no effective treatment against pruritus of cholestasis; however, promising clinical studies with KOR agonists are being developed (https://www.caratherapeutics.com/our-pipeline/; https://www.trevitherapeutics.com/pipeline/ (accessed on 10 August 2021)). Golpanian et al. [41] reported that butorphanol, a partial KOR agonist and mu opioid receptor antagonist, significantly reduced itch severity in five out of eight patients. We have previously reported that nalfurafine inhibits scratching in rats with cholestasis induced by chronic ethylene estradiol injections [42]. In a recently developed mice model of cholestasis (partial ligation of bile duct), authors reported that naloxone, U50,488, and clonidine (an α2-adrenoceptor agonist) significantly reduced scratching [43].

CQ has been shown to cause scratching in both humans and in rodents. CQ induce itch in healthy volunteers [44] and in patients during the treatment of malaria [45]. CQ elicits scratching behavior in rats [46] and in mice [29,47]. It was shown that CQ binds to Mas-related G-protein coupled receptor (Mrgprs) A3/X1 [48]. Multiple mediators and receptors are also involved in CQ-induced itch and are accepted as non-histaminergic itch [30]. Previously, we reported that CQ elicited-scratching was significantly reduced by pretreatment with nalfurafine in mice [29]. Munanairi et al. [49] reported that KOR and GRPR overlap at the spinal cord and activation of KOR inhibits GRPR-mediated itch in mice. Here, we showed that nalbuphine also inhibits CQ-induced scratching and antiscratch activity of nalbuphine is through KORs in mice.

In conclusion, nalbuphine is effective to reduce the itch like behavior induced by the TAT-HIV-1 protein (a protein is responsible for transcription of viruses and infection), DCA (one of the mediators responsible for cholestatic pruritus), and CQ in mice model acute itch. Since all these three conditions cause clinical itch in humans, we suggest that nalbuphine, a drug that has been in clinical use for over 40 years and is not a scheduled agent, will be effective for treating chronic itch in humans. Nalbuphine is already in clinical studies for cholestasis, but a clinical trial for chronic itch in HIV patients could be added.

4. Materials and Methods

4.1. Animals

Male Swiss–Webster mice (Taconic Biosciences, Germantown, NY, USA) and male C57BL/6J WT and KOR KO mice (007558-B6.129S2-Oprk1tm1Kff/J, Jackson Laboratories, Bar Harbor, ME, USA) weighing 25–30 g were used. WT and KOR KO mice were generated by homozygous breeding. Animals were housed in a temperature- and humidity-controlled environment with a 12-hr light–dark cycle. They were supplied with food and water ad libitum. Before any procedure was initiated, the mice were acclimated for a week in the animal facility. Behavioral testing was performed between 11:00 A.M. and 5:00 P.M. All animal care and experimental procedures were approved by the Institutional Animal Care and Use Committee of Temple University (protocol number 5021), conducted according to the NIH Guide for the Care and Use of Laboratory Animals. Between 6 and 8 animals/group were used for experiments.

4.2. Observation of Scratching Behavior

Acute scratching mouse model of itch described previously by Kuraishi et al. [50] was used. Mice were acclimated individually in rectangular observation boxes for at least an h before any injection or observation. Following acclimation, mice were injected s.c. in the area behind the neck with either saline or TAT-HIV-1 (0.1–1 mg/kg), deoxycholic acid (DCA, 0.3–10 mg/kg) to examine and develop dose–responses. One min after the injections, mice were observed for 30 min and the number of hindleg scratches directed to the back of the neck was counted by an observer. Since we have previously reported dose–response for CQ, we only used a submaximal dose (10 mg/kg) of CQ for the studies. To study whether nalbuphine would inhibit scratching induced by TAT-HIV, DCA, or CQ, mice were pretreated with nalbuphine (0.3–10 mg/kg, s.c.) at −30 min. Then, they were administered a fixed dose (submaximal dose) of pruritogen behind the neck area and they were observed, and scratching bouts were counted.

To study whether nalbuphine alleviates scratching acting on KORs, both genetic and pharmacologic approach was used to eliminate KORs. For the genetic approach, KOR knock out (KO) and wildtype (WT) littermates of C57BL/6J mice were used. CQ was chosen as pruritogen for this aim. Nalbuphine at 10 mg/kg, which significantly reduces scratching in Swiss–Webster, mice did not inhibit scratching induced by CQ in C57BL/6J mice. Then, we tried nalbuphine at 20 mg/kg, and we did not observe any behavioral depression following administration. Mice were injected with nalbuphine or saline and 30 min later they were administered CQ behind the neck and the number of scratches was counted for 30 min. For pharmacologic approach, Swiss–Webster mice were pretreated with either saline or norbinaltorphimine (nor-BNI, 20 mg/kg, intraperitoneally) at −20 h. The next day, mice were administered either saline or a fixed dose of nalbuphine (10 mg/kg). Thirty min later, saline or CQ was injected behind the neck of the mice. One min following injection, the scratching bouts were counted for 30 min.

4.3. Chemicals

Nalbuphine HCl, deoxycholic acid, and chloroquine were purchased from Sigma-Aldrich (St. Louis, MO, USA) and dissolved in saline. TAT-HIV-1 (32–62) was a generous gift from Phoenix Pharmaceuticals (Burlingame, CA, USA) and dissolved in saline. Compounds were administered as 0.1 mL/10 g body weight.

References

1. Fishbane, S.; Jamal, A.; Munera, C.; Wen, W.; Menzaghi, F. A phase 3 trial of difelikefalin in hemodialysis patients with pruritus. *N. Engl. J. Med.* **2020**, *382*, 222–232. [CrossRef]
2. Kamimura, K.; Yokoo, T.; Kamimura, H.; Sakamaki, A.; Abe, S.; Tsuchiya, A.; Takamura, M.; Kawai, H.; Yamagiwa, S.; Terai, S. Long-term efficacy and safety of nalfurafine hydrochloride on pruritus in chronic liver disease patients: Patient-reported outcome based analyses. *PLoS ONE* **2017**, *12*, e0178991. [CrossRef]
3. Ueno, Y.; Mori, A.; Yanagita, T. One year long-term study on abuse liability of nalfurafine in hemodialysis patients. *Int. J. Clin. Pharmacol. Ther.* **2013**, *51*, 823–831. [CrossRef]
4. Yagi, M.; Tanaka, A.; Namisaki, T.; Takahashi, A.; Abe, M.; Honda, A.; Matsuzaki, Y.; Ohira, H.; Yoshiji, H.; Takikawa, H. Is patient-reported outcome improved by nalfurafine hydrochloride in patients with primary biliary cholangitis and refractory pruritus? A post-marketing, single-arm, prospective study. *J. Gastroenterol.* **2018**, *53*, 1151–1158. [CrossRef]
5. Gmerek, D.E.; Cowan, A. An animal model for preclinical screening of systemic antipruritic agents. *J. Pharmacol. Methods* **1983**, *10*, 107–112. [CrossRef]
6. Sun, Y.G.; Chen, Z.F. A gastrin-releasing peptide receptor mediates the itch sensation in the spinal cord. *Nature* **2007**, *448*, 700–703. [CrossRef]
7. Fleming, M.S.; Ramos, D.; Han, S.B.; Zhao, J.; Son, Y.J.; Luo, W. The majority of dorsal spinal cord gastrin releasing peptide is synthesized locally whereas neuromedin B is highly expressed in pain- and itch-sensing somatosensory neurons. *Mol. Pain* **2012**, *8*, 52. [CrossRef]
8. Gmerek, D.E.; Cowan, A. In vivo evidence for benzomorphan-selective receptors in rats. *J. Pharmacol. Exp. Ther.* **1984**, *230*, 110–115.
9. Gmerek, D.E.; Dykstra, L.A.; Woods, J.H. Kappa opioids in rhesus monkeys. III. Dependence associated with chronic administration. *J. Pharmacol. Exp. Ther.* **1987**, *242*, 428–436.
10. Kardon, A.P.; Polgár, E.; Hachisuka, J.; Snyder, L.M.; Cameron, D.; Savage, S.; Cai, X.; Karnup, S.; Fan, C.R.; Hemenway, G.M.; et al. Dynorphin acts as a neuromodulator to inhibit itch in the dorsal horn of the spinal cord. *Neuron* **2014**, *82*, 573–586. [CrossRef]
11. Chiang, M.C.; Hachisuka, J.; Todd, A.J.; Ross, S.E. Insight into B5-I spinal interneurons and their role in the inhibition of itch and pain. *Pain* **2016**, *157*, 544–545. [CrossRef] [PubMed]
12. Peng, X.; Knapp, B.I.; Bidlack, J.M.; Neumeyer, J.L. Pharmacological properties of bivalent ligands containing butorphan linked to nalbuphine, naltrexone, and naloxone at mu, delta, and kappa opioid receptors. *J. Med. Chem.* **2007**, *50*, 2254–2258. [CrossRef]
13. Wentland, M.P.; Lou, R.; Lu, Q.; Bu, Y.; Denhardt, C.; Jin, J.; Ganorkar, R.; VanAlstine, M.A.; Guo, C.; Cohen, D.J.; et al. Syntheses of novel high affinity ligands for opioid receptors. *Bioorg. Med. Chem. Lett.* **2009**, *19*, 2289–2294. [CrossRef] [PubMed]
14. Obeng, S.; Yuan, Y.; Jali, A.; Selley, D.E.; Zhang, Y. In vitro and in vivo functional profile characterization of 17-cyclopropylmethyl-3,14β-dihydroxy-4,5α-epoxy-6α-(isoquinoline-3-carboxamido)morphinan (NAQ) as a low efficacy mu opioid receptor modulator. *Eur. J. Pharmacol.* **2018**, *827*, 32–40. [CrossRef]
15. Schmidt, W.K.; Tam, S.W.; Shotzberger, G.S.; Dewey, H.S.; Clark, R.; Vernier, V.G. Nalbuphine. *Drug Alcohol Depend.* **1985**, *14*, 339–362. [CrossRef]
16. Hawi, A.; Hunter, R.; Morpford, L.; Sciascia, T. Nalbuphine attenuates itch in the substance-P-induced mouse model. *Acta Derm. Venereol.* **2013**, *93*, 634.

17. Inan, S.; Huerto, A.T.; Jensen, L.E.; Dun, N.J.; Cowan, A. Nalbuphine, a kappa opioid receptor agonist and mu opioid receptor antagonist attenuates pruritus, decreases IL-31, and increases IL-10 in mice with contact dermatitis. *Eur. J. Pharmacol.* **2019**, *864*, 172702. [CrossRef] [PubMed]

18. Kopyciok, M.E.R.; Ständer, H.F.; Osada, N.; Steinke, S.; Ständer, S. Prevalence and characteristics of pruritus: A one-week cross-sectional study in a German dermatology practice. *Acta Derm. Venereol.* **2016**, *96*, 50–55. [CrossRef]

19. Matterne, U.; Apfelbacher, C.J.; Loerbroks, A.; Schwarzer, T.; Büttner, M.; Ofenloch, R.; Diepgen, T.L.; Weisshaar, E. Prevalence, correlates and characteristics of chronic pruritus: A population-based cross-sectional study. *Acta Derm. Venereol.* **2011**, *91*, 674–679. [CrossRef]

20. Ständer, S.; Schäfer, I.; Phan, N.Q.; Blome, C.; Herberger, K.; Heigel, H.; Augustin, M. Prevalence of chronic pruritus in Germany: Results of a cross-sectional study in a sample working population of 11,730. *Dermatology* **2010**, *221*, 229–235. [CrossRef] [PubMed]

21. Sheehan-Dare, R.A.; Henderson, M.J.; Cotterill, J.A. Anxiety and depression in patients with chronic urticaria and generalized pruritus. *Br. J. Dermatol.* **1990**, *123*, 769–774. [CrossRef] [PubMed]

22. Zachariae, R.; Zachariae, C.O.; Lei, U.; Pedersen, A.F. Affective and sensory dimensions of pruritus severity: Associations with psychological symptoms and quality of life in psoriasis patients. *Acta Derm. Venereol.* **2008**, *88*, 121–127. [CrossRef] [PubMed]

23. Cedeno-Laurent, F.; Gómez-Flores, M.; Mendez, N.; Ancer-Rodríguez, J.; Bryant, J.L.; Gaspari, A.A.; Trujillo, J.R. New insights into HIV-1-primary skin disorders. *J. Int. AIDS Soc.* **2011**, *14*, 5. [CrossRef] [PubMed]

24. Kaushik, S.; Teque, F.; Patel, M.; Fujimura, S.H.; Schmidt, B.; Levy, J.A. Plasmacytoid dendritic cell number and responses to Toll-like receptor 7 and 9 agonists vary in HIV Type 1-infected individuals in relation to clinical state. *AIDS Res. Hum. Retroviruses* **2013**, *29*, 501–510. [CrossRef] [PubMed]

25. Khan, N.A.; Di Cello, F.; Nath, A.; Kim, K.S. Human immunodeficiency virus type 1 tat-mediated cytotoxicity of human brain microvascular endothelial cells. *J. Neurovirol.* **2003**, *9*, 584–593. [CrossRef] [PubMed]

26. Bai, L.; Zhu, X.; Ma, T.; Wang, J.; Wang, F.; Zhang, S. The p38 MAPK NF-κB pathway, not the ERK pathway, is involved in exogenous HIV-1 Tat-induced apoptotic cell death in retinal pigment epithelial cells. *Int. J. Biochem. Cell Biol.* **2013**, *45*, 1794–1801. [CrossRef] [PubMed]

27. Hayashi, I.; Majima, M. Reduction of sodium deoxycholic acid-induced scratching behaviour by bradykinin B2 receptor antagonists. *Br. J. Pharmacol.* **1999**, *126*, 197–204. [CrossRef] [PubMed]

28. Lee, Y.C.; Lin, C.H.; Hung, S.Y.; Chung, H.Y.; Luo, S.T.; MacDonald, I.; Chu, Y.T.; Lin, P.L.; Chen, Y.H. Manual acupuncture relieves bile acid-induced itch in mice: The role of microglia and TNF-α. *Int. J. Med. Sci.* **2018**, *15*, 953–960. [CrossRef]

29. Inan, S.; Cowan, A. Kappa opioid agonists suppress chloroquine-induced scratching in mice. *Eur. J. Pharmacol.* **2004**, *502*, 233–237. [CrossRef]

30. Ajani, A.A.L. Itching, chloroquine, and malaria: A review of recent molecular and neuroscience advances and their contribution to mechanistic understanding and therapeutics of chronic non-histaminergic pruritus. *Int. J. Dermatol.* **2019**, *58*, 880–891.

31. Chao, C.C.; Gekker, G.; Hu, S.; Sheng, W.S.; Shark, K.B.; Bu, D.F.; Archer, S.; Bidlack, J.M.; Peterson, P.K. Kappa opioid receptors in human microglia downregulate human immunodeficiency virus 1 expression. *Proc. Natl. Acad. Sci. USA* **1996**, *93*, 8051–8056. [CrossRef] [PubMed]

32. Chao, C.C.; Hu, S.; Gekker, G.; Lokensgard, J.R.; Heyes, M.P.; Peterson, P.K. U50,488 protection against HIV-1-related neurotoxicity: Involvement of quinolinic acid suppression. *Neuropharmacol* **2000**, *39*, 150–160. [CrossRef]

33. Sheng, W.S.; Hu, S.; Lokensgard, J.R.; Peterson, P.K. U50,488 inhibits HIV-1 Tat-induced monocyte chemoattractant protein-1 (CCL2) production by human astrocytes. *Biochem. Pharmacol.* **2003**, *65*, 9–14. [CrossRef]

34. Parker, S.R. The skin and HIV: No superficial matter. *Top. Antivir. Med.* **2014**, *22*, 680–684.

35. Gelfand, J.M.; Rudikoff, D. Evaluation and treatment of itching in HIV-infected patients. *Mt. Sinai J. Med.* **2001**, *68*, 298–308. [PubMed]

36. Blanes, M.; Belinchón, I.; Portilla, J.; Betlloch, I.; Reus, S.; Sánchez-Payá, J. Pruritus in HIV-infected patients in the era of combination antiretroviral therapy: A study of its prevalence and causes. *Int. J. STD AIDS* **2012**, *23*, 255–257. [CrossRef] [PubMed]

37. Kaushik, S.B.; Cerci, F.B.; Miracle, J.; Pokharel, A.; Chen, S.C.; Chan, Y.H.; Wilkin, A.; Yosipovitch, G. Chronic pruritus in HIV-positive patients in the southeastern United States: Its prevalence and effect on quality of life. *J. Am. Acad. Dermatol.* **2014**, *70*, 659–664. [CrossRef] [PubMed]

38. Bender, A.M.; Tang, O.; Khanna, R.; Ständer, S.; Kang, S.; Kwatra, S.G. Racial differences in dermatologic conditions associated with HIV: A cross-sectional study of 4679 patients in an urban tertiary care center. *J. Am. Acad. Dermatol.* **2020**, *82*, 1117–1123. [CrossRef]

39. Bergasa, N.V. The pruritus of cholestasis: From bile acids to opiate agonists: Relevant after all these years. *Med. Hypotheses* **2018**, *110*, 86–89. [CrossRef]

40. Cifci, S.; Irak, K.; Bayram, M.; Ekmen, N.; Kazezoglu, C.; Acar, Z.; Sasani, H. Relationship between pruritus and autotaxin in intrahepatic cholestasis of pregnancy. *Gastroenterol. Hepatol.* **2021**, *44*, 96–102. [CrossRef] [PubMed]

41. Golpanian, R.S.; Yosipovitch, G.; Levy, C. Use of Butorphanol as Treatment for Cholestatic Itch. *Dig. Dis. Sci.* **2020**, *66*, 1693–1699. [CrossRef] [PubMed]

42. Inan, S.; Cowan, A. Nalfurafine, a kappa opioid receptor agonist, inhibits scratching behavior secondary to cholestasis induced by chronic ethynylestradiol injections in rats. *Pharmacol. Boichem. Behav.* **2006**, *85*, 39–43. [CrossRef] [PubMed]

43. Andoh, T.; Suzuki, K.; Konno, M.; Tsuneyama, K.; Kuraishi, Y. Pharmacological Characterization of a Novel Mouse Model of Cholestatic Pruritus. *Biol. Pharm. Bull.* **2020**, *43*, 1111–1117. [CrossRef]

44. Ezeamuzie, I.C.; Igbigbi, P.S.; Ambakederemo, A.W.; Abila, B.; Nwaejike, I.N. Halofantrine-induced pruritu amongst subjects who itch to chloroquine. *J. Trop. Med. Hyg.* **1991**, *94*, 184–188.

45. Osifo, N.G. Chloroquine-induced pruritus among patients with malaria. *Arch. Dermatol.* **1984**, *120*, 80–82. [CrossRef]

46. Onigbogi, O.; Ajayi, A.A.; Ukponmwan, O.E. Mechanisms of chloroquine-induced body-scratching behavior in rats: Evidence of involvement of endogenous opioid peptides. *Pharmacol. Biochem. Behav.* **2000**, *65*, 333–337. [CrossRef]

47. Green, A.D.; Young, K.K.; Lehto, S.G.; Smith, S.B.; Mogil, J.S. Influence of genotype, dose and sex on pruritogen-induced scratching behavior in the mouse. *Pain* **2006**, *124*, 50–58. [CrossRef] [PubMed]

48. Liu, Q.; Tang, Z.; Surdenikova, L.; Kim, S.; Patel, K.N.; Kim, A.; Ru, F.; Guan, Y.; Weng, H.J.; Geng, Y.; et al. Sensory neuron-specific GPCRs Mrgprs are itch receptors mediating chloroquine-induced pruritus. *Cell* **2009**, *139*, 1353–1365. [CrossRef] [PubMed]

49. Munanairi, A.; Liu, X.Y.; Barry, D.M.; Yang, Q.; Yin, J.B.; Jin, H.; Li, H.; Meng, Q.T.; Peng, P.H.; Wu, Z.Y.; et al. Non-canonical Opioid Signaling Inhibits Itch Transmission in the Spinal Cord of Mice. *Cell Rep.* **2018**, *23*, 866–877. [CrossRef] [PubMed]

50. Kuraishi, Y.; Nagasawa, T.; Hayashi, K.; Satoh, M. Scratching behavior induced by pruritogenic but not algesiogenic agents in mice. *Eur. J. Pharmacol.* **1995**, *275*, 229–233. [CrossRef]

molecules

Review

Epigenetic and Transcriptional Control of the Opioid Prodynorphine Gene: In-Depth Analysis in the Human Brain

Olga Nosova [1,*,†], Igor Bazov [1,†], Victor Karpyak [2], Mathias Hallberg [1] and Georgy Bakalkin [1,*]

1   Department of Pharmaceutical Biosciences, Uppsala University, 75124 Uppsala, Sweden;
    Igor.bazov@oru.se (I.B.); Mathias.Hallberg@farmbio.uu.se (M.H.)
2   Mayo Clinic, Rochester, MN 55905, USA; Karpyak.Victor@mayo.edu
*   Correspondence: Olga.Kononenko@farmbio.uu.se (O.N.); Georgy.Bakalkin@farmbio.uu.se (G.B.)
†   These authors contributed equally to this work.

Abstract: Neuropeptides serve as neurohormones and local paracrine regulators that control neural networks regulating behavior, endocrine system and sensorimotor functions. Their expression is characterized by exceptionally restricted profiles. Circuit-specific and adaptive expression of neuropeptide genes may be defined by transcriptional and epigenetic mechanisms controlled by cell type and subtype sequence-specific transcription factors, insulators and silencers. The opioid peptide dynorphins play a critical role in neurological and psychiatric disorders, pain processing and stress, while their mutations cause profound neurodegeneration in the human brain. In this review, we focus on the prodynorphin gene as a model for the in-depth epigenetic and transcriptional analysis of expression of the neuropeptide genes. Prodynorphin studies may provide a framework for analysis of mechanisms relevant for regulation of neuropeptide genes in normal and pathological human brain.

Keywords: prodynorphin; epigenetics; transcription; human brain

1. Introduction

Neuropeptides serve as neurohormones and local paracrine regulators. They control activity of neural circuits processing information relevant for behavioral, sensorimotor, endocrine and other processes [1]. Circuit functions and interaction between circuits are ultimately defined by cell-lineage and cell-type specific neuropeptide transcription that is regulated by epigenetic machinery.

Opioid peptides constitute the largest neuropeptide family. They include dynorphins, enkephalins, endorphins, and nociceptin/orphanin FQ that are processed from the prodynorphin (PDYN), proenkephalin, proopiomelanocortin, and pronociceptin precursor proteins. Effects of these peptides are mediated by κ- (KOR), δ-, μ-opioid receptors, and nociceptin receptor. Dynorphins are endogenous KOR ligands [2,3] acting through mitogen-activated protein kinases [4]. Dynorphins are expressed in the striatum, hippocampus, hypothalamus, amygdala and other brain areas, and, at the highest levels, in the pituitary gland suggesting their neuroendocrine functions [5,6].

The PDYN/KOR system regulates processing of reward, mood, nociception, stress response, and motor and cardiovascular functions [2,3,7–10]. Dysregulation of opioid peptides may cause depression, epilepsy and substance dependence [11–17]. Strikingly, mutations in dynorphins cause spinocerebellar ataxia SCA23 characterized by profound neurodegeneration in the brain of affected subjects [18–20]. Dynorphin expression and/or release is activated by stress [21]. The unique feature of KOR ligands is that they elicit dysphoric effects when administered to humans [22] and aversion in rodents [12,23,24]. Dysphoria and anxiety evoked by stress contribute to drug abuse in humans [25] and reinstatement of drug seeking in experimental animals [26]. Dysphoria induced by repeated stress is mediated by dynorphins [7]. The prodynorphin gene (*PDYN*) is identified as a hub

associated with the neuroticism that predicts psychological disorders [27]. Experiments with KOR antagonists and gene deletion demonstrate that the endogenous dynorphins are involved in regulation of alcohol consumption and alcohol dependence [12,28–31]. Withdrawal developed due to discontinuation of drug use is severely dysphoric. The KOR mediated dynorphin effects may lead to negative mood and trigger "relief craving", i.e., desire to suppress negative mood that often provokes drug-seeking in both human subjects and laboratory animals. Genetic studies associate polymorphisms in the *PDYN* gene and *OPRK1*, the KOR-encoding gene with heroin addiction, alcoholism, novelty seeking and positive reward traits [32–37]. *PDYN* variations are also linked to negative craving in alcohol-dependent subjects [38]. These pharmacological and genetic findings imply that KOR antagonists have a potential for treatment of depression and alcoholism including negative craving and relapse [39,40].

In this review, we focus on in-depth analysis of epigenetic and transcription mechanisms of *PDYN* regulation in the human brain. Understanding of these mechanisms could uncover general principles of regulation of neuropeptide genes that are specific for cell types, neuronal subtypes, and neural circuits. Selective regulation of neuropeptides by transcriptional and epigenetic mechanisms may underlie formation and rewiring of neural circuits in the human brain as the cellular basis of behavior and cognition.

2. Prodynorphin Transcripts and Proteins in the Human Brain

The human *PDYN* gene gives rise to mRNAs translated to the full-length (FL) and N-terminally truncated proteins (Figures 1 and 2).
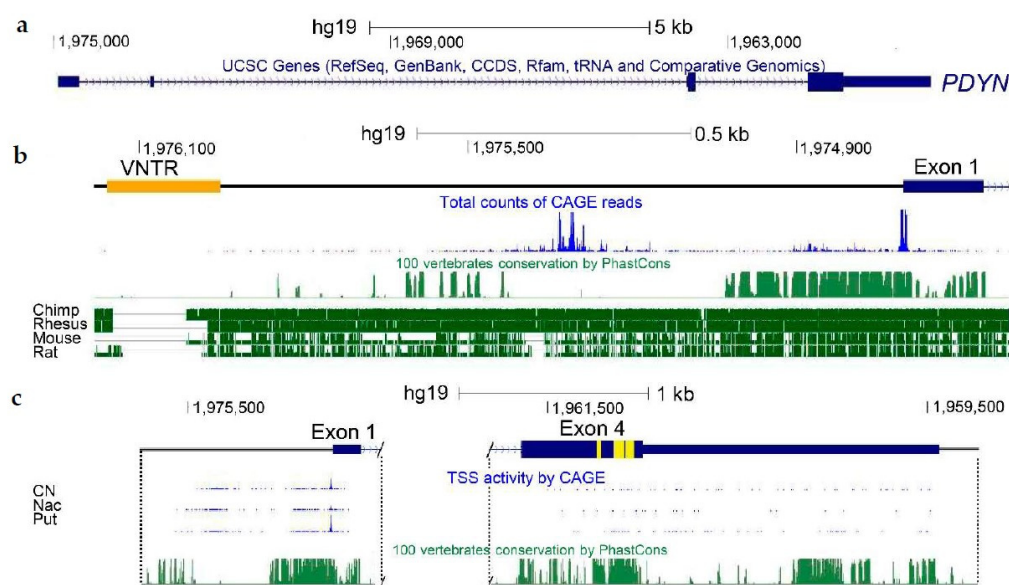
Figure 1. Human *PDYN* gene (modified screenshot from UCSC Genome Browser). (**a**) Gene structure. (**b**) Promoter *PDYN* region with VNTR and TSSs. Conservation across vertebrates. (**c**) Canonical *PDYN* mRNAs and transcripts initiated in exon 4. Their conservation across vertebrates. Noncoding sequences are shown by thin *dark blue* line; coding sequences by thick *dark blue* line; dynorphin peptides-encoding sequences by *yellow*. CN, caudate nucleus; NAc, nucleus accumbens; Put, putamen. Modified from [41].

Two transcription start sites (TSSs) were identified in the human *PDYN* gene by targeted gene analysis [42] and FANTOM transcriptome analysis [43] (Figure 1c). The first TSS cluster determines the 5′-end of exon 1, while the second cluster is located in the coding segment of exon 4. *PDYN* mRNA giving rise to the full-length protein (FL1-*PDYN* mRNA) consists of four exons and three introns (Figure 2a). Testis-specific transcripts with alternative first exons (Taf I and Taf II) and the second FL mRNA (FL2), all differ from FL1

in exon 1 structure [42,44]. Three variants (GTEx 1-3) of dominant FL-PDYN transcripts that differ in the length of exon 1, the presence of exon 2 were identified by RNA-Seq analysis (http://www.gtexportal.org/home/, accessed on 6 May 2021 and Figure 2a). Sp1 and Sp2, and T1-T3 mRNAs are alternatively spliced 5′-truncated transcripts giving rise to N-terminally truncated (T) proteins (Figure 2b). A fragment of coding exon 4 is absent in Sp1, while exons 2 and 3 and a fragment of exon 4 are missed in Sp2 [42]. T1 and T2 are transcribed from the sites located between sequences coding for α-neoendorphin and dynorphin A. TSSs in exons are not unique for PDYN and were identified in other genes (Figure 2b) [45].
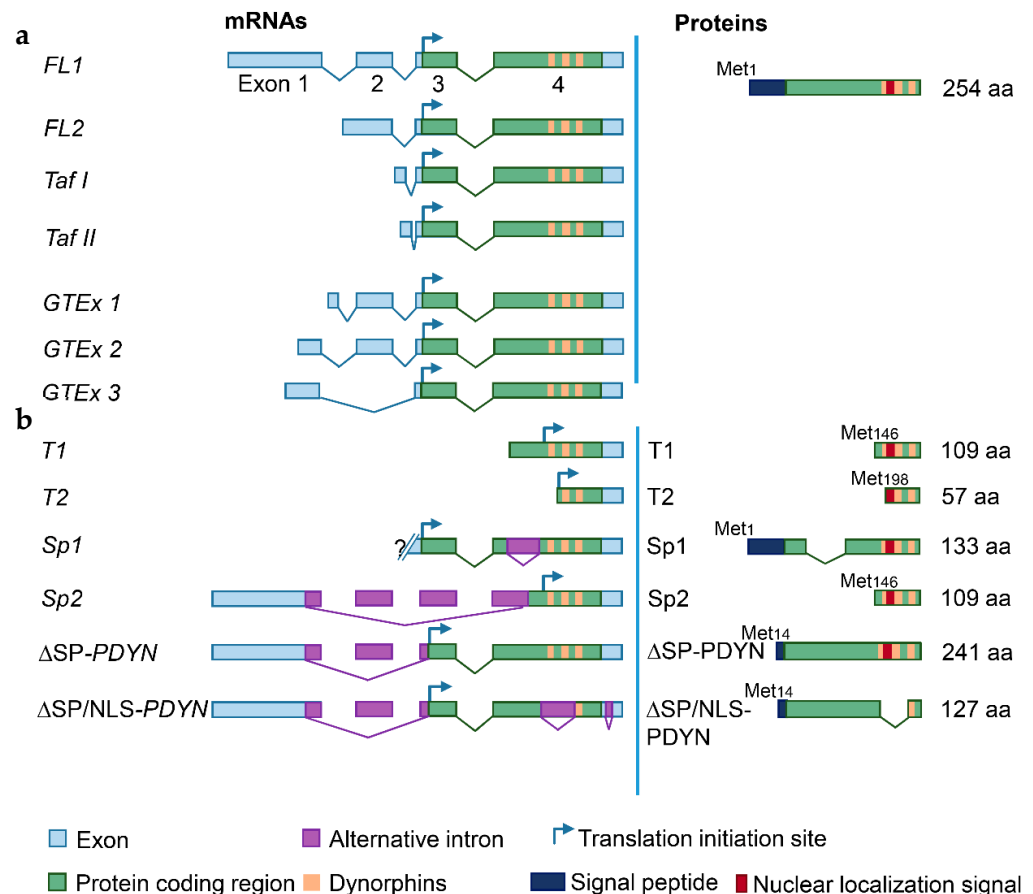
Figure 2. *PDYN* mRNAs coding for the full-length (FL, (**a**)) and truncated proteins (**b**). (**a**) Transcripts encoding FL-PDYN protein. The dominant FL1-*PDYN* and shorter transcripts including FL2-*PDYN* and *GTEx1-3* and testis-specific *Taf* I and *Taf* II transcripts differ in the first and second exons, and in TSS. (**b**) PDYN mRNAs encoding truncated PDYN proteins including alternatively spliced Sp1, Sp2, ΔSP-PDYN and ΔSP/NLS-PDYN transcripts, and transcripts initiated within the coding part of exon 4 (T1 and T2). Signal peptide is truncated in both ΔSP- and ΔSP/NLS-PDYN. Putative nuclear localization signal (NLS) is located in the dynorphin domain. Curved arrows show initiation of translation. Modified from [46].

Exon 4 of human *PDYN* contains neuropeptide-encoding sequences, and also exhibits a promoter activity enabling transcription of T1- and T2-*PDYN* mRNAs from the intragenic TSSs. These variants give rise to N-terminally truncated 12 and 6 kDa PDYNs that lack a signal peptide. In cellular models, T1- and T2-proteins are targeted to the cell nucleus suggesting their non-canonical functions [42]. Transcripts initiated in exon 4 are produced in the amygdala, striatum and hippocampus (Figure 1c). The dynorphin encoding sequences are also hot spot for mutations that cause the neurodegenerative disorder spinocerebellar ataxia type 23 [18–20] (Figure 3a).
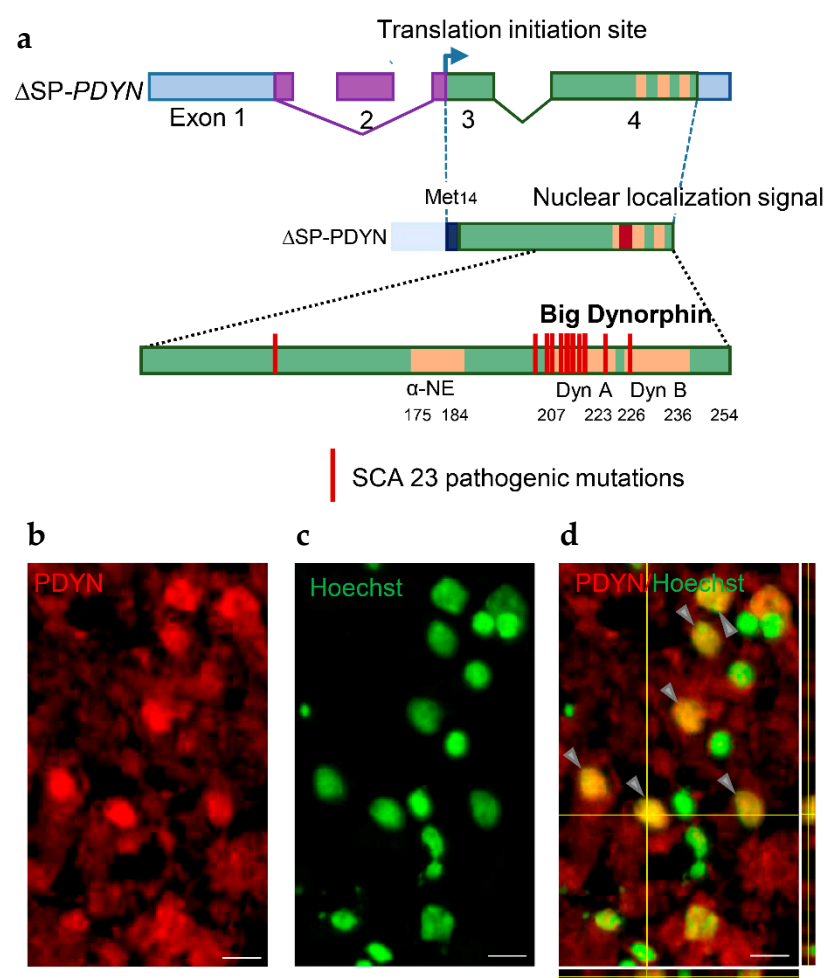
Figure 3. Structure of ΔSP-*PDYN* mRNA and protein, *PDYN* pathogenic mutations causing SCA23, and nuclear localization of ΔSP-PDYN protein. (**a**) ΔSP-*PDYN* encode ΔSP-PDYN protein with truncated signal peptide. Sequences of opioid peptides α-neoendorphin (α-NE), dynorphin A (Dyn A), dynorphinB (Dyn B), and big dynorphin (Big Dyn) are shown in yellow. Pathogenic mutations form a mutational hot spot that is localized within the pathogenic big dynorphin sequence with dynorphin A as a core. (**b**,**c**) PDYN immunoreactivity (red) in the nuclei (green) of neurons in the human caudate nucleus. (**d**) Double labeling (yellow) of neuronal nuclei (arrows) in 3D confocal reconstruction projections. Scale bar, 20 μm. Modified from [46].

Besides FL1-*PDYN* mRNA, the gene gives rise to ΔSP-*PDYN* and ΔSP/NLS-*PDYN* mRNAs that are alternatively spliced variants (Figure 2b). ΔSP-*PDYN* mRNA contains two introns and three exons, and produces the ΔSP-PDYN protein that is translated from the Met_{14} and therefore lacks thirteen amino acids of the signal peptide (Figures 2b and 3a). The ΔSP/NLS-PDYN protein in addition lacks α-neoendorphin and dynorphin A sequences [46]. ΔSP-*PDYN* mRNA is expressed in the striatum where its levels constitute approximately 30% of total *PDYN* mRNA, while in other brain areas its expression is negligible. ΔSP-PDYN protein has a putative bipartite nuclear localization signal (NLS) that has a high score and is located in the opioid domain [46]. The NLS targets ΔSP-PDYN protein to the cell nuclei. Biochemical methods and confocal imaging identified endogenous PDYN protein in the nucleus of neurons in the human striatum (Figure 3b–d) [46]. Consistently, electron microscopic analysis of rat nucleus accumbens demonstrated the presence of Pdyn protein and dynorphin A in the neuronal nuclei along with its location in the smooth endoplasmic reticulum [47]. Proenkephalin, another opioid peptide precursor, was found in the cell nucleus in several cell lines [48,49].

Bioinformatics analysis of PDYN, proenkephalin and proopiomelanocortin predicts that these opioid peptide precursors may serve as DNA-binding proteins. They have zinc-finger and helix-loop-helix domains that are similar to those of twist, hunchback, tal and lil-1 transcription factors [50]. The cystein-rich pattern is perfectly conserved in the opioid peptide precursors and fits to the pattern of zinc-finger domains of transcription factors. Furthermore, the enkephalin sequences represent heptapeptide repeats typical for helix-loop-helix DNA-binding motif.

Nuclear localization of neuropeptide precursor proteins is unusual phenomenon that along with structure similarity with transcription factors predicts a novel transcriptional and/or epigenetic function of these proteins. This function may be essential, at least for *PDYN*, for area-specific regulations. This is supported by the presence of ΔSP-*PDYN* mRNA in the human striatum but not in other human brain regions.

Long non-coding RNAs are RNA molecules that are not translated into proteins and may function as gene-specific regulators of transcription and epigenetic modifications. The *AK090681* gene is transcribed from the opposite strand relative to *PDYN* in the locus and gives rise to non-coding RNA [51]. The nucleus accumbens and cerebellum strongly differ in *PDYN* and *AK090681* expression. The levels of *PDYN* mRNA are 1,000-fold higher while those of the *AK090681* RNA are 20-fold lower in the nucleus accumbens vs. the cerebellum. Long non-coding *AK090681* RNA may be involved in regulation of *PDYN* transcription (see Section 5.1).

In conclusion, transcription of the human *PDYN* gene is highly plastic resulting in generation of a variety of mRNAs that give rise to several proteins serving as opioid peptide precursors, or nuclear proteins that may regulate transcriptional and epigenetic processes.

3. *PDYN* Promoter Mapping and Identification of Transcription Factors

The conservation of *PDYN* promoter is weak across vertebrates besides short, about 300 nucleotides segment located upstream of the main TSSs (Figure 1b). At the same time, the 1.25 kb *PDYN* promoter region shows similarity among humans, great apes and monkey (Figure 1b). This region may be an example of the recent unique positive selection of cis-regulation in human genome [52]. The low similarity between human and rodent suggests that rodent models are not suitable for analysis of *PDYN* regulation associated with human disorders.

The conserved 300 bp of human *PDYN* promoter fragment is responsible for basal and protein kinase A-activated transcription. This fragment includes a downstream response element (DRE) that mediates transcriptional repression. DRE is a DNA binding element for the transcriptional repressor downstream regulatory element antagonist modulator (DREAM), the Ca^{2+}-binding transcriptional repressor [53]. DREAM inhibits *PDYN* transcription while its genetic deletion results in upregulation of expression of this gene [54]. Complexing with alphaCREM, the CREM repressor isoform prevents DREAM–DRE binding and allows the cyclic AMP-dependent *PDYN* de-repression [55,56].

NF-κB, a nuclear factor kappa-light chain-enhancer of activated B cells, and YY1, Yin-Yang1 transcription factors may regulate *PDYN* transcription [57–59]. They target the exon 4 *PDYN* DNA sequences that encode dynorphin peptides. These findings suggest that the neuropeptide sequences that are short, well conserved and present in several copies in neuropeptide-encoding genes, may serve as binding elements for sequence-specific transcription factors. These unique sequences may represent DNA signatures—identifiers of the neuropeptide genes, allowing their selective transcriptional regulation. This hypothesis is supported by the findings that the neuropeptide encoding sequences in exon *PDYN* 4 may function as gene promoter and activate transcription of a reporter gene [42].

Animal studies suggest that *Pdyn* may be regulated by ΔFosB, a component of Activator protein 1 (AP-1) transcription factor that consists of two protein subunits [60]. ΔFosB, a truncated FosB protein was proposed as the major transcriptional integrator in addictive, stress and psychiatric disorders [61]. Still, no detailed transcriptional analysis of ΔFOSB

in human brain supports this hypothesis, and no study assessed yet if ΔFOSB is present in the AP-1 complex and regulates human *PDYN* transcription. The expression levels of ΔFOSB are very low or negligible in the human brain compared to those of two other FOSB proteins. No changes in the levels of this protein were detected in addicted human brain, and this protein is not present in the AP-1 transcription factor that targets the *PDYN* AP-1 binding element [62]. Instead, the AP-1 dimer consists of FOSB and JUND subunits in human brain. Thus, there is no evidence that ΔFosB is involved in human addiction disorders [62].

4. Genetic Factors Contributing to *PDYN* Regulation

Human studies identified strong associations of SNPs in *PDYN* with alcoholism, drug addiction, emotions and memory. Alcoholism and alcohol dependence are associated with several SNPs in the *PDYN* 5′-promoter, exons 3 and 4, and 3′-untranslated region (3′-UTR) [35]. The 3′-UTR contains of six SNPs that form a haplotype block associated with alcohol dependence [35]. The risk haplotype is also associated with combined cocaine dependence and cocaine–alcohol co-dependence along with cocaine dependence, and likely enables low *PDYN* expression in the caudate and nucleus accumbens [63]. The *PDYN* rs2281285-rs1997794 haplotype is associated with alcoholism and susceptibility for drinking in negative emotional states [38,64].

Variable number tandem repeats (VNTR) are often associated with complex disease traits. The 68 bp VNTR is located upstream of the *PDYN* main TSSs (Figure 4b). The VNTR copy number varies from one to five in humans while a single copy is present in nonhuman primates, and none in other animals [52]. The human VNTR elements have five substitutions that differentiate them from chimpanzees. The DNA sequence similar to the AP-1 binding element is located in the *PDYN* VNTR and may serve as a target for this transcription factor [65]. The VNTR elements may contribute to *PDYN* regulation that is dependent on their number, and cellular context [66]. The *PDYN* VNTR variants are associated with epilepsy [11,67], cocaine dependence and abuse [68], schizophrenia [69], opioid addiction [38,70,71], methamphetamine dependence [72,73], and cocaine/alcohol co-dependence [74]. However, attempts to replicate these studies were generally unsuccessful [6,75,76].
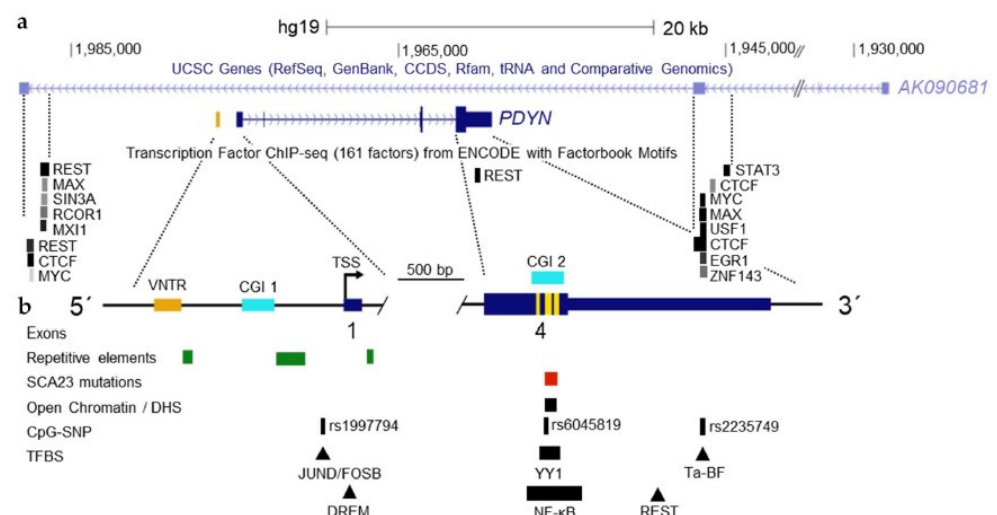
Figure 4. Locus of human *PDYN* with targets for transcription factors. (**a**) Genomic organization showing *PDYN*, the antisense *AK090681* transcript and transcription factor targets deposited on UCSC Genome Browser. (**b**) Verified and putative transcription factor binding elements, promoter VNTR, CpG islands 1 and 2 (CGI 1 and CGI 2), *PDYN* pathogenic mutations causing neurodegeneration, and DNase I hypersensitivity sequence (DHS), and CpG-SNPs association with alcoholism. Thin *light blue* line shows non-coding RNA, thick *dark blue* line coding region, vertical *yellow* lines dynorphin sequences. Modified from [41].

5. *PDYN* Epigenetic Mechanisms

5.1. PDYN Regulation in Chromosomal Context

Strong signals of CTCF, the CCCTC-binding factor in the *PDYN* locus were detected in a variety of cell lines in the genome-wide screen (Figure 4a). CTCF is a pleiotropic transcription factor that may activate or repress gene transcription, and contribute to gene insulation and imprinting. CTCF possesses eleven zinc fingers that may bind to diverse DNA sequences and, by this virtue, may mediate intra- and interchromosomal interactions by chromatin looping between insulators targeted by CTCF [77]. Chromatin domains in these loops may be either activated [78] or repressed for their gene transcription [77] through facilitation or inhibition of interactions of the enhancers and inhibitors with gene promoters. Strong peaks of CTCF are located at putative boundaries of the *PDYN* gene (Figure 4a) where they overlap with strong REST, MYC, MAX, USF1, EGR1 and ZNF143 signals. Localization of the sites occupied by CTCT corresponds to exons 3 and 4 of long non-coding *AK090681* RNA that are positioned on the complementary DNA strand (Figure 4a).

Besides CTCF, the *PDYN* locus is regulated by RE1-Silencing Transcription Factor (REST) that targets the neuron-restrictive silencer element RE-1 and acts as a transcriptional repressor (Figure 4a; see Section 5.4). REST forms two peaks with the first located upstream of the gene in proximity to the upstream CTCF site proximally to the gene. The second peak is in the 3′-UTR. The emerging mechanism is that these two transcription factors may control the locus specific *PDYN* transcription that is insulated from *AK090681* by formation of the chromatin loops due to CTCF binding (Figure 4a). Similar to other long non-coding RNAs, the *AK090681* long non-coding RNA may be involved in the regulation of gene transcription by coordinating intrachromosomal looping and recruiting the chromatin modifying factors.

Lack of cellular and animal models is a limiting factor in analysis of human *PDYN* transcription in chromosomal context. Cell lines of rodent and human origin do not generally express prodynorphin or transcribe it at much, approximately 1000-fold lower levels compared to the brain. Furthermore, in in vitro cellular models *PDYN* transcription is not responsive to pharmacological treatments that upregulate expression of this gene in animal models.

5.2. DNA Methylation

The *PDYN* gene is transcribed mostly in neurons in the human brain [79,80]. The neuronal expression may be controlled through methylation of two short adjacent differentially methylated regions, DMR1 and DMR2 in the promoter. Methylation patterns are opposite between neurons and glia for each DMR, and also between the DMRs (Figure 5). DMR1 comprises of a short, nucleosome size CpG island (CGI) that is hypomethylated and enriched in 5-hydroxymethylcytosine in neurons, while hypermethylated in other cell types.

The current paradigm is that DMRs are associated with CGI shores but not with core of the CGIs [81,82]. In contrast to this pattern, methylation of the *PDYN* CGI is different among neurons and other cell types. This CGI is also enriched in 5-hydroxymethylcytosine suggesting its function as active regulatory domain characterized by high cytosine methylation turnover rate [79]. Methylation of individual CpGs in the CGI is highly coordinated in neurons, that is not observed in other *PDYN* promoter areas in these and other cell types. This pattern in the *PDYN* CGI is analogous to contiguous methylation clusters characterized by high correlations among CpG methylation in other genes [83].

The CGI methylation may differ in its chromatin organization between neurons and glia. In cells that do not transcribe the *PDYN* gene, the CGI is wrapped in a nucleosome, a feature of the repressive chromatin [79]. Thus, the CGI may serve as the *PDYN* promoter module, which cycling between the methylated and occupied by a nucleosome state, and hydroxymethylated nucleosome free state, is locally regulated. These DNA and chromatin

modifications may allow interactions with sequence–specific transcription factors that could delineate cell-type specific *PDYN* transcription.

The opposite pattern is observed for DMR2 that is hypermethylated in neurons and hypomethylated in glia and other cell types (Figure 5). This pattern and also negative correlations between methylation of the two DMRs imply that the mechanisms that are autonomic for each DMR and coordinated between them, regulate their methylation, and consequently their complementary role in *PDYN* expression. Hypermethylation of DMR2 in neurons may enable binding of MeCP2 or other factors that binds to methylated DNA and activate gene transcription. In non-neuronal cells, *PDYN* may be repressed through interactions of DREAM, a methylation sensitive transcriptional repressor, with non-methylated DMR2 [84]. There epigenetic mechanism may control cell type-specific control of *PDYN* transcription in human brain.
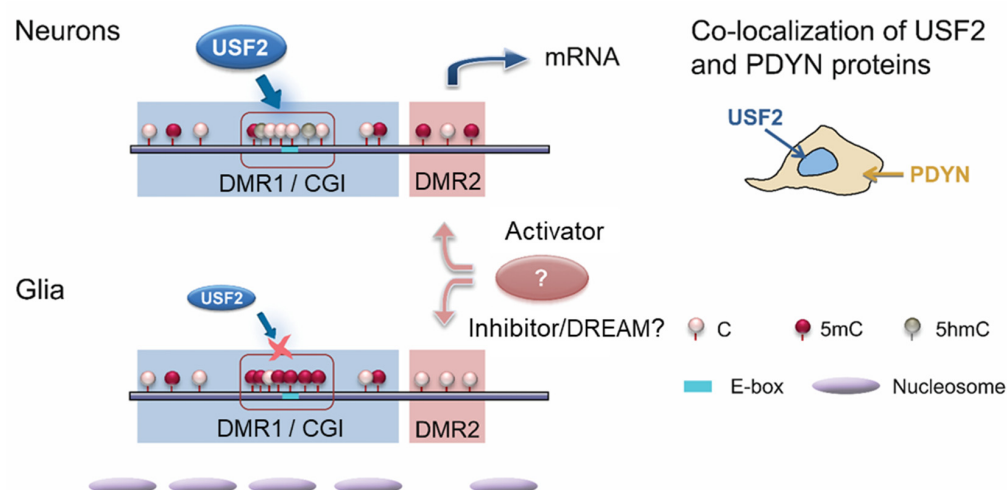
Figure 5. Model for epigenetic and transcriptional regulation of neuronal *PDYN* transcription. In neurons, USF2 binds to E-box in the promoter CGI that is hypomethylated and enriched in 5-hydroxymethylcytosine (5-hmC). In glia, the CGI is hypermethylated. DMR2 and DMR1/CGI exhibit methylation patterns that are opposite between them and between neurons and glia for each of them. In non-neuronal cells, DMR2 may be targeted by methylation-sensitive transcriptional repressor such as DREAM, while in neurons by a methylation-dependent transcriptional activator. In glia, the DMR1/CGI may be wrapped in a nucleosome, that prevents transcriptional initiation. These mechanisms may underlie contrasting *PDYN* expression in neurons and glia. Modified from [79].

One more CpG island is located in the coding part of exon 4 of the *PDYN* gene (Figure 4b). High methylation of cytosine residues in exons [85] were detected in many genes that was positively associated with gene transcription levels [86,87]. The exon 4 *PDYN* CpG island possesses a promoter activity, transcription factor binding sites, and the second cluster of TSSs, along with SNP associated with alcoholism [35,42,57–59]. This island is similarly hypermethylated in the brain and blood DNA in which the levels of FL-*PDYN* transcript are high or negligible, respectively [80]. DNA methylation profile in this domain is well conserved across human individuals, whereas differs among brain and peripheral tissues, and among brain regions [79]. Epigenetic mechanisms may remodel chromatin structure in the exon 4 *PDYN* CpG island that may result in transcription of this gene from intragenic TSSs or regulate elongation of transcription and mRNA splicing.

5.3. The CpG-SNP Hypothesis: Epialleles of PDYN SNPs Associated with Alcoholism

The current paradigm is that the environmental, epigenetic and genetic factors influence the phenotype and contribute to the propensity for disorders by altering gene transcription. SNPs are much more abundant at the CpG dinucleotides than predicted [88] and may form or disrupt a CpG sequence. Methylation and hydroxymethylation of CpG-

SNPs is allele-specific. Environmental, epigenetic and genetic factors may mechanistically integrate on CpG-SNPs which genetic variants may determine the phenotype while the cytosine methylation—the demethylation state may control transcription from the C-allele (Figure 6a). Two SNP alleles and three cytosine epialleles including its unmethylated, methylated and hydroxymethylated states may differentially contribute to a vulnerability of a disease.
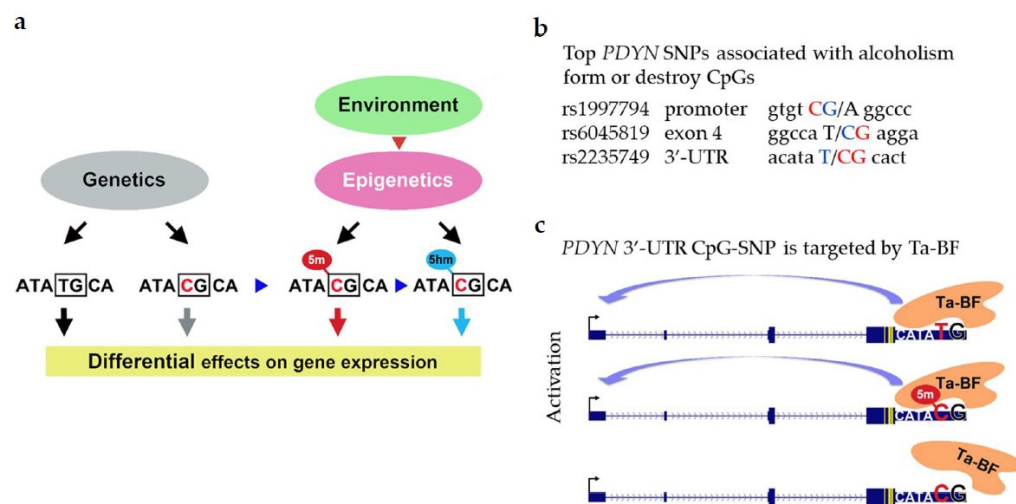
Figure 6. The CpG-SNP hypothesis. (**a**) Genetic, epigenetic and environmental factors are mechanistically integrated at CpG-SNPs that may be methylated and hydroxymethylated at the C-allele. Two alleles and three cytosine epialleles may differentially affect gene transcription and thereby differently contribute to deasease predisposition [89]. (**b**) *PDYN* SNPs variants associated with alcoholism are shown in *blue* while those forming CpGs in *red*. (**c**) T-allele-binding factor (Ta-BF) has high affinity for the T and methylated C alleles of the 3′-UTR CpG-SNP but not to unmethylated C allele. The high affinity interaction may be a basis for transcriptional activation by this DNA-binding protein.

Five *PDYN* SNPs are associated with alcoholism with high significance [89]. Three of them form or disrupt CpG sites (rs1997794; rs6045819 and rs2235749; Figure 6b). To test the CpG-SNP hypothesis we analyzed methylation of these three *PDYN* CpG-SNPs in the human dlPFC. Alcoholism is associated with hypermethylation of the C allele of 3′-UTR CpG-SNP rs2235749 (C > T) in the human brain, and its methylation levels positively correlate with *PDYN* expression suggesting a functional link between these two processes. Analysis of DNA-binding factors targeting this area identified a novel T-allele-binding factor (Ta-BF). This 63 kDa protein has high affinity for the T and methylated C alleles of the 3′-UTR CpG-SNP but not for unmethylated C allele (Figure 6c).

Positive correlation between the 3′-UTR CpG-SNP methylation and *PDYN* expression suggests that the Ta-BF binding to the 3′-UTR may activate *PDYN* transcription [89]. Thus, the environmental, epigenetic and genetic factors associated with alcoholism may be mechanistically integrated on the *PDYN* 3′-UTR CpG-SNP, and Ta-BF may read the resulting methylation signals and translate them into disease predisposition through changes in *PDYN* transcription.

Several gene-centric and genome wide human studies lend support for the CpG-SNP hypothesis. Many well-known polymorphic sites associated with psychiatric disorders form CpG-SNPs. CpG-SNPs of the catechol-O-methyltransferase, GABA(A) receptor beta(2) (*GABRB2*) and μ-opioid receptor genes are the examples. Methylation of the cytosine allele at these sites is a part of the mechanism that controls gene transcription and contributes to the phenotype [90–95]. Thus, modifications of CpG-SNPs may have an essential epigenetic function that mediates the effects of a changing environment on the polymorphism dependent genome expression.

5.4. PDYN Regulation by REST

REST is a master regulator of neuronal phenotype acting through neuron-restrictive silencer element (RE1) and inhibiting transcription of its target genes [96,97]. The REST effects are mediated by epigenetic mechanisms that recruit inhibitory enzymatic activities to its target elements leading to long-term alterations in gene transcription.

Chromatin immunoprecipitation data generated by ENCODE [98,99] demonstrate that *PDYN* has two binding sites for REST (Figure 4a) [100,101]. They are located 12 kb upstream of the *PDYN* gene and in its 3′-UTR, respectively [102]. Functional inactivation of REST with a dominant negative mutant REST protein [103,104] increases *PDYN* transcription in cellular models [104]. Consistently analysis of the human dlPFC by Chromatin Immunoprecipitation quantitative real-time PCR assay revealed REST bound to the RE1 located upstream of *PDYN*, while binding to the 3′-UTR RE1 element was negligible [104].

REST is regulated by the microRNA MIR-9, and they together control chromatin remodeling that determines cell phenotype [105,106]. Analysis of the human brain demonstrates that REST and MIR-9 negatively correlate suggesting the negative feedback mechanism. Thus, REST may repress *PDYN* transcription while this transcription factor is negatively controlled by MIR-9 microRNA [104].

5.5. Dual Epigenetic and Transcriptional Mechanism Controls Neuronal PDYN Expression

Expression of the neuropeptide genes including *PDYN* is confined to specific cell types and neuronal lineages that may be coordinated by epigenetic and transcriptional mechanisms. These mechanisms may permit and restrict, activate or inhibit gene transcription depending on cell type. We tested this hypothesis by the in-depth analysis of the opioid *PDYN* transcription in the human brain [79]. Our strategy was to detect sequences in the *PDYN* locus that are differentially methylated between neurons and other cell types, and to identify sequence-specific methylation-sensitive transcription factors that target these DMRs, and therefore may control the methylation-regulated *PDYN* expression in specific cell types.

The previous sections described that the *PDYN* promoter has the DMR1 with a short CGI as a core that is hypomethylated and enriched in 5-hydroxymethylcytosine in neurons (Figure 5) [79]. When unmethylated this CGI serves as a binding site for USF2, E-box transcription factor that does not interact with methylated sequences. USF2 activates *PDYN* transcription in model cell systems, and is physically associated with unmethylated E-box in the *PDYN* CGI in human brain. Consistently, expression of USF2 and *PDYN* is correlated (Figure 7a,b). USF2 and PDYN proteins are co-expressed in the same neurons in the human dlPFC; only USF2-producing cells synthesize dynorphins (Figure 7c–e). Thus, two conditions may be obligatory for the neuron-specific *PDYN* transcription that are the CGI hypomethylation and USF2 expression.
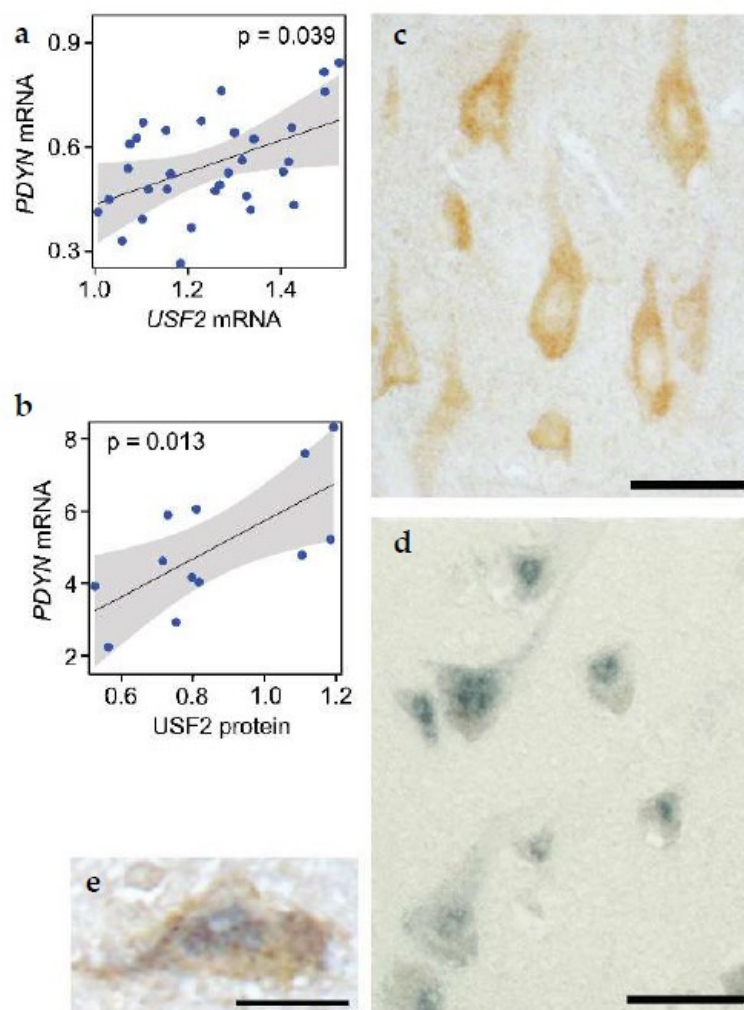
Figure 7. Correlation of USF2 and PDYN (**a**,**b**), and their co-localization (**c**–**e**) in the human dlPFC. (**a**,**b**) The estimated effect with 95% confidence interval. Immunoreactivity of (**c**) PDYN, and (**d**) USF2 in the cytoplasm and nuclei of the layer V neurons, respectively. (**e**) Double labeling of PDYN and USF2 in the same neuron. Scale bars, 50 μm (**c**,**d**); and 25 μm (**e**). Modified from [79].

In rodents, Ptf1a, Pax2, Neurod1/2/6 and Bhlhb5 transcription factors enable *Pdyn* expression in cell type and cell lineage-specific patterns in the dorsal spinal cord and Islet-1 in the striatum [107–112]. USF2 and these transcription factors are E-box proteins (USF2, Ptf1a and Neurod1/2/6), or regulate E-box dependent transcription. Thus, formation of cellular prodynorphin phenotype in the human and rodent central nervous system is determined by E-box transcription factors.

6. *PDYN* Transcriptional Adaptations Concomitant with Neuronal Decline in Human Alcoholics

Alcoholism is associated with cognitive impairments that may develop due to aberrant neurotransmission and neurodegeneration. Several lines of evidence suggest that dynorphin opioid peptides have a role in cognitive decline [113–117]. In animal experiments, dynorphins administered into the hippocampus impair spatial learning [118]. Dynorphins also contribute to the stress and age-related learning and memory deficits [113–115]. In elderly humans, *PDYN* polymorphism is associated with memory loss [116]. Dynorphins are elevated in the prefrontal cortex of patients with Alzheimer's disease, and their levels correlate with neuropathological score [117]. Consistently, it was hypothesized that the PDYN/KOR system is dysregulated in the dlPFC and hippocampus of alcoholics, and that these changes contribute to cognitive impairments [119,120]. This notion gains a support in animal model of cognitive deficits induced by alcohol binge drinking [120–122]. The

PDYN/KOR system mediated impairments of spatial learning and memory in this model while selective κ-antagonist nor-binaltorphimine reversed these impairments by decrease in the ethanol-induced elevation of glutamate overflow.

In line with these studies, changes in the PDYN/KOR system are considered as a molecular mechanism that underlies the long-term effects of addicted substances on behavior, cognitive impairment and loss of control over intake of addictive substances and alcohol [12,30,120,123–129]. This hypothesis was addressed by analysis of the expression levels and co-expression (transcriptionally coordinated) patterns of *PDYN* and *OPRK1* (KOR) genes in the dlPFC of alcoholics; 53 alcoholics were compared with 55 control subjects [127,128]. *PDYN* was found to be downregulated in the addicted brain, while the *OPRK1* expression was not altered. Thus, the effects of alcoholism on these two genes were not mechanistically coordinated.

Early postmortem morphological studies revealed marked reduction in the number of neurons in the dlPFC of alcoholics [130,131]. More recently this was confirmed by analysis of neuronal proportion in the epigenome-wide DNA methylation study, and by analysis of neuronal and glial markers [132]. Importantly, the *PDYN* mRNA levels were not affected by the decline in the neuronal number. Instead, their alterations were likely caused by transcriptional adaptations [79,127,128]. Another issue that is important for regulation of the PDYN/KOR system is that the absolute levels of *PDYN* mRNA were markedly lower compared to those of KOR (*OPRK1*). Thus, *PDYN* transcription may be a limiting factor in the PDYN/KOR signaling. Therefore, a decrease in *PDYN* transcription may further diminish efficacy of PDYN/KOR signaling in dlPFC of alcoholics. Resulting overactivation of neurotransmission in cortical neurocircuits that is negatively controlled by dynorphins, may be a gross effect of PDYN/KOR downregulation that contributes to formation of alcohol-induced impairments in behavior.

Addictive substances may cause similar downstream molecular adaptations—the general molecular syndrome that mediates the lasting nature of the addictive state [133]. *PDYN* transcription is downregulated in the dlPFC and dorsal striatum in alcoholics [127–129], and in the dorsal striatum in cocaine addicts [63]. These changes may be a part of the general adaptive syndrome caused by addictive substances.

7. Conclusions

The specific feature of neurons and neural circuits is their neuropeptide phenotype. In short, conserved and repetitive neuropeptide sequences are a distinctive feature of neuropeptide genes. In this property these sequences are similar to DNA-binding sites for sequence-specific transcription factors. The opioid peptide sequences in the *PDYN* gene overlap with or are situated in close proximity to multiple TSSs, splice junctions, and CpG-SNP that is associated with psychiatric phenotype (Figure 6b). YY1 and NF-κB through binding to these sequences may activate transcription from a cryptic promoter located in this area [42,57–59]. This region is hypersensitive to DNAase I, suggesting that chromatin is open in the short CpG island that is a core of this region (Figure 4b). Strikingly, the dynorphin-encoding sequences may be a mutational hot spot; their missense mutations cause profound neurodegeneration in human subjects with neurodegenerative disorder SCA23 [20,134–136]. SCA23 mutations are enriched in CpGs suggesting a link of their origin or a pathogenic mechanism with methylation/demethylation processes [79,137]. Together these findings lend support for the hypothesis that the neuropeptide-encoding sequences may have regulatory functions. They may have a role in transcriptional initiation, elongation, and RNA splicing leading to synthesis of transcripts that give rise to protein variants with non-canonical functions. A unique combination of transcriptional mechanisms regulated by conventional enhancer and promoter, and by the neuropeptide-encoding sequences may determine cell-type and cell lineage-specific gene expression. Whether neuropeptide-encoding sequences are gene signatures targeted by epigenetic mechanisms that define neuropeptide phenotype of neural circuits, is important to address in future studies.

Dysregulation of neural circuits expressing neuropeptides may cause neurological and psychiatric disorders including spinocerebellar ataxia 23, epilepsy, depression and substance dependence. Not all functions of neuropeptide precursors might have been identified. The unusual nuclear localization of PDYN and proenkephalin was demonstrated, and predicts novel epigenetic or transcriptional functions for nuclear variants of these proteins. Knowledge of the mechanisms that regulate epigenome and transcriptome in the neuropeptide producing neurons is essential for understanding of normal and dysfunctional neural circuits. Studies focused on individual neuropeptide genes and functions of their protein products complement, specify and further advance multi-omics analysis of human brain relevant for psychiatric disorders.

Conflicts of Interest: The authors declare no conflict of interest.

References

1. Nusbaum, M.P.; Blitz, D.M.; Marder, E. Functional consequences of neuropeptide and small-molecule co-transmission. *Nat. Rev. Neurosci.* **2017**, *18*, 389–403. [CrossRef]
2. Chavkin, C. Dynorphin—Still an extraordinarily potent opioid peptide. *Mol. Pharmacol.* **2013**, *83*, 729–736. [CrossRef]
3. Schwarzer, C. 30 years of dynorphins—New insights on their functions in neuropsychiatric diseases. *Pharmacol. Ther.* **2009**, *123*, 353–370. [CrossRef] [PubMed]
4. Bruchas, M.R.; Chavkin, C. Kinase cascades and ligand-directed signaling at the kappa opioid receptor. *Psychopharmacology* **2010**, *210*, 137–147. [CrossRef] [PubMed]
5. Hurd, Y.L. Differential messenger RNA expression of prodynorphin and proenkephalin in the human brain. *Neuroscience* **1996**, *72*, 767–783. [CrossRef]
6. Nikoshkov, A.; Drakenberg, K.; Wang, X.; Horvath, M.C.; Keller, E.; Hurd, Y.L. Opioid neuropeptide genotypes in relation to heroin abuse: Dopamine tone contributes to reversed mesolimbic proenkephalin expression. *Proc. Natl. Acad. Sci. USA* **2008**, *105*, 786–791. [CrossRef] [PubMed]
7. Knoll, A.T.; Carlezon, W.A., Jr. Dynorphin, stress, and depression. *Brain Res.* **2010**, *1314*, 56–73. [CrossRef]
8. Negrete, R.; García Gutiérrez, M.S.; Manzanares, J.; Maldonado, R. Involvement of the dynorphin/KOR system on the nociceptive, emotional and cognitive manifestations of joint pain in mice. *Neuropharmacology* **2017**, *116*, 315–327. [CrossRef]
9. Nogueiras, R.; Romero-Picó, A.; Vazquez, M.J.; Novelle, M.G.; López, M.; Diéguez, C. The opioid system and food intake: Homeostatic and hedonic mechanisms. *Obes. Facts.* **2012**, *5*, 196–207. [CrossRef]
10. Przewlocki, R.; Przewlocka, B. Opioids in chronic pain. *Eur. J. Pharmacol.* **2001**, *429*, 79–91. [CrossRef]
11. Zangrandi, L.; Schwarzer, C. The Kappa Opioid Receptor System in Temporal Lobe Epilepsy. *Handb. Exp. Pharmacol.* **2021**.
12. Shippenberg, T.S.; Zapata, A.; Chefer, V.I. Dynorphin and the pathophysiology of drug addiction. *Pharmacol. Ther.* **2007**, *116*, 306–321. [CrossRef] [PubMed]
13. Bazov, I.; Kononenko, O.; Watanabe, H.; Kuntić, V.; Sarkisyan, D.; Taqi, M.M.; Hussain, M.Z.; Nyberg, F.; Yakovleva, T.; Bakalkin, G. The endogenous opioid system in human alcoholics: Molecular adaptations in brain areas involved in cognitive control of addiction. *Addict. Biol.* **2013**, *18*, 161–169. [CrossRef] [PubMed]
14. Clark, S.D.; Abi-Dargham, A. The Role of Dynorphin and the Kappa Opioid Receptor in the Symptomatology of Schizophrenia: A Review of the Evidence. *Biol. Psychiatry* **2019**, *86*, 502–511. [CrossRef] [PubMed]
15. Li, X.; Marchant, N.J.; Shaham, Y. Opposing roles of cotransmission of dynorphin and hypocretin on reward and motivation. *Proc. Natl. Acad. Sci. USA* **2014**, *111*, 5765–5766. [CrossRef] [PubMed]

16. Muschamp, J.W.; Hollander, J.A.; Thompson, J.L.; Voren, G.; Hassinger, L.C.; Onvani, S.; Kamenecka, T.M.; Borgland, S.L.; Kenny, P.J.; Carlezon, W.A., Jr. Hypocretin (orexin) facilitates reward by attenuating the antireward effects of its cotransmitter dynorphin in ventral tegmental area. *Proc. Natl. Acad. Sci. USA* **2014**, *111*, 1648–1655. [CrossRef]

17. Tejeda, H.A.; Shippenberg, T.S.; Henriksson, R. The dynorphin/kappa-opioid receptor system and its role in psychiatric disorders. *Cell Mol. Life Sci.* **2012**, *69*, 857–896. [CrossRef] [PubMed]

18. Bakalkin, G.; Watanabe, H.; Jezierska, J.; Depoorter, C.; Verschuuren-Bemelmans, C.; Bazov, I.; Artemenko, K.A.; Yakovleva, T.; Dooijes, D.; Van de Warrenburg, B.P.; et al. Prodynorphin mutations cause the neurodegenerative disorder spinocerebellar ataxia type 23. *Am. J. Hum. Genet.* **2010**, *87*, 593–603. [CrossRef] [PubMed]

19. Smeets, C.J.; Jezierska, J.; Watanabe, H.; Duarri, A.; Fokkens, M.R.; Meijer, M.; Zhou, Q.; Yakovleva, T.; Boddeke, E.; den Dunnen, W.; et al. Elevated mutant dynorphin A causes Purkinje cell loss and motor dysfunction in spinocerebellar ataxia type 23. *Brain* **2015**, *138*, 2537–2552. [CrossRef]

20. Wu, F.; Wang, X.; Li, X.; Teng, H.; Tian, T.; Bai, J. Spinocerebellar ataxia type 23 (SCA23): A review. *J. Neurol.* **2020**. [CrossRef] [PubMed]

21. Mague, S.D.; Pliakas, A.M.; Todtenkopf, M.S.; Tomasiewicz, H.C.; Zhang, Y.; Stevens, W.C., Jr.; Jones, R.M.; Portoghese, P.S.; Carlezon, W.A., Jr. Antidepressant-like effects of kappa-opioid receptor antagonists in the forced swim test in rats. *J. Pharmacol. Exp. Ther.* **2003**, *305*, 323–330. [CrossRef]

22. Pfeiffer, A.; Brantl, V.; Herz, A.; Emrich, H.M. Psychotomimesis mediated by kappa opiate receptors. *Science* **1986**, *233*, 774–776. [CrossRef]

23. Land, B.B.; Bruchas, M.R.; Lemos, J.C.; Xu, M.; Melief, E.J.; Chavkin, C. The dysphoric component of stress is encoded by activation of the dynorphin kappa-opioid system. *J. Neurosci.* **2008**, *28*, 407–414. [CrossRef] [PubMed]

24. Todtenkopf, M.S.; Marcus, J.F.; Portoghese, P.S.; Carlezon, W.A., Jr. Effects of kappa-opioid receptor ligands on intracranial self-stimulation in rats. *Psychopharmacology* **2004**, *172*, 463–470. [CrossRef]

25. De Kloet, E.R.; Joels, M.; Holsboer, F. Stress and the brain: From adaptation to disease. *Nat. Rev. Neurosci.* **2005**, *6*, 463–475. [CrossRef] [PubMed]

26. Shaham, Y.; Erb, S.; Stewart, J. Stress-induced relapse to heroin and cocaine seeking in rats: A review. *Brain Res.* **2000**, *33*, 13–33. [CrossRef]

27. Xu, Q.; Liu, F.; Qin, W.; Jiang, T.; Yu, C. Multiscale neurobiological correlates of human neuroticism. *Hum. Brain Mapp.* **2020**. [CrossRef]

28. Altshuler, H.L.; Phillips, P.E.; Feinhandler, D.A. Alteration of ethanol self-administration by naltrexone. *Life Sci.* **1980**, *26*, 679–688. [CrossRef]

29. Cichelli, M.J.; Lewis, M.J. Naloxone nonselective suppression of drinking of ethanol, sucrose, saccharin, and water by rats. *Pharmacol. Biochem. Behav.* **2002**, *72*, 699–706. [CrossRef]

30. Walker, B.M.; Zorrilla, E.P.; Koob, G.F. Systemic kappa-opioid receptor antagonism by nor-binaltorphimine reduces dependence-induced excessive alcohol self-administration in rats. *Addict. Biol.* **2011**, *16*, 116–119. [CrossRef]

31. Gutierrez-Cuesta, J.; Burokas, A.; Mancino, S.; Kummer, S.; Martín-García, E.; Maldonado, R. Effects of genetic deletion of endogenous opioid system components on the reinstatement of cocaine-seeking behavior in mice. *Neuropsychopharmacology* **2014**, *39*, 2974–2988. [CrossRef]

32. Edenberg, H.J.; Wang, J.; Tian, H.; Pochareddy, S.; Xuei, X.; Wetherill, L.; Goate, A.; Hinrichs, T.; Kuperman, S.; Nurnberger, J.I.; et al. A regulatory variation in OPRK1, the gene encoding the kappa-opioid receptor, is associated with alcohol dependence. *Hum. Mol. Genet.* **2008**, *17*, 1783–1789. [CrossRef]

33. Egervari, G.; Jutras-Aswad, D.; Landry, J.; Miller, M.L.; Anderson, S.A.; Michaelides, M.; Jacobs, M.M.; Peter, C.; Yiannoulos, G.; Liu, X.; et al. A Functional 3′UTR Polymorphism (rs2235749) of Prodynorphin Alters microRNA-365 Binding in Ventral Striatonigral Neurons to Influence Novelty Seeking and Positive Reward Traits. *Neuropsychopharmacology* **2016**, *41*, 2512–2520. [CrossRef] [PubMed]

34. Ramchandani, V.A.; Umhau, J.; Pavon, F.J.; Ruiz-Velasco, V.; Margas, W.; Sun, H.; Damadzic, R.; Eskay, R.; Schoor, M.; Thorsell, A.; et al. A genetic determinant of the striatal dopamine response to alcohol in men. *Mol Psychiatry* **2011**, *16*, 809–817. [CrossRef]

35. Xuei, X.; Dick, D.; Flury-Wetherill, L.; Tian, H.J.; Agrawal, A.; Bierut, L.; Goate, A.; Bucholz, K.; Schuckit, M.; Nurnberger, J.; et al. Association of the kappa-opioid system with alcohol dependence. *Mol. Psychiatry* **2006**, *11*, 1016–1024. [CrossRef] [PubMed]

36. Xuei, X.; Flury-Wetherill, L.; Bierut, L.; Dick, D.; Nurnberger, J.; Nurnberger, J., Jr.; Foroud, T.; Edenberg, H.J. The opioid system in alcohol and drug dependence: Family-based association study. *Am. J. Med. Gene.t B. Neuropsychiatr. Genet.* **2007**, *144*, 877–884. [CrossRef]

37. Ji, Y.; Su, R.; Tang, H.; Cui, J.; Deji, C.; Shi, Y.; Wei, S. Genetic association analyses and meta-analysis of Dynorphin-Kappa Opioid system potential functional variants with heroin dependence. *Neurosci. Lett.* **2018**, *685*, 75–82. [CrossRef]

38. Karpyak, V.M.; Winham, S.J.; Preuss, U.W.; Zill, P.; Cunningham, J.M.; Walker, D.L.; Lewis, K.A.; Geske, J.R.; Colby, C.L.; Abulseoud, O.A.; et al. Association of the PDYN gene with alcohol dependence and the propensity to drink in negative emotional states. *Int. J. Neuropsychopharmacol.* **2013**, *16*, 975–985. [CrossRef] [PubMed]

39. Anderson, R.I.; Lopez, M.F.; Griffin, W.C.; Haun, H.L.; Bloodgood, D.W.; Pati, D.; Boyt, K.M.; Kash, T.L.; Becker, H.C. Dynorphin-kappa opioid receptor activity in the central amygdala modulates binge-like alcohol drinking in mice. *Neuropsychopharmacology* **2019**, *44*, 1084–1092. [CrossRef] [PubMed]

40. Li, S.; Zheng, M.Q.; Naganawa, M.; Gao, H.; Pracitto, R.; Shirali, A.; Lin, S.F.; Teng, J.K.; Ropchan, J.; Huang, Y. Novel Kappa Opioid Receptor Agonist as Improved PET Radiotracer: Development and in Vivo Evaluation. *Mol. Pharm.* **2019**, *16*, 1523–1531. [CrossRef]

41. Bazov, I.; Bakalkin, G. Prodynorphin Epialleles, in Epigenetics and Human Health, Clinical Focus on Psychiatry. *Springer* **2016**, *2*, 43–76.

42. Nikoshkov, A.; Hurd, Y.L.; Yakovleva, T.; Bazov, I.; Marinova, Z.; Cebers, G.; Pasikova, N.; Gharibyan, A.; Terenius, L.; Bakalkin, G. Prodynorphin transcripts and proteins differentially expressed and regulated in the adult human brain. *FASEB J.* **2005**, *19*, 1543–1545. [CrossRef]

43. Lizio, M.; Harshbarger, J.; Shimoji, H.; Severin, J.; Kasukawa, T.; Sahin, S.; Abugessaisa, I.; Fukuda, S.; Hori, F.; Ishikawa-Kato, S.; et al. Gateways to the FANTOM5 promoter level mammalian expression atlas. *Genome. Biol.* **2015**, *16*, 22. [CrossRef] [PubMed]

44. Telkov, M.; Geijer, T.; Terenius, L. Human prodynorphin gene generates several tissue-specific transcripts. *Brain Res.* **1998**, *804*, 284–295. [CrossRef]

45. Carninci, P.; Sandelin, A.; Lenhard, B.; Katayama, S.; Shimokawa, K.; Ponjavic, J.; Semple, C.A.; Taylor, M.S.; Engström, P.G.; Frith, M.C.; et al. Genome-wide analysis of mammalian promoter architecture and evolution. *Nat. Genet.* **2006**, *38*, 626–635. [CrossRef] [PubMed]

46. Kononenko, O.; Bazov, I.; Watanabe, H.; Gerashchenko, G.; Dyachok, O.; Verbeek, D.S.; Alkass, K.; Druid, H.; Andersson, M.; Mulder, J.; et al. Opioid precursor protein isoform is targeted to the cell nuclei in the human brain. *Biochim. Biophys. Acta. Gen. Subj.* **2017**, *1861*, 246–255. [CrossRef]

47. Hara, Y.; Yakovleva, T.; Bakalkin, G.; Pickel, V.M. Dopamine D1 receptors have subcellular distributions conducive to interactions with prodynorphin in the rat nucleus accumbens shell. *Synapse* **2006**, *60*, 1–19. [CrossRef] [PubMed]

48. Bottger, A.; Spruce, B.A. Proenkephalin is a nuclear protein responsive to growth arrest and differentiation signals. *J. Cell Biol.* **1995**, *130*, 1251–1262. [CrossRef]

49. McTavish, N.; Copeland, L.A.; Saville, M.K.; Perkins, N.D.; Spruce, B.A. Proenkephalin assists stress-activated apoptosis through transcriptional repression of NF-kappaB- and p53-regulated gene targets. *Cell Death. Differ.* **2007**, *14*, 1700–1710. [CrossRef] [PubMed]

50. Bakalkin, G.; Ponomariev, D.; Sarkisyan, R.A.; Terenius, L. Sequence similarity between opioid peptide precursors and DNA-binding proteins. *FEBS Lett.* **1991**, *282*, 175–177. [CrossRef]

51. Ota, T.; Suzuki, Y.; Nishikawa, T.; Otsuki, T.; Sugiyama, T.; Irie, R.; Wakamatsu, A.; Hayashi, K.; Sato, H.; Nagai, K.; et al. Complete sequencing and characterization of 21,243 full-length human cDNAs. *Nat. Genet.* **2004**, *36*, 40–45. [CrossRef]

52. Rockman, M.V.; Hahn, M.W.; Soranzo, N.; Zimprich, F.; Goldstein, D.B.; Wray, G.A. Ancient and recent positive selection transformed opioid cis-regulation in humans. *PLoS. Biol.* **2005**, *3*, 387. [CrossRef] [PubMed]

53. Carrion, A.M.; Link, W.A.; Ledo, F.; Mellström, B.; Naranjo, J.R. DREAM is a Ca2+-regulated transcriptional repressor. *Nature* **1999**, *398*, 80–84. [CrossRef]

54. Cheng, H.Y.; Pitcher, G.M.; Laviolette, S.R.; Whishaw, I.Q.; Tong, K.I.; Kockeritz, L.K.; Wada, T.; Joza, N.A.; Crackower, M.; Goncalves, J.; et al. DREAM is a critical transcriptional repressor for pain modulation. *Cell* **2002**, *108*, 31–43. [CrossRef]

55. Ledo, F.; Carrión, A.M.; Link, W.A.; Mellström, B.; Naranjo, J.R. DREAM-alphaCREM interaction via leucine-charged domains derepresses downstream regulatory element-dependent transcription. *Mol. Cell Biol.* **2000**, *20*, 9120–9126. [CrossRef]

56. Campos, D.; Jimenez-Diaz, L.; Carrion, A.M. Ca$^{(2+)}$-dependent prodynorphin transcriptional derepression in neuroblastoma cells is exerted through DREAM protein activity in a kinase-independent manner. *Mol. Cell Neurosci.* **2003**, *22*, 135–145. [CrossRef]

57. Bakalkin, G.; Telkov, M.; Yakovleva, T.; Terenius, L. [Leu5]enkephalin-encoding sequences are targets for a specific DNA-binding factor. *Proc. Natl. Acad. Sci. USA* **1995**, *92*, 9024–9028. [CrossRef] [PubMed]

58. Bakalkin, G.; Yakovleva, T.; Terenius, L. Prodynorphin gene expression relates to NF-kappa B factors. *Brain Res. Mol. Brain Res.* **1994**, *24*, 301–312. [CrossRef]

59. Bakalkin, G.; Yakovleva, T.; Terenius, L. The Leu-enkephalin-encoding sequence DNA-binding factor (LEF) is the transcription factor YY1. *Biochem. Biophys. Res. Commun.* **1997**, *231*, 135–139. [CrossRef] [PubMed]

60. McClung, C.A.; Ulery, P.G.; Perrotti, L.I.; Zachariou, V.; Berton, O.; Nestler, E.J. DeltaFosB: A molecular switch for long-term adaptation in the brain. *Brain Res. Mol. Brain Res.* **2004**, *132*, 146–154. [CrossRef] [PubMed]

61. Zachariou, V.; Bolanos, C.A.; Selley, D.E.; Theobald, D.; Cassidy, M.P.; Kelz, M.B.; Shaw-Lutchman, T.; Berton, O.; Sim-Selley, L.J.; Dileone, R.J.; et al. An essential role for DeltaFosB in the nucleus accumbens in morphine action. *Nat. Neurosci.* **2006**, *9*, 205–211. [CrossRef]

62. Taqi, M.M.; Bazov, I.; Watanabe, H.; Nyberg, F.; Yakovleva, T.; Bakalkin, G. Prodynorphin promoter SNP associated with alcohol dependence forms noncanonical AP-1 binding site that may influence gene expression in human brain. *Brain Res.* **2011**, *1385*, 18–25. [CrossRef]

63. Yuferov, V.; Ji, F.; Nielsen, D.A.; Levran, O.; Ho, A.; Morgello, S.; Shi, R.; Ott, J.; Kreek, M.J. A functional haplotype implicated in vulnerability to develop cocaine dependence is associated with reduced PDYN expression in human brain. *Neuropsychopharmacology* **2009**, *34*, 1185–1197. [CrossRef] [PubMed]

64. Preuss, U.W.; Winham, S.J.; Biernacka, J.M.; Geske, J.R.; Bakalkin, G.; Koller, G.; Zill, P.; Soyka, M.; Karpyak, V.M. PDYN rs2281285 variant association with drinking to avoid emotional or somatic discomfort. *PLoS ONE* **2013**, *8*, 78688. [CrossRef]

65. Zimprich, A.; Kraus, J.; Wöltje, M.; Mayer, P.; Rauch, E.; Höllt, V. An allelic variation in the human prodynorphin gene promoter alters stimulus-induced expression. *J. Neurochem.* **2000**, *74*, 472–477. [CrossRef]

66. Rouault, M.; Nielsen, D.A.; Ho, A.; Kreek, M.J.; Yuferov, V. Cell-specific effects of variants of the 68-base pair tandem repeat on prodynorphin gene promoter activity. *Addict. Biol.* **2011**, *16*, 334–346. [CrossRef]

67. Stogmann, E.; Zimprich, A.; Baumgartner, C.; Aull-Watschinger, S.; Höllt, V.; Zimprich, F. A functional polymorphism in the prodynorphin gene promotor is associated with temporal lobe epilepsy. *Ann. Neurol.* **2002**, *51*, 260–263. [CrossRef]

68. Chen, A.C.; LaForge, K.S.; Ho, A.; McHugh, P.F.; Kellogg, S.; Bell, K.; Schluger, R.P.; Leal, S.M.; Kreek, M.J. Potentially functional polymorphism in the promoter region of prodynorphin gene may be associated with protection against cocaine dependence or abuse. *Am. J. Med. Genet.* **2002**, *114*, 429–435. [CrossRef]

69. Zhang, C.S.; Tan, Z.; Lu, L.; Wu, S.N.; He, Y.; Gu, N.F.; Feng, G.Y.; He, L. Polymorphism of Prodynorphin promoter is associated with schizophrenia in Chinese population. *Acta. Pharmacol. Sin.* **2004**, *25*, 1022–1026.

70. Saify, K.; Saadat, I.; Saadat, M. Association between VNTR polymorphism in promoter region of prodynorphin (PDYN) gene and heroin dependence. *Psychiatry Res.* **2014**, *219*, 690–692. [CrossRef]

71. Ray, R.; Doyle, G.A.; Crowley, J.J.; Buono, R.J.; Oslin, D.W.; Patkar, A.A.; Mannelli, P.; DeMaria, P.A., Jr.; O'Brien, C.P.; Berrettini, W.H. A functional prodynorphin promoter polymorphism and opioid dependence. *Psychiatr Genet.* **2005**, *15*, 295–298. [CrossRef]

72. Nomura, A.; Ujike, H.; Tanaka, Y.; Otani, K.; Morita, Y.; Kishimoto, M.; Morio, A.; Harano, M.; Inada, T.; Yamada, M.; et al. Genetic variant of prodynorphin gene is risk factor for methamphetamine dependence. *Neurosci Lett.* **2006**, *400*, 158–162. [CrossRef]

73. Saify, K.; Saadat, M. Association between VNTR Polymorphism in Promoter Region of Prodynorphin (PDYN) Gene and Methamphetamine Dependence. *J. Med. Sci.* **2015**, *3*, 371–373. [CrossRef] [PubMed]

74. Williams, T.J.; LaForge, K.S.; Gordon, D.; Bart, G.; Kellogg, S.; Ott, J.; Kreek, M.J. Prodynorphin gene promoter repeat associated with cocaine/alcohol codependence. *Addict. Biol.* **2007**, *12*, 496–502. [CrossRef]

75. Bovo, G.; Diani, E.; Bisulli, F.; Di Bonaventura, C.; Striano, P.; Gambardella, A.; Ferlazzo, E.; Egeo, G.; Mecarelli, O.; Elia, M.; et al. Analysis of LGI1 promoter sequence, PDYN and GABBR1 polymorphisms in sporadic and familial lateral temporal lobe epilepsy. *Neurosci. Lett.* **2008**, *436*, 23–26. [CrossRef] [PubMed]

76. Dahl, J.P.; Weller, A.E.; Kampman, K.M.; Oslin, D.W.; Lohoff, F.W.; Ferraro, T.N.; O'Brien, C.P.; Berrettini, W.H. Confirmation of the association between a polymorphism in the promoter region of the prodynorphin gene and cocaine dependence. *Am. J. Med. Genet. B. Neuropsychiatr. Genet.* **2005**, *139*, 106–108. [CrossRef]

77. Hou, C.; Zhao, H.; Tanimoto, K.; Dean, A. CTCF-dependent enhancer-blocking by alternative chromatin loop formation. *Proc. Natl. Acad. Sci. USA* **2008**, *105*, 20398–20403. [CrossRef]

78. Majumder, P.; Gomez, J.A.; Chadwick, B.P.; Boss, J.M. The insulator factor CTCF controls MHC class II gene expression and is required for the formation of long-distance chromatin interactions. *J. Exp. Med.* **2008**, *205*, 785–798. [CrossRef]

79. Bazov, I.; Sarkisyan, D.; Kononenko, O.; Watanabe, H.; Taqi, M.M.; Stålhandske, L.; Verbeek, D.S.; Mulder, J.; Rajkowska, G.; Sheedy, D.; et al. Neuronal Expression of Opioid Gene is Controlled by Dual Epigenetic and Transcriptional Mechanism in Human Brain. *Cereb. Cortex.* **2018**, *28*, 3129–3142. [CrossRef]

80. Yuferov, V.; Nielsen, D.A.; Levran, O.; Randesi, M.; Hamon, S.; Ho, A.; Morgello, S.; Kreek, M.J. Tissue-specific DNA methylation of the human prodynorphin gene in post-mortem brain tissues and PBMCs. *Pharm. Genomics.* **2011**, *21*, 185–196. [CrossRef]

81. Doi, A.; Park, I.H.; Wen, B.; Murakami, P.; Aryee, M.J.; Irizarry, R.; Herb, B.; Ladd-Acosta, C.; Rho, J.; Loewer, S.; et al. Differential methylation of tissue- and cancer-specific CpG island shores distinguishes human induced pluripotent stem cells, embryonic stem cells and fibroblasts. *Nat. Genet.* **2009**, *41*, 1350–1353. [CrossRef]

82. Ciernia, A.V.; LaSalle, J. The landscape of DNA methylation amid a perfect storm of autism aetiologies. *Nat. Rev. Neurosci.* **2016**, *17*, 411–423. [CrossRef] [PubMed]

83. Liu, Y.; Li, X.; Aryee, M.J.; Ekström, T.J.; Padyukov, L.; Klareskog, L.; Vandiver, A.; Moore, A.Z.; Tanaka, T.; Ferrucci, L.; et al. GeMes, clusters of DNA methylation under genetic control, can inform genetic and epigenetic analysis of disease. *Am. J. Hum. Genet.* **2014**, *94*, 485–495. [CrossRef] [PubMed]

84. Naranjo, J.R.; Mellstrom, B. Ca^{2+}-dependent transcriptional control of Ca^{2+} homeostasis. *J. Biol. Chem.* **2012**, *287*, 31674–31680. [CrossRef] [PubMed]

85. Nguyen, C.; Liang, G.; Nguyen, T.T.; Tsao-Wei, D.; Groshen, S.; Lübbert, M.; Zhou, J.H.; Benedict, W.F.; Jones, P.A. Susceptibility of nonpromoter CpG islands to de novo methylation in normal and neoplastic cells. *J. Natl. Cancer Inst.* **2001**, *93*, 1465–1472. [CrossRef]

86. Ball, M.P.; Li, J.B.; Gao, Y.; Lee, J.H.; LeProust, E.M.; Park, I.H.; Xie, B.; Daley, G.Q.; Church, G.M. Targeted and genome-scale strategies reveal gene-body methylation signatures in human cells. *Nat. Biotechnol.* **2009**, *27*, 361–368. [CrossRef]

87. Moen, E.L.; Zhang, X.; Mu, W.; Delaney, S.M.; Wing, C.; McQuade, J.; Myers, J.; Godley, L.A.; Dolan, M.E.; Zhang, W. Genome-wide variation of cytosine modifications between European and African populations and the implications for complex traits. *Genetics* **2013**, *194*, 987–996. [CrossRef]

88. Tomso, D.J.; Bell, D.A. Sequence context at human single nucleotide polymorphisms: Overrepresentation of CpG dinucleotide at polymorphic sites and suppression of variation in CpG islands. *J. Mol. Biol.* **2003**, *327*, 303–308. [CrossRef]

89. Taqi, M.M.; Bazov, I.; Watanabe, H.; Sheedy, D.; Harper, C.; Alkass, K.; Druid, H.; Wentzel, P.; Nyberg, F.; Yakovleva, T.; et al. Prodynorphin CpG-SNPs associated with alcohol dependence: Elevated methylation in the brain of human alcoholics. *Addict. Biol.* **2011**, *16*, 499–509. [CrossRef]

90. Oertel, B.G.; Doehring, A.; Roskam, B.; Kettner, M.; Hackmann, N.; Ferreirós, N.; Schmidt, P.H.; Lötsch, J. Genetic-epigenetic interaction modulates mu-opioid receptor regulation. *Hum. Mol. Genet.* **2012**, *21*, 4751–4760. [CrossRef]

91. Pun, F.W.; Zhao, C.; Lo, W.S.; Ng, S.K.; Tsang, S.Y.; Nimgaonkar, V.; Chung, W.S.; Ungvari, G.S.; Xue, H. Imprinting in the schizophrenia candidate gene GABRB2 encoding GABA(A) receptor beta(2) subunit. *Mol. Psychiatry.* **2011**, *16*, 557–568. [CrossRef]

92. Ursini, G.; Bollati, V.; Fazio, L.; Porcelli, A.; Iacovelli, L.; Catalani, A.; Sinibaldi, L.; Gelao, B.; Romano, R.; Rampino, A.; et al. Stress-related methylation of the catechol-O-methyltransferase Val 158 allele predicts human prefrontal cognition and activity. *J. Neurosci.* **2011**, *31*, 6692–6698. [CrossRef]

93. Sigurdsson, M.I.; Smith, A.V.; Bjornsson, H.T.; Jonsson, J.J. HapMap methylation-associated SNPs, markers of germline DNA methylation, positively correlate with regional levels of human meiotic recombination. *Genome. Res.* **2009**, *19*, 581–589. [CrossRef]

94. Hellman, A.; Chess, A. Extensive sequence-influenced DNA methylation polymorphism in the human genome. *Epigenetics Chromatin.* **2010**, *3*, 11. [CrossRef]

95. Xie, H.; Wang, M.; Bischof, J.; Bonaldo, M.; Soares, M.B. SNP-based prediction of the human germ cell methylation landscape. *Genomics* **2009**, *93*, 434–440. [CrossRef]

96. Chong, J.A.; Tapia-Ramírez, J.; Kim, S.; Toledo-Aral, J.J.; Zheng, Y.; Boutros, M.C.; Altshuller, Y.M.; Frohman, M.A.; Kraner, S.D.; Mandel, G. REST: A mammalian silencer protein that restricts sodium channel gene expression to neurons. *Cell* **1995**, *80*, 949–957. [CrossRef]

97. Schoenherr, C.J.; Anderson, D.J. The neuron-restrictive silencer factor (NRSF): A coordinate repressor of multiple neuron-specific genes. *Science* **1995**, *267*, 1360–1363. [CrossRef]

98. Gerstein, M.B.; Kundaje, A.; Hariharan, M.; Landt, S.G.; Yan, K.K.; Cheng, C.; Mu, X.J.; Khurana, E.; Rozowsky, J.; Alexander, R.; et al. Architecture of the human regulatory network derived from ENCODE data. *Nature* **2012**, *489*, 91–100. [CrossRef]

99. Wang, J.; Zhuang, J.; Iyer, S.; Lin, X.; Whitfield, T.W.; Greven, M.C.; Pierce, B.G.; Dong, X.; Kundaje, A.; Cheng, Y.; et al. Sequence features and chromatin structure around the genomic regions bound by 119 human transcription factors. *Genome. Res.* **2012**, *22*, 1798–1812. [CrossRef] [PubMed]

100. Bruce, A.W.; Donaldson, I.J.; Wood, I.C.; Yerbury, S.A.; Sadowski, M.I.; Chapman, M.; Göttgens, B.; Buckley, N.J. Genome-wide analysis of repressor element 1 silencing transcription factor/neuron-restrictive silencing factor (REST/NRSF) target genes. *Proc. Natl. Acad. Sci. USA* **2004**, *101*, 10458–10463. [CrossRef]

101. Johnson, D.S.; Mortazavi, A.; Myers, R.M.; Wold, B. Genome-wide mapping of in vivo protein-DNA interactions. *Science* **2007**, *316*, 1497–1502. [CrossRef]

102. Rockowitz, S.; Lien, W.H.; Pedrosa, E.; Wei, G.; Lin, M.; Zhao, K.; Lachman, H.M.; Fuchs, E.; Zheng, D. Comparison of REST cistromes across human cell types reveals common and context-specific functions. *PLoS. Comput. Biol.* **2014**, *10*, 1003671. [CrossRef]

103. Tapia-Ramirez, J.; Eggen, B.J.; Peral-Rubio, M.J.; Toledo-Aral, J.J.; Mandel, G. A single zinc finger motif in the silencing factor REST represses the neural-specific type II sodium channel promoter. *Proc. Natl. Acad. Sci. USA* **1997**, *94*, 1177–1182. [CrossRef]

104. Henriksson, R.; Bäckman, C.M.; Harvey, B.K.; Kadyrova, H.; Bazov, I.; Shippenberg, T.S.; Bakalkin, G. PDYN, a gene implicated in brain/mental disorders, is targeted by REST in the adult human brain. *Biochim Biophys Acta.* **2014**, *1839*, 1226–1232. [CrossRef]

105. Packer, A.N.; Xing, Y.; Harper, S.Q.; Jones, L.; Davidson, B.L. The bifunctional microRNA miR-9/miR-9* regulates REST and CoREST and is downregulated in Huntington's disease. *J. Neurosci.* **2008**, *28*, 14341–14346. [CrossRef] [PubMed]

106. Yoo, A.S.; Staahl, B.T.; Chen, L.; Crabtree, G.R. MicroRNA-mediated switching of chromatin-remodelling complexes in neural development. *Nature* **2009**, *460*, 642–646. [CrossRef]

107. Brohl, D.; Strehle, M.; Wende, H.; Hori, K.; Bormuth, I.; Nave, K.A.; Müller, T.; Birchmeier, C. A transcriptional network coordinately determines transmitter and peptidergic fate in the dorsal spinal cord. *Dev. Biol.* **2008**, *322*, 381–393. [CrossRef]

108. Huang, M.; Huang, T.; Xiang, Y.; Xie, Z.; Chen, Y.; Yan, R.; Xu, J.; Cheng, L. Ptf1a, Lbx1 and Pax2 coordinate glycinergic and peptidergic transmitter phenotypes in dorsal spinal inhibitory neurons. *Dev. Biol.* **2008**, *322*, 394–405. [CrossRef] [PubMed]

109. Wildner, H.; Das Gupta, R.; Bröhl, D.; Heppenstall, P.A.; Zeilhofer, H.U.; Birchmeier, C. Genome-wide expression analysis of Ptf1a- and Ascl1-deficient mice reveals new markers for distinct dorsal horn interneuron populations contributing to nociceptive reflex plasticity. *J. Neurosci.* **2013**, *33*, 7299–7307. [CrossRef]

110. Lu, K.M.; Evans, S.M.; Hirano, S.; Liu, F.C. Dual role for Islet-1 in promoting striatonigral and repressing striatopallidal genetic programs to specify striatonigral cell identity. *Proc. Natl. Acad. Sci. USA* **2014**, *111*, 168–177. [CrossRef]

111. Kardon, A.P.; Polgár, E.; Hachisuka, J.; Snyder, L.M.; Cameron, D.; Savage, S.; Cai, X.; Karnup, S.; Fan, C.R.; Hemenway, G.M.; et al. Dynorphin acts as a neuromodulator to inhibit itch in the dorsal horn of the spinal cord. *Neuron* **2014**, *82*, 573–586. [CrossRef]

112. Huang, D.; Huang, D.; Grady, F.S.; Peltekian, L.; Geerling, J.C. Efferent projections of Vglut2, Foxp2, and Pdyn parabrachial neurons in mice. *J. Comp. Neurol.* **2020**. [CrossRef] [PubMed]

113. Jiang, H.K.; Owyang, V.V.; Hong, J.S.; Gallagher, M. Elevated dynorphin in the hippocampal formation of aged rats: Relation to cognitive impairment on a spatial learning task. *Proc. Natl. Acad. Sci. USA* **1989**, *86*, 2948–2951. [CrossRef]

114. Nguyen, X.V.; Masse, J.; Kumar, A.; Vijitruth, R.; Kulik, C.; Liu, M.; Choi, D.Y.; Foster, T.C.; Usynin, I.; Bakalkin, G.; et al. Prodynorphin knockout mice demonstrate diminished age-associated impairment in spatial water maze performance. *Behav. Brain Res.* **2005**, *161*, 254–262. [CrossRef] [PubMed]

115. Carey, A.N.; Lyons, A.M.; Shay, C.F.; Dunton, O.; McLaughlin, J.P. Endogenous kappa opioid activation mediates stress-induced deficits in learning and memory. *J. Neurosci.* **2009**, *29*, 4293–4300. [CrossRef] [PubMed]

116. Kolsch, H.; Wagner, M.; Bilkei-Gorzó, A.; Toliat, M.R.; Pentzek, M.; Fuchs, A.; Kaduszkiewicz, H.; van den Bussche, H.; Riedel-Heller, S.G.; Angermeyer, M.C.; et al. Gene polymorphisms in prodynorphin (PDYN) are associated with episodic memory in the elderly. *J. Neural Transm.* **2009**, *116*, 897–903. [CrossRef]

117. Yakovleva, T.; Marinova, Z.; Kuzmin, A.; Seidah, N.G.; Haroutunian, V.; Terenius, L.; Bakalkin, G. Dysregulation of dynorphins in Alzheimer disease. *Neurobiol. Aging.* **2007**, *28*, 1700–1708. [CrossRef]

118. Sandin, J.; Nylander, I.; Georgieva, J.; Schött, P.A.; Ogren, S.O.; Terenius, L. Hippocampal dynorphin B injections impair spatial learning in rats: A kappa-opioid receptor-mediated effect. *Neuroscience* **1998**, *85*, 375–382. [CrossRef]

119. Cippitelli, A.; Damadzic, R.; Frankola, K.; Goldstein, A.; Thorsell, A.; Singley, E.; Eskay, R.L.; Heilig, M. Alcohol-induced neurodegeneration, suppression of transforming growth factor-beta, and cognitive impairment in rats: Prevention by group II metabotropic glutamate receptor activation. *Biol. Psychiatry.* **2010**, *67*, 823–830. [CrossRef]

120. Kuzmin, A.; Chefer, V.; Bazov, I.; Meis, J.; Ögren, S.O.; Shippenberg, T.; Bakalkin, G. Upregulated dynorphin opioid peptides mediate alcohol-induced learning and memory impairment. *Transl. Psychiatry.* **2013**, *3*, 310. [CrossRef]

121. Kuzmin, A.; Liljequist, S.; Meis, J.; Chefer, V.; Shippenberg, T.; Bakalkin, G. Repeated moderate-dose ethanol bouts impair cognitive function in Wistar rats. *Addict. Biol.* **2012**, *17*, 132–140. [CrossRef]

122. Chefer, V.; Meis, J.; Wang, G.; Kuzmin, A.; Bakalkin, G.; Shippenberg, T. Repeated exposure to moderate doses of ethanol augments hippocampal glutamate neurotransmission by increasing release. *Addict. Biol.* **2011**, *16*, 229–237. [CrossRef]

123. Walker, B.M.; Koob, G.F. Pharmacological evidence for a motivational role of kappa-opioid systems in ethanol dependence. *Neuropsychopharmacology* **2008**, *33*, 643–652. [CrossRef]

124. Schlosburg, J.E.; Whitfield, T.W., Jr.; Park, P.E.; Crawford, E.F.; George, O.; Vendruscolo, L.F.; Koob, G.F. Long-term antagonism of kappa opioid receptors prevents escalation of and increased motivation for heroin intake. *J. Neurosci.* **2013**, *33*, 19384–19392. [CrossRef]

125. Nealey, K.A.; Smith, A.W.; Davis, S.M.; Smith, D.G.; Walker, B.M. kappa-opioid receptors are implicated in the increased potency of intra-accumbens nalmefene in ethanol-dependent rats. *Neuropharmacology* **2011**, *61*, 35–42. [CrossRef]

126. Kissler, J.L.; Sirohi, S.; Reis, D.J.; Jansen, H.T.; Quock, R.M.; Smith, D.G.; Walker, B.M. The one-two punch of alcoholism: Role of central amygdala dynorphins/kappa-opioid receptors. *Biol. Psychiatry* **2014**, *75*, 774–782. [CrossRef]

127. Bazov, I.; Sarkisyan, D.; Kononenko, O.; Watanabe, H.; Karpyak, V.M.; Yakovleva, T.; Bakalkin, G. Downregulation of the neuronal opioid gene expression concomitantly with neuronal decline in dorsolateral prefrontal cortex of human alcoholics. *Transl. Psychiatry* **2018**, *8*, 122. [CrossRef]

128. Bazov, I.; Sarkisyan, D.; Kononenko, O.; Watanabe, H.; Yakovleva, T.; Hansson, A.C.; Sommer, W.H.; Spanagel, R.; Bakalkin, G. Dynorphin and kappa-Opioid Receptor Dysregulation in the Dopaminergic Reward System of Human. *Alcoholics. Mol. Neurobiol.* **2018**, *55*, 7049–7061. [CrossRef]

129. Sarkisyan, D.; Hussain, M.Z.; Watanabe, H.; Kononenko, O.; Bazov, I.; Zhou, X.; Yamskova, O.; Krishtal, O.; Karpyak, V.M.; Yakovleva, T.; et al. Downregulation of the endogenous opioid peptides in the dorsal striatum of human alcoholics. *Front. Cell Neurosci.* **2015**, *9*, 187. [CrossRef]

130. De la Monte, S.M.; Kril, J.J. Human alcohol-related neuropathology. *Acta. Neuropathol.* **2014**, *127*, 71–90. [CrossRef]

131. Zahr, N.M.; Kaufman, K.L.; Harper, C.G. Clinical and pathological features of alcohol-related brain damage. *Nat. Rev. Neurol.* **2011**, *7*, 284–294. [CrossRef] [PubMed]

132. Sarkisyan, D.; Bazov, I.; Watanabe, H.; Kononenko, O.; Syvänen, A.C.; Schumann, G.; Yakovleva, T.; Bakalkin, G. Damaged reward areas in human alcoholics: Neuronal proportion decline and astrocyte activation. *Acta. Neuropathol.* **2017**. [CrossRef] [PubMed]

133. Robison, A.J.; Nestler, E.J. Transcriptional and epigenetic mechanisms of addiction. *Nat. Rev. Neurosci.* **2011**, *12*, 623–637. [CrossRef] [PubMed]

134. Nassel, D.R. Neuropeptide signaling near and far: How localized and timed is the action of neuropeptides in brain circuits? *Invert. Neurosci.* **2009**, *9*, 57–75. [CrossRef] [PubMed]

135. Gohler, T.; Reimann, M.; Cherny, D.; Walter, K.; Warnecke, G.; Kim, E.; Deppert, W. Specific interaction of p53 with target binding sites is determined by DNA conformation and is regulated by the C-terminal domain. *J. Biol. Chem.* **2002**, *277*, 41192–41203. [CrossRef]

136. Lai, J.; Ossipov, M.H.; Vanderah, T.W.; Malan, T.P.; Porreca, F. Neuropathic pain: The paradox of dynorphin. *Mol. Interv.* **2001**, *1*, 160–167.

137. Bazov, I.; Kononenko, O.; Watanabe, H.; Taqi, M.M.; Gerashchenko, G.; Yakovleva, T.; Bakalkin, G. Epigenetic mechanism of endogenous opioid peptide precursor prodynorphin upregulation in the brain of human alcoholics: Methylation of DNA in a single promoter nucleosome mediates USF2 effects. *Soc. Neurosci. Meet.* **2011**.

Mechanistic Characterization of the Pharmacological Profile of HS-731, a Peripherally Acting Opioid Analgesic, at the μ-, δ-, κ-Opioid and Nociceptin Receptors

Kristina Puls [1], Helmut Schmidhammer [2], Gerhard Wolber [1,*] and Mariana Spetea [2,*]

1 Department of Pharmaceutical Chemistry, Institute of Pharmcy, Freie Universität Berlin, Königin-Luise-Str. 2+4, D-14195 Berlin, Germany; kristina.puls@fu-berlin.de
2 Department of Pharmaceutical Chemistry, Institute of Pharmacy and Center for Molecular Biosciences Innsbruck (CMBI), University of Innsbruck, Innrain 80-82, 6020 Innsbruck, Austria; helmut.schmidhammer@uibk.ac.at
* Correspondence: gerhard.wolber@fu-berlin.de (G.W.); mariana.spetea@uibk.ac.at (M.S.); Tel.: +49-30-838-52686 (G.W.); +43-512-507-58277 (M.S.)

Abstract: Accumulated preclinical and clinical data show that peripheral restricted opioids provide pain relief with reduced side effects. The peripherally acting opioid analgesic HS-731 is a potent dual μ-/δ-opioid receptor (MOR/DOR) full agonist, and a weak, partial agonist at the κ-opioid receptor (KOR). However, its binding mode at the opioid receptors remains elusive. Here, we present a comprehensive in silico evaluation of HS-731 binding at all opioid receptors. We provide insights into dynamic interaction patterns explaining the different binding and activity of HS-731 on the opioid receptors. For this purpose, we conducted docking, performed molecular dynamics (MD) simulations and generated dynamic pharmacophores (dynophores). Our results highlight two residues important for HS-731 recognition at the classical opioid receptors (MOR, DOR and KOR), particular the conserved residue 5.39 (K) and the non-conserved residue 6.58 (MOR: K, DOR: W and KOR: E). Furthermore, we assume a salt bridge between the transmembrane helices (TM) 5 and 6 via K227$^{5.39}$ and E297$^{6.58}$ to be responsible for the partial agonism of HS-731 at the KOR. Additionally, we experimentally demonstrated the absence of affinity of HS-731 to the nociceptin/orphanin FQ peptide (NOP) receptor. We consider the morphinan phenol Y130$^{3.33}$ responsible for this affinity lack. Y130$^{3.33}$ points deep into the NOP receptor binding pocket preventing HS-731 binding to the orthosteric binding pocket. These findings provide significant structural insights into HS-731 interaction pattern with the opioid receptors that are important for understanding the pharmacology of this peripheral opioid analgesic.

Keywords: GPCR; opioid receptor; HS-731; peripheral opioid agonist; analgesia; binding; selectivity; molecular docking; molecular dynamics simulations

1. Introduction

Opioid receptors are membrane-bound receptors belonging to the family of G protein-coupled receptors (GPCRs) [1]. There are four opioid receptor subtypes, including the three classical opioid receptors, μ (MOR), δ (DOR) and κ (KOR), and the more recently discovered nociceptin/orphanin FQ peptide (NOP) receptor [1]. The central role of the opioid system (opioid receptors and their endogenous and exogenous ligands) in pain treatment has been long recognized, with activation of each opioid receptor subtype leading to pain relief [2,3]. Because of their therapeutic relevance, the opioid receptors are among the few GPCRs determined in different activation states [4].

The most common strategy for the treatment of severe pain is by targeting the MOR [2,3,5]. Clinically used MOR agonists (e.g., morphine, oxycodone and fentanyl) are capable of producing potent and effective analgesia, but they also cause unwanted

and numerous side effects, such as respiratory depression, constipation, sedation, nausea, tolerance, dependence and addiction [2–4]. Opioid misuse and opioid-induced overdoses and death have become a global medical and socioeconomical issue leading to the ongoing opioid epidemic [6,7]. Recently, it was reported that the overdose deaths from opioids was increased to 56,064 in 2020 in the USA [8]. Therefore, the development of safer analgesics with lower or no abuse liability and other undesirable side effects is highly needed [9–11]. Diverse approaches in the design of safer analgesics include targeting multiple receptors simultaneously (bi- and multifunctional ligands) [11–13], functional selectivity at GPCRs (biased agonists) [11,14–16] and peripheralization of opioid receptor agonists [2,11,17,18].

Opioid receptors are expressed in the central and peripheral nervous systems (CNS and PNS), and various non-neuronal tissues (immune, neuroendocrine and ectodermal cells) [2,3,19,20]. Preclinical and clinical studies have shown that selective activation of peripheral opioid receptors leads to effective pain relief and reduced CNS-mediated side effects [2,17,18,21–23]. Increasing the hydrophilicity of opioids to limit their access to the CNS, and thus to minimize the incidence of undesirable CNS effects comprises diverse chemical modifications, such as incorporation of quaternary or amphiphilic molecules, which contain hydrophilic and hydrophobic components, pH-sensitive activation of analgesic compounds and synthesis of peptide-derived analgesics. The goal of achieving analgesia while avoiding CNS penetration has focused on both small molecules and peptides [2,17,18,21,22,24].

Among the first generation of peripherally restricted opioid compounds was the MOR agonist loperamide [25] (clinically used in the control of diarrhea), which is completely excluded from the CNS by the action of P-glycoprotein [18]. Asimadoline [26], an amphiphilic molecule, was the first peripherally selective agonist with activity at the KOR evaluated in humans for the treatment of peripheral pain. Unfortunately, asimadoline did not achieve clinically relevant efficacy at doses that lacked CNS adverse effects [17,21]. Through computer simulations at low pH, the fluorinated fentanyl analogue, NFEEP, was identified as a potent antinociceptive activating specifically the MOR in acidified peripheral tissues and to lack the typical opioid side effects in animals [18,21,27]. Peripheral restriction can also be achieved with peptidic agonists that produce analgesia by activating the MOR or KOR in the periphery [17,22,28]. The most advanced peripherally restricted KOR agonist under clinical development for acute postoperative pain and chronic pain is the tetrapeptide CR845 (also known as difelikefalin) [17,22].

Chemical and pharmacological work from our laboratory in the field of peripheral opioid analgesics from the class of opioid morphinans targeted the attachment of amino acid residues and dipeptides at the C6 position of the centrally acting MOR agonist 14-*O*-methyloxymorphone [29–37]. It was established that inclusion of an ionizable group, such as amino acid residues and sulfate conjugates, in morphinans leads to increased hydrophylicity and consequently reduced penetration into the CNS, by having greater selectivity towards peripheral tissues [31,32,34,35,37–40]. Inclusion of an ionizable group, such as amino acid residues, leads to increased hydrophylicity and consequently reduced penetration into the CNS, by having greater selectivity towards peripheral tissues. Several zwitterionic analogues were profiled as very potent MOR/DOR agonists producing antinociception after systemic administration in various pain models in rodents (mice and rats) via activation of peripheral opioid receptors [37]. A prominent representative of the series is HS-731, the 6β-glycine substituted derivative of 14-*O*-methyloxymorphone (Figure 1) [29], showing high affinity, potent and full agonism at the MOR and DOR, and a weak, partial agonism at the KOR (Table 1). In addition, HS-731 has been demonstrated to effectively induce peripheral opioid antinociception in a multitude of pain conditions, including acute nociception (tail-flick test) [31], visceral pain (acetic acid-induced writhing assay) [34,37], inflammatory pain (formalin test [31,33] and carrageenan-induced hyperalgesia [32]), neuropathic pain (sciatic nerve ligation) [33] and migraine pain (eye-wiping trigeminal nociceptive test) [36] in rodents. In acute thermal nociception, HS-731 was up to 200-fold more potent than morphine and had similar potencies to fentanyl when given systemically subcutaneous (s.c.), with considerably long-lasting antinociceptive effects. A

significant and prolonged duration of the antinociceptive effect (up to 4 h) with a peripheral site of action was shown after oral administration of HS-731 to rats with carrageenan-induced inflammatory pain [32]. Recent data were reported on the absence of analgesic tolerance for HS-731 in rats upon chronic s.c. treatment for 14 days [23].
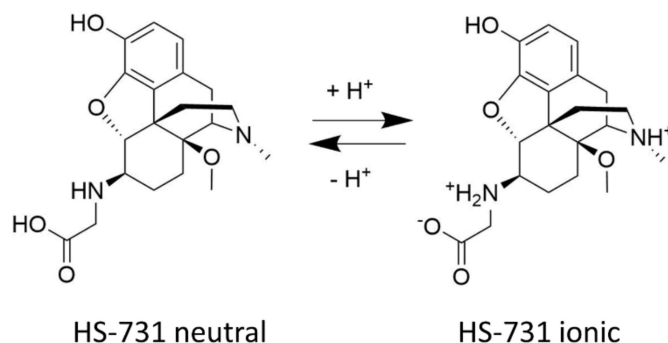
Figure 1. Structure of HS-731 and the acid-base equilibrium under physiological conditions.

Table 1. In vitro binding affinities and agonist activities of HS-731 at the opioid receptors.

Receptor	Rat Opioid Receptor	Human Opioid Receptor		
	Binding affinity K_i (nM)	Binding affinity K_i (nM)	Functional activity	
			EC_{50} (nM)	% stim.
MOR	0.83 ± 0.02 [a]	0.90 ± 0.14 [b]	3.78 ± 0.73 [b]	98 ± 9 [b]
DOR	7.86 ± 0.64 [a]	10.1 ± 2.7 [b]	7.92 ± 1.63 [b]	103 ± 7 [b]
KOR	44.8 ± 0.1 [a]	- [c]	361 ± 154 [b]	82 ± 9 [b]
NOP	- [c]	>10,000	- [d]	- [d]

[a] Binding affinities (K_i, nM) to the opioid receptors in the rat brain were determined in competitive radioligand binding assays; data from [30]. [b] Binding affinities (K_i, nM) to the human opioid receptors expressed in CHO cells were determined in competitive radioligand binding assays; data from [35]. Potencies (EC_{50}, nM) and efficacies (% stimulation expressed as percentage relative to the maximum effect of a selective, full opioid agonist) to the human opioid receptors expressed in CHO cells were determined in the [^{35}S]GTPγS binding assays; data from [35]. [c]—denotes not determined. [d]—denotes not applicable. Values are means $\pm$ SEM (n = 3 independent experiments performed in duplicate).

In the present study, we present the first mechanistic in silico investigation of the binding mode and interaction mechanisms of HS-731 to the three classical opioid receptors and rationalize why HS-731 does not bind to the NOP receptor.

2. Results and Discussion

2.1. HS-731 Shows No Specific Binding to the NOP Receptor

We have reported previously on the specific binding of HS-731 to the three classical opioid receptors, MOR, DOR and KOR, in the rat brain and to the recombinant human receptors expressed in Chinese hamster ovary (CHO) cells (Table 1). HS-731 shows high binding affinities in the low nanomolar range to the MOR and DOR, and reduced affinity to the KOR [30,35]. In the present study, the first data on the binding affinity of HS-731 to the NOP receptor is reported. Competitive inhibition of [^{3}H]nociceptin binding by HS-731 to the NOP receptor was assessed using in vitro competitive radioligand binding assays with membranes of CHO cells expressing the human NOP receptor. HS-731 displayed no substantial binding to the NOP receptor up to a concentration of 10 μM. In the same assay, the reference nociceptin ligand had a very high binding affinity ($K_i = 0.17 \pm 0.04$ nM) to the NOP receptor (Figure 2 and Table 1).
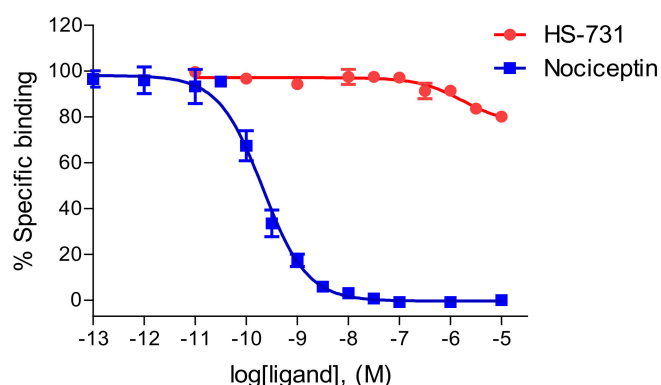
Figure 2. Binding curves of HS-731 to the human NOP receptor determined in the competitive radioligand binding assay. Concentration-dependent inhibition by HS-731 and nociceptin of [³H]nociceptin binding to membranes from CHO cells stably expressing the human NOP receptor. Values are means ± SEM (*n* = 3 independent experiments performed in duplicate).

2.2. Homology Modeling Is Suitable to Predict the Active State Human Nociceptin Receptor

In order to characterize binding of HS-731 in a comprehensive way, an investigation of both the inactive conformation, but also the active conformation is necessary. Since no active-state crystal structure of the NOP receptor is available we modeled the active state human NOP receptor structure using the crystal structure of the κ-opioid receptor (KOR, PDB-ID: 6B73 [41]). Model generation was carried out as described in the Section 3 and resulted in a model with a 0.7 Å root mean square deviation (RMSD) between the α-carbon atoms between NOP receptor and active conformation KOR template, indicating a correct global fold. The NOP receptor homology model contains no atom clashes and only two phi/psi angle outliers, suggesting a high-quality homology model (Figure 3, see Section 3 for details).
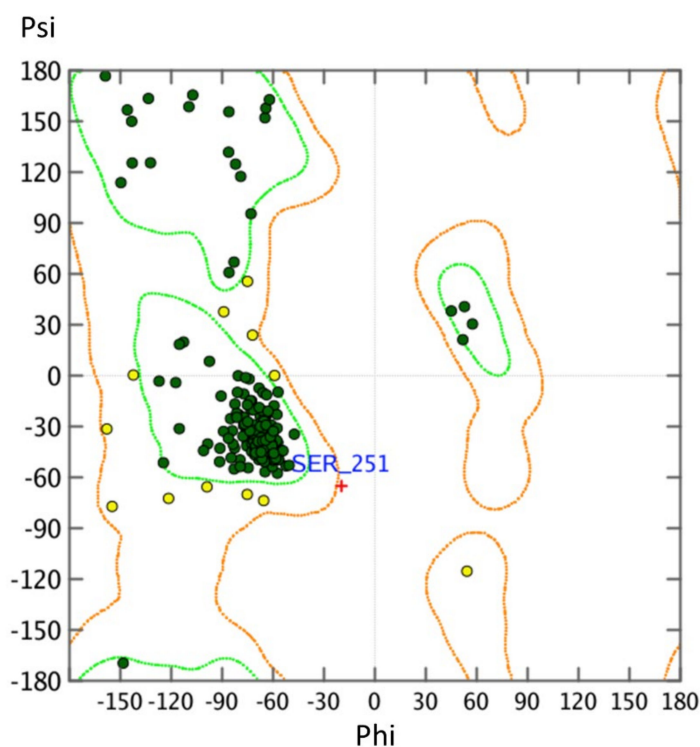
Figure 3. Ramachandran plot of the NOP receptor homology model. Angles within the orange range angles are plausible (yellow spheres) and angles within the green space are optimal (green spheres).

2.3. Water Molecules Are Important for HS-731 Binding to the Opioid Receptors

Water-mediated hydrogen bonds between ligand and receptor are known to occur within opioid receptor crystal structures [41–43]. Both MOR and DOR x-ray crystal structures [42,43] contain crystal water molecules. In the MOR, three polar interactions between ligand and protein are mediated by water molecules, namely those to K233[5.39], H297[6.52] and Y148[3.33] (the numbering refers to the mouse MOR; the respective residues in the human MOR are K235[5.39], H299[6.52] and Y150[3.33], superscripts denote Ballesteros-Weinstein numbering [44]) were reported [42]. Mutagenesis studies have revealed all three residues to be involved in MOR binding and selectivity [45]. Therefore, the water molecules in the MOR structure were retained. The DOR structure with PDB-ID 6PT2 published by Claff et al. [43] contains three water molecules, which mediate interactions to K214[5.39] and Y129[3.33]. In mutagenesis studies, Y129[3.33] was shown to contribute to affinity and activity of DOR agonists [43,46], while K214[5.39] contributes to agonist binding and selectivity [47]. Therefore, all three water molecules were retained. For the KOR, no crystal waters are experimentally resolved. 'Interaction potential maps' implemented in MOE were therefore used to identify a single potential conserved water position. The same workflow was applied to the NOP receptor homology model and the NOP receptor inactive crystal structure. For all three structures water molecule between the transmembrane helices 5 and 6 (TM5/TM6) were identified that are capable to mediate interactions to the backbone carbonyl of K5.39, an interaction highlighted previously in opioid receptors [41–43]. The predicted water molecule in the KOR occupies the same coordinates as a preserved water molecule present in the MOR (PDB-ID: 5C1M).

2.4. Docking Reveals a Common Binding Mode for HS-731 to the Opioid Receptors

HS-731 contains the same morphinan scaffold (Figure 4) as the co-crystallized ligands of the active X-ray crystal structures used in this study (KOR co-crystalized with MP1104, PDB-ID: 6B73 [41], and MOR co-crystalized with BU72, PDB-ID: 5C1M [42], Figure 4). In contrast, the active state DOR structure used in this study contains a peptidic ligand [43]. Nevertheless, MP1104 is known to be a potent agonist at the MOR, DOR and KOR [41,48]. Thus, a maximal scaffold overlay of HS-731 and MP1104 or BU72, and additionally a common binding mode within the opioid receptors was aimed.
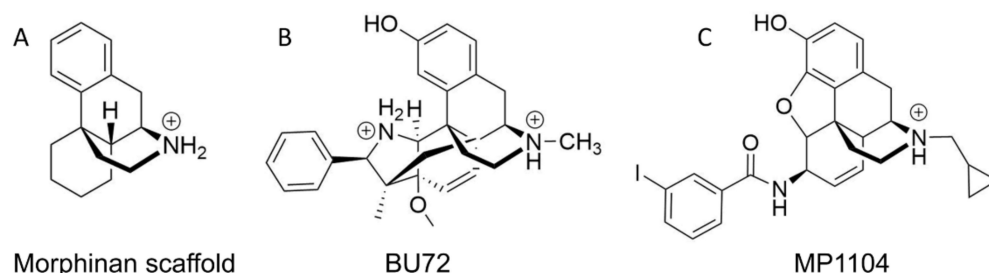
Figure 4. Chemical structures of (**A**) a morphinan scaffold and co-crystallized ligands (**B**) BU72 in MOR (PDB-ID: 5C1M) and (**C**) MP1104 in KOR (PDB-ID: 6B73) under physiological pH (7.4).

To obtain a common binding mode of HS-731 in all opioid receptors, we docked HS-731 into the prepared MOR, KOR, DOR x-ray crystal structures, as well as into the NOP receptor active state homology model and the NOP receptor inactive crystal structure. All protein structures contain water molecules in the TM5-6 region that is surmised to be important for ligand binding [41]. Docking revealed a common binding pose of HS-731 in the classical opioid receptors with the phenolic moiety establishing hydrogen bonding to the water molecules coordinating the K5.39 backbone carbonyl in TM5. The morphinan amine interacts with D3.32 via a salt bridge. The HS-731 carboxylate moiety points upwards to the extracellular domain (Figure 5A). An ionic interaction between the side chain of K5.39 and the carboxylate of HS-731 occurs in all the three classical opioid receptors. In the MOR, the carboxylate moiety also forms an ionic interaction with a second lysine positioned in

TM6 (K305$^{6.58}$). While K5.39 is conserved among the classical opioid receptors, residue 6.58 is not conserved, with the positively charged K305$^{6.58}$ in the MOR, neutral W284$^{6.58}$ in the DOR, and negatively charged E297$^{6.58}$ in the KOR. Thus, HS-731 is only able to form ionic interactions with both lysine residues in the MOR, explaining the highest affinity of HS-731 to this receptor. In contrast, HS-731 only can exhibit one ionic interaction to K5.39 in the KOR and DOR (Figure 5B–C).
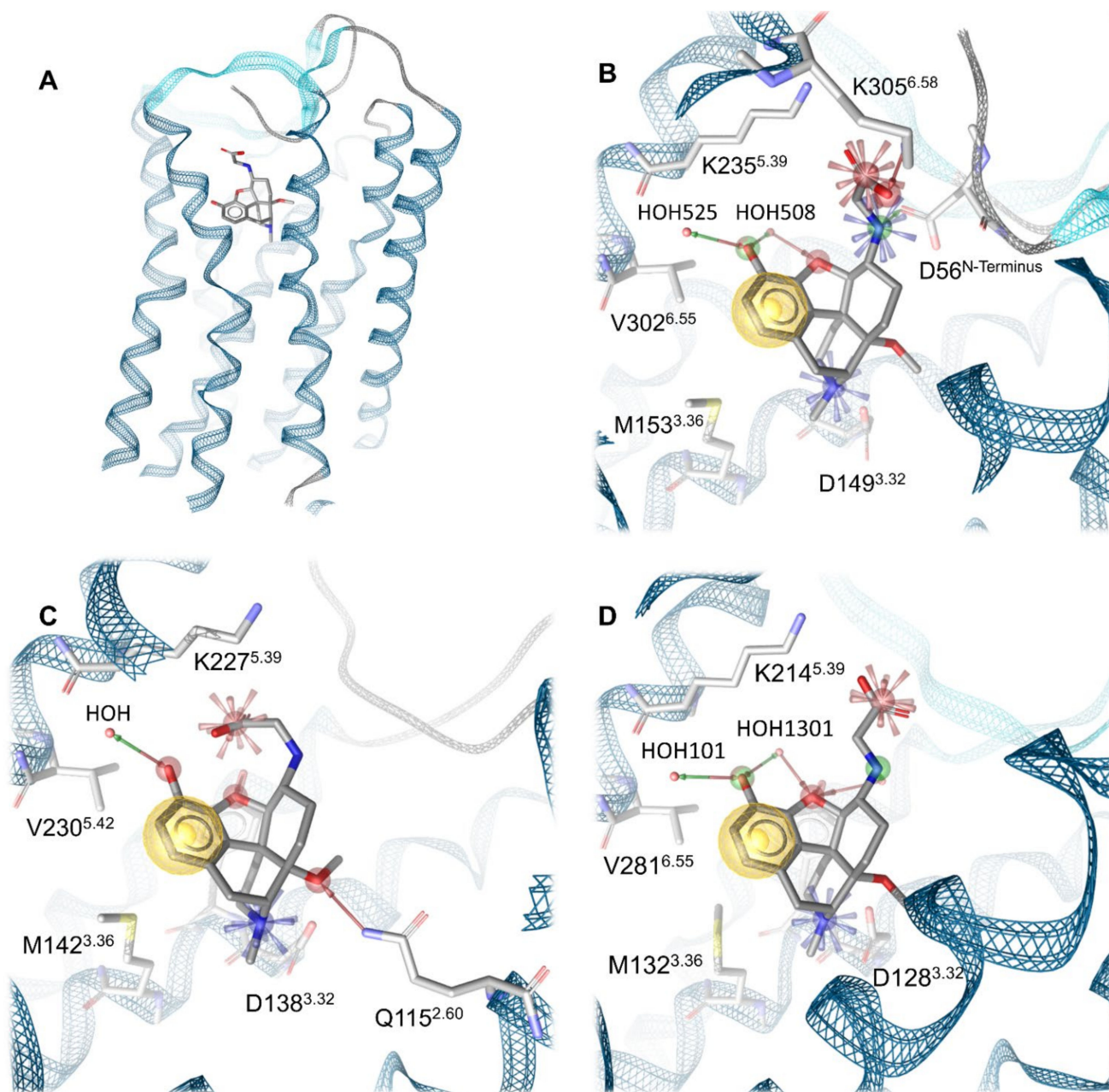
Figure 5. Binding modes of HS-731 to the classical opioid receptors. (**A**) Global view on the MOR binding pocket with docked HS-731. (**B**) Binding pocket of the MOR. Residues 297–303 and 322–325 are not shown for better visualization. (**C**) Binding pocket of the KOR. Residues 289–294 and 311–318 are not shown for better visualization. (**D**) Binding pocket of the DOR. Residues 275–282 are not shown for better visualization. Blue star indicates positive ionizable interactions, red stars negative ionizable interactions, yellow spheres lipophilic contacts, green arrow hydrogen bond donors and red arrows hydrogen bond acceptors. Water molecules are depicted as red spheres.

Even though residue 6.58 did not participate in an interaction with HS-731 in the KOR, it could have an influence on ligand binding. In the KOR, K227$^{5.39}$ and E297$^{6.58}$ could interact with each other in an ionic protein-protein-interaction. Subsequently the carboxylate of HS-731 would have to compete with E297$^{6.58}$ for K227$^{5.39}$ as interaction partner. This competition would likely weaken the strength of the ligand interaction to K227$^{5.39}$ and reduces HS-731's affinity to the KOR. The neutral W284$^{6.58}$ in the DOR cannot participate in an ionic interaction. Nonetheless, it could take part in a weaker π-cation interaction with K214$^{5.39}$. No geometrically plausible π-cation between W284$^{6.58}$ and K214$^{5.39}$ could be observed in our model. Subsequently, we surmise that W284$^{6.58}$ does not influence ligand binding resulting in a better affinity value compared to the KOR. Additionally the non-conserved residue 6.58 is a known selectivity-determinant at the classical opioid receptors [45,47,49], and therefore its influence on ligand binding could contribute to the affinity pattern of HS-731 at the opioid receptors.

A feature only visible in the binding hypothesis generated at the MOR is an ionic interaction between the secondary amine of HS-731 and D56 of the N-terminus. The MOR is currently the only solved opioid receptor crystal structure in which the N-terminus covers the binding site [42]. Thus, possible interactions between HS-731 and the N-terminus of the KOR or DOR were not detectable, even though the unresolved parts of the N-termini of both receptors contain negatively charged residues that could be oriented towards the binding pocket. Hence, the ionic interaction between the secondary amine of HS-731 and the N-terminus of the MOR was not investigated in this study.

Experimentally, HS-731 did not exhibit specific binding to the NOP receptor (Figure 2 and Table 1). Therefore, the generated binding hypothesis to the NOP receptor predominately served to give insights into the reasons for the lack of affinity to this receptor and to assess if HS-731 could be active in higher concentrations than experimentally tested. As there is no data about the activity profile of HS-731 at the NOP receptor available we conducted docking to the modeled active state NOP receptor as well as to the inactive state NOP receptor (crystal structure, PDB-ID: 5DGH). For the active state homology model no valid and plausible docking solution for the orthosteric binding pocket with the essential ionic interaction to D130$^{3.32}$ could be obtained. Residue Y130$^{3.33}$ is likely to cause this exclusion effect as it points deeper into the NOP receptor binding pocket than in the classical opioid receptors (Figure 6). A superimposition of NOP receptor with the classical opioid receptors in complex with HS-731 revealed atom clashes between the morphinan scaffold and Y130$^{3.33}$ (Figure 6). This steric hindrance precludes HS-731 from binding to the active state NOP receptor orthosteric binding pocket. Additionally, Akuzawa et al. [50] demonstrated abolished binding of the endogenous ligand nociceptin to the NOP receptor mutant Q280A, which indicates an important role of Q280 in anchoring NOP agonists. Residue Q280 is positioned deep in the orthosteric binding pocket; therefore, it could not mediate HS-731 binding to the active conformation of the NOP receptor. Also, for the inactive state NOP receptor (as obtained from the crystal structure with PDB-ID 5DGH), no reasonable binding mode could be obtained. The binding site in the inactive NOP receptor conformation is enlarged allowing HS-731 to bind to the lower part of the orthosteric binding pocket as does the co-crystallized antagonist C-35. However, HS-731 adopted a different orientation within the binding pocket and exhibited a distinct interaction pattern compared to known NOP antagonists [51,52] as no 3D pharmacophore overlay could be detected (Figure S2). Furthermore, HS-731 was not able to stabilize its two charged moieties outside the morphinan scaffold in ionic interactions resulting in an enthalpically unfavorable binding mode. Unlike endorphins, enkephalins and dynorphins, the endogenous NOP receptor ligand nociceptin contains FGGF instead of YGGF in its message domain [50,51,53]. The additional hydroxyl group is considered to function as a discriminator feature between classical opioid receptors and the NOP receptor [51] with dynorphin A (Y^1) showing no activity at the NOP receptor [54]. The phenyl group of nociceptin is considered to point deeply into the orthosteric binding pocket [51]. The discriminative hydroxyl group of HS-731 was similarly oriented further indicating an implausible binding mode for HS-731.
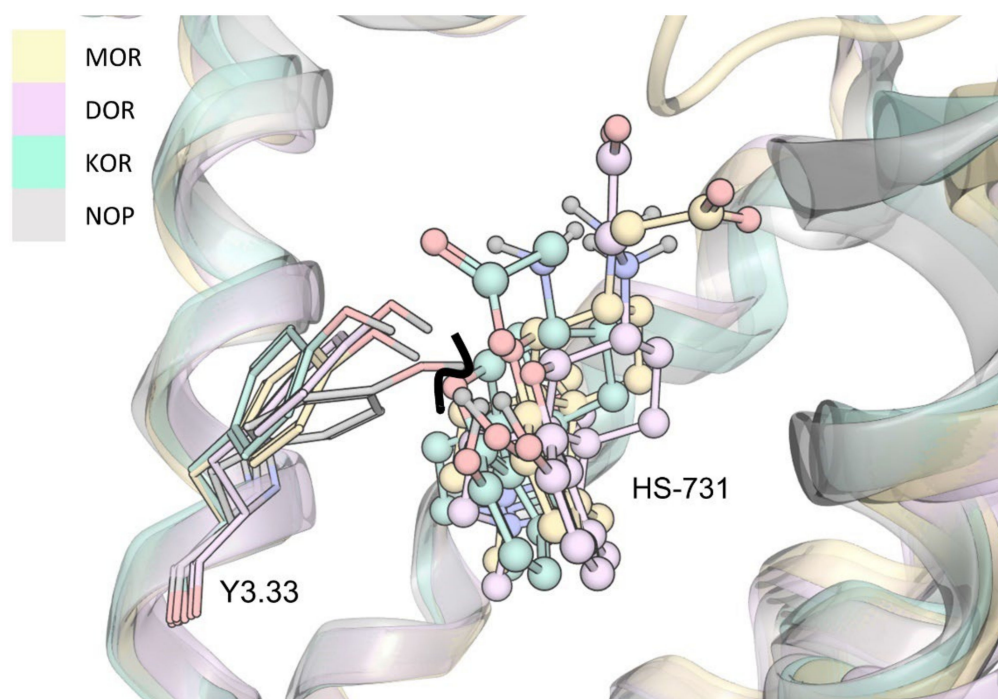
Figure 6. Superimposition of the NOP receptor and the classical opioid receptors in complex with HS-731. Atom clash is indicated by the bold black line.

Altogether, the absence of affinity of HS-731 to the NOP receptor is in line with reports indicating that NOP ligands often exhibit binding and activity patterns to the NOP receptor not observed in the classical opioid receptors [1]. Furthermore, the lack of plausible docking poses implies inactivity of HS-731 to the NOP receptor even for high ligand concentrations. Hence, the binding poses at the NOP receptor were not further assessed in MD simulations.

2.5. Molecular Dynamics Simulations Revealed Additional Interactions for HS-731 Binding to the Opioid Receptors

To obtain dynamic information for the opioid receptor-HS-731 complexes, we performed MD simulations and analyzed the interactions using the in-house developed Dynophore software [55], that calculates dynamic pharmacophores ('dynophores'). Table 2 shows the frequency of the ionic interactions between HS-731 and the three opioid receptors, MOR, DOR and KOR, during the simulations performed. Notably, the salt bridge between the morphinan amine and D3.32 that is known to be crucial for binding of positively charged ligands [56,57] occurred in 100% of the trajectory. In the case of the MOR, MD simulations resulted in the same four ionic interactions observed in the static model. The ionic interactions occurred with high frequencies, suggesting strong salt bridges between HS-731 and the MOR binding pocket (Table 2). Dynophore analysis obtained from the DOR and KOR complexes with HS-731 revealed additional, ionic interactions between the ligand and extracellular loops (DOR: R291[ECL3]; KOR: K200[ECL2]) that were not seen in the static model. The occurrence of ionic interactions with residues of the ECLs could be explained by a tilt of the loops towards the binding pocket during the simulations. Moreover, dynophore analysis revealed four stabilizing ionic interactions between ligand and protein in case of the KOR, but only three in case of the DOR (Table 2). Furthermore, the frequency of the ionic interaction between the morphinan amine and K5.39 is as frequent in the KOR as in the DOR, even though a lower frequency in case of the KOR was predicted due to possible intramolecular interaction between K227[5.39] and E297[6.58] as discussed in Section 2.4. The last two findings seem in disagreement with the higher affinity of HS-731 towards the DOR than to the KOR (Table 1). To explain these observations, we analyzed the geometry of

the stabilizing salt bridges between HS-731 and the opioid receptors residues (Table 2) as described in the next section.

Table 2. Ionic interaction occurrence between HS-731 and the three classical opioid receptors during MD simulations.

Interaction Type	Interaction Partners			
	HS-731	MOR	DOR	KOR
Cationic interaction	morphinan amine	D149$^{3.32}$ (100%)	D128$^{3.32}$ (100%)	D138$^{3.32}$ (100%)
Cationic interaction	secondary amine	D56$^{\text{N-terminus}}$ (73.7%)	Not present	E209$^{\text{ECL2}}$ (12.5%)
Anionic interaction	Carboxylate	K235$^{5.39}$ (81.3%)	K214$^{5.39}$ (65.0%)	K227$^{5.39}$ (63.3%)
		K305$^{6.58}$ (75.0%)	R291$^{\text{ECL3}}$ (9.2%)	K200$^{\text{ECL2}}$ (15.7%)

The frequency is given as an average of five simulation replicates per system.

Detailed root-mean-square deviation (RMSD) plots of HS-731 and the protein backbone can be found in the Supplementary Materials (Figures S3–S8). Additionally, the supportive information provide a comparison of the binding modes of HS-731 at the end of the simulation time with the docking pose (Figures S9–S11).

2.6. Interaction Distance Assessment Confirms Binding Hypothesis

We measured the distances between the interaction partner atoms to examine the quality of the ionic interactions occurring during MD simulations. Ionic interactions are known to be strongly distance-dependent and the energy of ionic interactions is determined by an exponential term, i.e., the strength of the interaction decreases rapidly by increasing distance [58]. The distance measurement between the carboxylate moiety of HS-731 and K5.39 at the MOR revealed short distances throughout the majority of the MD simulation (Figure 7A). The large extent of strong interactions implies stable ligand binding over the simulation time and the higher amount compared to the other opioid receptors contributes to the superior affinity of around one order of magnitude exhibited at the MOR.

The corresponding distance assessment at the DOR and KOR revealed far more short-distance interactions at the DOR than at the KOR (Figure 7B). Thus, even though the interaction frequency at the DOR and KOR was very similar, the interaction was much stronger at the DOR, explaining the increased affinity of HS-731 at the DOR compared to the KOR (Table 1). Additional interactions between the carboxylate and the basic residues in the ECLs in both receptors (R291$^{\text{ECL3}}$ in the DOR, K200$^{\text{ECL2}}$ in the KOR) only occurred with low frequency and long interaction distances rendering their effect on ligand binding negligible (Figure S12A). The ionic interaction in the KOR between E209$^{\text{ECL2}}$ and the secondary amine of HS-731 also only occurred with low frequency and again the distance assessment revealed mostly long distances, rendering its effect on ligand binding trivial (Figure S12B).

To explain the activity profile of HS-731 as a partial agonist at the KOR (Table 1), the possible interaction between K227$^{5.39}$ and E297$^{6.58}$ to the KOR was assessed. This is because a salt bridge between K227$^{5.39}$ and E297$^{6.58}$ at the KOR is assumed to hamper KOR activation in that the interaction between the TM5 and TM6 hinders TM6 from its outward movement [59]. At the same time, the translocation of TM6 is important for receptor activation at GPCRs like the opioid receptors [4,60] and interactions between TM5 and TM6 are considered to hamper activation in other GPCRs [61]. This hypothesis is supported by the fact that the salt bridge between K227$^{5.39}$ and E297$^{6.58}$ at the KOR only occurs in the inactive conformation (PDB-ID: 4DJH [56]), but was broken up in the active crystal structure (PDB ID: 6B73 [41]). The partial adoption of an intermediate state conformation with a less pronounced outward movement due to K227$^{5.39}$–E297$^{6.58}$ interaction would explain the partial agonism of HS-731 at the KOR. Our simulation shows that the two residues

interact with each other during 45.6% of the time indicating that the surmised intermediate state is indeed relevant. Furthermore, the proposed hindered TM6 outward movement at KOR was confirmed by a distance measurement between the alpha carbonyl atoms of the opposing residues 6.31 at the bottom of TM6 (MOR: R278[6.31], DOR: R257[6.31], KOR: R270[6.31]) and 4.40 at the bottom of TM4 (MOR: R184[4.40], DOR: A163[4.40], KOR: L173[4.40]) over the simulation time (Figure 8). Thus, the K227[5.39]–E297[6.58] interaction appears to induce a less active conformation at KOR explaining the observed partial agonism of HS-731 at the KOR. A comparison between the active state KOR (PDB-ID: 6B73) and one exemplary intermediate state conformation can be found in the Supplementary Materials (Figure S13).
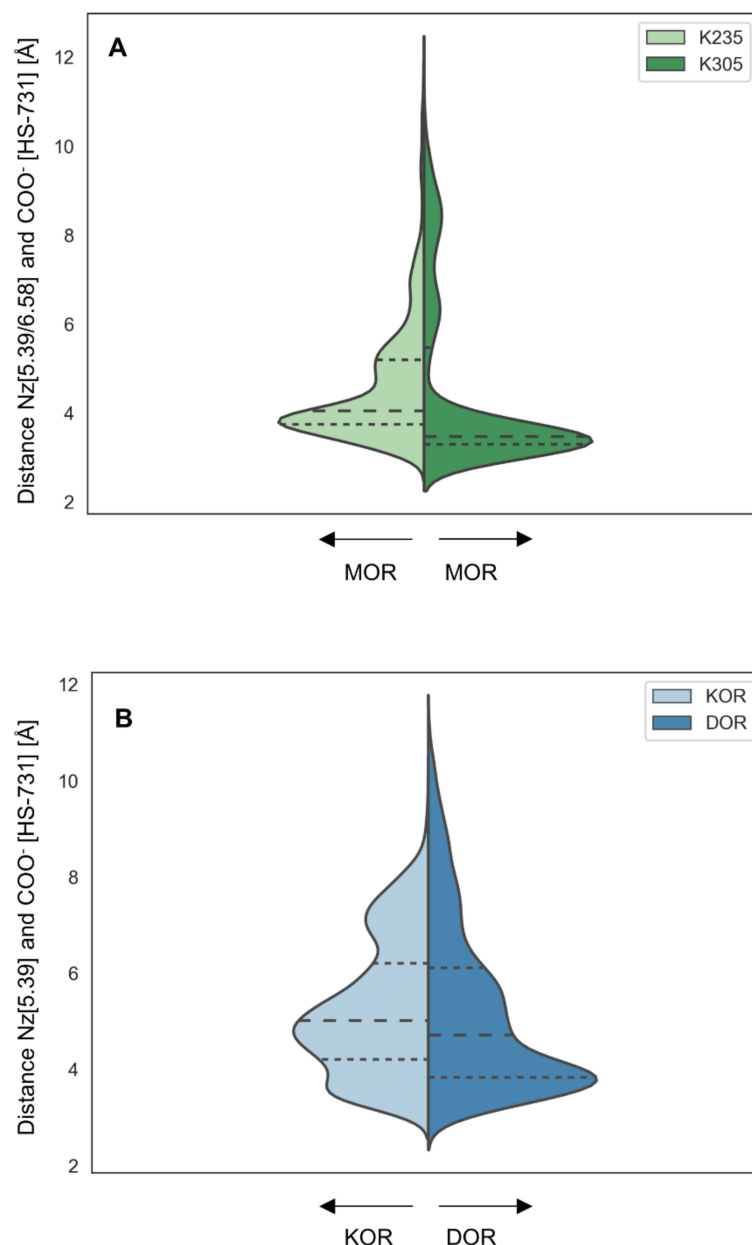
Figure 7. Ionic interaction distances. (**A**) Distances between K235[5.39] (Nz) or K305[6.58] (Nz) in the MOR and the carboxylate of HS-731. (**B**) Distances between K227[5.39] (KOR, Nz) or K214[5.39] (DOR, Nz) and the carboxylate moiety of HS-731. Dashed lines represent quantile. The width of the plot corresponds to the frequency of the measured distance.
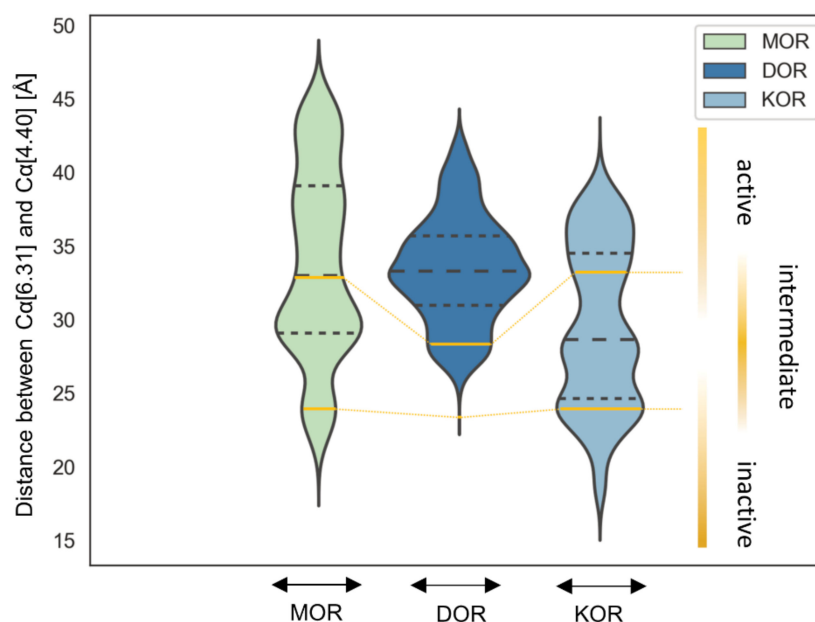
Figure 8. TM6 translocation. Measurement between the alpha carbon atoms of 6.31 at the bottom of TM6 (MOR: R278[6.31], DOR: R257[6.31], KOR: R270[6.31]) and 4.40 at the bottom of TM4 (MOR: R184[4.40], DOR: A163[4.40], KOR: L173[4.40]) over the simulation time. The width of the plot corresponds to the frequency of the measured distance. Dashed black lines represent quantile. Yellow solid lines indicate the analog measured distances at the active state crystal structures (PDB-ID: 5C1M for MOR, 6PT2 for DOR and 6B73 for KOR) and inactive state crystal structures (PDB-ID: 4DKL for MOR, 4N6H for DOR and 4DJH for KOR).

In the case of the MOR and DOR, which do not exhibit negatively charged residues in the upper half of TM6, no similar interaction occurred, in accordance with the HS-731 full agonism observed at these receptors (Table 1). To ensure that all influencing factors for TM5–TM6 interactions in the DOR were properly considered, the occurrence of cation–π-interactions between W284[6.58] and K214[5.39] were determined. As surmised this interaction was not detectable in MD simulations confirming the hypothesis of partial agonism in the presence of TM5–TM6 interactions.

Definition of the intermediate state for all opioid receptors based on the TM6 deflection measured between the alpha carbonyl atoms of the opposing residues 6.31 and 4.40 at the respective active state crystal structures (PDB-ID: 5C1M for MOR, 6PT2 for DOR and 6B73 for KOR) and inactive state crystal structures (PDB-ID: 4DKL for MOR, 4N6H for DOR and 4DJH for KOR) clearly indicates a maximum within the intermediate area for KOR, but also for MOR while DOR only very rarely adopts such a state (Figure 8). Nonetheless, the number of intermediate state conformations observed for all three opioid receptors during the simulation time reflects the order of activation potential measured in the [35S]GTPγS binding assay (Table 1). The KOR-HS-731 complex exhibits 51.9% of the time an intermediate state conformation corresponding to 82% stimulation in the [35S]GTPγS binding assay and partial agonism. The MOR-HS-731 complex in contrast only adopts an intermediate conformation in 44.6% of the simulation time correlating to 98% stimulation in the [35S]GTPγS binding assay and full agonism. The DOR-HS-731 complex reaches 103% stimulation in the [35S]GTPγS binding assay and full agonism with only 5.3% intermediate states.

3. Materials and Methods

3.1. Chemicals and Materials

HS-731 was prepared as previously described [29]. Radioligand [3H]nociceptin (119.4 Ci/mmol) was purchased from PerkinElmer (Boston, MA, USA). Tris(hydroxymethyl)

aminomethane (Tris), bovine serum albumin (BSA) polyethylenimine (PEI) and nociceptin were obtained from Sigma-Aldrich Chemicals (St. Louis, MO, USA). Cell culture media and supplements were obtained from Sigma-Aldrich Chemicals (St. Louis, MO, USA). All other chemicals were of analytical grade and obtained from standard commercial sources. Test compounds were prepared as 1 mM stocks in water and further diluted to working concentrations in 50 mM Tris-HCl buffer (pH 7.4).

3.2. Cell Culture and Membrane Preparation

CHO cells stably expressing the human NOP receptor (CHO-hNOP cell line) was kindly provided by Dr. Lawrence Toll (SRI International, Menlo Park, CA, USA). CHO-hNOP cells were grown at 37 °C in Dulbecco's Modified Eagle's Medium (DMEM) culture medium supplemented with 10% fetal bovine serum (FBS), 0.1% penicillin/streptomycin, 2 mM L-glutamine and 0.4 mg/mL geneticin (G418). Cells were maintained in a humidified atmosphere of 95% air and 5% CO_2. Membranes from CHO-hNOP cells were prepared as described previously [62]. Briefly, CHO-hNOP cells grown at confluence were removed from the culture plates by scraping, homogenized in 50 mM Tris-HCl buffer (pH 7.7) using a Polytron homogenizer, then centrifuged once and washed by an additional centrifugation at 27,000× g for 15 min at 4 °C. The final pellet was resuspended in 50 mM Tris-HCl buffer (pH 7.7) and stored at –80 °C until use. Protein content of cell membrane preparations was determined by the method of Bradford using BSA as the standard [63].

3.3. [^{3}H]NOP Receptor Binding Assay

Competitive binding assays at the human NOP receptor stably transfected into CHO cells were performed according to the published procedure [62]. Cell membranes (15 μg) were incubated in 50 mM Tris-HCl buffer (pH 7.4) with [^{3}H]nociceptin (0.1 nM) and various concentrations of test compounds in a final volume of 1 mL, for 60 min at 25 °C. Non-specific binding was determined using 10 μM of unlabeled nociceptin. After incubation, reactions were terminated by rapid filtration through 0.5% PEI-soaked Whatman GF/C glass fiber filters. Filters were washed three times with 5 mL of ice-cold 50 mM Tris-HCl buffer (pH 7.4) using a Brandel M24R cell harvester (Brandel, Gaithersburg, MD, USA). Radioactivity retained on the filters was counted by liquid scintillation counting using a Beckman Coulter LS6500 (Beckman Coulter Inc., Fullerton, CA, USA). Inhibition constant (K_i, nM) values were determined by the method of Cheng and Prusoff [64] from concentration-response curves by nonlinear regression analysis using the GraphPad Prism 5.0 Software (GraphPad Prism Software Inc., San Diego, CA, USA). All experiments were performed in duplicate and repeated three times with independently prepared samples. Data are presented as means ± SEM.

3.4. Protein Preparation and Modeling of the KOR Active Conformation

For classical opioid receptors, X-ray crystal structures of the active state proteins are published and provided in the protein data bank (PDB [65]). The respective structures with PDB-IDs 5C1M for the MOR [42], 6PT2 for the DOR [43] and 6B73 for the KOR [41] were prepared using MOE v2020.0901 [66]. The X-ray crystal structure of the inactive state NOP receptor (PDB-ID: 5DGH) was prepared analog. Only the chain with the best resolution was processed. Fusion proteins (antibody fragment in MOR, thermostabilized cytochrome b562 (BRIL) in the DOR, nanobody in the KOR) and the unresolved parts of the N-terminus, as well as of the C-terminus of the opioid receptors were deleted. Thermostabilizing mutations in the DOR and KOR were subsequently reverted to the human wild-type sequence obtained from the UniProt-Databank [67] (human DOR: P41143, human KOR: P41145). The MOR structure (PDB-ID: 5C1M) is of a murine receptor. Hence, the sequence was manually mutated to obtain the human wild-type MOR model (UniProt-ID: P35372). The NOP receptor structure already contained the human sequence. Missing side chain atoms were automatically generated using the protein builder integrated in MOE. The unresolved parts of ECL2, ECL3 and ICL3 of the KOR and ICL2 of the NOP receptor were

modeled using the loop modeler panel within MOE. To obtain high quality structures, Ramachandran outliers [68] and atom clashes were resolved using energy minimization with the OPLS-AA force field [69].

Homology modeling of the active state NOP receptor was performed using MOE v2020.0901 with default settings in a similar as described in [70]. The chain with the best resolution (3.10 Å) of the active KOR structure (PDB-ID: 6B73, sequence identity of 59% and sequence similarity of 73%) with the NOP receptor (Figure S1) served as a template. The protein target sequence (human NOP receptor) was obtained from the UniProt-Database (human NOP receptor P41146). Both Ramachandran outliers as shown in Figure 3 are located in flexible loops far away from the binding site (T206 of extracellular loop 2, ECL2, and S251 of intracellular loop 3, ICL3). Hence, we assume that these Ramachandran outliers are unlikely to influence ligand binding. Visual inspection revealed that the side chain orientations of the residues forming the orthosteric binding pocket, including D3.32 (number denote Ballesteros–Weinstein numbering [44]), responsible for the crucial ionic interaction between opioids and their receptors, show a similar orientation in the generated model as in the template.

'Interaction potential maps' as implemented in MOE v2020.0901 were used to determine putatively relevant water molecules inside the binding site of the KOR (resolution too low to determine co-crystallized waters) and the NOP receptor (homology model without water coordinates; too low resolution in the crystal structure). The interaction potential is an energy-based function that probes water molecules within the protein and calculates the interaction energy between water molecule and protein [66]. For this calculation the KOR binding site was defined as all residues within 4.5 Å around the crystalized ligand MP1104 in the KOR structure (PDB-ID: 6B73). Since the KOR and NOP receptor share a high sequence identity (59%) the same resides were used to define the NOP binding site in the active state homology model. For the NOP receptor crystal structure again, all residues within 4.5 Å around the crystalized ligand C-35 were used.

3.5. Protein-Ligand Docking

The starting conformation of HS-731 (IUPAC name: 2-[(4,5α-epoxy-3-hydroxy-14β-methoxy-17-methylmorphinan-6β-yl)amino]acetic acid) was generated using Corina v3.00 [71,72]. All five opioid receptor structures were protonated at a pH of 7.0 using the protonate 3D function [73] included in MOE (v2020.0901). GOLD v5.2 [74] was used for docking HS-731 into the receptors. The binding site was defined as a 20 Å sphere around the side chain carboxylate C (γC)-atom of D3.32 and restricted to the solvent-accessible surface. Pyramidal nitrogen atoms in the ligand were allowed to flip during the docking process. A total of 30 genetic algorithm runs per receptor structure were performed, generating diverse solutions (the root mean square deviation between docking poses was more than 1.5 Å). The generated binding hypotheses were scored using the GoldScore docking function [75,76]. The search efficiency was held at 100%. A constraint maintaining a maximum distance of 5.5 Å between the nitrogen in the morphinan scaffold and the γC-atom of D3.32 was set to ensure a crucial ionic interaction [41,56,57,77].

The obtained binding poses were energy-minimized in the protein environment using the MMFF94 force field [78] implemented in LigandScout v4.4.3 [79,80]. The binding poses of HS-731 in complex with the MOR, DOR and KOR were visually inspected and filtered according to the reported binding mode of the morphinan scaffold of opioid agonist BU72 co-crystallized with the MOR (PDB-ID: 5C1M [42]) and the morphinan scaffold of the opioid agonist MP1104 co-crystallized with the KOR (PDB-ID: 6B73 [41]). Additionally, MP1104-KOR interactions were used to score the DOR docking results as MP1104 also exhibits full agonism at the DOR. The relevant interactions are summarized in Table 3. Rescoring of the MOR and KOR clearly identified one docking result as most plausible that was chosen for further evaluation. At the DOR however, several docking results were scored equal. Thus, the pose with the lowest distance between the positively charged

nitrogen in the morphinan scaffold and the carboxylate of D3.32 out of the best scored docking results was chosen at the DOR.

Table 3. Ligand–receptor interactions used for rescoring of docking results.

Interaction	BU72	MP1104		
	MOR	DOR	KOR	NOP
PI	D149$^{3.32}$	D128$^{3.32}$	D138$^{3.32}$	D130$^{3.32}$
HY	M153$^{3.36}$	M132$^{3.36}$	M142$^{3.36}$	M134$^{3.36}$
HY	V238$^{5.42}$	V217$^{5.42}$	V230$^{5.42}$	I219$^{5.42}$
HY	I298$^{6.51}$	-	-	-
HY	V302$^{6.55}$	V281$^{6.55}$	I294$^{6.55}$	283$^{6.55}$
HY	W320$^{7.35}$	-	-	-
HBA	-	Y129$^{3.33}$	Y139$^{3.33}$	-
HBA/HBD	HOH525/508	HOH101/1301/1302	HOH	HOH

PI, positive ionizable interaction; HY, hydrophobic interaction; HBA, hydrogen bond acceptor; HBD, hydrogen bond donor; HOH refers to water molecules.

None of the crystallized opioid ligands exhibit agonist activity to the NOP receptor, but due to high identity and similarity to the classical opioid receptors (Figure S1) a similar binding mode of HS-731 in all active state opioid receptors was assumed. MP1104 shares the morphinan scaffold of HS-731 and an alignment and superposition of the KOR crystal structure and the NOP receptor homology model revealed the same orientation of the residues that interact with MP1104 in the MP1104-KOR-complex and their NOP receptor equivalent, with the exception of Y131$^{3.33}$. Therefore, the binding poses were evaluated according to the geometry of the other interactions detected in the MP1104-KOR complex (Table 3). For the inactive state NOP receptor (PDB-ID: 5DGH) the orientation and interaction pattern of the cocrystallized ligand C-35 was used to evaluate the docking poses. C-35 only exhibit the crucial ionic interaction towards D130$^{3.32}$ as well as several hydrophobic interactions (to I127$^{3.29}$, I129$^{3.31}$, Y131$^{3.33}$, M134$^{3.36}$, V279$^{6.51}$, V283$^{6.55}$).

3.6. Molecular Dynamics Simulations and Analysis to Evaluate Docking Poses

Five replicates of molecular dynamics (MD) simulations of 100 ns were performed for each receptor-ligand complex. The systems were set up using Maestro v2020-4 [81] and parametrized using the OPLS 2005 force field [82,83]. The MD simulations were performed using Desmond v2020-4 [84]. The protein was placed in a cubic box with 10 Å padding either side to the protein surface filled with TIP4P water molecules [85] and ions (0.15 M NaCl), to ensure isotonic conditions, and was embedded in a 1-palmitoyl-2-oleoylphosphatidylcholine (POPC) bilayer. The membrane placement was carried out according the OPM database (PDB-ID: 5C1M for the MOR, 6PT2 for the DOR, 6B73 for the KOR). The simulation was performed under periodic boundary conditions as an NPγT ensemble, i.e., a constant number of particles, pressure (1.01325 bar), lateral surface tension (0 N/m) and temperature (300 K) throughout the simulation. Each simulation resulted in 1000 system conformations, according to a 100 ps recording interval. VMD v1.9.3 [86] was used to center the protein and to align the trajectory onto the backbone heavy atoms of the starting protein conformation.

For MD simulation analysis, dynamic pharmacophores, so called dynophores [55,87], were calculated. Dynamic pharmacophores encompass pharmacophoric information derived from an ensemble of protein conformations obtained from MD simulations. Interactions are grouped into feature groups according to their interaction type (e.g., lipophilic interaction, hydrogen bond acceptor, hydrogen bond donor). The interaction occurrence over the trajectory of each interaction group is statistically determined and reported as percentages. The dynophore algorithm is implemented the ilib framework, on which also LigandScout [79,80] is based upon. To assess the quality of interactions occurring during the MD simulations distances between HS-731-COO-(C-atom)-KOR-K227$^{5.39}$ (Nz), HS-731-COO-(C-atom)-DOR-K214$^{5.39}$ (Nz), HS-731-COO-(C-atom)-MOR-K235$^{5.39}$ (Nz)

and HS-731-COO-(C-atom)-MOR-K305$^{6.58}$ (Nz), HS-731-COO-(C-atom)–DOR-R291 (Cz), HS-731-COO-(C-atom)-KOR-K200, and HS-731-secondary amine-KOR-E209 (CD) were measured using VMD. The violin plots (Figure 7) representing the distribution of measured distances were generated using the python v3.8.5 [88] packages seaborn v0.11.2 [89] and matplotlib v3.4.3 [90].

4. Conclusions

In this study, we assessed the difference in binding affinity and activity values of the peripheral opioid antinociceptive, HS-731, at the opioid receptors, and generated a binding hypothesis at each opioid receptor subtype. HS-731 shows extensive ionic interactions with the classical opioid receptors, MOR, DOR and KOR, and the differences in the frequency and quality of those interactions mediate differences in the affinity and activity of HS-731 to these receptors. At the MOR, HS-731 forms four ionic interactions over the majority of the MD simulations. At the DOR and KOR, there were only two noteworthy ionic interactions present. A closer examination of the interaction quality facilitated by an interaction distance assessment revealed by far the strongest ionic interactions at the MOR followed by the DOR. The quality at the KOR was much weaker than at the DOR. A salt bridge between K227$^{5.39}$ and E297$^{6.58}$ was observed in about 50% in the case of the KOR. This interaction is likely to cause the KOR to adopt an intermediate-state conformation as supported by the decreased distance between the bottom of TM6 and TM4 as a surrogate parameter for the TM6 translocation and GPCR activation, and therefore could explain the partial agonism of HS-731 to the KOR. The MOR and DOR that did not exhibit TM5-TM6 ionic interactions, and thus were not forced to adopt an intermediate state conformation are able to be fully activated by the agonist HS-731.The present results highlight the importance of ionic interactions for the binding of the 6β-glycine substituted agonist HS-731 to the opioid receptors, and accentuate the non-conserved residue 6.58 and the N-terminus, as important selectivity determinants for the classical opioid receptors. We experimentally demonstrate that HS-731 displayed no substantial binding to the NOP receptor. We surmise that Y131$^{3.33}$ is responsible for this observation, in that it points further into the active state binding pocket than in the classical opioid receptors and prevents HS-731 binding within the orthosteric binding pocket. Furthermore, the hydroxyl group of HS-731 is likely to abolish ligand binding to the NOP receptor in that it mimics the tyrosine within the message address of endogenous peptides for the classical opioid receptors instead of the phenylalanine within the message address of the NOP receptor agonist nociceptin.

In conclusion, our findings offer significant structural insights into HS-731 interactions with the opioid receptors that are important for understanding the pharmacology of this peripheral opioid analgesic.

Supplementary Materials: The following are available online, Figure S1: Sequence identity and similarity among the opioid receptors, Figure S2: Docking pose of HS-731 to the inactive NOP receptor, Figure S3: Root mean square deviation of HS-731 in complex with the MOR over the simulation time, Figure S4: Root mean square deviation of the MOR backbone atoms in complex with HS-731 over the simulation time, Figure S5: Root mean square deviation of HS-731 in complex with the DOR over the simulation time., Figure S6: Root mean square deviation of the DOR backbone atoms in complex with HS-731 over the simulation time, Figure S7: Root mean square deviation of HS-731 in complex with the KOR over the simulation time, Figure S8: Root mean square deviation of the KOR backbone atoms in complex with HS-731 over the simulation time, Figure S9: Comparison of the binding modes of HS-731 at the MOR derived by docking and after MD simulations, Figure S10: Comparison of the binding modes of HS-731 at the DOR derived by docking and after MD simulations. Figure S11: Comparison of the binding modes of HS-731 at the KOR derived by docking and after MD simulations. Figure S12: Ionic interaction distances. Figure S13: Comparison between the active state KOR and the intermediate state KOR.

Author Contributions: Conceptualization, M.S. and G.W.; methodology, K.P., H.S. and M.S.; formal analysis, K.P., H.S., G.W. and M.S.; investigation, K.P. and M.S.; resources, H.S., G.W. and M.S; writing—original draft preparation, K.P. and M.S.; writing—review and editing, all authors.; visual-

References

1. Waldhoer, M.; Bartlett, S.E.; Whistler, J.L. Opioid receptors. *Annu. Rev. Biochem.* **2004**, *73*, 953–990. [CrossRef] [PubMed]
2. Stein, C. Opioid receptors. *Annu. Rev. Med.* **2016**, *67*, 433–451. [CrossRef] [PubMed]
3. Corder, G.; Castro, D.C.; Bruchas, M.R.; Scherrer, G. Endogenous and exogenous opioids in pain. *Annu. Rev. Neurosci.* **2018**, *41*, 453–473. [CrossRef] [PubMed]
4. Ribeiro, J.M.L.; Filizola, M. Insights From molecular dynamics simulations of a number of G-protein coupled receptor targets for the treatment of pain and opioid use disorders. *Front. Mol. Neurosci.* **2019**, *12*, 207. [CrossRef] [PubMed]
5. Paul, A.K.; Smith, C.M.; Rahmatullah, M.; Nissapatorn, V.; Wilairatana, P.; Spetea, M.; Gueven, N.; Dietis, N. Opioid analgesia and opioid-induced adverse effects: A review. *Pharmaceuticals* **2021**, *14*, 1091. [CrossRef] [PubMed]
6. Zierk, K.A. The real antidote: A critical review of U.S. and Canadian drug treatment courts and a call for public health prevention tools as a solution to the opioid epidemic. *Ind. Intl Comp. L. Rev.* **2019**, *29*, 185–217. [CrossRef]
7. Sobczak, Ł.; Goryński, K. Pharmacological aspects of over-the-counter opioid drugs misuse. *Molecules* **2020**, *25*, 3905. [CrossRef]
8. Centers for Disease Control and Prevention; National Center for Health Statistics; Office of Communication. Drug Overdose Deaths in the U.S. Top 100,000 Annually. Available online: https://www.cdc.gov/nchs/pressroom/nchs_press_releases/2021/20211117.htm (accessed on 29 November 2021).
9. Volkow, N.D.; Blanco, C. The changing opioid crisis: Development, challenges and opportunities. *Mol. Psychiatry* **2021**, *26*, 218–233. [CrossRef]
10. Obeng, S.; Hiranita, T.; León, F.; McMahon, L.R.; McCurdy, C.R. Novel approaches, drug candidates, and targets in pain drug discovery. *J. Med. Chem.* **2021**, *64*, 6523–6548. [CrossRef]
11. Yekkirala, A.S.; Roberson, D.P.; Bean, B.P.; Woolf, C.J. Breaking barriers to novel analgesic drug development. *Nat. Rev. Drug Discov.* **2017**, *16*, 545–564. [CrossRef]
12. Günther, T.; Dasgupta, P.; Mann, A.; Miess, E.; Kliewer, A.; Fritzwanker, S.; Steinborn, R.; Schulz, S. Targeting multiple opioid receptors–improved analgesics with reduced side effects? *Br. J. Pharmacol.* **2018**, *175*, 2857–2868. [CrossRef] [PubMed]
13. Cunningham, C.W.; Elballa, W.M.; Vold, S.U. Bifunctional opioid receptor ligands as novel analgesics. *Neuropharmacology* **2019**, *151*, 195–207. [CrossRef] [PubMed]
14. Mores, K.L.; Cummins, B.R.; Cassell, R.J.; van Rijn, R.M. A review of the therapeutic potential of recently developed G protein-biased kappa agonists. *Front. Pharmacol.* **2019**, *10*, 407. [CrossRef] [PubMed]
15. Faouzi, A.; Varga, B.R.; Majumdar, S. Biased opioid ligands. *Molecules* **2020**, *25*, 4257. [CrossRef] [PubMed]
16. Bermudez, M.; Nguyen, T.N.; Omieczynski, C.; Wolber, G. Strategies for the discovery of biased GPCR ligands. *Drug Discov. Today* **2019**, *24*, 1031–1037. [CrossRef]
17. Albert-Vartanian, A.; Boyd, M.; Hall, A.; Morgado, S.; Nguyen, E.; Nguyen, V.; Patel, S.; Russo, L.; Shao, A.; Raffa, R. Will peripherally restricted kappa-opioid receptor agonists (pKORA s) relieve pain with less opioid adverse effects and abuse potential? *J. Clin. Pharm. Ther.* **2016**, *41*, 371–382. [CrossRef]
18. Martínez, V.; Abalo, R. Peripherally acting opioid analgesics and peripherally-induced analgesia. *Behav. Pharmacol.* **2020**, *31*, 136–158. [CrossRef]
19. Bidlack, J.M. Detection and function of opioid receptors on cells from the immune system. *Clin. Diagn. Lab.* **2000**, *7*, 719–723. [CrossRef] [PubMed]
20. Holzer, P. Opioids and opioid receptors in the enteric nervous system: From a problem in opioid analgesia to a possible new prokinetic therapy in humans. *Neurosci. Lett.* **2004**, *361*, 192–195. [CrossRef]
21. Machelska, H.; Celik, M.Ö. Advances in achieving opioid analgesia without side effects. *Front. Pharmacol.* **2018**, *9*, 1388. [CrossRef]

22. Beck, T.C.; Hapstack, M.A.; Beck, K.R.; Dix, T.A. Therapeutic potential of kappa opioid agonists. *Pharmaceuticals* **2019**, *12*, 95. [CrossRef] [PubMed]

23. Fürst, S.; Zádori, Z.S.; Zádor, F.; Király, K.; Balogh, M.; László, S.B.; Hutka, B.; Mohammadzadeh, A.; Calabrese, C.; Galambos, A.R. On the role of peripheral sensory and gut mu opioid receptors: Peripheral analgesia and tolerance. *Molecules* **2020**, *25*, 2473. [CrossRef] [PubMed]

24. DeHaven-Hudkins, D.L.; Dolle, R.E. Peripherally restricted opioid agonists as novel analgesic agents. *Curr. Pharm. Des.* **2004**, *10*, 743–757. [CrossRef] [PubMed]

25. Stokbroekx, R.A.; Vandenberk, J.; Van Heertum, A.H.; Van Laar, G.M.; Van der Aa, M.J.; Van Bever, W.F.; Janssen, P.A. Synthetic antidiarrheal agents. 2, 2-Diphenyl-4-(4′-aryl-4′-hydroxypiperidino) butyramides. *J. Med. Chem.* **1973**, *16*, 782–786. [CrossRef] [PubMed]

26. Barber, A.; Bartoszyk, G.; Bender, H.; Gottschlich, R.; Greiner, H.; Harting, J.; Mauler, F.; Minck, K.O.; Murray, R.; Simon, M. A pharmacological profile of the novel, peripherally-selective κ-opioid receptor agonist, EMD 61753. *Br. J. Pharmacol.* **1994**, *113*, 1317–1327. [CrossRef]

27. Spahn, V.; Del Vecchio, G.; Labuz, D.; Rodriguez-Gaztelumendi, A.; Massaly, N.; Temp, J.; Durmaz, V.; Sabri, P.; Reidelbach, M.; Machelska, H. A nontoxic pain killer designed by modeling of pathological receptor conformations. *Science* **2017**, *355*, 966–969. [CrossRef]

28. Schiller, P.W. Opioid peptide-derived analgesics. In *Drug Addiction*, 1st ed.; Rapaka, R.S., Sadée, W., Eds.; Springer: New York, NY, USA, 2008; pp. 357–366.

29. Schütz, J.; Brandt, W.; Spetea, M.; Wurst, K.; Wunder, G.; Schmidhammer, H. Synthesis of 6-amino acid Substituted derivatives of the highly potent analgesic 14-*O*-methyloxymorphone. *Helv. Chim. Acta* **2003**, *86*, 2142–2148. [CrossRef]

30. Spetea, M.; Friedmann, T.; Riba, P.; Schütz, J.; Wunder, G.; Langer, T.; Schmidhammer, H.; Fürst, S. In vitro opioid activity profiles of 6-amino acid substituted derivatives of 14-*O*-methyloxymorphone. *Eur. J. Pharmacol.* **2004**, *483*, 301–308. [CrossRef]

31. Fürst, S.; Riba, P.; Friedmann, T.; Tímar, J.; Al-Khrasani, M.; Obara, I.; Makuch, W.; Spetea, M.; Schütz, J.; Przewlocki, R. Peripheral versus central antinociceptive actions of 6-amino acid-substituted derivatives of 14-*O*-methyloxymorphone in acute and inflammatory pain in the rat. *J. Pharmacol. Exp. Ther.* **2005**, *312*, 609–618. [CrossRef]

32. Bileviciute-Ljungar, I.; Spetea, M.; Guo, Y.; Schütz, J.; Windisch, P.; Schmidhammer, H. Peripherally mediated antinociception of the mu-opioid receptor agonist 2-(4,5alpha-epoxy-3-hydroxy-14beta-methoxy-17-methylmorphinan-6beta-yl)aminoacetic acid (HS-731) after subcutaneous and oral administration in rats with carrageenan-induced hindpaw inflammation. *J. Pharmacol. Exp. Ther.* **2006**, *317*, 220–227. [CrossRef]

33. Obara, I.; Makuch, W.; Spetea, M.; Schütz, J.; Schmidhammer, H.; Przewlocki, R.; Przewlocka, B. Local peripheral antinociceptive effects of 14-*O*-methyloxymorphone derivatives in inflammatory and neuropathic pain in the rat. *Eur. J. Pharmacol.* **2007**, *558*, 60–67. [CrossRef] [PubMed]

34. Al-Khrasani, M.; Spetea, M.; Friedmann, T.; Riba, P.; Király, K.; Schmidhammer, H.; Furst, S. DAMGO and 6β-glycine substituted 14-*O*-methyloxymorphone but not morphine show peripheral, preemptive antinociception after systemic administration in a mouse visceral pain model and high intrinsic efficacy in the isolated rat vas deferens. *Brain Res. Bull.* **2007**, *74*, 369–375. [CrossRef] [PubMed]

35. Spetea, M.; Windisch, P.; Guo, Y.; Bileviciute-Ljungar, I.; Schütz, J.; Asim, M.F.; Berzetei-Gurske, I.P.; Riba, P.; Kiraly, K.; Fürst, S. Synthesis and pharmacological activities of 6-glycine substituted 14-phenylpropoxymorphinans, a novel class of opioids with high opioid receptor affinities and antinociceptive potencies. *J. Med. Chem.* **2011**, *54*, 980–988. [CrossRef]

36. Baillie, L.D.; Schmidhammer, H.; Mulligan, S.J. Peripheral µ-opioid receptor mediated inhibition of calcium signaling and action potential-evoked calcium fluorescent transients in primary afferent CGRP nociceptive terminals. *Neuropharmacology* **2015**, *93*, 267–273. [CrossRef]

37. Spetea, M.; Rief, S.B.; Haddou, T.B.; Fink, M.; Kristeva, E.; Mittendorfer, H.; Haas, S.; Hummer, N.; Follia, V.; Guerrieri, E. Synthesis, biological, and structural explorations of new zwitterionic derivatives of 14-*O*-methyloxymorphone, as potent µ/δ opioid agonists and peripherally selective antinociceptives. *J. Med. Chem.* **2019**, *62*, 641–653. [CrossRef] [PubMed]

38. Botros, S.; Lipkowski, A.; Larson, D.; Stark, P.; Takemori, A.; Portoghese, P.S. Opioid agonist and antagonist activities of peripherally selective derivatives of naltrexamine and oxymorphamine. *J. Med. Chem.* **1989**, *32*, 2068–2071. [CrossRef]

39. Mazak, K.; Noszal, B.; Hosztafi, S. Physicochemical and pharmacological characterization of permanently charged opioids. *Curr. Med. Chem.* **2017**, *24*, 3633–3648. [CrossRef]

40. Zádor, F.; Mohammadzadeh, A.; Balogh, M.; Zádori, Z.S.; Király, K.; Barsi, S.; Galambos, A.R.; László, S.B.; Hutka, B.; Váradi, A.; et al. Comparisons of in vivo and in vitro opioid effects of newly synthesized 14-methoxycodeine-6-*O*-sulfate and codeine-6-*O*-sulfate. *Molecules* **2020**, *25*, 1370. [CrossRef]

41. Che, T.; Majumdar, S.; Zaidi, S.A.; Ondachi, P.; McCorvy, J.D.; Wang, S.; Mosier, P.D.; Uprety, R.; Vardy, E.; Krumm, B.E.; et al. Structure of the nanobody-stabilized active state of the kappa opioid receptor. *Cell* **2018**, *172*, 55–67.e15. [CrossRef]

42. Huang, W.; Manglik, A.; Venkatakrishnan, A.J.; Laeremans, T.; Feinberg, E.N.; Sanborn, A.L.; Kato, H.E.; Livingston, K.E.; Thorsen, T.S.; Kling, R.C.; et al. Structural insights into µ-opioid receptor activation. *Nature* **2015**, *524*, 315–321. [CrossRef]

43. Claff, T.; Yu, J.; Blais, V.; Patel, N.; Martin, C.; Wu, L.; Han, G.W.; Holleran, B.J.; van der Poorten, O.; White, K.L.; et al. Elucidating the active δ-opioid receptor crystal structure with peptide and small-molecule agonists. *Sci. Adv.* **2019**, *5*, eaax9115. [CrossRef] [PubMed]

44. Ballesteros, J.A.; Weinstein, H. Integrated methods for the construction of three-dimensional models and computational probing of structure-function relations in G protein-coupled receptors. In *Methods in Neurosciences*; Academic Press: San Diego, USA; London, UK, 1995; Volume 25, pp. 366–428.

45. Chavkin, C.; McLaughlin, J.P.; Celver, J.P. Regulation of opioid receptor function by chronic agonist exposure: Constitutive activity and desensitization. *Mol. Pharmacol.* **2001**, *60*, 20–25. [CrossRef] [PubMed]

46. Befort, K.; Zilliox, C.; Filliol, D.; Yue, S.; Kieffer, B.L. Constitutive activation of the delta opioid receptor by mutations in transmembrane domains III and VII. *J. Biol. Chem.* **1999**, *274*, 18574–18581. [CrossRef] [PubMed]

47. Décaillot, F.M.; Befort, K.; Filliol, D.; Yue, S.; Walker, P.; Kieffer, B.L. Opioid receptor random mutagenesis reveals a mechanism for G protein-coupled receptor activation. *Nat. Struct. Biol.* **2003**, *10*, 629–636. [CrossRef]

48. Váradi, A.; Marrone, G.F.; Eans, S.O.; Ganno, M.L.; Subrath, J.J.; Le Rouzic, V.; Hunkele, A.; Pasternak, G.W.; McLaughlin, J.P.; Majumdar, S. Synthesis and characterization of a dual kappa-delta opioid receptor agonist analgesic blocking cocaine reward behavior. *ACS Chem. Neurosci.* **2015**, *6*, 1813–1824. [CrossRef]

49. Saleh, A.H.; Abdelwaly, A.; Darwish, K.M.; Eissa, A.A.H.M.; Chittiboyina, A.; Helal, M.A. Deciphering the molecular basis of the kappa opioid receptor selectivity: A molecular dynamics study. *J. Mol. Graph. Model.* **2021**, *106*, 107940. [CrossRef]

50. Akuzawa, N.; Takeda, S.; Ishiguro, M. Structural modelling and mutation analysis of a nociceptin receptor and its ligand complexes. *J. Biochem.* **2007**, *141*, 907–916. [CrossRef]

51. Thompson, A.A.; Liu, W.; Chun, E.; Katritch, V.; Wu, H.; Vardy, E.; Huang, X.-P.; Trapella, C.; Guerrini, R.; Calo, G.; et al. Structure of the nociceptin/orphanin FQ receptor in complex with a peptide mimetic. *Nature* **2012**, *485*, 395–399. [CrossRef]

52. Miller, R.L.; Thompson, A.A.; Trapella, C.; Guerrini, R.; Malfacini, D.; Patel, N.; Han, G.W.; Cherezov, V.; Caló, G.; Katritch, V.; et al. The importance of ligand-receptor conformational pairs in stabilization: Spotlight on the N/OFQ G protein-coupled receptor. *Structure* **2015**, *23*, 2291–2299. [CrossRef]

53. Mustazza, C.; Bastanzio, G. Development of nociceptin receptor (NOP) agonists and antagonists. *Med. Res. Rev.* **2011**, *31*, 605–648. [CrossRef]

54. Meunier, J.-C.; Mouledous, L.; Topham, C.M. The nociceptin (ORL1) receptor: Molecular cloning and functional architecture. *Peptides* **2000**, *21*, 893–900. [CrossRef]

55. Sydow, D. *Dynophores: Novel Dynamic Pharmacophores Implementation of Pharmacophore Generation Based on Molecular Dynamics Trajectories and Their Graphical Representation*; Freie Universität Berlin: Berlin, Germany, 2015.

56. Wu, H.; Wacker, D.; Mileni, M.; Katritch, V.; Han, G.W.; Vardy, E.; Liu, W.; Thompson, A.A.; Huang, X.-P.; Carroll, F.I.; et al. Structure of the human κ-opioid receptor in complex with JDTic. *Nature* **2012**, *485*, 327–332. [CrossRef] [PubMed]

57. Fenalti, G.; Zatsepin, N.A.; Betti, C.; Giguere, P.; Han, G.W.; Ishchenko, A.; Liu, W.; Guillemyn, K.; Zhang, H.; James, D.; et al. Structural basis for bifunctional peptide recognition at human δ-opioid receptor. *Nat. Struct. Mol. Biol.* **2015**, *22*, 265–268. [CrossRef] [PubMed]

58. Lee, K.K.; Fitch, C.A.; García-Moreno E., B. Distance dependence and salt sensitivity of pairwise, coulombic interactions in a protein. *Protein Sci.* **2002**, *11*, 1004–1016. [CrossRef]

59. Vardy, E.; Mosier, P.D.; Frankowski, K.J.; Wu, H.; Katritch, V.; Westkaemper, R.B.; Aubé, J.; Stevens, R.C.; Roth, B.L. Chemotype-selective modes of action of κ-opioid receptor agonists. *J. Biol. Chem.* **2013**, *288*, 34470–34483. [CrossRef] [PubMed]

60. Che, T.; English, J.; Krumm, B.E.; Kim, K.; Pardon, E.; Olsen, R.H.J.; Wang, S.; Zhang, S.; Diberto, J.F.; Sciaky, N.; et al. Nanobody-enabled monitoring of kappa opioid receptor states. *Nat. Commun.* **2020**, *11*, 1145. [CrossRef] [PubMed]

61. Wacker, D.; Wang, C.; Katritch, V.; Han, G.W.; Huang, X.-P.; Vardy, E.; McCorvy, J.D.; Jiang, Y.; Chu, M.; Siu, F.Y.; et al. Structural features for functional selectivity at serotonin receptors. *Science (New York, N.Y.)* **2013**, *340*, 615–619. [CrossRef]

62. Dumitrascuta, M.; Bermudez, M.; Trovato, O.; Neve, J.D.; Ballet, S.; Wolber, G.; Spetea, M. Antinociceptive efficacy of the μ-opioid/nociceptin peptide-based hybrid KGNOP1 in inflammatory pain without rewarding effects in mice: An experimental assessment and molecular docking. *Molecules* **2021**, *26*, 3267. [CrossRef] [PubMed]

63. Bradford, M.M. A rapid and sensitive method for the quantitation of microgram quantities of protein utilizing the principle of protein-dye binding. *Anal. Biochem.* **1976**, *72*, 248–254. [CrossRef]

64. Cheng, Y.-C.; Prusoff, W.H. Relationship between the inhibition constant (KI) and the concentration of inhibitor which causes 50 per cent inhibition (I50) of an enzymatic reaction. *Biochem. Pharmacol.* **1973**, *22*, 3099–3108. [CrossRef]

65. Berman, H.; Henrick, K.; Nakamura, H. Announcing the worldwide Protein Data Bank. *Nat. Struct. Biol.* **2003**, *10*, 980. [CrossRef] [PubMed]

66. Molecular Operating Environment (MOE). *Molecular Operating Environment (MOE), C.C.G.U.* Sherbooke St. West, Suite #910, Montreal, QC, Canada, H3A 2R7. 2021. Available online: https://www.chemcomp.com/Products.htm (accessed on 29 November 2021).

67. The UniProt Consortium. UniProt: The universal protein knowledgebase in 2021. *Nucleic Acids Res.* **2021**, *49*, D480–D489. [CrossRef] [PubMed]

68. Ramachandran, G.N.; Ramakrishnan, C.; Sasisekharan, V. Stereochemistry of polypeptide chain configurations. *J. Mol. Biol.* **1963**, *7*, 95–99. [CrossRef]

69. Zhu, S. Validation of the generalized force fields GAFF, CGenFF, OPLS-AA, and PRODRGFF by testing against experimental osmotic coefficient data for small drug-Like molecules. *J. Chem. Inf. Model.* **2019**, *59*, 4239–4247. [CrossRef] [PubMed]

70. Bermudez, M.; Rakers, C.; Wolber, G. Structural characteristics of the allosteric binding site represent a key to subtype selective modulators of muscarinic acetylcholine receptors. *Mol. Inform.* **2015**, *34*, 526–530. [CrossRef] [PubMed]

71. 3D Structure Generator CORINA Classic. Available online: https://mn-am.com/products/corina/ (accessed on 2 April 2021).

72. Gasteiger, J.; Rudolph, C.; Sadowski, J. Automatic generation of 3D-atomic coordinates for organic molecules. *Tetrahedron Comput. Methodol.* **1990**, *3*, 537–547. [CrossRef]

73. Labute, P. Protonate3D: Assignment of ionization states and hydrogen coordinates to macromolecular structures. *Proteins* **2009**, *75*, 187–205. [CrossRef]

74. Jones, G.; Willett, P.; Glen, R.C.; Leach, A.R.; Taylor, R. Development and validation of a genetic algorithm for flexible docking. *J. Mol. Biol.* **1997**, *267*, 727–748. [CrossRef]

75. Evers, A.; Hessler, G.; Matter, H.; Klabunde, T. Virtual screening of biogenic amine-binding G-protein coupled receptors: Comparative evaluation of protein- and ligand-based virtual screening protocols. *J. Med. Chem.* **2005**, *48*, 5448–5465. [CrossRef]

76. Verdonk, M.L.; Cole, J.C.; Hartshorn, M.J.; Murray, C.W.; Taylor, R.D. Improved protein-ligand docking using GOLD. *Proteins* **2003**, *52*, 609–623. [CrossRef]

77. Vo, Q.N.; Mahinthichaichan, P.; Shen, J.; Ellis, C.R. How μ-opioid receptor recognizes fentanyl. *Nat. Commun.* **2021**, *12*, 984. [CrossRef] [PubMed]

78. Halgren, T.A. Merck molecular force field. I. Basis, form, scope, parameterization, and performance of MMFF94. *J. Comput. Chem.* **1996**, *17*, 490–519. [CrossRef]

79. Wolber, G.; Dornhofer, A.A.; Langer, T. Efficient overlay of small organic molecules using 3D pharmacophores. *J. Comput. Aided Mol. Des.* **2006**, *20*, 773–788. [CrossRef] [PubMed]

80. Wolber, G.; Langer, T. LigandScout: 3-D pharmacophores derived from protein-bound ligands and their use as virtual screening filters. *J. Chem. Inf. Model.* **2005**, *45*, 160–169. [CrossRef]

81. *Schrödinger Release -4: Maestro, version Release -4*; Schrödinger, LLC: New York, NY, USA, 2020.

82. Jorgensen, W.L.; Maxwell, D.S.; Tirado-Rives, J. Development and Testing of the OPLS all-atom force field on conformational energetics and properties of organic liquids. *J. Am. Chem. Soc.* **1996**, *118*, 11225–11236. [CrossRef]

83. Ponder, J.W.; Case, D.A. Force fields for protein simulations. In *Advances in Protein Chemistry*; Academic Press: Cambridge, MA, USA, 2003; Volume 66, pp. 27–85.

84. Bowers, K.J.; Chow, E.; Xu, H.; Dror, R.O.; Eastwood, M.P.; Gregersen, B.A.; Klepeis, J.L.; Kolossvary, I.; Moraes, M.A.; Sacerdoti, F.D.; et al. Scalable algorithms for molecular dynamics simulations on commodity clusters. In Proceedings of the Proceedings of the ACM/IEEE Conference on Supercomputing (SC06), Tampa, FL, USA, 11–17 November 2006.

85. Jorgensen, W.L.; Chandrasekhar, J.; Madura, J.D.; Impey, R.W.; Klein, M.L. Comparison of simple potential functions for simulating liquid water. *J. Chem. Phys.* **1983**, *79*, 926–935. [CrossRef]

86. Humphrey, W.; Dalke, A.; Schulten, K. VMD: Visual molecular dynamics. *J. Mol. Graph.* **1996**, *14*, 33–38. [CrossRef]

87. Bock, A.; Bermudez, M.; Krebs, F.; Matera, C.; Chirinda, B.; Sydow, D.; Dallanoce, C.; Holzgrabe, U.; Amici, M.d.; Lohse, M.J.; et al. Ligand binding ensembles determine graded agonist efficacies at a G protein-coupled receptor. *J. Biol. Chem.* **2016**, *291*, 16375–16389. [CrossRef]

88. van Rossum, G.; Drake, F. *Python 3 Reference Manual*; CreateSpace: Scotts Valley, CA, USA, 2009.

89. Waskom, M. Seaborn: Statistical data visualization. *J. Open Source Softw.* **2021**, *6*, 3021. [CrossRef]

90. Hunter, J.D. Matplotlib: A 2D Graphics environment. *Comput. Sci. Eng.* **2007**, *9*, 90–95. [CrossRef]

Review

Spotlight on Nociceptin/Orphanin FQ Receptor in the Treatment of Pain

Amal El Daibani [1] and Tao Che [1,2,*]

1   Department of Anesthesiology, Washington University School of Medicine, St. Louis, MO 63110, USA;
    aeldaibani@wustl.edu
2   Center for Clinical Pharmacology, University of Health Sciences and Pharmacy in St. Louis,
    St. Louis, MO 63110, USA
*   Correspondence: taoche@wustl.edu; Tel.: +1-(314)-446-8016

Abstract: In our society today, pain has become a main source of strain on most individuals. It is crucial to develop novel treatments against pain while focusing on decreasing their adverse effects. Throughout the extent of development for new pain therapies, the nociceptin/orphanin FQ receptor (NOP receptor) has appeared to be an encouraging focal point. Concentrating on NOP receptor to treat chronic pain with limited range of unwanted effects serves as a suitable alternative to prototypical opioid morphine that could potentially lead to life-threatening effects caused by respiratory depression in overdose, as well as generate abuse and addiction. In addition to these harmful effects, the uprising opioid epidemic is responsible for becoming one of the most disastrous public health issues in the US. In this article, the contributing molecular and cellular structure in controlling the cellular trafficking of NOP receptor and studies that support the role of NOP receptor and its ligands in pain management are reviewed.

Keywords: nociceptin/orphanin FQ receptor; NOP receptor; ligands; opioid receptor; nociceptin; N/OFQ; analgesia

---

1. Introduction

Persistent pain affects more than 30% of North America's population throughout their life and it attributes to substantial expense in the US with annual costs ranging between $560 and $635 billion, which is larger than the cost of the nation's priority health conditions [1]. This main socio-economic issue is expected to have a two-fold increase within the next 10 years especially in the elderly, as reported by the 2010 Medical Expenditure Panel Survey (MEPS). Despite the life- threatening effect caused by respiratory depression in overdose and the potential of high abuse, opioid analgesics stand as the conventional choice of treatment for moderate to severe pain [2–6]. As a result of misuse and extensive diversion, the use of opioids has become a leading crisis in the US, which was declared by the United States Department of Health and Human Service (HHS) in 2017 [7,8]. According to the Centers for Disease Control and Prevention (CDC), a significant increase in overdose-related deaths occurred in 2020 in which the involvement of synthetic opioids was over 60% [9]. For this reason, several research institutes have made it a priority to develop safe, effective, and non-addictive therapeutics for chronic pain management and address opioid-use disorders with innovative medications, to save lives and encourage recovery.

Opioids exert their effect via opioid receptors, a member of a large superfamily of seven-transmembrane-spanning (7TM) G-protein-coupled receptors (GPCRs), mu (MOP receptor), kappa (KOP receptor), delta (DOP receptor), and nociceptin (NOP receptor) [10]. Since NOP receptors are distributed in various regions (dorsal root ganglia (DRG), spinal dorsal horn (SDH), and brain) that are involved in pain transmission, NOP receptor ligands are under investigation primarily as an alternative for MOP receptor opioid analgesic in addition to their anxiolysis and antidepressant-like effect [11–13]. However, the NOP

receptor was considered a controversial drug target for analgesics because of its unique pharmacological effects in pain modulation (antinociceptive vs. nociceptive effects) in the earlier phases of discovering nociceptin [14–19]. Currently, the NOP receptor has become a main focus as a promising target for analgesics as NOP receptor ligands have reported to show antinociceptive effects in non-human primates regardless of their administered doses and administration routes (spinal or supraspinal).

Moreover, the bifunctional and multifunctional NOP/opioid receptor agonists have recently displayed potent antinociceptive activity with favorable side effect profiles. Among these agonists, cebranopadol represents a promising therapeutic candidate for pain, according to the results of its clinical trials. In this article, the current literature for NOP receptor's crystal structure, distribution, signaling pathway, and the rational design of NOP receptor ligands with various pharmacological profiles as a promising alternative for conventional opioid analgesic is reviewed to assess its therapeutic potential as analgesics.

2. Structure of NOP Receptor

In the mid 1990s, the human cDNA clone that encodes the NOP receptor was first isolated from the human and mouse brainstem and was then identified in several murine genomes including rat, pig, and guinea pig [20–25]. It was previously known as "orphanin FQ", "nociceptin,", or "ORL-1" for opioid receptor-like 1 receptor, due to the lack of its endogenous peptide ligand in the binding assays; however, nociceptin or orphanin FQ (N/OFQ) that closely resemble dynorphin A, a selective KOP receptor endogenous peptide, was characterized a year later by applying reverse pharmacology as the endogenous neuropeptide for NOP receptor [14,15]. This endogenous neuropeptide has 17 amino acids, Phe-Gly-Gly-Phe-Thr-Gly-Ala-Arg-Lys-Ser-Ala-Arg-Lys-Leu-Ala-Asn-Gln, which have quite unique features. The Phe-Gly-Gly-Phe amino terminal is noticeably comparable to the Tyr-Gly-Gly-Phe that is conserved in other classical opioid peptides [26,27]. Moreover, the number of Lys and Arg residues that are found in N/OFQ are similar to dynorphin A. Along with this resemblance, the gene structure of opioid peptide genes (preprodynorphin and preproenkephalin) and nociceptin precursor gene are also similar [27,28]. Multiple conserved amino acid residues and motifs specifically in the transmembrane helices and the intracellular loops have been identified by comparing the cDNA-derived amino acid sequence of the NOP receptor protein with that of other opioid receptors, indicating that NOP receptor belongs to GPCR Class A (rhodopsin-like) receptors, as the fourth and last characterized opioid receptor [29]. Consequently, the IUPHAR nomenclature defined this receptor and its peptide which are currently named NOP receptor and N/OFQ [30].

To date, three crystal structures of human NOP receptor have been solved with three piperidine-based antagonists (Banyn Compound-24 (C24), SB-612111, and Compound-35 (C-35)) at a resolution of 3 Å [31,32]. These crystal structures provide a perspective into the atomic details of the molecular structure of the NOP receptor and support previous homology models developed to further understand the functional mechanism of NOP receptor. In all three structures, the protonated nitrogen of the piperidine interacts with the D130$^{3.32}$ (superscripts indicate the Ballesteros Weinstein TM helix residue numbering) residue in NOP receptor which leads to the formation of a salt bridge, implying the high affinity for these ligands. Consistent with NOP receptor crystal structure in its inactive state, the previous homology models of NOP receptor in complex with N/OFQ further support that the N-terminal amino groups of an endogenous neuropeptide agonist, N/OFQ, interact with D130$^{3.32}$ [33–35]. This indicates the important role of this residue which is conserved in other canonical opioid receptors on the binding of NOP receptor ligands. Moreover, the replacement of D130$^{3.32}$ into alanine or asparagine in the mutagenesis studies abolished N/OFQ binding, emphasizing the negative charge essentiality at this location [32].

Computer aided molecular docking studies of the selective NOP receptor agonist Ro 64-6198 into the first active state NOP receptor homology model, have also indicated signs for the mentioned NOP receptor selectivity enhancing of interactivity [34]. In this model, the amide hydrogen in Ro 64-6198 directly interacts with T305$^{7.39}$ to form a hydrogen

bond that takes place at the extracellular end of the orthosteric binding site, while the phenalenyl ring of Ro 64-6198 and the hydrophobic V279$^{6.51}$ residue interact together inside the binding site.

Despite these studies that have highlighted the key residues and structures that are involved with ligand binding, receptor activation, and signaling, the determination of NOP receptor in its active state is required to illuminate the conformational changes in receptor's architecture.

3. The Distribution and Signaling Pathway of NOP Receptor

Several techniques and animal model including in situ hybridization, immunohisto-chemistry, autoradiography, RT-PCR, knock-in mice with a fluorescent-tagged NOP receptor (NOP receptor-eGFP) in place of the native NOP receptor, and [^{35}S]-GTPγS assay were employed to reveal the tissue distribution of NOP receptor. It is widely expressed in the human and other animal species both in the central and peripheral nervous systems [12,36]. Peripherally, the human immune cells (lymphocytic B and T-cell lines, monocytic cell lines, and circulating lymphocytes and monocytes) express NOP receptor mRNA [37]. Centrally, the NOP receptor mRNA is detected in the cortical areas, hypothalamus, mammillary bodies, the substantia nigra, thalamus nuclei, limbic structures (the hippocampus and amygdala), brainstem (colliculi, the ventral tegmental area, the locus coeruleus), and the pituitary gland [37,38].

Because NOP receptor activation modulates several physiological functions and pharmacological roles including, but not limited to, pain sensation, mood, learning, memory, cardiovascular control, and immune response [39], it is important to understand its signaling pathways and subsequent trafficking events. NOP receptor has shown a high sequence identity and homology in the TM helices and intracellular loops with other classical opioid receptors (DOP receptor, MOP receptor, and KOP receptor) which couple to inhibitory G proteins, suggesting a similar activation mechanism upon ligand binding. This binding triggers the heterotrimeric dissociation of Gαβγ subunits following the replacement of guanosine diphosphate (GDP) by guanosine triphosphate (GTP) at Gα subunit and subsequently induces multiple intracellular signaling pathways [40,41]. The dissociated Gα subunit suppresses adenyl cyclase and cAMP production, while Gβγ subunits directly couple with different ion channels such as Ca^{2+} and Kir3 [42–44]. NOP receptor also regulates the voltage-dependent Ca^{2+} channels by modulating Rho-associated coiled-coil-containing protein kinase (ROCK) and LIM domain kinase (LIMK) [45]. Like canonical opioid receptor, the suppression of pre and postsynaptic Ca^{2+} influx, the activation of G protein gated inward rectifying potassium (GIRKs) conductance, as well as the inhibition of various ions channels such as Na$^+$ channel resulted in cellular hyperpolarization and attenuation of neuronal excitability and nociceptive stimuli transmission, thus producing antinociceptive effects [46]. In addition to ion channels, the activation of NOP receptors also modulates all three mitogen-activated protein kinase (MAPK). MAPK activity thereby regulates cell proliferation, progression, and differentiation (ERK1/ERK2), as well as the response to cellular stressors (p38 and JNK1/JNK2/JNK3) [47,48]. Moreover, the neurotransmitter release of serotonin, noradrenaline and glutamate, as well as the phospholipase (PLC) A2 and C signaling, are induced by NOP receptor activation [49–52].

Within minutes of NOP receptor activation, the uncoupling of NOP receptor to G protein is facilitated by a desensitization process, a feedback mechanism to control the receptor overstimulation during acute and chronic exposure to the ligand [53]. This process is regulated by various kinases such as GPCR kinases (GRKs) that mediate the phosphorylation, and the arrestin ligation to the C-terminus of the opioid receptor. Besides GRKs, second messenger-dependent protein kinases including protein kinase A (PKA), protein kinase C (PKC), and calcium/calmodulin-dependent protein kinase II have also been shown to phosphorylate and desensitize the NOP receptor [54,55]. The receptor desensitization is suppressed through the inhibition of mitogen activated protein dependent kinase that could interfere with the arrestin recruitment. After the GRK/arrestin recruitment, the

NOP receptor is translocated into the intracellular compartment through clathrin-mediated endocytosis into which the receptor is recycled and re-sensitized to restore the receptor function back again.

4. Ligands of NOP Receptor

Analgesia is one of the potential clinical indications of NOP receptor due to its wide distribution in the nervous system (central and peripheral) which are involved in the pain processing pathways. In this review, NOP receptor ligands including N/OFQ-related peptides, nonpeptidic, and bifunctional compounds with different pharmacological profiles (full agonist, partial agonist, and antagonist) that represent viable drug target for pain are spotlighted. Initially, intrathecally (i.t) administered N/OFQ produces dose-dependent analgesia in the tail flick assay and flinching behavior in the formalin test without causing sedation as well as promotes antinociceptive effect of morphine in both rats and monkey [16–19]. Whereas opposite effects like hyperalgesia and a decrease in locomotor activity are produced as a result of the intracerebroventricular (i.c.v) N/OFQ administration in the hot plate test and the tail flick test in mice [14,15]. The unexpected action of i.c.v. N/OFQ administration resulted from both the anti-opioid activity (antagonizing MOP receptor, DOP receptor, and KOP receptor antinociception activity) via NOP receptor stimulation in the periaqueductal gray (PAG) neurons and the reversal of opioid induced analgesia of N/OFQ opposed to the nociceptive activity as proposed previously [56–58]. These findings indicate the dual actions of N/OFQ that mainly depend on the administered dose, pain models (chronic or acute), examined species, and the route of administration as illustrated in Figure 1. The reason behind this discrepancy across species is not known yet; however, some studies (reviewed in [29,59]) suggest that the difference in neuronal circuitry of pain between different species could be the reason for NOP receptor system having opposite effects in pain processing. Furthermore, the effectiveness of NOP receptor agonists in addressing chronic pain (over acute pain), can be explained by the varying levels of NOP receptor mRNA and NFQ peptide induced by chronic inflammation.
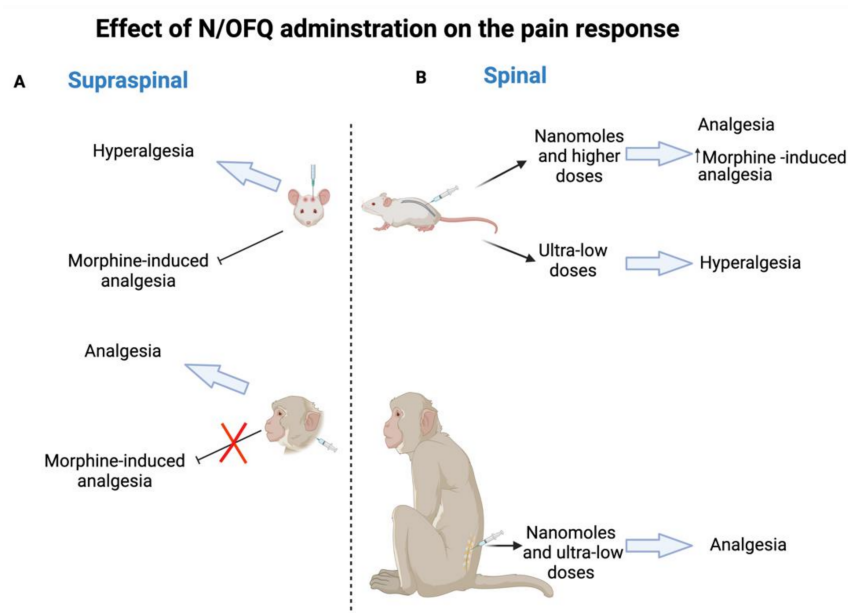
Figure 1. N/OFQ effect in rodent and non-human primates on pain response. (**A**) Supraspinal administration of N/OFQ produces hyperalgesia and blocks morphine-induced analgesia in rodent, whereas the opposite effect of analgesia and the promotion of an antinociceptive effect are produced in non-human primates. (**B**) Spinal administration of N/OFQ produces dose-dependent analgesia in both rodent (nanomoles and higher doses) and non-human primates (nanomoles and ultra-low doses) as well as promotes an antinociceptive effect of morphine, while ultra-low doses of N/OFQ induce hyperalgesia in rodent.

In this section, the relevant pharmacological features of NOP receptor ligands including peptide, nonpeptide, and bifunctional and mixed NOP receptor compounds are explored with a focus on their role in modulating pain to further comprehend the nature of the N/OFQ–NOP receptor system within these processes.
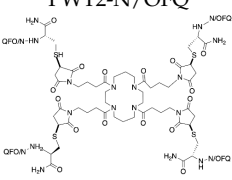
4.1. Peptide Ligands Related to N/OFQ Targeting Pain

Earlier systematic SAR studies revealed that both truncation and amidation of N/OFQ are required to sustain the biological activity of N/OFQ and avoid the N-terminus degradation by proteases, respectively [60]. As a result, N/OFQ(1-13)-NH2, which is the shortest peptide sequence that maintains the potency, efficacy, and affinity as N/OFQ, has been used as a template to design a new series of N/OFQ analogues. In the frame of SAR studies, several peptides with distinct pharmacological activity have been identified such as [Phe1Ψ(CH2-NH)Gly2]N/OFQ(1-13)NH2, UFP-101, and [Nphe1]N/OFQ(1-13)NH2 (NOP receptor antagonists), UFP-112 (highly potent NOP receptor agonist), and UFP-113 (partial NOP receptor agonist) [61–65]. The peptides that have antinociceptive activity are summarized in Table 1 and described below.

Table 1. The peptides that have antinociceptive activity are summarized.

Name/Structure	Category	In Vitro Human NOP Receptor			In Vivo		Ref
		Receptor Binding pKi	$[^{35}S]GTP\gamma S$ pK_B/pA_2	Ca^{+2} Mobilization pK_B/pA_2	Administration Route/Dose/Species	Effect	
[Nphe^1]N/OFQ(113)NH$_2$	Selective NOP receptor antagonist	8.39	7.33	6.29	(30 nmol) i.c.v. mice	Analgesia Promote morphine-induced analgesia.	[61]
[Nphe^1, Arg^{14}, Lys^{15}]N/OFQ-NH$_2$ (UFP-101)	Selective NOP receptor antagonist	10.24	8.85	7.66	(10 nmol) i.c.v. mice	Long lasting analgesia Block N/OFQ effect on locomotor activity	[62]
					(10 nmol) i.t. mice	Block N/OFQ (i.t.1 nmol) analgesic effect	[66]
[(pF)Phe^{4}Aib^{7}Arg^{14}Lys^{15}]N/OFQ-NH$_2$ (UFP-112)	Selective NOP receptor agonist	10.55	10.55	9.05	(1–100 pmol) i.c.v. mice	Hyperalgesia Decrease locomotor activity	[67]
					(1–100 pmol) i.t. mice	Long lasting dose dependent analgesia	[67]
					(0.1 and 10 nmol/kg) Intravenous (i.v.) rats	Decrease heart rate Decrease blood pressure Decrease urinary sodium excretion Increase urine flow	[67]
					(1–10 nmol) i.t. monkey	Dose-dependent analgesia without inducing itch Promotes morphine-induced analgesia without increasing itch response	[68]

Table 1. *Cont.*

Name/Structure	Category	In Vitro Human NOP Receptor			In Vivo		Ref
		Receptor Binding pKi	[35S]GTPγS pK$_B$/pA$_2$	Ca^{+2} Mobilization pK$_B$/pA$_2$	Administration Route/Dose/Species	Effect	
[Phe$^{1\Psi}$(CH$_2$-NH)Gly^2(pF)Phe^{4}Aib^{7}Arg^{14}Lys^{15}] N/OFQ-NH$_2$ (UFP-113)	Selective NOP receptor partial agonist	10.26	9.72	7.97	(0.001–1 nmol) i.t. rats	Analgesia	[69]
PWT2-N/OFQ	Selective NOP receptor agonist	10.3	10.12	8.83	(250 pmol) i.c.v. mice	Decease locomotor activity	[70]
					(2.5–250 pmol) i.t. mice	Dose-dependent analgesia	[71]
					(0.3, 1, and 3 nmol) i.t. monkey	Analgesia No itching No sedation No impairment in motor activity	[71]

4.1.1. [Nphe^1]N/OFQ(1-13)NH2

A preliminary hypothesis regarding the behavior of NOP receptor-active compounds stated that if N/OFQ induces pain, antagonists are likely to exhibit antinociceptive activity. To test this, [Nphe^1]N/OFQ(1-13)-NH$_2$, the first reported peptide with antagonist activity, was generated by shifting the side chain of Phe^1 from C to N atom in the amidated N/OFQ. A binding assay using Chinese hamster ovary (CHO) cells that express recombinant human NOP receptor and cyclic AMP accumulation in CHO cells identified the antagonistic properties of [Nphe^1]N/OFQ(1-13)-NH$_2$. The mouse tail withdrawal assay revealed that a single i.c.v. administration of [Nphe^1]N/OFQ(1-13)NH2 increased the tail withdrawal latency time, while a combinational administration of [Nphe^1]N/OFQ(1-13)NH2 with N/OFQ and morphine inverted the reduction of tail withdrawal latency time latency and promoted the antinociceptive effect of morphine, respectively, implying the analgesic action of this ligand [61,72].

4.1.2. [Nphe^1, Arg^{14}, Lys^{15}]N/OFQ-NH$_2$ (UFP-101)

Previous studies have shown that the binding of C-terminus-amidated N/OFQ to the acidic restudies at the ECL2 of NOP receptor was enhanced by inserting Arg and Lys [35,73]. Combination of [Nphe^1]N/OFQ(1-13)-NH$_2$ and [Arg^{14}, Lys^{15}]N/OFQ-NH$_2$ led to the generation of a new peptide [Nphe^1, Arg^{14}, Lys^{15}]N/OFQ-NH$_2$, also called UFP-101 [62]. In vitro assays including functional binding assays using (CHO cells expressing human NOP receptor and [35S]-GTPγS), cyclic AMP accumulation experiment, and Schild regression analysis of electrically stimulated isolated peripheral (rats, mice, and guinea pigs) and central tissues (rat) showed that UFP-101 competitively antagonized the effects of N/OFQ. Similar to [Nphe^1]N/OFQ(1-13)-NH$_2$, i.c.v. administration of 10 nmol UFP-101 produced antinociceptive effect in the mouse tail withdrawal assay, but with higher potency and longer duration of action, indicating that the presence of Arg^{14} and Lys^{15} may promote either the binding of UFP-101 to NOP receptor and/or the UFP-101 metabolic stability. Since UFP-101 is a selective NOP receptor antagonist, it has been also used as a research tool to confirm that NOP receptor mediates both the inhibition of spinal excitatory transmission in vitro as well as the spinal antinociception in vivo [66].

4.1.3. [(pF)Phe^{4}Aib^{7}Arg^{14}Lys^{15}]N/OFQ-NH$_2$ (UFP-112)

The chemical modifications of the phenyl ring in Phe4 residue that is essential for NOP receptor activation by inserting pF along with the replacement of Ala at position 7 by α-aminoisobutyric acid (Aib) in N/OFQ sequence resulted in generation of more potent lig-

ands [74–76]. By applying these two chemical modifications to [Arg^{14}, Lys^{15}]N/OFQ-NH$_2$, [(pF)Phe^{4}Aib^{7}Arg^{14}Lys^{15}]N/OFQ-NH$_2$, also known as (UFP-112), was synthesized [67]. This ligand acts as a potent (100-fold higher than N/OFQ) and a selective NOP receptor agonist. A long-lasting dose dependent antinociceptive effect was observed after the i.t. administration of UFP-112 (1–100 pmol) in the mouse tail withdrawal assay. In contrast, the same dose of UFP-112 produced a pronociceptive effect and a long-lasting reduction in the locomotor activity when it was administered intracerebroventricularly. Subsequent to intravenous (i.v.) administration of UFP-112 in rats, diuresis as well as reduction in heart rate, blood pressure, and urinary sodium excretion were significantly observed. Consistent with the mouse tail withdrawal assay finding, a long-lasting dose dependent antinociceptive effect was also observed after the i.t. administration of UFP-112 (1–10 nmol) in monkeys without inducing itching by using acute and chronic primate pain modalities (acute noxious stimulus and capsaicin-induced thermal hyperalgesia, respectively) [68]. Notably, the spinal administration of a subthreshold dose of UFP-112 (1 nmol) synergized a morphine analgesic effect without increasing pruritus.

4.1.4. [Phe$^{1\Psi}$(CH$_2$-NH)Gly^2(pF)Phe^{4}Aib^{7}Arg^{14}Lys^{15}]N/OFQ-NH$_2$ (UFP-113)

The combination of [Phe$^{1\Psi}$(CH$_2$-NH)Gly^2](N/OFQ-NH$_2$ that was synthesized to further avoid the protease degradation [63] and the mentioned above [(pF)Phe^{4}Aib^{7}Arg^{14}Lys^{15}] N/OFQ-NH$_2$, UFP-112, led to the generation of [Phe$^{1\Psi}$(CH$_2$-NH)Gly^2(pF)Phe^{4}Aib^{7}Arg^{14} Lys^{15}]N/OFQ-NH$_2$, also referred to as UFP-113 [77]. In vitro pharmacological characterization studies that include the functional [^{35}S]-GTPγS binding in CHO cells that express the human NOP receptor and electrically stimulated mouse and rat vas deferens and guinea pig ileum tissues, reveals that UFP-113 acts as a selective partial agonist for NOP receptor [77]. The spinal catheterization of UFP-113 induced an analgesic response in rats at doses that range between (0.001 and 1 nmol); however, in the knockout of rats for the NOP receptor gene the analgesic effect no longer persisted, implying that the antinociceptive effect of UFP-113 is mediated through the NOP receptor stimulation [69].

4.1.5. PWT2-N/OFQ

By employing a novel chemical strategy using peptide wilding approach (PWT), three tetrabranched derivatives of N/OFQ that include PWT1-N/OFQ, PWT2-N/OFQ, and PWT3-N/OFQ were generated [78]. Both in vitro ([^{35}S]-GTPγS binding, calcium mobilization, and electrically stimulated mouse vas deferens assays) and in vivo studies using NOP receptor gene knocked out [NOP receptor (−/−)], revealing that these PWT derivatives act as full NOP receptor agonists that have high potency and a long duration of action of, particularly in PWT2-N/OFQ (40-fold more potent than N/OFQ) [70]. Additionally, analgesic effects were reported after the spinal administration of PWT2-N/OFQ using the nociceptive pain model (tail withdrawal assay) and the neuropathic pain model (chronic constriction injury) in mice and monkeys [71]. PWT2-N/OFQ exhibited higher potency (40-fold more potent) and longer duration (10-fold longer duration of action) in comparison to N/OFQ.
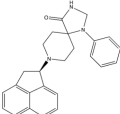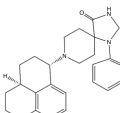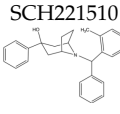
Despite having high potency and selectivity of the previously mentioned NOP receptor peptides in targeting NOP receptor, their pharmacokinetic properties, specifically their poor penetration across the blood-brain barrier have limited their therapeutic indications. However, these peptides have substantially contributed to the detailed understanding of the various responses of the peripheral (respiratory, gastrointestinal, genitourinary, immune, and cardiovascular systems) and central (pain transmission, anxiety, food intake, locomotion, and drug addiction) systems that are related to the N/OFQ–NOP receptor system.

4.2. *Non-Peptide NOP Receptor Ligands Targeting Pain*

To overcome the poor metabolic stability of peptide ligands related to N/OFQ and require to be administered either intrathecally or intracerebroventricularly, several studies were conducted to identify new selective non-peptide ligands that are suitable for in-

traperitoneal or oral administration. High-throughput screening and medicinal chemistry research have led to the discovery of multiple classes of chemical compounds including piperidines, spiropiperidines, nortropanes, 4-amino-quinolines, and quinazolines that act as NOP receptor ligands with enhanced metabolic stability. The non-peptides that have antinociceptive activity are summarized in Table 2 and described below.

Table 2. Non-peptide NOP receptor ligands targeting pain.

Name/Structure	Category	In Vitro Human NOP Receptor			In Vivo		Ref
		Receptor Binding pKi	[^{35}S]GTPγS pEC$_{50}$	Ca^{+2} MobilizationpEC$_{50}$	Administration Route/Dose/Species	Effect	
Ro 65-6570	NOP receptor non peptide agonist	8.6			(0.1–1 mg/kg) (0.03 to 1 μmol/kg) i.v. mice	Analgesia	[79,80]
Ro 64-6198	NOP receptor nonpeptide agonist	9.41	8.09	7.98	(3 mg/kg) (1 mg/kg) intraperitoneal (i.p) mice (0.3 to 3 mg/kg) i.p. mice	Analgesia Additive analgesia anxiolytic-like effects	[81–83]
					(0.001–0.06 mg/kg), subcutaneous (s.c.) monkey	Analgesia No depression No itching No reinforcing	[17]
SCH221510	Selective NOP receptor nonpeptide agonist	0.3	12		1–30 mg/kg) peroral (p.o.) rat	anxiolytic-like effects	[84]
					(0.1–3.0 mg/kg) i.p., p.o., intracolonic mice	potent anti-inflammatory and analgesic effect	[85]

4.2.1. Ro 65-6570

The high-throughput screening of 8-acenaphthene-l-yl-l-phenyl-l,3,8-triaza-spiro[4.5]decan-4-one was performed to develop Ro 65-6570, 8-(1,2-dihydroacenaphthylen-1-yl)-1-phenyl-1,3,8-triazaspiro[4,5]decan-4-one, by a group of scientists at Roche laboratories [86]. In vitro studies that include radioligand binding and cAMP inhibition assays in (CHO) cells expressing the recombinant human NOP receptor indicated that Ro 65-6570 acts as a NOP receptor full agonist with poor selectivity in comparison to other opioid receptors [87]. In mice, i.v. administration of Ro 65-6570 resulted in dose-dependent antinociceptive effects without modifying motor coordination using formalin paw and orofacial formalin (OFF) tests [79,80]. Further in vitro functional selectivity studies such as the BRET-based assay revealed that Ro 65-6570 is a G protein-biased agonist which exhibited antinociceptive effects in β-arrestin 2 knockout mice as compared to the wild-type [88,89].

4.2.2. Ro 64-6198

In an effort to develop a new NOP receptor agonist with high selectivity (greater than 100-fold over canonical opioid receptors) and potency, [(1*S*,3a*S*)-8-(2,3,3a,4,5, 6- hexahydro-1*H*-phenalen-1-yl)-1-phenyl-1,3,8-triaza- spiro[4.5] decan-4-one], also known as Ro 64-6198, was identified by a group of scientists at Hoffman La Roche in Switzerland [81,90,91]. Using Ro 64-6198 as a valuable pharmacological tool highlighted therapeutic applications for NOP receptor agonist such as anxiety, neuropathic pain, addiction, cough, and anorexia, in addition to the undesirable effects it has on learning, memory, motor activity, and body temperature (hypothermia) [92]. Similar to morphine, analgesic effects in the hot plate and shock threshold assays were observed after the systemic administration of Ro 64-6198 (3 mg/kg, intraperitoneal (i.p)) in wild-type mice but not in NOP receptor

knockout mice [82,83]. Conversely, increased pain sensitivity was observed as an opposite effect in the tail flick assay, implying the complex role of NOP receptor in pain processing. Furthermore, coadministration of low doses (1 mg/kg) of Ro 64-6198 and morphine resulted in an additive analgesic effect [83]. Consistent with these findings, analgesic effects without causing depression, itching, and reinforcing responses were observed after the subcutaneous (s.c.) administration of Ro 64-6198 (0.001–0.06 mg/kg) in both acute (acute noxious stimulus) and chronic (capsaicin-induced neuropathic pain) pain modalities in monkeys [93]. Pretreatment with J-113397 (0.1 mg/kg), a selective nonpeptidic NOP receptor antagonist, blocked Ro 64-6198-induced antinociception, emphasizing that the antinociceptive actions of Ro 64-6198 is mediated via NOP receptor. Despite the robust analgesic effects of systemically administered Ro 64-6198 in non-human primates, several in vivo studies using tail flick and immersion, tactile or cold water stimulation and foot shock assays revealed that Ro 64-6198 does not modulate pain processing in rodents, except mouse hot plate assay [81,83,93–95].

4.2.3. SCH221510

SCH221510 is a potent and selective non-peptide NOP receptor agonist that was reported to induce analgesia in neuropathic pain when administered orally and intrathecally in mice and rat models, respectively [96–98]. It is also reported to attenuate the respiratory depression and itch response that were observed after the systemic administration of buprenorphine to a non-human primate, as well as reinforcing MOP receptor agonists induced responses in rats [97,99]. Conversely, a s.c. administration of SCH221510 (3 and 10 mg/kg) in hot-plate test did not produce analgesia, while SCH221510 administration (3 mg/kg) reduced morphine-induced analgesia. The co-administration of SCH221510 (3 mg/kg) and morphine (10 mg/kg) accelerated the tolerance development to the antinociceptive effect of morphine in female mice [100].

4.3. Bifunctional and Mixed NOP Receptor Compounds

Considering the potential ability of intracerebroventricularly administered N/OFQ to attenuate morphine tolerance and suppress drug reinforcing response, the development of new synthetic agonists may constitute an innovative pharmacological approach for analgesics that target both MOP receptor and NOP receptor to enhance their analgesic effect and minimize their side effects as depicted in Figure 2 [99,101–105]. Additionally, multiple pathophysiological pathways are involved in the pain process, so developing analgesic agents with multiple mechanisms of actions could be an innovative strategy for developing new effective and safe analgesics [106]. Accordingly, several compounds including AT-121 (a partial agonist of NOP receptor and MOP receptor), buprenorphine (semisynthetic multifunctional opioid), and its analogue BU08028 were synthesized (reviewed in [107–109]).

4.3.1. SR 16435

SR 16435 (Figure 3), also referred to as [1-(1-(bicyclo[3.3.1]nonan-9-yl)piperidin-4-yl)indolin-2-one] behaved as a bi-functional NOP receptor /MOP receptor partial agonist with high binding affinity was synthesized by Toll group [110]. In mice, SR 16435 administration produced an analgesic effect (s.c. and i.t.) which was effective and potent in attenuating both neuropathic and inflammatory pain (i.t) with diminished tolerance development to the antinociceptive effect of SR 16435 [96,110]. Nonetheless, the conditioned place preference (CPP) that was primarily mediated by MOP receptor activation was induced after the administration of SR 16435. This finding emphasizes that full agonistic activity at NOP receptor could be required to reduce the rewarding properties associated with MOP receptor [110].
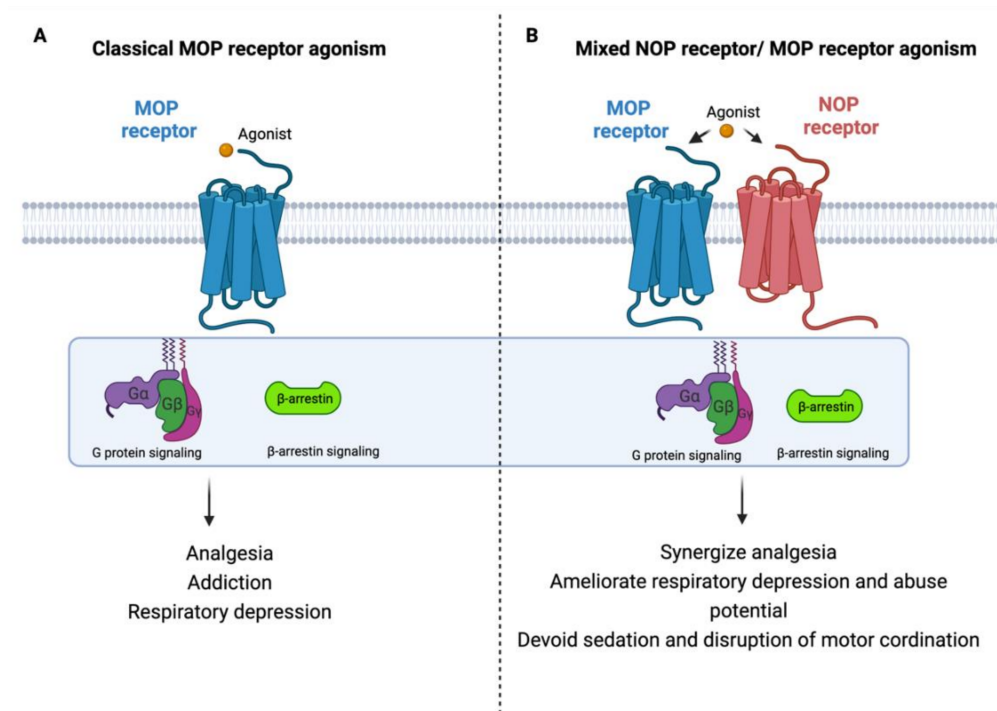
Figure 2. Rational design of new safer analgesics. (**A**) Beneficiary and side effects produced by MOP receptor activation. (**B**) Beneficiary (synergizing analgesic effect) and protective (ameliorating typical-opioid side effect profile) effects produced by developing a new compound with simultaneous agonistic activity at NOP receptor and MOP receptor.

Cebranopadol

Ki (NOP) = 0.9 nM
Ki (MOP) = 0.7 nM
NOP EC$_{50}$ =13 nM [^{35}S]GTPγS
MOP EC$_{50}$ = 1.2 nM
NOP E$_{max}$ = 88.9%
MOP E$_{max}$ = 103.5%
ED$_{50}$ = 0.5-5.6 μg/kg (i.v., rat)
ED$_{50}$ =25.1 μg/kg (oral, rat)

SR 16435

Ki (NOP) = 7.5 nM
Ki (MOP) EC50 =2.7 nM
NOP EC$_{50}$ =28.7 nM [^{35}S]GTPγS
MOP EC$_{50}$ = 29.5 nM [^{35}S]GTPγS
NOP E$_{max}$ = 45%
MOP E$_{max}$ = 30%

AT-121

Ki (NOP) = 3.7 nM
Ki (MOP) = 16.5 nM
NOP EC$_{50}$ = 34.7 nM [^{35}S]GTPγS
MOP EC$_{50}$ = 19.6 nM [^{35}S]GTPγS
NOP E$_{max}$ = 41.1%
MOP E$_{max}$ = 14.2%

Buprenorphine

Ki (NOP) = 285 nM
Ki (MOP) = 0.08 nM
Ki (KOP)= 0.11 nM
Ki (DOP) = 0.42 nM
NOP EC$_{50}$ = 35 nM [^{35}S]GTPγS
MOP EC$_{50}$ = 0.08 nM [^{35}S]GTPγS
KOP EC$_{50}$ = 0.04 nM [^{35}S]GTPγS
ED$_{50}$ = 0.044 mg/kg (monkey)
NOP E$_{max}$ = 60%
MOP E$_{max}$ = 38%
KOP E$_{max}$ = 10%

BU08028

Ki (NOP) = 8.5 nM
Ki (MOP) EC50 = 2.1 nM
NOP EC$_{50}$ =78.6 nM [^{35}S]GTPγS
MOP EC$_{50}$ =6 nM [^{35}S]GTPγS
NOP E$_{max}$ = 48%
MOP E$_{max}$ = 21.1%

BU10038

Ki (NOP) = 14.8 nM
Ki (MOP) = 0.9 nM
Ki (KOP) = 1.2 nM
NOP EC$_{50}$ = 44 nM [^{35}S]GTPγS
NOP E$_{max}$ = 34%

BPR1M97

Ki (NOP) = 4.2 nM
Ki (MOP) = 1.8 nM
NOP EC$_{50}$ = 1.8 nM (cAMP assay)
MOP EC$_{50}$ = 0.6 nM (cAMP assay)
NOP E$_{max}$ =109% (cAMP assay)
MOP E$_{max}$ = 97.5% (cAMP assay)

JTC-801

Ki (NOP) = 8.2 nM

Figure 3. Chemical structures and in vitro pharmacological profiles of bifunctional and mixed NOP receptor ligands that target pain [99,110–119].

4.3.2. AT-121

AT-121 (Figure 3) is a non- morphinan compound which acts as a bifunctional NOP receptor /MOP receptor partial agonist with high binding affinity [114]. It was synthesized to optimize the pharmacological profile of MOP receptor agonists by synergizing their therapeutic effects (analgesia and treatment of substance abuse) and minimizing their side effects (respiratory depression, tolerance dependent, and abuse liability) via targeting NOP receptor. In monkeys, s.c. administration of AT-121 produced morphine-like analgesic and antiallodynic effects using the warm water tail-withdrawal assay and capsaicin-induced allodynia, respectively, without trigging itch, physical dependence, respiratory depression, and hyperalgesia mediated by opioid. These effects were confirmed to be mediated by MOP receptor and NOP receptor activation by using selective dose of MOP receptor and NOP receptor antagonists, J-113397 (0.1 mg/kg) and naltrexone (0.03 mg/kg), respectively. Additionally, AT-121 could be therapeutically implicated for opioid addiction as it lacks the abuse potential (reinforcing effects) and diminished oxycodone reinforcing response.

4.3.3. Buprenorphine and Its Analog BU08028

Buprenorphine (Figure 3) is a natural derived alkaloid of the opium poppy with a mixed pharmacological activity (MOP receptor /NOP receptor partial agonist and DOP receptor /KOP receptor low partial agonist) clinically approved to treat pain and substance abuse [99,115]. In rodent, full analgesic effects were produced after the administration of buprenorphine in both chronic and acute pain models [120]. After a systemic administration of 0.01–0.1 mg/kg to a non-human primate, an antinociceptive effect was present in a dose-dependent manner. A resultant respiratory depression and itch were observed and subsequently confirmed to be induced by MOP receptor activation. These side effects associated with buprenorphine were found to be attenuated by the co-administration of an NOP receptor selective agonist such as Ro 64-6198 and SCH 221510 [99]. As such, the combination emphasized the therapeutic potential of mixed MOP receptor /NOP receptor agonists as innovative analgesics. A buprenorphine analog that is known as BU08028 (Figure 3) demonstrated a similar binding profile to buprenorphine with improved binding affinity and efficacy to NOP receptor. In mice, an intrathecal administration of BU08028 produced an analgesic effect, which was more potent than morphine in attenuating both neuropathic and inflammatory pain [96]. Consistent with these results, a systemic administration of BU08028 to a non-human primate produced a long-lasting analgesic effect (>24 h) with a reduced reinforcing effect as compared to cocaine, remifentanil, or buprenorphine and without causing respiratory depression and CVS adverse effects [121].

4.3.4. BPR1M97

By applying a high-throughput screening, BPR1M97 (Figure 3) was identified as a dual agonist that produced a significant analgesic effect in a tail-flick assay in mice [122]. Both in vitro assays (radioligand binding, c-AMP production, membrane potential, β-Arrestin-2 recruitment, and internalization assays) and in vivo behavior assays (tail flick and clip, respiratory and cardiovascular functional, acetone drop, von Frey hair, charcoal meal, glass bead, locomotor activity, conditioned place preference (CPP) and naloxone precipitation assays) proved that BPR1M97 behaved as a dual agonist for MOP receptor (full agonist) and NOP receptor (G-protein biased agonist) [118]. Notably, rapid analgesic actions (more potent than morphine in cancer-induced sensory allodynia) were observed after the BPR1M97 s.c. administration with less undesirable side effect as compared to morphine.

4.3.5. BU10038

A naltrexone-derived bifunctional MOP receptor /NOP receptor agonist, also referred to as BU10038 (Figure 3), behaved as a partial MOP receptor and NOP receptor agonist was synthesized by Husbands and Ko groups [117]. In non-human primate, both systemic (0.001–0.01 mg/kg) and intrathecal (3 mg) administrations of BU10038 resulted in a

long-lasting antinociceptive with neither reinforcing effects nor other effects like itching, respiratory depression, and tolerance when administered repeatedly.

4.3.6. JTC-801

JTC-801 (Figure 3), also referred to as [N-(4-amino-2-methylquinolin-6-yl)-2-(4-ethylphenoxymethyl) benzamide hydrochloride], behaved as a NOP receptor antagonist and was developed by a group of scientists at the Central Pharmaceutical Research Institute [119]. JTC-801 produced antinociceptive effects in a hot plate test and a formalin test using mice and rats, respectively. Although the injectable and oral formulations of JTC-801 entered Phase II of its clinical trials in both Japan and the UK to treat the neuropathic and postoperative pain, it was suspended for unknown reasons [123].

4.3.7. Cebranopadol

The rational optimization strategy of spiro[cyclohexanedihydropyrano[3,4-b]indole]-amine resulted in the discovery of cebranopadol (Figure 3) that represents the first in its class to be a highly potent and efficacious antinociceptive agent with combined agonistic activity at MOP receptor, NOP receptor (subnanomolar affinity), KOP receptor, and DOP receptor (low nanomolar affinity) [111,112,124]. Behavior in vivo studies including acute and chronic pain models in rodents (tail-flick, formalin test, rheumatoid arthritis, bone cancer, spinal nerve ligation, diabetic neuropathy) further indicated the high potency and extremely long-lasting analgesic effect of cebranopadol in comparison with selective MOP receptor agonist, particularly in the chronic pain model [111,125]. Extensive preclinical safety and tolerability studies have been conducted on rodent models to reveal the possible side effects on the CNS, the respiratory system, and the gastrointestinal system (reviewed in [126]). Limited range of unwanted effects were also observed, as cebranopadol did not decrease respiratory rate, develop a tolerance, or impair the motor coordination, unlike the effects of morphine. The G-protein-biased agonistic activity at NOP receptor could be the reason behind these favorable side effect profiles of cebranopadol [125]. Notably, cebranopadol is equipotent and equi-efficacious toward the G protein activation at both MOP receptor and NOP receptor without inducing phosphorylation or NOP receptor internalization and without recruiting B-arrestin2 at NOP receptor only in BRET assay [125,127]. The noncompartmental analysis in phase I and phase II clinical trials was used to assess the pharmacokinetics profiles of cebranopadol. The maximum plasma concentration [Cmax] (4–6 h) with a long half-value duration (14–15 h) was reached after oral administration of immediate release formulation of cebranopadol. After the administration of multiple once-daily oral doses of cebranopadol in patients, the steady state was reached in nearly 2 weeks. Following single- and multiple-doses administration of cebranopadol in healthy subjects and patients, a two-compartment disposition model with first-order elimination process and a two lagged transition compartments was observed [128]. Several phase II clinical trials were conducted and listed as complete in patients suffering from acute (bunionectomy trial) and chronic (diabetic neuropathy, osteoarthritis, chronic low back pain, and diabetic polyneuropathy) pain to evaluate the efficacy, safety, and tolerability of a single oral dose of cebranopadol [129–135]. While most phase III clinical trials have recently proven the effectiveness, safety, and tolerability of cebranopadol when administered orally (200–1000 μg per day) to cancer patients who suffer from moderate to severe chronic pain [136,137].

5. Future Directions and Conclusions

In this review, the rational design of NOP receptor ligands with various pharmacological profiles as a promising alternative for conventional opioid analgesic is discussed. The crystal structure, distribution, and signaling pathway of NOP receptor are also highlighted. It is important to note that other therapeutic indications for NOP receptor in the treatment of various neurological disorders and alcohol abuse have not been explored in this review. Notably, NOP receptor-related peptides have substantially attributed in expanding our

knowledge regarding the various peripheral and central responses related to N/OFQ–NOP receptor system, but their poor bioavailability has limited their therapeutic implications. Regardless of the controversial results between the spinal and supraspinal administration of endogenous neuropeptide of NOP receptor that remains poorly understood, the NOP receptor ligands exhibit favorable pharmacological activity and side effects, particularly the mixed which target multiple opioid receptors. So far, cebranopadol represents the most promising NOP receptor ligand to treat acute and chronic pain without reducing respiratory rate, developing a tolerance, or impairing the motor coordination as compared to the clinically approved opioid analgesic. However, further work needs to be done to resolve the high-resolution structure of NOP receptor in its active state to elucidate the distinct residues responsible for NOP receptor agonist binding [138]. Conceivably, a deep understanding of the NOP receptor signaling pathway and structure along with computer-aided molecular docking and behavior studies will facilitate the discovery of polypharmacological ligands that target multiple receptors including NOP receptor as new effective and safe analgesics.

References

1. Gaskin, D.J.; Richard, P. The economic costs of pain in the United States. *J. Pain* **2012**, *13*, 715–724. [CrossRef]
2. Brownstein, M.J. A brief history of opiates, opioid peptides, and opioid receptors. *Proc. Natl. Acad. Sci. USA* **1993**, *90*, 5391–5393. [CrossRef] [PubMed]
3. Volkow, N.D.; Collins, F.S. The Role of Science in Addressing the Opioid Crisis. *N. Engl. J. Med.* **2017**, *377*, 391–394. [CrossRef]
4. Ballantyne, J.C.; Kalso, E.; Stannard, C. WHO analgesic ladder: A good concept gone astray. *BMJ* **2016**, *352*, i20. [CrossRef] [PubMed]
5. Bruchas, M.R.; Roth, B.L. New Technologies for Elucidating Opioid Receptor Function. *Trends Pharmacol. Sci.* **2016**, *37*, 279–289. [CrossRef]
6. Khademi, H.; Kamangar, F.; Brennan, P.; Malekzadeh, R. Opioid Therapy and its Side Effects: A Review. *Arch. Iran. Med.* **2016**, *19*, 870–876. [PubMed]
7. Iwanicki, J.L.; Severtson, S.G.; Margolin, Z.; Dasgupta, N.; Green, J.L.; Dart, R.C. Consistency between Opioid-Related Mortality Trends Derived From Poison Center and National Vital Statistics System, United States, 2006–2016. *Am. J. Public Health* **2018**, *108*, 1639–1645. [CrossRef] [PubMed]
8. Kirson, N.Y.; Scarpati, L.M.; Enloe, C.J.; Dincer, A.P.; Birnbaum, H.G.; Mayne, T.J. The Economic Burden of Opioid Abuse: Updated Findings. *J. Manag. Care Spec. Pharm.* **2017**, *23*, 427–445. [CrossRef]
9. Available online: https://www.cdc.gov/nchs/nvss/vsrr/drug-overdose-data.htm (accessed on 12 January 2022).
10. Wacker, D.; Stevens, R.C.; Roth, B.L. How Ligands Illuminate GPCR Molecular Pharmacology. *Cell* **2017**, *170*, 414–427. [CrossRef]
11. Anton, B.; Fein, J.; To, T.; Li, X.; Silberstein, L.; Evans, C.J. Immunohistochemical localization of ORL-1 in the central nervous system of the rat. *J. Comp. Neurol.* **1996**, *368*, 229–251. [CrossRef]
12. Mollereau, C.; Mouledous, L. Tissue distribution of the opioid receptor-like (ORL1) receptor. *Peptides* **2000**, *21*, 907–917. [CrossRef]
13. Neal, C.R., Jr.; Mansour, A.; Reinscheid, R.; Nothacker, H.P.; Civelli, O.; Akil, H.; Watson, S.J., Jr. Opioid receptor-like (ORL1) receptor distribution in the rat central nervous system: Comparison of ORL1 receptor mRNA expression with (125)I-[(14)Tyr]-orphanin FQ binding. *J. Comp. Neurol.* **1999**, *412*, 563–605. [CrossRef]
14. Meunier, J.C.; Mollereau, C.; Toll, L.; Suaudeau, C.; Moisand, C.; Alvinerie, P.; Butour, J.L.; Guillemot, J.C.; Ferrara, P.; Monsarrat, B.; et al. Isolation and structure of the endogenous agonist of opioid receptor-like ORL1 receptor. *Nature* **1995**, *377*, 532–535. [CrossRef] [PubMed]
15. Reinscheid, R.K.; Nothacker, H.P.; Bourson, A.; Ardati, A.; Henningsen, R.A.; Bunzow, J.R.; Grandy, D.K.; Langen, H.; Monsma, F.J., Jr.; Civelli, O. Orphanin FQ: A neuropeptide that activates an opioidlike G protein-coupled receptor. *Science* **1995**, *270*, 792–794. [CrossRef]
16. Xu, X.J.; Hao, J.X.; Wiesenfeld-Hallin, Z. Nociceptin or antinociceptin: Potent spinal antinociceptive effect of orphanin FQ/nociceptin in the rat. *Neuroreport* **1996**, *7*, 2092–2094.
17. Ko, M.C.; Naughton, N.N. Antinociceptive effects of nociceptin/orphanin FQ administered intrathecally in monkeys. *J. Pain* **2009**, *10*, 509–516. [CrossRef]
18. Ko, M.C.; Wei, H.; Woods, J.H.; Kennedy, R.T. Effects of intrathecally administered nociceptin/orphanin FQ in monkeys: Behavioral and mass spectrometric studies. *J. Pharmacol. Exp. Ther.* **2006**, *318*, 1257–1264. [CrossRef] [PubMed]

19. Yamamoto, T.; Nozaki-Taguchi, N.; Kimura, S. Analgesic effect of intrathecally administered nociceptin, an opioid receptor-like1 receptor agonist, in the rat formalin test. *Neuroscience* **1997**, *81*, 249–254. [CrossRef]

20. Bunzow, J.R.; Saez, C.; Mortrud, M.; Bouvier, C.; Williams, J.T.; Low, M.; Grandy, D.K. Molecular cloning and tissue distribution of a putative member of the rat opioid receptor gene family that is not a mu, delta or kappa opioid receptor type. *FEBS Lett.* **1994**, *347*, 284–288. [CrossRef]

21. Fukuda, K.; Kato, S.; Mori, K.; Nishi, M.; Takeshima, H.; Iwabe, N.; Miyata, T.; Houtani, T.; Sugimoto, T. cDNA cloning and regional distribution of a novel member of the opioid receptor family. *FEBS Lett.* **1994**, *343*, 42–46. [CrossRef]

22. Mollereau, C.; Parmentier, M.; Mailleux, P.; Butour, J.L.; Moisand, C.; Chalon, P.; Caput, D.; Vassart, G.; Meunier, J.C. ORL1, a novel member of the opioid receptor family. Cloning, functional expression and localization. *FEBS Lett.* **1994**, *341*, 33–38. [CrossRef]

23. Nishi, M.; Takeshima, H.; Mori, M.; Nakagawara, K.; Takeuchi, T. Structure and chromosomal mapping of genes for the mouse kappa-opioid receptor and an opioid receptor homologue (MOR-C). *Biochem. Biophys. Res. Commun.* **1994**, *205*, 1353–1357. [CrossRef] [PubMed]

24. Osinski, M.A.; Pampusch, M.S.; Murtaugh, M.P.; Brown, D.R. Cloning, expression and functional role of a nociceptin/orphanin FQ receptor in the porcine gastrointestinal tract. *Eur. J. Pharmacol.* **1999**, *365*, 281–289. [CrossRef]

25. Wick, M.J.; Minnerath, S.R.; Lin, X.; Elde, R.; Law, P.Y.; Loh, H.H. Isolation of a novel cDNA encoding a putative membrane receptor with high homology to the cloned mu, delta, and kappa opioid receptors. *Brain Res. Mol.* **1994**, *27*, 37–44. [CrossRef]

26. Mollereau, C.; Moisand, C.; Butour, J.L.; Parmentier, M.; Meunier, J.C. Replacement of Gln280 by His in TM6 of the human ORL1 receptor increases affinity but reduces intrinsic activity of opioids. *FEBS Lett.* **1996**, *395*, 17–21. [CrossRef]

27. Mollereau, C.; Simons, M.J.; Soularue, P.; Liners, F.; Vassart, G.; Meunier, J.C.; Parmentier, M. Structure, tissue distribution, and chromosomal localization of the prepronociceptin gene. *Proc. Natl. Acad. Sci. USA* **1996**, *93*, 8666–8670. [CrossRef] [PubMed]

28. Nothacker, H.P.; Reinscheid, R.K.; Mansour, A.; Henningsen, R.A.; Ardati, A.; Monsma, F.J., Jr.; Watson, S.J.; Civelli, O. Primary structure and tissue distribution of the orphanin FQ precursor. *Proc. Natl. Acad. Sci. USA* **1996**, *93*, 8677–8682. [CrossRef]

29. Toll, L.; Bruchas, M.R.; Calo, G.; Cox, B.M.; Zaveri, N.T. Nociceptin/Orphanin FQ Receptor Structure, Signaling, Ligands, Functions, and Interactions with Opioid Systems. *Pharmacol. Rev.* **2016**, *68*, 419–457. [CrossRef]

30. Cox, B.M.; Christie, M.J.; Devi, L.; Toll, L.; Traynor, J.R. Challenges for opioid receptor nomenclature: IUPHAR Review 9. *Br. J. Pharmacol.* **2015**, *172*, 317–323. [CrossRef]

31. Miller, R.L.; Thompson, A.A.; Trapella, C.; Guerrini, R.; Malfacini, D.; Patel, N.; Han, G.W.; Cherezov, V.; Caló, G.; Katritch, V.; et al. The Importance of Ligand-Receptor Conformational Pairs in Stabilization: Spotlight on the N/OFQ G Protein-Coupled Receptor. *Structure* **2015**, *23*, 2291–2299. [CrossRef]

32. Thompson, A.A.; Liu, W.; Chun, E.; Katritch, V.; Wu, H.; Vardy, E.; Huang, X.P.; Trapella, C.; Guerrini, R.; Calo, G.; et al. Structure of the nociceptin/orphanin FQ receptor in complex with a peptide mimetic. *Nature* **2012**, *485*, 395–399. [CrossRef]

33. Akuzawa, N.; Takeda, S.; Ishiguro, M. Structural modelling and mutation analysis of a nociceptin receptor and its ligand complexes. *J. Biochem.* **2007**, *141*, 907–916. [CrossRef]

34. Daga, P.R.; Zaveri, N.T. Homology modeling and molecular dynamics simulations of the active state of the nociceptin receptor reveal new insights into agonist binding and activation. *Proteins* **2012**, *80*, 1948–1961. [CrossRef]

35. Topham, C.M.; Moulédous, L.; Poda, G.; Maigret, B.; Meunier, J.C. Molecular modelling of the ORL1 receptor and its complex with nociceptin. *Protein Eng.* **1998**, *11*, 1163–1179. [CrossRef] [PubMed]

36. Ozawa, A.; Brunori, G.; Mercatelli, D.; Wu, J.; Cippitelli, A.; Zou, B.; Xie, X.S.; Williams, M.; Zaveri, N.T.; Low, S.; et al. Knock-In Mice with NOP-eGFP Receptors Identify Receptor Cellular and Regional Localization. *J. Neurosci.* **2015**, *35*, 11682–11693. [CrossRef]

37. Peluso, J.; LaForge, K.S.; Matthes, H.W.; Kreek, M.J.; Kieffer, B.L.; Gavériaux-Ruff, C. Distribution of nociceptin/orphanin FQ receptor transcript in human central nervous system and immune cells. *J. Neuroimmunol.* **1998**, *81*, 184–192. [CrossRef]

38. Neal, C.R., Jr.; Akil, H.; Watson, S.J., Jr. Expression of orphanin FQ and the opioid receptor-like (ORL1) receptor in the developing human and rat brain. *J. Chem. Neuroanat.* **2001**, *22*, 219–249. [CrossRef]

39. Lambert, D.G. The nociceptin/orphanin FQ receptor: A target with broad therapeutic potential. *Nat. Rev. Drug Discov.* **2008**, *7*, 694–710. [CrossRef]

40. Childers, S.R.; Creese, I.; Snowman, A.M.; Synder, S.H. Opiate receptor binding affected differentially by opiates and opioid peptides. *Eur. J. Pharmacol.* **1979**, *55*, 11–18. [CrossRef]

41. Childers, S.R.; Snyder, S.H. Guanine nucleotides differentiate agonist and antagonist interactions with opiate receptors. *Life Sci.* **1978**, *23*, 759–761. [CrossRef]

42. Connor, M.; Christie, M.J. Modulation of Ca^{2+} channel currents of acutely dissociated rat periaqueductal grey neurons. *J. Physiol.* **1998**, *509*, 47–58. [CrossRef] [PubMed]

43. Darlison, M.G.; Greten, F.R.; Harvey, R.J.; Kreienkamp, H.J.; Stühmer, T.; Zwiers, H.; Lederis, K.; Richter, D. Opioid receptors from a lower vertebrate (Catostomus commersoni): Sequence, pharmacology, coupling to a G-protein-gated inward-rectifying potassium channel (GIRK1), and evolution. *Proc. Natl. Acad. Sci. USA* **1997**, *94*, 8214–8219. [CrossRef]

44. Zhang, N.R.; Planer, W.; Siuda, E.R.; Zhao, H.C.; Stickler, L.; Chang, S.D.; Baird, M.A.; Cao, Y.Q.; Bruchas, M.R. Serine 363 is required for nociceptin/orphanin FQ opioid receptor (NOPR) desensitization, internalization, and arrestin signaling. *J. Biol. Chem.* **2012**, *287*, 42019–42030. [CrossRef] [PubMed]

45. Mittal, N.; Roberts, K.; Pal, K.; Bentolila, L.A.; Fultz, E.; Minasyan, A.; Cahill, C.; Pradhan, A.; Conner, D.; DeFea, K.; et al. Select G-protein-coupled receptors modulate agonist-induced signaling via a ROCK, LIMK, and beta-arrestin 1 pathway. *Cell Rep.* **2013**, *5*, 1010–1021. [CrossRef]

46. Stein, C. Opioid Receptors. *Annu. Rev. Med.* **2016**, *67*, 433–451. [CrossRef]

47. Al-Hasani, R.; Bruchas, M.R. Molecular mechanisms of opioid receptor-dependent signaling and behavior. *Anesthesiology* **2011**, *115*, 1363–1381. [CrossRef] [PubMed]

48. Parker, K.E.; Bruchas, M.R. NOP Receptor Signaling Cascades. *Handb. Exp. Pharmacol.* **2019**, *254*, 131–139.

49. Armstead, W.M. Differential activation of ERK, p38, and JNK MAPK by nociceptin/orphanin FQ in the potentiation of prostaglandin cerebrovasoconstriction after brain injury. *Eur. J. Pharmacol.* **2006**, *529*, 129–135. [CrossRef]

50. New, D.C.; Wong, Y.H. The ORL1 receptor: Molecular pharmacology and signalling mechanisms. *Neurosignals* **2002**, *11*, 197–212. [CrossRef] [PubMed]

51. Marti, M.; Stocchi, S.; Paganini, F.; Mela, F.; De Risi, C.; Calo, G.; Guerrini, R.; Barnes, T.A.; Lambert, D.G.; Beani, L.; et al. Pharmacological profiles of presynaptic nociceptin/orphanin FQ receptors modulating 5-hydroxytryptamine and noradrenaline release in the rat neocortex. *Br. J. Pharmacol.* **2003**, *138*, 91–98. [CrossRef]

52. Nicol, B.; Lambert, D.G.; Rowbotham, D.J.; Smart, D.; McKnight, A.T. Nociceptin induced inhibition of K+ evoked glutamate release from rat cerebrocortical slices. *Br. J. Pharmacol.* **1996**, *119*, 1081–1083. [CrossRef] [PubMed]

53. Ferguson, S.S. Evolving concepts in G protein-coupled receptor endocytosis: The role in receptor desensitization and signaling. *Pharmacol. Rev.* **2001**, *53*, 1–24.

54. Krupnick, J.G.; Benovic, J.L. The role of receptor kinases and arrestins in G protein-coupled receptor regulation. *Annu Rev. Pharmacol. Toxicol.* **1998**, *38*, 289–319. [CrossRef]

55. Waldhoer, M.; Bartlett, S.E.; Whistler, J.L. Opioid receptors. *Annu. Rev. Biochem.* **2004**, *73*, 953–990. [CrossRef]

56. Mogil, J.S.; Grisel, J.E.; Reinscheid, R.K.; Civelli, O.; Belknap, J.K.; Grandy, D.K. Orphanin FQ is a functional anti-opioid peptide. *Neuroscience* **1996**, *75*, 333–337. [CrossRef]

57. Mogil, J.S.; Grisel, J.E.; Zhangs, G.; Belknap, J.K.; Grandy, D.K. Functional antagonism of mu-, delta- and kappa-opioid antinociception by orphanin FQ. *Neurosci. Lett.* **1996**, *214*, 131–134. [CrossRef]

58. Morgan, M.M.; Grisel, J.E.; Robbins, C.S.; Grandy, D.K. Antinociception mediated by the periaqueductal gray is attenuated by orphanin FQ. *Neuroreport* **1997**, *8*, 3431–3434. [CrossRef] [PubMed]

59. Toll, L.; Ozawa, A.; Cippitelli, A. NOP-Related Mechanisms in Pain and Analgesia. *Handb. Exp. Pharmacol.* **2019**, *254*, 165–186. [PubMed]

60. Guerrini, R.; Calo, G.; Rizzi, A.; Bianchi, C.; Lazarus, L.H.; Salvadori, S.; Temussi, P.A.; Regoli, D. Address and message sequences for the nociceptin receptor: A structure-activity study of nociceptin-(1-13)-peptide amide. *J. Med. Chem.* **1997**, *40*, 1789–1793. [CrossRef] [PubMed]

61. Calo, G.; Guerrini, R.; Bigoni, R.; Rizzi, A.; Marzola, G.; Okawa, H.; Bianchi, C.; Lambert, D.G.; Salvadori, S.; Regoli, D. Characterization of [Nphe(1)]nociceptin(1-13)NH(2), a new selective nociceptin receptor antagonist. *Br. J. Pharmacol.* **2000**, *129*, 1183–1193.

62. Calo, G.; Rizzi, A.; Rizzi, D.; Bigoni, R.; Guerrini, R.; Marzola, G.; Marti, M.; McDonald, J.; Morari, M.; Lambert, D.G.; et al. [Nphe1,Arg14,Lys15]nociceptin-NH2, a novel potent and selective antagonist of the nociceptin/orphanin FQ receptor. *Br. J. Pharmacol.* **2002**, *136*, 303–311. [CrossRef] [PubMed]

63. Guerrini, R.; Calo, G.; Rizzi, A.; Bigoni, R.; Bianchi, C.; Salvadori, S.; Regoli, D. A new selective antagonist of the nociceptin receptor. *Br. J. Pharmacol.* **1998**, *123*, 163–165. [CrossRef] [PubMed]

64. Rizzi, A.; Salis, M.B.; Ciccocioppo, R.; Marzola, G.; Bigoni, R.; Guerrini, R.; Massi, M.; Madeddu, P.; Salvadori, S.; Regoli, D.; et al. Pharmacological characterisation of [(pX)Phe4]nociceptin(1-13)NH2 analogues. 2. In vivo studies. *Naunyn Schmiedebergs Arch. Pharmacol.* **2002**, *365*, 450–456. [CrossRef]

65. Bigoni, R.; Rizzi, D.; Rizzi, A.; Camarda, V.; Guerrini, R.; Lambert, D.G.; Hashiba, E.; Berger, H.; Salvadori, S.; Regoli, D.; et al. Pharmacological characterisation of [(pX)Phe4]nociceptin(1-13)amide analogues. 1. In vitro studies. *Naunyn Schmiedebergs Arch. Pharmacol.* **2002**, *365*, 442–449. [CrossRef] [PubMed]

66. Nazzaro, C.; Rizzi, A.; Salvadori, S.; Guerrini, R.; Regoli, D.; Zeilhofer, H.U.; Calo, G. UFP-101 antagonizes the spinal antinociceptive effects of nociceptin/orphanin FQ: Behavioral and electrophysiological studies in mice. *Peptides* **2007**, *28*, 663–669. [CrossRef]

67. Rizzi, A.; Spagnolo, B.; Wainford, R.D.; Fischetti, C.; Guerrini, R.; Marzola, G.; Baldisserotto, A.; Salvadori, S.; Regoli, D.; Kapusta, D.R.; et al. In vitro and in vivo studies on UFP-112, a novel potent and long lasting agonist selective for the nociceptin/orphanin FQ receptor. *Peptides* **2007**, *28*, 1240–1251. [CrossRef] [PubMed]

68. Hu, E.; Calò, G.; Guerrini, R.; Ko, M.C. Long-lasting antinociceptive spinal effects in primates of the novel nociceptin/orphanin FQ receptor agonist UFP-112. *Pain* **2010**, *148*, 107–113. [CrossRef]

69. Micheli, L.; Di Cesare Mannelli, L.; Guerrini, R.; Trapella, C.; Zanardelli, M.; Ciccocioppo, R.; Rizzi, A.; Ghelardini, C.; Calò, G. Acute and subchronic antinociceptive effects of nociceptin/orphanin FQ receptor agonists infused by intrathecal route in rats. *Eur. J. Pharmacol.* **2015**, *754*, 73–81. [CrossRef]

70. Rizzi, A.; Malfacini, D.; Cerlesi, M.C.; Ruzza, C.; Marzola, E.; Bird, M.F.; Rowbotham, D.J.; Salvadori, S.; Guerrini, R.; Lambert, D.G.; et al. In vitro and in vivo pharmacological characterization of nociceptin/orphanin FQ tetrabranched derivatives. *Br. J. Pharmacol.* **2014**, *171*, 4138–4153. [CrossRef]

71. Rizzi, A.; Sukhtankar, D.D.; Ding, H.; Hayashida, K.; Ruzza, C.; Guerrini, R.; Calò, G.; Ko, M.C. Spinal antinociceptive effects of the novel NOP receptor agonist PWT2-nociceptin/orphanin FQ in mice and monkeys. *Br. J. Pharmacol.* **2015**, *172*, 3661–3670. [CrossRef]

72. Guerrini, R.; Caló, G.; Bigoni, R.; Rizzi, A.; Varani, K.; Toth, G.; Gessi, S.; Hashiba, E.; Hashimoto, Y.; Lambert, D.G.; et al. Further studies on nociceptin-related peptides: Discovery of a new chemical template with antagonist activity on the nociceptin receptor. *J. Med. Chem.* **2000**, *43*, 2805–2813. [CrossRef] [PubMed]

73. Okada, K.; Sujaku, T.; Chuman, Y.; Nakashima, R.; Nose, T.; Costa, T.; Yamada, Y.; Yokoyama, M.; Nagahisa, A.; Shimohigashi, Y. Highly potent nociceptin analog containing the Arg-Lys triple repeat. *Biochem. Biophys. Res. Commun.* **2000**, *278*, 493–498. [CrossRef]

74. Dooley, C.T.; Houghten, R.A. Orphanin FQ: Receptor binding and analog structure activity relationships in rat brain. *Life Sci.* **1996**, *59*, PL23-9. [CrossRef]

75. Reinscheid, R.K.; Ardati, A.; Monsma, F.J., Jr.; Civelli, O. Structure-activity relationship studies on the novel neuropeptide orphanin FQ. *J. Biol. Chem.* **1996**, *271*, 14163–14168. [CrossRef] [PubMed]

76. Zhang, C.; Miller, W.; Valenzano, K.J.; Kyle, D.J. Novel, potent ORL-1 receptor agonist peptides containing alpha-Helix-promoting conformational constraints. *J. Med. Chem.* **2002**, *45*, 5280–5286. [CrossRef]

77. Arduin, M.; Spagnolo, B.; Calò, G.; Guerrini, R.; Carrà, G.; Fischetti, C.; Trapella, C.; Marzola, E.; McDonald, J.; Lambert, D.G.; et al. Synthesis and biological activity of nociceptin/orphanin FQ analogues substituted in position 7 or 11 with Calpha, alpha-dialkylated amino acids. *Bioorg. Med. Chem.* **2007**, *15*, 4434–4443. [CrossRef] [PubMed]

78. Guerrini, R.; Marzola, E.; Trapella, C.; Pela', M.; Molinari, S.; Cerlesi, M.C.; Malfacini, D.; Rizzi, A.; Salvadori, S.; Calo', G. A novel and facile synthesis of tetra branched derivatives of nociceptin/orphanin FQ. *Bioorg. Med. Chem.* **2014**, *22*, 3703–3712. [CrossRef] [PubMed]

79. Byford, A.J.; Anderson, A.; Jones, P.S.; Palin, R.; Houghton, A.K. The hypnotic, electroencephalographic, and antinociceptive properties of nonpeptide ORL1 receptor agonists after intravenous injection in rodents. *Anesth. Analg.* **2007**, *104*, 174–179. [CrossRef]

80. Rizzi, A.; Ruzza, C.; Bianco, S.; Trapella, C.; Calo', G. Antinociceptive action of NOP and opioid receptor agonists in the mouse orofacial formalin test. *Peptides* **2017**, *94*, 71–77. [CrossRef] [PubMed]

81. Jenck, F.; Wichmann, J.; Dautzenberg, F.M.; Moreau, J.L.; Ouagazzal, A.M.; Martin, J.R.; Lundstrom, K.; Cesura, A.M.; Poli, S.M.; Roever, S.; et al. A synthetic agonist at the orphanin FQ/nociceptin receptor ORL1: Anxiolytic profile in the rat. *Proc. Natl. Acad. Sci. USA* **2000**, *97*, 4938–4943. [CrossRef] [PubMed]

82. Chang, S.D.; Brieaddy, L.E.; Harvey, J.D.; Lewin, A.H.; Mascarella, S.W.; Seltzman, H.H.; Reddy, P.A.; Decker, A.M.; McElhinny, C.J., Jr.; Zhong, D.; et al. Novel Synthesis and Pharmacological Characterization of NOP Receptor Agonist 8-[(1S,3aS)-2,3,3a,4,5,6-Hexahydro-1H-phenalen-1-yl]-1-phenyl-1,3,8-triazaspiro[4.5]decan-4-one (Ro 64-6198). *ACS Chem. Neurosci.* **2015**, *6*, 1956–1964. [CrossRef] [PubMed]

83. Reiss, D.; Wichmann, J.; Tekeshima, H.; Kieffer, B.L.; Ouagazzal, A.M. Effects of nociceptin/orphanin FQ receptor (NOP) agonist, Ro64-6198, on reactivity to acute pain in mice: Comparison to morphine. *Eur. J. Pharmacol.* **2008**, *579*, 141–148. [CrossRef] [PubMed]

84. Varty, G.B.; Lu, S.X.; Morgan, C.A.; Cohen-Williams, M.E.; Hodgson, R.A.; Smith-Torhan, A.; Zhang, H.; Fawzi, A.B.; Graziano, M.P.; Ho, G.D.; et al. The anxiolytic-like effects of the novel, orally active nociceptin opioid receptor agonist 8-[bis(2-methylphenyl)methyl]-3-phenyl-8-azabicyclo[3.2.1]octan-3-ol (SCH 221510). *J. Pharmacol. Exp. Ther.* **2008**, *326*, 672–682. [CrossRef] [PubMed]

85. Sobczak, M.; Mokrowiecka, A.; Cygankiewicz, A.I.; Zakrzewski, P.K.; Sałaga, M.; Storr, M.; Kordek, R.; Małecka-Panas, E.; Krajewska, W.M.; Fichna, J. Anti-inflammatory and antinociceptive action of an orally available nociceptin receptor agonist SCH 221510 in a mouse model of inflammatory bowel diseases. *J. Pharmacol. Exp. Ther.* **2014**, *348*, 401–409. [CrossRef]

86. Röver, S.; Adam, G.; Cesura, A.M.; Galley, G.; Jenck, F.; Monsma, F.J., Jr.; Wichmann, J.; Dautzenberg, F.M. High-affinity, non-peptide agonists for the ORL1 (orphanin FQ/nociceptin) receptor. *J. Med. Chem.* **2000**, *43*, 1329–1338. [CrossRef] [PubMed]

87. Hashiba, E.; Harrison, C.; Galo', G.; Guerrini, R.; Rowbotham, D.J.; Smith, G.; Lambert, D.G. Characterisation and comparison of novel ligands for the nociceptin/orphanin FQ receptor. *Naunyn Schmiedebergs Arch. Pharmacol.* **2001**, *363*, 28–33. [CrossRef] [PubMed]

88. Azevedo Neto, J.; Ruzza, C.; Sturaro, C.; Malfacini, D.; Pacifico, S.; Zaveri, N.T.; Calò, G. Functional Selectivity Does Not Predict Antinociceptive/Locomotor Impairing Potencies of NOP Receptor Agonists. *Front. Neurosci.* **2021**, *15*, 657153. [CrossRef] [PubMed]

89. Ferrari, F.; Malfacini, D.; Journigan, B.V.; Bird, M.F.; Trapella, C.; Guerrini, R.; Lambert, D.G.; Calo', G.; Zaveri, N.T. In vitro pharmacological characterization of a novel unbiased NOP receptor-selective nonpeptide agonist AT-403. *Pharmacol. Res. Perspect.* **2017**, *5*, e00333. [CrossRef]

90. Wichmann, J.; Adam, G.; Röver, S.; Cesura, A.M.; Dautzenberg, F.M.; Jenck, F. 8-acenaphthen-1-yl-1-phenyl-1,3,8-triaza-spiro[4.5]decan-4-one derivatives as orphanin FQ receptor agonists. *Bioorg. Med. Chem. Lett.* **1999**, *9*, 2343–2348. [CrossRef]

91. Wichmann, J.; Adam, G.; Röver, S.; Hennig, M.; Scalone, M.; Cesura, A.M.; Dautzenberg, F.M.; Jenck, F. Synthesis of (1S,3aS)-8-(2,3,3a,4,5, 6-hexahydro-1H-phenalen-1-yl)-1-phenyl-1,3,8-triaza-spiro[4. 5]decan-4-one, a potent and selective orphanin FQ (OFQ) receptor agonist with anxiolytic-like properties. *Eur. J. Med. Chem.* **2000**, *35*, 839–851. [CrossRef]

92. Shoblock, J.R. The pharmacology of Ro 64-6198, a systemically active, nonpeptide NOP receptor (opiate receptor-like 1, ORL-1) agonist with diverse preclinical therapeutic activity. *CNS Drug Rev.* **2007**, *13*, 107–136. [CrossRef]

93. Ding, H.; Hayashida, K.; Suto, T.; Sukhtankar, D.D.; Kimura, M.; Mendenhall, V.; Ko, M.C. Supraspinal actions of nociceptin/orphanin FQ, morphine and substance P in regulating pain and itch in non-human primates. *Br. J. Pharmacol.* **2015**, *172*, 3302–3312. [CrossRef] [PubMed]

94. Obara, I.; Przewlocki, R.; Przewlocka, B. Spinal and local peripheral antiallodynic activity of Ro64-6198 in neuropathic pain in the rat. *Pain* **2005**, *116*, 17–25. [CrossRef] [PubMed]

95. Varty, G.B.; Hyde, L.A.; Hodgson, R.A.; Lu, S.X.; McCool, M.F.; Kazdoba, T.M.; Del Vecchio, R.A.; Guthrie, D.H.; Pond, A.J.; Grzelak, M.E.; et al. Characterization of the nociceptin receptor (ORL-1) agonist, Ro64-6198, in tests of anxiety across multiple species. *Psychopharmacology* **2005**, *182*, 132–143. [CrossRef] [PubMed]

96. Sukhtankar, D.D.; Zaveri, N.T.; Husbands, S.M.; Ko, M.C. Effects of spinally administered bifunctional nociceptin/orphanin FQ peptide receptor/μ-opioid receptor ligands in mouse models of neuropathic and inflammatory pain. *J. Pharmacol. Exp. Ther.* **2013**, *346*, 11–22. [CrossRef]

97. Sukhtankar, D.D.; Lagorio, C.H.; Ko, M.C. Effects of the NOP agonist SCH221510 on producing and attenuating reinforcing effects as measured by drug self-administration in rats. *Eur. J. Pharmacol.* **2014**, *745*, 182–189. [CrossRef] [PubMed]

98. Wu, Q.; Liu, L. ORL$_1$ Activation Mediates a Novel ORL$_1$ Receptor Agonist SCH221510 Analgesia in Neuropathic Pain in Rats. *J. Mol. Neurosci.* **2018**, *66*, 10–16. [CrossRef]

99. Cremeans, C.M.; Gruley, E.; Kyle, D.J.; Ko, M.C. Roles of mu-opioid receptors and nociceptin/orphanin FQ peptide receptors in buprenorphine-induced physiological responses in primates. *J. Pharmacol. Exp. Ther.* **2012**, *343*, 72–81. [CrossRef]

100. Hao, X.Q.; Wang, Z.Y.; Chen, J.M.; Wu, N.; Li, J. Involvement of the nociceptin opioid peptide receptor in morphine-induced antinociception, tolerance and physical dependence in female mice. *Metab. Brain Dis.* **2021**, *36*, 2243–2253. [CrossRef]

101. Kiguchi, N.; Ko, M.C. Effects of NOP-Related Ligands in Nonhuman Primates. *Handb. Exp. Pharmacol.* **2019**, *254*, 323–343. [PubMed]

102. Lutfy, K.; Hossain, S.M.; Khaliq, I.; Maidment, N.T. Orphanin FQ/nociceptin attenuates the development of morphine tolerance in rats. *Br. J. Pharmacol.* **2001**, *134*, 529–534. [CrossRef] [PubMed]

103. Murphy, N.P.; Lee, Y.; Maidment, N.T. Orphanin FQ/nociceptin blocks acquisition of morphine place preference. *Brain Res.* **1999**, *832*, 168–170. [CrossRef]

104. Murphy, N.P.; Ly, H.T.; Maidment, N.T. Intracerebroventricular orphanin FQ/nociceptin suppresses dopamine release in the nucleus accumbens of anaesthetized rats. *Neuroscience* **1996**, *75*, 1–4. [CrossRef]

105. Rutten, K.; De Vry, J.; Bruckmann, W.; Tzschentke, T.M. Effects of the NOP receptor agonist Ro65-6570 on the acquisition of opiate- and psychostimulant-induced conditioned place preference in rats. *Eur. J. Pharmacol.* **2010**, *645*, 119–126. [CrossRef]

106. Raffa, R.B.; Pergolizzi, J.V., Jr.; Tallarida, R.J. The determination and application of fixed-dose analgesic combinations for treating multimodal pain. *J. Pain* **2010**, *11*, 701–709. [CrossRef] [PubMed]

107. Kiguchi, N.; Ding, H.; Kishioka, S.; Ko, M.C. Nociceptin/Orphanin FQ Peptide Receptor-Related Ligands as Novel Analgesics. *Curr. Top. Med. Chem.* **2020**, *20*, 2878–2888. [CrossRef] [PubMed]

108. Kiguchi, N.; Ding, H.; Ko, M.C. Therapeutic potentials of NOP and MOP receptor coactivation for the treatment of pain and opioid abuse. *J. Neurosci. Res.* **2020**, *100*, 191–202. [CrossRef]

109. Mustazza, C.; Pieretti, S.; Marzoli, F. Nociceptin/Orphanin FQ Peptide (NOP) Receptor Modulators: An Update in Structure-Activity Relationships. *Curr. Med. Chem.* **2018**, *25*, 2353–2384. [CrossRef] [PubMed]

110. Khroyan, T.V.; Zaveri, N.T.; Polgar, W.E.; Orduna, J.; Olsen, C.; Jiang, F.; Toll, L. SR 16435 [1-(1-(bicyclo[3.3.1]nonan-9-yl)piperidin-4-yl)indolin-2-one], a novel mixed nociceptin/orphanin FQ/mu-opioid receptor partial agonist: Analgesic and rewarding properties in mice. *J. Pharmacol. Exp. Ther.* **2007**, *320*, 934–943. [CrossRef]

111. Linz, K.; Christoph, T.; Tzschentke, T.M.; Koch, T.; Schiene, K.; Gautrois, M.; Schröder, W.; Kögel, B.Y.; Beier, H.; Englberger, W.; et al. Cebranopadol: A novel potent analgesic nociceptin/orphanin FQ peptide and opioid receptor agonist. *J. Pharmacol. Exp. Ther.* **2014**, *349*, 535–548. [CrossRef]

112. Schunk, S.; Linz, K.; Hinze, C.; Frormann, S.; Oberbörsch, S.; Sundermann, B.; Zemolka, S.; Englberger, W.; Germann, T.; Christoph, T.; et al. Discovery of a Potent Analgesic NOP and Opioid Receptor Agonist: Cebranopadol. *ACS Med. Chem. Lett.* **2014**, *5*, 857–862. [CrossRef]

113. Zaveri, N.T.; Jiang, F.; Olsen, C.; Deschamps, J.R.; Parrish, D.; Polgar, W.; Toll, L. A novel series of piperidin-4-yl-1,3-dihydroindol-2-ones as agonist and antagonist ligands at the nociceptin receptor. *J. Med. Chem.* **2004**, *47*, 2973–2976. [CrossRef] [PubMed]

114. Ding, H.; Kiguchi, N.; Yasuda, D.; Daga, P.R.; Polgar, W.E.; Lu, J.J.; Czoty, P.W.; Kishioka, S.; Zaveri, N.T.; Ko, M.C. A bifunctional nociceptin and mu opioid receptor agonist is analgesic without opioid side effects in nonhuman primates. *Sci. Transl. Med.* **2018**, *10*, eaar3483. [CrossRef]

115. Huang, P.; Kehner, G.B.; Cowan, A.; Liu-Chen, L.Y. Comparison of pharmacological activities of buprenorphine and norbuprenorphine: Norbuprenorphine is a potent opioid agonist. *J. Pharmacol. Exp. Ther.* **2001**, *297*, 688–695. [PubMed]

116. Khroyan, T.V.; Polgar, W.E.; Cami-Kobeci, G.; Husbands, S.M.; Zaveri, N.T.; Toll, L. The first universal opioid ligand, (2S)-2-[(5R,6R,7R,14S)-N-cyclopropylmethyl-4,5-epoxy-6,14-ethano-3-hydroxy-6-methoxymorphinan-7-yl]-3,3-dimethylpentan-2-ol (BU08028): Characterization of the in vitro profile and in vivo behavioral effects in mouse models of acute pain and cocaine-induced reward. *J. Pharmacol. Exp. Ther.* **2011**, *336*, 952–961.

117. Kiguchi, N.; Ding, H.; Cami-Kobeci, G.; Sukhtankar, D.D.; Czoty, P.W.; DeLoid, H.B.; Hsu, F.C.; Toll, L.; Husbands, S.M.; Ko, M.C. BU10038 as a safe opioid analgesic with fewer side-effects after systemic and intrathecal administration in primates. *Br. J. Anaesth.* **2019**, *122*, e146–e156. [CrossRef]

118. Chao, P.K.; Chang, H.F.; Chang, W.T.; Yeh, T.K.; Ou, L.C.; Chuang, J.Y.; Tsu-An Hsu, J.; Tao, P.L.; Loh, H.H.; Shih, C.; et al. BPR1M97, a dual mu opioid receptor/nociceptin-orphanin FQ peptide receptor agonist, produces potent antinociceptive effects with safer properties than morphine. *Neuropharmacology* **2020**, *166*, 107678. [CrossRef]

119. Shinkai, H.; Ito, T.; Iida, T.; Kitao, Y.; Yamada, H.; Uchida, I. 4-Aminoquinolines: Novel nociceptin antagonists with analgesic activity. *J. Med. Chem.* **2000**, *43*, 4667–4677. [CrossRef] [PubMed]

120. Christoph, T.; Kögel, B.; Schiene, K.; Méen, M.; De Vry, J.; Friderichs, E. Broad analgesic profile of buprenorphine in rodent models of acute and chronic pain. *Eur. J. Pharmacol.* **2005**, *507*, 87–98. [CrossRef] [PubMed]

121. Ding, H.; Czoty, P.W.; Kiguchi, N.; Cami-Kobeci, G.; Sukhtankar, D.D.; Nader, M.A.; Husbands, S.M.; Ko, M.C. A novel orvinol analog, BU08028, as a safe opioid analgesic without abuse liability in primates. *Proc. Natl. Acad. Sci. USA* **2016**, *113*, E5511–E5518. [CrossRef]

122. Chen, S.R.; Ke, Y.Y.; Yeh, T.K.; Lin, S.Y.; Ou, L.C.; Chen, S.C.; Chang, W.T.; Chang, H.F.; Wu, Z.H.; Hsieh, C.C.; et al. Discovery, structure-activity relationship studies, and anti-nociceptive effects of N-(1,2,3,4-tetrahydro-1-isoquinolinylmethyl)benzamides as novel opioid receptor agonists. *Eur. J. Med. Chem.* **2017**, *126*, 202–217. [CrossRef] [PubMed]

123. Zaveri, N.T. Nociceptin Opioid Receptor (NOP) as a Therapeutic Target: Progress in Translation from Preclinical Research to Clinical Utility. *J. Med. Chem.* **2016**, *59*, 7011–7028. [CrossRef] [PubMed]

124. Lambert, D.G.; Bird, M.F.; Rowbotham, D.J. Cebranopadol: A first in-class example of a nociceptin/orphanin FQ receptor and opioid receptor agonist. *Br. J. Anaesth.* **2015**, *114*, 364–366. [CrossRef]

125. Rizzi, A.; Cerlesi, M.C.; Ruzza, C.; Malfacini, D.; Ferrari, F.; Bianco, S.; Costa, T.; Guerrini, R.; Trapella, C.; Calo', G. Pharmacological characterization of cebranopadol a novel analgesic acting as mixed nociceptin/orphanin FQ and opioid receptor agonist. *Pharmacol. Res. Perspect.* **2016**, *4*, e00247. [CrossRef] [PubMed]

126. Tzschentke, T.M.; Linz, K.; Koch, T.; Christoph, T. Cebranopadol: A Novel First-in-Class Potent Analgesic Acting via NOP and Opioid Receptors. *Handb. Exp. Pharmacol.* **2019**, *254*, 367–398.

127. Mann, A.; Moulédous, L.; Froment, C.; O'Neill, P.R.; Dasgupta, P.; Günther, T.; Brunori, G.; Kieffer, B.L.; Toll, L.; Bruchas, M.R.; et al. Agonist-selective NOP receptor phosphorylation correlates in vitro and in vivo and reveals differential post-activation signaling by chemically diverse agonists. *Sci. Signal.* **2019**, *12*, eaau8072. [CrossRef] [PubMed]

128. Kleideiter, E.; Piana, C.; Wang, S.; Nemeth, R.; Gautrois, M. Clinical Pharmacokinetic Characteristics of Cebranopadol, a Novel First-in-Class Analgesic. *Clin. Pharmacokinet.* **2018**, *57*, 31–50. [CrossRef]

129. Available online: https://clinicaltrials.gov/ct2/show/NCT00872885 (accessed on 12 January 2022).

130. Available online: https://clinicaltrials.gov/ct2/show/NCT01939366 (accessed on 12 January 2022).

131. Available online: https://clinicaltrials.gov/ct2/show/NCT01357837 (accessed on 12 January 2022).

132. Available online: https://clinicaltrials.gov/ct2/show/NCT01709214 (accessed on 12 January 2022).

133. Available online: https://clinicaltrials.gov/ct2/show/NCT01725087 (accessed on 12 January 2022).

134. Available online: https://clinicaltrials.gov/ct2/show/NCT01347671 (accessed on 12 January 2022).

135. Available online: https://clinicaltrials.gov/ct2/show/NCT00878293 (accessed on 12 January 2022).

136. Eerdekens, M.H.; Kapanadze, S.; Koch, E.D.; Kralidis, G.; Volkers, G.; Ahmedzai, S.H.; Meissner, W. Cancer-related chronic pain: Investigation of the novel analgesic drug candidate cebranopadol in a randomized, double-blind, noninferiority trial. *Eur. J. Pain* **2019**, *23*, 577–588. [CrossRef]

137. Koch, E.D.; Kapanadze, S.; Eerdekens, M.H.; Kralidis, G.; Létal, J.; Sabatschus, I.; Ahmedzai, S.H. Cebranopadol, a Novel First-in-Class Analgesic Drug Candidate: First Experience With Cancer-Related Pain for up to 26 Weeks. *J. Pain Symptom. Manag.* **2019**, *58*, 390–399. [CrossRef]

138. Che, T.; Roth, B.L. Structural Insights Accelerate the Discovery of Opioid Alternatives. *Annu. Rev. Biochem.* **2021**, *90*, 739–761. [CrossRef] [PubMed]

molecules

Shedding Light on the Pharmacological Interactions between μ-Opioid Analgesics and Angiotensin Receptor Modulators: A New Option for Treating Chronic Pain

Kornél Király [1,*,†], Dávid Á. Karádi [1,†], Ferenc Zádor [1,2], Amir Mohammadzadeh [1], Anna Rita Galambos [1], Mihály Balogh [1], Pál Riba [1], Tamás Tábi [2], Zoltán S. Zádori [1], Éva Szökő [2], Susanna Fürst [1] and Mahmoud Al-Khrasani [1,*]

1   Department of Pharmacology and Pharmacotherapy, Faculty of Medicine, Semmelweis University, Nagyvárad tér 4, P.O. Box 370, H-1445 Budapest, Hungary; karadi.david_arpad@med.semmelweis-univ.hu (D.Á.K.); zador.ferenc@pharma.semmelweis-univ.hu (F.Z.); mohammadzadeh.amir@med.semmelweis-univ.hu (A.M.); galambos.anna@pharma.semmelweis-univ.hu (A.R.G.); balogh.mihaly@med.semmelweis-univ.hu (M.B.); riba.pal@med.semmelweis-univ.hu (P.R.); zadori.zoltan@med.semmelweis-univ.hu (Z.S.Z.); furst.zsuzsanna@med.semmelweis-univ.hu (S.F.)
2   Department of Pharmacodynamics, Faculty of Pharmacy, Semmelweis University, Nagyvárad tér 4, H-1089 Budapest, Hungary; tabi.tamas@pharma.semmelweis-univ.hu (T.T.); szoko.eva@pharma.semmelweis-univ.hu (É.S.)
*   Correspondence: kiraly.kornel@med.semmelweis-univ.hu (K.K.); al-khrasani.mahmoud@med.semmelweis-univ.hu (M.A.-K.); Tel.: +36-1-210-4416-56273 (K.K.); +36-1-210-4416-56285 (M.A.-K.)
†   These authors equally contributed to this work.

Abstract: The current protocols for neuropathic pain management include μ-opioid receptor (MOR) analgesics alongside other drugs; however, there is debate on the effectiveness of opioids. Nevertheless, dose escalation is required to maintain their analgesia, which, in turn, contributes to a further increase in opioid side effects. Finding novel approaches to effectively control chronic pain, particularly neuropathic pain, is a great challenge clinically. Literature data related to pain transmission reveal that angiotensin and its receptors (the AT1R, AT2R, and MAS receptors) could affect the nociception both in the periphery and CNS. The MOR and angiotensin receptors or drugs interacting with these receptors have been independently investigated in relation to analgesia. However, the interaction between the MOR and angiotensin receptors has not been excessively studied in chronic pain, particularly neuropathy. This review aims to shed light on existing literature information in relation to the analgesic action of AT1R and AT2R or MASR ligands in neuropathic pain conditions. Finally, based on literature data, we can hypothesize that combining MOR agonists with AT1R or AT2R antagonists might improve analgesia.

Keywords: μ-opioid analgesics; angiotensin receptors; chronic pain; neuropathic pain

1. Introduction

Among different types of chronic pain, neuropathic pain is defined by the International Association for the Study of Pain (IASP) as pain caused by a lesion or disease of the somatosensory nervous system (IASP 2012). There are many available treatment approaches for the management of neuropathic pain. Yet, despite these advances, it remains an unmet medical need because most of the treatment approaches intended to halt this pain condition are not effective enough or sometimes effective but limited by side effects. Thus, finding new targets and innovative future strategies that might help to improve neuropathic pain control are of clinical need.

μ-Opioid receptor (MOR) agonists are the mainstay treatment for different forms of chronic pain [1–4]. However, their efficacy in the management of neuropathic pain is a long-standing question of debate. Yet, international guidelines restrict opioids to second- or third-

line therapy, with no clear consensus on their effect [5–7]. MOR agonists with significantly higher intrinsic efficacy than morphine produced acceptable analgesia in preclinical models of neuropathic pain [8,9]; however, this has not been successfully utilized clinically because clinical trials showed controversial results related to their efficacy and liability for side effects [10–13]. In response to this argument, many studies have been conducted to increase the efficacy and decrease the side effects of opioids when used in the management of neuropathic pain. Some of the encouraging strategies that aim to improve the analgesic effect and decrease the side effects of currently used analgesics, such as opioids, are based on combining two or more different agents. However, so far, clinical research data that is based on combination strategies have not met expectations [14]. Chaparro et al., reviewed clinical trials on the efficacy and safety of various agent combinations for neuropathic pain [14]. Their analysis revealed that the combination of opioids with gabapentin was significantly better than gabapentin alone in reducing the symptoms. However, the number of treated patients that was required for a single patient to benefit was still 9.5, and significantly more participants experienced side effects and thus dropped out of the studies with opioids plus gabapentin than with gabapentin alone [14]. On the other hand, studies assessing the effects of opioids in combination with other sensory-sensitization blocking agents could be of high clinical value. Thus, continuing preclinical research based on the application of multi-target drugs or combination strategies that involve implementing different agents might bring a new treatment option for neuropathic pain. In the former case, for instance, applying opioid receptor ligands that display agonist and non-opioid effects, such as tapentadol, display both the MOR agonist and norepinephrine reuptake inhibitory effects in the same molecule [15]. Recently, our group reported on the promising effect of the combination of glycine transporter 1 and 2 inhibitors in the management of neuropathic pain evoked by sciatic nerve ligation [16]. In such a strategy, we need to consider how the individual drugs affect pain transmission.

Accumulating evidence has proven that drugs affecting the renin–angiotensin system can modulate pain transmission [17–34]. Recent studies have also shown that drugs mimic or antagonize angiotensin type 1 and 2 (AT1R and AT2R) receptor-mediated actions do produce a beneficial analgesic effect in rodent models of chronic pain types [17,20,22,28,29,35–38]. The analgesic effect of ligands affecting angiotensin receptors in neuropathic pain is explained by the contribution of these receptors to neuroregeneration and neuroprotection—partially by reducing neural inflammatory processes [18,24,37,39–41]. Nevertheless, much remains unclear regarding the role and clinical utility of these receptors in analgesia.

This review briefly highlights how the effect of MOR agonist-induced analgesia is altered under neuropathic pain conditions, showing the advantages and drawbacks, as well as principal factors that negatively impact the analgesic effect of MOR analgesics in this pain entity. The next sections review the implication of angiotensin and its receptors in chronic pain, particularly that associated with neuropathy, and also the neuroanatomical overlap between MORs and angiotensin receptors in relation to pain. Finally, according to the reviewed data, perspectives on the future drug combination-based research strategy to treat neuropathic pain are provided. With respect to angiotensin IV and its receptor, the presence of the peptide has been reported in human dorsal root ganglia (DRG) and trigeminal nucleus (TG) [42,43]. However, there are little data related to their analgesic effect. Thus, they will not be discussed in the present review.

2. The Opioid System and the μ-Opioid Receptor in Different Pain Entities

The opioid system is a physiological system for controlling pain, but it also participates in addictive behaviors and immune defense, among others. Mammalian endogenous opioid peptides and exogenous natural, semisynthetic and synthetic opioid agonists can produce their effects through the activation of opioid receptors, namely μ-(MOR), δ-(DOR), and κ-(KOR) opioid receptors. Opioid receptors belong to the class A G-proteins of the pertussis toxin-sensitive Gi/Go family. Their effectors include adenylyl cyclase, N- and L-type Ca^{2+} channels, and inwardly rectifying K^+ channels. Upon activation, adenylyl

cyclase and Ca^{2+} channels are inhibited, whereas K^+ channels are activated. Thus, both the limitation of Ca^{2+} entry and the hyperpolarization of the cells may give a tenable explanation for the inhibition of transmitter release at pain traffic points [44,45]. With respect to pain, central MORs are the principal target for mediating the analgesic effects of opioids. As in MOR-knockout mice, selective MOR agonists failed to produce analgesia as well as MOR-induced opioid side effects, such as respiratory depression, gastrointestinal transit inhibition, and addiction liability [46,47]. Since the identification of functional peripheral MORs, it has become obvious that the analgesic effects of opioids do not solely depend on MORs at the central nervous system (CNS) [48]. It is worth noting that achieving peripheral analgesia requires prerequisite factors that are related both to the physicochemical properties of opioid analgesics (limited CNS penetration) and pain entity. In the case of the latter, the pathological state of pain largely reflects the effects of opioid analgesics. In inflammatory or acute non-inflammatory pain, MORs number is increased or maintained at normal level, respectively [9,48–50]. Several opioid researchers have proven that functional MORs in the periphery are targetable, particularly in inflammatory pain types [51–54]. However, under neuropathic pain conditions, several studies have demonstrated the downregulation of MORs in the dorsal spinal cord and DRG [9,55]. The efficacy of currently available MOR agonists in neuropathic pain is a question of debate. Taken together, in cases of acute or inflammatory pain types, opioid analgesics can provide adequate pain control, which is somewhat hampered by above mentioned unwanted effects. However, in the case of neuropathic pain, the desired analgesia itself is often unachievable, consequently demanding dose-escalation, therefore causing more pronounced side effects (Figure 1A) (Karádi and Al-Khrasani, unpublished data) and (Figure 1B) (adopted from our previous work [16]).
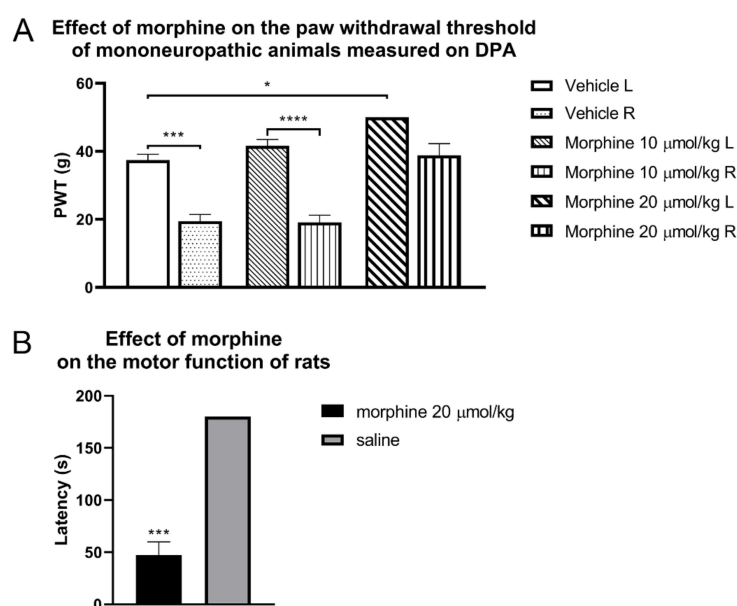
Figure 1. (**A**) The analgesic effect of morphine measured on a dynamic plantar aesthesiometer (DPA) test at 30 min, after s.c. administration to mononeuropathic animals. Columns represent the paw withdrawal threshold of the animals in grams ± S.E.M. Asterisks indicate the significant differences between treatment groups or operated (R) and non-operated (L) hind paws (* $p < 0.05$; *** $p < 0.001$ and **** $p < 0.0001$). Statistical differences were determined with one-way ANOVA and Tukey post-hoc test. Data represent means ± S.E.M ($n = 5$–12 per group). (Karádi, D.Á.; Al-Khrasani, M.; unpublished data). (**B**) Effect of the systemic administration of morphine to the motor function of rats. Columns represent the time latency of the animals in sec ± S.E.M. at 30 min post-treatment in the rotarod test. Asterisks indicate the significant differences compared to the saline group (one-way ANOVA, Newman–Keuls post-hoc test; *** $p < 0.001$). In each treatment group, 4–7 animals were used. These results were adopted from our previous work [16].

For restoring the effect of opioids in neuropathic pain, many attempts have been focused on the mechanisms related to changes in the number of functional MORs on sensory neurons in subjects with painful neuropathy. In our and other studies carried out in rats with neuropathic pain induced either by streptozotocin (STZ) or chronic constriction injury (CCI), the number of MORs was found to be decreased in DRG and spinal tissue [9,56,57]. This reduction in MOR number was accompanied by a decrease in the analgesic effects of opioids.

3. Angiotensin Receptor Mimetics and Antagonists in Relation to Pain

3.1. Endogenous Angiotensin Ligands and Angiotensin Receptors

Components of the renin–angiotensin system (RAS) have been previously reviewed or discussed extensively [19,24,58–64]. Nevertheless, the main findings are briefly summarized here for an overview. Among the endogenous peptides of the RAS, neuronal angiotensin II (Ang II) is the most significant in relation to pain. Ang II is an octapeptide derived from the inactive precursor angiotensinogen, which is initially cleaved by renin, resulting in the inactive intermediate angiotensin I (Ang I). Ang II is cleaved from Ang I by the angiotensin-converting enzyme 1 (ACE1). Ang II equally binds to and activates the AT1R and AT2R (see later on). Another relevant endogenous peptide of the RAS to this review is angiotensin 1-7 (Ang (1-7)), which is cleaved by the angiotensin-converting enzyme 2 (ACE2) from Ang II or by ACE1 from Ang I via the intermediate angiotensin 1-9. Ang (1-7) activates the Ang (1-7) receptor or MAS receptor, but it can also bind with lower affinity to AT2R.

There are four angiotensin receptor types known so far within the RAS; namely angiotensin II type 1 and 2 receptors, the angiotensin IV receptor, and the Ang (1-7) receptor or MAS receptor (abbreviated as AT1R, AT2R, AT4R, and AT7R or MASR, respectively). Additionally, in mice and rats, two AT1R isoforms have been identified, namely AT1aR and AT1bR [65,66]. In relation to the RAS, this review will focus on data of AT1R, AT2R, and MASR, with respect to pain, particularly from preclinical studies. They all belong to the rhodopsin-like G-protein coupled receptor family (GPCR); however, they differ significantly in terms of activation of signaling pathways and cellular and tissue distribution patterns. The latter will be discussed in detail in a separate section. The AT1R is a prime example of a GPCR that upon activation can be dependent and independent from heterotrimeric G-proteins, allowing the receptor to have a wide range of signaling responses to Ang II. In terms of G-protein dependent signaling pathways, the AT1R couples to multiple types of Gα, (Gq/11, Gi, G12, and G13), but it also includes the activation of small G-proteins. G-protein independent signaling of AT1R involves β-arrestin 1 and 2, tyrosine kinase-related signaling, reactive oxygen species signaling, receptor-interacting scaffold proteins, or heterodimerization with AT2R or MASR. In the case of AT2R, signaling pathways are still not fully elucidated, in spite of the intensive research. In fact, it is one of the least understood areas of the renin–angiotensin system. Most interestingly, it fails to demonstrate classic GPCR signaling features, such as affecting second messengers (e.g., cAMP, diacylglycerol) or the lack of phosphorylation-induced receptor desensitization, or internalization in most tissue types. However, it has been proven that AT2R is sensitive to GTPγS and pertussis toxin in rat locus coeruleus, indicating Gi/o coupling [67]. AT2R can also stimulate protein phosphatases and nitric oxide production. In addition, AT2R mediates the inactivation of mitogen-activated protein kinase (MAPK) inhibition which is important in the induction of apoptosis [60,67]. The AT2R and Ang II interaction leads to neurite formation and growth via the modulation of polymerized β-tubulin, microtubule-associated proteins (MAP), the activation of the p42/p44 MAPK phosphorylation of trkA. MASR, similar to AT1R and AT2R, can couple to many downstream signaling pathways via Ang (1-7) activation. These include the activation of phospholipase C and A2, arachidonic acid release, or calcium-independent nitric oxide synthase activation. MASR also modulates several kinase-related pathways/effectors, such as the p38 MAPK, ERK1/2, phosphatidylinositol 3-kinase/Akt, RhoA, and cAMP/PKA, in different cell lines. MASR was also demonstrated

to constitutively couple to Gαi, Gαq, and Gα12/13 [63]. On the other hand, similar to AT2R, in most cases, MASR fails to induce the conventional G-protein mediated signaling response, defined by the levels of classical second messengers, such Ca^{2+}, or inositol trisphosphate (IP3), despite belonging to the GPCR family.

3.2. AT1 and AT2 Receptor Agonists

Following the discovery of the neuronal RAS, numerous studies have reported on the implication of AT1R/AT2R agonists on nociception [27,30,33,68–76]. In spite of the high number of studies conducted, literature data remain highly controversial. Some publications describe the analgesic activity of AngII, AngIII, or renin on acute pain tests following central (intracerebroventricular [27,69,71,72,76] or intrathecal [33]) administration. These reports proposed different possible mechanisms of action behind the observed effects. Many of them indicate the role of the endogenous opioid system as the analgesic activity of test compounds was naloxone-sensitive [27,33,69,71,72]. Next, Shimamura et al., suggested a kinetic interaction between AngIII and met-enkephalin, namely the inhibition of cleavage of the latter [71]. Georgieva et al., found that AngII administered intracerebroventricularly (icv.) produced an antinociceptive effect in the acetic-acid writhing pain model, yet the AngII-induced antinociception was blocked by PD123319, an AT2R selective antagonist but not by losartan, an AT1R antagonist [75]. In this study, the authors concluded that AT2Rs but not AT1Rs are involved in the mechanism behind the analgesic action in acute inflammatory pain. Since then, studies assessing the effects of RAS peptides (angiotensinogen, AngI, AngII, or AngIII) microinjected into different regions of the periaqueductal gray (PAG) were conducted in rats. In these studies, all test peptides were proven to be analgesic on the tail-flick assay, and their effect was AT1R or AT2R antagonist reversible [77]. Another observation is that spontaneously hypertensive rats show longer latency on the hot plate but not on the tail-flick test, when compared to wild-type animals. Moreover, this increase in latency can be reversed by orally administered captopril or losartan, but not by antihypertensive agents which are acting on targets other than the RAS [73]. In contrast to the above-mentioned studies, Cridland et al., reported that AngII failed to show either anti- or pronociceptive effect [72]. However, at present, we cannot judge this issue because, to the best of our knowledge, there is no other study that supports Cridland's observations. It is also worth considering the article of Pavel et al., which examined the effect of AngII and losartan in rats undergoing CCI. In these animals, intraperitoneal AngII was found to be pronociceptive in the von Frey test (mechanical stimuli), constant hot- and cold-plate tests and decremental cold plate test (thermal stimuli). Losartan fully reversed the effect of AngII in case of mechanical stimuli, partially reversed it in case of constant cold-plate test, but further aggravated it in the decremental cold plate test. In the incremental hot plate test, the pain threshold was unchanged both following AngII or AngII + losartan administration [78]. The differences observed in this study between the effect of angiotensin in response to constant or decremental/incremental thermal stimuli is difficult to explain.

Further on, the direct pronociceptive activity of AngII and AngIII was described as spontaneous painful behavior (scratching) was observed following intrathecal administration [40,41]. It is worth noting that the study of Cridland et al., showed neither anti- nor pronociceptive action of AngII, whereas Nemoto and coworkers reported a pronociceptive action. Despite the similar administration route, the phenotype of the animals, as well as the dose applied, was different in these studies [40,41,73]. Therefore, further studies are needed to elucidate the effect of AngII at the spinal level. Indirectly supporting the pronociceptive action of AngII, Kaneko et al., reported icv. administered AngII to attenuate the analgesic activity of morphine in a dose-dependent manner in hot plate and tail pinch tests [69]. Similarly, Yamada et al., found that icv. administrated AngII or the AT2R agonist novokin decreased the antinociceptive effect of morphine in the tail-pinch test [79]. Shepherd et al., also reported an increased mechanical but not thermal allodynia following intraplantar AngII administration in mice after spared nerve injury (SNI) [80].

There is large literature data on neural regeneration and differentiation mediated by the AT2R, which were recently reviewed by Danigo et al. [24]. From this aspect, activating the AT2R induces positive changes in terms of neural injury. This neuroprotective action linked to the AT2R has been associated with an increase in neuronal BDNF expression by several reports. The AT2R agonist "compound 21" (C21) has been reported to increase neurite growth following spinal nerve injury [81] and to improve survival while attenuating post-stroke neurological deficit in mice [82]. Under these conditions, the common feature was an increase in neuronal BDNF expression. In contrast, increasing BDNF level is not necessarily beneficial in cases of peripheral nerve injury from the aspect of pathological pain, since Madara et al., showed that BDNF could induce glutamate release by enhancing the action of presynaptic NMDA receptors [83]. BDNF release governs the spinal long-term potentiation of C-fibers [84]. Long-term potentiation and a consequently increased glutamatergic tone, involving the increased activity of spinal NMDA receptors, are hallmarks of neuropathic pain or other chronic pain states [85,86]. Furthermore, Chen et al., proved that spinal NMDA receptor-potentiation on primary afferents in neuropathic pain could be blocked either by the BDNF scavenger trkB-Fc or by the trkB receptor antagonist ANA-12 [87]. The contribution of BDNF to pain was validated by Sikandar et al., where they demonstrated that the conditional knockout of BDNF from mouse sensory neurons results in unchanged response to most acute pain types and displayed hypoalgesia in chronic inflammatory or neuropathic pain [88].

3.3. MAS Receptor Agonists

Primarily the Ang (1-7)-MASR branch of RAS acts as an antagonist of the AngII-AT1R activity. The activity linked to AT2Rs is similar in general; however, with respect to pain transmission, this is not the case. The possible analgesic effect of Ang (1-7) was investigated following mostly local (intraplantar [21,23] or intrathecal [34,89–93]) administration. Studies using intraplantar administration reported that Ang (1-7) attenuated PGE2 [21,23,90,91] or carrageenan [23] induced inflammatory mechanical hyperalgesia. The antihyperalgesic effect of Ang (1-7) was lost in MASR KO mice [23] and was reversible by MASR, nNOS, guanylyl cyclase, or ATP-sensitive potassium channel blockers [94] as well as by different adrenergic antagonists [21], but not by naloxone [95].

Intrathecal administration of Ang (1-7) resulted in a decrease in spontaneous nociceptive behavior induced by intrathecal AngII [91], AngIII [92], substance P or NMDA [34]. Furthermore, intrathecal Ang (1-7) showed an antiallodynic and antihyperalgesic effect in neuropathic pain induced by CCI [89], STZ [90], or genetic model of diabetes (ob/ob mice) [93]. Moreover, several authors reported that Ang (1-7) effectively decreased the pathological increased p38 phosphorylation in the spinal cord [90–92,96]. Similar results were reported following intrathecal administration of ACE2 activator DIZE, namely reduced nociceptive behavior in the formalin test and decreased spinal p38 phosphorylation [96]. On the other hand, intraplantar Ang (1-7) was ineffective in the treatment of CCI induced neuropathic pain [23].

The effect of systemic (ip.) administration of Ang (1-7) on bone cancer pain was investigated by Forte et al., In this model, Ang (1-7) reduced spontaneous pain reactions, increased von Frey threshold and tail immersion latency following acute or chronic administration. The authors reported no anti-tumor activity [97].

3.4. AT1 and AT2 Receptor Antagonists

A growing body of literature data supports that antagonists of the AT1R, such as losartan, candesartan, or telmisartan, among others, display analgesic action in different pain models, including acute thermal, inflammatory, or neuropathic pain [17,23,30,35,36,39–41]. With respect to the analgesic effect of telmisartan, our unpublished results also support such findings because it could reduce the partial sciatic nerve CCI-induced allodynia after systemic administration in rats (Figure 2) (Karádi and Al-Khrasani, unpublished data)).
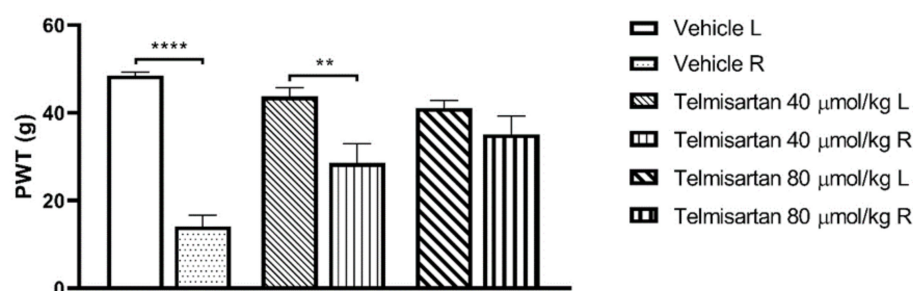
Figure 2. The analgesic effect of telmisartan measured on a dynamic plantar aesthesiometer (DPA) test at 120 min, after p.o. administration to mononeuropathic animals induced by partial sciatic nerve ligation rat model described by Seltzer et al. [98]. Columns represent the paw withdrawal threshold (PWT) of the animals in grams $\pm$ S.E.M. Asterisk indicates the significant differences between treatment groups or operated (R) and non-operated (L) hind paws (** $p < 0.01$ and **** $p < 0.0001$). Statistical differences were determined with one-way ANOVA and Tukey post-hoc test. Data represent means $\pm$ S.E.M ($n = 5$ per group). (Karádi, D.Á.; Al-Khrasani, M.; unpublished data).

In addition, intrathecal administration of losartan has been reported to block AngII-induced spontaneous pain [39], both phases of formalin test [41], and STZ-induced allodynia [99]. On the other hand, microinjection of AT1R and AT2R antagonists into the PAG has been reported to aggravate incisional allodynia [26,77]. Local administration of losartan was also investigated by Costa et al., In this study, intraplantar (ipl.) losartan effectively reversed prostaglandin E2 (PGE2) and carrageenan-induced mechanical hyperalgesia but was ineffective in CCI induced neuropathic pain [23]. In contrast, numerous publications have reported that systemic administration of AT1R antagonists to be beneficial [17,20,35,36,79]. Most of these reports suggest that blocking AT1R could also attenuate the inflammatory reaction in DRG [35,36] or the sciatic nerve [17] and elevate the decreased BDNF level in the sciatic nerve [17] following neuronal damage.

Bessaguet et al., investigated the effect of candesartan on resiniferatoxin-induced neurotoxic thermal hypoalgesia in mice and proved that intraperitoneal candesartan was able to reverse the evoked hypoalgesia in this assay, yet the same effect was achieved following the treatment with AT2R antagonist, EMA200 (PD123319). The authors proposed that candesartan may increase the AT2R binding of endogenous AngII, thus lowering the thermal threshold of animals. This proposal is further supported by the lack of efficacy of candesartan in AT2R KO mice [20]. In agreement with these results, Hashikawa-Hobara et al., reported that hypoesthesia caused by fructose induced diabetes was reversible by orally administered candesartan [100]. Obagata et al., showed that intrathecal losartan can attenuate the allodynia evoked by STZ in mice. In addition, they found that Ang II, as well as ACE expression, were increased, indicating the involvement of AngII in neuropathic pain conditions. It has also been reported that candesartan is capable of inducing neuroprotective, anti-inflammatory, and pro-angiogenetic effects accompanied by an increase in BDNF expression [101,102]. In these studies, the beneficial effects of AT1R antagonism were reversible by the AT2 receptor antagonist, EMA200 [101,102]. Similar to the above-mentioned studies, the authors hypothesized that AT1R antagonism causes a shift in endogenous AngII binding from the AT1R to the AT2R, thus indirectly causing AT2R activation.

There are numerous studies indicating that AT2R antagonism can be beneficial in treating different pain entities. In case of inflammatory pain types, the proposal that reduction in hyperinnervation can attenuate pain is in agreement with literature data [103,104]. Chakrabarty et al., reported that EMA200 reduced thermal hyperalgesia, mechanical allodynia, and pathological hyperinnervation of inflamed tissue in a model of inflammatory pain induced by complete Freund's Adjuvant (CFA) [18,22]. The same compound was also effective in the treatment of cancer-induced bone pain, which is mostly an inflam-

matory pain type, strongly depending on local inflammatory mediators [105]. The most clinically promising results, however, came from the investigation of the analgesic effect of EMA200 and its analogs in neuropathic pain, partially contradicting the above-mentioned data [28,29,37,38,80,106–108]. These include rodent models of mononeuropathic pain and even human clinical trials. AT2R antagonists were shown to be able to attenuate mechanical [37,38,81,107,108] and cold [107] allodynia in different mononeuropathic models, such as CCI or SNI. Moreover, the effect of EMA200 was validated on complex behavioral pain assays as well [109]. The most clinically relevant result, however, is that the analgesic effect of EMA401, the orally available analog of EMA200, was tested in clinical trials for postherpetic neuralgia [28,29] and diabetic neuropathy [28]. The efficacy in attenuating symptoms of the patients enrolled was acceptable in both conditions; however, two of the three studies were prematurely terminated because of preclinical data on the possible hepatotoxic effect of the test compound upon long-term administration [28]. There is no clear consensus whether AT2Rs are expressed on sensory neurons creating a direct pharmacological target for analgesia [18,37,38,106,107,110], or the observed beneficial effect is mediated by immune cells infiltrating injured nerves [80,107]. The neuro-immune cross-talk proposed by the latter studies was recently reviewed by Balogh et al. [19].

4. Neuroanatomical Distribution of the μ-Opioid and Angiotensin Receptors in Areas Related to Pain

4.1. The μ-Opioid Receptor

The neuroanatomical distribution of the MOR is now well-established by immunohistochemistry, autoradiography, in situ hybridization, and fluorescence techniques [109–113]. Accordingly, MORs can be found at supraspinal, spinal, and peripheral levels [114–116]. MORs are enriched in the descending pain modulatory pathway, involving the periaqueductal gray (PAG) matter, rostral ventromedial medulla (RVM), locus coeruleus (LC), and the dorsal horn of the spinal cord [115,117]. In addition, they can be found in brain regions that are strongly related to pain perception and integration, such as the cerebral cortex, thalamus, striatum, amygdala, hippocampus, nucleus accumbens, and the ventral tegmental area (VTA) [115,117]. Within the dorsal horn of the spinal cord, MORs are densely localized in the lamina I-II superficial layers on interneurons and projection neurons [115,118]. The dorsal root ganglia are also a significant locus for MORs attributed to pain [115,119]. MORs can also be found on C- and A-fibers and near primary afferent nociceptors [117].

4.2. Angiotensin Receptors and Endogenous Angiotensin Ligands

The components of neuronal angiotensin system are found in anatomical regions hosting different key points in pain pathways, including the dorsal horn of the spinal cord, dorsal root ganglia (DRG and identical structures, such as the spinal trigeminal tract and trigeminal ganglion), or peripheral nerves. Angiotensinogen mRNA can be found ubiquitously in the mammalian brain [120], spinal cord [99], and almost all cells in the DRG [42,43]. The angiotensinogen level in the CNS is not affected by STZ treatment-induced diabetes; however, it is elevated following peripheral inflammation [22,121].

There are contradictory data in the literature about the localization of neuronal renin, the primary activating enzyme of the renin–angiotensin system [42,43,100]. AngI mRNA is present in the human DRG and trigeminal ganglion (TG) [42,43], whereas its protein form was described in rat DRG [121]. AngII was found in rat and human DRG [18,37,43,106,107], TG [42], neurons, satellite cells, and CD3+ T-cells [106]. The colocalization of AngII alongside components involved in pain sensation, such as substance P (SP) and vanilloid transient receptor potential channels, was reported as well on small and medium neurons [18,37,42,43,106]. In rodent, AngII can be found ubiquitously in the spinal cord; its level was highest in the superficial laminae of the dorsal horn, which could suggest a possible role of AngII in nociception [41,99]. Furthermore, AngII levels have been reported to be increased following mono- or polyneuropathic pain evoked by CCI [106] or

STZ, respectively [41,99]. Furthermore, this change in AngII levels was also seen in pain conditions induced by intraplantar formalin injection [41,99] or in bone cancer pain [105].

With respect to the receptors, several studies have reported on the distribution of AT1R on key points related to nociceptive transmission both in mice [39,40] and rats [31,36,43,122–129]. These areas include sciatic nerve [31,127,130], DRG [36,43,123, 125,127–131], and spinal cord [22,39,40,129,132]. Moreover, it can be found in different brain regions, such as the spinal trigeminal tract and raphe nuclei [122]. These data also provide strong evidence on a large amount of AT1aR, and smaller amounts of AT1bR mRNA [43,127,129,132], and the receptor protein [31,36,39,40,123,125,127–129] was also shown in the mentioned regions. In the DRG, the receptor protein was found on satellite cells and neurons of all sizes with a greater extent on smaller ones [36,110,128,130]. In the spinal cord, similarly to AngII, AT1R level was the highest in the superficial dorsal horn [39,128].

In contrast to AT1R, AT2R localization and the above-mentioned function in relation to nociception are controversial subjects. At present, little data are available on the ganglional or sensory neural expression of AT2R as many of the currently commercially available AT2R antibodies used for immunohistochemistry seem to show inappropriate specificity [131]. Therefore, it is important to evaluate the results of studies using antibodies with appropriate criticism—especially in case of earlier works.

Early autoradiographic studies found significant inhibition of AngII binding by AT1R but not by AT2R antagonists on the sciatic nerve, spinal cord, and (upper cervical) sensory ganglion [31,128]. AT2 mRNA was found in the DRG and sciatic nerve of rats [43,127]. The receptor protein was found by many research groups on neurons (IB4+ [132]), satellite cells [106,127], and CD3+ T-cells [106] and in the rat DRG as well [101,106,107,110,125,130]. Indeed, in a few studies, the AT2 antibody specificity was verified on AT2R KO mice, further reinforcing the results [37,123]. On the other hand, Shepherd and colleagues were not able to find AT2R mRNA or protein in the DRG of mice or humans [80]. In their study using Agtr2^{GFP} reporter mice, the AT2 positivity in the sciatic nerve was detectable and increased after SNI but because of macrophage infiltration instead of neural expression. Taken together, Shepherd's group claims that AT2R is not expressed on sensory neurons involved in nociception [107]. In contrast, Benitez et al., found AT2 immunoreactivity in rat DRG mostly on non-peptidergic (IB4+) C- and Aδ-fibers showing high colocalization to AT1 yet using an antibody with specificity verified on AT2R KO mice. In their study, the level of AT2 increased in an inflammatory state following treatment with CFA [123]. It is important to mention that mice were used in the study conducted by Shepherd in contrast to rats used by Benitez. A very recent review published in 2021 by Danigo et al., provides detail on how to solve this contradiction and lists species differences as well as the possible gene duplication of AT2R (similar to AT1R) in mice which could cause a lack of signal in the reporter mice [24].

Angiotensin-converting enzyme 2 (ACE2) is a carboxypeptidase enzyme regulating the local levels of AngII and Ang 1-7 (metabolizes AngII to Ang 1-7). Its mRNA and protein were found in human DRG samples, colocalizing with nociceptor neuronal markers [133]. It is also expressed in mouse spinal cord, where it is localized on neurons and microglia but not on astrocytes [93]. Finally, MASR expression was shown in rat DRG [91,92], PAG [134] and in mouse spinal cord [93]. However, to the best of our knowledge, the localization of the Ang (1-7) peptide has not been fully described. The neuroanatomical localization of key elements of the RAS and μ-opioid receptors have been summarized in Table 1.

Table 1. Neuroanatomical distribution of ligands and receptors in the renin–angiotensin system with importance in pain transmission and the μ-opioid receptor (MOR).

Ligand/Receptor	Species	mRNA /Peptide/ Protein	Method	Details	Changes		References
					Inflammation	Neuropathy	
Peripheral nerves							
Angiotensinogen	rat	p	IHC	detected	increased	-	[22]
AT1 receptor	rat	p	autorad	detected	-	-	[31]
	rat	r	PCR	detected	-	increased	[124]
AT2 receptor	rat	p	autorad	not detected	-	-	[31]
	rat	r	PCR	detected	-	increased	[124]
	AgtrGFP reporter mouse	p	reporter mouse	detected on thick non-peptidergic neurons	-	increased (macrophage infiltration)	[107]
MAS receptor	mouse	p	IHC	detected	-	increased	[135]
MOR	rat	p	IHC	detected	increased	-	[136]
	human	p	IHC	detected on CGRP positive skin sensory nerves	no change	-	[137]
Dorsal root ganglia							
Angiotensinogen	rat	p	IHC	detected	increased	-	[22]
	rat	r and p	PCR and IHC	detected	-	-	[121]
	rat	r	PCR and ISH	detected on all cells	-	-	[43]
Angiotensin I	human	p	RIA	detected	-	-	[43]
Angiotensin II	rat and human	p	IHC and RIA	colocalized with SP and CGRP	-	-	[43]
	rat	p	IHC	colocalized with neuronal markers	increased (bone metastasis)	-	[105]
	rat	p	IHC and WB	colocalized with SP and NF200	-	increased	[37]
	human	p	IHC	colocalized with TRPV1 on small and medium neurons	-	-	[18]
	rat	p	IHC	on neurons, satellite cells, and T cells	-	increased	[106]
Angiotensin (1-7)	human	p	IHC	not detected	-	-	[18]
AT1 receptor	rat	r	PCR	detected	-	no change	[124]
	rat	r	PCR	detected	-	-	[43]
	rat	p	IHC	detected on Schwann cells, satellite cells, and neurons	-	decreased (DM)	[127]
	rat (isolated neurons)	r and p	PCR, WB, and RB	detected	decreased (TNFα)	-	[129]
	rat	p	IHC	detected on small and large neurons	-	increased	[125]
	rat	p	IHC	detected on neurons and satellite cells	-	-	[36]
	rat	p	IHC	detected on all neurons, higher expression on small	increased on large neurons	-	[123]

Table 1. *Cont.*

Ligand/Receptor	Species	mRNA /Peptide/ Protein	Method	Details	Changes Inflammation	Changes Neuropathy	References
AT2 receptor	rat	r	PCR	detected	-	increased	[124]
	rat	r and p	PCR and IHC	detected	-	-	[121]
	rat	r	PCR	detected	-	-	[43]
	rat	p	IHC	detected on Schwann cells, satellite cells, and neurons	-	increased (DM)	[127]
	rat (cell culture)	p	WB	detected	-	increased (DM)	[100]
	rat	p	IHC	colocalized with neural markers	-	-	[37,105]
	rat (neonatal)	r and p	PCR, WB, and IHC	detected on IB4+ neurons	-	-	[132]
	rat	p	IHC	detected on neurons, satellite cells, and T-cells	-	no change	[106]
	rat	p	IHC	detected on all neurons, mostly non-peptidergic C and Aδ, high colocalization with AT1	increased	-	[123]
	AgtrGFP reporter mouse and human	r and p	PCR and reporter mouse	not detected	-	-	[80]
	AgtrGFP reporter mouse	p	reporter mouse	not detected	-	no change	[107]
MAS receptor	rat	p	IHC	detected	-	-	[95]
	rat	r and p	PCR and WB	detected	-	increased	[89]
	rat	r and p	PCR and WB	detected	-	-	[138]
	mouse	p	WB	detected	increased (bone metastasis)	-	[97]
MOR	rat	p	IHC	detected mainly on small neurons	increased	-	[136]
	rat	p	IHC	detected on small and medium neurons, highly colocalized with CGRP and SP	-	-	[139]
	rat	p	IHC	detected	increased	-	[50]
	rat	r	PCR	detected	increased	decreased	[140]
	human	r	PCR	detected on approx. 50% of neurons, mainly capsaicin-responsive small neurons	-	-	[119]

Table 1. *Cont.*

Ligand/Receptor	Species	mRNA /Peptide/ Protein	Method	Details	Changes Inflammation	Changes Neuropathy	References
				Spinal cord			
Angiotensin II	mouse	p	IHC	detected ubiquitously, highest in laminae I and II	increased	increased	[41,99]
AT1 receptor	rat	p	IHC, autorad, and ISH	detected in the superficial DH and on cholinergic neurons in the VH	-	-	[126,128]
	mouse	p	IHC	detected in the superficial DH	-	-	[39,40]
AT2 receptor	rat	p	IHC	detected in laminae I and II and colocalized with IB4 and SP in	-	-	[123]
	AgtrGFP reporter mouse	p	reporter mouse	detected in the deep DH and VH and colocalized with neuronal markers	-	no change	[107]
MAS receptor	mouse	p	WB	detected	-	-	[93]
	mouse	p	IHC	detected and colocalized with NK1 and NMDA receptors	-	-	[34]
MOR	rat/guinea pig	p	autorad	detected in the superficial dorsal horn	-	-	[113]
	rat	p	IHC	detected on laminae I-II	increased	-	[136]
	rat	p	IHC	present	-	-	[139]
	rat	p	IHC	postsynaptic MOR is restricted to lamina II	-	-	[141]
	rat	p	IHC	detected, half of MOR immunoreactivity in the SC is on primary afferents	-	-	[142]
	rat	r	PCR	detected	no change	no change	[140]
	rat	p	IHC	detected	-	decreased (reversible by NGF)	[57]

Abbreviations: p: peptide/protein; r: mRNA; IHC: immunohistochemistry; autorad: autoradiography; PCR: polymerase chain reaction; ISH: in situ hybridization; RIA: radioimmunoassay; WB: Western blot; DM: diabetes mellitus; DH: dorsal horn; VH: ventral horn; SP: substance P; CGRP: calcitonin gene-related peptide; NF200: neurofilament protein 200; TRPV1: transient receptor potential cation channel subfamily V member 1; IB4: isolectin B4; NK1: neurokinin 1; NMDA: N-methyl D-aspartate. A hyphen indicates no assessment by the indicated studies.

5. Possible Link between MOR Analgesics and Ligands Affecting Angiotensin Receptors in Relation to Pain

Rather than dose escalation of MORs analgesics which is associated with an increase in the incidence of side effects, augmenting MORs-mediated analgesia would be an important strategy in the management of neuropathic pain. In regard to the interaction between opioid and angiotensin systems, to the best of our knowledge, the first study published in 1983 by Haulica et al., described that AngII produced naloxone reversible analgesia following icv. administration in rat tail-flick test; therefore, these results showed the implication of endogenous opioid system in the effect of AngII [68]. In a later study, the same research group also reported that naloxone or saralasin attenuates stress analgesia in rats [70]. Based on another study by Han et al., icv. administered AngII was able to reverse the antinociceptive action of sc. morphine [76]. Similarly, Yamada et al., showed

that AT2R activation decreases the analgesic effect of morphine [79]. On the other hand, a previous study by Mojaverian et al., reported that orally administered ACE inhibitor enalapril failed to influence morphine analgesia [143]. Recently, Taskiran and Avci reported that systemic captopril alone was able to increase tail-flick and hot plate latency, and it also increased the analgesic effect of systemic morphine. Furthermore, the co-treatment with captopril reduced morphine-induced analgesic tolerance development. Captopril also reduced the inflammatory and endoplasmatic stress response in the DRG caused by acute or chronic morphine treatment [32]. It is important to note however, that ACE inhibition could result in a diverse molecular effect, partly independent from RAS—such as the inhibition of the catabolism of endogenous opioids and peptide mediators, among others. Next, connection between Ang (1-7), MASRs and the opioid system is unclear as to the best of our knowledge there are little data available at present. In this respect, Costa et al., reported that endogenous opioids do not play a role in the analgesic action of Ang (1-7) as it was not sensitive to naloxone [95]. This does not necessarily mean that there are no possible interactions between the two systems. Indeed, there are several reports, indicating opioids are capable of changing physiological parameters, most notably changes in the blood pressure [144–148] or drinking-response to AngII [149–151]. However, regarding the relationship between RAS and the opioid system only a small proportion of these address the role of interactions in analgesia. We have summarized the outcomes of relevant studies in Table 2.

Table 2. Reported connections between the opioid and renin–angiotensin systems in relation to pain.

RAS Ligand/Receptor	Method	Outcome	Reference
Angiotensin II	rat tail-flick test	AngII mediated analgesia is reversible by naloxone.	Haulica et al., 1983 [68]
	rat tail-flick test	AngII is able to attenuate morphine analgesia.	Han et al., 2000 [76]
Angiotensin-converting enzyme	rat tail-flick test	ACE-inhibition cannot influence morphine analgesia.	Mojaverian et al., 1984 [143]
	rat tail-flick and hot plate test	ACE-inhibition enhances morphine analgesia and decreases the development of opioid analgesic tolerance.	Taskiran et al., 2021 [32]
	ELISA	ACE-inhibition decreases inflammatory cytokine levels in the DRG of morphine tolerant animals.	Taskiran et al., 2021 [32]
AT2 receptor	mouse tail/pinch test	AT2 activation decreases morphine analgesia	Yamada et al., 2009 [79]
	rat tail-flick test	Saralasin (AT2 partial agonist) decreases stress analgesia.	Haulica et al., 1986 [70]

Abbreviations: ELISA: enzyme-linked immunosorbent assay.

With respect to neuropathic pain, Khan and coworkers showed that allodynia caused by CCI of the sciatic nerve was attenuated by a systemic single dose of EMA300, a small molecule AT2R antagonist [106]. In this study, the authors also proved that the nerve growth factor (NGF) level was significantly reduced in the ipsilateral lumbar DRGs of neuropathic rats. In addition, treatment with EMA300 could restore the decreased NGF level. Furthermore, several studies have shown that MOR reserve in the spinal cord and DRG is decreased in rodents with neuropathic pain. It is worth noting that administration of exogenous NGF does restore both MOR numbers and their analgesia at main relay points along the pain pathways, such as the spinal cord [58]. These results support a hypothesis on the possible existence of a link between MORs and angiotensin receptor affecting ligands which may provide a new strategy for the treatment of neuropathic pain. Namely, AT2R blockade was reported to restore pathologically decreased NGF levels in neuropathy, which, in turn, could positively influence the MOR number in the DRG and spinal cord, thus restoring the analgesic effect of MOR agonists (Figure 3). An opposing

viewpoint is the implication of NGF in pain induction which is not the scope of the present review but has been reported by other researchers [152–154]. Finally, whether activation or blockade of AT2R would be of value in managing neuropathic pain, we could propose that AT2R inhibition attenuates pain mediated by largely unidentified pathways. On the other hand, the neural growth and remodeling induced by AT2R activation may be beneficial for neuroregeneration, though undesired effects on the symptoms of neuropathy may occur.

To the best of our knowledge, so far, no publication has investigated the possible connections between the opioid system and the Ang (1-7)—MAS receptor branch of the RAS.
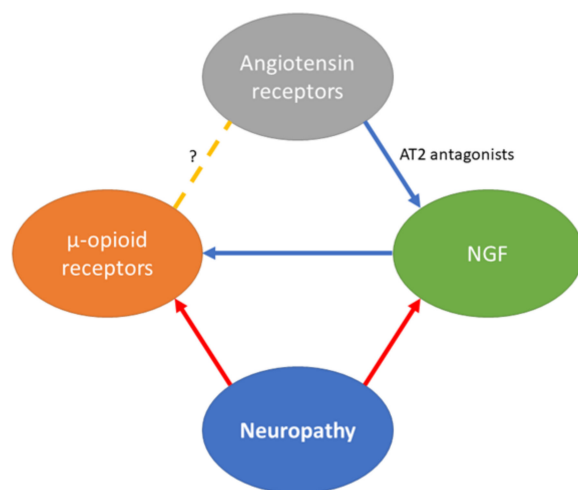

Figure 3. Possible links between neuropathy, the renin–angiotensin system, MORs and NGF. Red arrows indicate a reducing effect, while the blue ones indicate an increasing effect. In neuropathic conditions, the MOR reserve is decreased, resulting in impaired opioid analgesia. The receptor number can be restored by administration of NGF, the level of which is also reduced in the spinal cord in neuropathy. AT2 antagonists are capable of restoring the lowered NGF level, thus possibly restoring the analgesic effect of opioids. To the best of our knowledge, there is no evidence of the direct connection between MORs and the renin–angiotensin system. The figure was constructed based on literature discussed in Section 5.

6. Concluding Remarks and Future Directions

MOR analgesics alleviate neuropathic pain; however, high doses are needed, which, in turn, result in serious side effects both in preclinical and human studies. Current evidence indicates that AT1, AT2, and MASRs are involved in the control of neuropathic pain; however, their mechanism of action related to neuropathic pain has not yet been fully verified. Nevertheless, AT1, AT2, and MASRs are expressed in key areas related to pain where MORs agonists halt pain sensation. In neuropathic conditions, peripheral and central AT1 blockade and spinal MASRs activation appear to be beneficial. Data on the impact of AT2R in neuropathic pain are contradictory, though its activation or inhibition can result in neuroprotection or analgesia, respectively; however, future studies are needed to justify this issue. So far, there are no angiotensin receptor affecting agents that have been utilized clinically; however, there are clinical studies on AT2R inhibitors that have entered phase II trials but did not proceed further due to their toxicity. It is important to note that these clinical studies prove that such AT2R inhibitors showed equipotent efficacy with gabapentin. In neuropathic pain, the MOR receptors and NGF levels are decreased. Treatment with NGF results in restoring MOR and their analgesic activity in preclinical pain studies. On the other hand, there are studies reporting the increase in pain sensation upon NGF use, which is not the scope of the present review. Furthermore, some studies revealed that angiotensin AT2R inhibitors do increase NGF in neuropathic pain and thus normalize MOR levels. Therefore, we can speculate that drugs affecting angiotensin receptors could restore the effect of MOR analgesics, which results in avoiding dose escalation of opioids

upon the treatment of neuropathic pain. Finally, these strategies might offer a bridge upon titration of drugs with delay in onset used in the treatment of neuropathic pain.

References

1. Chou, R.; Fanciullo, G.J.; Fine, P.G.; Adler, J.A.; Ballantyne, J.C.; Davies, P.S.; Donovan, M.I.; Fishbain, D.A.; Foley, K.M.; Fudin, J.; et al. Clinical Guidelines for the Use of Chronic Opioid Therapy in Chronic Noncancer Pain. *J. Pain* **2009**, *10*, 113–130.e22. [CrossRef]

2. Hoskin, P. Opioids in context: Relieving the pain of cancer. The role of comprehensive cancer management. *Palliat. Med.* **2008**, *22*, 303–309. [CrossRef]

3. Quigley, C. The role of opioids in cancer pain. *BMJ* **2005**, *331*, 825–829. [CrossRef] [PubMed]

4. Fukshansky, M.; Are, M.; Burton, A.W. The Role of Opioids in Cancer Pain Management. *Pain Pr.* **2005**, *5*, 43–54. [CrossRef] [PubMed]

5. Bates, D.; Schultheis, B.C.; Hanes, M.C.; Jolly, S.M.; Chakravarthy, K.V.; Deer, T.R.; Levy, R.M.; Hunter, C.W. A Comprehensive Algorithm for Management of Neuropathic Pain. *Pain Med.* **2019**, *20*, S2–S12. [CrossRef]

6. Attal, N.; Cruccu, G.; Baron, R.; Haanpää, M.; Hansson, P.; Jensen, T.S.; Nurmikko, T. EFNS guidelines on the pharmacological treatment of neuropathic pain: 2010 revision. *Eur. J. Neurol.* **2010**, *17*, 1113-e88. [CrossRef]

7. O'Connor, A.B.; Dworkin, R.H. Treatment of Neuropathic Pain: An Overview of Recent Guidelines. *Am. J. Med.* **2009**, *122*, S22–S32. [CrossRef] [PubMed]

8. Przewłocka, B.; Mika, J.; Łabuz, D.; Toth, G.; Przewłocki, R. Spinal analgesic action of endomorphins in acute, inflammatory and neuropathic pain in rats. *Eur. J. Pharmacol.* **1999**, *367*, 189–196. [CrossRef]

9. Balogh, M.; Zádor, F.; Zádori, Z.S.; Shaqura, M.; Király, K.; Mohammadzadeh, A.; Varga, B.; Lázár, B.; Mousa, S.A.; Hosztafi, S.; et al. Efficacy-Based Perspective to Overcome Reduced Opioid Analgesia of Advanced Painful Diabetic Neuropathy in Rats. *Front. Pharmacol.* **2019**, *10*, 347. [CrossRef] [PubMed]

10. Wu, C.L.; King, A.B.; Geiger, T.M.; Grant, M.C.; Grocott, M.P.W.; Gupta, R.; Hah, J.M.; Miller, T.; Shaw, A.D.; Gan, T.J.; et al. American Society for Enhanced Recovery and Perioperative Quality Initiative Joint Consensus Statement on Perioperative Opioid Minimization in Opioid-Naïve Patients. *Anesthesia Analg.* **2019**, *129*, 567–577. [CrossRef] [PubMed]

11. Els, C.; Hagtvedt, R.; Kunyk, D.; Sonnenberg, B.; Lappi, V.G.; Straube, S. High-dose opioids for chronic non-cancer pain: An overview of Cochrane reviews. *Cochrane Database Syst. Rev.* **2016**, *7*, CD012299. [CrossRef]

12. Cooper, T.E.; Chen, J.; Wiffen, P.J.; Derry, S.; Carr, D.B.; Aldington, D.; Cole, P.; Moore, R.A. Morphine for chronic neuropathic pain in adults. *Cochrane Database Syst. Rev.* **2017**, *2019*, CD011669. [CrossRef]

13. Morgan, M.M.; Christie, M.J. Analysis of opioid efficacy, tolerance, addiction and dependence from cell culture to human. *Br. J. Pharmacol.* **2011**, *164*, 1322–1334. [CrossRef] [PubMed]

14. Gilron, I.; Wiffen, P.J.; Moore, R.A. Combination pharmacotherapy for the treatment of neuropathic pain in adults. *Cochrane Database Syst. Rev.* **2011**, *1*, CD008943. [CrossRef]

15. Schroder, W.; Tzschentke, T.M.; Terlinden, R.; De Vry, J.; Jahnel, U.; Christoph, T.; Tallarida, R.J. Synergistic Interaction between the Two Mechanisms of Action of Tapentadol in Analgesia. *J. Pharmacol. Exp. Ther.* **2011**, *337*, 312–320. [CrossRef] [PubMed]

16. Mohammadzadeh, A.; Lakatos, P.P.; Balogh, M.; Zador, F.; Karadi, D.A.; Zadori, Z.S.; Kiraly, K.; Galambos, A.R.; Barsi, S.; Riba, P.; et al. Pharmacological Evidence on Augmented Antiallodynia Following Systemic Co-Treatment with GlyT-1 and GlyT-2 Inhibitors in Rat Neuropathic Pain Model. *Int. J. Mol. Sci.* **2021**, *22*, 2479. [CrossRef]

17. Al-Rejaie, S.S.; Abuohashish, H.M.; Ahmed, M.M.; Arrejaie, A.; Aleisa, A.M.; AlSharari, S.D. Telmisartan inhibits hyperalgesia and inflammatory progression in a diabetic neuropathic pain model of Wistar rats. *Neurosciences* **2015**, *20*, 115–123. [CrossRef] [PubMed]

18. Anand, U.; Yiangou, Y.; Sinisi, M.; Fox, M.; MacQuillan, A.; Quick, T.; Korchev, Y.E.; Bountra, C.; McCarthy, T.; Anand, P. Mechanisms underlying clinical efficacy of Angiotensin II type 2 receptor (AT2R) antagonist EMA401 in neuropathic pain: Clinical tissue and in vitro studies. *Mol. Pain* **2015**, *11*, s12990-015. [CrossRef]

19. Balogh, M.; Aguilar, C.; Nguyen, N.T.; Shepherd, A.J. Angiotensin receptors and neuropathic pain. *PAIN Rep.* **2021**, *6*, e869. [CrossRef]

20. Bessaguet, F.; Danigo, A.; Magy, L.; Sturtz, F.; Desmoulière, A.; Demiot, C. Candesartan prevents resiniferatoxin-induced sensory small-fiber neuropathy in mice by promoting angiotensin II-mediated AT2 receptor stimulation. *Neuropharmacology* **2017**, *126*, 142–150. [CrossRef]

21. Castor, M.G.M.; Santos, R.A.; Duarte, I.D.; Romero, T.R. Angiotensin-(1-7) through Mas receptor activation induces peripheral antinociception by interaction with adrenoreceptors. *Peptides* **2015**, *69*, 80–85. [CrossRef]

22. Chakrabarty, A.; Liao, Z.; Smith, P.G. Angiotensin II Receptor Type 2 Activation Is Required for Cutaneous Sensory Hyper-innervation and Hypersensitivity in a Rat Hind Paw Model of Inflammatory Pain. *J. Pain* **2013**, *14*, 1053–1065. [CrossRef] [PubMed]

23. Costa, A.C.; Romero, T.R.; Pacheco, D.F.; Perez, A.C.; Savernini, A.; Santos, R.R.; Duarte, I.D. Participation of AT1 and Mas receptors in the modulation of inflammatory pain. *Peptides* **2014**, *61*, 17–22. [CrossRef] [PubMed]

24. Danigo, A.; Rovini, A.; Bessaguet, F.; Bouchenaki, H.; Bernard, A.; Sturtz, F.; Bourthoumieu, S.; Desmouliere, A.; Magy, L.; Demiot, C. The Angiotensin II Type 2 Receptor, a Target for Protection and Regeneration of the Peripheral Nervous System? *Pharmaceuticals* **2021**, *14*, 175. [CrossRef] [PubMed]

25. Danser, A.J.; Anand, P. The Angiotensin II Type 2 Receptor for Pain Control. *Cell* **2014**, *157*, 1504–1506. [CrossRef] [PubMed]

26. Pelegrini-Da-Silva, A.; Martins, A.; Prado, W. A new role for the renin—Angiotensin system in the rat periaqueductal gray matter: Angiotensin receptor-mediated modulation of nociception. *Neuroscience* **2005**, *132*, 453–463. [CrossRef]

27. Raghavendra, V.; Chopra, K.; Kulkarni, S. Brain renin angiotensin system (RAS) in stress-induced analgesia and impaired retention. *Peptides* **1999**, *20*, 335–342. [CrossRef]

28. Rice, A.S.C.; Dworkin, R.H.; Finnerup, N.B.; Attal, N.; Anand, P.; Freeman, R.; Piaia, A.; Callegari, F.; Doerr, C.; Mondal, S.; et al. Efficacy and safety of EMA401 in peripheral neuropathic pain: Results of 2 randomised, double-blind, phase 2 studies in patients with postherpetic neuralgia and painful diabetic neuropathy. *Pain* **2021**, *162*, 2578–2589.

29. Rice, A.S.C.; Dworkin, R.H.; McCarthy, T.D.; Anand, P.; Bountra, C.I.; McCloud, P.; Hill, J.; Cutter, G.; Kitson, G.; Desem, N.; et al. EMA401, an orally administered highly selective angiotensin II type 2 receptor antagonist, as a novel treatment for postherpetic neuralgia: A randomised, double-blind, placebo-controlled phase 2 clinical trial. *Lancet* **2014**, *383*, 1637–1647. [CrossRef]

30. Takai, S.; Song, K.; Tanaka, T.; Okunishi, H.; Miyazaki, M. Antinociceptive effects of angiotensin-converting enzyme inhibitors and an angiotensin II receptor antagonist in mice. *Life Sci.* **1996**, *59*, PL331–PL336. [CrossRef]

31. Tang, H.; Pavel, J.; Saavedra, J.M.; Brimijoin, S. Type-1 angiotensin receptors are expressed and transported in motor and sensory axons of rat sciatic nerves. *Neuropeptides* **2009**, *43*, 81–92. [CrossRef]

32. Taskiran, A.S.; Avci, O. Effect of captopril, an angiotensin-converting enzyme inhibitor, on morphine analgesia and tolerance in rats, and elucidating the inflammation and endoplasmic reticulum stress pathway in this effect. *Neurosci. Lett.* **2020**, *741*, 135504. [CrossRef] [PubMed]

33. Toma, N.; Sgambato, V.; Couture, R. Effect of Angiotensin Ii on a Spinal Nociceptive Reflex in the Rat: Receptor and Mechanism of Action. *Life Sci.* **1997**, *61*, 503–513. [CrossRef]

34. Yamagata, R.; Nemoto, W.; Fujita, M.; Nakagawasai, O.; Tan-No, K. Angiotensin (1-7) Attenuates the Nociceptive Behavior Induced by Substance P and NMDA via Spinal MAS1. *Biol. Pharm. Bull.* **2021**, *44*, 742–746. [CrossRef] [PubMed]

35. Kalynovska, N.; Diallo, M.; Sotakova-Kasparova, D.; Palecek, J. Losartan attenuates neuroinflammation and neuropathic pain in paclitaxel-induced peripheral neuropathy. *J. Cell. Mol. Med.* **2020**, *24*, 7949–7958. [CrossRef]

36. Kim, E.; Hwang, S.-H.; Kim, H.-K.; Abdi, S.; Kim, H.K. Losartan, an Angiotensin II Type 1 Receptor Antagonist, Alleviates Mechanical Hyperalgesia in a Rat Model of Chemotherapy-Induced Neuropathic Pain by Inhibiting Inflammatory Cytokines in the Dorsal Root Ganglia. *Mol. Neurobiol.* **2019**, *56*, 7408–7419. [CrossRef]

37. Smith, M.T.; Woodruff, T.; Wyse, B.D.; Muralidharan, A.; Walther, T. A Small Molecule Angiotensin II Type 2 Receptor (AT2R) Antagonist Produces Analgesia in a Rat Model of Neuropathic Pain by Inhibition of p38 Mitogen-Activated Protein Kinase (MAPK) and p44/p42 MAPK Activation in the Dorsal Root Ganglia. *Pain Med.* **2013**, *14*, 1557–1568. [CrossRef]

38. Smith, M.T.; Wyse, B.D.; Edwards, S.R. Small molecule angiotensin II type 2 receptor (AT(2)R) antagonists as novel analgesics for neuropathic pain: Comparative pharmacokinetics, radioligand binding, and efficacy in rats. *Pain Med.* **2013**, *14*, 692–705. [CrossRef]

39. Nemoto, W.; Nakagawasai, O.; Yaoita, F.; Kanno, S.-I.; Yomogida, S.; Ishikawa, M.; Tadano, T.; Tan-No, K. Angiotensin II Produces Nociceptive Behavior through Spinal AT1 Receptor-Mediated p38 Mitogen-Activated Protein Kinase Activation in Mice. *Mol. Pain* **2013**, *9*, 38. [CrossRef]

40. Nemoto, W.; Ogata, Y.; Nakagawasai, O.; Yaoita, F.; Tadano, T.; Tan-No, K. Involvement of p38 MAPK activation mediated through AT1 receptors on spinal astrocytes and neurons in angiotensin II- and III-induced nociceptive behavior in mice. *Neuropharmacology* **2015**, *99*, 221–231. [CrossRef]

41. Nemoto, W.; Ogata, Y.; Nakagawasai, O.; Yaoita, F.; Tanado, T.; Tan-No, K. The intrathecal administration of losartan, an AT1 receptor antagonist, produces an antinociceptive effect through the inhibiton of p38 MAPK phosphorylation in the mouse formalin test. *Neurosci. Lett.* **2015**, *585*, 17–22. [CrossRef]

42. Imboden, H.; Patil, J.; Nussberger, J.; Nicoud, F.; Hess, B.; Ahmed, N.; Schaffner, T.; Wellner, M.; Muller, D.N.; Inagami, T.; et al. Endogenous angiotensinergic system in neurons of rat and human trigeminal ganglia. *Regul. Pept.* **2009**, *154*, 23–31. [CrossRef] [PubMed]

43. Patil, J.; Schwab, A.; Nussberger, J.; Schaffner, T.; Saavedra, J.M.; Imboden, H. Intraneuronal angiotensinergic system in rat and human dorsal root ganglia. *Regul. Pept.* **2010**, *162*, 90–98. [CrossRef] [PubMed]

44. Connor, M.; Christie, M. Opioid Receptor Signalling Mechanisms. *Clin. Exp. Pharmacol. Physiol.* **1999**, *26*, 493–499. [CrossRef]

45. Jordan, B.; Devi, L.A. Molecular mechanisms of opioid receptor signal transduction. *Br. J. Anaesth.* **1998**, *81*, 12–19. [CrossRef]

46. Loh, H.H.; Liu, H.C.; Cavalli, A.; Yang, W.; Chen, Y.F.; Wei, L.N. μ Opioid receptor knockout in mice: Effects on ligand-induced analgesia and morphine lethality. *Brain Res. Mol. Brain Res.* **1998**, *54*, 321–326. [CrossRef]

47. Matthes, H.W.; Maldonado, R.; Simonin, F.; Valverde, O.; Slowe, S.; Kitchen, I.; Befort, K.; Dierich, A.; le Meur, M.; Dolle, P. Loss of morphine-induced analgesia, reward effect and withdrawal symptoms in mice lacking the mu-opioid-receptor gene. *Nature* **1996**, *383*, 819–823. [CrossRef] [PubMed]

48. Stein, C.; Schäfer, M.; Machelska, H. Attacking pain at its source: New perspectives on opioids. *Nat. Med.* **2003**, *9*, 1003–1008. [CrossRef]

49. Lackó, E.; Riba, P.; Giricz, Z.; Váradi, A.; Cornic, L.; Balogh, M.; Király, K.; Csekő, K.; Mousa, S.A.; Hosztafi, S.; et al. New morphine analogs produce peripheral antinociception within a certain dose range of their systemic administration. *J. Pharmacol. Exp. Ther.* **2016**, *359*, 171–181. [CrossRef]

50. Zollner, C.; Shaqura, M.A.; Bopaiah, C.P.; Mousa, S.; Stein, C.; Schafer, M. Painful inflammation-induced increase in mu-opioid receptor binding and G-protein coupling in primary afferent neurons. *Mol. Pharmacol.* **2003**, *64*, 202–210. [CrossRef]

51. Khalefa, B.I.; Mousa, S.A.; Shaqura, M.; Lacko, E.; Hosztafi, S.; Riba, P.; Schafer, M.; Ferdinandy, P.; Furst, S.; Al-Khrasani, M. Peripheral antinociceptive efficacy and potency of a novel opioid compound 14-O-MeM6SU in comparison to known peptide and non-peptide opioid agonists in a rat model of inflammatory pain. *Eur. J. Pharmacol.* **2013**, *713*, 54–57. [CrossRef]

52. Al-Khrasani, M.; Lacko, E.; Riba, P.; Kiraly, K.; Sobor, M.; Timar, J.; Mousa, S.; Schafer, M.; Furst, S. The central versus peripheral antinociceptive effects of mu-opioid receptor agonists in the new model of rat visceral pain. *Brain Res. Bull.* **2012**, *87*, 238–243. [CrossRef]

53. Al-Khrasani, M.; Spetea, M.; Friedmann, T.; Riba, P.; Király, K.; Schmidhammer, H.; Furst, S. DAMGO and 6β-glycine substituted 14-O-methyloxymorphone but not morphine show peripheral, preemptive antinociception after systemic administration in a mouse visceral pain model and high intrinsic efficacy in the isolated rat vas deferens. *Brain Res. Bull.* **2007**, *74*, 369–375. [CrossRef]

54. Balogh, M.; Zádori, Z.S.; Lázár, B.; Karádi, D.; László, S.; Mousa, S.A.; Hosztafi, S.; Zádor, F.; Riba, P.; Schäfer, M.; et al. The Peripheral Versus Central Antinociception of a Novel Opioid Agonist: Acute Inflammatory Pain in Rats. *Neurochem. Res.* **2018**, *43*, 1250–1257. [CrossRef]

55. Mizoguchi, H.; Watanabe, C.; Yonezawa, A.; Sakurada, S. Chapter 19 New Therapy for Neuropathic Pain. *Int. Rev. Neurobiol.* **2009**, *85*, 249–260. [CrossRef]

56. Shaqura, M.; Khalefa, B.; Shakibaei, M.; Zöllner, C.; Al-Khrasani, M.; Fürst, S.; Schäfer, M.; Mousa, S.A. New insights into mechanisms of opioid inhibitory effects on capsaicin-induced TRPV1 activity during painful diabetic neuropathy. *Neuropharmacology* **2014**, *85*, 142–150. [CrossRef] [PubMed]

57. Shaqura, M.; Khalefa, B.I.; Shakibaei, M.; Winkler, J.; Al-Khrasani, M.; Fürst, S.; Mousa, S.A.; Schäfer, M. Reduced Number, G Protein Coupling, and Antinociceptive Efficacy of Spinal Mu-Opioid Receptors in Diabetic Rats Are Reversed by Nerve Growth Factor. *J. Pain* **2013**, *14*, 720–730. [CrossRef] [PubMed]

58. Eckenstaler, R.; Sandori, J.; Gekle, M.; Benndorf, R.A. Angiotensin II receptor type 1—An update on structure, expression and pathology. *Biochem Pharmacol.* **2021**, *192*, 114673. [CrossRef] [PubMed]

59. Burghi, V.; Echeverria, E.B.; Sosa, M.H.; Quiroga, D.T.; Munoz, M.C.; Davio, C.; Monczor, F.; Fernandez, N.C.; Dominici, F.P. Participation of Galphai-Adenylate Cyclase and ERK1/2 in Mas Receptor Signaling Pathways. *Front Pharmacol.* **2019**, *10*, 146. [CrossRef]

60. Forrester, S.J.; Booz, G.W.; Sigmund, C.D.; Coffman, T.M.; Kawai, T.; Rizzo, V.; Scalia, R.; Eguchi, S. Angiotensin II Signal Transduction: An Update on Mechanisms of Physiology and Pathophysiology. *Physiol. Rev.* **2018**, *98*, 1627–1738. [CrossRef]

61. Karnik, S.S.; Singh, K.D.; Tirupula, K.; Unal, H. Significance of angiotensin 1-7 coupling with MAS1 receptor and other GPCRs to the renin-angiotensin system: IUPHAR Review 22. *Br. J. Pharmacol.* **2017**, *174*, 737–753. [CrossRef] [PubMed]

62. Takezako, T.; Unal, H.; Karnik, S.S.; Node, K. Structure-Function Basis of Attenuated Inverse Agonism of Angiotensin II Type 1 Receptor Blockers for Active-State Angiotensin II Type 1 Receptor. *Mol. Pharmacol.* **2015**, *88*, 488–501. [CrossRef] [PubMed]

63. Bader, M.; Alenina, N.; Andrade-Navarro, M.A.; Santos, R.A. MAS and its related G protein-coupled receptors, Mrgprs. *Pharmacol. Rev.* **2014**, *66*, 1080–1105. [CrossRef] [PubMed]

64. Porrello, E.R.; Delbridge, L.M.; Thomas, W.G. The angiotensin II type 2 (AT2) receptor: An enigmatic seven transmembrane receptor. *Front. Biosci.* **2009**, *14*, 958–972. [CrossRef]

65. Iwai, N.; Inagami, T.; Ohmichi, N.; Nakamura, Y.; Saeki, Y.; Kinoshita, M. Differential regulation of rat AT1a and AT1b receptor mRNA. *Biochem. Biophys. Res. Commun.* **1992**, *188*, 298–303. [CrossRef]

66. Zhou, Y.; Chen, Y.; Dirksen, W.P.; Morris, M.; Periasamy, M. AT1b Receptor Predominantly Mediates Contractions in Major Mouse Blood Vessels. *Circ. Res.* **2003**, *93*, 1089–1094. [CrossRef]

67. Karnik, S.S.; Unal, H.; Kemp, J.R.; Tirupula, K.C.; Eguchi, S.; Vanderheyden, P.M.; Thomas, W.G. International Union of Basic and Clinical Pharmacology. XCIX. Angiotensin Receptors: Interpreters of Pathophysiological Angiotensinergic Stimuli. *Pharmacol. Rev.* **2015**, *67*, 754–819. [CrossRef]

68. Haulică, I.; Neamţu, C.; Petrescu, G.; Cringu, A.; Nacu, C.; Topoliceanu, F.; Lozneanu, S. Possible opioid participation in the analgesic effects of the renin-angiotensin system. *Physiol. (Bucarest)* **1983**, *20*, 149–156.

69. Kaneko, S.; Mori, A.; Tamura, S.; Satoh, M.; Takagi, H. Intracerebroventricular administration of angiotensin II attenuates morphine-induced analgesia in mice. *Neuropharmacology* **1985**, *24*, 1131–1134. [CrossRef]

70. Haulică, I.; Neamţţu, C.; Stratone, A.; Petrescu, G.; Brănişteanu, D.; Roşca, V.; Slătineanu, S. Evidence for the involvement of cerebral renin-angiotensin system (RAS) in stress analgesia. *Pain* **1986**, *27*, 237–245. [CrossRef]

71. Shimamura, M.; Kawamuki, K.; Hazato, T. Angiotensin III: A Potent Inhibitor of Enkephalin-Degrading Enzymes and an Analgesic Agent. *J. Neurochem.* **1987**, *49*, 536–540. [CrossRef]

72. Cridland, R.; Henry, J. Effects of intrathecal administration of neuropeptides on a spinal nociceptive reflex in the rat: VIP, galanin, CGRP, TRH, somatostatin and angiotensin II. *Neuropeptides* **1988**, *11*, 23–32. [CrossRef]

73. Irvine, R.J.; White, J.; Head, R. The renin angiotensin system and nociception in spontaneously hypertensive rats. *Life Sci.* **1995**, *56*, 1073–1078. [CrossRef]

74. Irvine, R.J.; White, J. The Effects of Central and Peripheral Angiotensin on Hypertension and Nociception in Rats. *Pharmacol. Biochem. Behav.* **1997**, *57*, 37–41. [CrossRef]

75. Georgieva, D.; Georgiev, V. The role of angiotensin II and of its receptor subtypes in the acetic acid-induced abdominal constriction test. *Pharmacol. Biochem. Behav.* **1999**, *62*, 229–232. [CrossRef]

76. Han, N.-L.; Luo, F.; Bian, Z.-P.; Han, J.-S. Synergistic effect of cholecystokinin octapeptide and angiotensin II in reversal of morphine induced analgesia in rats. *Pain* **2000**, *85*, 465–469. [CrossRef]

77. Prado, W.A.; Pelegrini-Da-Silva, A.; Martins, A.R. Microinjection of renin-angiotensin system peptides in discrete sites within the rat periaqueductal gray matter elicits antinociception. *Brain Res.* **2003**, *972*, 207–215. [CrossRef]

78. Pavel, J.; Oroszova, Z.; Hricova, L.; Lukacova, N. Effect of Subpressor Dose of Angiotensin II on Pain-Related Behavior in Relation with Neuronal Injury and Activation of Satellite Glial Cells in the Rat Dorsal Root Ganglia. *Cell. Mol. Neurobiol.* **2013**, *33*, 681–688. [CrossRef] [PubMed]

79. Yamada, Y.; Ohinata, K.; Lipkowski, A.W.; Yoshikawa, M. Angiotensin AT2 receptor agonists act as anti-opioids via EP3 receptor in mice. *Peptides* **2009**, *30*, 735–739. [CrossRef] [PubMed]

80. Shepherd, A.J.; Copits, B.A.; Mickle, A.D.; Karlsson, P.; Kadunganattil, S.; Haroutounian, S.; Tadinada, S.M.; De Kloet, A.D.; Valtcheva, M.V.; McIlvried, L.A.; et al. Angiotensin II Triggers Peripheral Macrophage-to-Sensory Neuron Redox Crosstalk to Elicit Pain. *J. Neurosci.* **2018**, *38*, 7032–7057. [CrossRef]

81. Namsolleck, P.; Boato, F.; Schwengel, K.; Paulis, L.; Matho, K.; Geurts, N.; Thöne-Reineke, C.; Lucht, K.; Seidel, K.; Hallberg, A.; et al. AT2-receptor stimulation enhances axonal plasticity after spinal cord injury by upregulating BDNF expression. *Neurobiol. Dis.* **2013**, *51*, 177–191. [CrossRef] [PubMed]

82. Schwengel, K.; Namsolleck, P.; Lucht, K.; Clausen, B.H.; Lambertsen, K.L.; Valero-Esquitino, V.; Thöne-Reineke, C.; Müller, S.; Widdop, R.; Denton, K.; et al. Angiotensin AT2-receptor stimulation improves survival and neurological outcome after experimental stroke in mice. *J. Mol. Med.* **2016**, *94*, 957–966. [CrossRef] [PubMed]

83. Madara, J.C.; Levine, E.S. Presynaptic and Postsynaptic NMDA Receptors Mediate Distinct Effects of Brain-Derived Neurotrophic Factor on Synaptic Transmission. *J. Neurophysiol.* **2008**, *100*, 3175–3184. [CrossRef] [PubMed]

84. Zhou, L.-J.; Zhong, Y.; Ren, W.-J.; Li, Y.-Y.; Zhang, T.; Liu, X.-G. BDNF induces late-phase LTP of C-fiber evoked field potentials in rat spinal dorsal horn. *Exp. Neurol.* **2008**, *212*, 507–514. [CrossRef] [PubMed]

85. Al-Khrasani, M.; Mohammadzadeh, A.; Balogh, M.; Király, K.; Barsi, S.; Hajnal, B.; Köles, L.; Zádori, Z.S.; Harsing, L.G. Glycine transporter inhibitors: A new avenue for managing neuropathic pain. *Brain Res. Bull.* **2019**, *152*, 143–158. [CrossRef]

86. Nickel, F.T.; Seifert, F.; Lanz, S.; Maihofner, C. Mechanisms of neuropathic pain. *Eur. Neuropsychopharmacol.* **2012**, *22*, 81–91. [CrossRef]

87. Chen, W.; Walwyn, W.; Ennes, H.S.; Kim, H.; McRoberts, J.A.; Marvizón, J.C.G. BDNF released during neuropathic pain potentiates NMDA receptors in primary afferent terminals. *Eur. J. Neurosci.* **2014**, *39*, 1439–1454. [CrossRef]

88. Sikandar, S.; Minett, M.S.; Millet, Q.; Varela, S.S.; Lau, J.; Wood, J.N.; Zhao, J. Brain-derived neurotrophic factor derived from sensory neurons plays a critical role in chronic pain. *Brain* **2018**, *141*, 1028–1039. [CrossRef]

89. Zhao, Y.; Qin, Y.; Liu, T.; Hao, D. Chronic nerve injury-induced Mas receptor expression in dorsal root ganglion neurons alleviates neuropathic pain. *Exp. Ther. Med.* **2015**, *10*, 2384–2388. [CrossRef]

90. Ogata, Y.; Nemoto, W.; Yamagata, R.; Nakagawasai, O.; Shimoyama, S.; Furukawa, T.; Ueno, S.; Tan-No, K. Anti-hypersensitive effect of angiotensin (1-7) on streptozotocin-induced diabetic neuropathic pain in mice. *Eur. J. Pain* **2019**, *23*, 739–749. [CrossRef]

91. Nemoto, W.; Ogata, Y.; Nakagawasai, O.; Yaoita, F.; Tadano, T.; Tan-No, K. Angiotensin (1-7) prevents angiotensin II-induced nociceptive behaviour via inhibition of p38 MAPK phosphorylation mediated through spinal Mas receptors in mice. *Eur. J. Pain* **2014**, *18*, 1471–1479. [CrossRef] [PubMed]

92. Nemoto, W.; Yamagata, R.; Ogata, Y.; Nakagawasai, O.; Tadano, T.; Tan-No, K. Inhibitory effect of angiotensin (1-7) on angiotensin III-induced nociceptive behaviour in mice. *Neuropeptides* **2017**, *65*, 71–76. [CrossRef] [PubMed]

93. Yamagata, R.; Nemoto, W.; Nakagawasai, O.; Takahashi, K.; Tan-No, K. Downregulation of spinal angiotensin converting enzyme 2 is involved in neuropathic pain associated with type 2 diabetes mellitus in mice. *Biochem. Pharmacol.* **2020**, *174*, 113825. [CrossRef] [PubMed]

94. Costa, A.; Galdino, G.; Romero, T.; Silva, G.; Cortes, S.; Santos, R.; Duarte, I. Ang-(1-7) activates the NO/cGMP and ATP-sensitive K+ channels pathway to induce peripheral antinociception in rats. *Nitric Oxide* **2014**, *37*, 11–16. [CrossRef]

95. Costa, A.C.; Becker, L.K.; Moraes, R.; Romero, T.R.; Guzzo, L.; Santos, R.A.; Duarte, I.D. Angiotensin-(1-7) Induces Peripheral Antinociception through Mas Receptor Activation in an Opioid-Independent Pathway. *Pharmacology* **2012**, *89*, 137–144. [CrossRef]

96. Nemoto, W.; Yamagata, R.; Nakagawasai, O.; Nakagawa, K.; Hung, W.-Y.; Fujita, M.; Tadano, T.; Tan-No, K. Effect of spinal angiotensin-converting enzyme 2 activation on the formalin-induced nociceptive response in mice. *Eur. J. Pharmacol.* **2020**, *872*, 172950. [CrossRef]

97. Forte, B.L.; Slosky, L.M.; Zhang, H.; Arnold, M.R.; Staatz, W.D.; Hay, M.; Largent-Milnes, T.M.; Vanderah, T.W. Angiotensin-(1-7)/Mas receptor as an antinociceptive agent in cancer-induced bone pain. *Pain* **2016**, *157*, 2709–2721. [CrossRef]

98. Seltzer, Z.; Dubner, R.; Shir, Y. A novel behavioral model of neuropathic pain disorders produced in rats by partial sciatic nerve injury. *Pain* **1990**, *43*, 205–218. [CrossRef]

99. Ogata, Y.; Nemoto, W.; Nakagawasai, O.; Yamagata, R.; Tadano, T.; Tan-No, K. Involvement of Spinal Angiotensin II System in Streptozotocin-Induced Diabetic Neuropathic Pain in Mice. *Mol. Pharmacol.* **2016**, *90*, 205–213. [CrossRef] [PubMed]

100. Hashikawa-Hobara, N.; Hashikawa, N.; Inoue, Y.; Sanda, H.; Zamami, Y.; Takatori, S.; Kawasaki, H. Candesartan Cilexetil Improves Angiotensin II Type 2 Receptor-Mediated Neurite Outgrowth via the PI3K-Akt Pathway in Fructose-Induced Insulin-Resistant Rats. *Diabetes* **2012**, *61*, 925–932. [CrossRef]

101. Alhusban, A.; Kozak, A.; Ergul, A.; Fagan, S.C. AT1 Receptor Antagonism Is Proangiogenic in the Brain: BDNF a Novel Mediator. *J. Pharmacol. Exp. Ther.* **2012**, *344*, 348–359. [CrossRef]

102. Goel, R.; Bhat, S.A.; Hanif, K.; Nath, C.; Shukla, R. Angiotensin II Receptor Blockers Attenuate Lipopolysaccharide-Induced Memory Impairment by Modulation of NF-kappaB-Mediated BDNF/CREB Expression and Apoptosis in Spontaneously Hypertensive Rats. *Mol. Neurobiol.* **2018**, *55*, 1725–1739. [CrossRef] [PubMed]

103. Chakrabarty, A.; McCarson, K.; Smith, P.G. Hypersensitivity and hyperinnervation of the rat hind paw following carrageenan-induced inflammation. *Neurosci. Lett.* **2011**, *495*, 67–71. [CrossRef] [PubMed]

104. De Lima, J.; Alvares, D.; Hatch, D.J.; Fitzgerald, M. Sensory hyperinnervation after neonatal skin wounding: Effect of bupivacaine sciatic nerve block. *Br. J. Anaesth.* **1999**, *83*, 662–664. [CrossRef] [PubMed]

105. Muralidharan, A.; Wyse, B.D.; Smith, M.T. Analgesic Efficacy and Mode of Action of a Selective Small Molecule Angiotensin II Type 2 Receptor Antagonist in a Rat Model of Prostate Cancer-Induced Bone Pain. *Pain Med.* **2014**, *15*, 93–110. [CrossRef]

106. Khan, N.; Muralidharan, A.; Smith, M.T. Attenuation of the Infiltration of Angiotensin II Expressing CD3(+) T-Cells and the Modulation of Nerve Growth Factor in Lumbar Dorsal Root Ganglia—A Possible Mechanism Underpinning Analgesia Produced by EMA300, An Angiotensin II Type 2 (AT2) Receptor Antagonist. *Front. Mol. Neurosci.* **2017**, *10*, 389.

107. Shepherd, A.J.; Mickle, A.; Golden, J.; Mack, M.R.; Halabi, C.; de Kloet, A.; Samineni, V.; Kim, B.S.; Krause, E.; Gereau, R.W.; et al. Macrophage angiotensin II type 2 receptor triggers neuropathic pain. *Proc. Natl. Acad. Sci. USA* **2018**, *115*, E8057–E8066. [CrossRef]

108. Shepherd, A.J.; Mohapatra, D.P. Attenuation of Unevoked Mechanical and Cold Pain Hypersensitivities Associated with Experimental Neuropathy in Mice by Angiotensin II Type-2 Receptor Antagonism. *Anesthesia Analg.* **2019**, *128*, e84–e87. [CrossRef]

109. Erbs, E.; Faget, L.; Scherrer, G.; Matifas, A.; Filliol, D.; Vonesch, J.-L.; Koch, M.; Kessler, P.; Hentsch, D.; Birling, M.-C.; et al. A mu–delta opioid receptor brain atlas reveals neuronal co-occurrence in subcortical networks. *Brain Struct. Function* **2014**, *220*, 677–702. [CrossRef]

110. Sim, L.J.; Childers, S.R. Anatomical distribution of mu, delta, and kappa opioid- and nociceptin/orphanin FQ-stimulated [35S]guanylyl-5'-O-(gamma-thio)-triphosphate binding in guinea pig brain. *J. Comp. Neurol.* **1997**, *386*, 562–572. [CrossRef]

111. Mansour, A.; Fox, C.A.; Akil, H.; Watson, S.J. Opioid-receptor mRNA expression in the rat CNS: Anatomical and functional implications. *Trends Neurosci.* **1995**, *18*, 22–29. [CrossRef]

112. Delfs, J.M.; Kong, H.; Mestek, A.; Chen, Y.; Yu, L.; Reisine, T. Expression of Mu opioid receptor mRNA in rat brain: An in situ hybridization study at the single cell level. *J. Comp. Neurol.* **1994**, *345*, 46–68. [CrossRef]

113. Gouarderes, C.; Cros, J.; Quirion, R. Autoradiographic localization of mu, delta and kappa opioid receptor binding sites in rat and guinea pig spinal cord. *Neuropeptides* **1985**, *6*, 331–342. [CrossRef]

114. Valentino, R.J.; Volkow, N.D. Untangling the complexity of opioid receptor function. *Neuropsychopharmacology* **2018**, *43*, 2514–2520. [CrossRef]

115. Corder, G.; Castro, D.C.; Bruchas, M.R.; Scherrer, G. Endogenous and Exogenous Opioids in Pain. *Annu. Rev. Neurosci.* **2018**, *41*, 453–473. [CrossRef]

116. Stein, C.; Machelska, H.; Schäfer, M. Peripheral analgesic and antiinflammatory effects of opioids. *Z. Rheumatol.* **2001**, *60*, 416–424. [CrossRef]

117. Lueptow, L.; Fakira, A.; Bobeck, E.N. The Contribution of the Descending Pain Modulatory Pathway in Opioid Tolerance. *Front. Neurosci.* **2018**, *12*, 886. [CrossRef]

118. Arvidsson, U.; Riedl, M.; Chakrabarti, S.; Lee, J.H.; Nakano, A.H.; Dado, R.J.; Loh, H.H.; Law, P.Y.; Wessendorf, M.W.; Elde, R. Distribution and targeting of a mu-opioid receptor (MOR1) in brain and spinal cord. *J. Neurosci.* **1995**, *15*, 3328–3341. [CrossRef] [PubMed]

119. Moy, J.K.; Hartung, J.E.; Duque, M.G.; Friedman, R.; Nagarajan, V.; Loeza-Alcocer, E.; Koerber, H.R.; Christoph, T.; Schröder, W.; Gold, M.S. Distribution of functional opioid receptors in human dorsal root ganglion neurons. *Pain* **2020**, *161*, 1636–1649. [CrossRef]

120. Campbell, D.J.; Bouhnik, J.; Ménard, J.; Corvol, P. Identity of angiotensinogen precursors of rat brain and liver. *Nature* **1984**, *308*, 206–208. [CrossRef] [PubMed]

121. Chakrabarty, A.; Blacklock, A.; Svojanovsky, S.; Smith, P.G. Estrogen Elicits Dorsal Root Ganglion Axon Sprouting via a Renin-Angiotensin System. *Endocrinology* **2008**, *149*, 3452–3460. [CrossRef]

122. Arce, M.; Sanchez, S.; Seltzer, A.; Ciuffo, G. Autoradiographic localization of angiotensin II receptors in developing rat cerebellum and brainstem. *Regul. Pept.* **2001**, *99*, 53–60. [CrossRef]

123. Benitez, S.G.; Seltzer, A.M.; Messina, D.N.; Foscolo, M.R.; Patterson, S.I.; Acosta, C.G. Cutaneous inflammation differentially regulates the expression and function of Angiotensin-II types 1 and 2 receptors in rat primary sensory neurons. *J. Neurochem.* **2019**, *152*, 675–696. [CrossRef] [PubMed]

124. Gallinat, S.; Yu, M.; Dorst, A.; Unger, T.; Herdegen, T. Sciatic nerve transection evokes lasting up-regulation of angiotensin AT2 and AT1 receptor mRNA in adult rat dorsal root ganglia and sciatic nerves. *Mol. Brain Res.* **1998**, *57*, 111–122. [CrossRef]

125. Oroszova, Z.; Hricova, L.; Stropkovska, A.; Lukacova, N.; Pavel, J. The Characterization of AT1 Expression in the Dorsal Root Ganglia After Chronic Constriction Injury. *Cell. Mol. Neurobiol.* **2016**, *37*, 545–554. [CrossRef] [PubMed]

126. Pavel, J.; Tang, H.; Brimijoin, S.; Moughamian, A.; Nishioku, T.; Benicky, J.; Saavedra, J.M. Expression and transport of Angiotensin II AT1 receptors in spinal cord, dorsal root ganglia and sciatic nerve of the rat. *Brain Res.* **2008**, *1246*, 111–122. [CrossRef]

127. Sugimoto, K.; Kojima, K.; Baba, M.; Yasujima, M. Olmesartan ameliorates peripheral nerve dysfunction in Zucker diabetic fatty rats. *J. Hypertens.* **2011**, *29*, 1337–1346. [CrossRef]

128. Tang, H.; Pavel, J.; Saavedra, J.M.; Brimijoin, S. Angiotensin II type 1 receptors may not influence response of spinal autonomic neurons to axonal damage. *Neurol. Res.* **2008**, *30*, 751–760. [CrossRef]

129. Yang, Y.; Wu, H.; Yan, J.Q.; Song, Z.B.; Guo, Q.L. Tumor necrosis factor-alpha inhibits angiotensin II receptor type 1 expression in dorsal root ganglion neurons via beta-catenin signaling. *Neuroscience* **2013**, *248*, 383–391. [CrossRef]

130. Lucius, R.; Gallinat, S.; Rosenstiel, P.; Herdegen, T.; Sievers, J.; Unger, T. The Angiotensin II Type 2 (AT2) Receptor Promotes Axonal Regeneration in the Optic Nerve of Adult Rats. *J. Exp. Med.* **1998**, *188*, 661–670. [CrossRef]

131. Hafko, R.; Villapol, S.; Nostramo, R.; Symes, A.; Sabban, E.L.; Inagami, T.; Saavedra, J.M. Commercially Available Angiotensin II At2 Receptor Antibodies Are Nonspecific. *PLoS ONE* **2013**, *8*, e69234. [CrossRef]

132. Benitez, S.; Seltzer, A.; Acosta, C. Nociceptor-like rat dorsal root ganglion neurons express the angiotensin-II AT2 receptor throughout development. *Int. J. Dev. Neurosci.* **2016**, *56*, 10–17. [CrossRef]

133. Shiers, S.; Ray, P.R.; Wangzhou, A.; Sankaranarayanan, I.; Tatsui, C.E.; Rhines, L.D.; Li, Y.; Uhelski, M.L.; Dougherty, P.M.; Price, T.J. ACE2 and SCARF expression in human dorsal root ganglion nociceptors: Implications for SARS-CoV-2 virus neurological effects. *Pain* **2020**, *161*, 2494–2501. [CrossRef]

134. Xing, J.; Kong, J.; Lu, J.; Li, J. Angiotensin-(1-7) inhibits neuronal activity of dorsolateral periaqueductal gray via a nitric oxide pathway. *Neurosci. Lett.* **2012**, *522*, 156–161. [CrossRef]

135. Assis, A.D.; Araújo, F.D.A.; dos Santos, R.A.S.; Andrade, S.P.; Zanon, R.G. Pattern of Mas expression in acute and post-acute stage of nerve injury in mice. *Peptides* **2017**, *96*, 15–19. [CrossRef] [PubMed]

136. Ji, R.-R.; Zhang, Q.; Law, P.; Low, H.; Elde, R.; Hokfelt, T. Expression of mu-, delta-, and kappa-opioid receptor-like immunoreactivities in rat dorsal root ganglia after carrageenan-induced inflammation. *J. Neurosci.* **1995**, *15*, 8156–8166. [CrossRef] [PubMed]

137. Stander, S.; Gunzer, M.; Metze, D.; Luger, T.; Steinhoff, M. Localization of mu-opioid receptor 1A on sensory nerve fibers in human skin. *Regul. Pept.* **2002**, *110*, 75–83. [CrossRef]

138. Cao, L.; Xun, J.; Jiang, X.; Tan, R. Propofol up-regulates Mas receptor expression in dorsal root ganglion neurons. *Die Pharm.* **2013**, *68*, 677–680.

139. Li, J.L.; Ding, Y.Q.; Li, Y.Q.; Li, J.S.; Nomura, S.; Kaneko, T.; Mizuno, N. Immunocytochemical localization of mu-opioid receptor in primary afferent neurons containing substance P or calcitonin gene-related peptide. A light and electron microscope study in the rat. *Brain Res.* **1998**, *794*, 347–352. [CrossRef]

140. Obara, I.; Parkitna, J.R.; Korostynski, M.; Makuch, W.; Kaminska, D.; Przewlocka, B.; Przewlocki, R. Local peripheral opioid effects and expression of opioid genes in the spinal cord and dorsal root ganglia in neuropathic and inflammatory pain. *Pain* **2009**, *141*, 283–291. [CrossRef] [PubMed]

141. Spike, R.C.; Puskár, Z.; Sakamoto, H.; Stewart, W.; Watt, C.; Todd, A.J. MOR-1-immunoreactive neurons in the dorsal horn of the rat spinal cord: Evidence for nonsynaptic innervation by substance P-containing primary afferents and for selective activation by noxious thermal stimuli. *Eur. J. Neurosci.* **2002**, *15*, 1306–1316. [CrossRef]

142. Abbadie, C.; Lombard, M.-C.; Besson, J.-M.A.; Trafton, J.; Basbaum, I.A. Mu and delta opioid receptor-like immunoreactivity in the cervical spinal cord of the rat after dorsal rhizotomy or neonatal capsaicin: An analysis of pre- and postsynaptic receptor distributions. *Brain Res.* **2002**, *930*, 150–162. [CrossRef]

143. Mojaverian, P.; Swanson, B.N.; Ferguson, R.K. Enalapril, a new nonsulfhydryl angiotensin converting enzyme inhibitor, does not potentiate morphine analgesia. *Eur. J. Pharmacol.* **1984**, *98*, 303–306. [CrossRef]

144. Fukuhara, M.; Matsumura, K.; Abe, I.; Fujishima, M. Interaction of opioids and vasopressin in central action of angiotensin II in conscious rabbits. *Hypertens Res.* **1998**, *21*, 89–95. [CrossRef]

145. Kirby, D.A.; Spealman, R.D. Attenuation by naloxone of the pressor effects of angiotensin II in conscious cynomolgus monkeys. *Life Sci.* **1988**, *43*, 453–458. [CrossRef]

146. Wilkinson, D.L.; Scroop, G.C. The Effect of Naloxone on Pressor Responses To Angiotensin Ii In Anaesthetized Greyhounds. *Clin. Exp. Pharmacol. Physiol.* **1986**, *13*, 179–186. [CrossRef]

147. Innanen, V.; Jobb, E.; Korogyi, N. Naloxone reversal of hemorrhagic hypotension in the conscious guinea-pig is impeded by inhibition of the renin-angiotensin II system. *Neuroscience* **1987**, *22*, 313–315. [CrossRef]

148. Rabkin, S.W. Endogenous kappa opioids mediate the action of brain angiotensin II to increase blood pressure. *Neuropeptides* **2007**, *41*, 411–419. [CrossRef]

149. Summy-Long, J.Y.; Keil, L.C.; Deen, K.; Rosella, L.; Severs, W.B. Endogenous opioid peptide inhibition of the central actions of angiotensin. *J. Pharmacol. Exp. Ther.* **1981**, *217*, 619–629. [PubMed]

150. Summy-Long, J.Y.; Keil, L.C.; Deen, K.; Severs, W.B. Opiate regulation of angiotensin-induced drinking and vasopressin release. *J. Pharmacol. Exp. Ther.* **1981**, *217*, 630–637. [PubMed]

151. Yu, W.-Z.; Bodnar, R.J. Interactions Between Angiotensin II and Delta Opioid Receptor Subtype Agonists Upon Water Intake in Rats. *Peptides* **1997**, *18*, 241–245. [CrossRef]

152. Lewin, G.R.; Rueff, A.; Mendell, L.M. Peripheral and Central Mechanisms of NGF-induced Hyperalgesia. *Eur. J. Neurosci.* **1994**, *6*, 1903–1912. [CrossRef] [PubMed]

153. Deising, S.; Weinkauf, B.; Blunk, J.; Obreja, O.; Schmelz, M.; Rukwied, R. NGF-evoked sensitization of muscle fascia nociceptors in humans. *Pain* **2012**, *153*, 1673–1679. [CrossRef]

154. Rukwied, R.; Mayer, A.; Kluschina, O.; Obreja, O.; Schley, M.; Schmelz, M. NGF induces non-inflammatory localized and lasting mechanical and thermal hypersensitivity in human skin. *Pain* **2010**, *148*, 407–413. [CrossRef] [PubMed]

Non-Peptide Opioids Differ in Effects on Mu-Opioid (MOP) and Serotonin 1A (5-HT$_{1A}$) Receptors Heterodimerization and Cellular Effectors (Ca^{2+}, ERK1/2 and p38) Activation

Vlad Radoi [1], Gerd Jakobsson [2], Vinko Palada [3], Andrej Nikosjkov [1], Henrik Druid [2,4], Lars Terenius [1], Eva Kosek [1,5] and Vladana Vukojević [1,*]

[1] Department of Clinical Neuroscience, Karolinska Institute, 171 76 Stockholm, Sweden; vlad.radoi@su.se (V.R.); andrej.nikosjkov@ki.se (A.N.); lars.terenius@ki.se (L.T.); eva.kosek@ki.se (E.K.)
[2] Department of Forensic Genetics and Forensic Toxicology, National Board of Forensic Medicine, 587 58 Linköping, Sweden; gerd.jakobsson@liu.se (G.J.); henrik.druid@ki.se (H.D.)
[3] Department of Physiology, SleepWell Research Program, Faculty of Medicine, University of Helsinki, 00290 Helsinki, Finland; vinko.palada@helsinki.fi
[4] Department of Oncology-Pathology, Karolinska Institute, 171 77 Stockholm, Sweden
[5] Department of Surgical Sciences, Uppsala University, 752 36 Uppsala, Sweden
* Correspondence: vladana.vukojevic@ki.se

Abstract: The importance of the dynamic interplay between the opioid and the serotonin neuromodulatory systems in chronic pain is well recognized. In this study, we investigated whether these two signalling pathways can be integrated at the single-cell level via direct interactions between the mu-opioid (MOP) and the serotonin 1A (5-HT$_{1A}$) receptors. Using fluorescence cross-correlation spectroscopy (FCCS), a quantitative method with single-molecule sensitivity, we characterized in live cells MOP and 5-HT$_{1A}$ interactions and the effects of prolonged (18 h) exposure to selected non-peptide opioids: morphine, codeine, oxycodone and fentanyl, on the extent of these interactions. The results indicate that in the plasma membrane, MOP and 5-HT$_{1A}$ receptors form heterodimers that are characterized with an apparent dissociation constant K_d^{app} = (440 ± 70) nM. Prolonged exposure to all non-peptide opioids tested facilitated MOP and 5-HT$_{1A}$ heterodimerization and stabilized the heterodimer complexes, albeit to a different extent: $K_{d, Fentanyl}^{app}$ = (80 ± 70) nM), $K_{d,Morphine}^{app}$ = (200 ± 70) nM, $K_{d, Codeine}^{app}$ = (100 ± 70) nM and $K_{d, Oxycodone}^{app}$ = (200 ± 70) nM. The non-peptide opioids differed also in the extent to which they affected the mitogen-activated protein kinases (MAPKs) p38 and the extracellular signal-regulated kinase (Erk1/2), with morphine, codeine and fentanyl activating both pathways, whereas oxycodone activated p38 but not ERK1/2. Acute stimulation with different non-peptide opioids differently affected the intracellular Ca^{2+} levels and signalling dynamics. Hypothetically, targeting MOP–5-HT$_{1A}$ heterodimer formation could become a new strategy to counteract opioid induced hyperalgesia and help to preserve the analgesic effects of opioids in chronic pain.

Keywords: chronic pain; fluorescence cross-correlation spectroscopy (FCCS); G protein-coupled receptor (GPCR); opioid; serotonin

1. Introduction

Chronic pain is a major health issue worldwide [1] that enacts considerable suffering [2,3]. Despite the limited effects of available drugs for the treatment of pain, chronic pain patients are often treated with opioids, which have a controversial role in chronic pain management. In fact, patient follow-ups and population studies reveal the low long-term analgesic efficacy of opioids that is accompanied by the development of tolerance, opioid induced hyperalgesia (OIH), adverse side-effects, addiction, and opioid-related

deaths [4,5]. New strategies to avoid the aversive effects of opioids while preserving their analgesic properties are therefore needed.

In this perspective, the serotonin 1 A receptor (5-HT_{1A}) emerges as a promising candidate. 5-HT_{1A} is an inhibitory presynaptic autoreceptor on serotonergic neurons and is also expressed postsynaptically in terminal regions innervated by serotonergic neurons [6]. In animal studies, 5-HT_{1A} agonists have been reported to counteract opioid-induced hyperalgesia, opioid tolerance and to improve the analgesic potency of opioids while reducing their rewarding effects [6–8]. Contrary to opioids, a first order pronociceptive effect followed by an analgesic effect was documented for 5-HT_{1A} agonists, suggesting opposing effects between opioids and 5-HT_{1A} agonists [8]. Therefore, hypothetically, 5-HT_{1A}/opioid interactions could be time-dependent with 5-HT_{1A} antagonists initially enhancing opioid analgesia [9,10] and 5-HT_{1A} agonists, having beneficial long-term effects when OIH has developed [6–8]. In agreement with this, a genetically inferred reduction of serotonergic signalling was associated with an increased analgesic response to the opioid drug fentanyl in healthy human subjects [11]. Furthermore, gene-to-gene interactions between the mu-opioid receptor (MOP) gene (*OPRM1*) and the serotonin transporter (*5-HTT*) or 5-HT_{1A} (*HTR1A*) genes had antagonistic effects on endogenous descending pain modulation in healthy subjects and in fibromyalgia patients [12].

In the human brain, high densities of 5-HT_{1A} [13] and MOP [14] have been reported in regions implicated in pain modulation, and high 5-HT_{1A} binding potential was associated with more efficient endogenous pain inhibition [15]. Moreover, significant positive associations were found between the serotonin and the opioid systems in networks known to regulate pain and mood, including the cingulate cortex, thalamus, dorsolateral prefrontal cortex, amygdala, and the left parietal cortex [16]. The exact mechanisms responsible for the physiological, pain-related interactions between the opioid and the serotonergic signalling systems are not known [6]. One possible mechanism is the opioid-induced activation of 5-HT_{1A}–expressing glial cells through the Toll-like receptor 4 [17], as activated glia has been implicated in the development of OIH and opioid tolerance [18,19]. In accordance with this reasoning, extensive cortical glia activation was documented in patients suffering from fibromyalgia [20], a chronic pain syndrome with aberrations in cerebral opioid signalling [21]. An additional explanation might be the co-localization of MOP and 5-HT_{1A} receptors on the same neurons. In fact, Kishimoto et al. presented electrophysiological evidence of their co-localization on individual presynaptic GABAergic nerve terminals, and demonstrated that they synergistically inhibited GABA release in the periaqueductal gray (PAG), a structure that mediates opioid-based pain control [22]. In addition, the activation of $GABA_A$ receptors in PAG projecting neurons was shown to have a net pronociceptive effect [23]. Further support for interactions between MOP and 5-HT_{1A} at the cellular level comes from a study showing that they can form functional heterodimers and that signalling of one receptor in the heterodimer is inhibited by the activation of the other [24]. We thus hypothesize that opioid induced heterodimerization of MOP and 5-HT_{1A} inactivates the receptors, which then become unable to inhibit GABA release and promote pronociceptive pathways.

The primary aim of this study was to challenge this hypothesis by quantitatively characterizing interactions between the MOP and 5-HT_{1A} receptors in live cells expressing near physiological levels of these receptors, and to assess the effects of commonly used non-peptide opioid drugs such as morphine, oxycodone, codeine, and fentanyl, on the extent of these interactions and their downstream effects. In particular, we have focused on intracellular Ca^{2+} levels and signalling dynamics, and on mitogen-activated protein kinases (MAPKs) p38 and the extracellular signal-regulated kinase (Erk1/2), both previously associated with the adverse effects of opioids [25,26].

2. Results

The effects of non-peptide opioids on the extent of interactions between the mu-opioid receptor fused with the enhanced Green Fluorescent Protein (MOP-eGFP) and the sero-

tonin 1 A receptor fused with the red fluorescent protein Tomato (5-HT$_{1A}$-Tomato) were examined in live cells using confocal laser scanning microscopy (CLSM) and fluorescence cross-correlation spectroscopy (FCCS). FCCS, a quantitative analytical method with single-molecule sensitivity, is succinctly described in Section 4. Materials and Methods. Primary data, temporal autocorrelation curves (tACCs) and cross-correlation curves (tCCC) acquired using FCCS are shown in Figure 1. Determination of the so-called relative cross-correlation amplitude (RCCA) and its use to assess the apparent dissociation constant is described in Section 4. Materials and Methods and in the Supplementary Materials, Section S2. Calculation of the apparent dissociation constant and S3. Relative Cross-Correlation Amplitude (RCCA) increased upon opioid treatment. Verification by switching FCCS. More information can also be found in [27].
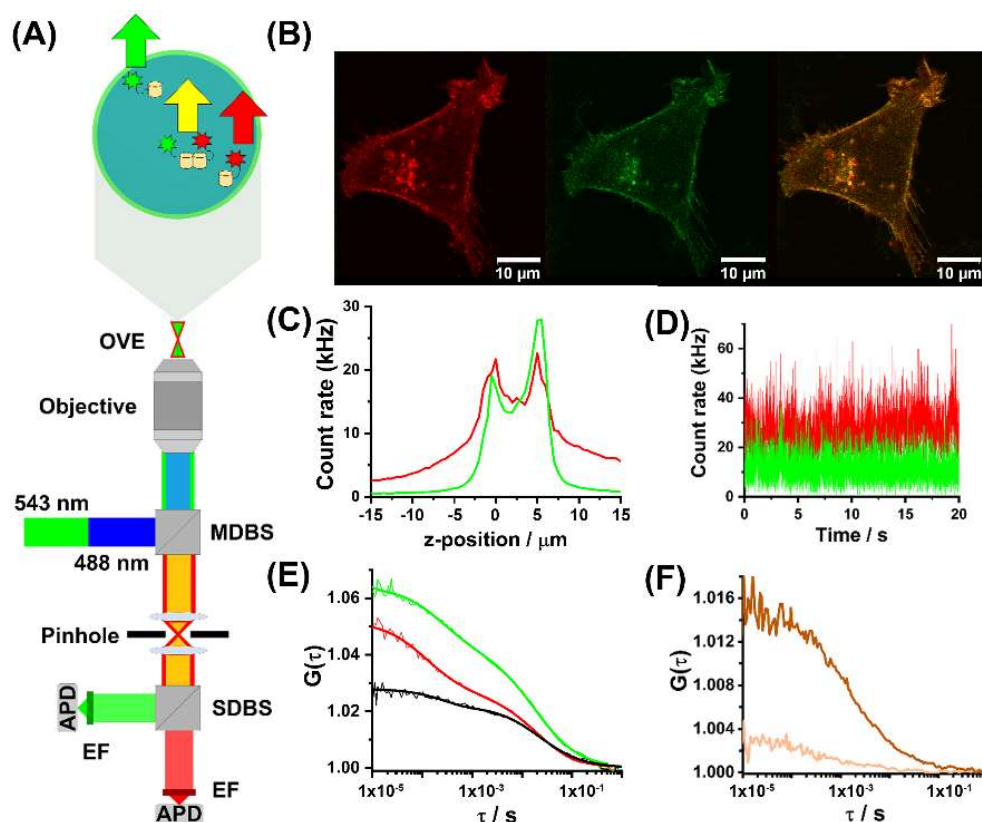
Figure 1. Fluorescence cross-correlation spectroscopy (FCCS). (**A**) Schematic presentation of the instrumental setup for dual colour CLSM imaging and FCCS. Incident laser light, 488 nm (blue) and 543 nm (green), is reflected by the main dichroic beam splitter (MDBS, 488/453/633) and focused by the objective into the sample. Fluorescence and scattered light are collected by the same objective and fluorescence is separated from the elastically scattered light by the MDBS. The fluorescence is spectrally separated by the secondary dichroic beam splitter (SDBS, 545) and further spectrally narrowed by emission filters (EF) before being recorded by avalanche photo diodes (APD) detectors. *Magnified insert:* Cross section through the observation volume element (OVE) in the radial (*xy*) plane in the sample. Fluctuations in fluorescence intensity are generated as fluorescently labelled molecules diffuse through the OVE (arrows). (**B**) CLSM image of a HEK293 cell genetically modified to stably express MOP-eGFP (green) and 5-HT$_{1A}$-Tomato (red). Scale bar 10 μm. (**C**) Fluorescence intensity scan through a HEK293 cell expressing MOP-eGFP (green) and 5-HT$_{1A}$-Tomato (red) in the axial (*z*-axis direction). The first peak in fluorescence intensity indicates the position of the basal (*z* = 0) and the second one the apical (*z* = 5 μm) plasma membrane of the same cell. Fluorescence intensity drops when the apical plasma membrane is crossed, as the OVE is now positioned in the surrounding cell culture medium. (**D**) Fluorescence intensity fluctuations recorded at the apical membrane of a HEK293

cell, originating from MOP-eGFP (green) and 5-HT$_{1A}$-Tomato (red) lateral diffusion in the plasma membrane. (**E**) Representative auto- (green and red) and cross-correlation (black) curves recorded at the apical membrane of a HEK293 cell. (**F**) Cross-correlation curves recorded in live HEK293 cells expressing the positive (brown) and negative (champagne) control constructs. For detailed information see Section 4. Materials and Methods and Supplementary Materials, Section S1. Transfection, positive and negative control cells (Figures S1 and S2).

2.1. Non-Peptide Opioids Potentiate MOP and 5-HT1A Heterodimerization to a Different Extent

CLSM imaging showed clear co-localization of both receptors, MOP-eGFP (green) and 5-HT$_{1A}$-Tomato (red), in the plasma membrane in both the HEK293 (Figure 1B) and the PC12 (Figure 2A) cells. It also showed that treatment with non-peptide opioids did not cause the internalization of individual receptors or of heterodimer receptor complexes (Figure 2B). This contrasts with the effects of treatment with the opioid peptide DAMGO, which promoted MOP internalization, but not the internalization of the heterodimer MOP-eGFP–5-HT$_{1A}$-Tomato complex (Figure 2C).
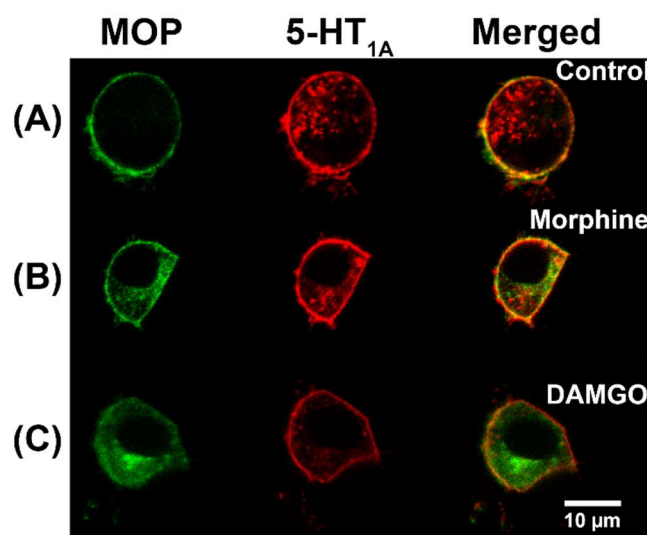
Figure 2. Non-peptide opioids neither induce MOP-eGFP nor MOP-eGFP-5-HT$_{1A}$-Tomato heterodimers internalization, whereas the opioid peptide DAMGO induces strong MOP-eGFP internalization. CLSM images of live PC12 cells stably expressing MOP-eGFP (green) and 5-HT1A-Tomato (red). (**A**) Cultured under standard conditions, without opioid treatment (control). (**B**) Treated for 18 h with 750 nM morphine. (**C**) Treated for 18 h with 500 nM DAMGO. Scale bar 10 µm.

For FCCS analysis, data collected on cells expressing similar (within the experimental error of FCS measurements) receptor levels, $N_{MOP} = (27 \pm 6)$ and $N_{5\text{-}HT1A} = (25 \pm 3)$, were compared. At these expression levels, corresponding to concentrations: $c_{MOP} = (320 \pm 70)$ nM and $c_{5\text{-}HT1A} = (300 \pm 40)$ nM, FCCS analysis showed that MOP-eGFP and 5-HT$_{1A}$-Tomato receptors not only co-localized in the plasma membrane, but also formed heterodimers, as evidenced by tCCCs (Figure 1E, black). FCCS showed that in untreated cells about 33% (RCCA = 0.33) of the 5-HT$_{1A}$-Tomato receptors are bound in heterodimer complexes with MOP-eGFP (Figure 3A). Based on this, the apparent dissociation constant for a heterodimer receptor complex of MOP-eGFP–5-HT$_{1A}$-Tomato with a 1:1 stoichiometry was estimated to be $K_d^{app} = (440 \pm 70)$ nM.

Figure 3. Opioids differ in their potency to induce heterodimer formation between MOP-eGFP and 5-HT$_{1A}$-Tomato in HEK293 cells. (**A**) Fentanyl induces a dose-dependent increase in MOP-eGFP and 5-HT$_{1A}$-Tomato receptor heterodimer formation in the concentration range $0 < c_{Fentanyl} < 750$ nM. For fentanyl concentrations ≥ 1 μM, the extent of heterodimer formation 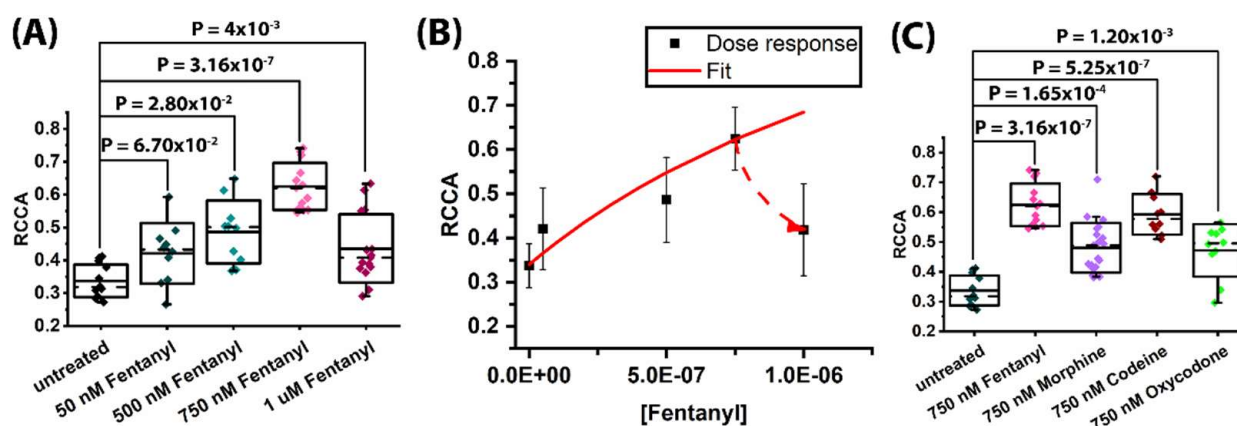drops significantly. (**B**) Fentanyl dose response curve calculated from the experimentally obtained RCCA values in A and the known concentrations of fentanyl. (**C**) 18 h treatment with equimolar concentrations of different opioids, c = 750 nM induces in cells expressing the same levels of MOP-eGFP and 5-HT$_{1A}$-Tomato different extent of receptor heterodimer formation. Relative cross-correlation amplitude (RCCA), defined as the limiting value, when the lag time $\tau \to 0$, of the amplitude of the cross-correlation curve relative to the amplitude of the green autocorrelation curve, yields the number of dually-labelled, i.e., heterodimer receptor complexes (N_{rg}) relative to the total number of the red labelled 5-HT$_{1A}$-Tomato receptors ($N_r^{total} = N_r + N_{rg}$), where N_r is the number of unbound, single-labelled 5-HT$_{1A}$-Tomato receptors, and N_{rg} is the number of double-labelled MOP-eGFP and 5-HT$_{1A}$-Tomato complexes. To reduce the effect of noise and minimize the contribution of afterpulsing, the RCCAs values were calculated as an average value of five points, starting with the value at the lag time of 10 μs to the lag time of 50 μs. In the box-and-whisker plot, the solid line shows the mean value, the dashed line shows the median, box represents the standard deviation, and the whiskers give the 5-95 percentiles. Statistical analysis: a Student's *t*-test was used to determine whether the difference between the mean values measured in untreated and treated cells, or in cells treated with different opioids, are significantly different from each other. The results are reported using a two-tailed *p*-value (*p*). The Benjamini–Hochberg method to control the false discovery rate (FDR) in sequential modified Bonferroni correction for multiple hypothesis testing showed that at an FDR value of 5%, $p \leq 0.012$ was statistically significant.

Moreover, FCCS showed that treatment with different concentrations of fentanyl increased the fraction of 5-HT$_{1A}$-Tomato receptors in heterodimer complexes with MOP-eGFP (Figure 3A,B). For fentanyl, the number of heterodimer receptor-receptor complexes increased in a dose dependent manner, as evident from the increase in RCCA from $RCCA_{Fentanyl}^{50\,nM} = 0.42 \pm 0.09$, which was not significantly different from the RCCA value measured in untreated cells ($p = 0.067$), to $RCCA_{Fentanyl}^{500\,nM} = 0.49 \pm 0.09$ ($p = 0.028$) in cells treated with 500 nM fentanyl, and $RCCA_{Fentanyl}^{750\,nM} = 0.62 \pm 0.07$ ($p = 3.16 \times 10^{-7}$) in cells treated with 750 nM fentanyl. From the experimentally determined concentration of heterodimer complexes and the known concentration of fentanyl, the effect of fentanyl on the extent of MOP-eGFP and 5-HT$_{1A}$-Tomato heterodimerization could be quantified (Figure 3B, solid red line).

By applying the standard mathematical formalism of ligand binding assays in the absence of competing reactions [28], and considering the concentration of heterodimer complexes as an dependent variable and the concentration of fentanyl as an independent variable, the concentration of fentanyl at which the number of heterodimer complexes would be doubled was determined to be (1.90 ± 0.05) μM. Unexpectedly, treatment with such high fentanyl concentrations showed a decrease, rather than the expected increase in

the concentration of heterodimer complexes (Figure 3B, dashed red line) and the RCCA decreased to 0.45 (SD = 0.11, p = 0.004). This suggested that other processes, such as receptor homodimer formation and/or higher-order receptor heterooligomer formation [29,30] and/or desensitization or feedback processes [30] may occur at high fentanyl concentrations. Finally, it may also happen that fentanyl at such high concentrations may be toxic to cells [31], but we have not observed any such indication.

Due to this, concentrations higher than 750 nM were not investigated, and this concentration was selected in further studies to compare the effects of different opioids. FCCS showed that for treatment with 750 nM fentanyl, the RCCA was $\text{RCCA}_{\text{Fentanyl}}^{750\,\text{nM}} = 0.62 \pm 0.07$, which was significantly different from the RCCA value measured in untreated cells ($p = 3.16 \times 10^{-7}$); $\text{RCCA}_{\text{Morphine}}^{750\,\text{nM}} = 0.47 \pm 0.08$ ($p = 1.65 \times 10^{-4}$); $\text{RCCA}_{\text{Codeine}}^{750\,\text{nM}} = 0.59 \pm 0.07$ ($p = 5.25 \times 10^{-7}$) and $\text{RCCA}_{\text{Oxycodone}}^{750\,\text{nM}} = 0.47 \pm 0.09$ ($p = 0.0117$) (Figure 3C). Moreover, the RCCA value measured for cells treated with fentanyl was significantly higher than that measured in cells treated with equimolar concentrations of morphine ($p = 2.48 \times 10^{-4}$) or oxycodone ($p = 6.99 \times 10^{-4}$), but not significantly higher than that for codeine ($p = 0.24$). The difference in RCCA values measured in cells treated with codeine was significantly higher than that in cells treated by morphine ($p = 3.66 \times 10^{-3}$). Based on these measurements and using Equation (6), the apparent dissociation constants for the MOP-eGFP–5-HT$_{1A}$-Tomato heterodimer complex in the presence of equimolar concentrations (750 nM) of different non-peptide opioids could be estimated: $K_{\text{d, Fentanyl}}^{\text{app}} = (80 \pm 70)$ nM, $K_{\text{d,Morphine}}^{\text{app}} = (200 \pm 70)$ nM, $K_{\text{d, Codeine}}^{\text{app}} = (100 \pm 70)$ nM and $K_{\text{d, Oxycodone}}^{\text{app}} = (200 \pm 70)$ nM. Likewise, the apparent heterodimer dissociation constants in the presence of different concentrations of fentanyl were determined to be: $K_{\text{d, 50 nM Fentanyl}}^{\text{app}} = (260 \pm 70)$ nM, $K_{\text{d, 500 nM Fentanyl}}^{\text{app}} = (180 \pm 70)$ nM, $K_{\text{d, 750 nM Fentanyl}}^{\text{app}} = (80 \pm 70)$ nM, and $K_{\text{d, 1 }\mu\text{M Fentanyl}}^{\text{app}} = (220 \pm 70)$ nM.

2.2. Non-Peptide Opioids Increase to a Different Extent the Brightness of eGFP and Tomato

Prolonged treatment with non-peptide opioids increased eGFP brightness, as evident from the measured counts per second per molecule (CPM). In untreated cells, average eGFP brightness was $\text{CPM}_{\text{Untreated}}^{\text{eGFP}} = (1.1 \pm 0.3)$ kHz. In treated cells, eGFP brightness nearly doubled, showing statistically significant difference for all treatments: $\text{CPM}_{\text{Fentanyl}}^{\text{eGFP}} = (1.9 \pm 0.7)$ kHz ($p = 0.015$), $\text{CPM}_{\text{Morphine}}^{\text{eGFP}} = (2.0 \pm 0.5)$ kHz ($p = 9.6 \times 10^{-3}$), $\text{CPM}_{\text{Codeine}}^{\text{eGFP}} = (1.9 \pm 0.5)$ kHz ($p = 5.8 \times 10^{-3}$), and $\text{CPM}_{\text{Oxycodone}}^{\text{eGFP}} = (1.8 \pm 0.7)$ kHz ($p = 0.027$). Interestingly, an increase in Tomato brightness was also observed in cells treated with 750 nM fentanyl or morphine, but not in cells treated with codeine or oxycodone. However, the increase in Tomato brightness was not as pronounced as for eGFP, and changed from $\text{CPM}_{\text{Untreated}}^{\text{Tomato}} = (0.8 \pm 0.2)$ kHz in untreated cells to: $\text{CPM}_{\text{Fentanyl}}^{\text{Tomato}} = (1.1 \pm 0.3)$ kHz ($p = 0.021$) for treatment with 750 nM fentanyl; $\text{CPM}_{\text{Morphine}}^{\text{Tomato}} = (1.3 \pm 0.3)$ kHz ($p = 3.0 \times 10^{-3}$) for treatment with 750 nM morphine, whereas it remained unchanged (within the limits of the experimental error) for treatment with 750 nM codeine, $\text{CPM}_{\text{Codeine}}^{\text{Tomato}} = (1.0 \pm 0.3)$ kHz ($p = 0.20$), or 750 nM oxycodone, $\text{CPM}_{\text{Oxycodone}}^{\text{Tomato}} = (0.9 \pm 0.3)$ kHz ($p = 0.12$). While we do not know why the brightness of fluorescence reporters has changed following treatment with non-peptide opioids, two processes can independently and jointly cause such effects, receptor homodimerization and/or alteration of fluorescence lifetime due to environmental changes. However, to discern the contribution of one effect from the other, a stringent number and brightness analysis and fluorescence lifetime measurements would be needed. We reflect on this in more detail in Section 3.

2.3. Non-Peptide Opioids Elicit Different Intracellular Ca^{2+} Signalling Dynamics

Time-lapse CLSM imaging of intracellular Ca^{2+} levels using the cell-permeant Fura Red ratiometric dye (Figure 4A), showed that stimulation with equimolar concentrations of different non-peptide opioids acutely induced different changes in the intracellular

Ca^{2+} levels in HEK293 cells expressing MOP-eGFP and 5-HT$_{1A}$-Tomato (Figure 4B). In untreated cells, stationary state intracellular Ca^{2+} levels were observed. Following the addition of 750 nM morphine, the stationary state appeared to have lost its stability and sinusoidal oscillations in Ca^{2+} levels with smoothly increasing amplitudes and a period of about 5 min, emerged. Treatment with 750 nM codeine also induced oscillations in intracellular Ca^{2+} levels. However, these oscillations showed features of so-called relaxation oscillations [32], which are characterized by a relatively long relaxation period during which the system remained in a stationary state, alternating with a short period in which the abrupt decrease in fluorescence intensity, i.e., the increase in intracellular Ca^{2+} level was observed. Treatment with 750 nM fentanyl did not cause any oscillations in intracellular Ca^{2+} levels, but a four-fold increase in Fura Red fluorescence intensity was noted, indicating that intracellular Ca^{2+} levels decreased markedly following the addition of fentanyl. Finally, treatment with 750 nM oxycodone induced small-amplitude relaxation oscillations with gradually increasing amplitudes over a period of about 5 min. Of note, while the time series shown in Figure 4 was recorded in individual cells, the dynamic behaviour is representative, as it is most often encountered in the analysed population of cells.
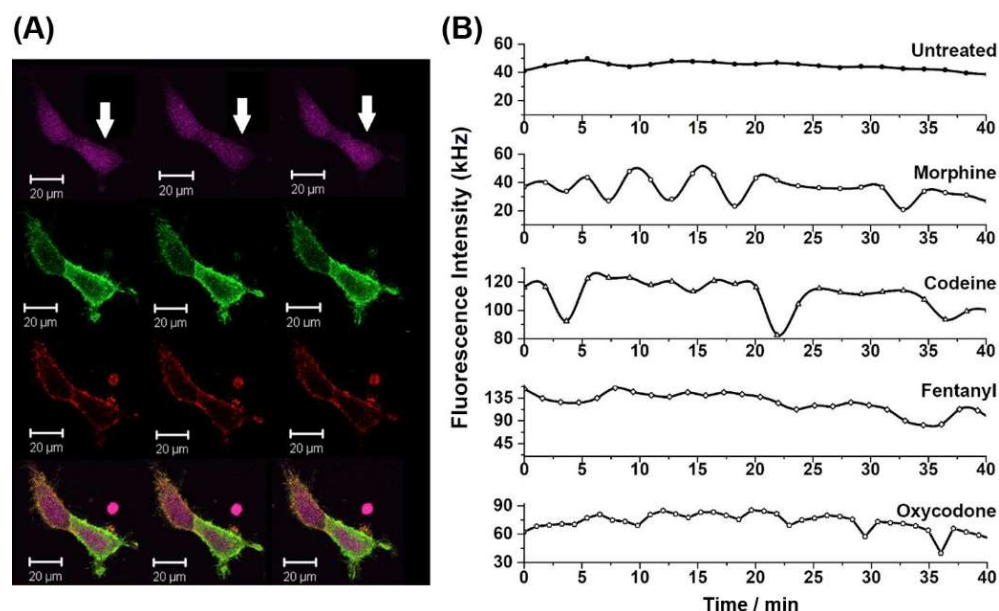

Figure 4. Stimulation with non-peptide opioids causes different intracellular Ca^{2+} signalling dynamics in HEK293 cells stably expressing MOP-eGFP and 5-HT$_{1A}$-Tomato. (**A**) CLSM time-lapse imaging of Ca^{2+} levels (Fura Red, dark violet) in HEK293 cells expressing MOP-eGFP (green) and 5-HT$_{1A}$-Tomato (red) after 30 min treatment with 750 nM oxycodone. White arrows indicate oscillatory changes in Fura Red fluorescence intensity, where a transient decrease in fluorescence intensity reflects an increase in the concentration of Ca^{2+} ions. (**B**) Fluctuations in Fura Red fluorescence intensity over time following treatment of HEK293 cells expressing MOP-eGFP and 5-HT$_{1A}$-Tomato with equimolar concentrations of different opioids.

2.4. Non-Peptide Opioids Differ in the Extent to Which They Activate Major Signal Transduction Pathways

In order to assess the downstream effects of non-peptide opioids in HEK293 cells expressing MOP-eGFP and 5-HT$_{1A}$-Tomato, phosphorylation of MAPKs ERK1/2 and p38 was probed because MOP activation was shown to trigger the phosphorylation of both ERK1/2 [33] and p38 [34]. Western blot analysis showed an increase in phosphorylated ERK1/2 and p38 in cells that had been treated with 750 nM of morphine, oxycodone, codeine, or fentanyl when compared to untreated cells (Figure 5).
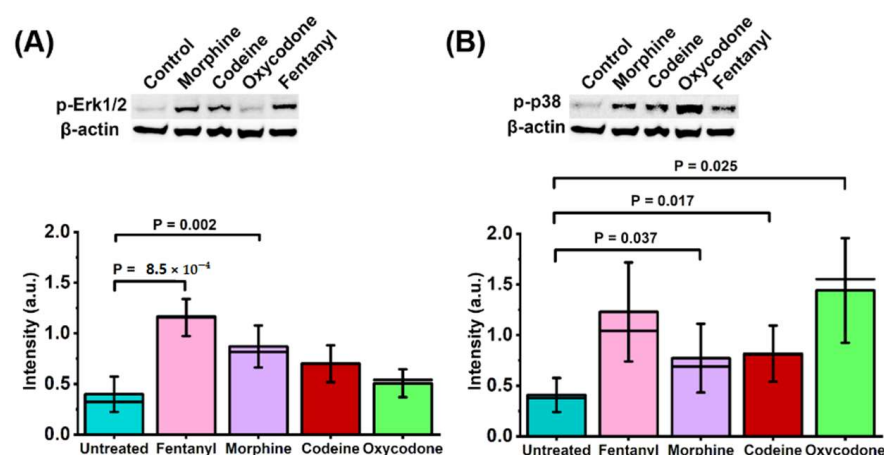
Figure 5. Opioids differ in their capacity to activate extracellular signal-regulated kinase (ERK) and p38 mitogen-activated protein kinase (MAPK) signalling pathways in HEK293 cells stably expressing MOP-eGFP and 5-HT$_{1A}$-Tomato. Top: HRP chemiluminescence images of western blotting membranes showing different levels p-ERK1/2 (**A**) and p-p38 (**B**) following 18 h treatment using equimolar concentrations of different opioids. Bottom: Protein level of phosphorylated-Erk1/2 relative to β-actin (**A**) and the protein level of phosphorylated-p38 relative to β-actin (**B**), following 18 h treatment with 750 nM of morphine (red), codeine (green), oxycodone (blue) or fentanyl (magenta), as compared to untreated cells (grey). Statistical analysis: Paired *t*-test. Experiments were carried out in triplicate (see Supplementary Materials, Section S4. Western blotting (Figure S5)).

Fentanyl elicited the strongest ERK1/2 activation (mean = 1.156, SD = 0.183, $p = 8.52 \times 10^{-4}$), unlike oxycodone (mean = 0.506, SD = 0.139, N.S). In contrast, oxycodone elicited the strongest p38 activation (mean = 1.441, SD = 0.517, $p = 0.025$), while the effects of fentanyl, morphine, and codeine were similar. Interestingly, LC-MS/MS metabolite analysis indicated that these effects are likely attributed to the primary non-peptide opioid compounds in their own right, as there were no common opioid metabolites detected either in the cell culture medium or in the cell lysate (Supplementary Materials, Section S6, Table S2).

3. Discussion

Advanced fluorescence microscopy-based techniques allow us to quantitatively characterize molecular interactions in live cells and bring about new understanding of dynamical processes that underlie complex biological functions [35–37]. They also enable us to test with unprecedented precision new mechanistic hypotheses. In this study, FCCS, a quantitative time-resolved analytical method with single-molecule sensitivity, was used to examine in live cells the hypothesis that prolonged exposure to non-peptide opioids promotes heterodimer formation between MOP and 5-HT$_{1A}$. This hypothesis, derived from preclinical [6–8] and clinical studies [11,12,20], further asserts that altered cellular signalling due to receptor heterodimer formation may contribute to neuroplastic changes that, eventually, lead to sensitization of pronociceptive pathways at the organism level.

To test the initial statement in this hypothesis, FCCS was used to quantitatively characterize in live cells interactions between MOP and 5-HT$_{1A}$ receptors and the effects of some of the most commonly used non-peptide opioid drugs: morphine, oxycodone, codeine and fentanyl, on the extent of these interactions. The CLSM imaging, biochemical assays and LC-MS/MS were used to assess the downstream consequences of these interactions. The most important results are summarized in Table 1 and discussed below.

We found that MOP and 5-HT$_{1A}$ receptors associate in the plasma membrane (Figures 1B, 2A and 3A), building heterodimer complexes characterized by an apparent dissociation constant, $K_d^{app} = (440 \pm 70)$ nM. This result, obtained nondestructively in live cells, confirms the findings by Cussac et al. who have shown using co-immunoprecipitation

and Bioluminescence Resonance Energy Transfer (BRET) that functional MOP and 5-HT$_{1A}$ heterodimers are formed in overexpressing cells [24]. We have verified this finding in cells expressing physiologically relevant levels of the investigated receptors and determined the apparent dissociation constants for MOP–5-HT$_{1A}$ heterodimers in live cells, K_d^{app} = (440 ± 70) nM. Moreover, in agreement with the results obtained by Cussac et al. [24], we have also observed that DAMGO induces prominent MOP internalization but not the internalization of MOP–5-HT$_{1A}$ heterodimer complexes, whereas the non-peptide opioids did not cause internalization, neither of individual receptors, nor of heterodimer MOP–5-HT$_{1A}$ complexes (Figure 2).

Table 1. Equimolar concentrations of non-peptide opioids differently affect the apparent dissociation constant of MOP–5-HT$_{1A}$, fluorophore brightness, ERK1/2 and p38 activation, and Ca^{2+} levels and signalling dynamics.

Treatment (750 nM)	K_d (nM)	CPM$_{eGFP}$ (kHz)	CPM$_{Tomato}$ (kHz)	ERK1/2	p38	CR (kHz)	Ca^{2+} Dynamics
Untreated	440 ± 70	1.1 ± 0.3	0.8 ± 0.2			40	Stationary state
Fentanyl	80 ± 70	1.9 ± 0.7	1.1 ± 0.3	+	+	40	Stationary state
Morphine	200 ± 70	2.0 ± 0.5	1.3 ± 0.7	+	+	120	Small-amplitude oscillations
Codeine	100 ± 70	1.9 ± 0.5	1.0 ± 0.3	+	+	135	Relaxation oscillations
Oxycodone	200 ± 70	1.8 ± 0.7	0.9 ± 0.3	0	+	60	Relaxation oscillations

Prolonged exposure to all opioids tested facilitated heterodimer formation between MOP and 5-HT$_{1A}$ receptors, albeit to a different extent (Figure 3), differently altered intracellular Ca^{2+} levels and signalling dynamics (Figure 4) and activated ERK1/2 and p38 signal transduction pathways to a different extent (Figure 5). Fentanyl, the most potent off all non-peptide opioids tested here, exhibited in the concentration range 50–750 nM, a dose-dependent effect on MOP–5-HT$_{1A}$ heterodimer formation (Figure 3A,B) and stabilized significantly the heterodimer complexes, as evident from the five-fold decrease in the apparent dissociation constant from K_d^{app} = (440 ± 70) nM in untreated cells, to $K_{d,\,Fentanyl}^{app}$ = (80 ± 70) nM in cells treated with 750 nM fentanyl. It also elicited the highest activation of the ERK1/2 and a comparably strong activation of the p38 (Figure 5). Finally, fentanyl caused an acute decrease in Ca^{2+} levels, as evident from the pronounced increase in Fura Red fluorescence (Figure 4, Table 1), which is in line with previously reported findings [38]. In contrast, oxycodone elicited the weakest stabilizing effect on MOP–5-HT$_{1A}$ heterodimer formation, as evident from the two-fold reduction in $K_{d,\,Oxycodone}^{app}$ = (200 ± 70) nM (Figure 3C) and elicited the highest activation of the p38 (Figure 5B), while causing an insignificant activation of the ERK1/2 (Figure 5A, Table 1). Treatment with 750 nM oxycodone did not significantly affect Ca^{2+} signalling dynamics, although a small reduction in Ca^{2+} level and the appearance of small-amplitude relaxation oscillations were noted. The very strong activation of the p38 observed in our study is in line with recent findings in rats showing increased p38 activity during chronic oxycodone exposure [39]. p38 activation may also be relevant for the aversive, addictive effects of oxycodone—p38 activation was shown to underlie opioid reward behaviour in mice [40] and the kappa opioid receptor (KOP)-induced p38 activation has been shown to reinstate drug seeking behavior in mice [41]. Based on this, a recent study argued that the addictive qualities of oxycodone outweighed its benefits as a prescription drug [42].

Morphine and codeine showed significant differences in their potency to stabilize MOP–5-HT$_{1A}$ heterodimer complexes, with codeine eliciting a higher stabilizing effect than morphine, $K_{d,Morphine}^{app}$ = (200 ± 70) nM and $K_{d,\,Codeine}^{app}$ = (100 ± 70) nM (Figure 3C, Table 1). Codeine also elicited more dramatic effects on intracellular Ca^{2+} signalling, reducing to a larger extent intracellular Ca^{2+} levels and causing more dramatic changes in Ca^{2+} signalling dynamics than morphine (Figure 4B). However, they activated the

ERK1/2 and p38 signalling pathways to a similar extent. The unexpected observation that codeine more strongly stabilized MOP and 5-HT$_{1A}$ heterodimer complexes than morphine is contrary to the general view that codeine is an inactive prodrug with a low affinity for MOP, the effect of which is obtained first after its metabolic conversion to morphine [43–45] and dihydrocodeine-6-O-gluconoride [46,47]. To interrogate this further, an LC-MS/MS analysis was deployed. The LC-MS/MS showed that the concentration of codeine metabolites in the cell culture medium and the cell lysate, if present at all, is below the detection limit of the applied method (Supplementary Materials, Section S6, Table S1). This finding is in line with the fact that HEK293 cells do not express the CYP2D6 gene (https://www.proteinatlas.org/ENSG00000100197-CYP2D6/cell, 3 February 2022), which is crucial for metabolizing codeine [48]. Taken together, our data indicate that codeine is an active compound in its own right. Recent studies showed that codeine has a 6-fold higher permeability and crosses the plasma membrane faster than morphine [49], which could potentially explain the strong response elicited in our cell model. This finding suggests that the pharmacodynamics of codeine is not yet fully elucidated and warrants further studies.

Moreover, FCCS analysis revealed that all non-opioid peptides tested nearly doubled eGFP brightness, while Tomato brightness was not affected to the same extent and treatment with oxycodone and codeine did not alter Tomato brightness (Table 1). The following processes: homodimerization of MOP and, to a lesser extent, of 5-HT$_{1A}$; homo- and heterooligomerization of MOP and 5-HT$_{1A}$; and changes in fluorescence lifetime of eGFP and Tomato due to intracellular environment changes caused by signal transduction, can independently or jointly increase the brightness of eGFP/Tomato. Further studies are, however, needed to distinguish the contribution of these possible mechanisms. Most notably, stringent number and brightness analysis and fluorescence lifetime measurements would be needed to discern the contribution of one effect from the other. Having said this, we point out that changes in brightness consistent with the presence of higher order oligomers were not observed.

The possibility to quantitatively characterize MOP/5-HT$_{1A}$ interactions in live cells is a significant achievement of great general interest—the stability of G protein-coupled receptor (GPCR) homo/heterodimer complexes is measured in live cells for a handful of GPCRs, see for example [34–36,50], even though it is well recognized that numerous GPCRs form homo- and heterodimers and that these interactions are important targets for drug development [51]. However, some limitations of our approach are inevitably present and warrant further discussion. Most notably, FCS/FCCS cannot detect endogenous nonfluorescent receptors, receptor constructs with irreversibly photobleached fluorophores or with fluorophores residing for various reasons in dark states. This affects the actual value of the apparent dissociation constants. However, in the context of our study, this limitation does not affect the conclusions of our work, since relative differences are analysed.

Another limitation of our study is that the work was performed using transfected cells that express the proteins of interest through powerful promoters, which may lead to artefacts due to over-expression. To mitigate this risk, we have generated stably transformed cell lines—it is commonly known that stably transformed cells do not yield as high expression as transiently transfected cells. Besides, we have selected for our analysis cells expressing low levels of MOP-eGFP and 5-HT$_{1A}$-Tomato—the average number of molecules in the OVE of N$_{MOP}$ = (27 ± 6) and N$_{5-HT1A}$ = (25 ± 3) corresponds to a surface density of about (130 ± 10) molecules/μm^2. For comparison, many studies of GPCRs class A show that the average surface density of endogenous GPCRs is typically low, <5 molecules/μm^2, in healthy but increase severalfold in disease states—a recent study showed endogenous MOP levels of 4 molecules/μm^2 [52]. However, as cautioned by the authors, one needs to bear in mind that this value may be underestimated due to low antibody binding efficiency—theoretical studies show that at GPCRs surface densities < 5 molecules/μm^2 the receptors may be too far apart from each other to allow for the efficient build-up of Gβγ to concentrations needed to modulate the activity of other intracellular proteins and show

that G protein signalling occurs within nanodomains where the local density of GPCRs is easily > 50 molecules/μm^2 [53].

Furthermore, an important limitation of our study is that the effects of one concentration of non-peptide opioids is tested. A dose-response analysis is needed to characterize cellular responses to varied amounts of the selected non-peptide opioids and stringent control experiments are needed to examine to what extent the observed effects are mediated via the monomeric fraction of the receptor pool and what the contribution of the receptor heterodimer is. In the light of our work, it is important to point out that while the affinity of the tested non-peptide opioids for binding to MOP is in the range 1–750 nM [54] and to 5-HT$_{1A}$ in the 2–20 μM range [55], pharmacologically relevant concentrations of non-peptide opioids are considerably higher [56]. For example, in opioid-naive postoperative patients, an analgesic effect of fentanyl is achieved at the lowest blood plasma fentanyl concentration levels of about 1.8–4.4 nM (0.6–1.5 ng/mL) [57]. However, much higher concentrations were measured in cancer patients treated for pain; on average 530 nM (178 ng/mL) [56,58]. The concentrations used in our study are therefore in the pharmacologically relevant range. Moreover, in this study we chose to study equimolar concentrations of opioids, rather than equipotent concentrations. Although there are several conversion tables for opioid potency, they are perceived as unreliable [59]. The few studies that have addressed opioid equianalgesic dose/potency ratios are heterogeneous with respect to size, subjects, specific aims, settings, and study method [60]. Thus, Rennick et al. have concluded from their findings that there is no true universal way to accurately perform equianalgesic conversions for opioids [60]. Given that the aim of our work was to assess the effect of non-peptide opioids on the extent of MOP-eGFP and 5-HT$_{1A}$-Tomato association in live cells, the study design where cells with similar receptor surface density levels are used and the effects of equimolar concentrations of non-peptide opioids are compared is correct. It may, however, be interesting to examine in the future the effect of equipotent concentrations of non-peptide opioids, determined with regard to a quantifiable effect, such as the ability to alter intracellular Ca^{2+}, ERK1/2 or p38 phosphorylation levels.

Furthermore, the treatment time length is an important variable. We have chosen 18 h, taking into consideration the cell doubling time, which is under the condition of our experiments ~36 h for HEK293 cells and ~72 h for PC12 cells. In this way, the cells were exposed to treatment for a considerable fraction, 0.25–0.50, of their cycle time and the effect of the number of divisions during the course of an assay is small [61]. In future studies it may, however, be interesting to examine the effect of treatment time length on MOP-eGFP and 5-HT$_{1A}$-Tomato association in live cells in order to understand the relevance of this phenomenon in acute vs chronic treatment with non-peptide opioids.

Finally, we have not used in our study antagonists of MOP and 5-HT$_{1A}$ receptors to block effects mediated via monomeric receptors. Consequently, we cannot discern to what extent Ca^{2+} level and dynamics, and ERK1/2 or p38 phosphorylation levels change via heterodimer-mediated pathways and whether these effects can also be blocked by the selective antagonists of MOP and 5-HT$_{1A}$.

4. Materials and Methods

4.1. Cell Culture and Transfection

Human embryonic kidney (HEK293) and rat phaeochromocytoma (PC12) cell lines (American Type Culture Collection (ATCC)), were used because they are capable of post-translational folding and modifications required to express MOP and 5-HT$_{1A}$ [62–64]. The experiments were first performed in HEK293 cells, and key findings were validated in PC12 cells. The HEK293 and PC12 cells were stably transformed to simultaneously express the human MOP receptor genetically fused at the C-terminus with the enhanced Green Fluorescent Protein (MOP-eGFP) and the human 5-HT$_{1A}$ receptor genetically fused at the C-terminus with the Tomato Red Fluorescent Protein (5-HT$_{1A}$-Tomato). Both constructs were cloned into the pBudCE4.1 vector (Thermo Fisher, Munich, Germany), with the MOP-eGFP gene being expressed under the control of the hEF-1 promoter (KpnXho) and

5-HT$_{1A}$-Tomato gene under the control of the CMV promoter (HindXba). For details, see Supplementary Materials (Section S1, Figure S1A).

For cultivation, untransformed and stably transformed HEK293 and PC12 cells were cultured in collagen coated T25 flasks (Sarsted) at 37 °C in a humidified atmosphere containing 5% CO$_2$. HEK293 cells were cultured in DMEM medium supplemented with 10% Fetal Bovine Serum (FBS), 100 U/mL penicillin and 100 µg/mL streptomycin (PenStrep). For PC12 cells, the RPMI 1640 medium supplemented with 10% Horse Serum (HS) and 5% FBS, 100 U/mL penicillin and 100 µg/mL streptomycin was used. All cell culture reagents were from Invitrogen, Stockholm, Sweden.

For generating the stably transformed cell lines, the HEK293 and PC12 cells were grown to 70% confluence in 8-well chambered cover slides (Nalge Nunc International, Rochester, NY, USA) and transfected using Lipofectamine 2000 (Invitrogen), following the transfection protocol provided by the manufacturer. Stably expressing cell lines were isolated through selection using culture medium supplemented with phleomycin D1 antibiotic (0.4 mg/mL, Thermo Fisher). Positive and negative control cells were cultured and transfected in the same way. For details, see Supplementary Materials (Section S1, Figure S1A,B). The functionality of MOP-eGFP and 5-HT$_{1A}$-Tomato receptors was validated by assessing how treatment with the selected agonists morphine, serotonin or buspirone or their combination: morphine and serotonin, or morphine and buspirone, affects phosphorylation of Erk1/2 and p38 MAPKs. The data show that all tested compounds and their combination increase the protein levels of p-ERK1/2 and p-p38 as compared to their levels in untreated cells (Section S1, Figure S1C).

4.2. Confocal Laser Scanning Microscopy (CLSM) Imaging and Fluorescence Correlation and Cross-Correlation Spectroscopy (FCS/FCCS)

The CLSM imaging and FCS/FCCS were performed using an individually modified ConfoCor 3 system (Carl Zeiss, Jena, Germany), as previously described [65,66]. Briefly, the system comprises an inverted microscope for transmitted light and epifluorescence (Axiovert 200 M); a VIS-laser module housing the Ar/ArKr (458, 477, 488 and 514 nm), HeNe 543 nm and HeNe 633 nm lasers; a scanning module LSM 510 META modified to enable imaging using silicon avalanche photodiodes (SPCM-AQR-1X, PerkinElmer, Waltham, MA, USA) in order to allow studies of cells expressing low levels of the proteins of interest; and an FCS/FCCS module with two detection channels. The C-Apochromat 40×/1.2 W UV-VIS-IR objective was used throughout. A stage incubator consisting of a heated microscope stage (Heating insert P), incubator box (Incubator S), atmosphere-controller (CTI-Controller 3700) and a temperature regulator (Temp control 37-2 digital), was used to maintain the cells at 37.0 °C and supply them with heated humidified air containing 5.0% CO$_2$. The temperature and CO$_2$ levels were continuously monitored and regulated via a digital feedback control algorithm, allowing temperature control within ±0.2 °C and atmosphere control within ±0.1% CO$_2$.

The CLSM images were acquired in a sequential, i.e., dual track mode, one channel at a time. The eGFP fluorescence was excited using the 488 nm line of the Ar/ArKr laser. A band pass 505–530 nm emission filter was used to spectrally narrow the emitted fluorescence. Tomato fluorescence was excited using the 543 nm HeNe laser, and a long pass 580 nm emission filter was used to collect the emitted fluorescence. Incident and emitted light were separated using the main dichroic beam splitter HFT 488/543/633. The eGFP and Tomato fluorescence were separated using a secondary dichroic beam splitter NFT 545 (Figure 1A). Images were acquired without averaging, using a pixel dwell time of 51.2 µs and a 512 × 512 pixels format (Figure 1B).

The optical setup for FCCS was the same as for CLSM imaging described above. Fluorescence intensity fluctuations were recorded at the apical plasma membrane of live cells identified by an axial fluorescence intensity scan (Figure 1C). Time series were collected in an array of 10 consecutive measurements, each measurement lasting 20 s (Figure 1D).

4.3. Brief Background on FCS/FCCS

Fluorescence cross-correlation spectroscopy (FCCS) is a dual color variant of fluorescence correlation spectroscopy (FCS). The FCS measures with sub-microsecond temporal resolution spontaneous fluctuations in fluorescence intensity around a steady state to extract quantitative information about the concentration and diffusion/size of fluorescent molecules [67–69]. The FCS is well suited for biological applications, as it is non-destructive and allows quantitative measurements to be performed in sub-cellular compartments [70]. The fluctuations in fluorescence intensity are recorded in a very small observation volume element (OVE) that is typically about V_{OVE} = 0.1–2 fL ((0.1–2) $\times$ 10^{-15} L). The OVE is generated by tightly focusing the incident laser light into the sample using a high numerical aperture objective. Fluorescence is collected through the same objective, and the volume from which fluorescence is being collected is reduced by placing a pinhole in the optically conjugate plane in front of the detector [69,71]. The spontaneous diffusion of fluorescent molecules in and out of the OVE gives rise to fluctuations in fluorescence intensity. The size and volume of the OVE is specific for each instrument and is determined in calibration experiments using a reference molecule with a known diffusion coefficient, such as Rhodamine 6G (Rh6G). Using a standard 10 nM Rh6G solution, and following the procedure described in detail in [71], the OVE volume in our system was determined to be V_{OVE} = 0.2 fL [68]. For a quick estimate of the concentration, note that for a 10 nM solution and V_{OVE} = 0.17 fL, the average number of molecules in the OVE (N) is N = 1 [71,72].

The FCS/FCCS works best at low, sub-micromolar concentrations [71], where the signal from a bright fluorescent molecule generates a substantial increase in fluorescence intensity that is well above the background signal from the surrounding molecules. From the recorded fluorescence intensity fluctuations, which are generated by the translational diffusion of fluorescent molecules, one can extract the average number of molecules in the OVE (N), i.e., their concentration and their average translational diffusion time (τ_D), which is defined by the diffusion coefficient (D), i.e., the size of the molecule (Stokes-Einstein equation). To extract this information from fluorescence intensity fluctuation analysis, the most commonly employed method, which is also used here, is temporal autocorrelation analysis. In temporal autocorrelation analysis, the signal is compared to a copy of itself delayed for a certain lag time (τ) using the autocorrelation function:

$$G(\tau) = 1 + \frac{\langle \delta F(t) \cdot \delta F(t+\tau) \rangle}{\langle F(t) \rangle^2} \qquad (1)$$

In Equation (1), chevron brackets denote average values of the analyzed variables over time, and fluorescence intensity fluctuation ($\delta(F(t))$ is the deviation of the fluorescence intensity at time t (F(t)) from the mean fluorescence intensity ($\langle F(t) \rangle$), $\delta F(t) = F(t) - \langle F(t) \rangle$. Accordingly, $\delta F(t + \tau) = F(t + \tau) - \langle F(t) \rangle$. When the fluctuations are not random, temporal autocorrelation analysis yields a temporal autocorrelation curve (tACC). The tACC is characterized by a maximal limiting value of $G(\tau)$ as $\tau \to 0$ and decreases to the value $G(\tau) = 1$ at long lag times, indicating that correlation between the fluorescence intensities is being lost (Figure 1E, green and red). If there is only one process that gives rise to fluorescence intensity fluctuations, the tACC shows one inflection point, that is, one characteristic decay time. If there are more processes giving rise to fluorescence intensity fluctuations, which occur at different time scales, the tACC assumes a more complex shape with more than one characteristic decay time (Figure 1E, green and red). The zero-lag amplitude of the tACC, ($G_0 = G(0) - 1$) provides information about the concentration of fluorescent molecules as it equals the inverse average number of molecules in the OVE (1/N). Thus, the amplitude of the tACC decreases when N increases. The characteristic decay time of the tACC gives information about the rates at which processes that give rise to the fluorescence intensity fluctuations occur. When fluorescence intensity fluctuations are generated by molecular diffusion, the characteristic decay time of the tACC reflects the average time it takes for a molecule to cross through the OVE by translational diffusion.

For dual colour FCCS, two spectrally distinct fluorescent molecules, such as eGFP and Tomato, are used to render the molecules of interest visible. Fluorescence intensity fluctuations are then simultaneously recorded for both fluorophores using overlaying excitation pathways, but separate detector pathways (Figure 1A). The fluorescence intensity fluctuations observed in FCCS (Figure 1D) are subjected to temporal auto- and cross-correlation analysis. This generates two tACCs, one for each fluorophore (Figure 1E, red and green) and, when the molecules of interest bind, one temporal cross-correlation curve (tCCC; Figure 1E, black), which reflects the population of dually labelled molecules diffusing as one [36,73,74]. As in FCS, the amplitudes of the individual tACCs contain information about the total average number of green- and red-labelled molecules in the OVE, now being the sum of unbound singly labelled molecules and the bound dually labelled complexes. Thus, for the eGFP-labelled MOP receptors, $N_g^{total} = N_g + N_{gr}$, and for the Tomato-labelled 5-HT$_{1A}$ receptors, $N_r^{total} = N_r + N_{gr}$ (Figure 1E). Only the dually labelled receptor-receptor heterodimer molecules give rise to fluorescence intensity fluctuations in both detectors at the same time, and are thus the only ones to contribute to the tCCC, obtained by calculating the cross-correlation function:

$$G_{CC}(\tau) = 1 + \frac{\langle \delta F_{green}(t) \cdot \delta F_{red}(t+\tau) \rangle}{\langle F_{green}(t) \rangle \langle F_{red}(t) \rangle} \tag{2}$$

In contrast to the amplitudes of the tACCs (Equation (1)), which are inversely proportional to the average number of molecules in the OVE (see detailed explanation in [71,75], the zero-lag amplitude of the tCCC (Equation (2)) is directly proportional to the number of dually labelled molecules (N_{gr}) and thus increases as N_{gr} increases:

$$G_{CC}(0) - 1 \propto \frac{N_{gr}}{(N_g + N_{gr}) \cdot (N_r + N_{gr})} \tag{3}$$

In order to characterize the degrees of binding between MOP-eGFP and 5-HT$_{1A}$-Tomato, i.e., to determine the number of the heterodimer receptor complexes, FCCS data are further analysed to obtain a dimensionless value known as the relative cross-correlation amplitude (RCCA) [75]. The RCCA is defined as the limiting value, when the lag time approaches zero ($\tau \rightarrow 0$), of the cross-correlation curve relative to the autocorrelation curve for a single fluorophore. For example, the number of bound, dually labelled molecules carrying both the green and the red label, relative to the total number of molecules carrying the red label ($N_r^{total} = N_r + N_{gr}$), equals the amplitude of the cross-correlation curve ($G_{CC}(0) - 1$) relative to the amplitude of the green autocorrelation curve ($G_{AC,g}(0) - 1$) [75]:

$$RCCA = \frac{G_{cc}(0) - 1}{G_{AC,g}(0) - 1} = \frac{N_{gr}}{N_r^{total}} = \frac{N_{gr}}{N_r + N_{gr}} \tag{4}$$

Knowing the concentration of MOP-eGFP and 5-HT$_{1A}$-Tomato molecules, and the concentration of heterodimer MOP-eGFP–5-HT$_{1A}$-Tomato complexes, the apparent dissociation constant for the receptor-receptor heterodimer complex can be calculated:

$$K_d^{app} = \frac{c_{free}^{MOP} \cdot c_{free}^{5-HT1A}}{c_{MOP-5-HT1A}} \tag{5}$$

or, when expressed using the quantities determined by FCCS:

$$K_d^{app} = \frac{\left(N_g^{total} - N_r^{total} \cdot RCCA \right) \cdot (1 - RCCA)}{RCCA} \cdot \frac{1}{N_A \cdot V_{OVE}} \tag{6}$$

In Equation (6), N_A is the Avogadro number. For determining the dynamic range of the RCCA, i.e., the smallest and the largest RCCA values that could be reliably measured,

see control experiments described in Supplementary Materials (Section S1. Transfection, positive and negative control cells (Figure S2)). Derivation of Equation (6) is given in Supplementary Materials, Section S2. Calculation of the apparent dissociation constant).

One challenge in dual-color FCCS that is particularly important to consider when fluorescence proteins are being used is the risk of false-positives due to spectral crosstalk between channels, which may lead to overestimation of the cross-correlation amplitude [75]. In order to ascertain that this error is minimized, we have validated the optical setting using control cells—cells expressing eGFP and Tomato were used as negative control (Supplementary Materials, Section S1. Transfection, positive and negative control cells (Figure S2C)) and cells expressing genetically fused eGFP-Tomato were used as positive control (Supplementary Materials, Section S1. Transfection, positive and negative control cells (Figure S2A)). The corresponding tCCCs are shown in Figure 1F. Control experiments showed that the dynamic range in dual-color FCCS differed from the theoretical range, $0 \leq \text{RCCA} \leq 1$, and was determined to be, $(0.10 \pm 0.07) \leq \text{RCCA} \leq (0.80 \pm 0.08)$. The RCCA value determined in the negative control experiments, $\text{RCCA}_{nc} = (0.10 \pm 0.07)$, indicated that only values that are significantly larger then RCCA_{nc} should be considered as a positive indication of binding. Positive control experiments indicated that RCCA values higher than $\text{RCCA}_{pc} = (0.80 \pm 0.08)$ may not be reached for reasons explained in (Supplementary Materials, Section S1. Transfection, positive and negative control cells (Figure S2E,F), and that RCCA values as high as RCCA_{pc} indicate that 100% binding between the investigated receptors has been reached.

In order to ascertain that errors due to spectral crosstalk are minimized, the optical setting was further validated using the so-called switching mode. In the switching mode, the sample is alternatingly (every 240 µs) illuminated with one laser at a time to excite one fluorophore only [69,71]. By using the switching mode, we could adjust the optical setting so that the crosstalk is minimal when the non-switching mode is being used, as explained in detail in [71], thus ascertaining that increased RCCA are actually being observed following treatment with non-peptide opioids (Supplementary Materials, Section S3. Relative cross-correlation amplitude (RCCA) increased upon opioid treatment. Verification was done by switching FCCS (Figures S3 and S4). Finally, in order to account for the, while minimized, inevitably present cross-talk-induced cross-correlation, the RCCA was corrected by subtracting the cross-talk-induced cross-correlation from the RCCA and scaled up as follows [36,75,76]:

$$\text{RCCA}_{\text{corrected}} = \frac{\text{RCCA} - \kappa \cdot f}{1 - \kappa \cdot f} \tag{7}$$

where κ is the so-called bleed-through ratio, i.e., brightness as reflected by the counts per second and per molecule (CPM) of the green dye in the red channel ($\text{CPM}_{g/r}$) when the red fluorophore is not present, divided by its brightness in the green channel $\text{CPM}_{g/g}$, $\kappa = \text{CPM}_{g/r}/\text{CPM}_{g/g}$, and f is the count rate (CR) ratio in the green and red channels, $f = \text{CR}_g/\text{CR}_r$. For the optical setting used in our studies, $\kappa = 0.1$ and $f \leq 1.2$. Following treatment, a two-fold increase in eGFP brightness was observed, while Tomato brightness remained largely unchanged (Table 1). To account for this, the κ factor was accordingly scaled. Thus $0.1 \leq \kappa \leq 0.2$, and the product $0.12 \leq \kappa \cdot f \leq 0.24$.

4.4. Opioid Treatment

Cells stably expressing MOP-eGFP and 5-HT$_{1A}$-Tomato were cultured in 8-well chambered coverslides (Nalge Nunc International, USA) at 37 °C in a humidified atmosphere containing 5% CO_2 using phenol red-free media, supplemented in the same way as described above. To ascertain that MOP-eGFP is functional and integrated into cellular physiology, the selective MOP receptor peptide agonist DAMGO ([D-Ala^2, N-MePhe^4, Gly-ol^5] enkephalin), was used (Figure 2) [77]. For experiments with non-peptide opioids, the cells were incubated for 18 h with different concentrations of fentanyl (50 nM, 500 nM, 750 nM or 1 µM) or morphine (250 nM, 500 nM or 750 nM). Based on the results of these experiments (explained in the Section 2), the 750 nM concentration was selected as suitable

for further studies. Hence, the cells were subsequently treated with 750 nM codeine or oxycodone. Non-peptide opioids and the peptide opioid DAMGO were all purchased from Sigma-Aldrich.

4.5. Intracellular Ca^{2+} Imaging

In order to measure acute opioid-induced changes in Ca^{2+} levels, cells were incubated for 30 min with Fura Red (Invitrogen), a ratiometric Ca^{2+} fluorescent indicator [78,79] stimulated with 750 nM opioids and Ca^{2+} levels were monitored using sequential, i.e., dual-track time-lapse CLSM imaging. In the first track, the 488 nm line of the Ar/ArKr laser was used to excite eGFP and Fura Red. The eGFP signal was collected using the band pass 505-530 nm emission filter, and the Fura Red signal was collected using the long pass 680 nm emission filter. In response to changes in Ca^{2+} concentrations, the excitation wavelength of Fura Red shifts from 472 nm at low Ca^{2+} concentration to 436 nm at high Ca^{2+} concentration [78]. As a result, the intensity of the Fura Red fluorescence signal decreases when intracellular Ca^{2+} levels increase and increases as they fall again. In the second track, the 543 nm HeNe laser was used to excite Tomato, and fluorescence was collected using the band pass 580–620 nm emission filter. The images were collected every 30 s for 40 min (in some cases up to 80 min). The pixel dwell time was 51.2 µs, and the images were collected without averaging.

4.6. Western Blotting

Transfected HEK293 cells expressing MOP-eGFP and 5-HT$_{1A}$-Tomato were cultured in collagen-coated T25 flasks (Sarstedt) as described in the *Cell culture and transfection* section. At around 90% confluence, the cells were treated with opioids following the protocol described in the *Opioid treatment* section. Adherent cells were removed from the flasks with trypsin-EDTA (0.05%, Thermo Fisher Scientific), washed with ice-cold PBS and centrifuged at 1500 rpm for 5 min at 4 °C. The cell pellets were solubilized in RIPA lysate buffer (10×10^6 cells/mL) containing protease inhibitor and phosphatase inhibitor (Sigma-Aldrich) and incubated for 30 min on ice. The cell solution was transferred to Eppendorf tubes and centrifuged at 10 000 rpm for 10 min. The total protein content was determined colorimetrically using the BioRad RC DC Protein Assay (Bio-Rad). Samples (20 µg protein) were denatured at 70 °C for 10 min with 4X LDS Sample Buffer, 10X Sample Reducing Agent (Invitrogen) and water was added to a final volume of 30 µL. Samples were loaded on precast polyacrylamide gels (Invitrogen) along with 5 µL of pre-stained standard protein ladder (Thermo Fisher Scientific), electrophoresed and transferred onto a nitrocellulose membrane (Thermo Fisher Scientific). The membrane was probed overnight with antibodies against ERK1/2 (Invitrogen and Cell Signaling Technology, Inc., Danvers, MA, USA), phospho-ERK1/2 (Invitrogen and Cell Signaling Technology, Inc.), p38 (Cell Signaling Technology, Inc.), phospho-p38 (Cell Signaling Technology, Inc.) or β-actin (Invitrogen and Cell Signaling Technology, Inc.). Only one primary antibody was used at a time and the membrane was stripped for 15 min with a western blot stripping buffer (Thermo Fisher Scientific) in between the different primary antibodies. Depending on the primary antibody, either biotin or horseradish peroxidase conjugated secondary antibody (Invitrogen) was used for detection. Western blot experiments were repeated three times, starting from different cell cultures. The same trend was observed in all repetitions. Data from one representative experiment are shown (Supplementary Materials, Section S4. Western blotting (Figure S5)).

4.7. LC-MS/MS Opioid Metabolite Analysis

In order to assess whether opioids were active compounds in their own right, HEK293 cells expressing MOP-eGFP and 5-HT$_{1A}$-Tomato were cultured in collagen-coated T25 flasks (Sarstedt) as described in the Section 4.1. At 90% confluence, the cell media was supplemented with 750 nM of morphine, oxycodone, codeine or fentanyl. After 18 h of incubation, the cell media was collected, the cells were lysed, and the cell culture medium

and the lysate were stored at -20 °C. Prior to LC-MS/MS analysis, the samples were thawed and allowed to reach room temperature, diluted $10\times$ with MilliQ water and filtered using Agilent/Whatman MiniUniPrep vials 0.2 µm PP (p/n 5190-1421). The samples were aliquoted (in triplicate) and subjected to LC-MS/MS for metabolite analysis. To this aim, a general protocol initially developed for urine analysis was used [80]. An LC-MS/MS analysis tested for the presence of morphine, morphine-3-glucuronide, morphine-6-glucuronide, normorphine, codeine, codeine-6-glucuronide, norcodeine, 6-acetylmorphine and ethylmorphine (Supplementary Materials, Section S5. Liquid chromatography-tandem mass spectrometry (LC-MS/MS) analysis (Tables S1 and S2)).

The analysis was performed using an ACQUITY UPLC I-Class system from Waters (Milford, MA, USA) coupled to a Waters Xevo TQD (Waters). All systems were controlled by MassLynx (Waters, version 4.1 SCN 940). Chromatographic separation was achieved on an ACE Excel 2 C18-PFP column (100 mm $\times$ 2.1 mm, 1.8 µm, Aberdeen, Scotland) kept at 60°C. Mobile phase A consisted of 0.001% formic acid in 10 mM ammonium formate pH 5.2 and mobile phase B consisted of 0.001% formic acid in methanol. Initial gradient conditions were 1% B held for 1.5 min, then increasing to 5% B during 0.1 min following a ramping of B to 41% until 7.5 min. The following gradient steps were 95% B until 8 min following 95% B during 1 min before reaching 1% B again and equilibration during 1 min. Total run time was 10.1 min and LC flow was 0.5 mL/min. The injection volume was 3 µL. The electro spray ionization (ESI) interface was operating in positive mode and the mass spectrometer was operating in multiple reaction monitoring (MRM) mode with two transitions for each analyte and one transition for each internal standard according to the table below. Both quadrupoles were set in unit resolution. Data were processed using TargetLynx TM (MassLynx version 4.1 SCN940).

Analytes were identified by their retention time and transition ratio. Quantification of the analytes in the samples was performed using calibration samples with eleven concentrations of the analyte, as shown in Supplementary Materials (Section S6, Table S1).

4.8. Statistical Analysis

A student's *t*-test was used to determine whether the difference between the mean values measured in untreated and treated cells, or in cells treated with different opioids, are significantly different from each other. The results are reported using a two-tailed *p*-value (*p*). The Benjamini–Hochberg method to control the False Discovery Rate (FDR) in sequential modified Bonferroni correction for multiple hypothesis testing was thereafter applied. At an FDR value of 5%, $p \leq 0.012$ was determined to be statistically significant.

5. Conclusions

The long-term usefulness of opioids in chronic pain treatment is hampered by side effects. Drugs targeting 5-HT_{1A} have been shown to alleviate the adverse effects of prolonged opioid use, suggesting interactions between MOP- and 5-HT_{1A}-mediated pathways. However, details of underlying mechanisms remain obscure. The aim of our study was to investigate whether these pathways can be integrated at the single-cell level by MOP- and 5-HT_{1A} heterodimerisation. Our quantitative characterization of MOP-eGFP and 5-HT_{1A}-Tomato interactions in live cells shows that these receptors can indeed form heterodimers in the plasma membrane of cells expressing physiologically relevant levels of these receptors. Our data show that under the conditions of our study, a surface density of (130 ± 10) molecules/µm^2, about 33% of the 5-HT_{1A}-Tomato receptors are bound in heterodimer complexes with MOP-eGFP in untreated cells.

In line with our hypothesis, we found an increase in MOP–5-HT_{1A} heterodimer formation in cells simultaneously expressing MOP and 5-HT_{1A} receptors following 18 h of incubation with fentanyl, morphine, codeine and oxycodone. All tested non-peptide opioids stabilized the heterodimer complexes and elicited a distinct down-stream cellular signalling response, as evidenced by Ca^{2+} imaging and ERK1/2 and p38 activation. An opi-

oid metabolites analysis did not show any traces of common opioid metabolites, indicating that codeine was an active compound with a similar strength to morphine.

Taken together, our findings suggest that treatments hindering MOP–5-HT$_{1A}$ heterodimer formation could provide potentially new strategies to treat opioid induced hyperalgesia and help to preserve the analgesic effects of opioids. The development of new drugs targeting these mechanisms is therefore of interest.

Supplementary Materials: The following supporting information can be downloaded at: https://www.mdpi.com/article/10.3390/molecules27072350/s1. Subsections: S1. Transfection, positive and negative control cells, S2. Calculation of the apparent dissociation constant (derivation of Equation (6) given in the main text), S3. Relative Cross-Correlation Amplitude (RCCA) increased upon opioid treatment. Verification by switching FCCS, S4. Western blotting and S5. Liquid chromatography-tandem mass spectrometry (LC-MS/MS) analysis. Figures: Figure S1. Transfection and cellular model generation; Figure S2. Determination of the RCCA for positive and negative control cells; Figure S3. RCCA increases upon opioid treatment; Figure S4. Switching FCCS; Figure S5. Western blots showing the activation of extracellular signal-regulated kinase (Erk1/2 and p-Erk1/2) and the p38 mitogen-activated protein kinase (p38/p-p38 MAPK) in HEK293 cells expressing MOP-eGFP and 5-HT$_{1A}$-Tomato. Loading control: β-actin. Tables: Table S1. Calibration standards for LC-MS/MS; Table S2. LC-MS/MS data for morphine (MOR), normorphine (NMOR), Morphine-3-glucuronide (M3G), Morphine-6-glucuronide (M6G), codeine (COD), norcodeine (NCOD), Codeine-6-glucuronide (C6G), Ethyl-morphine (EMOR) and 6-acetyl-morphine (6MAM). For every analyte two transitions (denoted 1 and 2) are measured, where one determines the concentration (underlined) and the other identity. In the measurements internal standards are also measured (denoted D3).

Author Contributions: Conceptualization, V.V. and E.K.; methodology, V.V., L.T., H.D. and E.K.; investigation, V.R., G.J., V.P. and A.N.; data analysis, V.R., G.J., V.P. and A.N.; writing—original draft preparation, V.R., V.V. and E.K.; writing—review and editing, all authors; resources and funding, V.V. and E.K. All authors have read and agreed to the published version of the manuscript.

Institutional Review Board Statement: Not applicable.

Informed Consent Statement: Not applicable.

Data Availability Statement: Not applicable.

Conflicts of Interest: The authors have no conflicts of interest to declare.

Sample Availability: Samples of the compounds are not available from the authors.

References

1. Collett, B. The burden of chronic pain. *Curr. Med. Res. Opin.* **2011**, *27*, 2065–2066. [CrossRef] [PubMed]
2. Basbaum, A.I.; Bautista, D.M.; Scherrer, G.; Julius, D. Cellular and molecular mechanisms of pain. *Cell* **2009**, *139*, 267–284. [CrossRef] [PubMed]
3. Gosselin, R.D.; Suter, M.R.; Ji, R.R.; Decosterd, I. Glial cells and chronic pain. *Neuroscientist* **2010**, *16*, 519–531. [CrossRef] [PubMed]
4. Kalso, E.; Edwards, J.E.; Moore, A.R.; McQuay, H.J. Opioids in chronic non-cancer pain: Systematic review of efficacy and safety. *Pain* **2004**, *112*, 372–380. [CrossRef] [PubMed]
5. Ballantyne, J.C. Opioids for the Treatment of Chronic Pain: Mistakes Made, Lessons Learned, and Future Directions. *Anesth. Analg.* **2017**, *125*, 1769–1778. [CrossRef]
6. Haleem, D.J. Serotonin-1A receptor dependent modulation of pain and reward for improving therapy of chronic pain. *Pharmacol. Res.* **2018**, *134*, 212–219. [CrossRef]
7. Xu, X.J.; Colpaert, F.; Wiesenfeld-Hallin, Z. Opioid hyperalgesia and tolerance versus 5-HT1A receptor-mediated inverse tolerance. *Trends Pharmacol. Sci.* **2003**, *24*, 634–639. [CrossRef]

8. Colpaert, F.C.; Deseure, K.; Stinus, L.; Adriaensen, H. High-efficacy 5-hydroxytryptamine 1A receptor activation counteracts opioid hyperallodynia and affective conditioning. *J. Pharmacol. Exp. Ther.* **2006**, *316*, 892–899. [CrossRef]

9. Rojas-Corrales, M.O.; Berrocoso, E.; Micó, J.A. Role of 5-HT1A and 5-HT1B receptors in the antinociceptive effect of tramadol. *Eur. J. Pharmacol.* **2005**, *511*, 21–26. [CrossRef]

10. Mico, J.A.; Berrocoso, E.; Ortega-Alvaro, A.; Gibert-Rahola, J.; Rojas-Corrales, M.O. The role of 5-HT1A receptors in research strategy for extensive pain treatment. *Curr. Top. Med. Chem.* **2006**, *6*, 1997–2003. [CrossRef]

11. Kosek, E.; Jensen, K.B.; Lonsdorf, T.B.; Schalling, M.; Ingvar, M. Genetic variation in the serotonin transporter gene (5-HTTLPR, rs25531) influences the analgesic response to the short acting opioid Remifentanil in humans. *Mol. Pain.* **2009**, *5*, 37. [CrossRef] [PubMed]

12. Tour, J.; Löfgren, M.; Mannerkorpi, K.; Gerdle, B.; Larsson, A.; Palstam, A.; Bileviciute-Ljungar, I.; Bjersing, J.; Martin, I.; Ernberg, M.; et al. Gene-to-gene interactions regulate endogenous pain modulation in fibromyalgia patients and healthy controls-antagonistic effects between opioid and serotonin-related genes. *Pain* **2017**, *158*, 1194–1203. [CrossRef] [PubMed]

13. Møller, M.; Jakobsen, S.; Gjedde, A. Parametric and regional maps of free serotonin 5HT1A receptor sites in human brain as function of age in healthy humans. *Neuropsychopharmacology* **2007**, *32*, 1707–1714. [CrossRef] [PubMed]

14. Petrovic, P.; Ingvar, M. Imaging cognitive modulation of pain processing. *Pain* **2002**, *95*, 1–5. [CrossRef]

15. Martikainen, I.K.; Hirvonen, J.; Kajander, J.; Hagelberg, N.; Mansikka, H.; Någren, K.; Hietala, J.; Pertovaara, A. Correlation of human cold pressor pain responses with 5-HT(1A) receptor binding in the brain. *Brain Res.* **2007**, *1172*, 21–31. [CrossRef]

16. Tuominen, L.; Nummenmaa, L.; Keltikangas-Järvinen, L.; Raitakari, O.; Hietala, J. Mapping neurotransmitter networks with PET: An example on serotonin and opioid systems. *Hum. Brain Mapp.* **2014**, *35*, 1875–1884. [CrossRef]

17. Azmitia, E.C.; Gannon, P.J.; Kheck, N.M.; Whitaker-Azmitia, P.M. Cellular localization of the 5-HT1A receptor in primate brain neurons and glial cells. *Neuropsychopharmacology* **1996**, *14*, 35–46. [CrossRef]

18. Grace, P.M.; Maier, S.F.; Watkins, L.R. Opioid-induced central immune signaling: Implications for opioid analgesia. *Headache* **2015**, *55*, 475–489. [CrossRef]

19. Roeckel, L.A.; Le Coz, G.M.; Gavériaux-Ruff, C.; Simonin, F. Opioid-induced hyperalgesia: Cellular and molecular mechanisms. *Neuroscience* **2016**, *338*, 160–182. [CrossRef]

20. Albrecht, D.S.; Forsberg, A.; Sandström, A.; Bergan, C.; Kadetoff, D.; Protsenko, E.; Lampa, J.; Lee, Y.C.; Höglund, C.O.; Catana, C.; et al. Brain glial activation in fibromyalgia—A multi-site positron emission tomography investigation. *Brain Behav. Immun.* **2019**, *75*, 72–83. [CrossRef]

21. Schrepf, A.; Harper, D.E.; Harte, S.E.; Wang, H.; Ichesco, E.; Hampson, J.P.; Zubieta, J.-K.; Clauw, D.J.; Harris, R.E. Endogenous opioidergic dysregulation of pain in fibromyalgia: A PET and fMRI study. *Pain* **2016**, *157*, 2217–2225. [CrossRef] [PubMed]

22. Kishimoto, K.; Koyama, S.; Akaike, N. Synergistic mu-opioid and 5-HT1A presynaptic inhibition of GABA release in rat periaqueductal gray neurons. *Neuropharmacology* **2001**, *41*, 529–538. [CrossRef]

23. Jasmin, L.; Wu, M.V.; Ohara, P.T. GABA puts a stop to pain. *Curr. Drug Targets CNS Neurol. Disord.* **2004**, *3*, 487–505. [CrossRef] [PubMed]

24. Cussac, D.; Rauly-Lestienne, I.; Heusler, P.; Finana, F.; Cathala, C.; Bernois, S.; De Vries, L. μ-Opioid and 5-HT1A receptors heterodimerize and show signalling crosstalk via G protein and MAP-kinase pathways. *Cell Signal.* **2012**, *24*, 1648–1657. [CrossRef] [PubMed]

25. Liu, J.G.; Prather, P.L. Chronic exposure to mu-opioid agonists produces constitutive activation of mu-opioid receptors in direct proportion to the efficacy of the agonist used for pretreatment. *Mol. Pharmacol.* **2001**, *60*, 53–62. [CrossRef]

26. Tsai, R.-Y.; Tai, Y.-H.; Tzeng, J.-I.; Lin, S.-L.; Shen, C.-H.; Yang, C.-P.; Hsin, S.-T.; Wang, C.-B.; Wong, C.-S. Ultra-low dose naloxone restores the antinociceptive effect of morphine in pertussis toxin-treated rats and prevents glutamate transporter downregulation by suppressing the p38 mitogen-activated protein kinase signaling pathway. *Neuroscience* **2009**, *159*, 1244–1256. [CrossRef]

27. Radoi, V. Interactions between the opioid and serotonin systems in chronic pain. Quantitative Live Cell Study by Fluorescence Cross-Correlation Spectroscopy (FCCS). Ph.D. Thesis, Karolinska Institutet, Stockholm, Sweden, 2019.

28. Hulme, E.C.; Trevethick, M.A. Ligand binding assays at equilibrium: Validation and interpretation. *Br. J. Pharmacol.* **2010**, *161*, 1219–1237. [CrossRef]

29. Watabe, M.; Arjunan, S.N.V.; Chew, W.X.; Kaizu, K.; Takahashi, K. Cooperativity transitions driven by higher-order oligomer formations in ligand-induced receptor dimerization. *Phys. Rev. E* **2019**, *100*, 062407. [CrossRef]

30. Heusler, P.; Tardif, S.; Cussac, D. Agonist stimulation at human μ opioid receptors in a [(35)S]GTPγS incorporation assay: Observation of "bell-shaped" concentration-response relationships under conditions of strong receptor G protein coupling. *J. Recept. Signal Transduct. Res.* **2016**, *36*, 158–166. [CrossRef]

31. McIntyre, I.M.; Anderson, D.T. Postmortem Fentanyl Concentrations: A Review. *J. Forensic Res.* **2012**, *3* (Suppl. S1), 2. [CrossRef]

32. Goldbeter, A. *Biochemical Oscillations and Cellular Rhythms: The Molecular Bases of Periodic and Chaotic Behaviour*; Cambridge University Press: Cambridge, UK, 1996; pp. 89–160, 349–406.

33. Macey, T.A.; Lowe, J.D.; Chavkin, C. Mu opioid receptor activation of ERK1/2 is GRK3 and arrestin dependent in striatal neurons. *J. Biol. Chem.* **2006**, *281*, 34515–34524. [CrossRef] [PubMed]

34. Tan, M.; Walwyn, W.M.; Evans, C.J.; Xie, C.W. p38 MAPK and beta-arrestin 2 mediate functional interactions between endogenous micro-opioid and alpha2A-adrenergic receptors in neurons. *J. Biol. Chem.* **2009**, *284*, 6270–6281. [CrossRef]

35. Kasai, R.S.; Kusumi, A. Single-molecule imaging revealed dynamic GPCR dimerization. *Curr. Opin. Cell Biol.* **2014**, *27*, 78–86, Correction in *Curr. Opin. Cell Biol.* **2014**, *27*, 144. [CrossRef] [PubMed]

36. Petersen, J.; Wright, S.; Rodríguez, D.; Matricon, P.; Lahav, N.; Vromen, A.; Friedler, A.; Strömqvist, J.; Wennmalm, S.; Carlsson, J.; et al. Agonist-induced dimer dissociation as a macromolecular step in G protein-coupled receptor signaling. *Nat. Commun.* **2017**, *8*, 226. [CrossRef] [PubMed]

37. Foster, S.R.; Bräuner-Osborne, H. Investigating Internalization and Intracellular Trafficking of GPCRs: New Techniques and Real-Time Experimental Approaches. *Handb. Exp. Pharmacol.* **2018**, *245*, 41–61. [CrossRef]

38. Kanaya, N.; Zakhary, D.R.; Murray, P.A.; Damron, D.S. Differential effects of fentanyl and morphine on intracellular Ca^{2+} transients and contraction in rat ventricular myocytes. *Anesthesiology* **1998**, *89*, 1532–1542. [CrossRef]

39. Fan, R.; Schrott, L.M.; Snelling, S.; Ndi, J.; Arnold, T.; Korneeva, N.L. Chronic oxycodone induces integrated stress response in rat brain. *BMC Neurosci.* **2015**, *16*, 58. [CrossRef]

40. Hutchinson, M.R.; Northcutt, A.L.; Hiranita, T.; Wang, X.; Lewis, S.S.; Thomas, J.; Van Steeg, K.; Kopajtic, T.A.; Loram, L.C.; Sfregola, C.; et al. Opioid activation of toll-like receptor 4 contributes to drug reinforcement. *J. Neurosci.* **2012**, *32*, 11187–11200. [CrossRef]

41. Al-Hasani, R.; Bruchas, M.R. Molecular mechanisms of opioid receptor-dependent signaling and behavior. *Anesthesiology* **2011**, *115*, 1363–1381. [CrossRef]

42. Remillard, D.; Kaye, A.D.; McAnally, H. Oxycodone's Unparalleled Addictive Potential: Is it Time for a Moratorium? *Curr. Pain Headache Rep.* **2019**, *23*, 15. [CrossRef]

43. Yue, Q.Y.; Hasselström, J.; Svensson, J.O.; Säwe, J. Pharmacokinetics of codeine and its metabolites in Caucasian healthy volunteers: Comparisons between extensive and poor hydroxylators of debrisoquine. *Br. J. Clin. Pharmacol.* **1991**, *31*, 635–642. [CrossRef] [PubMed]

44. Cortazzo, M.H.; Copenhaver, D.; Fishman, S.M. Major Opioids and Chronic Opioid Therapy. In *Practical Management of Pain*, 5th ed.; Benzon, H.T., Rathmell, J.P., Wu, C.L., Turk, D.C., Argoff, C.E., Hurley, R.W., Eds.; Elsevier Inc.: Amsterdam, The Netherlands, 2013; pp. 495–507.e493. [CrossRef]

45. Johnson, J.L.; Rolan, P.E.; Johnson, M.E.; Bobrovskaya, L.; Williams, D.; Johnson, K.F.; Tuke, J.; Hutchinson, M. Codeine-induced hyperalgesia and allodynia: Investigating the role of glial activation. *Transl. Psychiatry* **2014**, *4*, e482. [CrossRef] [PubMed]

46. Mignat, C.; Wille, U.; Ziegler, A. Affinity profiles of morphine, codeine, dihydrocodeine and their glucuronides at opioid receptor subtypes. *Life Sci.* **1995**, *56*, 793–799. [CrossRef]

47. Schmidt, H.; Vormfelde, S.V.; Klinder, K.; Gundert-Remy, U.; Gleiter, C.H.; Skopp, G.; Aderjan, R.; Fuhr, U. Affinities of dihydrocodeine and its metabolites to opioid receptors. *Pharmacol. Toxicol.* **2002**, *91*, 57–63. [CrossRef] [PubMed]

48. Ingelman-Sundberg, M. Genetic polymorphisms of cytochrome P450 2D6 (CYP2D6): Clinical consequences, evolutionary aspects and functional diversity. *Pharm. J.* **2005**, *5*, 6–13. [CrossRef]

49. Tzvetkov, M.V.; dos Santos Pereira, J.N.; Meineke, I.; Saadatmand, A.R.; Stingl, J.C.; Brockmöller, J. Morphine is a substrate of the organic cation transporter OCT1 and polymorphisms in OCT1 gene affect morphine pharmacokinetics after codeine administration. *Biochem. Pharmacol.* **2013**, *86*, 666–678. [CrossRef] [PubMed]

50. Kasai, R.S.; Suzuki, K.G.N.; Prossnitz, E.R.; Koyama-Honda, I.; Nakada, C.; Fujiwara, T.K.; Kusumi, A. Full characterization of GPCR monomer-dimer dynamic equilibrium by single molecule imaging. *J. Cell Biol.* **2011**, *192*, 463–480. [CrossRef]

51. Casadó-Anguera, V.; Moreno, E.; Mallol, J.; Ferré, S.; Canela, E.I.; Cortés, A.; Casadó, V. Reinterpreting anomalous competitive binding experiments within G protein-coupled receptor homodimers using a dimer receptor model. *Pharmacol. Res.* **2019**, *139*, 337–347. [CrossRef]

52. Jorand, R.; Biswas, S.; Wakefield, D.L.; Tobin, S.J.; Golfetto, O.; Hilton, K.; Ko, M.; Ramos, J.W.; Small, A.R.; Chu, P.; et al. Molecular signatures of mu opioid receptor and somatostatin receptor 2 in pancreatic cancer. *Mol. Biol. Cell* **2016**, *27*, 3659–3672. [CrossRef]

53. Touhara, K.K.; MacKinnon, R. Molecular basis of signaling specificity between GIRK channels and GPCRs. *eLife* **2018**, *7*, e42908. [CrossRef]

54. Volpe, D.A.; Tobin, G.A.M.; Mellon, R.D.; Katki, A.G.; Parker, R.J.; Colatslcy, T.; Kropp, T.J.; Verbois, S.L. Uniform assessment and ranking of opioid Mu receptor binding constants for selected opioid drugs. *Regul. Toxicol. Pharmacol.* **2011**, *59*, 385–390. [CrossRef] [PubMed]

55. Rickli, A.; Liakoni, E.; Hoener, M.C.; Liechti, M.E. Opioid-induced inhibition of the human 5-HT and noradrenaline transporters in vitro: Link to clinical reports of serotonin syndrome. *Br. J. Pharmacol.* **2018**, *175*, 532–543. [CrossRef] [PubMed]

56. Heiskanen, T.; Langel, K.; Gunnar, T.; Lillsunde, P.; Kalso, E.A. Opioid Concentrations in Oral Fluid and Plasma in Cancer Patients with Pain. *J. Pain Symptom Manag.* **2015**, *50*, 524–532. [CrossRef] [PubMed]

57. Christrup, L.L.; Foster, D.; Popper, L.D.; Troen, T.; Upton, R. Pharmacokinetics, efficacy, and tolerability of fentanyl following intranasal versus intravenous administration in adults undergoing third-molar extraction: A randomized, double-blind, double-dummy, two-way, crossover study. *Clin Ther.* **2008**, *30*, 469–481. [CrossRef] [PubMed]

58. Trescot, A.M. Review of the role of opioids in cancer pain. *J. Natl. Compr. Cancer Netw.* **2010**, *8*, 1087–1094. [CrossRef] [PubMed]

59. Pereira, J.; Lawlor, P.; Vigano, A.; Dorgan, M.; Bruera, E. Equianalgesic dose ratios for opioids: A critical review and proposals for long-term dosing. *J. Pain Symptom Manag.* **2001**, *22*, 672–687. [CrossRef]

60. Rennick, A.; Atkinson, T.; Cimino, N.M.; Strassels, S.A.; McPherson, M.L.; Fudin, J. Variability in Opioid Equivalence Calculations. *Pain Med.* **2016**, *17*, 892–898. [CrossRef]

61. Hafner, M.; Niepel, M.; Chung, M.; Sorger, P.K. Growth rate inhibition metrics correct for confounders in measuring sensitivity to cancer drugs. *Nat. Methods* **2016**, *13*, 521–527. [CrossRef] [PubMed]

62. Thomas, P.; Smart, T.G. HEK293 cell line: A vehicle for the expression of recombinant proteins. *J. Pharmacol. Toxicol. Methods* **2005**, *51*, 187–200. [CrossRef]

63. Westerink, R.H.; Ewing, A.G. The PC12 cell as model for neurosecretion. *Acta Physiol.* **2008**, *192*, 273–285. [CrossRef]

64. Khan, K.H. Gene expression in Mammalian cells and its applications. *Adv. Pharm. Bull.* **2013**, *3*, 257–263. [CrossRef]

65. Vukojevic, V.; Heidkamp, M.; Ming, Y.; Johansson, B.; Terenius, L.; Rigler, R. Quantitative single-molecule imaging by confocal laser scanning microscopy. *Proc. Natl. Acad. Sci. USA* **2008**, *105*, 18176–18181. [CrossRef]

66. Vukojevic, V.; Papadopoulos, D.K.; Terenius, L.; Gehring, W.J.; Rigler, R. Quantitative study of synthetic Hox transcription factor-DNA interactions in live cells. *Proc. Natl. Acad. Sci. USA* **2010**, *107*, 4093–4098. [CrossRef]

67. Schwille, P. Fluorescence correlation spectroscopy and its potential for intracellular applications. *Cell Biochem. Biophys.* **2001**, *34*, 383–408. [CrossRef]

68. Vukojević, V.; Pramanik, A.; Yakovleva, T.; Rigler, R.; Terenius, L.; Bakalkin, G. Study of molecular events in cells by fluorescence correlation spectroscopy. *Cell Mol. Life Sci.* **2005**, *62*, 535–550. [CrossRef]

69. Kim, S.A.; Heinze, K.G.; Schwille, P. Fluorescence correlation spectroscopy in living cells. *Nat. Methods* **2007**, *4*, 963–973. [CrossRef]

70. Tian, Y.; Martinez, M.M.; Pappas, D. Fluorescence correlation spectroscopy: A review of biochemical and microfluidic applications. *Appl. Spectrosc.* **2011**, *65*, 115A–124A. [CrossRef]

71. Rogacki, M.K.; Golfetto, O.; Tobin, S.J.; Li, T.; Biswas, S.; Jorand, R.; Zhang, H.; Radoi, V.; Ming, Y.; Svenningsson, P.; et al. Dynamic lateral organization of opioid receptors (kappa, mu$_{wt}$ and mu$_{N40D}$) in the plasma membrane at the nanoscale level. *Traffic* **2018**, *19*, 690–709. [CrossRef]

72. Schwille, P.; Ries, J. Principles and Applications of Fluorescence Correlation Spectroscopy (Fcs). In *Biophotonics: Spectroscopy, Imaging, Sensing, and Manipulation*; NATO Security through Science Series B: Physics and Biophysics; Springer: Dordrecht, The Netherlands, 2011; pp. 63–85. [CrossRef]

73. Bacia, K.; Kim, S.A.; Schwille, P. Fluorescence cross-correlation spectroscopy in living cells. *Nat. Methods* **2006**, *3*, 83–89. [CrossRef]

74. Krieger, J.W.; Singh, A.P.; Bag, N.; Garbe, C.S.; Saunders, T.; Langowski, J.; Wohland, T. Imaging fluorescence (cross-) correlation spectroscopy in live cells and organisms. *Nat. Protoc.* **2015**, *10*, 1948–1974. [CrossRef]

75. Bacia, K.; Petrášek, Z.; Schwille, P. Correcting for spectral cross-talk in dual-color fluorescence cross-correlation spectroscopy. *Chemphyschem* **2012**, *13*, 1221–1231. [CrossRef]

76. Du, Z.; Yu, J.; Li, F.; Deng, L.; Wu, F.; Huang, X.; Bergstrand, J.; Widengren, J.; Dong, C.; Ren, J. In Situ Monitoring of p53 Protein and MDM2 Protein Interaction in Single Living Cells Using Single-Molecule Fluorescence Spectroscopy. *Anal. Chem.* **2018**, *90*, 6144–6151. [CrossRef]

77. Xu, H.; Partilla, J.S.; Wang, X.; Rutherford, J.M.; Tidgewell, K.; Prisinzano, T.E.; Bohn, L.M.; Rothman, R.B. A comparison of noninternalizing (herkinorin) and internalizing (DAMGO) mu-opioid agonists on cellular markers related to opioid tolerance and dependence. *Synapse* **2007**, *61*, 166–175. [CrossRef] [PubMed]

78. Burchiel, S.W.; Edwards, B.S.; Kuckuck, F.W.; Lauer, F.T.; Prossnitz, E.; Ransom, J.T.; Sklar, L.A. Analysis of free intracellular calcium by flow cytometry: Multiparameter and pharmacologic applications. *Methods* **2000**, *21*, 221–230. [CrossRef]

79. Tinning, P.W.; Franssen, A.J.P.M.; Hridi, S.U.; Bushell, T.J.; McConnell, G. A 340/380 nm light-emitting diode illuminator for Fura-2 AM ratiometric Ca^{2+} imaging of live cells with better than 5 nM precision. *J. Microsc.* **2018**, *269*, 212–220. [CrossRef]

80. Murphy, C.M.; Huestis, M.A. LC-ESI-MS/MS analysis for the quantification of morphine, codeine, morphine-3-beta-D-glucuronide, morphine-6-beta-D-glucuronide, and codeine-6-beta-D-glucuronide in human urine. *J. Mass Spectrom.* **2005**, *40*, 1412–1416, Correction in *J. Mass Spectrom.* **2006**, *41*, 127. [CrossRef]

Article

Characterization of the Synergistic Effect between Ligands of Opioid and Free Fatty Acid Receptors in the Mouse Model of Colitis

Agata Binienda [1](ID), Adam Makaro [1](ID), Marcin Talar [1](ID), Julia B. Krajewska [1], Aleksandra Tarasiuk [1](ID), Adrian Bartoszek [1], Adam Fabisiak [1,2](ID), Paula Mosińska [1], Karolina Niewinna [1], Katarzyna Dziedziczak [1], Mikołaj Świerczyński [1], Radzisław Kordek [3], Maciej Salaga [1](ID) and Jakub Fichna [1,*](ID)

[1]   Department of Biochemistry, Faculty of Medicine, Medical University of Lodz, 92-215 Lodz, Poland;
      agata.binienda@gmail.com (A.B.); adam.makaro@stud.umed.lodz.pl (A.M.);
      marcin.talar@umed.lodz.pl (M.T.); krajewskajulia@gmail.com (J.B.K.); tarasiuk.aleksandra@gmail.com (A.T.);
      adrian.bartoszek@stud.umed.lodz.pl (A.B.); adam.fabisiak@umed.lodz.pl (A.F.);
      paula.mosinska@gmail.com (P.M.); karolina.niewinna@umed.lodz.pl (K.N.);
      katarzyna.dziedziczak@umed.lodz.pl (K.D.); mikolaj.swierczynski@stud.umed.lodz.pl (M.Ś.);
      salaga.maciej@gmail.com (M.S.)
[2]   Department of Digestive Tract Diseases, Medical University of Lodz, 93-281 Lodz, Poland
[3]   Department of Pathology, Medical University of Lodz, 92-215 Lodz, Poland; radzislaw.kordek@umed.lodz.pl
[*]   Correspondence: jakub.fichna@umed.lodz.pl; Tel.: +48-42-272-57-07

Abstract: Background: Recent studies suggest that lipids, including free fatty acids (FFAs), are necessary for proper μ opioid receptor (MOR) binding and that activation of opioid receptors (ORs) improves intestinal inflammation. The objective of the study was to investigate a possible interaction between the ORs and FFA receptors (FFARs) ligands in the colitis. Methods: The potential synergistic effect of ORs and FFARs ligands was evaluated using mouse model of acute colitis induced by dextran sulfate sodium (DSS, 4%). Compounds were injected intraperitoneally (i.p.) once or twice daily at the doses of 0.01 or 0.02 mg/kg body weight (BW) (DAMGO—an MOR agonist), 0.3 mg/kg BW (DPDPE—a δ OR (DOR) agonist) and 1 mg/kg BW (naloxone—a non-selective OR antagonist, GLPG 0974—a FFAR2 antagonist, GSK 137647—a FFAR4 agonist and AH 7614—a FFAR4 antagonist) for 4 days. Results: Myeloperoxidase (MPO) activity was significantly decreased after DAMGO (0.02 mg/kg BW) and GSK 137647 (1 mg/kg BW) administration and co-administration as compared to DSS group. Conclusions: Treatment with ligands of ORs and FFARs may affect the immune cells in the inflammation; however, no significant influence on the severity of colitis and no synergistic effect were observed.

Keywords: free fatty acid receptors; lipids; opioid receptor; DAMGO; colitis

1. Introduction

Inflammatory bowel disease (IBD), represented by Crohn's disease (CD) and ulcerative colitis (UC), is one of the most common gastrointestinal (GI) disorders with unknown etiology. Chronic inflammation, visceral pain, recurrent and alternating diarrhea and constipation are typical symptoms of IBD. Pharmacological treatment includes non-steroid anti-inflammatory drugs (NSAIDs), corticosteroids and biological therapies, e.g., anti-tumor necrosis factor α (anti-TNFα) and anti-α4β7 integrin antibodies. Additionally, surgical procedures, such as resection of the intestine's inflamed part, may be applied in severe cases [1,2]. Unfortunately, these methods are not fully effective (only about 50% of patients achieve remission), and they may cause serious adverse events (SAEs) [3].

Free fatty acids (FFAs) belong to signaling molecules which act through G protein-coupled receptors (GPCRs) [4]. There are four types of receptors for FFAs: FFAR1 (former nomenclature: GPR40), FFAR2 (GPR43), FFAR3 (GPR41) and FFAR4 (GPR120). FFAR2

and FFAR3 are activated by short chain fatty acids (SCFAs), while FFAR1 and FFAR4 are activated by medium and long chain fatty acids (MCFAs and LCFAs, respectively). FFAR ligands are involved in the regulation of metabolism and in inflammatory processes, also in the gut [5]. Recent studies showed that activation of FFAR1 and FFAR4 might decrease inflammation. In addition, it was showed that FFAR2 ligands are engaged in neutrophil inhibition and subsequently alleviate the severity of inflammation [6–8]. These findings suggest that FFARs have the potential to become new pharmacological targets in the treatment of IBD.

Ligands of the μ opioid receptor (MOR) and δ opioid receptor (DOR), including endogenous opioid peptides, such as β-endorphin and plant-derived opiates, are known for their central and peripheral analgesic effects [9,10]. In line, endogenous opioids were shown to be potentially engaged in pain regulation in chronic IBD [11]. Furthermore, Valdez-Morales et al. [12] proved that the release of endogenous opioids during dextran sulfate sodium (DSS)-induced chronic colitis in mice suppressed the excitability of nociceptive dorsal root ganglia neurons. Interestingly, there is evidence that endogenous opioid peptides are locally produced at the site of inflammation [13]. Consequently, Philippe et al. [14] showed anti-inflammatory properties of MOR agonists in the treatment of colonic inflammation in the mouse models of colitis. Furthermore, DiCello et al. [15] discovered that DOR signaling is enhanced in the enteric nervous system in DSS-induced acute colitis, suggesting that DORs can also be regarded as a potential pharmacological target in IBD treatment.

On the other hand, current studies claim that lipids, including FFAs, are necessary for proper MOR binding [16]. However, the literature on this potentially pharmacologically relevant subject is very scarce. Based on the data summarized above, we hypothesized that the co-administration of opioid receptor (OR) and FFAR ligands may exhibit synergy in alleviation of inflammation and, consequently, influence the course of IBD. Therefore, the aim of the study was to investigate a possible interaction between opioid receptor and FFAR ligands in the mouse model of colitis.

2. Results

2.1. FFAR2 Antagonist and MOR Agonist Decreased MPO Activity, but Did Not Display Synergistic Anti-Inflammatory Effect

To investigate the possible synergistic anti-inflammatory effect of a MOR agonist DAMGO and a FFAR2 antagonist GLPG 0974 in the mouse GI tract, we used a well-known mouse model of colitis induced by DSS which mimics UC. As shown in Figure 1, animals exposed to DSS developed a severe colonic injury, evidenced by—among others—increased macroscopic damage score and elevated MPO level compared with controls. DAMGO (0.02 mg/kg BW) and GLPG 0974 (1 mg/kg BW), injected once daily did not influence BW loss (Figure 1a), macroscopic score (Figure 1b), colon length (Figure 1c) and colon weight (Figure 1d). However, the co-administration of DAMGO and GLPG 0974 non-significantly decreased MPO activity as compared to DSS group and the compounds alone (Figure 1e).

Bootstrap for hypothesis testing revealed that $P_{bootstrap}$ in case of obtained difference in means between DSS + DAMGO vs DSS + DAMGO and GLPG 0974 ligands in macroscopic colon damage score (Figure 1b), colon length (Figure 1c), colon weight (Figure 1d) and MPO activity (Figure 1e) were 0.7928 (calculated absolute difference in means 0.2670), 0.5614 (calculated absolute difference in means 0.2310 cm), 0.7761 (calculated absolute difference in means 0.0132 g) and 0.2105 (calculated absolute difference in means 3.6200 μU/g tissue), respectively.
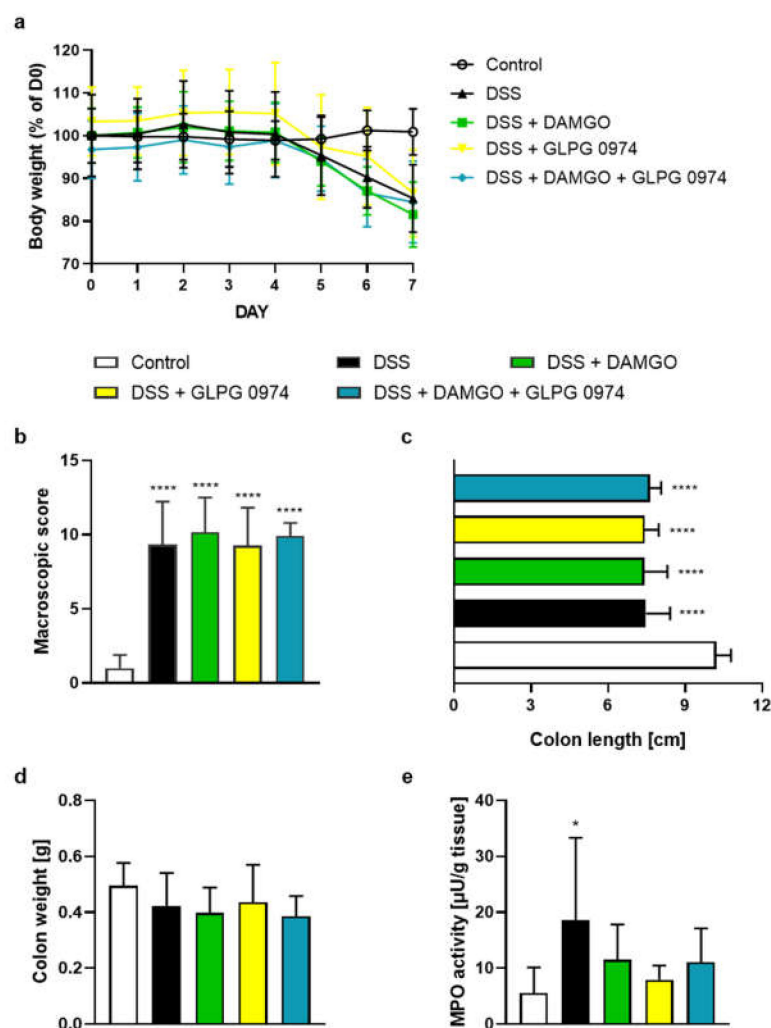
Figure 1. The i.p. administration of MOR agonist DAMGO (0.02 mg/kg BW) and FFAR2 antagonist GLPG 0974 (1 mg/kg BW) from day 3 to day 6, both once daily alleviate MPO activity, marker of DSS-induced colitis in mice. Figure shows data for body weight loss (**a**), macroscopic score (**b**), colon length (**c**), colon weight (**d**) and MPO activity (**e**). * $p < 0.05$, **** $p < 0.0001$, as compared to control mice. Data represent mean ± SEM of 5–10 mice per group. Abbreviations: DSS—dextran sulfate sodium, FFAR4—free fatty acid receptor type 4, i.p.—intraperitoneally, MOR—µ opioid receptor, MPO—myeloperoxidase.

2.2. FFAR4 Antagonist Did Not Influence the Effect of MOR Agonist

MOR agonist DAMGO administered twice daily at the dose of 0.02 mg/kg BW (i.p.) and FFAR4 antagonist AH 7614 administered twice daily at the dose of 1 mg/kg BW (i.p.) did not attenuate DSS-induced colitis alone or in co-administration, as indicated by inflammatory indicators (Figure 2a–d).

Bootstrap for hypothesis testing revealed that $P_{bootstrap}$ in case of obtained difference in means between DSS + DAMGO vs DSS + DAMGO and AH 7614 ligand in macroscopic colon damage score (Figure 2b), colon length (Figure 2c) and colon weight (Figure 2d) were 0.2445 (calculated absolute difference in means 1.300), 0.6970 (calculated absolute difference in means 0.1240 cm) and 0.5535 (calculated absolute difference in means 0.0239 g), respectively.
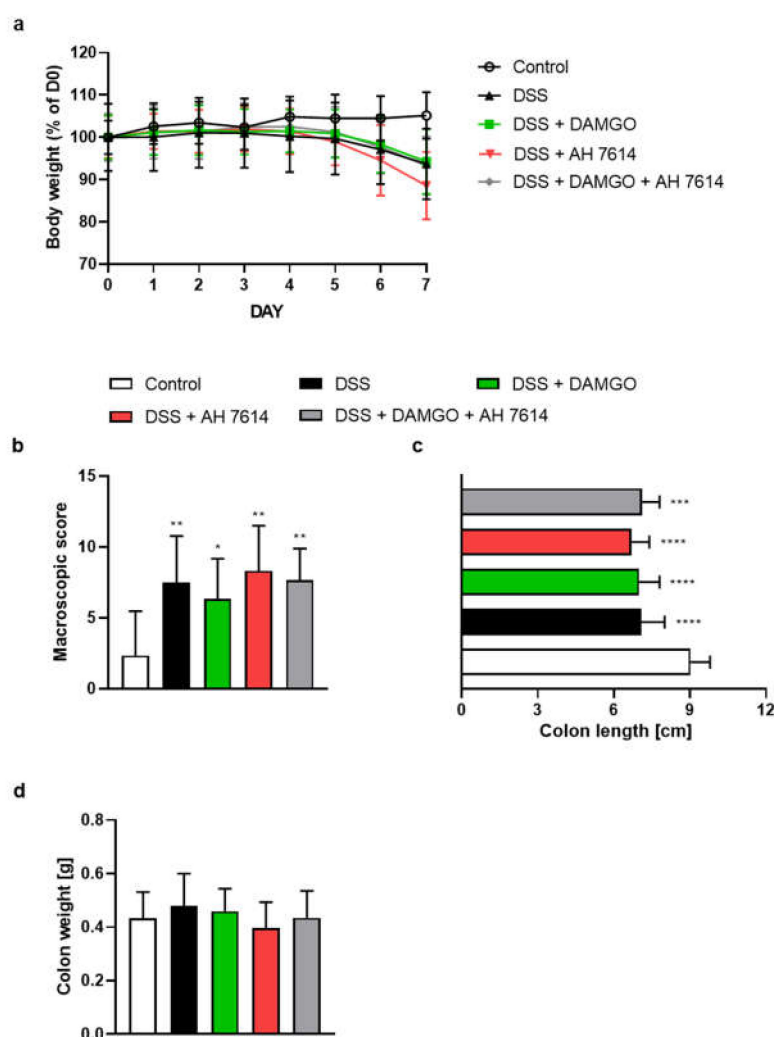
Figure 2. The i.p. administration of MOR agonist DAMGO (0.02 mg/kg BW) and FFAR4 antagonist AH 7614 (1 mg/kg BW) from day 3 to day 6, both twice daily did not alleviate symptoms of DSS-induced colitis in mice. Figure shows data for body weight loss (**a**), macroscopic score (**b**), colon length (**c**) and colon weight (**d**). * $p < 0.05$, ** $p < 0.01$, *** $p < 0.001$ and **** $p < 0.0001$ as compared to control mice. Data represent mean ± SEM of 5–10 mice per group. Abbreviations: DSS—dextran sulfate sodium, FFAR4—free fatty acid receptor type 4, i.p.—intraperitoneally, MOR—µ opioid receptor, MPO–myeloperoxidase.

2.3. FFAR4 Antagonist Did Not Influence the Effect of DOR Agonist

To test the anti-inflammatory activity of DOR agonist DPDPE and FFAR4 antagonist AH 7614 in the mouse model mimicking UC, a DSS-induced colitis was used. The i.p. administration of DPDPE (0.3 mg/kg BW) and the i.p. administration of AH 7614 (1 mg/kg BW), both twice daily between days 3 and 6 did not induce any improvement in the disease score, as demonstrated by the BW loss (Figure 3a), macroscopic colon damage score (Figure 3b), colon length (Figure 3c), colon weight (Figure 3d) and MPO activity (Figure 3e).

Bootstrap for hypothesis testing revealed that $P_{bootstrap}$ in case of obtained difference in means between DSS + DPDPE vs. DSS + DPDPE and AH 7614 ligands in macroscopic colon damage score (Figure 3b), colon length (Figure 3c), colon weight (Figure 3d), and MPO activity (Figure 3e) were 0.8040 (calculated mean absolute difference in means 0.2500), 0.5160 (calculated mean absolute difference in means 0.1800 cm), 0.8918 (calculated mean absolute difference in means 0.0044 g) and 0.6638 (calculated absolute difference in means 1.21 µU/g tissue), respectively.
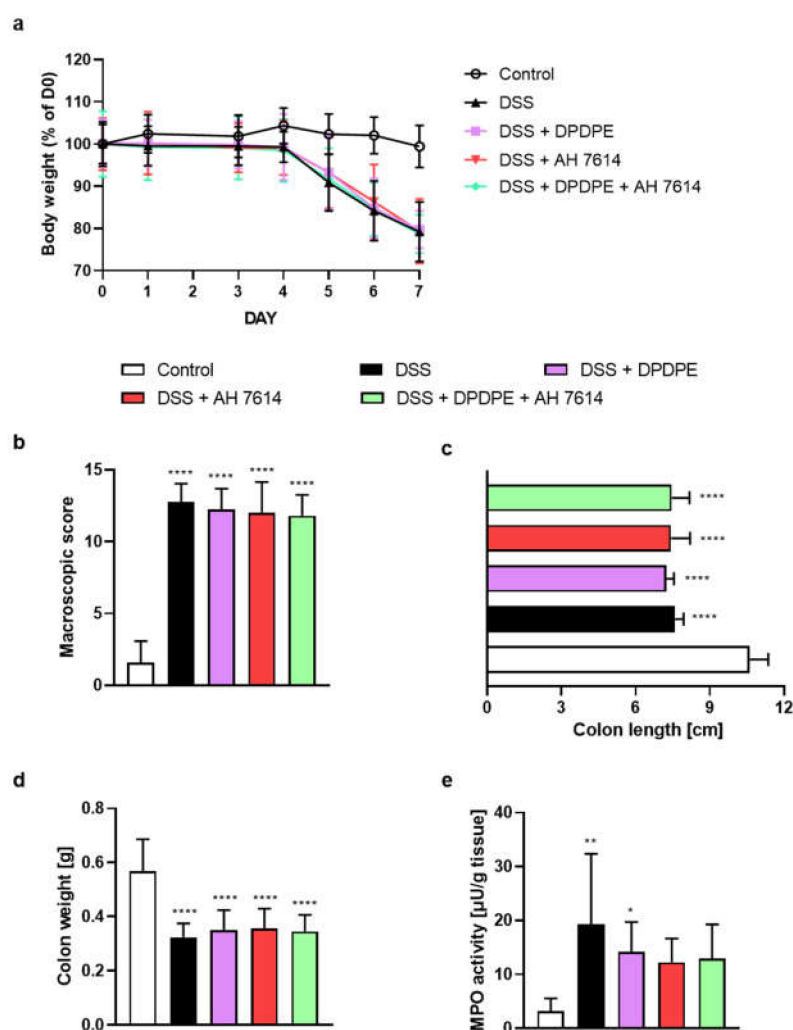
Figure 3. The i.p. administration of DOR agonist DPDPE (0.3 mg/kg BW) and FFAR4 antagonist AH 7614 (1 mg/kg BW) from day 3 to day 6, both twice daily did not alleviate symptoms of DSS-induced colitis in mice. Figure shows data for the body weight loss (**a**), macroscopic score (**b**), colon length (**c**), colon weight (**d**) and MPO activity (**e**). * $p < 0.05$, ** $p < 0.01$ and **** $p < 0.0001$, as compared to control mice. Data represent mean ± SEM of 5–10 mice per group. Abbreviations: DOR—δ opioid receptor, DSS—dextran sulfate sodium, FFAR4—free fatty acid receptor type 4, i.p.—intraperitoneally, MPO—myeloperoxidase.

2.4. FFAR4 and MOR Agonists Decreased MPO Activity, but Did Not Display Any Synergistic Effect

MOR agonist DAMGO at the dose of 0.02 mg/kg BW and FFAR4 agonist GSK 137647 at the dose of 1 mg/kg BW were administered i.p. twice daily from day 3 to day 6. Clinical and macroscopic indicators of colitis, such as BW loss (Figure 4a), macroscopic colon damage score (Figure 4b), colon length (Figure 4c) and colon weight (Figure 4d), were not altered as compared to DSS-treated group.

Noteworthy, the anti-inflammatory effects of DAMGO and GSK 137647 alone and the combination of DAMGO and GSK 137647 were observed on MPO activity (Figure 4e). However, no synergistic effect between MOR and FFAR4 agonists was noted. Moreover, investigated compounds did not influence the microscopic total damage score (Figure 4f,g).

Bootstrap for hypothesis testing revealed that $P_{bootstrap}$ in case of obtained difference in means between DSS + DAMGO vs. DSS + DAMGO and GSK 137647 ligands in macroscopic colon damage score (Figure 4b), colon length (Figure 4c), colon weight (Figure 4d), and MPO activity (Figure 4e) were as follows 0.2297 (calculated absolute difference between

means 0.7340), 0.8861 (calculated absolute difference in means 0.0441 cm), 0.4470 (calculated absolute difference in means 0.0320 g) and 0.8692 (calculated absolute difference in means 0.0400 µU/g tissue), respectively.
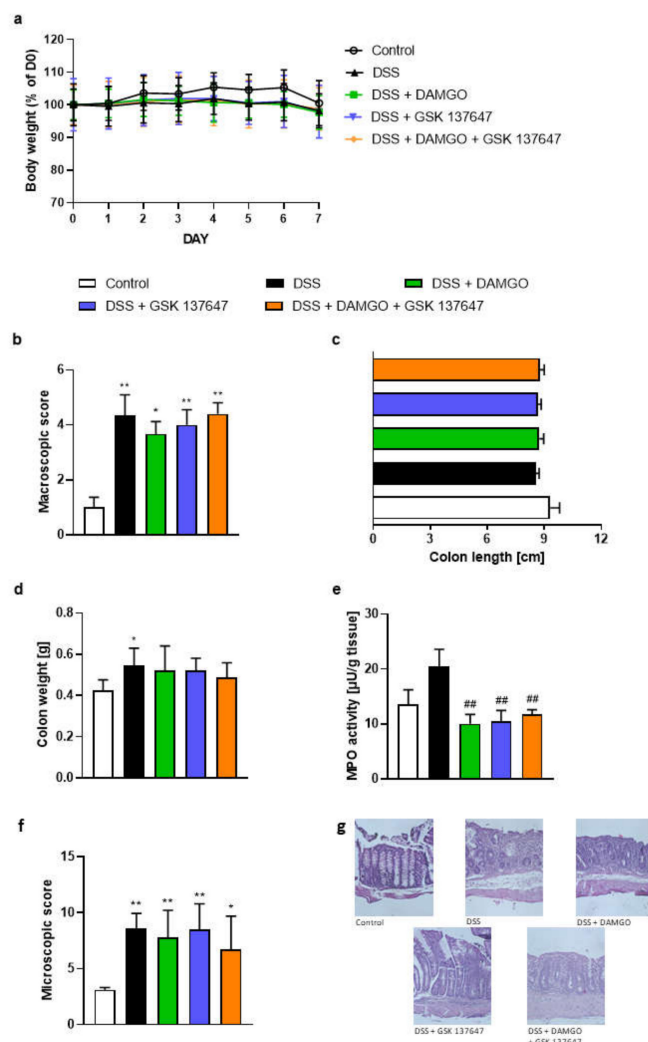

Figure 4. The i.p. administration of MOR agonist DAMGO (0.02 mg/kg BW) and FFAR4 agonist GSK 137647 (1 mg/kg BW) from day 3 to day 6, twice daily alleviated established DSS-induced colitis in mice. Figure shows data for body weight loss (**a**), macroscopic score (**b**), colon length (**c**), colon weight (**d**), MPO activity (**e**) and microscopic score (**f**). Representative photos of hematoxylin and eosin staining of colon samples (**g**). Scale bar = 100 µm. * $p < 0.05$, ** $p < 0.01$ as compared to control mice, whereas ## $p < 0.01$, as compared to DSS-treated mice. Data represent mean ± SEM of 5–10 mice per group. Abbreviations: DSS—dextran sulfate sodium, FFAR4—free fatty acid receptor type 4, i.p.—intraperitoneally, MOR—µ opioid receptor, MPO—myeloperoxidase.

2.5. FFAR4 Agonist Did Not Influence the Effect of Opioid Antagonist

A non-selective opioid receptor antagonist naloxone and FFAR4 agonist GSK 137647, both at the dose 1 mg/kg BW, were administered twice daily from day 3 to 6. The co-administration of naloxone and GSK 137647 in DSS-induced mouse model of colitis did not alleviate symptoms of disease (Figure 5a–e).

Bootstrap for hypothesis testing revealed that $P_{bootstrap}$ in case of obtained difference in means between DSS + naloxone vs. DSS + naloxone and GSK 137647 ligands in macroscopic colon damage score (Figure 5b), colon length (Figure 5c), colon weight (Figure 5d), and MPO activity (Figure 5e) were 0.1158 (calculated mean absolute difference in means 2.1),

0.1221 (calculated mean absolute difference in means 0.651 cm), 0.3317 (calculated mean absolute difference in means 0.0455 g) and 0.5067 (calculated absolute difference in means 1.1000 µU/g tissue), respectively.
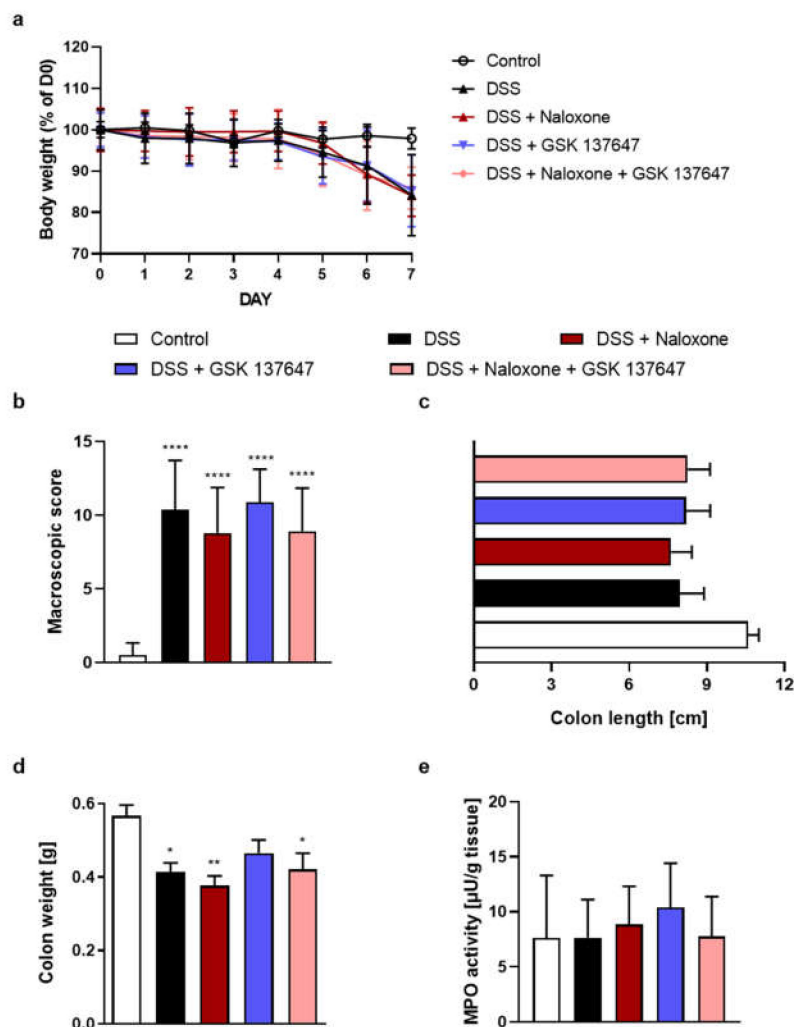

Figure 5. The i.p. administration of opioid receptor antagonist naloxone and FFAR4 agonist GSK 137647 (from day 3 to day 6, both 1 mg/kg BW, twice daily) did not alleviate symptoms of DSS-induced colitis in mice. Figure shows data for body weight loss (**a**), macroscopic score (**b**), colon length (**c**), colon weight (**d**) and MPO activity (**e**). * $p < 0.05$, ** $p < 0.01$ and **** $p < 0.0001$ as compared to control mice. Data represent mean $\pm$ SEM of 5–10 mice per group. Abbreviations: DSS—dextran sulfate sodium, FFAR4—free fatty acid receptor type 4, i.p.—intraperitoneally, MPO—myeloperoxidase.

3. Discussion

Several lines of evidence suggest the interplay between the endogenous opioid system and FFAs. In the early 1980s, the first reports showed that endogenous opioids contribute to the pathophysiology of central nervous system trauma [17,18]. The opioid mechanism was proved using naloxone, which significantly reversed hypotension and reduced pulse pressure after experimental brain injury. Noteworthy, it was also demonstrated that brain trauma might cause the release of FFAs. In 1990, Bakshi et al. [19] showed that the κ opioid receptor (KOR) agonist (dynorphin)-induced spinal cord tissue damage was connected with the increase in the level of total FFAs, reflecting changes in both saturated and unsaturated fatty acids. It was also evidenced that phospholipid hydrolysis may contribute to this type of injury. In further experiments it was indicated that dynorphin-

induced spinal cord tissue damage may be reversed with dynorphin antagonists or non-selective opioid antagonists. Moreover, pretreatment with nalmefene, an opioid receptor antagonist significantly attenuated the increase in total FFAs and individual increases in palmitic acid, stearic acid and oleic acid in spinal cord tissue, providing a potential link between opioids and membrane lipid-dependent mechanism. Finally, Hasegawa et al. [16] suggested that both unsaturated fatty acids and phospholipids can enhance binding of a purified MOR. Additionally, recent studies established that bioactive lipids and MOR cooperate in diabetes [20]. Namely, chronic oral administration of the lipid, 12(*S*)-hydroxyeicosatetraenoic [12(*S*)-HETE] reduced duodenal contractions and improved glucose tolerance. This effect was blocked by the peroxisome proliferator-activated receptor γ (PPARγ) antagonist GW 9662. Since 12(*S*)-HETE is considered as a second messenger that transmits signals from activated MOR, further experiments examined whether MOR is a receptor controlling intestinal contractions and glucose metabolism. The results showed that MOR agonist DAMGO significantly decreased frequency and contraction amplitude of the duodenum of diabetic mice; moreover, this effect was dependent on PPARγ [20].

SCFAs, which modulate FFAR2-dependent pathways, also play an important role in IBD pathophysiology through neutrophil chemotaxis, T cell differentiation and activation and production of cytokines, including tumor necrosis factor α (TNF-α), interleukin (IL)-1β and IL-8 [21,22]. Pizzonero et al. [23] demonstrated that the FFAR2 antagonist GLPG 0974 contributes to inhibition of acetate-induced neutrophil migration and is responsible for reduction of a neutrophil-based pharmacodynamics marker and CD11b activation-specific epitope in a human whole blood assay, suggesting that FFAR2 could be a potential pharmacological target for anti-IBD drugs. Two consecutive randomized, double-blind, placebo-controlled, single-center phase 1 studies (NCT01496937 and NCT01721980) evaluated the safety, tolerability and efficacy of GLPG 0974 in healthy subjects. Results showed that this compound was safe and well-tolerated up to a daily dose of 400 mg [24]. In addition, GLPG 0974 induced substantial and sustained inhibition of acetate-stimulated neutrophil activation. In phase 2 (NCT01829321), patients with mild-to-moderate UC were treated with GLPG 0974 at the dose of 200 mg, twice daily for 28 days. The aim of the study was to examine potential side effects (safety and tolerability) and efficacy of the FFAR2 antagonist. Although reduction of neutrophil activation and infiltration in GLPG 0974-treated individuals were observed, compared to those who received placebo, there were no differences in clinical responses, including Mayo score, or histopathology scoring of colon biopsies.

Recently, the nutritional therapy has begun to play a critical role in IBD course, emphasizing the role of—among others—FFAs in IBD [8,25,26]. Several studies suggest that activation of FFAR4 leads to an anti-inflammatory effect [27,28]. Moreover, patients with IBD have increased expression of FFAR4, which positively correlates with TNF-α level in the gut [29]. However, first reports showed contradictory properties of the selective GPR120/FFAR4 agonist, called compound A in IBD. Oh et al. [30] showed that compound A displays high selectivity and affinity, and is orally available; moreover, it produced potent anti-inflammatory effect on macrophages in vitro and in vivo in obese mice. In contrast, Wannick et al. [31] suggested that oral administration of compound A did not alleviate tissue inflammation in the mouse models of prototypical autoimmune diseases. On the other hand, a synthetic FFAR4 agonist GSK 137647 (administered at the dose of 1 mg/kg BW, i.p., twice daily) alleviated DSS-induced intestinal inflammation in mice, as indicated by significantly reduced MPO activity and macroscopic parameters, such as BW loss [28].

New therapeutics are urgently needed for patients with IBD and current research includes compounds targeting the opioid system [11,13]. Many in vitro and in vivo studies proved that peripherally active opioids decrease the release of pro-inflammatory cytokines or neuropeptides and improve wound healing [21,32,33]. For example, a synthetic MOR agonist DAMGO at the dose of 0.02 mg/kg BW administered in DSS-induced acute colitis significantly decreased disease activity index (DAI) and MPO activity and other parameters of inflammation, such as expression of cytokines and nuclear transcription factor-κB (NF-

κB) [34]. Interestingly, lower (0.01 mg/kg BW) and higher (0.04 or 0.08 mg/kg BW) doses of DAMGO did not affect the parameters of inflammation, including DAI and MPO activity suggesting a narrow therapeutic window for the anti-inflammatory properties of this compound [34]. Concurrently, Leanez et al. [35] discovered that a DOR agonist DPDPE demonstrated antinociceptive effect in peripheral inflammation and suggested that it was mainly mediated by nitric oxide derived from nitric oxide synthase 1. DPDPE is also engaged in inhibition of plasma extravasation during chronic intestinal inflammation [36]. Finally, MOR and DOR were found to be expressed by neurons and immune cells in the GI tract, especially in the colon [37] and they have since been considered as attractive pharmacological targets in IBD treatment.

In the present study, the possible synergistic effect of MOR/DOR and FFAR ligands was investigated. Of all the setups examined, the most interesting observation was that the treatment with DAMGO and GSK 137647 alone and in co-administration may affect the immune function in the colonic inflammation through reduction of MPO activity. Furthermore, we evaluated the microscopic total damage to analyze the reduction of neutrophil infiltration in tissues; however, no statistically significant results were obtained. In addition, in our experiments we have not observed any synergistic effects. This may be caused by the fact that no positive, anti-inflammatory effects of DAMGO alone were seen. The probable reason for such outcomes could be the severity of inflammation or doses of tested compounds used in our study (please see Study Limitations below).

To ensure that the revealed mean differences between MOR/DOR ligands alone and in co-administration with FFAR ligands were not observed due to pure chance, we used the bootstrap hypothesis testing technique with 10,000 iterations (see below Equation (1)). The bootstrap method is a statistical procedure that resamples a single dataset to create many simulated samples. Such approach is one of the ways to control and check the stability of the obtained results, especially when we have relatively small sample sizes. It is also a convenient method, often used in life sciences, that avoids the cost of repeating the experiment to obtain other groups of sample data; moreover, it follows 3R recommendations. Hypothesis testing is a fundamental statistical procedure on which all inference is based. It evaluates two mutually exclusive statements about differences in data sets to determine which statement is best supported by the gathered data. We believed that using this technique would support our results and increase the power of our inference.

As indicated above, although DAMGO and GSK 137647 alone and in co-administration decreased MPO activity, when compared to untreated group, we did not observe synergy in their action. On the other hand, the high values of the bootstrap statistics (there were no $P_{\text{bootstrap}} \leq 0.05$) in our experiments indicated that there is still a chance in further experiments of obtaining values of differences between the mean MOR and MOR + FFAR that were greater than or equal to the results we presented.

4. Materials and Methods

4.1. Animals

Experimentally naive male BALB/c mice obtained from the vivarium of the University of Lodz, Poland, were used in all experiments. Mice weighed 22–26 g (6–8 weeks of age) and were housed at a constant temperature (22–23 °C) and maintained under a 12-h light/dark cycle (lights on at 6.00 am) in sawdust-lined plastic cages with free access to chow pellets and tap water. All animal protocols were approved by the local Animal Care Committee (Protocols 3/ŁB124/2019 and 11/ŁB128/2019). All efforts were made to minimize animal suffering and to reduce the number of animals used. Groups of 5–10 animals were used in all in vivo experiments.

4.2. Drugs

MOR agonist—DAMGO was purchased from Sigma-Aldrich (Poznan, Poland), whereas DOR agonist—DPDPE was obtained from TriMen Chemicals (Lodz, Poland). FFAR ligands, including a FFAR4 agonist—GSK 137647, a FFAR4 antagonist—AH 7614 and a FFAR2

antagonist—GLPG 0974 and naloxone were obtained from Tocris Bioscience (Bristol, UK). DSS (MW 40,000) was purchased from PanReac AppliChem, Lot No.9J013322 (Darmstadt, Germany). All drugs were dissolved in 5% dimethyl sulfoxide (DMSO) in saline, which was used as a vehicle; DSS was dissolved in tap water. The vehicle in the used concentration had no effects on the observed parameters.

4.3. Induction of Colitis

Colonic inflammation in this model was induced by DSS (4% wt/vol). DSS was added to drinking water from day 0 to day 5. On days 6 and 7 DSS solution was changed to tap water. Control animals were receiving tap water throughout the whole experiment. Animal body weight and general health and disease progression were monitored daily.

4.4. Pharmacological Treatments

In the DSS model, mice were treated with various combinations of opioid receptor and FFAR ligands, namely: DAMGO (0.02 mg/kg BW, intraperitoneally (i.p.), once or twice daily), DPDPE (0.3 mg/kg BW, i.p., twice daily), naloxone (1 mg/kg BW, i.p., twice daily), GLPG 0974 (1 mg/kg BW, i.p., once daily), GSK 137647 (1 mg/kg BW, i.p., twice daily) and AH 7614 (1 mg/kg BW, i.p., twice daily), from day 3 to day 6. On day 7, animals were sacrificed, and evaluation of colonic damage was performed. In all experiments control animals received vehicle (100 μL, i.p.) alone. The doses of opioid receptor and FFAR ligands used in this study were selected based on literature and preliminary studies.

4.5. Evaluation of Colonic Damage

Disease parameters were evaluated on day 7 of the experiment. After euthanasia, the entire colon was isolated and weighed with fecal content; colon length was measured using a caliper. Then, the colon was opened longitudinally and cleaned from the fecal content. A total macroscopic damage score was calculated for each animal based on the (i) stool consistency (where 0 means normal well-shaped fecal pellets and 3 means diarrhea), (ii) colon epithelial damage based on a number of ulcers (0–3), (iii) colon length and weight scores expressed as a percentage change of each parameter in relation to the control group (0 points, ≤5% change; 1 point, 5–14% change; 2 points, 15–24% change; 3 points, 25–35% change; and 4 points, ≥35% change). The presence (score = 1) or absence (score = 0) of fecal blood was also recorded. Total score = 0 means no inflammation.

4.6. Determination of Tissue Myeloperoxidase Activity

Myeloperoxidase (MPO) activity was quantified with the method described earlier by Salaga et al. [38]. In brief, 0.3 cm segments of colon were weighed and rapidly homogenized in hexadecyltrimethylammonium bromide (HTAB) buffer (0.5% HTAB in 50 mM potassium phosphate buffer, pH 6.0; approx. 30 mg of tissue/mL). Then, the homogenate was centrifuged for 15 min (13,200 g, 4 °C) and the supernatant was used in the subsequent steps. On a 96-well plate, 200 μL of 50 mM potassium phosphate buffer (pH 6.0), containing 0.167 mg/mL of *O*-dianisidine hydrochloride and 0.05 μL of 1% hydrogen peroxide was added to 7 μL of the supernatant. Absorbance was measured (in triplicate) at 450 nm (iMARK Microplate Reader, Biorad, United Kingdom) at 0, 30 and 60 s after initiation of reaction. MPO was expressed in milliunits per gram of wet tissue, 1 unit being the quantity of enzyme able to convert 1 μmol of hydrogen peroxide to water in 1 min at room temperature. Units of MPO activity per 1 min were calculated from a standard curve prepared with the use of purified peroxidase enzyme.

4.7. Histology

Segments of the distal colon were stapled flat, mucosal side up, onto cardboard and fixed in 10% neutral-buffered formalin for 24 h at 4 °C. Then, samples were dehydrated in sucrose, embedded in paraffin, sectioned at 5 μm and mounted onto slides. Subsequently sections were stained with hematoxylin and eosin and examined using (Axio Imager A2

microscope, Carl Zeiss, Berlin, Germany). Microscopic total damage score was determined based on the following parameters: presence (score = 1) or absence (score = 0) of goblet cell depletion, the presence (score = 1) or absence (score = 0) of crypt abscesses, the destruction of mucosal architecture (normal = 1, moderate = 2, extensive = 3), the extent of muscle thickening (normal = 1, moderate = 2, extensive = 3) and the presence and degree of immune cell infiltration (normal = 1, moderate = 2, transmural = 3).

4.8. Bootstrap for Hypothesis Testing in R Software

To compare numeric variables for two groups/datasets, bootstrap approach to hypothesis testing was implemented. This approach was taken as an alternative to the two-sided t-test for two samples comparing independent groups (all datasets had normal distribution). All calculations were made in RStudio software with utilizing R programing language. Specific code for all computations was written for this purpose, according to guidelines from Marinstats lectures from the University of British Columbia (https://statslectures.com/r-scripts-datasets, accessed on 1 April 2021). Program code was attached in Supplementary Materials. Calculation of the absolute difference in means for MOR vs. MOR + FFAR ligand or DOR vs. DOR + FFAR ligand in colitis was the first step in our approach (observed_test_stat). Next, the matrix of 10,000 bootstrap resamples with replacement from our datasets were made. Each pair of data (column) was a single bootstrap sample. For each of such new random resampled column, the absolute difference in means for MOR vs. MOR + FFAR ligand or DOR vs. DOR + FFAR ligand was calculated through loop (bootstrap_test_stat [n, n + 1, n = 10,000]). Eventually, P value of bootstrap ($P_{\text{bootstrap}}$) was calculated as follows (Equation (1)):

$$P_{\text{bootstrap}} = \frac{\text{bootstrap}_{\text{test}_{\text{stat1}}} \geq \text{observed\_test\_stat} + \ldots + \text{bootstrap}_{\text{test}_{\text{stat10000}}} \geq \text{observed\_test\_stat}}{10000} \quad (1)$$

where P value denotes the number of the bootstrap test statistics that were greater than or equal to the observed test statistic divided by the total number of bootstrap test statistics. For example, $P_{\text{bootstrap}}$ = 0.25 (for calculated absolute difference in means = 13 units) was interpreted as out of the 10,000 bootstrap test statistics calculated, 2500 (25%) of them had test statistic greater than 13 units. This, in turn, was interpreted as follows: if there was no difference between two groups, we would see a test statistic equal or higher than the value of observed_test_stat (absolute difference in the sample means; in the example above: 13) by chance 25% of the time. More generically *p*-values of bootstrap have told us what the probability is of getting the test statistic we got, or if the null hypothesis is true (there is no difference between two groups/datasets).

4.9. Statistics

Statistical analysis was performed using Prism 9.0.1 (GraphPad Software Inc., La Jolla, CA, USA) and RStudio software. The data are expressed as means ± SEM. The Shapiro–Wilk test was used to test the normality of data distribution. One-way analysis of variance (ANOVA) followed by Bonferroni post-hoc test and student t-test were used for analysis. To better evaluate the synergy of the opioid receptor and FFAR ligands, mainly due to relatively small sample sizes and the low statistical power of the estimated inferences, we employed the bootstrap hypothesis testing technique (10,000 iterations) to ensure that the revealed differences in means between MOR vs. MOR + FFAR ligand or DOR vs. DOR + FFAR ligand, in colitis were not observed due to pure chance. P values and P value of bootstrap ($P_{\text{bootstrap}}$) < 0.05 were considered as statistically significant.

5. Conclusions

Our results showed that treatment with ligands of MOR and FFAR separately and in combination may affect immune function in the inflammation seen by altering MPO activity even though these ligands had no significant influence on the severity of colitis. However, MOR/DOR and FFAR ligands did not exhibit synergistic effect in colonic inflammation,

including immune aspect. This study indicates that the interaction between the endogenous opioid system and FFARs, although suggested by some reports, does not take place in colonic inflammation. Nevertheless, there are some premises to continue this research; one of them is the high values of $P_{\text{bootstrap}}$ statistics in the conducted experiments. Further validation of this interaction as a potential therapeutic target in IBD is thus needed. One of the necessary future experiments should include higher doses of compounds (e.g., DAMGO). Moreover, a new possible interactions should be tested, e.g., for FFAR and hormone binding sites.

6. Study Limitations

Although the doses of opioid receptors and FFARs ligands used in our study were selected based on literature [14,29,35] and our preliminary results, we did not obtain any beneficial impact on mouse colitis. Moreover, we concluded the study by investigating whether the co-administration of opioid antagonist naloxone and FFAR4 agonist GSK 137647 may influence parameters of colitis in mice. This opposite direction of our research also did not show any differences between treated and un-treated groups. In line, bootstrap hypothesis testing for DOR ligand and DOR + FFAR ligands revealed the same trend of randomness as mentioned in case of MOR ligand and MOR + FFAR ligands.

References

1. Sobolewska-Włodarczyk, A.; Włodarczyk, M. Pathogenesis of IBD. In *Introduction to Gastrointestinal Diseases*; Fichna, J., Ed.; Springer: Cham, Switzerland, 2017; Volume 1, pp. 83–93.
2. Raine, T. Vedolizumab for inflammatory bowel disease: Changing the game, or more of the same? *United Eur. Gastroenterol. J.* **2014**, *2*, 333–344. [CrossRef] [PubMed]
3. McLean, L.P.; Cross, R.K. Adverse events in IBD: To stop or continue immune suppressant and biologic treatment. *Expert Rev. Gastroenterol. Hepatol.* **2014**, *8*, 223–240. [CrossRef] [PubMed]
4. Milligan, G.; Stoddart, L.A.; Brown, A.J. G protein-coupled receptors for free fatty acids. *Cell. Signal.* **2006**, *18*, 1360–1365. [CrossRef] [PubMed]
5. Pongkorpsakol, P.; Moonwiriyakit, A.; Muanprasat, C. Fatty acid and mineral receptors as drug targets for gastrointestinal disorders. *Future Med. Chem.* **2017**, *9*, 315–334. [CrossRef]
6. Calder, P.C. Polyunsaturated fatty acids, inflammatory processes and inflammatory bowel diseases. *Mol. Nutr. Food Res.* **2008**, *52*, 885–897. [CrossRef]
7. Maslowski, K.M.; Vieira, A.T.; Ng, A.; Kranich, J.; Sierro, F.; Yu, D.; Schilter, H.C.; Rolph, M.S.; MacKay, F.; Artis, D. Regulation of inflammatory responses by gut microbiota and chemoattractant receptor GPR43. *Nature* **2009**, *461*, 1282–1286. [CrossRef]

8. Bartoszek, A.; Von Moo, E.; Binienda, A.; Fabisiak, A.; Krajewska, J.B.; Mosińska, P.; Niewinna, K.; Tarasiuk, A.; Martemyanov, K.; Salaga, M.; et al. Free Fatty Acid Receptors as new potential therapeutic target in inflammatory bowel diseases. *Pharmacol. Res.* **2020**, *152*, 104604. [CrossRef]

9. Wang, D.; Tawfik, V.L.; Corder, G.; Low, S.A.; François, A.; Basbaum, A.I.; Scherrer, G. Functional Divergence of Delta and Mu Opioid Receptor Organization in CNS Pain Circuits. *Neuron* **2018**, *98*, 90–108.e5. [CrossRef]

10. Abdallah, K.; Gendron, L. The Delta Opioid Receptor in Pain Control. In *Handbook of Experimental Pharmacology*; Springer: Cham, Switzerland, 2017; pp. 147–177. ISBN 978-3-319-29806-1.

11. Kienzl, M.; Storr, M.; Schicho, R. Cannabinoids and Opioids in the Treatment of Inflammatory Bowel Diseases. *Clin. Transl. Gastroenterol.* **2020**, *11*, e00120. [CrossRef]

12. Valdez-Morales, E.; Guerrero-Alba, R.; Ochoa-Cortes, F.; Benson, J.; Spreadbury, I.; Hurlbut, D.; Miranda-Morales, M.; Lomax, A.E.; Vanner, S. Release of endogenous opioids during a chronic IBD model suppresses the excitability of colonic DRG neurons. *Neurogastroenterol. Motil.* **2013**, *25*, 5–7. [CrossRef]

13. Stein, C. Targeting pain and inflammation by peripherally acting opioids. *Front. Pharmacol.* **2013**, *4*, 1–3. [CrossRef]

14. Philippe, D.; Dubuquoy, L.; Groux, H.; Brun, V.; Van Chuoï-Mariot, M.T.; Gaveriaux-Ruff, C.; Colombel, J.F.; Kieffer, B.L.; Desreumaux, P. Anti-inflammatory properties of the μ opioid receptor support its use in the treatment of colon inflammation. *J. Clin. Investig.* **2003**, *111*, 1329–1338. [CrossRef]

15. DiCello, J.J.; Saito, A.; Rajasekhar, P.; Eriksson, E.M.; McQuade, R.M.; Nowell, C.J.; Sebastian, B.W.; Fichna, J.; Veldhuis, N.A.; Canals, M.; et al. Inflammation-associated changes in DOR expression and function in the mouse colon. *Am. J. Physiol. Liver Physiol.* **2018**, *315*, G544–G559. [CrossRef]

16. Hasegawa, J.-I.; Loh, H.H.; Lee, N.M. Lipid Requirement for μ Opioid Receptor Binding. *J. Neurochem.* **1987**, *49*, 1007–1012. [CrossRef]

17. Faden, A.; Jacobs, T.; Holaday, J. Opiate antagonist improves neurologic recovery after spinal injury. *Science* **1981**, *211*, 493–494. [CrossRef]

18. Hayes, R.L.; Galinat, B.J.; Kulkarne, P.; Becker, D.P. Effects of naloxone on systemic and cerebral responses to experimental concussive brain injury in cats. *J. Neurosurg.* **1983**, *58*, 720–728. [CrossRef]

19. Bakshi, R.; Newman, A.H.; Faden, A.I. Dynorphin A-(1-17) induces alterations in free fatty acids, excitatory amino acids, and motor function through an opiate-receptor-mediated mechanism. *J. Neurosci.* **1990**, *10*, 3793–800. [CrossRef]

20. Abot, A.; Wemelle, E.; Laurens, C.; Paquot, A.; Pomie, N.; Carper, D.; Bessac, A.; Mas Orea, X.; Fremez, C.; Fontanie, M.; et al. Identification of new enterosynes using prebiotics: Roles of bioactive lipids and mu-opioid receptor signalling in humans and mice. *Gut* **2021**, *70*, 1078–1087. [CrossRef]

21. Stein, C.; Kuchler, S. Non-Analgesic Effects of Opioids: Peripheral Opioid Effects on Inflammation and Wound Healing. *Curr. Pharm. Des.* **2012**, *18*, 6053–6069. [CrossRef]

22. Kovarik, J.J.; Tillinger, W.; Hofer, J.; Hölzl, M.A.; Heinzl, H.; Saemann, M.D.; Zlabinger, G.J. Impaired anti-inflammatory efficacy of n-butyrate in patients with IBD. *Eur. J. Clin. Investig.* **2011**, *41*, 291–298. [CrossRef]

23. Pizzonero, M.; Dupont, S.; Babel, M.; Beaumont, S.; Bienvenu, N.; Blanqué, R.; Cherel, L.; Christophe, T.; Crescenzi, B.; De Lemos, E.; et al. Discovery and optimization of an azetidine chemical series as a free fatty acid receptor 2 (FFA2) antagonist: From hit to clinic. *J. Med. Chem.* **2014**, *57*, 10044–10057. [CrossRef] [PubMed]

24. Namour, F.; Galien, R.; Van Kaem, T.; Van der Aa, A.; Vanhoutte, F.; Beetens, J.; van't Klooster, G. Safety, pharmacokinetics and pharmacodynamics of GLPG0974, a potent and selective FFA2 antagonist, in healthy male subjects. *Br. J. Clin. Pharmacol.* **2016**, *82*, 139–148. [CrossRef] [PubMed]

25. Ma, C.; Vasu, R.; Zhang, H. The Role of Long-Chain Fatty Acids in Inflammatory Bowel Disease. *Mediators Inflamm.* **2019**, *2019*, 8495913. [CrossRef] [PubMed]

26. Marton, L.T.; Goulart, R.A.; de Carvalho, A.C.A.; Barbalho, S.M. Omega fatty acids and inflammatory bowel diseases: An overview. *Int. J. Mol. Sci.* **2019**, *20*, 4851. [CrossRef]

27. Lee, J.; Moraes-Vieira, P.M.; Castoldi, A.; Aryal, P.; Yee, E.U.; Vickers, C.; Parnas, O.; Donaldson, C.J.; Saghatelian, A.; Kahn, B.B. Branched fatty acid esters of hydroxy fatty acids (FAHFAs) protect against colitis by regulating gut innate and adaptive immune responses. *J. Biol. Chem.* **2016**, *291*, 22207–22217. [CrossRef]

28. Salaga, M.; Bartoszek, A.; Binienda, A.; Krajewska, J.B.; Fabisiak, A.; Mosińska, P.; Dziedziczak, K.; Niewinna, K.; Talar, M.; Tarasiuk, A.; et al. Activation of free fatty acid receptor 4 affects intestinal inflammation and improves colon permeability in mice. *Nutrients* **2021**, *13*, 2716. [CrossRef]

29. Tsukahara, T.; Watanabe, K.; Watanabe, T.; Yamagami, H.; Sogawa, M.; Tanigawa, T.; Shiba, M.; Tominaga, K.; Fujiwara, Y.; Maeda, K.; et al. Tumor necrosis factor α decreases glucagon-like peptide-2 expression by up-regulating G-protein-coupled receptor 120 in crohn disease. *Am. J. Pathol.* **2015**, *185*, 185–196. [CrossRef]

30. Oh, D.Y.; Walenta, E.; Akiyama, T.E.; Lagakos, W.S.; Lackey, D.; Pessentheiner, A.R.; Sasik, R.; Hah, N.; Chi, T.J.; Cox, J.M.; et al. A Gpr120-selective agonist improves insulin resistance and chronic inflammation in obese mice. *Nat. Med.* **2014**, *20*, 942–947. [CrossRef]

31. Wannick, M.; Bezdek, S.; Guillen, N.; Thieme, M.; Meshrkey, F.; Mousavi, S.; Seeling, M.; Nimmerjahn, F.; Mócsai, A.; Zillikens, D.; et al. Oral administration of the selective GPR120/FFA4 agonist compound A is not effective in alleviating tissue inflammation in mouse models of prototypical autoimmune diseases. *Pharmacol. Res. Perspect.* **2018**, *6*, 1–8. [CrossRef]

32. Stein, C.; Küchler, S. Targeting inflammation and wound healing by opioids. *Trends Pharmacol. Sci.* **2013**, *34*, 303–312. [CrossRef]
33. Ciotu, C.I.; Fischer, M.J.M. Novel Analgesics with Peripheral Targets. *Neurotherapeutics* **2020**, *17*, 784–825. [CrossRef]
34. Anselmi, L.; Huynh, J.; Duraffourd, C.; Jaramillo, I.; Vegezzi, G.; Saccani, F.; Boschetti, E.; Brecha, N.C.; De Giorgio, R.; Sternini, C. Activation of μ opioid receptors modulates inflammation in acute experimental colitis. *Neurogastroenterol. Motil.* **2015**, *27*, 509–523. [CrossRef]
35. Leánez, S.; Hervera, A.; Pol, O. Peripheral antinociceptive effects of μ- and δ -opioid receptor agonists in NOS2 and NOS1 knockout mice during chronic in fl ammatory pain. *Eur. J. Pharmacol.* **2009**, *602*, 41–49. [CrossRef]
36. Jiménez, N.; Puig, M.M.; Pol, O. Antiexudative Effects of Opioids and Expression of κ- and δ- Opioid Receptors during Intestinal Inflammation in Mice: Involvement of Nitric Oxide. *J. Pharmacol. Exp. Ther.* **2006**, *316*, 261–270. [CrossRef]
37. Galligan, J.J.; Sternini, C. Insights into the role of opioid receptors in the GI tract: Experimental evidence and therapeutic relevance. *Handb. Exp. Pharmacol.* **2017**, *239*, 363–378. [CrossRef]
38. Sałaga, M.; Lewandowska, U.; Sosnowska, D.; Zakrzewski, P.K.; Cygankiewicz, A.I.; Piechota-Polańczyk, A.; Sobczak, M.; Mosinska, P.; Chen, C.; Krajewska, W.M.; et al. Polyphenol extract from evening primrose pomace alleviates experimental colitis after intracolonic and oral administration in mice. *Naunyn. Schmiedebergs. Arch. Pharmacol.* **2014**, *387*, 1069–1078. [CrossRef]